NASA/CR—2005-213584/VOL3

Critical Propulsion Components
Volume 3: Exhaust Nozzle

Pratt & Whitney
West Palm Beach, Florida

General Electric Aircraft Engines
Cincinnati, Ohio

May 2005

The NASA STI Program Office . . . in Profile

Since its founding, NASA has been dedicated to the advancement of aeronautics and space science. The NASA Scientific and Technical Information (STI) Program Office plays a key part in helping NASA maintain this important role.

The NASA STI Program Office is operated by Langley Research Center, the Lead Center for NASA's scientific and technical information. The NASA STI Program Office provides access to the NASA STI Database, the largest collection of aeronautical and space science STI in the world. The Program Office is also NASA's institutional mechanism for disseminating the results of its research and development activities. These results are published by NASA in the NASA STI Report Series, which includes the following report types:

- TECHNICAL PUBLICATION. Reports of completed research or a major significant phase of research that present the results of NASA programs and include extensive data or theoretical analysis. Includes compilations of significant scientific and technical data and information deemed to be of continuing reference value. NASA's counterpart of peer-reviewed formal professional papers but has less stringent limitations on manuscript length and extent of graphic presentations.

- TECHNICAL MEMORANDUM. Scientific and technical findings that are preliminary or of specialized interest, e.g., quick release reports, working papers, and bibliographies that contain minimal annotation. Does not contain extensive analysis.

- CONTRACTOR REPORT. Scientific and technical findings by NASA-sponsored contractors and grantees.

- CONFERENCE PUBLICATION. Collected papers from scientific and technical conferences, symposia, seminars, or other meetings sponsored or cosponsored by NASA.

- SPECIAL PUBLICATION. Scientific, technical, or historical information from NASA programs, projects, and missions, often concerned with subjects having substantial public interest.

- TECHNICAL TRANSLATION. English-language translations of foreign scientific and technical material pertinent to NASA's mission.

Specialized services that complement the STI Program Office's diverse offerings include creating custom thesauri, building customized databases, organizing and publishing research results . . . even providing videos.

For more information about the NASA STI Program Office, see the following:

- Access the NASA STI Program Home Page at ***http://www.sti.nasa.gov***

- E-mail your question via the Internet to help@sti.nasa.gov

- Fax your question to the NASA Access Help Desk at 301–621–0134

- Telephone the NASA Access Help Desk at 301–621–0390

- Write to:
  NASA Access Help Desk
  NASA Center for AeroSpace Information
  7121 Standard Drive
  Hanover, MD 21076

NASA/CR—2005-213584/VOL3

Critical Propulsion Components
Volume 3: Exhaust Nozzle

Pratt & Whitney
West Palm Beach, Florida

General Electric Aircraft Engines
Cincinnati, Ohio

Prepared under Contract NAS3–27235

National Aeronautics and
Space Administration

Glenn Research Center

May 2005

Document History

This research was originally published internally in September 2000.

Available from

NASA Center for Aerospace Information
7121 Standard Drive
Hanover, MD 21076

National Technical Information Service
5285 Port Royal Road
Springfield, VA 22100

Available electronically at http://gltrs.grc.nasa.gov

Abstract

Several studies have concluded that a supersonic aircraft, if environmentally acceptable and economically viable, could successfully compete in the 21st century marketplace. However, before industry can commit to what is estimated as a 15-to-20 billion dollar investment, several barrier issues must be resolved. In an effort to address these barrier issues, NASA and Industry teamed to form the High-Speed Research (HSR) program. As part of this HSR program, the Critical Propulsion Components (CPC) element was created and assigned the task of developing those propulsion component technologies necessary to: (1) reduce cruise emissions by a factor of 10 and (2) meet the ever-increasing airport noise restrictions with an economically viable propulsion system. The CPC-identified critical components were ultra-low-emission combustors, low-noise/high-performance exhaust nozzles, low-noise fans, and stable/high-performance inlets. Propulsion cycle studies (coordinated with NASA–Langley sponsored airplane studies) were conducted throughout this CPC program to help evaluate candidate components and select the best concepts for the more complex and larger scale research efforts. The propulsion cycle and components ultimately selected were a mixed-flow turbofan (MFTF) engine employing a lean, premixed, prevaporized (LPP) combustor coupled to a two-dimensional mixed compression inlet and a two-dimensional mixer/ejector nozzle.

The CPC program began in 1994 and was planned for completion in 2002. Unfortunately, in 1999 NASA chose to prematurely end the HSR program. Although terminated early, the HSR program demonstrated that an economically viable and environmentally acceptable supersonic aircraft (and propulsion system) was achievable. The purpose of this document is to document the CPC findings in support of those visionaries in the future who have the courage to once again pursue a supersonic passenger airplane.

Due to the large amount of material presented in this report, it was prepared in four volumes:

Volume 1: Section 1 – Summary
Section 2 – Introduction
Section 3 – Propulsion System Studies

Volume 2: Section 4 – Combustor

Volume 3: Section 5 – Exhaust Nozzle

Volume 4: Section 6 – Inlet
Section 7 – Fan/Inlet Acoustic Team

Table of Contents

Table of Contents (Continued)

Table of Contents (Continued)

Table of Contents (Continued)

Table of Contents (Concluded)

List of Illustrations

List of Illustrations (Continued)

List of Illustrations (Continued)

List of Illustrations (Continued)

List of Illustrations (Continued)

List of Illustrations (Continued)

List of Illustrations (Continued)

List of Illustrations (Continued)

List of Illustrations (Continued)

List of Illustrations (Continued)

List of Illustrations (Continued)

List of Illustrations (Continued)

List of Illustrations (Concluded)

List of Tables

List of Tables (Concluded)

Lexicon

16TT	NASA–Langley 16-ft transonic wind tunnel
2D	Configuration similar to two back-to-back letter D's, also two dimensional
2DB	Two-dimensional bifurcated (inlet concept)
2DCD	Two-dimensional convergent/ divergent (exhaust nozzle)
2DFC	Two-dimensional fixed chute
2E	Two excitations per rotor revolution (vibration mode)
A_8	Exhaust nozzle throat area
A8CD	Exhaust nozzle effective jet area
A_9	Exhaust nozzle exit area
A16, A_{16}	Variable-area fan/core mixer duct-side area
A56	Mixer-exit area, core stream
AACE	Aeroacoustics collaborative effort
AAPL	Aeroacoustic Propulsion Laboratory
ACE	Axisymmetric coannular ejector (exhaust nozzle)
ADP	Aerodynamic design point
AE8, A_{E8}	Effective exhaust nozzle throat area
AEDC	Arnold Engineering Development Center
AFRL–MMD	Air Force Research Laboratory, Materials and Manufacturing Directorate
AIP	Aerodynamic interface plane (between inlet and engine)
AJ2	Exhaust nozzle suppressed throat area
ALMMC	Aluminum metal-matrix composite
AMEN	Axisymmetric mixer/ejector nozzle
AMT	Airframe Management Team
AN^2	Blade root stress parameter
ANSYS	GEAE design-analysis tool (software)
AR	Aspect ratio, also area ratio
ARP	Aerospace Recommended Practice
ASAR	Flowpath area aft of ejector mixer
ASME	American Society of Mechanical Engineers
AST	Advanced subsonic technology
A_t/A_{mix}	Ratio of acoustic treatment area to mixing area
ATC	Axi-tilt chute
ATCB	Axisymmetric translating centerbody (engine inlet)
AV	Arc valve
AVP	Active-volume parameter
BAC	Boeing Aircraft Company
BCAE	Boeing Commercial Aircraft Group
BDSM	"Best" downstream mixer (exhaust nozzle)
BLISK	Blade on disk (rotor type)
BOAS	Blade outer air seals
BPF	Blade-passing frequency
BPR	Bypass ratio
BS&D	Bearings, seals, and drives
BTSSI	Bifurcated two-stage supersonic inlet
C&A	Controls and accessories
CAFD	Circumferentially averaged flow determination (computer program)
CAM	Cold acoustic model, cold aerodynamic model
CASL	Chute aerodynamics with stereolithography
CB	Customer bleed
CBM	Computation-based method
CDA	Controlled-diffusion airfoil
CDP	Compressor-discharge plane
CER	Chute expansion ratio
CFD	Computational fluid dynamics
CFG, C_{FG}, C_{fg}	Coefficient of gross thrust
CFN, C_{FN}, C_{fn}	Coefficient of net thrust

CG	Center of gravity
CG1	Turbomachinery center of gravity
CG2	Exhaust nozzle center of gravity
CG3	Overall engine center of gravity
CM	Coordination memo
CMC	Ceramic-matrix composite
CMMR	Critical major milestone review
CMT	CPC management team
CO	Carbon monoxide
COTR	Contracting Officer's Technical Representative
CPC	Critical Propulsion Components
CPR	Compressor pressure ratio
CR	Contractor report
CRAFT	Combustion Research and Flow Technology Inc.
CTOL	Conventional takeoff and landing
dB	Decibels
DEN	Double-edge notch
$\Delta H/T$	Specific work
DOC	Direct operating cost
DOC+I	Direct operating cost + interest
DoD	Department of Defense
DOE	Design of experiments
DOSS	Design optimization synthesis system (Boeing)
DP	Pressure drop or differential
DPC	Circumferential pressure distortion
DPC/Pmx	Circumferential-distortion parameter (total pressure)
DPE	Perfluoroalkyldiphenylether
DPR	Radial pressure distortion
DPR/Pmx	Radial-distortion parameter (total pressure)
DR&O	Design requirements and objectives (Boeing document)
DRD	Documentation requirements document
DS	Directionally solidified
DSM	Downstream mixer (exhaust nozzle)
DTR	Diffuser test rig
DVM	Discrete-vortex method
EB	Electron beam
EDM	Electrical-discharge machining (or machined)
EFH	Engine flight hour(s)
EI	Emissions index: g of pollutant per kg of fuel burned; also, environmental impact
EICO	CO emissions index: g CO/kg fuel
EIHC	HC emissions index: g of unburned hydrocarbons per kg of fuel burned
EINOx	NOx emissions index: g of NOx/kg fuel
EPM	Enabling Propulsion Materials
EPNdB	Effective perceived noise decibels
EPNL	Effective perceived noise level
ER	Extraction ratio: P_{16}/P_{56}
ESF	Engine scale factor
ESP	Electronically scanned pressure
ETA (η)	Efficiency
f/a	Fuel/air ratio
F/C	Fan/core
FA&M	Florida Agricultural and Mechanical University
FADEC	Full-authority digital electronic control
FAR	Fuel/air ratio, also Federal Aviation Regulation
FC	Fixed chute (mixer/ejector nozzle)
FCG	Fatigue crack growth
FCM	Fixed-chute mixer
FCN	Fixed-chute nozzle
FEGV	Fan exit guide vane
FEM	Finite-element model
FENTD	Full-scale engine nozzle technology demonstration/demonstrator (more frequently called FSD)

FH	Flight hour(s)
FIAT	Fan inlet/acoustics team (ITD team)
FLABI	"FLADE" bypass injector valve
FLADE	Fan-on-blade HSCT engine concept
FN, F_N, F_n	Net thrust
FNAA	Fan average
FNDAB	Net thrust with afterbody drag removed
FNP	Fixed chute, no plug; unsuppressed primary (idle) thrust; uninstalled net thrust
FNS	Full Navier–Stokes
$F_{n\ sup}$	Net thrust with nozzle in noise-suppression mode
FOD	Foreign-object damage
FPR	Fan pressure ratio
FSD	Full-scale demonstrator
FSN	Fluid-shield nozzle
FSPSTD	Full-scale propulsion system technology demonstrator
FTR	Formal test report
γ	Gamma titanium aluminide (TiAl)
GC/MS	Gas chromatography/mass spectrometry
GE AE	GE Aircraft Engines
GFY	Government fiscal year
GI	Ground idle
GOCAP	Goals, objectives, challenges, approaches, and programs
GOTCHA	Goals, objectives, technical challenges, and approaches
GRA	Geared rotary actuator
GRC	Glenn Research Center
HAM	Hot acoustic model
HART	Hot acoustic rig test
HARW	High aspect ratio wing
HC	Hydrocarbons (unburned, in exhaust gas)
HCF	High-cycle fatigue
HEAT	High-lift engine aeroacoustic technology
HIN	HEAT isolated nacelle
HISCAT	Highly integrated supersonic cruise airplane technology
HMMRA	Highly mixed multistage radial/axial
HP	High pressure, also horsepower
HPC	High-pressure compressor
HPT	High-pressure turbine
HPX	Horsepower extraction
HPXH	Customer (aircraft) power extraction
HPX(2)	Customer (aircraft) power extraction plus engine parasitic requirements
HS	High speed; also, Hamilton Sundstrand
HSCT	High Speed Civil Transport
HSR	High Speed Research
HSS	HEAT semispan
IBR	Integrally bladed rotor
ICAO	International Civil Aviation Organization
ICD	Interface control document
ID	Inner diameter
IFV	Inverter flow valve
IGV	Inlet guide vane(s)
IHPTET	Integrated High Performance Turbine Engine Technology
ILT	Interlaminar tension
IMFH	Integrated mixer/flameholder
IML	Increased mixer length (exhaust nozzle)
IMT	Industry method test-bed
IR&D	Independent Research and Development
IRR	Internal rate of return
ITD	Integrated technology development
JBTS	Jet burner test stand (UTRC facility)
JER	Jet exit rig
JN8, Jn8B2	Jet-noise prediction models (P&W)

JNL	Jet Noise Laboratory (NASA–Langley
KCAS	Knots, calibrated air speed
KEAS	Knots, equivalent air speed
KIVA II	A multidimensional CFD code
KONA	NASA database Unix server
KTAS	Knots, true air speed
L/D	Lift/drag ratio, also length/diameter ratio
LAPIN	Large-amplitude perturbation inlet (model)
LaRC	Langley Research Center
LBO	Lean blowout
LCF	Low-cycle fatigue
LDI	Lean direct (fuel) injection
LDV	Laser doppler velocimeter
LE, Le	Leading edge
LeRC	Lewis Research Center
LET	Large Engine Technology
LF	Linked flap
LHV	Latent heat value
LOL, LoL	Lobe on lobe
LP	Low pressure
LPC	Low-pressure compressor (main engine fan)
LPP	Lean premixed/prevaporized
LPT	Low-pressure turbine
LSAF	Low-speed aeroacoustic facility (Boeing)
LSAWT	Low-speed aeroacoustic wind tunnel
LSM	Large-scale model
LSMS	LSM similitude
LSWT	Low-speed wind tunnel
LTO	Landing/takeoff
LV	Laser velocimeter
M	Mach number
M_∞	Ambient Mach number
M_0	Free-stream Mach number
M14	Mach number at bypass duct inlet
M15	Mach number at bypass duct average area
M155, $M_{15.5}$	Maximum Mach number in fan duct (bypass duct over rear frame)
M16, M_{16}	Mach number at fan duct mixing plane (fan/core mixer duct side)
M2	Mach number at engine inlet
M21ID	Mach number at fan discharge ID
M21OD	Mach number at fan discharge OD
M25	Mach number at compressor inlet
M3	Mach number at compressor discharge
M36	Mach number at combustor inlet
M4	Mach number at HPT vane inlet
M49	Mach number at LPT rotor 1 inlet
M5	Mach number at LPT exit
M54	Mach number at rear frame/diffuser average area
M55	Mach number at mixer entrance, core stream
M56	Mach number at mixer exit, core stream
M68	Mach number at miniaugmentor exit
MAR	Mixing area ratio (duct)
MCP	Modular component predictor
MCTCB	Mixed compression translating centerbody (inlet)
MDA	McDonnell Douglas Aircraft
MDC	McDonnell Douglas Corporation
MDO	Multidiscipline optimization
M–E, M/E	Mixer/ejector (exhaust nozzle)
MFTF	Mixed-flow turbofan
MIDIS	Mixer/ejector inlet distortion study
MIT	Massachusetts Institute of Technology
MITCFA	MIT compound flow analysis (computer program)
MMC	Metal-matrix composite
Mn	Mach number

MPC	Multiple-component predictor
MRA	Multistage radial/axial
M&S	Materials and structure
MTF	Mid-tandem fan
MTOGW	Maximum takeoff gross weight
MTOW	Maximum takeoff weight
N1	Low-pressure rotor speed
N1C2	Low-pressure rotor speed corrected to station 2
N2C2.5	High-pressure rotor speed corrected to station 25 (compressor inlet)
N4	HP spool speed
N5	LP spool speed
NASA	National Aeronautics and Space Administration
NASA LaRC	NASA Langley Research Center
NASA LeRC	NASA Lewis Research Center (now NASA Glenn)
NASTRAN	Computer modeling software
NATR	Nozzle acoustic test rig
Nc, N_c	Corrected engine (shaft) speed
NCP	National cycle program
NFM	Nearly fully mixed
NOx	Oxides of nitrogen
Noy	Acoustic annoyance parameter
NPD	Noise power distance
NPSS	Numerical propulsion-system simulation
NPR	Nozzle pressure ratio
NRA	NASA Research Announcement
OAC	Optimized aeroelastic concept
OD	Outer diameter
OEW	Operating empty weight (no fuel, oil, etc.)
OEW–PR	OEW minus propulsion-system weight
OGV	Outlet guide vane(s)
OML	Outer mold line
OPR	Overall pressure ratio
P_{16}	Pressure exiting bypass duct
P16Q56	Extraction ratio
P_{56}	Pressure exiting core engine
PAI	Propulsion/airframe integration
PAIT	Propulsion/airframe integration technology
PC	Power code
PCC	Precision Castparts Co.
PDF	Probability density function
PDPA	Phase Doppler particle analyzer
PDR	Preliminary design (or data) review
PFPAE	Perfluoropolyakylether
PH3	Tri-perfluoropolyalkylether-phenyl-phosphine
PIC	Pressure-infiltration casting
PLIF	Planar laser-induced fluoresence
PLR	Programmable lapse rate
PMT	Propulsion Management Team
PMC	Polymer-matrix composite
PNLT	Tone-controlled perceived noise level
P&O	Performance and operability
PSET	Propulsion System Evaluation Team
PSI	Propulsion system integration, also Pressure Systems Inc.
PST	Propulsion selection team
PT, P_T	Total pressure
PT8	Exhaust gas total pressure at nozzle throat
PT14	Total pressure at bypass duct inlet
PT15	Total pressure at bypass duct average area
PT155	Total pressure at bypass duct over turbines and rear frame (mixer entrance)
PT16	Total pressure at mixer exit, bypass stream side
PT21	Total pressure at fan discharge
PT21A	Average total pressure at fan discharge

PT21ID	Total pressure at fan discharge inner diameter
PT21ID	Total pressure at fan discharge outer diameter
PT25	Total pressure at compressor inlet
PT3	Total pressure at compressor discharge
PT36, P_{T36}	Total pressure at compressor inlet
PT4	Total pressure at HPT vane inlet
PT5	Total pressure at LPT exit
PT55	Total pressure at mixer entrance, core stream side
PT56	Total pressure at mixer exit, core stream side
PT68	Total pressure at miniaugmentor exit
PT7	Total pressure at convergent nozzle inlet
PT8	Total Pressure at nozzle throat
PTC	Preliminary technology configuration
Q	Dynamic pressure
R1	First-stage rotor
R2	Second-stage rotor
R3	Third-stage rotor
RAN	Reynolds-averaged Navier–Stokes
RC	Round convergent (exhaust nozzle)
RM	Relative “mixedness”
ROM	Rough order of magnitude
RPM	Revolutions per minute
RQL	Rich (burn), quick (quench), lean (burn)
RR	Rolls Royce
RSQ	Reduced-scale quench
RTI	Reversing through inlet
RTO	Refused takeoff
Rx4	HPT pitch reaction
S/MTD	STOL and maneuvering technology demonstratior
S1	First-stage stator
S2	Second-stage stator
S3	Third-stage stator
SAE	Society of Automotive Engineers
SAR	Suppressor area ratio
SAVE	Systematic approach to value engineering
SCC	Sizing-code calibration
SCID	Supersonic cruise integrated design
SCN	Sliding-chute nozzle
SD	Stepped dome
SDOF	Single degree of freedom
SERN	Single-expansion-ramp nozzle
SFC	Specific fuel consumption: lbm of fuel per hour per lbf
SFCDAB	SFC based on FNDAB
SI_{cp}	Stability index
SLA	Stereolithographic apparatus
SLS	Sea-level static
SLTO	Sea level takeoff
SMFAN	Stall margin, fan
SOAPP	State-of-the-art performance program (P&W)
SPFDB	Superplastic formed, diffusion bonded
SPL	Sound power level
SRP	Separate reverser port
SSC	Supersonic cruise
SST	Supersonic transport
STMT	System technology management team
STOL	Short takeoff and landing
SW	Sidewall
SWET	Substrate welding at elevated temperature
SW	Toal wing planform area
SwRI	Southwest Research Institute
SWT	Supersonic wind tunnel
T/b	Thickness-to-chord ratio
T/O	Takeoff

T_3	High-pressure compressor exit temperature
T_4	Combustor exit temperature
T_{41}, $T_{4.1}$	High-pressure turbine rotor inlet temperature
TAC	Total accumulated cycles
TBC	Thermal-barrier coating
TBE	Turbine bypass engine
TC	Technology configuration
TCA	Technology concept aircraft
TCB	Translating centerbody (inlet)
TCE	Technology concept engine
TCLA	Turbine cooling air
TCS	Turbulence control structure, also technology concept solution
TE	Trailing edge
TF	Turbofan
TF–IFV	Turbofan-inverter flow valve
TI	Technical integration (team)
TIC	Transient inlet/compressor (model)
TJ	Turbojet
TJ–IFV	Turbojet-inverter flow valve
TLID	Thrust-lapse parameter
TMT	Technology management team
TOBI	Tangential on-board bleed injection
TOC	Top of climb
TOGW	Takeoff gross weight
TP3	GEAE performance-analysis software
TPS	Thermal-protection system, also turbulence-prevention structure
TRF	Turbine rear frame
TRL	Technology readiness level
TSI	Triton Systems Inc.
TT, T_T	Total temperature
TT3	Compressor discharge total temperature
TT4	Total temperature at HPT vane inlet
TT4.1	High-pressure turbine rotor inlet total temperature
T_{T7}	Augmentor-exit total temperature
TT8	Exhaust gas total temperature at nozzle throat
TTC	Technology transition (or tracking) chart
TTR	Total-temperature ratio
UHB	Ultrahigh bypass
UHC	Unburned hydrocarbons
UPS	Universal propulsion simulator
UTRC	United Technology Research Center
VABI	Variable-area bypass injector
VAM	Variable-area mixer
VAMP	Variable-area mixing plane
VCE	Variable-cycle engine
VCF	Variable-capacity fan
VDC	Variable-diameter centerbody
VDVP	Variable-displacement vane pump
VEN	Variable exhaust nozzle
VFX	Variable-capacity fan, experimental
VG	Variable geometry
VJIP	Primary ideal jet velocity
VPI	Virginia Polytechnic Institute
W2AR	Engine corrected airflow
W5GR	LPT exit gas flow function
W_a	Airflow
WAE, W_{AE}	Engine airflow
WB3	Customer bleed
WBS	Work breakdown structure
W_c	Corrected airflow, also coolant flow
WG	Air (gas) flow
WG36	Airflow at combustor inlet
W_p	Primary flow, lbm/s
W_s	Secondary flow, lbm/s
XNH	Rotor speed (high-pressure spool)
XNL	Rotor speed (low-pressure spool)

5.0 Exhaust Nozzle

5.1 Overview

5.1.1 Goals, Objectives, Challenges, Approaches, and Programs

The goal, objectives, technical challenges, approaches, and programs of the HSR exhaust nozzle task are depicted in Figure 1. The goal has been to develop a low-noise nozzle for the HSCT propulsion system. One of the objectives of the low-noise nozzle was to achieve acoustic suppression levels of –1, –3, –1 EPNdB relative to the FAR36 Stage III noise-level requirements at the sideline, cutback, and approach measuring points respectively (Reference 1). In addition to achieving high levels of acoustic suppression, the exhaust nozzle must achieve high thrust performance — specifically a thrust coefficient at takeoff greater than 95%.

The technical challenges addressed as part of the HSR exhaust nozzle task involved developing a low-noise nozzle with high aerodynamic performance, low weight, and long life. The approach to meeting these technical challenges involved both configuration and materials technology development. The downselected nozzle concept was a two-dimensional, mixer/ejector nozzle referred to as the fixed-chute nozzle (FCN). The term “fixed chute” refers to the fact that the primary mixer chutes remain in the exhaust path throughout the entire mission (as opposed to rotating/sliding out of the hot-gas stream when the engine is operating in other than takeoff mode). The Enabling Propulsion Materials (EPM) program was responsible for developing the advanced materials required by the nozzle in order to meet weight and life requirements.

The final level of Figure 1 shows the programs used to develop the exhaust nozzle configuration and materials. The dashed box on the lower right lists the advanced materials that were developed as part of the EPM program. The Critical Propulsion Components (CPC) program was responsible for developing the aerodynamic, acoustic, and mechanical design of the FCN concept. The CPC exhaust

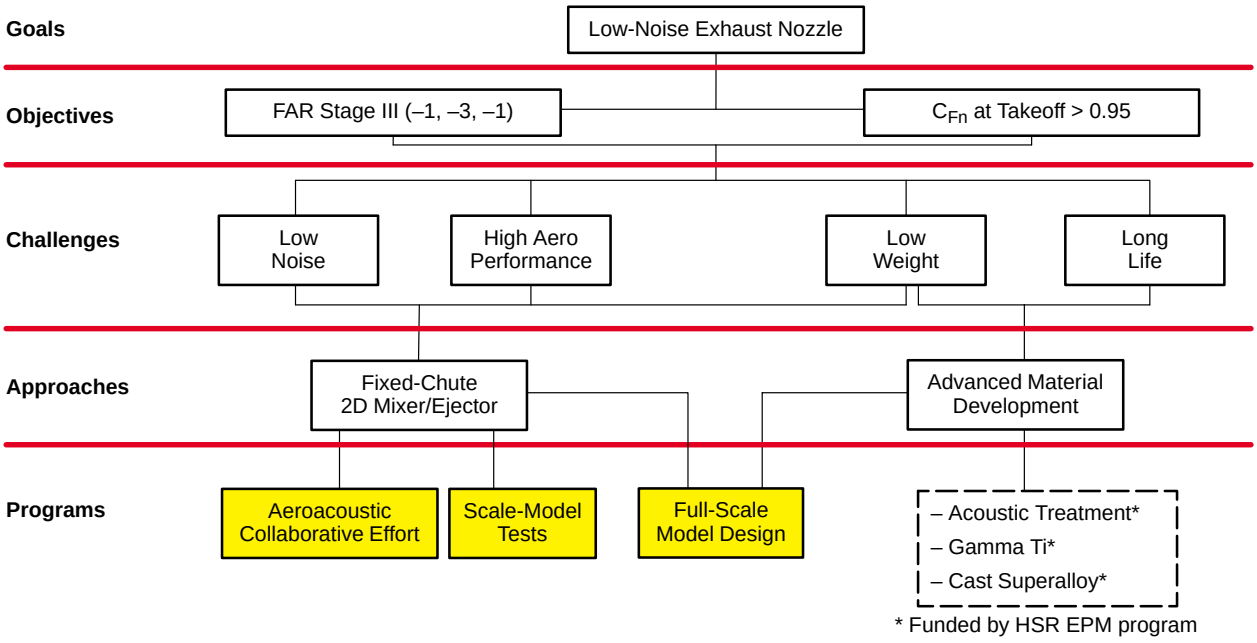

Figure 1. Exhaust Nozzle Goals, Objectives, Challenges, Approaches, and Programs

nozzle task consisted of three programs aimed at addressing the stated objectives and technical challenges: Full-Scale Nozzle Design, Scale-Model Tests, and the Aeroacoustic Collaborative Effort (shaded boxes in Figure 1). The work represented by these programs will be reported in this Exhaust Nozzle section of the final CPC report.

5.1.2 Technology Development Logic

The nozzle logic charts in Figures 2 and 3 show the key program tasks, the relationships of the tasks to one another, and the roadmap established through the CPC Program to achieve Technology Readiness for a full-scale production exhaust nozzle. These charts describe the overall program as defined through the 1998 replan, just prior to program termination. The roadmap was based on conceptual, preliminary, and detail design activities; subscale technology and validation testing; tools and methods development; and engine testing at approximately 50% scale. Nozzle design and test activities were integrated with the EPM Program to take advantage of and guide the development of advanced materials for this exhaust nozzle configuration.

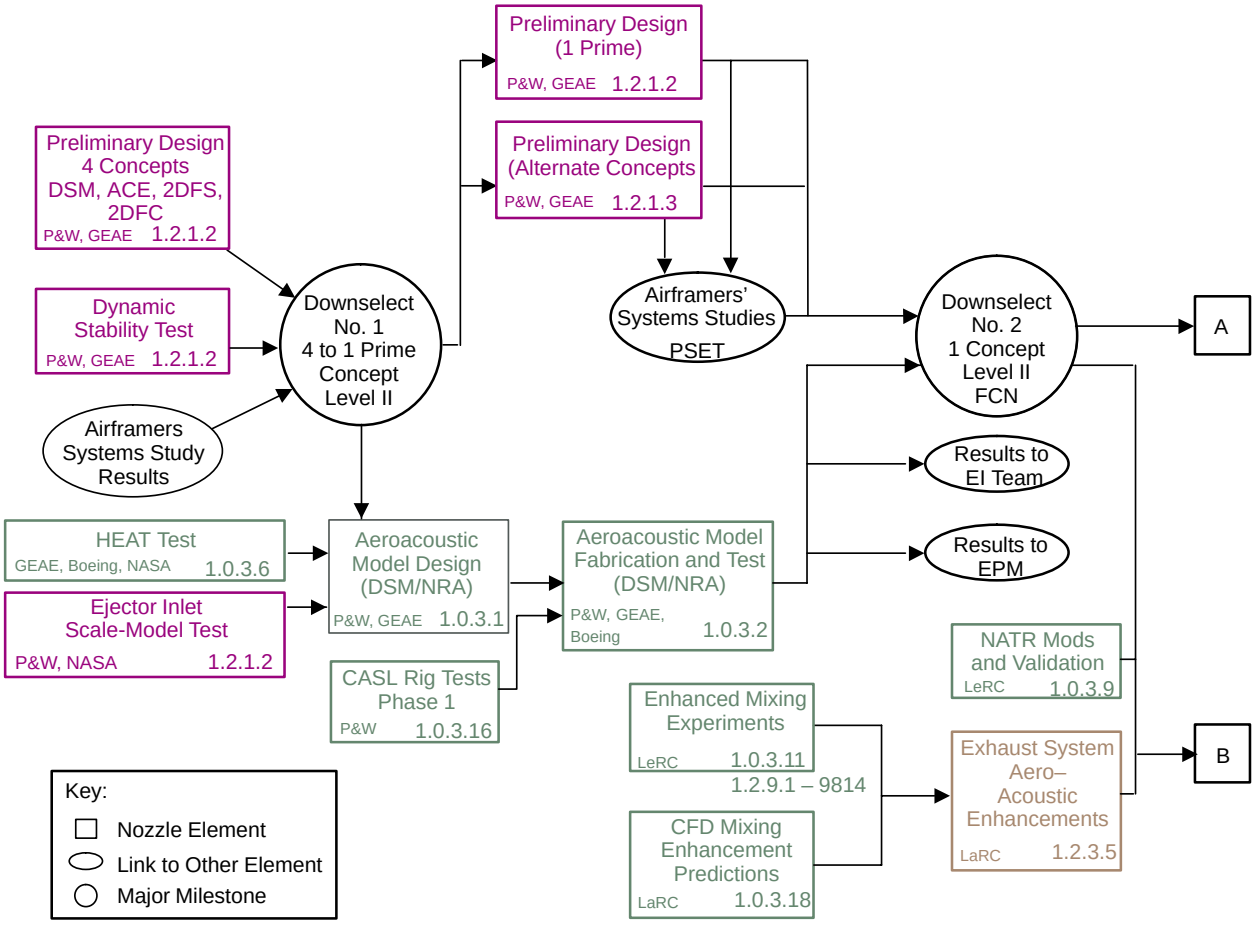

Figure 2. CPC Nozzle Logic Chart 1, 4Q98

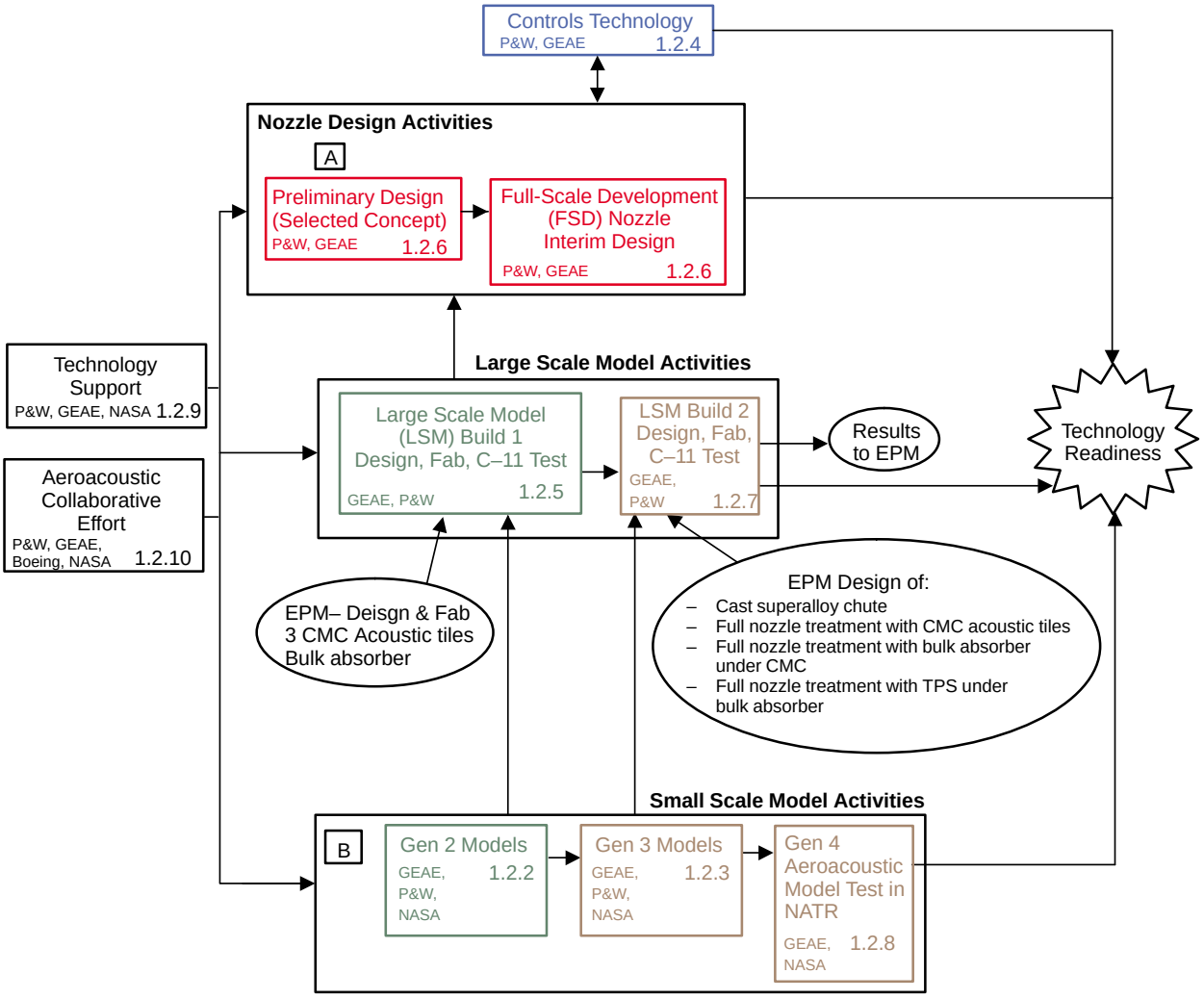

Figure 3. CPC Nozzle Logic Chart 2, 4Q98

5.1.3 Exhaust Nozzle Rationale

The selection of the exhaust nozzle concept was directly related to the noise requirements imposed on the HSCT. The HSCT aircraft must operate with community noise levels equivalent to those of the subsonic aircraft that will constitute the fleet at the time of the HSCT introduction, and the economics must be close to those of the subsonic aircraft. Since jet exhaust is the primary noise source at the sideline and community measurement locations, one of the major challenges for an HSCT aircraft is to develop an exhaust nozzle concept that will allow the aircraft to meet the noise goal without undue weight and performance penalties. To achieve the required noise levels, it is necessary that the final nozzle exhaust velocity be no greater than about 1400 ft/s. While it is possible to achieve this velocity with high-bypass turbofans, the weight and cruise drag of such engines has proven to be too costly. A mixer/ejector (M/E) nozzle was chosen to provide the means to reduce nozzle exhaust velocity without undue weight and performance penalties.

The M/E nozzle entrains ambient air to mix with the high-velocity engine exhaust, resulting in a lower nozzle exhaust velocity (Figure 4). The design requirements for the M/E nozzle are closely related to the engine cycle characteristics. For engine cycles producing high unsuppressed exhaust velocities, more suppression is required of the nozzle. For such cycles, much more ambient air must be entrained to produce the lower exhaust velocity required. Many of the early nozzles tested in this program were designed to be compatible with these high-velocity cycles. As the HSCT engine evolved to cycles having less extreme velocities, the M/E design also evolved to require more moderate amounts of entrained air.

To mix entrained ambient air with the engine exhaust within a reasonable nozzle length, multilobed mixers are used to enhance the mixing process. One of the early lessons learned in the nozzle program was that, in addition to the classical jet noise of the nozzle exhaust, the M/E concept introduces new sources of noise. One of these is high-frequency noise generated within the ejector due to the initial mixing of entrained ambient air with the high-velocity engine exhaust. Another new source is midfrequency noise resulting from continued larger scale mixing of the entrained air with the engine exhaust. The midfrequency source is directly related to the degree of "unmixedness" at the nozzle exit. To reduce the high-frequency noise, acoustic treatment is required within the nozzle. Increasing the nozzle length or enhancing the mixing process increases the "mixedness" at the nozzle exit and reduces noise from the midfrequency source. Increasing the length also allows more acoustic treatment; however, added length increases weight and drag. This just one example of the many trades required in the design of the M/E nozzle.

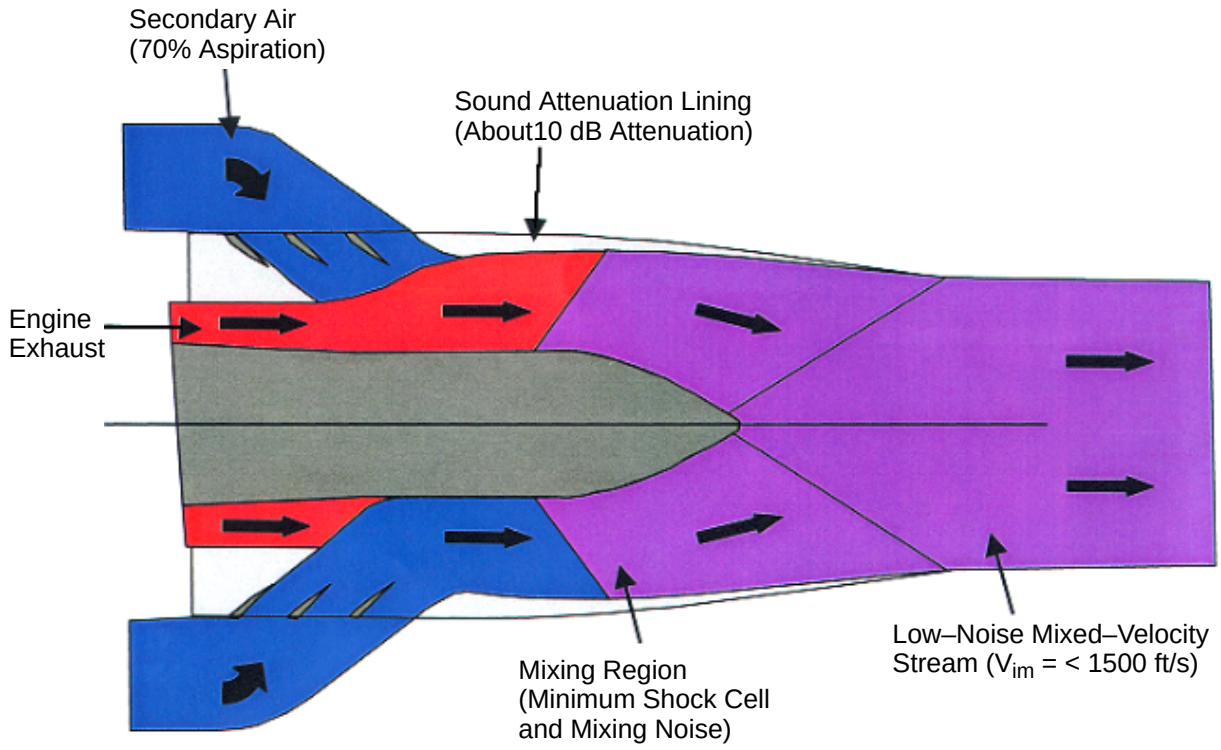

Figure 4. Internally Mixed Ejector Suppressor Exhaust Nozzle Concept

5.1.4 Exhaust Nozzle Technology Metrics

The HSR CPC nozzle program progress was tracked against 10 nozzle technology metrics as summarized in Table 1. For each nozzle metric a time history figure, called a "technology tracking chart" (TTC), was maintained and updated yearly. Figures 5 through 14 define the metrics listed in Table 1 and show the 10 nozzle TTC's as last updated in March, 1999.

Table 1. HSR CPC Nozzle Metrics Summary

	P–5 dB	P–6 dB	P–7 C_{fg}	P–8 C_{fg}	P–9 lb/in^2	P–10 A_{10}/A_{mix}	P–17 ΔBoatail Drag/F_{id}	P–18 ΔBoattail Drag/F_{id}	P–19 C_{fg}	P–20 C_{fg}
End of HSR II (2001 – 2002)	94.8	92.4	0.96	0.9830	2.25	2.050	0.024	0.056	0.9813	0.9837
Technology Configuration	94.8	92.4	0.96	0.9830	2.25	2.002	0.038	0.1328	0.9813	0.9837
Best Case	94.8	92.4	0.965	0.9845	2.09	1.983	0.017	0.039	0.9823	0.9847
Worst Case	96	93.7	0.93	0.981	2.51	2.071	0.038	0.1328	0.9783	0.981
Status 01/99	96.0*	93.7*	0.93–0.95	0.981–0.983	2.46	2.050	0.038	0.1328	0.978–0.982	0.981–0.985

Each TTC plots the metric status as a function of fiscal year. Major highlights (such as significant tests, analyses, and designs) that have contributed to or changed the metric status timeline are noted on each figure. For model testing, the bar is indicative of the range of the data collected.

Program *Technology Readiness Levels* are also shown on each TTC. The last Technology Readiness Level, at program end, is an expected level based on continued funding levels.

5.2 Exhaust Nozzle Concepts

Development of the HSCT exhaust system involved evaluation of a multitude of concepts. At the outset of the development process, the underlying exhaust system design parameters were established. The parameters chosen were those that were used to define the acoustic, aerodynamic, and mechanical properties of the nozzle and were used to develop the design of various exhaust nozzle concepts. Outlines of the parameters are listed in Tables 2 through 4. Throughout this process, the values of these parameters were revised as required to stay consistent with the knowledge gained from the aerodynamic and acoustic development activities and to reflect the requirements of the overall propulsion system and HSCT aircraft.

The exhaust system development proceeded in stages; at any given stage, a set of nozzle concepts was created by the nozzle mechanical team and developed under the existing groundrules. These nozzles were developed to a level of detail sufficient to allow ranking of the concepts and determination of the impact of each concept on the overall aircraft system objectives. The most favorable nozzle concept was downselected as the baseline for the next stage of development.

The following subsections provide a brief description of the various nozzle concepts considered at some point during the program. The process of eliminating concepts during the program and selecting a final concept will be described in Section 5.3.

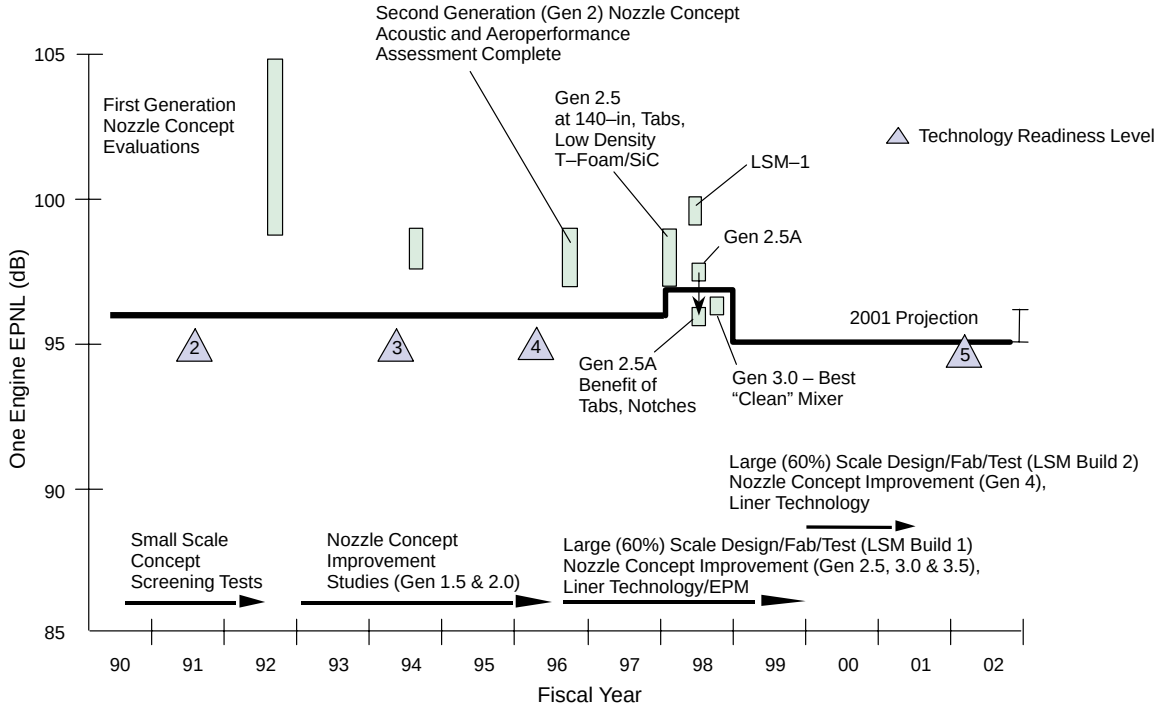

Figure 5. Nozzle Technology Metric P–5 (Sideline Noise Level)

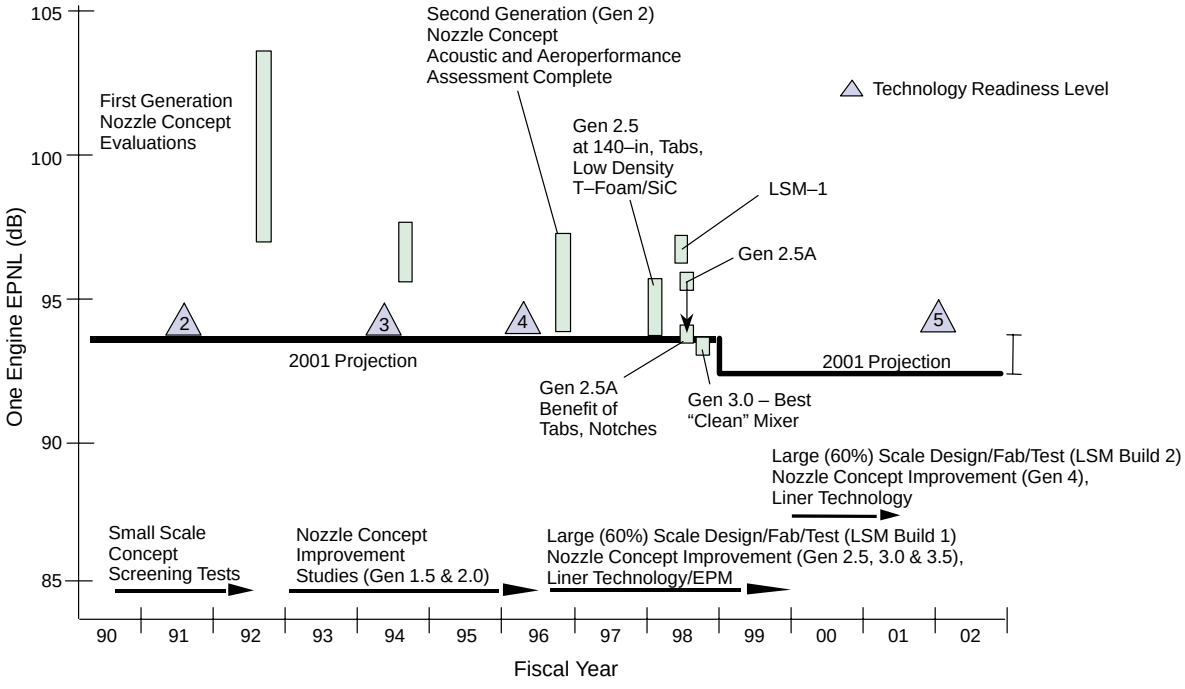

Figure 6. Nozzle Technology Metric P–6 (Cutback Noise Level)

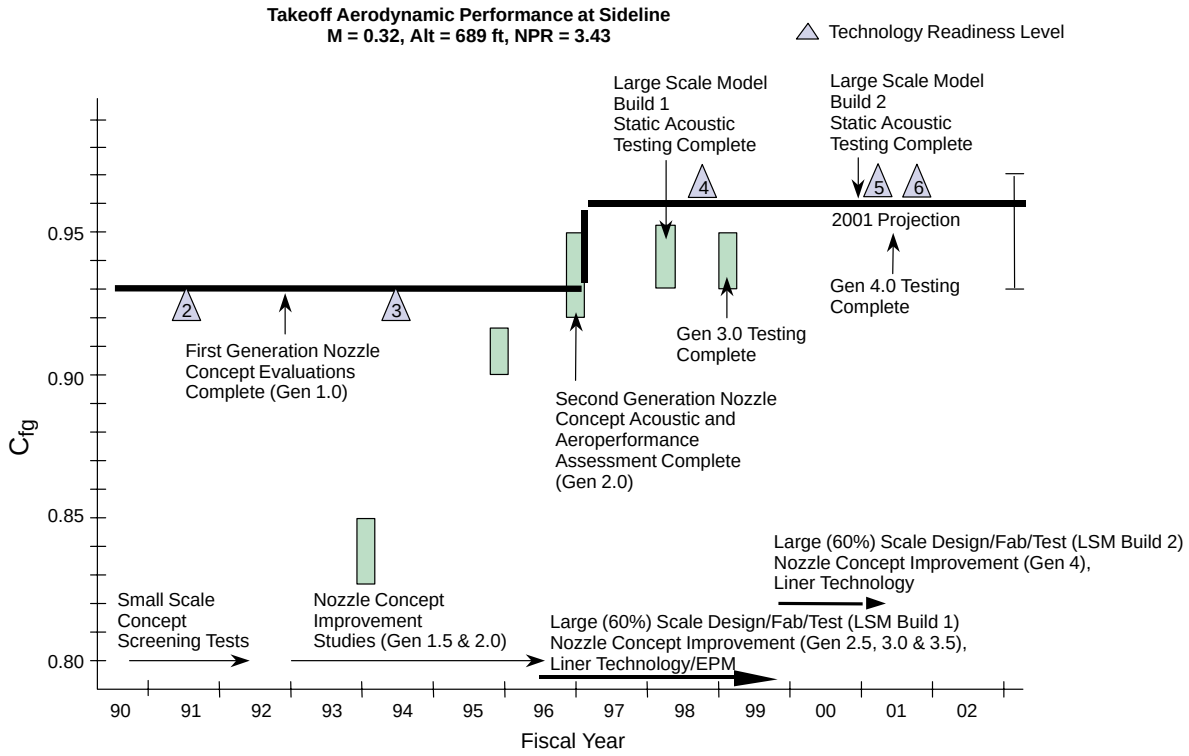

Figure 7. Nozzle Technology Metric P–7 (Sideline Aerodynamic Performance)

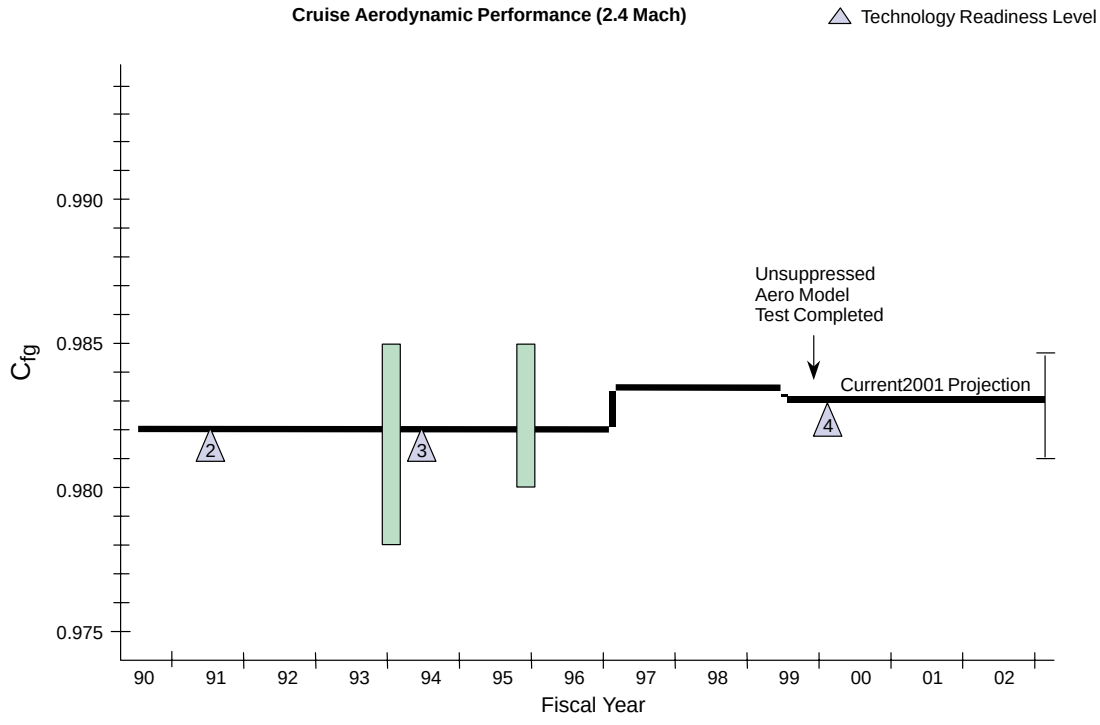

Figure 8. Nozzle Technology Metric P–8 (Supercruise Aerodynamic Performance)

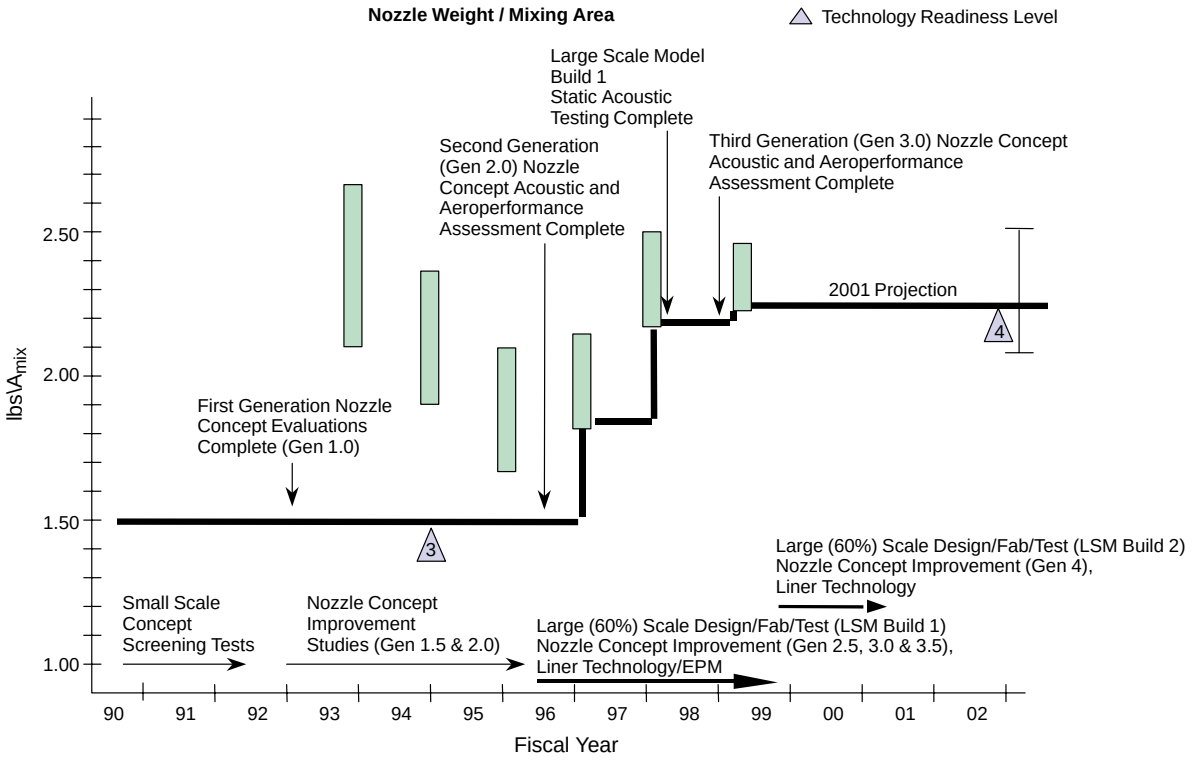

Figure 9. Nozzle Technology Metric P–9 (Nozzle Weight per Area)

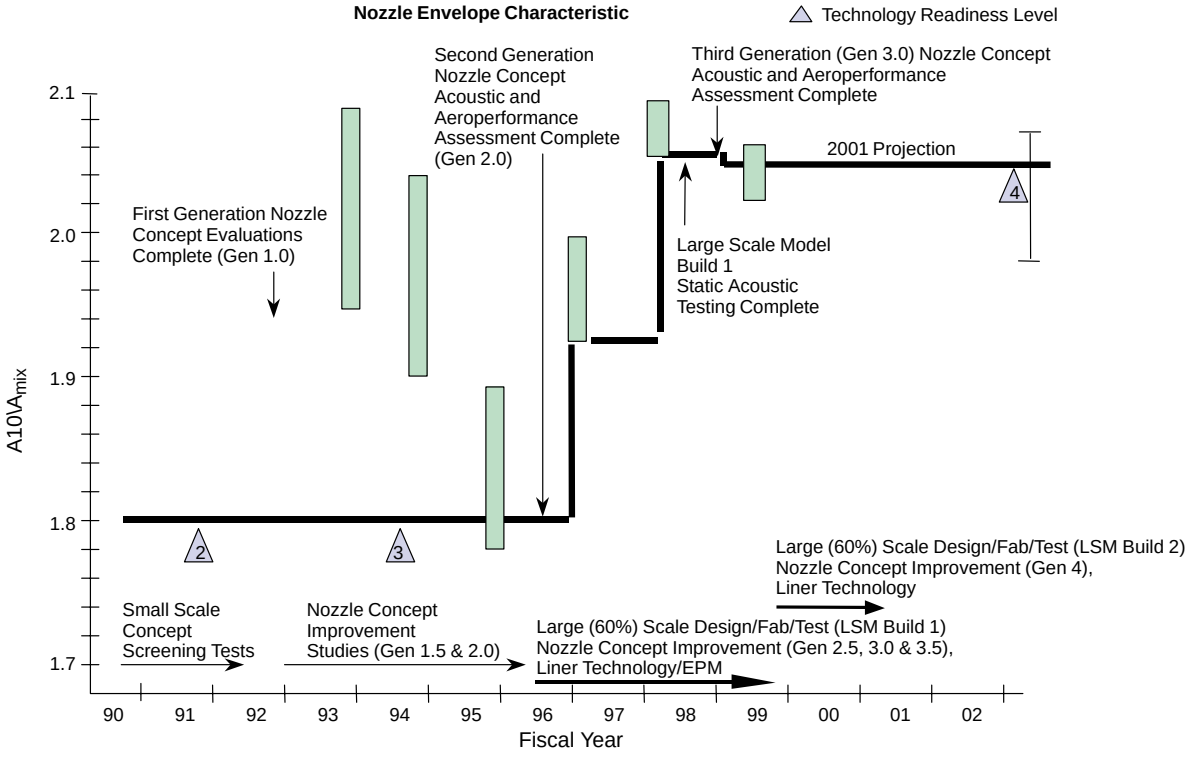

Figure 10. Nozzle Technology Metric P–10 (Envelope Characteristic)

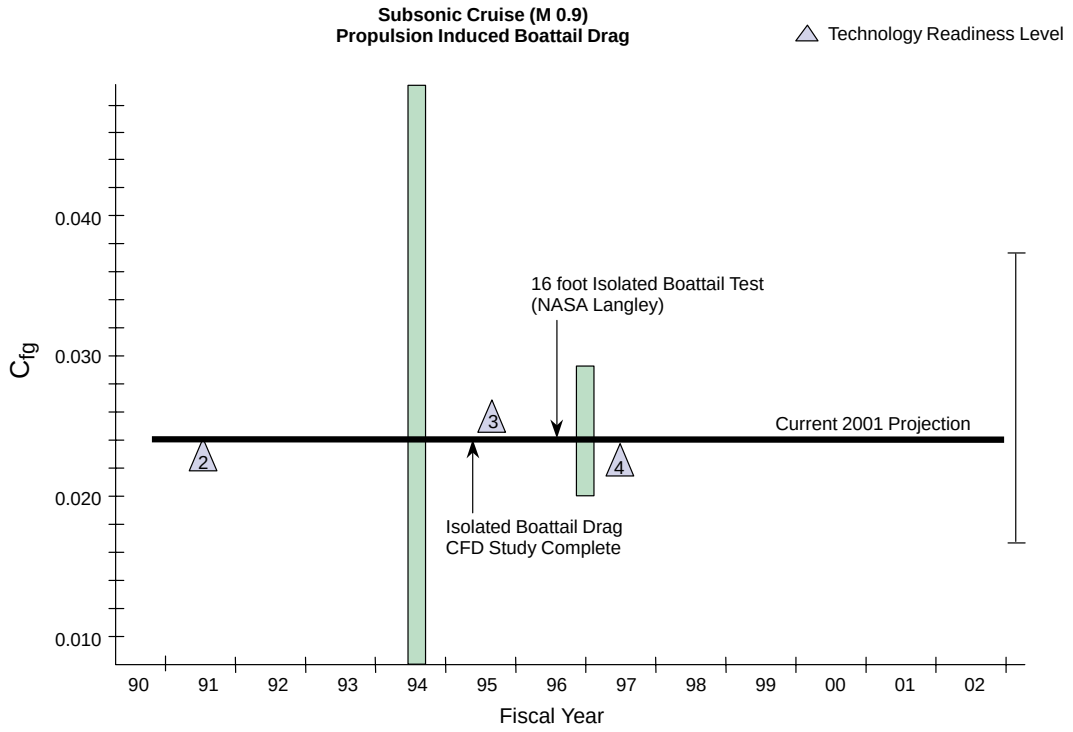

Figure 11. Nozzle Technology Metric P–17 (Subcruise Boattail Drag)

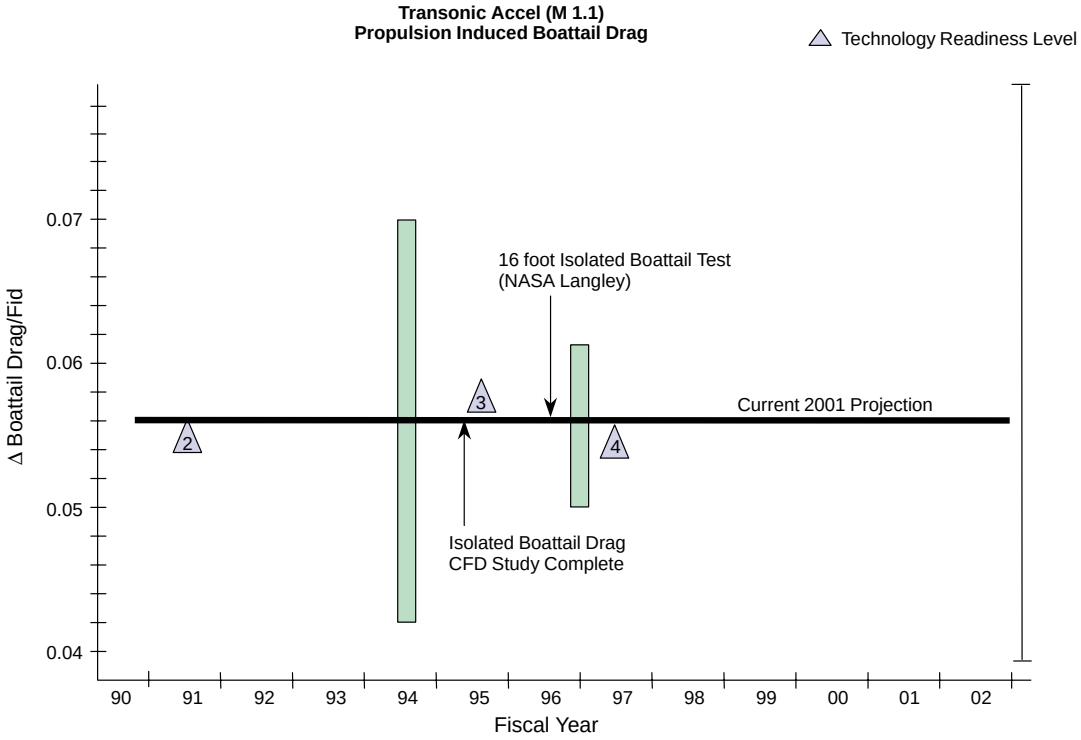

Figure 12. Nozzle Technology Metric P–18 (Transonic Boattail Drag)

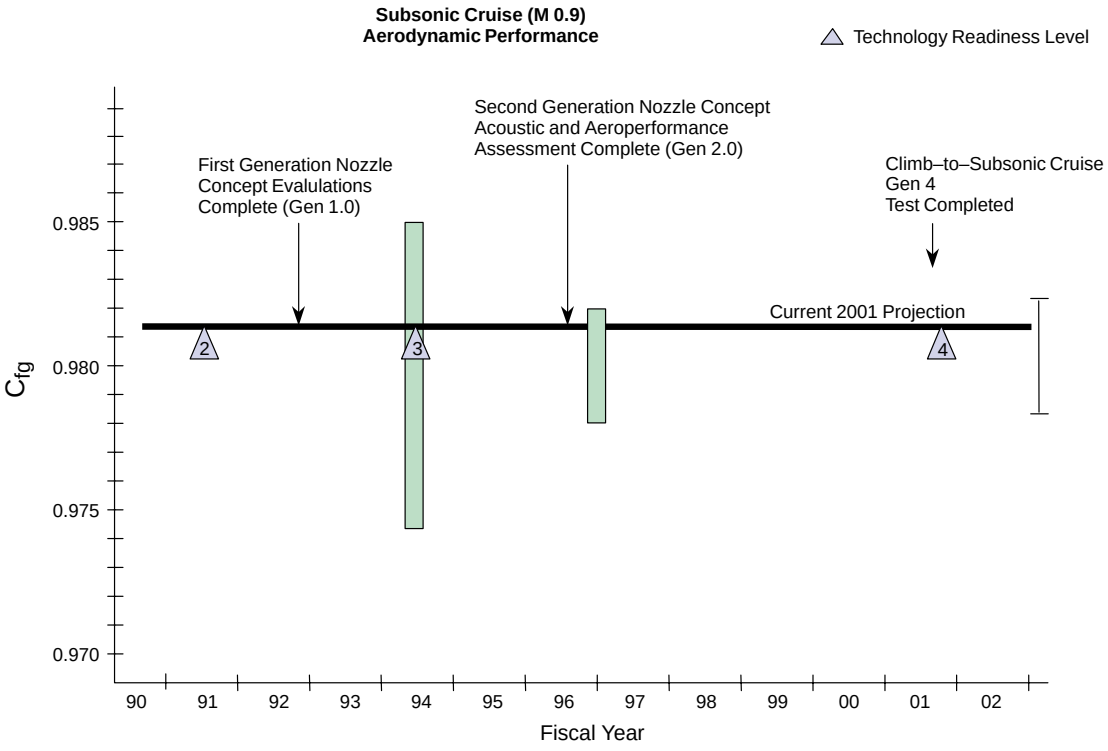

Figure 13. Nozzle Technology Metric P–19 (Subcruise Aerodynamic Performance)

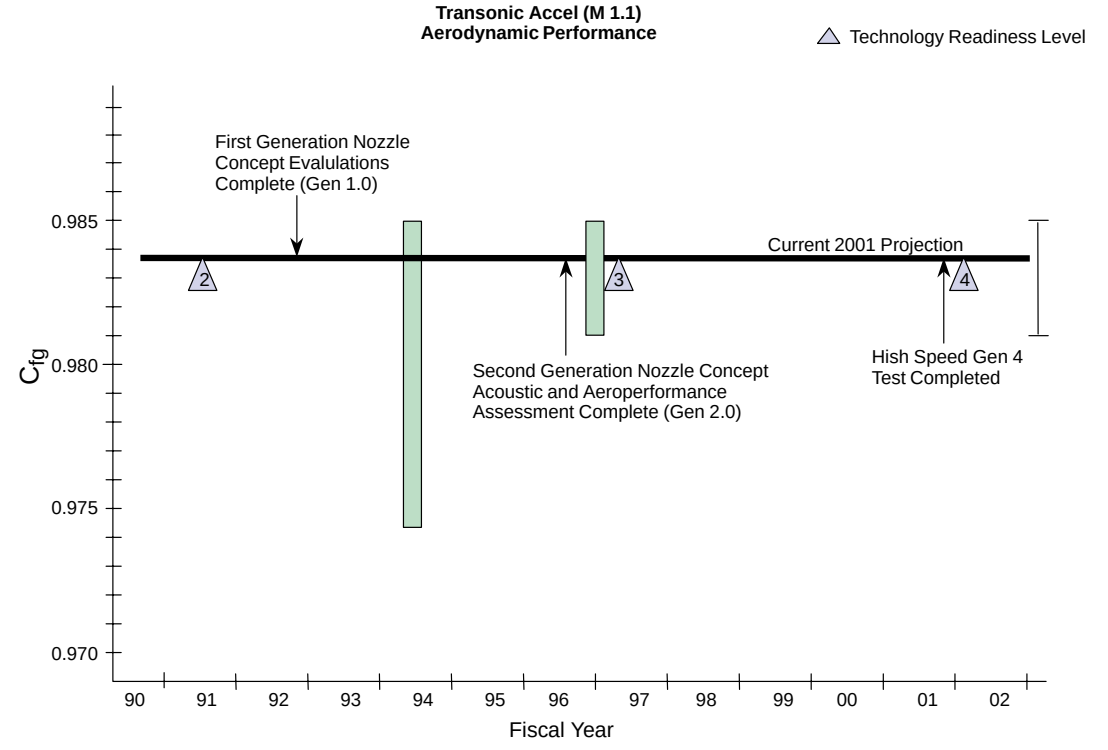

Figure 14. Nozzle Technology Metric P–20 (Transonic Aerodynamic Performance)

Table 2. Nozzle Acoustic Design Criteria

Criteria	Effect on Nozzle Mechanical Development
SAR, ASAR (or A_{mix})	Size of flowpath area aft of ejector mixer
	Internal width
Acoustic Treatment Area (A_{treat}/A_{mix})	Area of acoustic treatment
Aspect Ratio	Internal width
MAR	Position of divergent flap at the suppressed takeoff design point
	Internal width
Acoustic Treatment Thickness	Location of acoustic treatment within structural envelope of nozzle components
Chute Penetration	Location of outboard edge of ejector mixer chutes relative to convergent-flap flowpath surface
	Location of the forward edge of acoustic treatment (used in determining hot-lobe width of ejector mixer chutes)
Mixing Length	Minimum length of aft sidewall and resulting sidewall boattail angle
Number of Lobes per Ejector Mixer Rack	Location of the forward edge of acoustic treatment (used in determining hot-lobe width of ejector mixer chutes)
CER	Location of the forward edge of acoustic treatment (used in determining hot-lobe width of ejector mixer chutes)
Location of Forward Edge of Acoustic Treatment	Extent of acoustic treatment

Table 3. Nozzle Mechanical Design Criteria

Criteria	Effect on Nozzle Mechanical Development
Acoustic Treatment Area Efficiency	Physical area of acoustic treatment
Ejector Mixer Rack Gap at Centerline	Clearance between convergent flaps at reverse
	Location of reverser port opening aft edge
Minimum Distance for Aft Edge of Acoustic Treatment	Extent of acoustic treatment
	Structural envelope
Envelope for Actuation	Location of actuation components
	Size of actuation components
	Kinematics of flap-actuation system
Envelope for Seals	Location and sizing of reverser port
Sidewall Envelope/Contour	Envelope for structure and actuation
Nacelle Height at Nozzle Fore Flange	Envelope at forward end of nozzle
	Upper and lower forward OML
Boattail Angles	Sidewall envelope for structure and actuation
Control System Stackup and Error	Nozzle exit/throat area ratio (A_9/A_8) ratio at subcruise

Table 4. Nozzle Aerodynamic Design Criteria

Criteria	Effect on Nozzle Mechanical Development
Engine Cycle A_8 (Nozzle Throat Area)	Hot-lobe width of ejector mixer chutes
Engine Cycle Pressure and Temperature	Structural envelope of components
	Nozzle weight and center of gravity
Ejector Inlet Ramp Angle	Length of nozzle forward of the ejector mixer
	Size of cusp formed at the upper and lower OML's during cruise at hinge location of ejector inlet doors
	Length of ejector inlet doors
Ejector Inlet Area	Minimum inlet height between ejector inlet door ramp and ejector inlet aft lip
	Ejector inlet door length and allowable ejector inlet ramp angle
	A_7 (nozzle inlet area)
Ejector Mixer Chute Length	Nozzle length
	Axial location of reverser port and flap train
	Location of forward edge of acoustic treatment
Ejector Mixer Chute Shape	Envelope for mixer tie beam
Ejector Inlet Forward Shoulder Geometry	Size of cusp formed at the upper and lower OML's during cruise at hinge location of ejector inlet doors Shape of ejector inlet aft lip
Mar Range	Actuation system envelope for divergent flap
Ejector Inlet Aft Lip Contour	Convergent flap structural envelope and flowpath contour
Divergent Flap Angle (Length)	Location and kinematics of actuation system for divergent flap
	Location of forward hinge point of external flap
	Length of external flaps
	Upper and lower OML's of aft sidewalls
Convergent Flap Angle (Maximum)	Minimum length of convergent flap
Convergent/Divergent Hinge Radius	Location of convergent/divergent hinge
A_7/A_8 Ratio	Minimum height of the forward end of the ejector mixer
Reverser Port Area	Minimum reverser port dimensions
	Positional/kinematic constraints for convergent flap
	Positional/kinematic constraints for convergent flap Location of convergent flap nose seals
Reverser Flow Efflux Angles	Reverser port dimensions
	Reverser cascade configuration

5.2.1 Axisymmetric Coannular-Ejector Nozzle

The axisymmetric coannular-ejector (ACE) nozzle is a plug (boattail) nozzle with an ejector designed to provide aspiration of about 20% of the engine flow (Figure 15). The ACE concept produces higher performance by avoiding the use of lobes or chutes to force the aspirated and engine flows to mix using vorticity. In addition, ejector losses are reduced by the design-point aspiration of 20% as compared to some suppressor systems that aspirate as much as 120%. A variety of enhancers were designed to promote mixing of the engine flow and the aspirated flow. These included delta tabs (Figure 16), tone-injection rods, and wheeler ramps.

Model-scale acoustic and propulsion performance testing of the ACE nozzle were conducted in the Boeing Low-Speed Aeroacoustic Facility (LSAF). This facility consists of a free-jet wind tunnel in an anechoic chamber. Mixing-enhancement devices (micromanipulators) in the form of delta tabs, tone-injection rods, and wheeler ramps attached to the primary nozzle trailing edge and the ejector cowl trailing edge were tested. Performance and noise were evaluated both with and without the mixing-enhancement devices.

Although the ACE nozzle configuration achieved relatively high-thrust performance, the acoustic suppression, 6 to 8 EPNdB, would have required a higher bypass ratio engine to meet the system noise goals.

Further detail and background are available in References 2 and 3.

5.2.2 Fluid-Shield Nozzle

The fluid-shield nozzle (FSN) was considered as a potential suppressor for the fan-on blade (FLADE) engine. At takeoff and cutback, this engine cycle used an auxiliary airstream, in an annular duct surrounding the fan, pressurized by fan tip blade extensions. This auxiliary airflow increased the total airflow and decreased the jet velocity. The FSN consisted of an axisymmetric mixer plug nozzle surrounded by a 220° annular sector for the auxiliary airflow, providing an intermediate shear step between the core flow and ambient air (Figure 17). The FSN is shown in Figure 18 in the 2D plug (boattail) fan-on-blade configuration for the takeoff mode. Here the entering external air is mixed with the core flow to reduce the noise of the exiting jet. The mixing flow area is adjusted to meet engine cycle requirements by expansion or contraction of a 2D plug. For reverser operation, the plug is expanded to block the axial flow of the core, and the exiting core flow passes out sideways and forward as guided by reverser cascades.

Relative to a simple conic nozzle, at takeoff conditions, suppressions of approximately 8 EPNdB were achieved by the use of the suppressor nozzle alone. An additional 4 to 8 EPNdB were obtained with the fluid shield, depending on the particular geometry employed. Suppression increased with shield thickness and with increasing velocity ratio and/or mass flow ratio. However, when the comparisons were made at the same mixed-jet velocity, the benefit of the fluid shield was only about 1 EPNdB. As could be expected, noise benefits are at the expense of thrust, and tradeoffs would be required.

The aerodynamic tests investigated chute design parameters as well as shield thickness and cycle effects. Shadowgraphs were used to screen the configurations prior to more intensive laser velocimeter data acquisition and flow visualization using a planar laser sheet. The shadowgraphs provided insight into the highly complex 3D shock structures identified in the fluid shield and along the plug (simulated by a wedge here); the LV gave details of the flow within the shield and along the wedge, and the planar laser sheet allowed some insight to be gained into the mixing process.

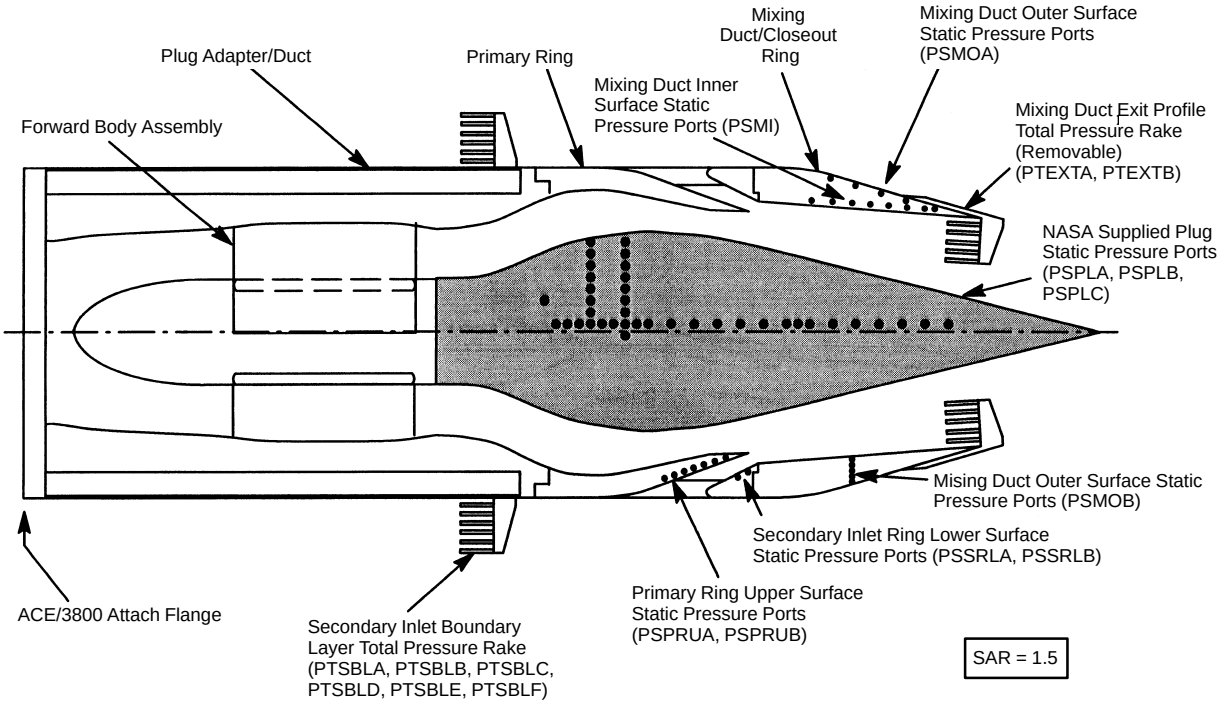

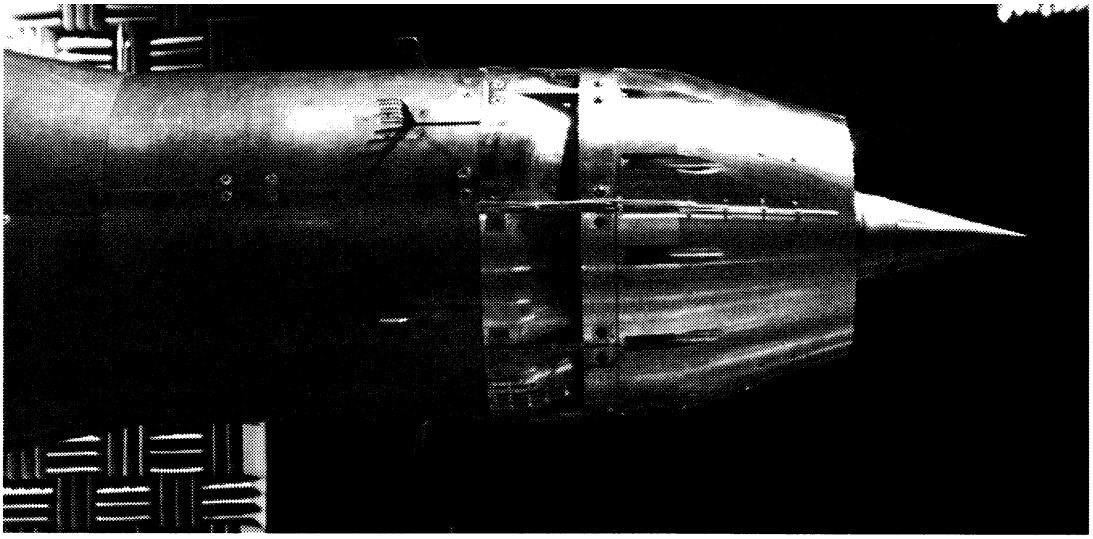

Figure 15. ACE Nozzle

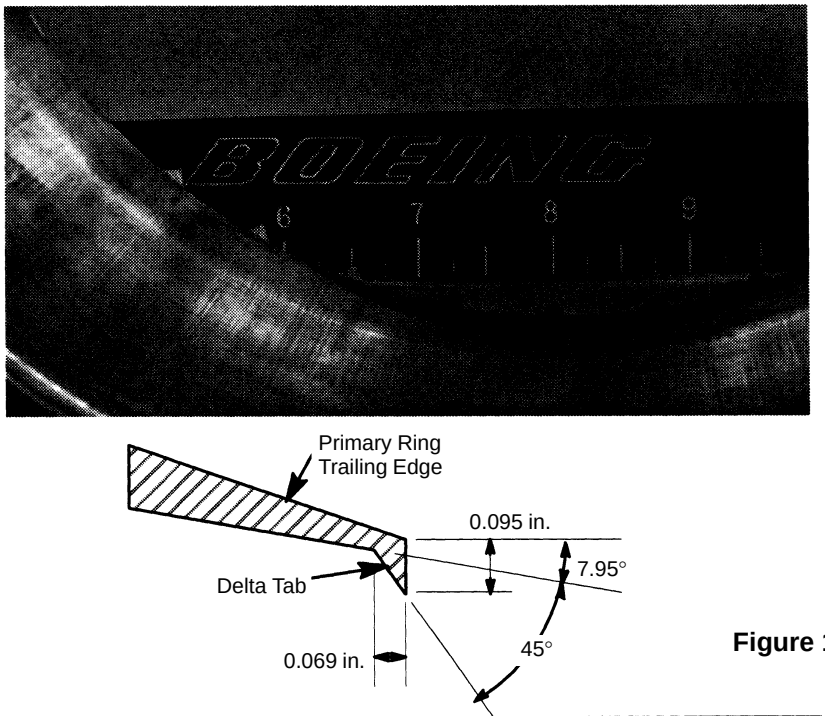

Figure 16. Delta Tab Mixing Device

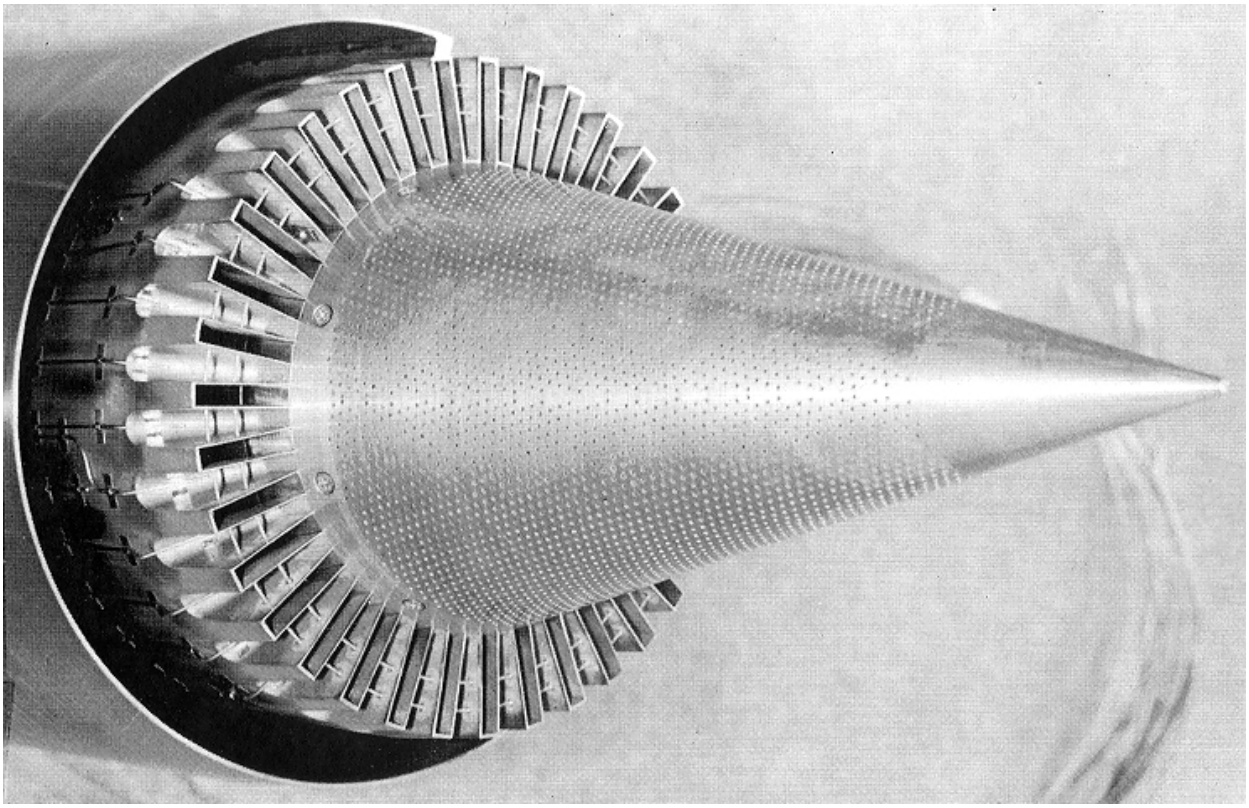

Figure 17. Fluid Shield Nozzle

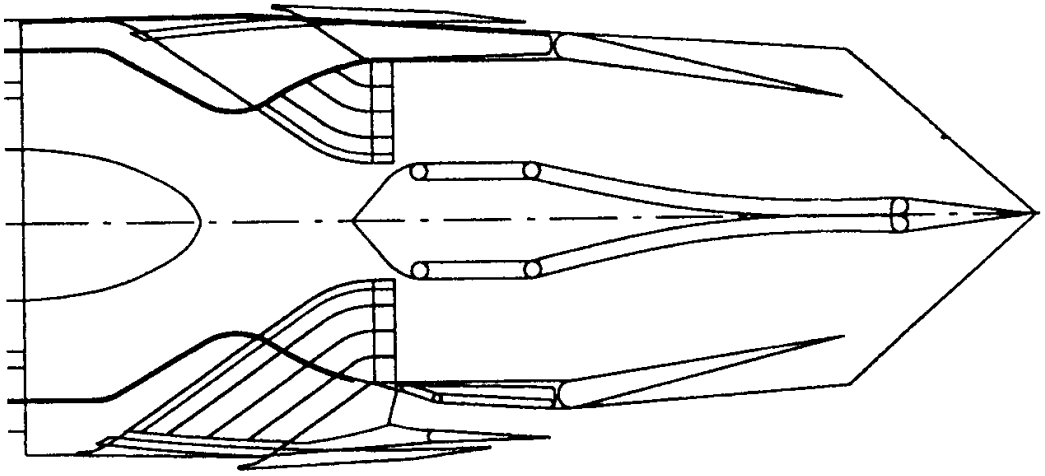

Figure 18. Schematic of Fluid Shield Nozzle Concept

5.2.3 Axi-Tilt Chute Nozzle

The axi-tilt chute (ATC) nozzle is an axisymmetric, convergent/divergent mixer/ejector nozzle. The ATC concept is defined in Figure 19, showing the component nomenclature, and Figure 20, illustrating the four key operating modes. The flap train design reflects a conventional overlapping flap and seal configuration similar to current military axisymmetric exhaust nozzles, with the exception of the integration of acoustic treatment within the structure of the flaps and seals. This concept incorporates a set of circumferentially segmented ejector/mixer chutes that are not stowable and therefore are always exposed to the gas flow. This concept provided an opportunity to investigate any possible advantages that may be associated with an axisymmetric nozzle in terms of installation and integration with the airframe, as well as the potential for added flexibility for the design of the reverser efflux and splay angles. No aerodynamic or acoustic testing was conducted with this concept.

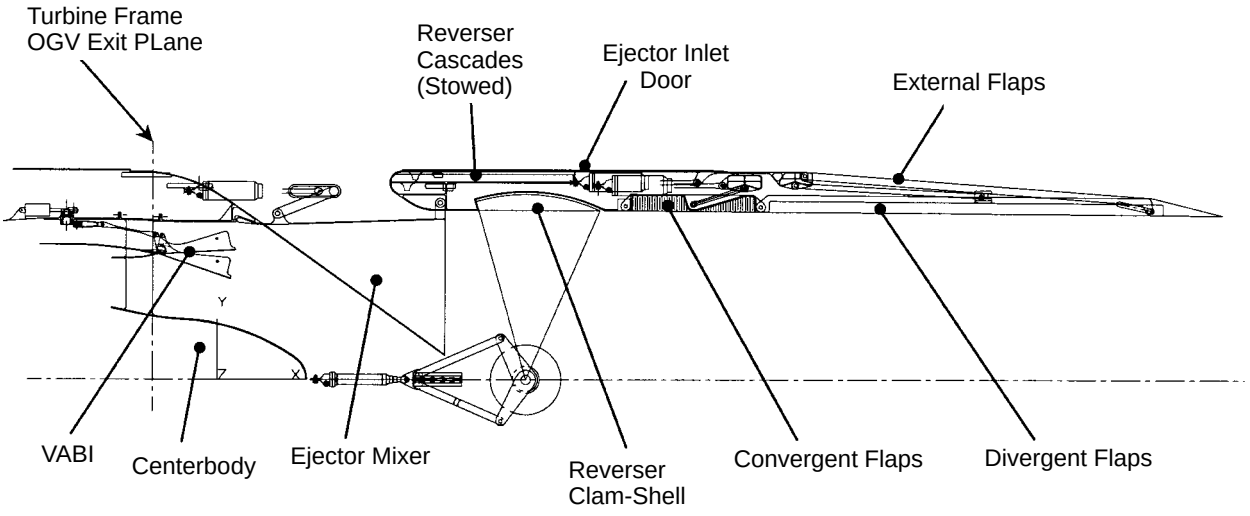

Figure 19. Component Nomenclature for the Axi-Tilt Chute Nozzle

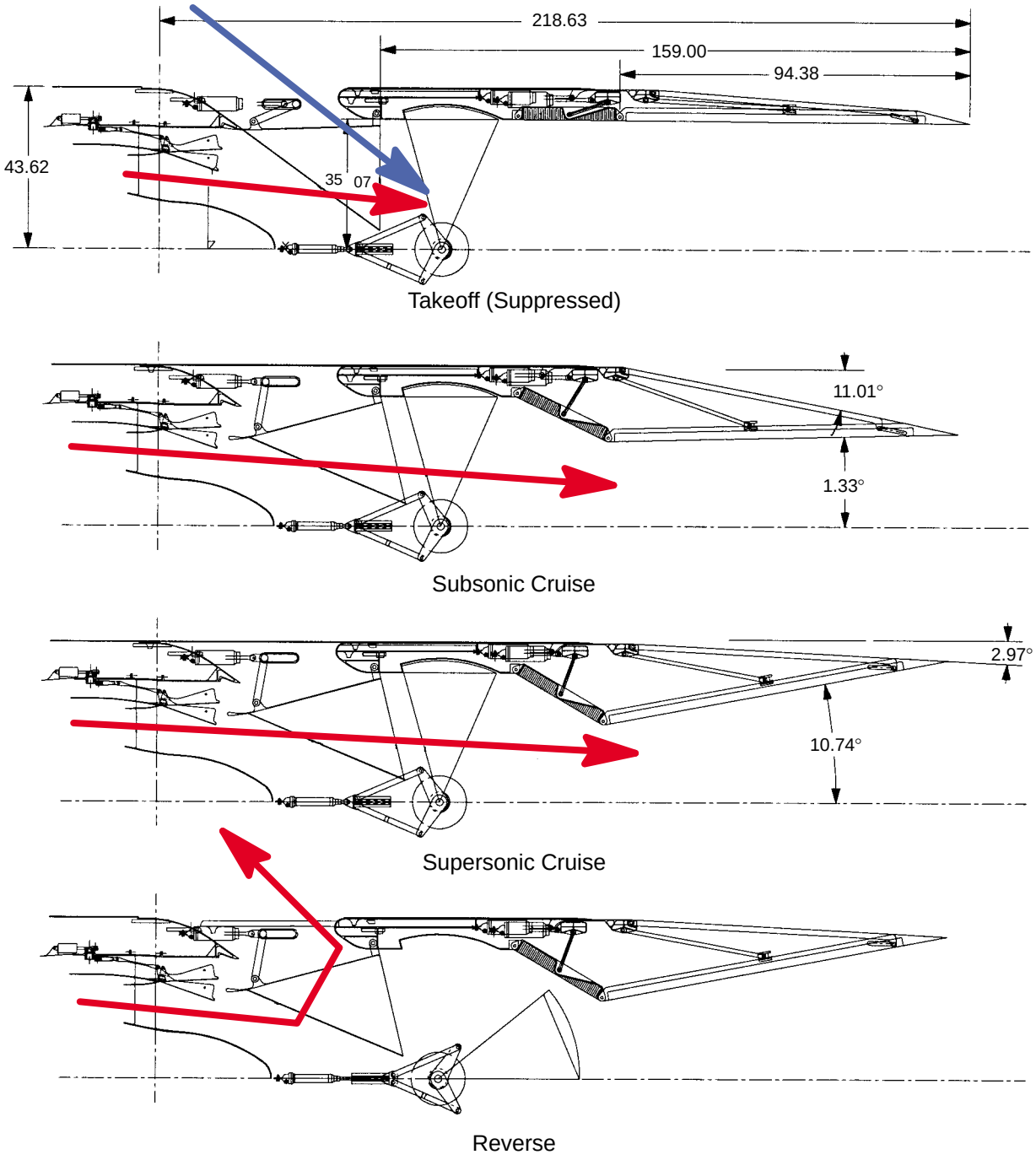

Figure 20. Layout of the ATC Nozzle at Four Flight Conditions

26

5.2.4 Variable-Area Axisymmetric (VAM) Nozzle Design

A conceptual design was developed for an axisymmetric nozzle incorporating variable throat and exit areas. The variable throat area is used to implement the desired engine inlet flow schedule and throttle the engine at constant inlet flow. The throat area is varied between 780 and 1240 in^2. The nozzle exit area is varied between 1100 and 5100 in^2 to provide the best overall nozzle performance throughout the flight envelope.

Figure 21 presents the conceptual design of this mixer/ejector nozzle, which entrains 120% secondary airflow during takeoff to achieve an average exit velocity of 1470 ft/s. The top section of Figure 21 illustrates the takeoff geometry with the secondary air scoops opened and the mixer deployed. The bottom of Figure 21 illustrates the supersonic cruise mode of operation with the secondary air doors closed and the mixer stowed.

During the landing/reverse-thrust mode of operation, the mixer is deployed and rotated to act as a flow blocker (see dashed mixer in Figure 21), and the reverser doors are opened to exhaust the TBE flow.

An X-shaped acoustic splitter is used to absorb the noise created in mixing the secondary air and TBE exhaust flow during takeoff. Acoustic treatment is applied to both the X-splitter and the divergent flaps.

Figure 22 shows a cross-sectional view of the X-splitter and mixer. In the top view, the mixer is stowed and the splitter and convergent flaps are shown. The bottom part of Figure 22 shows the geometry of the mixer. There are four mixer segments, each of which contain two core-stream lobes. During reverser operation, these mixer segments are rotated 90° to block the TBE exhaust flow and divert it out the secondary air inlet/reverser exhaust ports.

The mixer movement is controlled by two independent actuation systems. A synchronous ring/crane trolley system with three actuators is used to translate the four mixer segments forward or aft in unison between the conical convergent flap and divergent flap as shown in Figure 21. The reverser actuation system to rotate the four mixer segments consists of four actuators connected to a common control that synchronizes the movements with the translation actuation system.

Four intake/reverser doors are linked to the divergent flap actuation system so they can be opened or closed in unison with deployment of the mixer.

The convergent and divergent flap system comprises eight flaps with overlapping seals. A synchronous ring and three actuators are used to rotate the flaps in a track/roller system to achieve the throat area variation of 780 to 1240 in^2.

The divergent flap system has eight flaps with overlapping seals. These divergent flaps are linked with eight external flaps by a track roller system to achieve variable exit areas between 1100 and 5100 in^2. The divergent flap actuation system has three actuators, a rollered syncronization ring, and four rollers and tracks. The external flap actuation system has three actuators, a rollered sync ring, and eight rollers and tracks.

5.2.4.1 Dimensions

Table 5 presents the dimensions for the nozzle components for the original (8) and the revised (13) treatment/mixer area ratios.

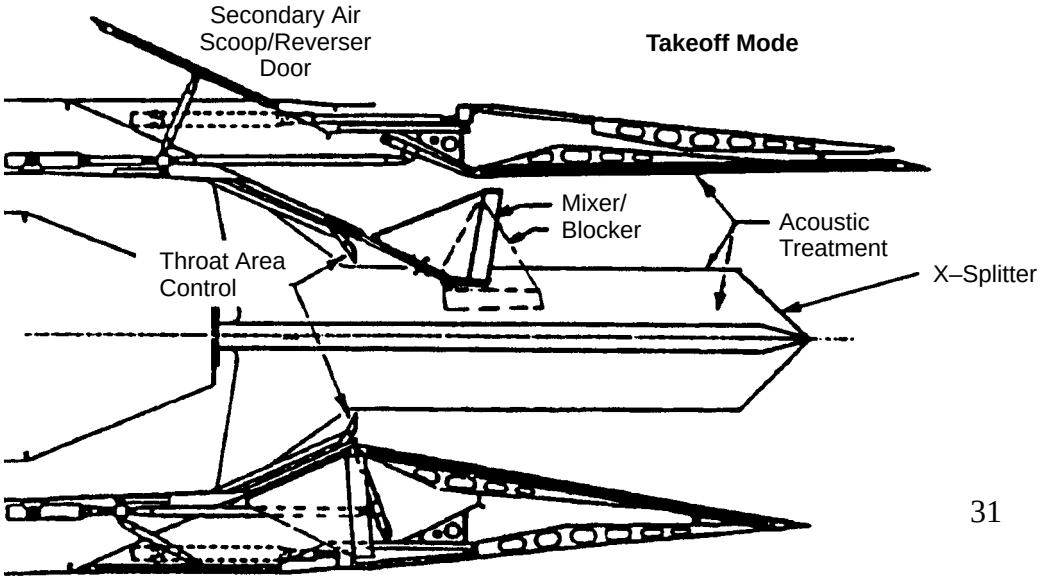

Figure 21. Variable-Exit-Area, Axisymmetric-Nozzle Conceptual Design

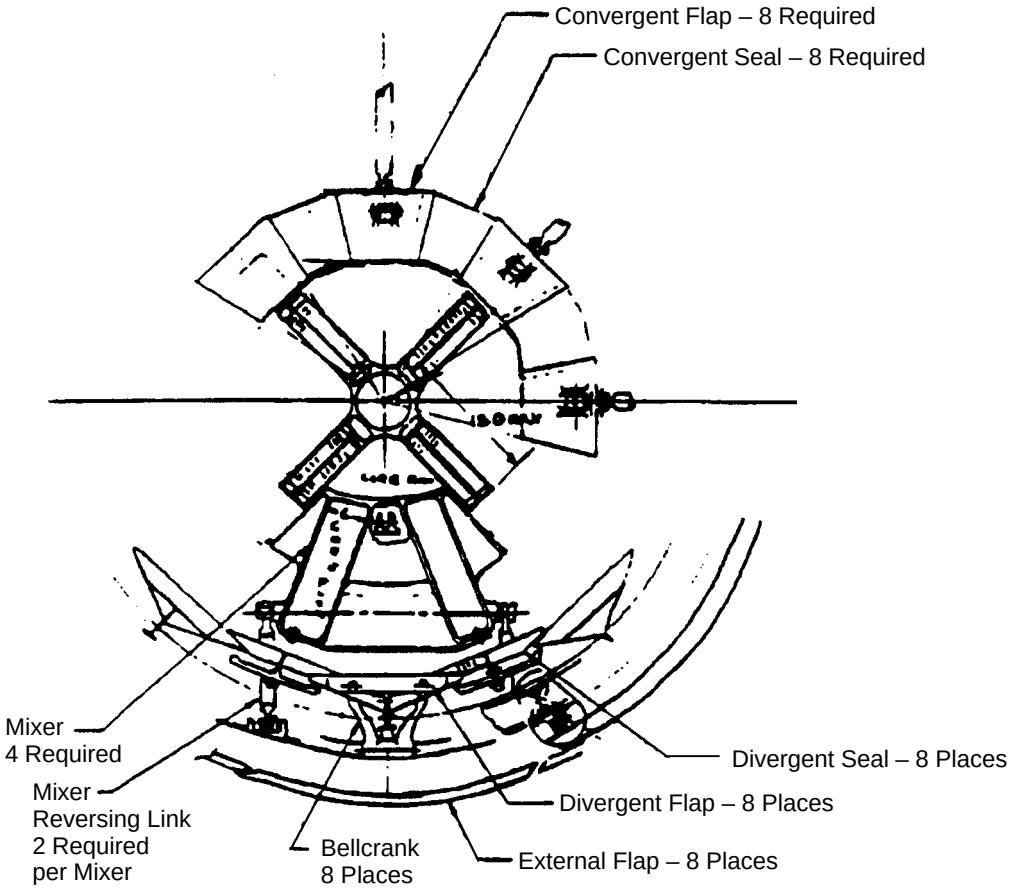

Figure 22. Mixer/Splitter Concept for Axisymmetric Nozzle

Table 5. Variable Axisymmetric Nozzle Dimensions

Dimension	Acoustic Treatment / Mixer Area Ratio	
	8	13
Acoustic Treatment Area, ft^2	219	356
Acoustic Treatment Thickness, in	2.0	3.25
Splitter Thickness, in	4.0	7.5
Nozzle Length (Mach 2.4) in	158	230
Nozzle Length (Mixer Deployed), in	182	254
Divergent Flap Length, in	95	167
External Flap Length, in	95	167
Maximum Diameter, in	113	115.5

When the acoustic treatment requirements were increased, the thickness of the acoustic material was also increased from 2.0 to 3.25 inches, which resulted in the maximum diameter increasing from 113 to 115.5 inches and the nozzle increasing from 158 to 230 inches.

The maximum cross-sectional diameter of this nozzle concept is set up by the requirement to stow the mixer during nonsuppression operation. This mixer is designed to produce full mixing of the streams with 20 hot lobe widths, or 120 inches of the mixer exit plane. As such, the mixer lobes are designed to fully penetrate the secondary flow stream as illustrated in Figure 22. The lobe height is 15.2 inches, and the lobe width is 6 inches. Storage of this mixer, and nozzle actuator requirements, produce a maximum diameter of 113 inches for the original acoustic guidelines and 115.5 inches for the revised acoustic treatment requirements.

The nozzle length is controlled by the deployable mixer design and the acoustic treatment surface area requirements. The distance from the turbine exit plane to the nozzle throat is 63 inches when the mixer is stowed. When the 24-inch mixer is deployed, this length increases to 79 inches.

The divergent flap length is set by the amount of acoustic treatment required to absorb the mixing noise, not performance considerations. The treatment is applied to both the X-splitter and divergent flap. To be effective, the treatment begins 3 lobe widths or 18 inches downstream of the mixer exit. Table 6 shows the acoustic treatment distribution between the splitter and divergent flaps.

Table 6. Variable Axisymmetric Nozzle Acoustic Treatment

Treatment / Mixer Area	Acoustic Treatment / Mixer Area Ratio	
	8	13
X–Splitter Treatment Area, ft^2	82	133
Divergent Flap Treatment Area, ft^2	137	223
Total Treatment Surface Area, ft^2	219	356

5.2.4.2 Performance

Installed nozzle performance was calculated for this nozzle concept at subsonic cruise (Mach 0.9, 36,089 ft), transonic acceleration (Mach 1.1, 32,700 ft), and supersonic cruise (Mach 2.4, 55,000 ft) conditions. The nozzle performance analysis accounted for the following losses:

- Friction drag on all internal surfaces downstream of the nozzle throat (flaps, seals, and acoustic splitters)
- Isolated external boattail drag (includes pressure and friction drag and jet effects)

Not included in the analyses were leakage losses or additional friction drag for the acoustic treatment. P&W's supersonic nozzle performance program was used to make these evaluations.

Figure 23 illustrates the nozzle geometry at the three flight conditions for the original (A_{treat}/A_{mixer} = 8) and revised (A_{treat}/A_{mixer} = 13) acoustic treatment groundrules. In this performance analysis, the exit area (A_9) is varied to achieve the maximum overall thrust minus drag coefficient (C_{Fmax}), where $C_{Fmax} = [F_{G(ideal)} - Drag] / F_{G(ideal)}$. Figure 23 shows that the nozzle with the higher acoustic treatment requirement will have a longer external flap and therefore will have a smaller boattail angle, which will reduce the external pressure drag. However, since both the internal and external surface areas are increased, the friction drag levels will increase.

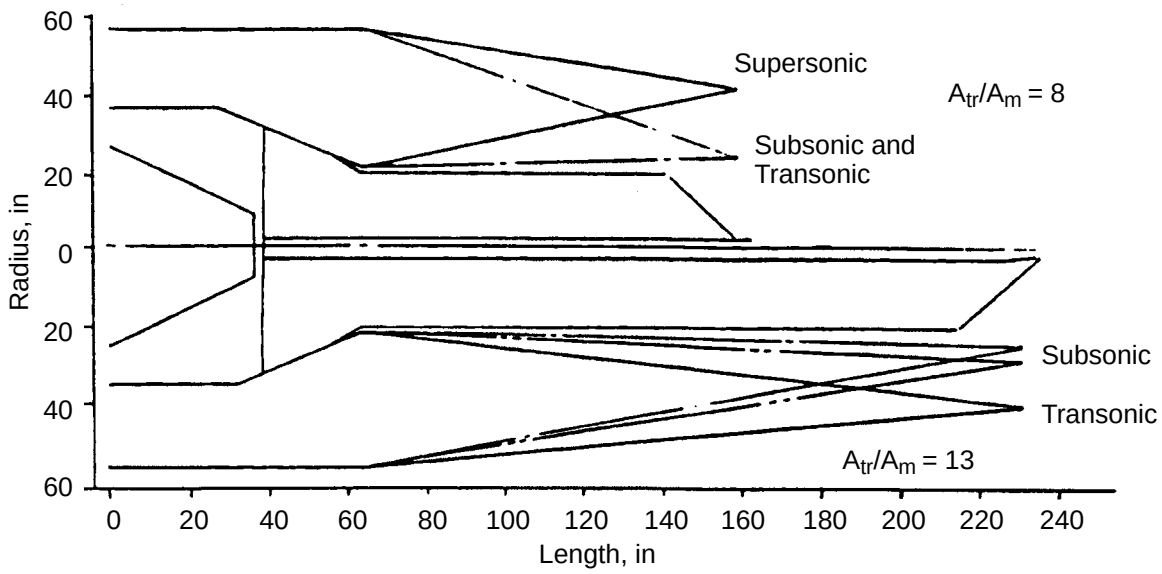

Figure 23. Variable-Exit-Area, Axisymmetric-Nozzle Flap Positions

Table 7 is a summary of the nozzle performance analysis.

5.2.4.3 Weight

The nozzles designed in this study incorporate an advanced material in the inner convergent and divergent flaps that is capable of withstanding the 1900°F maximum exhaust temperature of the TBE without requiring cooling air. The external flap and structure not exposed to the hot exhaust gases are constructed of Titanium (Ti 6–4). The acoustic treatment panels are constructed of an advanced honeycomb material that weighs 3.2 lbm/ft^2. Table 8 summarizes the variable-area axisymmetric nozzle weight.

Table 7. Variable-Area Axisymmetric Nozzle Performance

Parameter	A_{treat}/A_{mixer} = 8			A_{treat}/A_{mixer} = 13		
Mach Number	0.9	1.1	2.4	0.9	1.1	2.4
Effective Throat Area, in^2	1092	851	1006	1092	851	1006
Nozzle Pressure Ratio	4.5	10.3	29.4	4.5	10.3	29.4
Maximum Diameter, in	113	113	113	115.5	115.5	115.5
Exit Area, in^2	1471	1455	5058	1415	2293	4953
Exit Diameter, in	43.28	43.04	80.25	42.45	54.03	79.41
External Flap Length, in	95	95	95	167	167	167
Boattail Angle, Degrees	21.52	21.60	9.93	12.63	10.60	6.20
Treatment Surface Area, ft^2	219	219	219	356	356	356
Ideal Gross Thrust, lbf	17,070	42,985	56,535	17,070	42,985	56,535
Nozzle Drag, lbf	2,640	5,700	2,060	580	3,870	1510
Coefficient of Gross Thrust	0.964	0.963	0.964	0.940	0.941	0.963
Coefficient of Maximum Thrust	0.810	0.831	0.927	0.906	0.851	0.936
Gross Thrust, lbf	16,455	41,395	55,000	16,045	40,450	54,445
Ram Drag, lbf	6,310	12,110	31,770	6,310	12,110	31,770
Net Thrust, lbf	10,145	29,285	22,730	9,735	28,340	22,675
Fuel Flow, lbm/hr	9,577	34,790	29,680	9,577	34,790	29,680
Specific Fuel Consumption, lbm/hr/lbf	0.944	1.19	1.306	0.984	1.23	1.309

Table 8. Variable-Area Axisymmetric Nozzle Weight Summary

Weight	Acoustic Treatment / Mixer Area Ratio	
	8	13
Acoustic Splitter Weight, lbm	911	1061
Static Structure Weight, lbm	2139	2389
Convergent Flap Weight, lbm	110	110
Divergent Flap Weight, lbm	1153	1553
External Flap Weight, lbm	397	497
Mixer Weight, lbm	96	122
Scoop/Reverser Doors Weight, lbm	286	286
Actuation Systems Weight, lbm	1059	1059
Total Weight, lbm	6151	7077

5.2.5 Downstream-Mixer Nozzle

The downstream-mixer nozzle (DSM) is a 2D mixer/ejector nozzle designed to entrain ambient air amounting to 60 to 80% of the engine flow. The mixer was designed to be movable, rotating into the flow at takeoff and retrieved and stowed during supercruise.

The divergent part of the nozzle was divided into two sections with the forward section supporting the mixer and slotted to allow the chutes to extend and retract into and away from the flow. Linear

actuators housed between the forward divergent flap and the exterior surface actuate the mixer. Two sidewall disks position the aft divergent flap. These disks carry rollers that run in a track integral with the aft divergent flap. Disk position combinations determine the position of the divergent flap within the nozzle. The convergent flap sets its position along the divergent flap line, with the forward divergent flap acting as the kinematic link between them. The external flap of the nozzle constitutes the external contour. The interface of the external flap and divergent flap is located at the aft portion of each flap via a hinge interface that allows relative motion of the flaps. There are three sets of doors, all actuated. The reverser doors are hinged along the forward edges and open inward like a blow-in door. The ejector doors are hinged longitudinally along the sides and open out like a bomb-bay door.

After the DSM nozzle concept had been downselected in December 1994, a new engineering effort was initiated. This effort was referred to as the *Best Downstream Mixer* (Best DSM) nozzle study, with the objective of defining a nozzle that would configure a DSM into the most efficient package, thereby enabling the most favorable DSM nozzle/aircraft system. The resulting nozzle concept would then become the baseline for the ongoing development of the demonstrator (Demo) and full-scale product nozzles.

Two concepts, described in the following subsections, were developed in sufficient detail to allow a selection to be made: (1) the translating-chute concept (also called the sliding-chute concept) and (2) the rotating-chute concept.

5.2.5.1 Translating-Chute Concept

The translating-chute concept (also referred to as the sliding-chute concept) offers flexibility in the aerodynamic shaping and design of the ejector mixer chutes and provides a significant reduction in flowpath seal leakage. Unlike the rotating-chute concept (Subsection 5.2.5.2), the ejector mixer is completely stowed during unsuppressed operation and thereby does not have to integrate with the nozzle internal flowpath. In addition to the flexibility in ejector chutes shaping, it offers low parts count and demonstrated acoustic performance. Figure 24 shows components and nomenclature, and Figure 25 illustrates four operating modes.

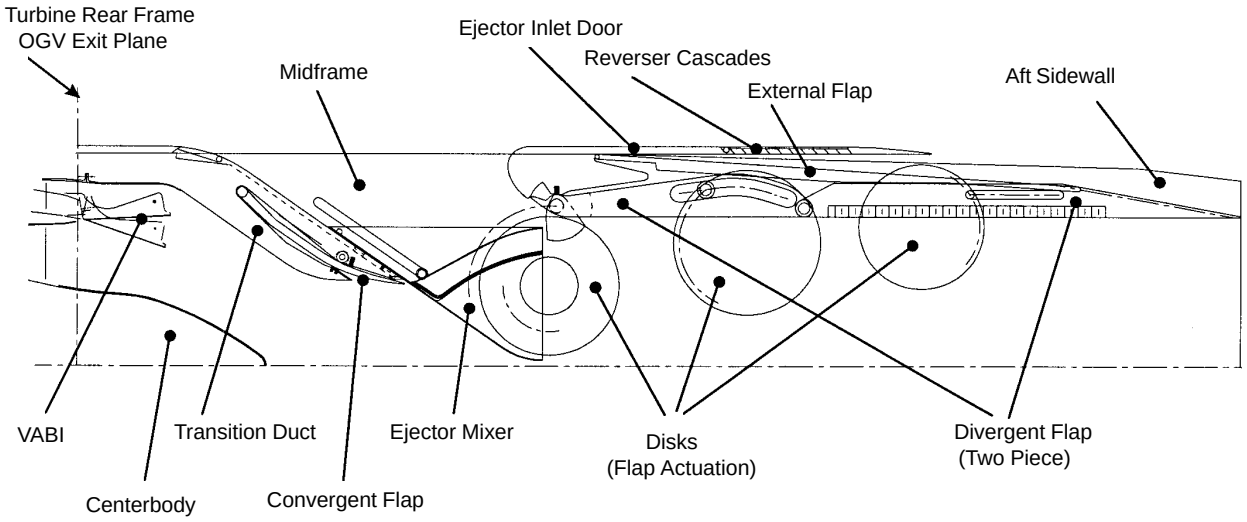

Figure 24. Component Nomenclature for the Sliding-Chute Nozzle

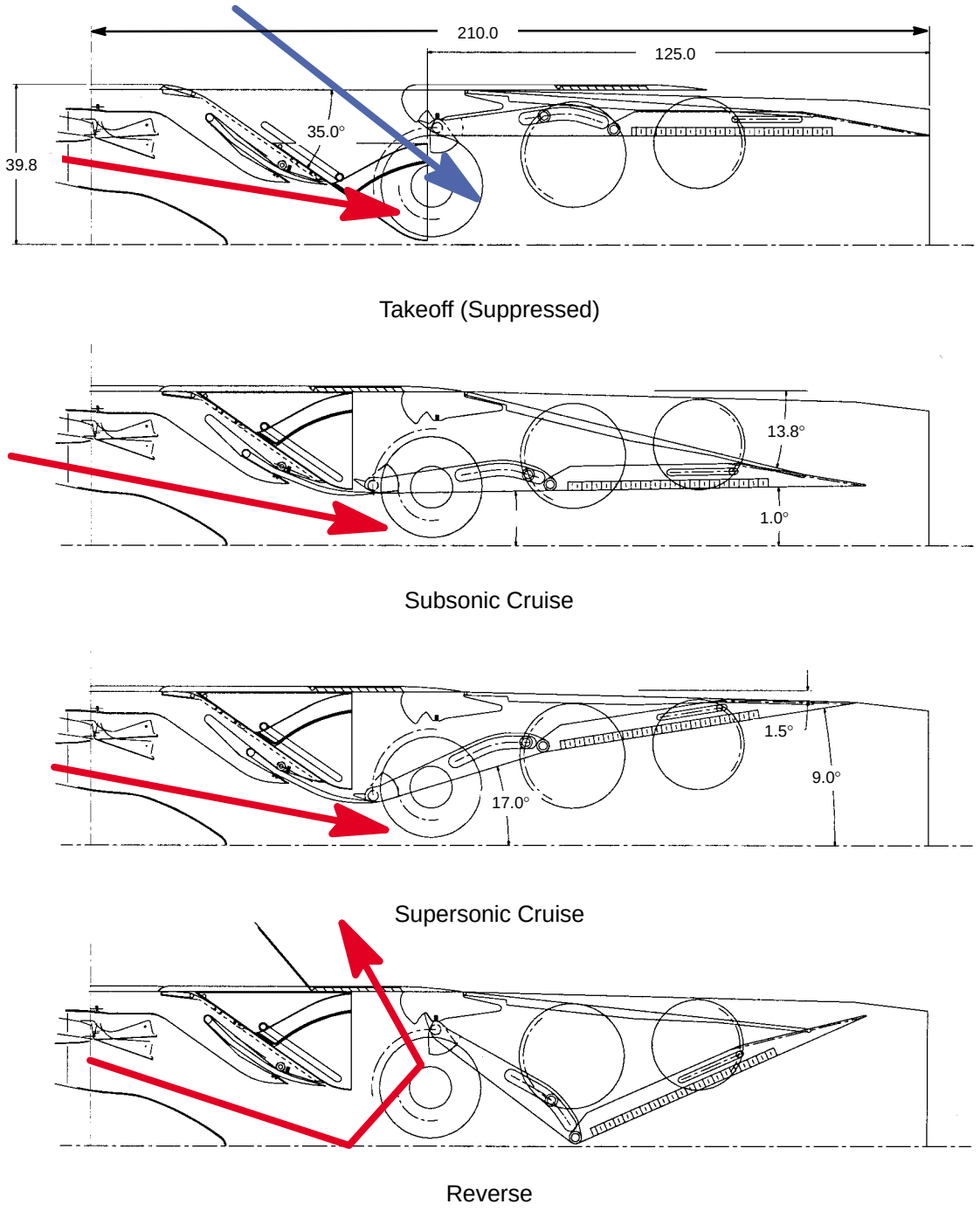

Figure 25. Layout of the Sliding Chute Nozzle at Four Flight Conditions

The nozzle is a 2DCD configuration. The cross section is circular at the variable-area bypass injector (VABI) exit plane. Between this plane and the entrance plane of the ejector mixer, the cross section transitions from circular to rectangular. Aft of the ejector, the cross section remains rectangular (2D) while the flow area converges to the throat and then diverges to the nozzle exit plane.

This concept incorporates an ejector/mixer chute that translates inboard into the flowpath for the suppressed takeoff mode. The ejector inlet doors are translated aft, thereby allowing ambient air to be entrained into the nozzle through the ejector inlet opening.

For unsuppressed operating modes (except reverse, which is unique), the ejector mixer chute is completely stowed outside of the gas flowpath, within the ejector inlet region of the midframe.

Transition between the suppressed and unsuppressed operating modes is achieved by simultaneous actuation of the ejector inlet doors, ejector mixers, and the convergent and divergent flaps. The ejector inlet doors are translated forward to close the ejector inlet opening. The ejector mixers are translated outboard, out of the flowpath, while the convergent flaps are translated inward into the flowpath and the divergent flaps are actuated inboard to meet with the convergent flaps through the rotation of the disks.

The reverse-thrust operating mode is implemented by simultaneous actuation of the ejector inlet doors, the reverser cascades, and the divergent and convergent flaps. The ejector inlets are opened by translation of the ejector inlet doors in the aft direction. The reverser cascades are translated together into the ejector inlet opening, while the convergent flaps are translated outboard into a stowed position. The aft flow of gas is blocked by the forward portions of the divergent flaps. Gas flow is thereby directed through the reverser cascades then continues outboard and forward through the ejector inlet opening.

5.2.5.2 Rotating-Chute Concept

The rotating-chute concept is shown in Figure 26, with the flaps in the supersonic cruise positions. It has a disk-mounted convergent flap that also acts as an axial-flow blocker during thrust reverse operation. The upper and lower convergent flaps are driven by common actuator and link mechanisms housed in the sidewalls. Hinged to the aft end of the convergent flaps aft end is a two-piece divergent flap. The forward divergent flap supports the flow mixer and actuation system and is hinged at the aft end to the aft divergent flap. The aft divergent flap is positioned by two sidewall disks, a large forward and a smaller aft disk. These disks carry rollers that run in tracks integral with the aft divergent flap. The particular combination of disk positions determines the line of action on which the aft divergent flap lies. The convergent flap position location is set along this line, with the forward divergent flap acting as the kinematic link. Each upper disk is paired with a lower counter-

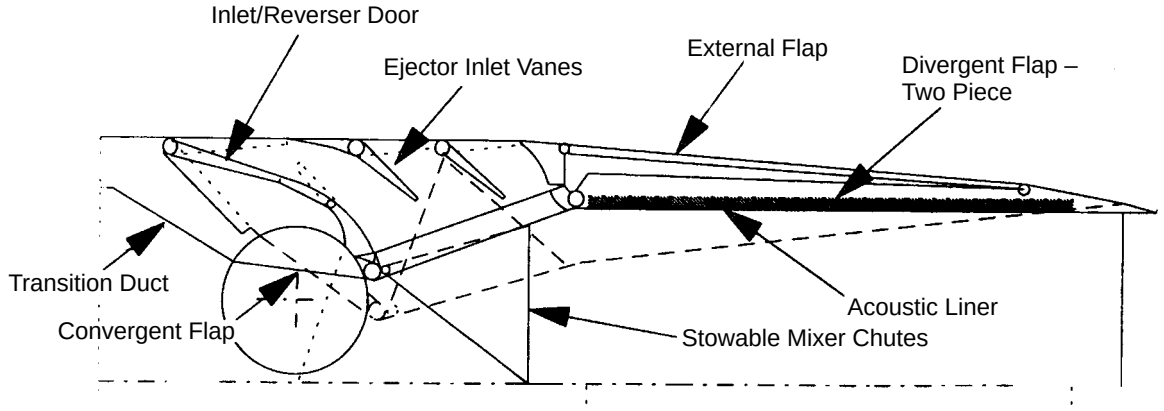

Figure 26. Downstream Rotating-Chute Mixer Nozzle

part, and they are driven by a common actuator and link system (not shown). There are a total of four divergent actuators per nozzle. The aft end of the aft divergent flap is also hinged to the aft end of the external flap. A roller running in a track fixed to the static structure supports the forward end of this flap. Therefore, the aft divergent flap passively positions it.

During takeoff, Figure 27, the mixer rotates into position. The mixer and actuation system are mounted on the forward divergent flap as shown in Figure 28. Each mixer is positioned by three actuators, for a total of six per nozzle. Both ejector door and reverser door open, and the auxiliary

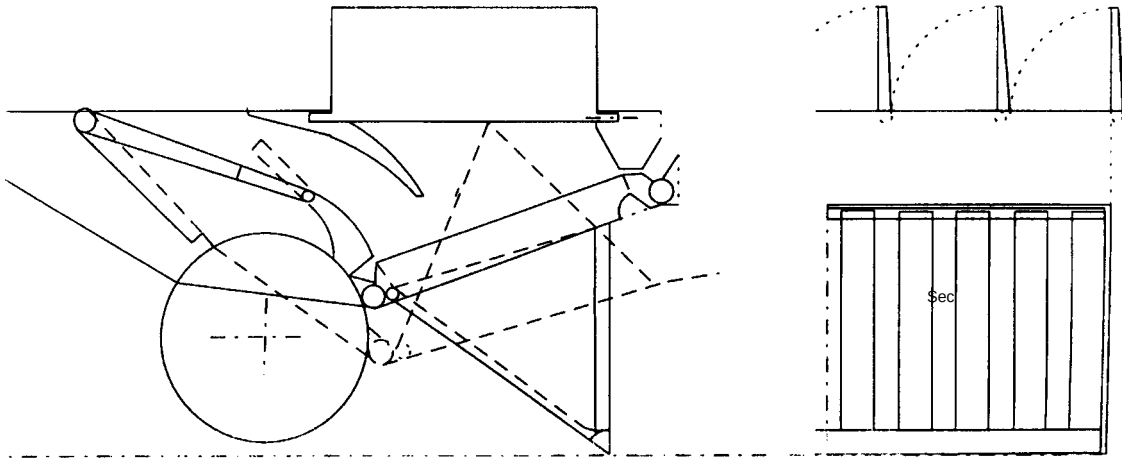

Figure 27. Details of Rotating Secondary Mixer Chutes

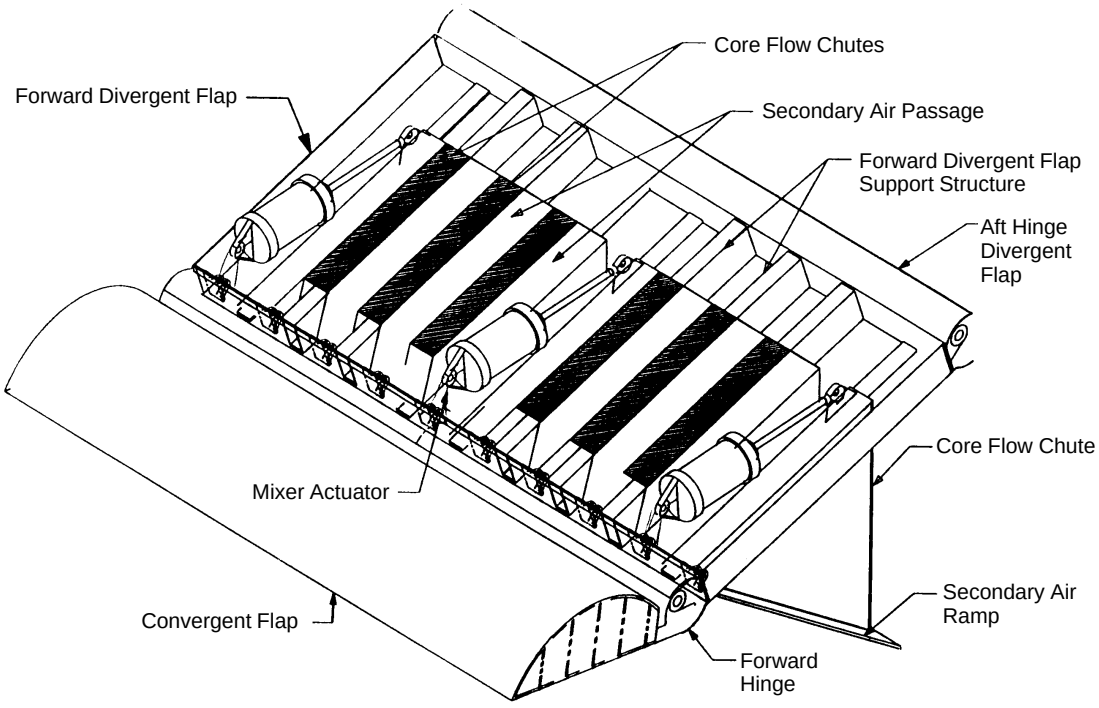

Figure 28. Isometric View of Downstream Mixer

door is set to the forward position. In this position, the forward edge meets up with the aft edge of the reverser door. This directs air entering through the reverser door into the ejector chamber, thereby increasing ejector capacity. In this position, the reverser chamber is closed at both ends and not used.

5.2.6 Two-Dimensional, Fixed-Chute (2DFC) Nozzle

The two-dimensional, fixed chute nozzle (2DFC) differs from the DSM in that the mixer remains in the flowpath during unsuppressed operation. The nozzle was originally designed with a plug to allow variable throat area. Later versions of this nozzle were designed without the plug. The following subsections describe this nozzle, the various stages of its development, and options for some of the major components.

5.2.6.1 Fixed-Chute Nozzle With Plug

For this concept, the ejector mixer chutes are fixed within the internal flowpath and thus do not require the added complexity of structurally integrating and stowing the mixer. However, a centrally located plug is required in order to control engine flow area during different modes of operation. Because the ejector mixer chutes are fixed, the configuration allows more flexibility in the aerodynamic shaping and mechanical design.

The 2DFC nozzle concept is defined in Figure 29, along with component nomenclature. The nozzle is a two-dimensional, convergent/divergent configuration (2DCD). The nozzle cross section is circular at the turbine rear frame OGV exit plane. Between this plane and the entrance plane of the ejector mixer, the cross section transitions from circular to rectangular. Aft of the ejector, the cross section remains rectangular (2D) while the flow area converges to the throat and then diverges to the nozzle exit plane.

This concept incorporates a set of ejector inlet doors that translate forward, thereby opening the ejector inlet for the suppressed modes of operation. Simultaneoulsy, the plug is translated to the

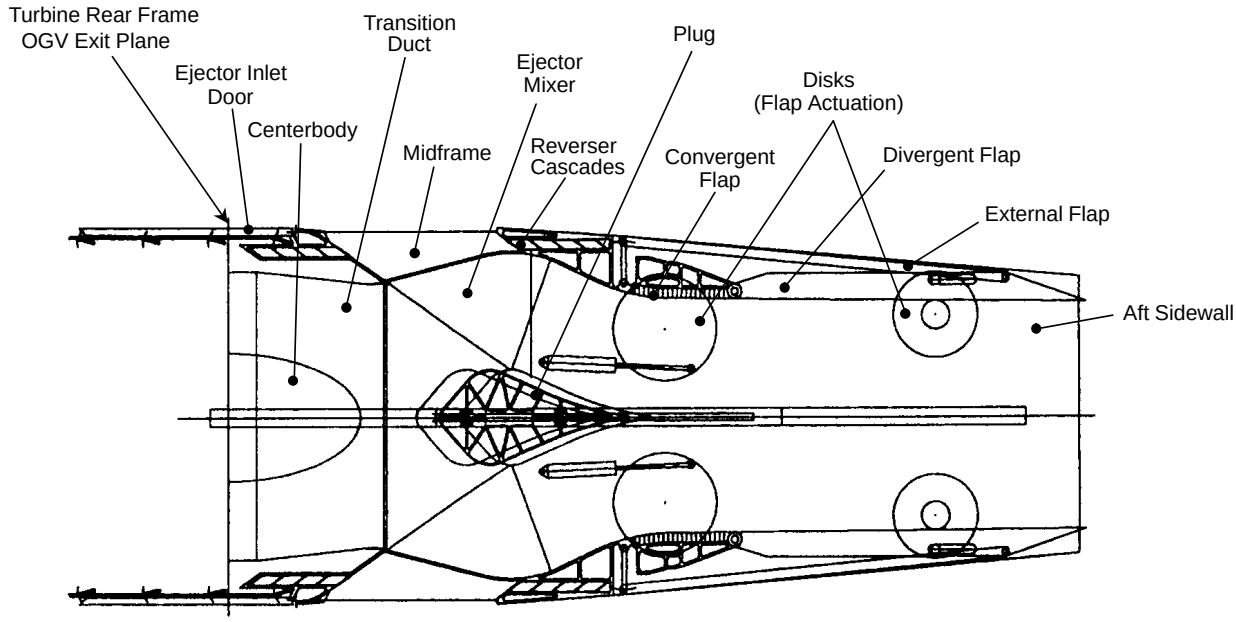

Figure 29. Component Nomenclature for the 2DFC Nozzle

aft-most position to create the throat for the engine flow, within the ejector mixer. This creates an ejector nozzle, where the engine gas flow is directed to the inboard side of the ejector mixer chutes and the ambient airflow is entrained into the nozzle on the outboard surface of the ejector mixer chutes. For the unsuppressed operating modes, the ejector inlet doors are translated aft, thereby closing the ejector inlet, while the plug is translated forward to allow the throat position to change to the convergent flaps.

The transition between suppressed and unsuppressed operating modes is achieved by simultaneous actuation of the ejector inlet doors, the plug, and the convergent and divergent flaps. The ejector inlet doors are translated aft to close the ejector inlet opening. Simultaneously, the plug is translated forward and the convergent and divergent flaps are positioned inward into the flowpath by rotation of the respective disks.

The reverse-thrust operating mode is implemented by simultaneous actuation of the ejector inlet doors, the plug, the reverser cascades, and the divergent and convergent flaps. The ejector inlets are opened by translation of the ejector inlet doors in the forward direction. The reverser cascades are translated together into the ejector inlet opening. The aft flow of gas is then blocked by the convergent flaps, while the divergent flaps are actuated simultaneously to allow this positioning. The gas flow is thereby directed through the reverser cascades, then continues outboard and forward through the ejector inlet openings.

5.2.6.2 Fixed-Chute, No-Plug Nozzle

The FNP nozzle concept is defined in Figure 30, showing the component nomenclature, and Figure 31, illustrating the four key operating modes.

The 2DCD nozzle cross section is circular at the VABI exit plane. Between this plane and the entrance plane of the ejector mixer, the cross section transitions from circular to rectangular. Aft of the ejector, the cross section remains rectangular (2D), while the flow area converges to the throat and then diverges to the nozzle exit plane.

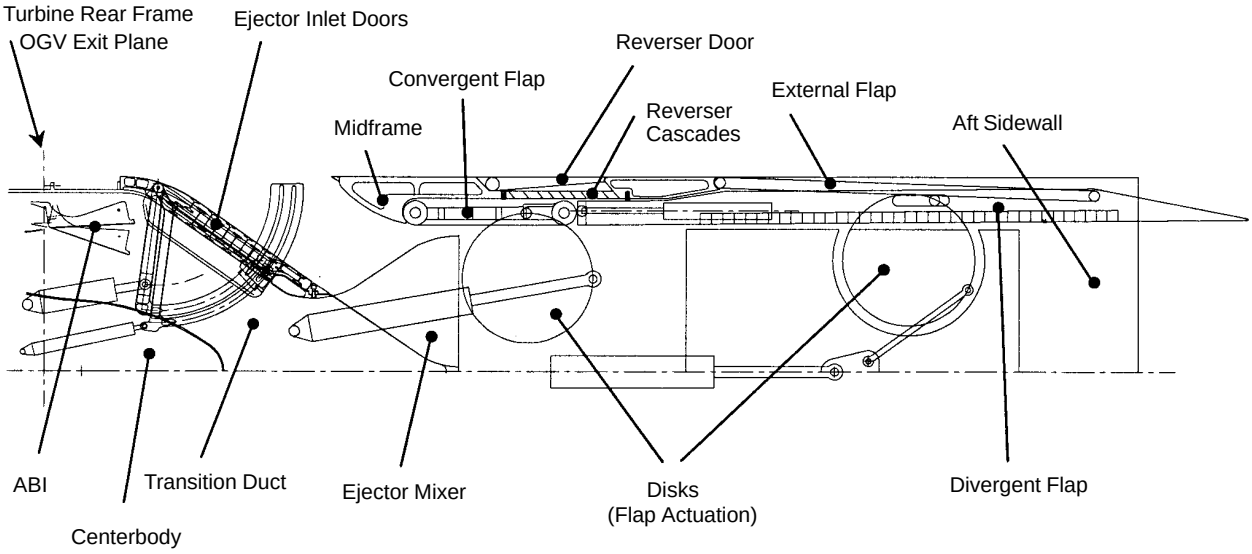

Figure 30. Component Nomenclature for the Fixed-Chute, No-Plug Nozzle (FCN)

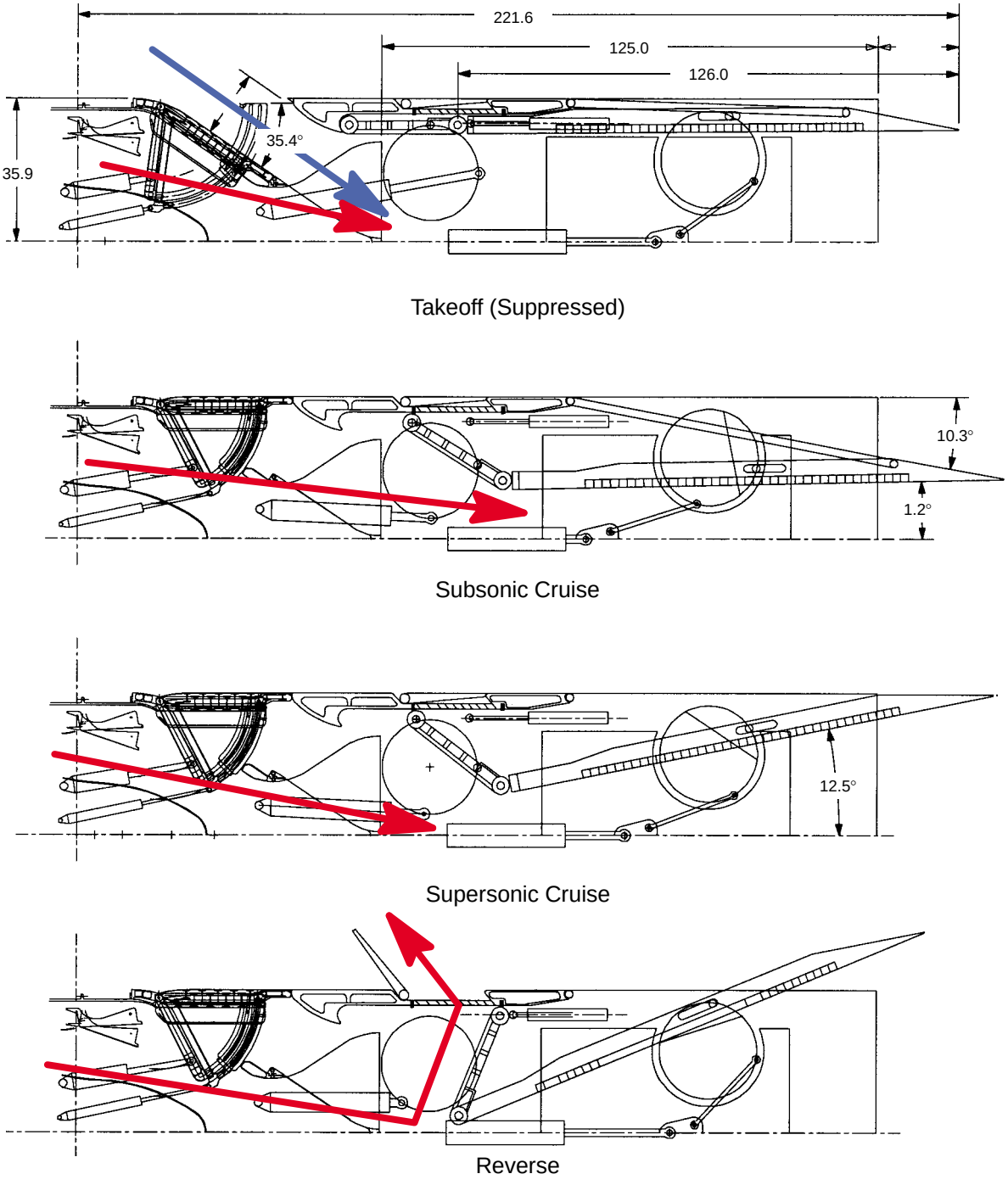

Figure 31. Layout of the FCN Nozzle at Four Flight Conditions

This concept incorporates a set of ejector inlet doors that rotate, or pivot, inboard into the flowpath for the suppressed takeoff mode. This creates an ejector nozzle, where the engine gas flow is directed to the inboard side of the ejector mixer chutes and the ambient airflow is entrained into the nozzle on the outboard surface of the ejector mixer chutes.

For the unsuppressed operating modes, the ejector inlet doors are rotated or pivoted outboard, closing off the ejector inlet and allowing engine gas flow to be directed along both the inboard and outboard surfaces of the ejector mixer chutes.

Transition between suppressed and unsuppressed operating modes is effected by simultaneous actuation of the ejector inlet doors and the convergent and divergent flaps. The ejector inlet doors are used to compensate for changes in flow area requirements during this transition. The ejector inlet doors are sequentially rotated outboard, about pivot points on the nozzle duct, to close the ejector inlet opening. The convergent and divergent flaps are positioned inward into the flowpath through rotation of the respective disks.

The reverse-thrust operating mode is implemented by simultaneous actuation of the ejector inlet doors, the reverser doors, and the divergent and convergent flaps. The reverser port is opened through the inboard rotation of the convergent flaps and subsequent outboard rotation of the reverser doors. The aft flow of gas is then blocked off by the convergent flaps, while the divergent flaps are actuated simultaneously to allow this type of positioning. The gas flow is thereby directed out through the reverser port opening.

5.2.6.3 Improved Fixed-Chute Nozzle

After the August 1995 selection of the FNP nozzle, development of the concept continued. This development involved subtle changes and improvements, culminating in establishment of a new version of the concept as the baseline for both the Demo and the full-scale product nozzles. The resulting configuration was designated as the fixed-chute nozzle concept (FCN). This new baseline configuration was subsequently presented at the Critical Propulsion Components Exhaust System PDR in December 1995.

The *Parallel Effort* was initiated after the December 1995 PDR of the baseline FCN in order to address key design improvements to the convergent flap and associated interfaces. Specifically, this effort focused on structurally integrating the convergent flap with the convergent actuation disk. Four concepts were developed to the level of detail necessary to allow a selection to be made:

- Separate Reverser Port (SRP)
- Linked Flap (LF)
- Arc Valve (AV)
- Reversing Through Inlet (RTI)

The nozzle development guidelines for these four nozzles are listed in Table 9.

Separate Reverser Port

This is a modified version of the FNP and FCN concepts and is therefore sometimes referred to as the FCN–SRP nozzle concept.

The SRP nozzle concept is defined in Figure 32, showing the component nomenclature, and Figure 33, illustrating the four key operating modes.

Table 9. Nozzle Development Guidelines for the Parallel Effort Nozzles

Criteria	Parameter	Value
Acoustic	ASAR SAR Aspect Ratio A_{mix} ($in^{2)}$ MAR Penetration Mixing Length (in) CER Forward Edge Treatment (in from A_{me})	2.79 2.65 1.35 3536 0.95 0.925 122.0 1.10 48.0 (15 Hot-Lobe Widths)
Aerodynamic	Cycle Flowpath Width (in) Divergent Flap Length (in) Inlet Door Length (in)	3570.80; Oct. 18, 1995 67.342 116.0 49.256
Mechanical	Aft Disk Envelope (in) Nacelle Half Ht. at Nozzle for Flange (in) Aft Edge Treatment (in from aft end of SW Divergent Flap) Forward OML	5.5 min from OML, 35.7 min. from SW Aft Edge 40.74 22.5 (SW), 13.0 (Divergent Flap) Horzontal

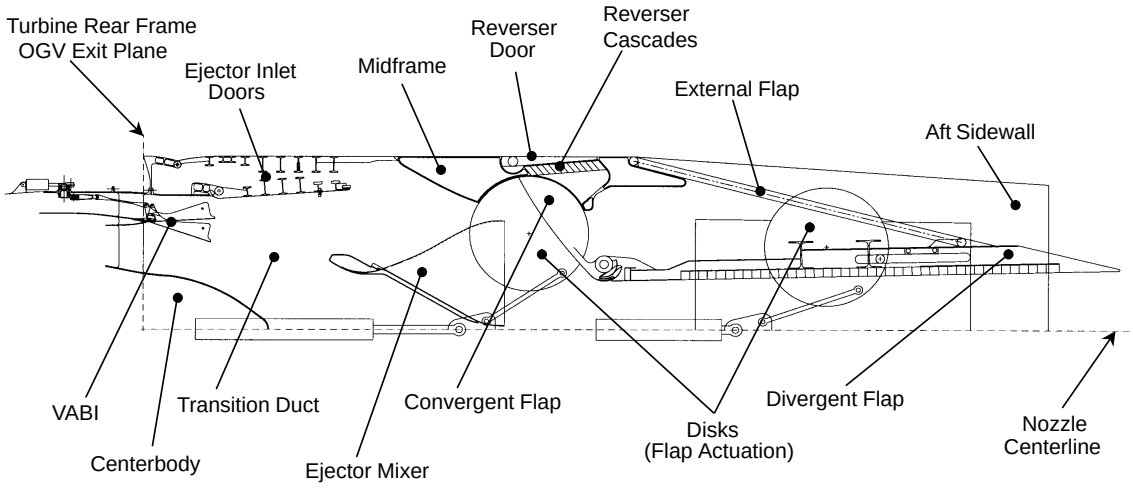

Figure 32. Component Nomenclature for the Separate Reverser Port Nozzle

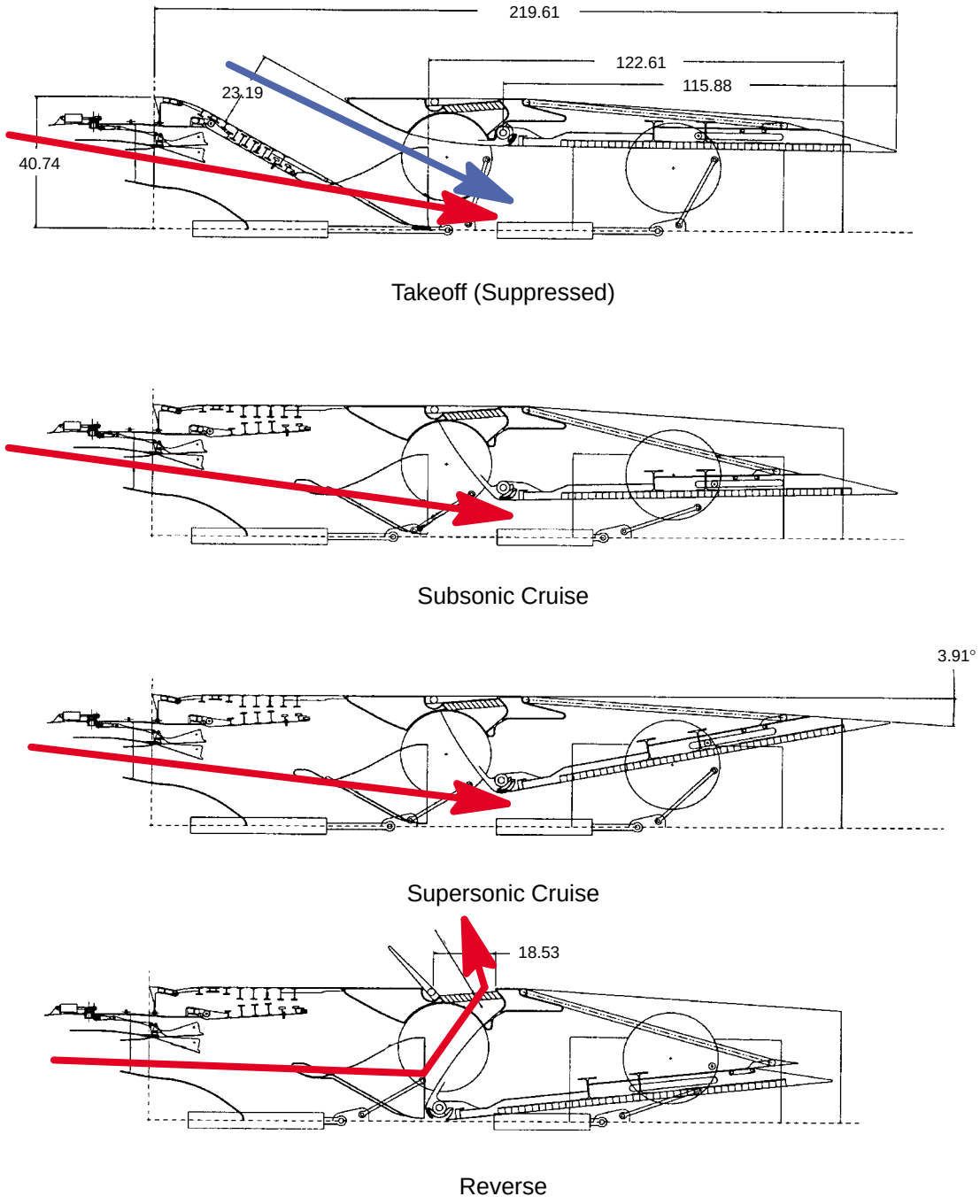

Figure 33. Layout of the Separate Reverser Port Nozzle at Four Flight Conditions

For the SRP, the convergent flap configuration and actuation system have been changed to reflect a flap that is structurally integrated with the convergent disks. Additionally, the number of actuators was reduced from four to two per nozzle, by placement of the actuators at the nozzle centerline, thereby resulting in different kinematics.

This change in the convergent flap kinematics affects two other aspects of the nozzle configuration. First, it eliminates the need for a separate reverser actuation system. Second, it provides for a simpler sealing configuration between the forward edge of the convergent flap and the midframe.

For the SRP the convergent flap and corresponding disks are one structural component; whereas, for the FNP the convergent flap is a separate component from the disks and is driven by the disks through a pin connection.

The characteristics, operation, and remaining features of the SRP nozzle are the same as described previously for the FNP.

Linked Flap

Like the SRP nozzle, this concept is another modified version of the FNP and FCN concepts and is therefore sometimes referred to as the FCN–LF nozzle concept.

The LF nozzle concept is defined in Figure 34, showing the component nomenclature, and Figure 35, illustrating the four key operating modes.

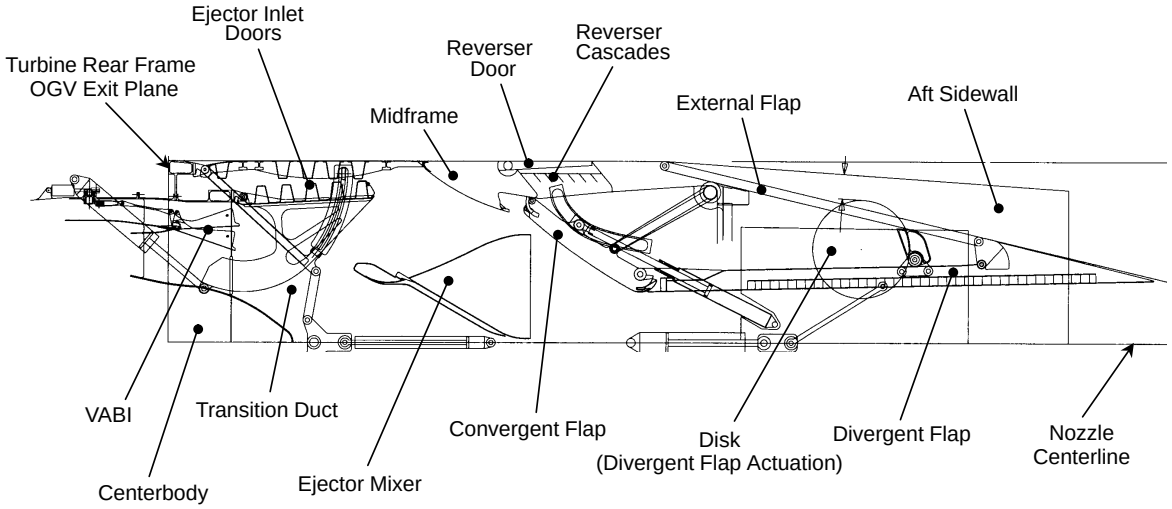

Figure 34. Component Nomenclature for the Linked Flap Nozzle

For the LF, the convergent flap configuration and actuation system have been changed to reflect a flap mounted to the nozzle structure by a link frame and actuated by a direct connection with the linear actuators, thereby eliminating the convergent disks and resulting in different kinematics.

This change in the convergent flap kinematics affects three other aspects of the nozzle configuration. First, it eliminates the need for a separate reverser actuation system. Second, it allows a simpler interface between the external flap and the divergent flap at the aft hinge connection. Third, a more

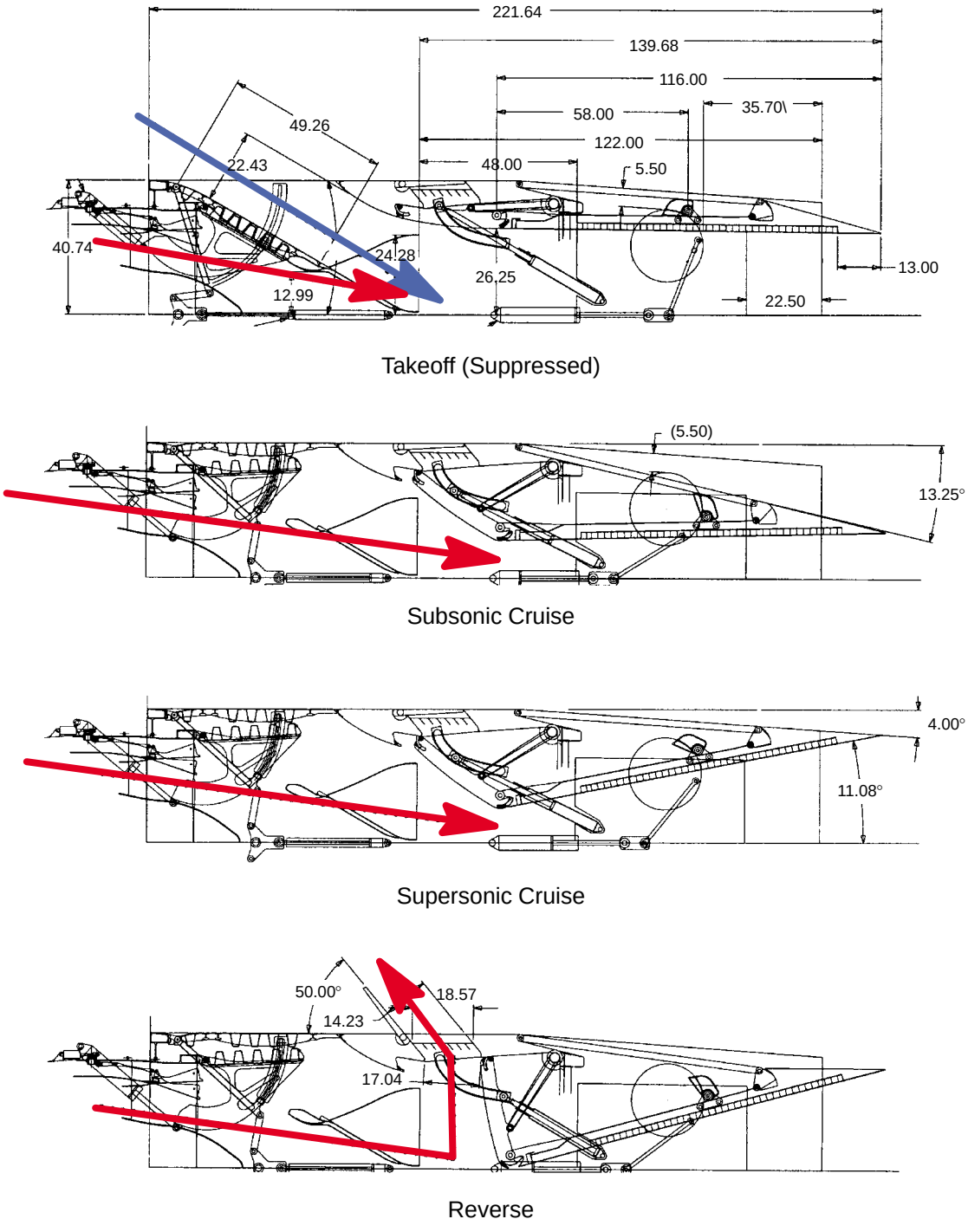

Figure 35. Layout of the Linked-Flap Nozzle at Four Flight Conditions

complicated sealing configuration is required between the forward edge of the convergent flap and the midframe.

The LF concept also reflects a change to the actuation system for the ejector inlet doors. The actuators for the inner ejector doors have been placed forward of the nozzle in the region of the turbine rear frame of the engine. The number of actuators for the outer ejector inlet doors has been reduced from four to two per nozzle, by the placement of the actuators at the nozzle centerline.

It should be noted that this change to the ejector inlet door actuation system could also be incorporated into the FNP or the FCN concepts and is therefore not solely dependent on the LF configuration. Additionally, the LF concept eliminates the need for a separate reverser actuation system.

The characteristics, operation, and remaining features of the LF nozzle are the same as described previously for the FNP.

Separate Reverser Port Fixed-Chute Nozzle

Figure 36 is a schematic of the separate reverser port (SRP) nozzle. One of the most distinctive differences between the SRP and the 1995 baseline is the integrated convergent flap and convergent disk of the SRP. This feature improved the structural integrity of these components; it also decreased the leakage potential into the flap cavity because the seam between the flap and the disk was eliminated in four places (four disks per nozzle). The drawback to integrating the convergent flap and disk is that the divergent flap is pulled forward during reverse, mandating a sliding-joint

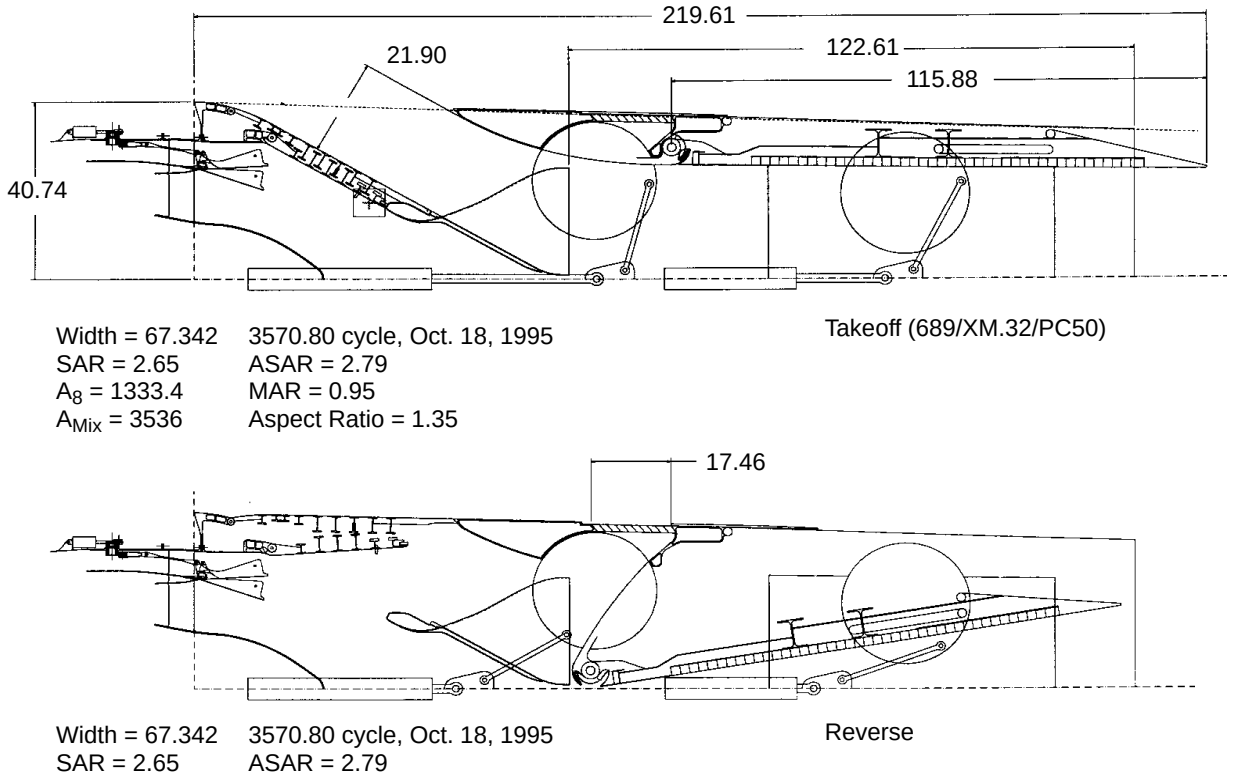

Figure 36. Separate Reverser Port (SRP) Nozzle *Integral convergent flap and disk with separate reverser.*

connection between the divergent flaps and external flaps. This is a major disadvantage relative to the link-flap scheme that uses a pin joint between the divergent and external flaps.

Another advantage is that the reversing is done through a separate port than the inlet; however, it can also be reversed through the inlet if so desired. This flexibility is an added bonus with the SRP. Reversing through a separate port is the preferred approach because it allows the reverser flow to be splayed in any desired direction to protect the aircraft wing structure.

Another advantage the SRP had over the link-flap type designs is that it needed only 10 actuators compared to the 12 needed to actuate the link-flap designs. By eliminating the two extra actuators in the convergent section, the convergent flaps could be synchronized through a track, trolley, and linkages located along the engine centerline. The only disadvantage to this reduction in actuator count was that the stroke on the convergent flap actuators increased from 22 to 30 inches. Also, the loading on the inlet doors is lower than other concepts because the doors are modulated at a low power setting.

The "parallel efforts" task ended with a downselect between the fixed-chute baseline, *reverse through the inlet* (RTI), *linked flap* (LF), and *separate reverser port* nozzles. The SRP was eventually dropped in favor of the LF. For a description of the LF and rationale for selection refer to the discussion on page 33.

Arc Valve Concept

A revue of the HSCT baseline nozzle (linked flap) revealed a serious under-area condition that occurred during transition to reverse. Transition to reverse is effected by bringing together the upper and lower convergent flaps at the nozzle centerline, completely blocking flow in the primary nozzle. Flow is then redirected to the reverse vane packs in the upper and lower sections of the nozzle. To prevent "back pressuring" the engine, the reverse mechanism must provide the engine-required jet area at all times during the transition to reverse mode. A first-pass look at the under-area problem was done for the 3570.80, October 1995 engine cycle for PC50 conditions. Jet area required for this condition is 1300 in^2. During reverse, the effective jet area was calculated to be 900 in^2. Actual reversing will occur at lower power settings, increasing the area required to be above 1300 in^2.

The "arc valve" was introduced as an area-compensating device. The arc valve is sandwiched between the rotating convergent flap and the static structure. Simultaneous with flap closure, the arc valve telescopes open to admit gas flow into the reverse cavities — opening additional area to compensate for the under-area produced by the convergent flaps alone. The arc valve motion is synchronized by mechanical linkage connected directly to the convergent flap. Figure 37 shows how the arc valve is nested in the nozzle structure. Figure 38 illustrates the arc valve configuration.

5.2.6.4 Fixed-Chute Nozzle, Alternate Kinematics

This effort was initiated in response to the results of the nozzle *Systematic Approach to Value Engineering* (SAVE) event (refer to Subsection NO TAG). The SAVE event predicted that nozzle weight would be reduced substantially by using an alternate kinematic approach that obviates the convergent and divergent actuation disks. Therefore, this effort was designated as the *Alternate Kinematics* nozzle study. The objectives were to (1) develop a FCN configuration that eliminated the use of the flap actuation disks and (2) verify any resulting weight reduction. Two concepts were developed to a level of detail to allow a selection to be made:

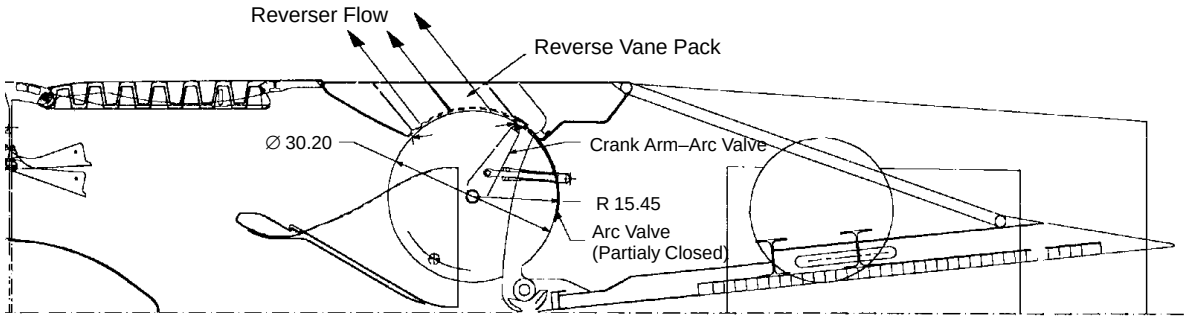

Figure 37. Arc Valve Nozzle Assembly

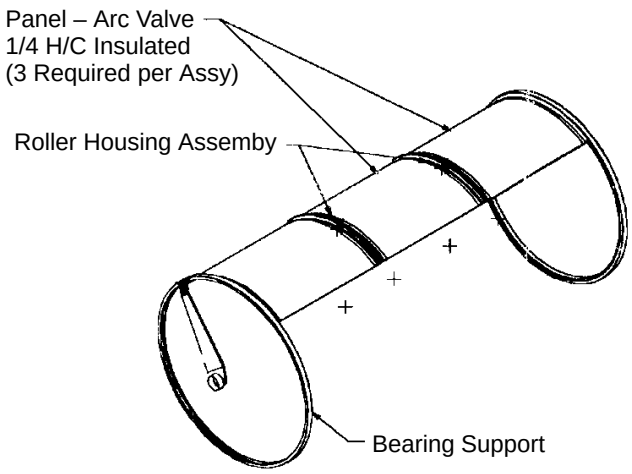

Figure 38. Arc Valve

- Linear Actuation System
- Rotary Actuation System

The functional components of each nozzle were laid out at product size to enable evaluation of ability to meet operational requirements, comparative weights, and reliability/maintainability. The nozzle development guidelines are presented in Table 10. The weight estimates were established for each component based on the results of the structural analyses.

Linear Actuation System

The linear actuation system nozzle concept is defined in Figures 39 and 40, showing the component nomenclature, and Figure 41, illustratuing the four key operating modes.

For the linear actuation system, the convergent flap configuration and actuation system have been changed to reflect a flap mounted to the nozzle structure by a set of links and cranks. The number of linear actuators increased from two to four per nozzle, with the actuators located off the nozzle centerline.

With these changes, the convergent disks have been eliminated, and different kinematics are realized. Likewise, the divergent flap configuration and actuation system have been changed to reflect elimination of the divergent disks, with the divergent flap being directly hinged to and actuated through the external flap. The divergent linear actuators remain at the nozzle centerline.

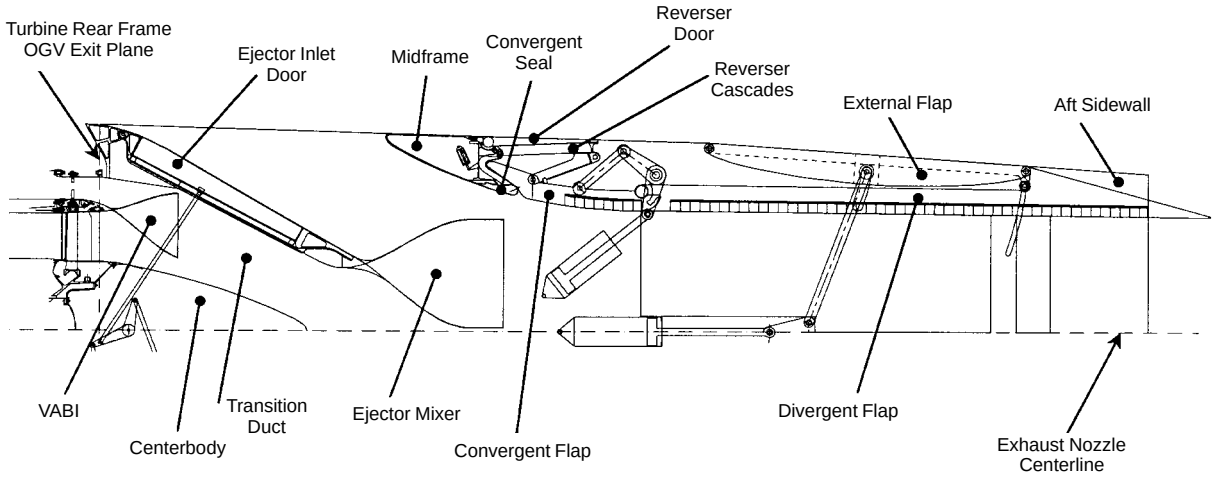

Figure 39. Component Nomenclature for the Alternate Kinematics – Linear Actuation System Nozzle

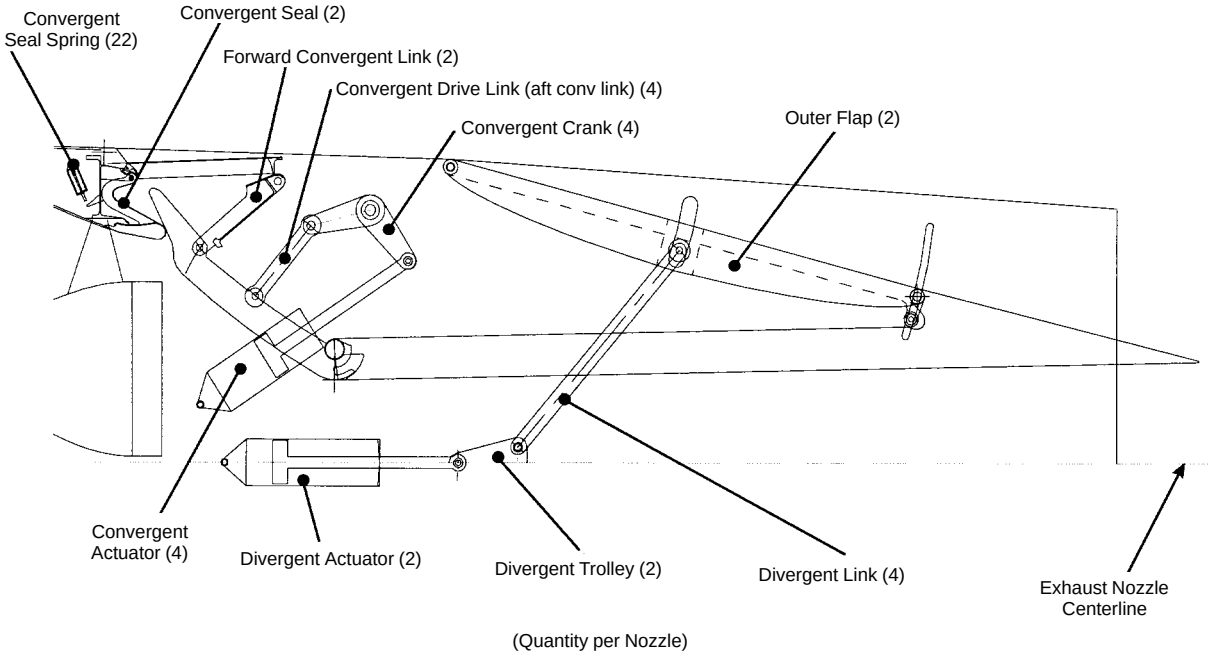

Figure 40. Additional Component Nomenclature for the Alternate Kinematics – Linear Actuation System Nozzle

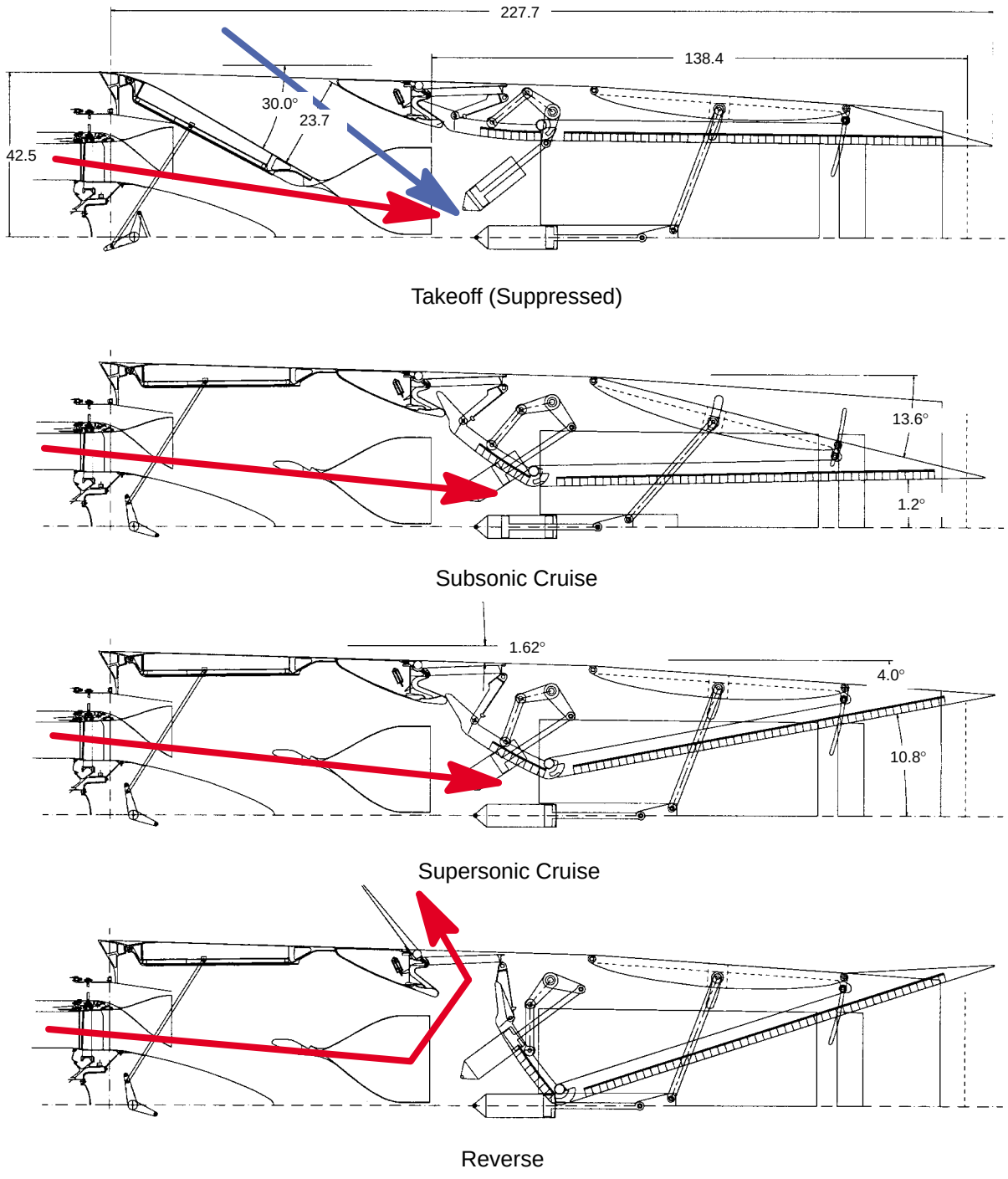

Figure 41. Layout of the Alternate Kinematics – Linear Actuation System Nozzle at Four Flight Conditions

Table 10. Nozzle Development Guidelines for the Alternate Kinematics Nozzles

Criteria	Parameter	Value
Acoustic	SAR	2.9
	Aspect Ratio	1.5
	Amix (in^2)	3570
	MAR	0.95
	Penetration	0.925
	Mixing Length (in.)	135
	$Atrt/A_{mix}$	>60
	Forward-Edge Treatment (in. from Ame)	(5 Hot Lobe Widths)
Aerodynamic	Cycle	3770.60; April 22, 1996
	Flowpath Width (in.)	71.33
	Divergent Flap Length (in.)	116.8
Mechanical	Nacelle Half Height at Nozzle Forwrad Flange (in.)	40.74
	Aft Edge Treatment (in. from Aft End of SW and Divergent Flap	22.5 (SW), 13.0 (Div. Flap)
	Aft OML Boattail Angle at Supersonic Cruise	4° maximum
	Aft OML Boattail Angle at Subsonic Cruise	15° maximum
	Sidewall Boattail Angle	5°
Nozzle System Requirements	Achieve all Mission Points	
	Meet Cycle Areas Kinematically	
	Meet Structural Envelope	
	Be Fail Safe	
	Meet Reversing Flow Area	

This change in the flap train kinematics affects three other aspects of the nozzle configuration. First, it allows a simpler interface between the external flap and the divergent flap at the aft hinge connection. Second, a more complicated sealing configuration is required between the forward edge of the convergent flap and the midframe (that is, the convergent seal). Third, the divergent actuators do not require activation for a refused takeoff (RTO) situation. The linear actuation system concept also reflects a change to the ejector inlet door configurations and actuation systems. The number of doors has been reduced from two to one door per ejector inlet (a reduction in total of four to two ejector inlet doors per nozzle). Along with this change, the number of actuators reduced from eight linear actuators per nozzle to two rotary actuators and one power drive unit per nozzle.

It should be noted that this change to the ejector inlet door configurations and actuation systems could also be incorporated into other derivatives of FCN–SRP concept and therefore is not solely dependent on the linear actuation system concept.

The characteristics, operation, and remaining features of the linear actuation system nozzle are the same as described previously for the FCN–SRP concept.

Rotary Actuation System

An attempt to reduce the weight of the baseline disk-driven HSCT nozzle resulted in consideration of an alternate nozzle structure, flap train, and flap support and actuation system. This system (Figure 42) uses rotary actuators instead of traditional linear actuators to move the flap train and,

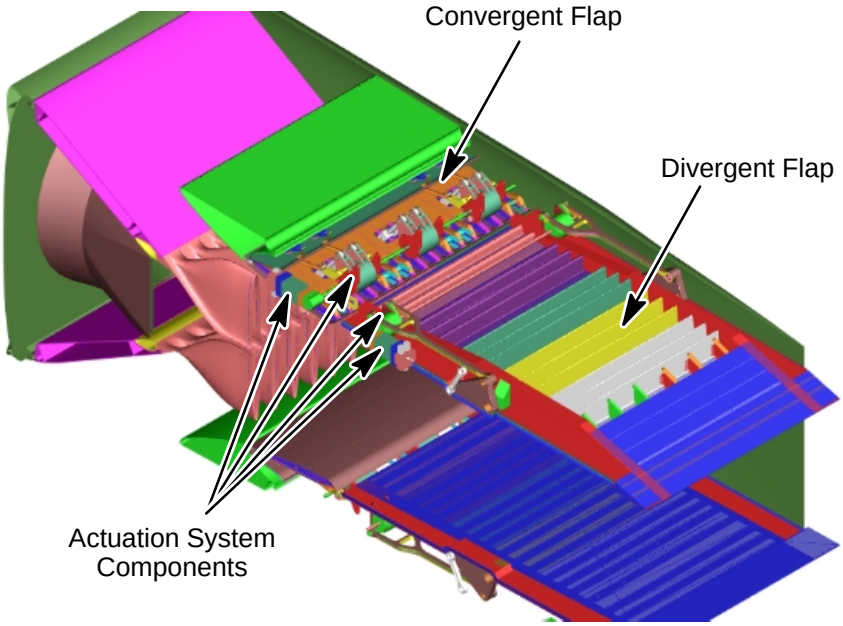

Figure 42. Rotary Actuated 2D/CD Nozzle

in an effort to improve the structural efficiency of flap and sidewall structures, locates these actuators in unused nozzle cavities instead of inside the structures.

Additionally, a more complex flap drive mechanism was developed in an effort to reduce the hydraulic power demands associated with operating the HSCT baseline nozzle.

Although significantly reducing weight and hydraulic demand of the baseline nozzle, this concept was dismissed in favor of the linear actuation system. The linear actuation system was selected as the "going forward" concept and presented at the CPC conceptual design review held June 2–3, 1999 at NASA Lewis.

5.3 Nozzle Selection Process

5.3.1 December 1994 Propulsion Downselect

The objective of the December 1994 propulsion downselect was to identify an exhaust nozzle concept that offered a combination of high performance and confidence in achieving this performance. High acoustic performance was needed to meet noise goals, and high aerodynamic performance was needed to assure economic viability (fuel costs). Along with high performance, it was desired that nozzle weight be minimized by the use of advanced materials being developed under the Enabling Propulsion Materials (EPM) program. High confidence was also desired in the manufacturability of these EPM's and in the accuracy of noise-suppression prediction methods.

Nozzle layout groundrules for these concepts are listed in Table 11. Four nozzle concepts were defined to meet the goals:

- Downstream mixer (DSM)
- Two-dimensional fixed chute (2DFC)
- Fluid shield
- Axisymmetric coannular ejector (ACE)

Table 11. Nozzle Layout Groundrules for December 1994 Nozzles

Parameter		Goal
Acoustics		FAR 36 Stage III Noise at Sideline and Community
Performance	Takeoff Subsonic Cruise Supersonic Cruise	C_{fg} = 0.950 C_{fg} = 0.982 C_{fg} = 0.982 at Supersonic Cruise
Manufacturing		Use Advanced Techniques and State-of-the-Art Materials
Maintainability, Reliability, and Supportability		Similar to Current Commercial Aircraft
Life		35,000 Hours and 9000 Cycles

The nozzle ITD concluded that 2D nozzles offer the best chance of meeting noise and performance goals. This conclusion was based on axisymmetrical nozzle test data from previous programs that suggested no advantages from an aerodynamic or acoustic perspective over 2D geometry. This eliminated both the fluid shield and the ACE nozzle from consideration.

Earlier evaluations also concluded that, to meet mechanical life criteria, the mixer/ejector must be retrieved and sheltered from high temperatures during the supercruise portion of the mission. This evaluation resulted in the choice of the DSM nozzle — for which the mixer was designed to be movable, rotating into the flow at takeoff and retrieved and stowed during supercruise.

5.3.2 Final Exhaust Nozzle Downselect (1995)

Because of the complexity of the original DSM and Best DSM nozzles, the HSCT nozzle team decided that studies of alternate nozzle concepts should be performed. This effort was referred to as the *Alternate Nozzle* study, with the objective of defining a less complex nozzle configuration with increased performance in terms of aerodynamics, acoustics, and airframe system integration. The resulting nozzle concept would then be considered the baseline for ongoing development of the Demo and full-scale product nozzles. Four concepts were developed to the level of detail necessary to allow a selection to be made.:

- Axi-Tilt Chute (ATC)
- Best DSM
- Fixed-Chute, No-Plug (FNP)
- Variable Axi-Mixer (VAM)

The selection criterion were that the nozzle provide undisputed, significant advantages to the HSCT program in the areas of system weight, system performance, mechanical simplicity, and acoustic risk. The nozzle development guidelines are listed in Table 12.

Table 12. Nozzle Development Guidelines for the Alternate Nozzle Concept Studies

Criteria	Parameter	Axi-Tilt Chute (ATC)	Best DSM	Fixed Chute No-Plug (FNP)	Variable Axi-Mixer (VAM)
Acoustic	SAR	2.7	2.5	2.5	2.2
Aerodynamic	Cycle	3765	3765	3765	3765
	A_8 at Takeoff (in^2)	1431	1431	1431	1431
	Minimum Divergent Flap Length (in)	90	100	100	90

The selected nozzle concept was to be demonstrated behind a F414–GE–100 engine at cruise and takeoff conditions. Selection of this demonstrator nozzle concept was based on three tollgate reviews (Figure 43) involving evaluation of the four alternate nozzle concepts and the DSM rotating-chute nozzle concept defined in Subsection 5.2.5.2. The demonstrator nozzle was to be fully functional and flight-like but not flight-weight. Additionally, a set of performance nozzles was included in the evaluation process to assess the airframe weight penalty associated with meeting noise goals; these represented the highest performance nozzles that could be achieved without design considerations or features for noise reduction.

The nozzle design tollgate reviews were conducted to evaluate the effects on the airplane TOGW due to aerodynamic performance, acoustics, weight, and drag of the different nozzle configurations. A mechanical “Red Team Review” of the development risk of the concepts was also conducted based on the P&W and GEAE experience with nozzle demonstrator programs.

Based on the three tollgate reviews and the Red Team review, a nozzle downselect was made in August 1995. The Red Team’s recommendation of the FNP nozzle was chosen as the downselected concept.

5.3.3 Tollgates 1, 2, and 3

The tollgates (Figure 43) used information from the nozzle data packs and airplane system studies to select a concept for demonstration on an F414 engine. Nozzle data packs provided geometry, weight, center of gravity, thrust coefficient, and engine cycle parameters such as thrust. System studies provided engine and nozzle sizing and airplane TOGW to meet the noise and mission goals. For Tollgate 1, data were developed for the performance, DSM sliding-chute, and DSM rotating-chute nozzles. For Tollgate 2, data were evaluated for the four alternate nozzle concepts. For Tollgate 3, data from three of the Tollgate 2 nozzles and the DSM rotating chute nozzle were updated and refined to perform more rigorous system studies for selection of the demonstrator nozzle.

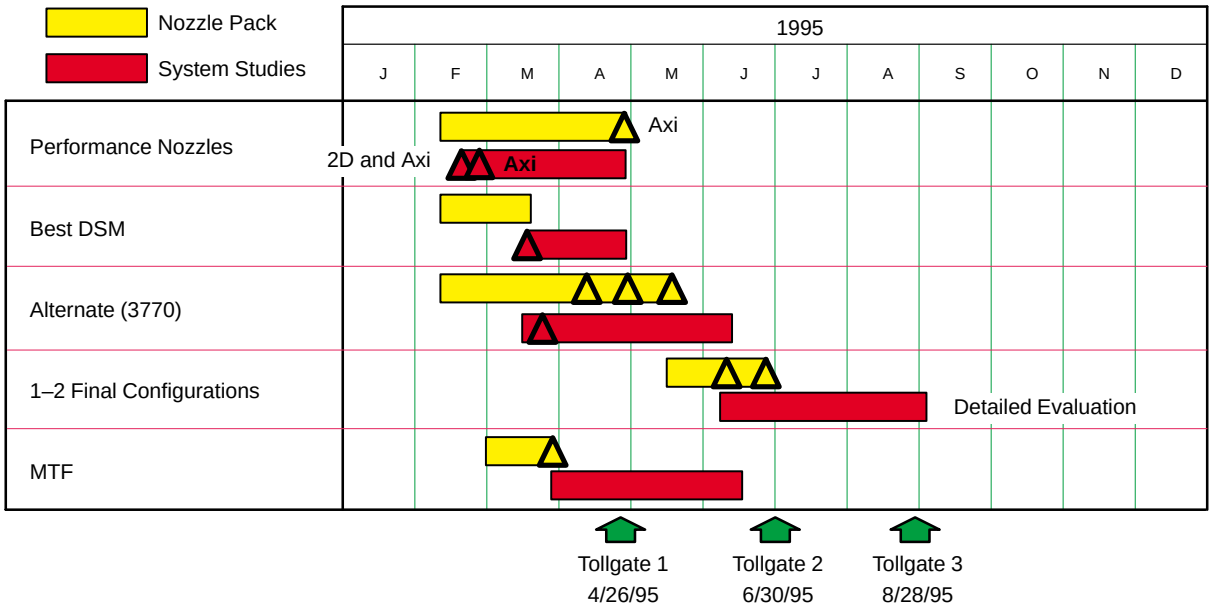

Figure 43. Tollgates for Nozzle Review

5.3.3.1 Tollgate 1

Objectives for Tollgate 1 were to:

1. Provide updated weight estimates for the Boeing and Douglas baseline airplanes with an improved DSM nozzle (the DSM sliding-chute and the DSM rotating-chute concepts) to determine whether or not work on the DSM nozzle should continue.
2. Estimate the weight of baseline airplanes with performance nozzles that are not noise constrained, thereby establishing the weight penalty associated with meeting noise goals.
3. Identify alternate nozzle and cycle concepts that have potential for further reducing TOGW for noise-constrained airplane concepts.

Example geometries for the axi and 2D configurations are illustrated in Figures 44 and 45, and Table 13 is a summary of the performance nozzles design parameters.

Table 13. Performance Nozzle Summary

Nozzle	Divergent Flap Length, in	Weight, lbm	Center of Gravity, in	Overall* Length, in	Boattail Angle at Supercruise (°)	Coefficient of Gross Thrust (C_{fg})	
						Takeoff	Supercruise
Axi 3770 w/o rev	100	2325	62	143	0.0	0.974	0.980
3770	100	3185	70	166	0.0	0.974	0.980
3770 w/o rev	110	2432	66	153	0.0	0.972	0.981
3770	110	3391	74	176	0.0	0.972	0.981
3770 w/o rev	123.6	2852	72	167	0.0	0.968	0.981
3770	123.6	3711	80	190	0.0	0.968	0.981
Axi 3270 w/o rev	113.59	2511	69	163	0.9	0.961	0.982
3270	113.59	3532	70	189	0.9	0.961	0.982
3270 w/o rev	124.59	2732	73	175	0.9	0.957	0.982
3270	124.59	3753	75	201	0.9	0.957	0.982
3270 w/o rev	140.40	3072	80	190	0.8	0.948	0.983
3270	140.40	4093	82	216	0.8	0.948	0.983
Axi 2970 w/o rev	122.14	2743	72	176	1.7	0.937	0.982
2970	122.14	3714	72	204	1.7	0.937	0.982
2970 w/o rev	134.35	2988	77	188	1.5	0.931	0.983
2970	134.35	3938	78	216	1.5	0.931	0.983
2970 w/o rev	150.97	3147	85	205	1.3	0.917	0.983
2970	150.97	4280	85	233	1.3	0.917	0.983
Axi 4370 w/o rev	84	1923	55	121	0.0	0.981	0.98
4370	84	2556	62	141	0.0	0.981	0.98
0.0	92.4	2038	58	129	0.0	0.979	0.981
0.0	92.4	2672	65	149	0.0	0.979	0.981
4370 w/o rev	103.8	2285	64	141	0.0	0.976	0.982
4370	103.8	2919	70	161	0.0	0.976	0.982
2D 3770	100	3080	73	184	0.0	0.977	0.977
3770	110	3270	77	194	0.0	0.971	0.987
3770	123.6	3510	82	198	0.0	0.965	0.980
* Measured from the trailing edge of the turbine frame outlet guide vane to the end of the divergent flap.							

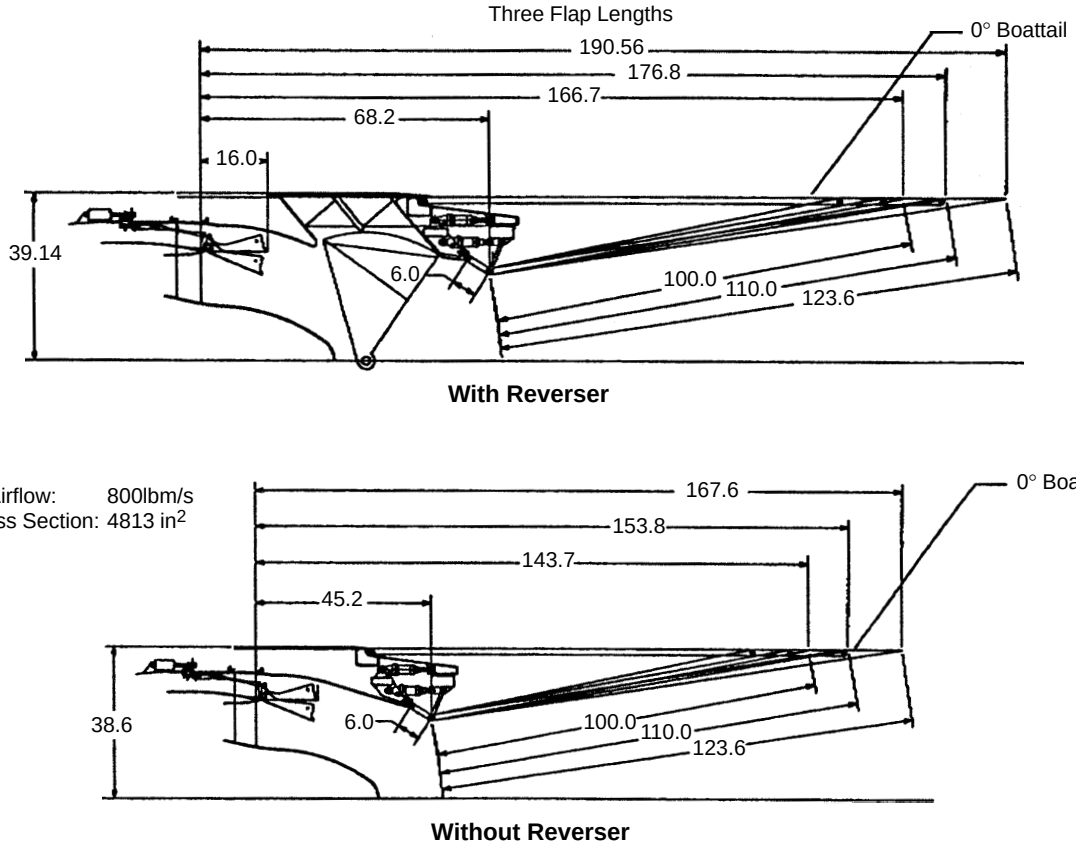

Figure 44. Performance Nozzle Geometry: 3770.100 Axi

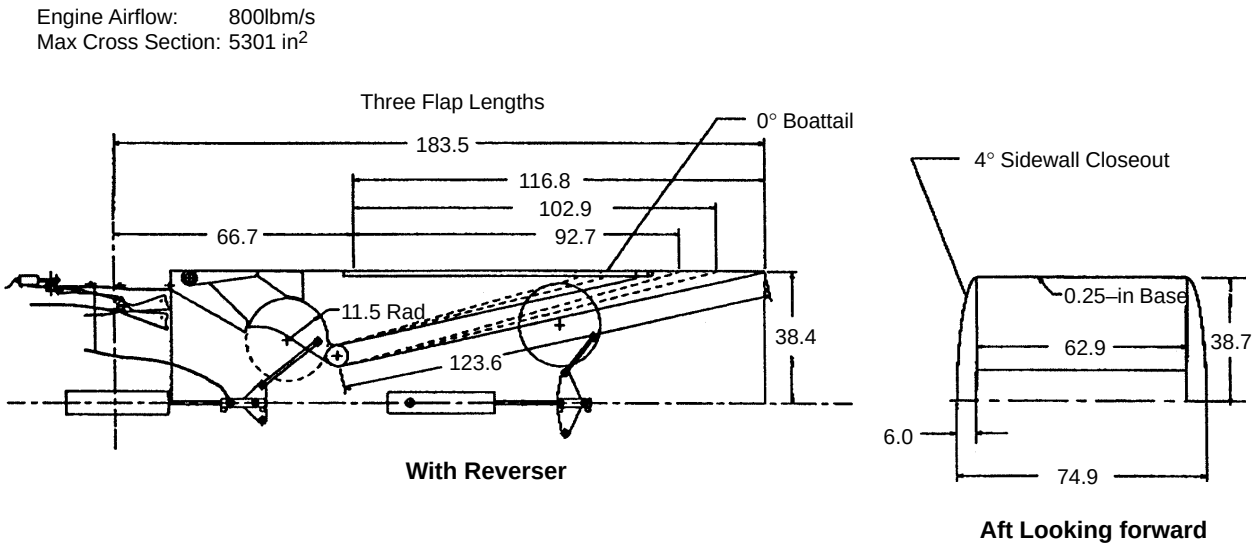

Figure 45. Performance Nozzle Geometry: 3770.100 2D

A summary of the DSM nozzle design parameters is given in Table 14. Example geometries for the sliding chute and rotating chute are presented in Figures 46 and 47.

Table 14. MFTF 3770.100 DSM Nozzle: Comparison Summary

Data Pack Release Date		March '95	Sept '94
Nozzle Type		Sliding Chute DSM–2D	Rotating Chute DSM–2D
Suppression	SAR, Acoustic Liner (L/D)	2.5, 1.0	2.82, 1.51
	W_s/W_p	0.566	0.717
	V_{exit}, ft/s	1679	1550
Envelope	Maximum Uninstalled Cross-Sectional Area, in^2	5804 (–9.5%)	6355
	Nozzle Length, in.	197.5	218.3 (with 16 in fan/ core mixer)
	Nozzle Weight (lbm) and CG (in)	5524, 82.3	5990, 88.3
Aerodynamic Performance	*C_{fn}, Sideline Noise Condition (M0.32/36,089-ft/60% Power)	0.928 (–4.2 %)	0.969
	C_{fg}, Subsonic Cruise (M0.9/36,089-ft/60% Power)	0.9838	0.9766
	C_{fg}, Transonic Accel (M1.1/30,000-ft/100% Power)	0.9856	0.9816
	C_{fg}, Supersonic TOC (M2.4/55,000-ft /100% Power)	0.9819	0.9816
Equivalent Conical Boattail Angle		20.9°	2.7°
* Coefficient of Net Thrust: $C_{fn} = (F_g$ – Ram Drag) / F_{idp}			

The Boeing airframe study results for the performance and rotating chute DSM are compared in Figure 48. For the performance nozzles, the axi results in lower TOGW than the 2D. Also, the short flap results in a lighter TOGW than the long flap. The DSM rotating chute results in the heaviest system TOGW. Figure 49 shows updated TOGW values for the rotating-chute concept as well as for the status DSM sliding-chute concept.

The conclusion of this tollgate was that work should continue on the DSM sliding-chute nozzle as planned through Tollgate 2. This included the best DSM F414 size demo nozzle preliminary design work under the CPC program. Also, the DSM sliding-chute nozzle had a 10 to 15% TOGW penalty relative to the performance nozzles (to meet noise goals). Finally, the tollgate evaluations were continued including alternate engine cycles and nozzles.

5.3.3.2 Tollgate 2

For Tollgate 2, nozzle design and engine cycle data were made available for airplane system evaluation. The nozzles included the four CPC alternate nozzle concepts, designated as the Best DSM, ATC, FNP, and VAM concepts. The geometric characteristics of these four nozzles are given in Table 15 and the installed performance in Table 16. A comparison of the resulting mission and noise sized airplane TOGW is presented in Figure 50. The Best DSM, FNP, and ATC were the three nozzles that resulted in the lowest TOGW airplanes and were therefore selected for continued design evaluation for downselect in Tollgate 3.

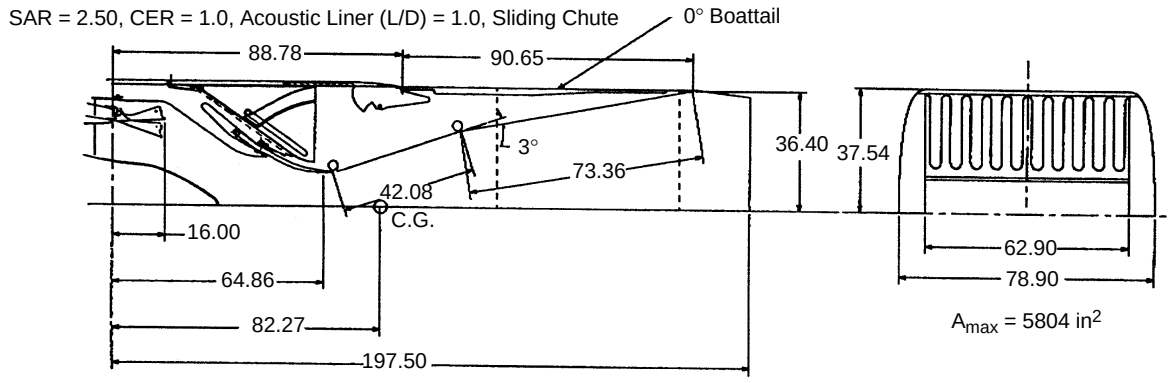

Figure 46. MFTF3770.100 DSM Sliding Chute Nozzle Geometry

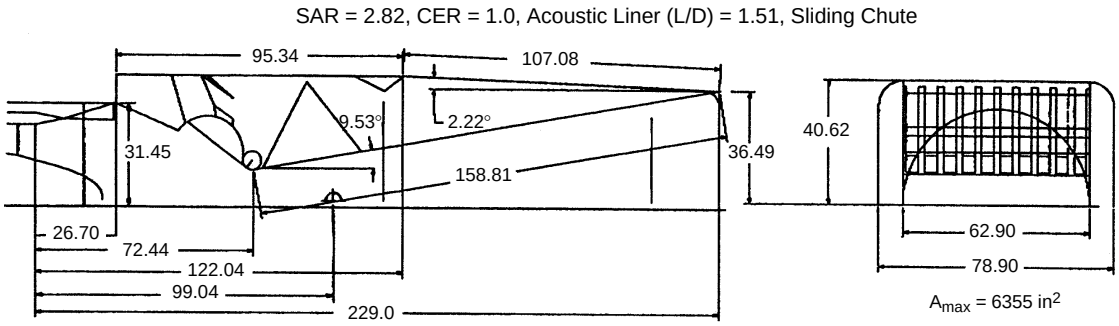

Figure 47. MFTF3770.100 DSM Rotating Chute Nozzle Geometry

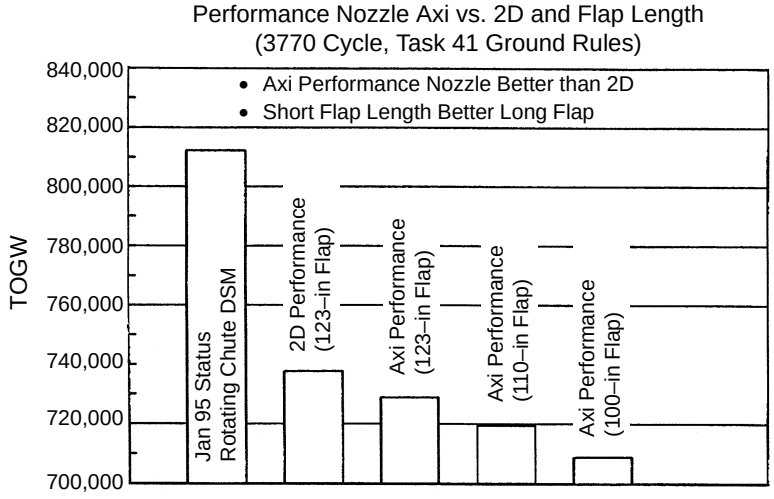

Figure 48. Boeing Airframe Systems Study Results

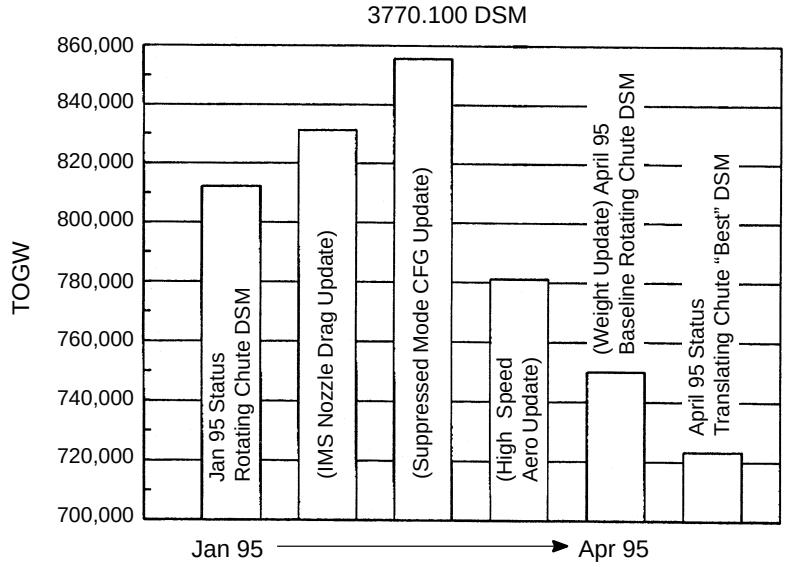

Figure 49. Boeing Airframe Systems Study Evolution

Table 15. Geometric Characteristics of CPC Alternate Nozzles

Best Downstream Mixers (BSDM)	2D Mixer/Ejector	2.5 SAR
	Sliding Chute	Variable A_8
Fixed Chute, No Plug (FNP)	2D Mixer/Ejector	2.5 SAR
	Fixed Chute	Fixed A_8
Axi Tilt Chute (ATC)	Axi Mixer/Ejector	2.7 SAR
	Fixed Chute	Fixed A_8
Variable-Area Mixer (VAM)	Axi Mixer/Ejector	2.1 SAR
	Fixed Chute	Variable A_8
	Secondary Flow Pressurized with Additional Turbomachinery	

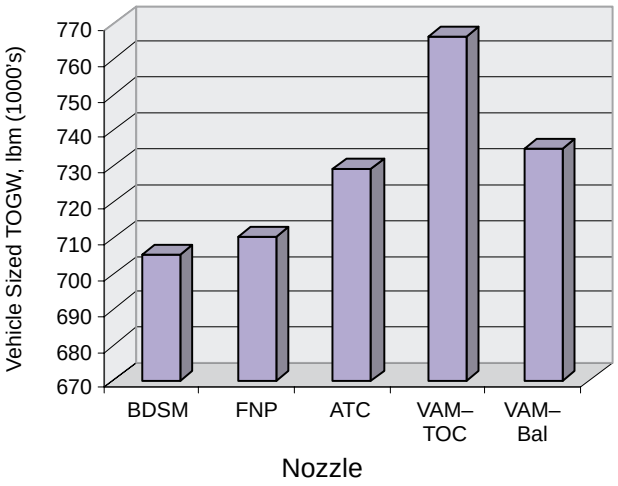

Figure 50. Comparison of Aircraft TOGW for Alternate Nozzles

Table 16. Comparison of Nozzle Installed Performance

Nozzle	BDSM	FNP	ATC	VAM or PN	VAM or PN*
Weight, lbm	6171	6200	5800	6600	6900
Length, in	208	21	219	258	258
Cruise C_{fg}	0.983	0.98	0.979	0.978	0.978
Cruise Installed SFC	1.240	1.251	1.261	1.261	1.272
Subsonic Installed SFC	0.90	0.90	0.915	0.94	0.93
% Transonic Boattail Drag	12	10	13	16	16
Sized TOGW, lbm (1000's)	705	710	729	766	735
* Updated Ref. H Interim Baseline = TOC thrust adjusted to "3768"					

5.3.3.3 Tollgate 3

At Tollgate 3, selection was made of the nozzle for the Technology Integration airplane. The candidate nozzles were the Best DSM, FNP and ATC (described in the Tollgate 2 discussion) along with the DSM rotating-chute nozzle. Five teams reviewed the candidate nozzle designs and installed system performance. The five teams, along with their major areas of concern, were as follows:

1. Red Team (see Subsection 5.3.4) – Relative development risk
2. Propulsion System Evaluation Team (PSET) – Mission takeoff gross weight (MTOGW)
3. Acoustic Team – Chute shaping flexibility, acoustic treatment area, A_8 at cutback, and aspect ratio
4. Aerodynamic Team – Chute shaping, ejector inlet design, chute stowability, takeoff C_{fg}, and cruise C_{fg}
5. Mechanical Design Team – Funtionality, weight, and life

The Red team identified two serious problems associated with the DSM sliding-chute concept:

1. A_8 throat at transition
2. A_{jet} control during cruise mode

Red Team overall recommendations were:

1. Cool all hot parts upstream of the throat
2. Downselect to the FNP nozzle

The PSET team concluded that differences in MTOGW among the concepts was within the inaccuracy of their estimate. Thus no nozzle could be deemed the clear winner from a systems perspective.

The Acoustic team's order of preference (most preferred ⧫ least preferred) was: Best DSM ⧫ FNP ⧫ DSM Rotating Chute.

The Aero team preference was: DSM Sliding Chute and the DSM Rotating Chute.

The ITD team agreed with the Red Team's assessment of the potential problems associated with the DSM Sliding Chute (the Best DSM) nozzle.

Since there were no overriding concerns from the other groups involved, the nozzle ITD team decided to recommend the fixed-chute, no-plug (FNP) as the downselected concept.

5.3.4 Mechanical Red Team Review

The Mechanical Red Team comprised a group of six experienced (over 150 years collectively) mechanical designers, three from P&W and three from GEAE. They were tasked by the Nozzle ITD team to evaluate the relative development risk of three nozzle concepts (DSM sliding chute, DSM rotating chute, and FNP) based on their experience with nozzle demonstrator programs. The objectives were to (1) identify any high-risk development features on each concept and (2) rank the concepts by development risk.

The mechanical scoring criteria developed by the designers for the three concepts are presented in Table 17. The level of development risk is given for each concept, with 0 denoting that the risk for a particular criteria is not an issue ranging to 12 being a potential showstopper.

Table 17. Mechanical Scoring Criteria

0: Not an Issue 4: Issue 8: Significant Issue 12: Potential Show Stopper			
Criteria	**Fixed Chute**	**Rotating Chute**	**Sliding Chute**
A_8 Throat at Transition	7	5	11
Control Complexity	4	7	9
Actuators	3	7	9
Thermal Distortion	5	9	4
Sidewall Distortion	6	8	8
Leakage	6	7	9
A_{jet} Control and P_S	5	3	12
Cam Slot Wear/Bind	6	4	9
Cooling Complexity	6	5	8
Total	**48**	**55**	**78**

Examination of the risk levels shows that the DSM sliding chute had two potential showstoppers: (1) A_8 (nozzle throat area) at transition and (2) A_{jet} control and P_S (during cruise mode only). Risk concerns and recommendations for the fixed-chute concept are:

- Concerns
  - Creep/distortion and cooling-air trades on the chutes
  - Large internal volume with high temperatures
  - Difficult to bring cooling air into current convergent-flap configuration
- Recommendations
  - Consider STOL and maneuvering demonstrator (S/MTD) approach to convergent-flap design
  - Change double door to single (slave) door

Risk concerns for the rotating-chute concept are:

- Concerns
  - Prone to chute leakage
  - Most difficult concept in terms of chute cooling
  - Hot actuators on divergent flap and use of flex lines
- Recommendations
  - Define cooling scheme for chutes
  - Conduct finite-element analyses of chutes for temperature/pressure loads
  - Define alternate chute-actuation system (obviate hot actuators and flex lines

General comments for all designs are:

- Demonstration should include provisions for actively cooling hot parts forward of the throat:
  - Reduce risk from engine temperature distortions and thermal transients
  - Help control warpage and deflection problems
- Long, unsupported sidewall is undesirable — major problem seen with divergent-flap-to-sidewall attachments (rollers, seals, pin connections).
- Demo schedule considered feasible if the mechanism is in place to make decisions quickly.
- Weight containment will be a threat to product development schedule but not demo nozzle schedule.
- Shifting of throat location during suppressed/unsuppressed transition is a potential trouble area.
- Will everything fit in sidewalls while maintaining structural integrity?

Finally, the Red Team recommended that the downselect be made to the fixed-chute nozzle because of lower overall mechanical risk. However, a recommendation was also made to make a backup, parallel design effort on the rotating-chute nozzle to reduce the noted significant risk of leakage and distortion and to move the rotating chutes upstream of the nozzle throat if dictated by thrust performance.

5.3.5 Results

Based on the absence of overriding concerns from the PSET, Aero, and Acoustics groups, the nozzle ITD team decided to go with the Red Team recommendation of the FNP concept downselect.

5.4 Fixed-Chute Nozzle Flowpath Description

The HSCT exhaust system is a variable-geometry, two-dimensional, converging/diverging nozzle that is capable of operating in three steady-state modes: (1) noise-suppression mode for takeoff and approach, (2) cruise mode for normal forward-thrust operation over most of the flight regime, and

(3) reverse-thrust mode. An isometric cutaway view of the exhaust system is shown in Figure 51 in the noise-suppression mode, and buttline cross sections of all three modes are shown in Figure 52. The exhaust system flowpath is completely symmetrical about the horizontal and vertical centerlines, thus only half of the nozzle is shown in most cross sections. In this program, the weight of an engine fan/core mixer component was book-kept in the weight of the exhaust system, and design and analysis for that component were performed as part of the exhaust. Detailed descriptions of the exhaust system flowpath follow.

5.4.1 Fan/Core Mixer

A side view, end view, and isometric view of the fan/core mixer are shown in Figures 53, 54, and 55 respectively. The mixer is a fixed-geometry design with deep lobes to mix the fan and core engine gas streams effectively. The key aerodynamic goals of this component are a high level of mixing effectiveness at cruise (80% or greater) with minimal pressure loss while matching the engine cycle bypass ratio requirements. The mixing would not only improve cruise specific fuel consumption (SFC) but would also reduce flow nonuniformities within the ejector mixer which would in turn reduce thermal gradients in the mixer walls for mechanical design considerations and reduce noise by eliminating/reducing local high-velocity streaks.

5.4.2 Suppressed-Mode Operation

A side view of the exhaust system in the noise suppression mode is shown in Figure 56. In this mode, the prime function of the nozzle is to use a 2D lobed ejector mixer to efficiently entrain ambient air and mix it with the hot engine gas stream to reduce external jet noise during takeoff.

Transition of the axisymmetric engine flowpath to the 2D nozzle occurs in the transition duct (T-duct) shown in more detail in Figure 57. The T-duct consists of flat, D-shaped sidewalls that diverge from the fan/core mixer exit to the nozzle maximum internal width, and flat top and bottom surfaces that converge to the acoustic mixer. The flat top and bottom surfaces are formed by doors that rotate outward to close the secondary air inlet for cruise operation. The four “corners” of the T-duct are composed of circular arcs connecting the flat side and top portions.

The acoustic mixer consists of a series of convoluted lobes aerodynamically shaped to efficiently entrain secondary air for acoustic mixing. End and side views of the lobes are shown in Figure 58 for clarity. There are 20 lobes, 10 each on the top and bottom halves of the nozzle. The lobes are shaped to avoid any flow separation on either the engine or secondary air side and to discharge both streams in a near-axial direction. The flow area on the engine side of the lobes remains nearly constant, maintaining a Mach number of about 0.5 until near the end of the lobes where there is an area contraction to the throat, or minimum area. This throat occurs upstream of the exit of the mixer, and the area from this station to the exit of the mixer diverges to provide a small area ratio within the lobes ($A_{exit}/A_{throat} \simeq 1.05$). This divergence occurs in the shaping of the mixer walls in the horizontal plane. Therefore, during the suppressed mode, the ejector mixer forms a constant-area throat for all engine power settings. Three turning vanes are included in each lobe on the secondary side to provide structural rigidity and retain mixer shape and flow area in the noise-suppression mode. The vanes are intentionally aligned with the secondary flow streamlines to make them nonintrusive to the normal flowfield (without the vanes) to minimize any aerodynamic pressure loss. The leading edges are elliptical to provide robustness for any variation in the incoming-flow angle of attack as engine power setting and aircraft Mach number change in the suppressed mode. The flow

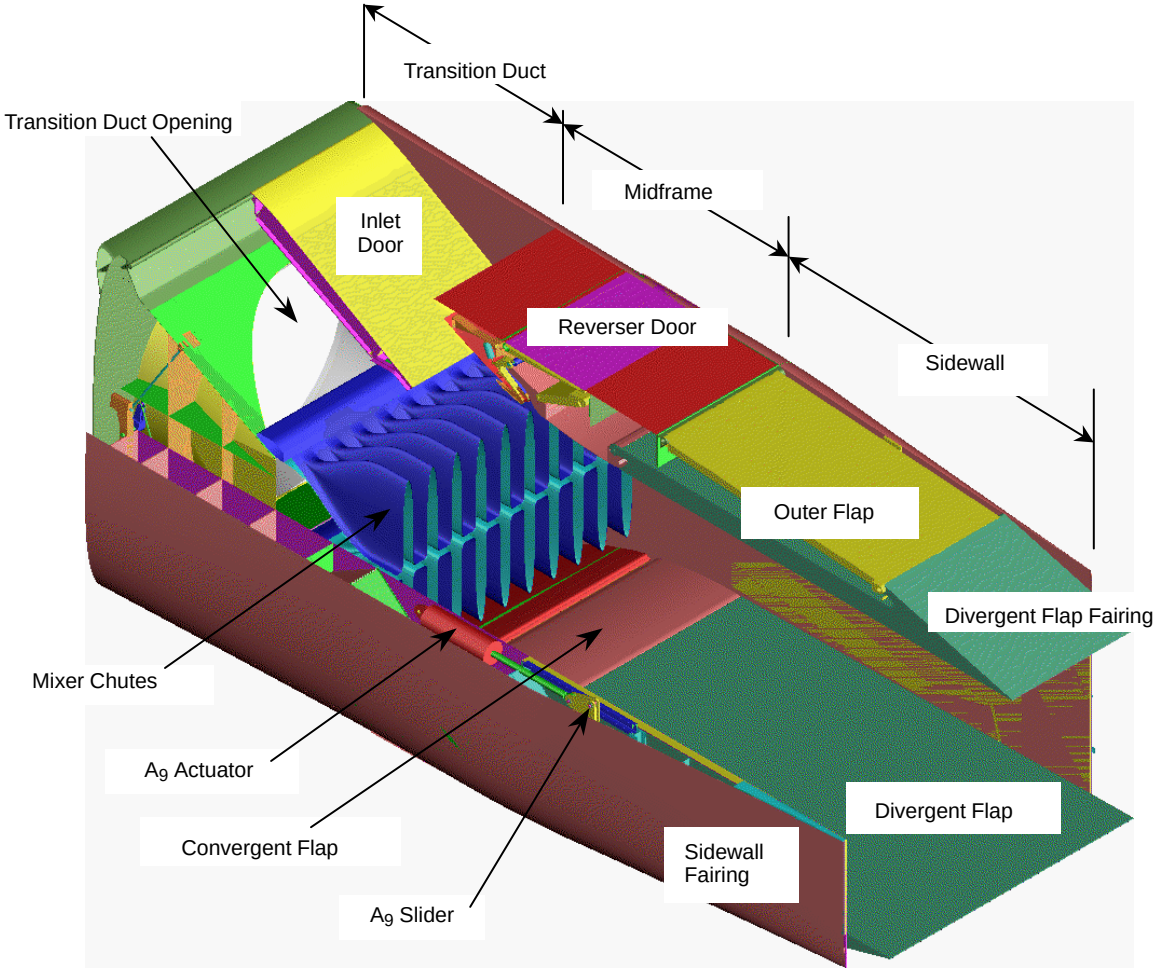

Figure 51. Isometric Cutaway View, Noise-Suppression Mode

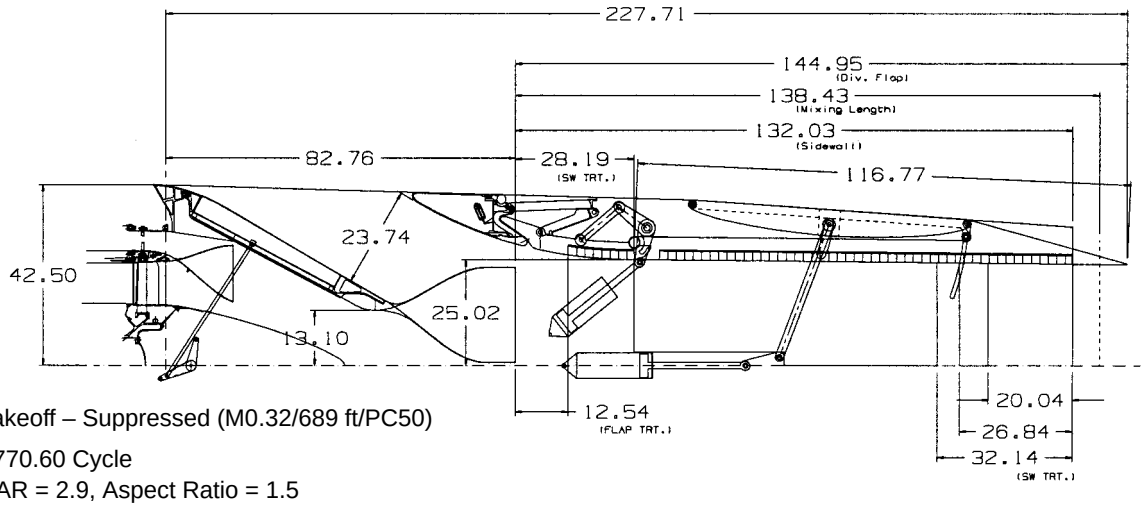

Takeoff – Suppressed (M0.32/689 ft/PC50)

3770.60 Cycle
SAR = 2.9, Aspect Ratio = 1.5
MAR = 0.95, Width = 71.33 in (Flowpath)
A_8 = 1230.6 in^2

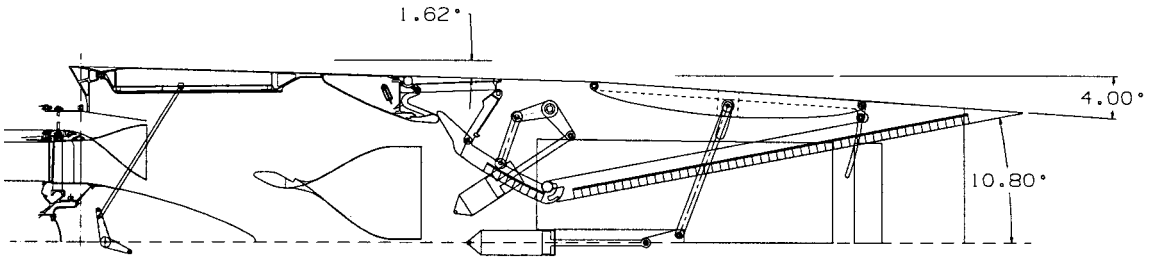

Supersonic Cruise (M2.4/55,000 ft/PC50)

3770.60 Cycle
SAR = 2.9, Aspect Ratio = 1.5
Width = 71.33 in (Flowpath)
A_8 = 1360.8 in^2, A_9 = 4487.1 in^2

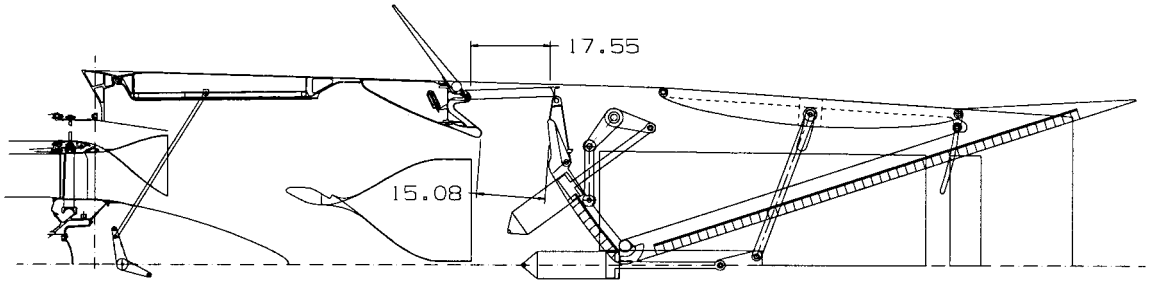

Reverse (M0.2/0 ft)

3770.60 Cycle
SAR = 2.9, Aspect Ratio = 1.5
Width = 71.33 in (Flowpath)

Figure 52. Buttline Cross Sections of Nozzle in Three Operating Modes

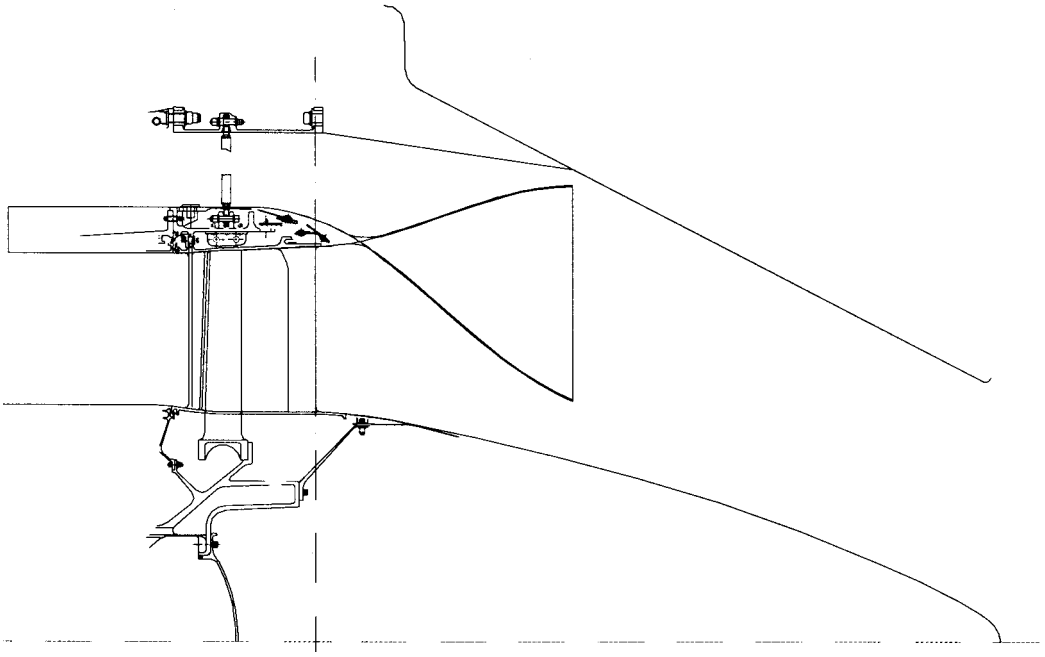

Figure 53. Fan/Core Mixer Side View (Buttline Cross Section)

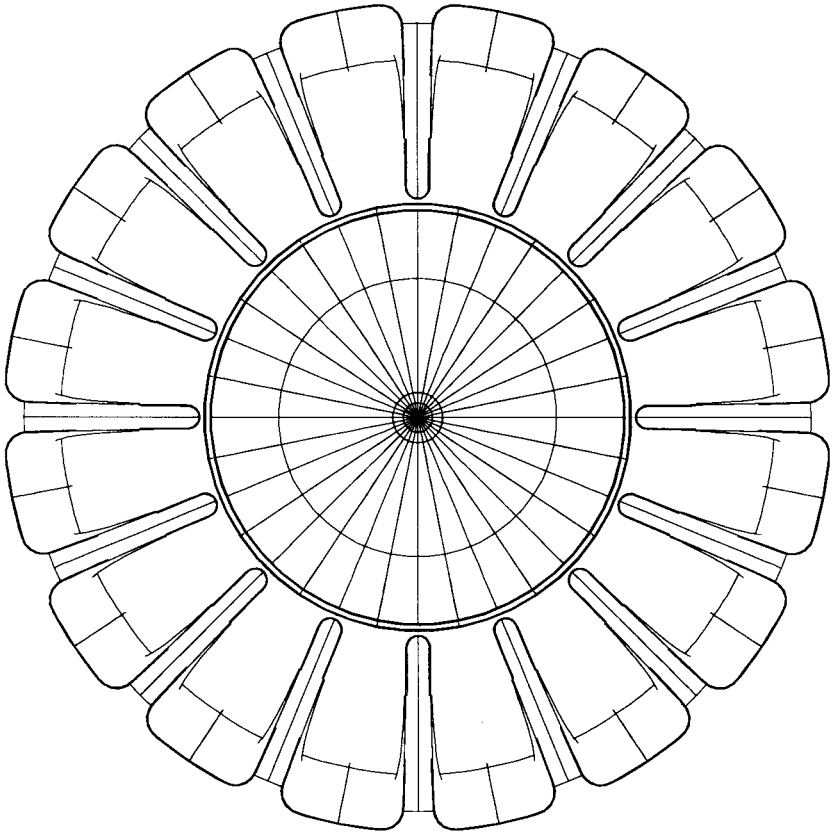

Figure 54. Fan/Core Mixer End View, Aft Looking Forward

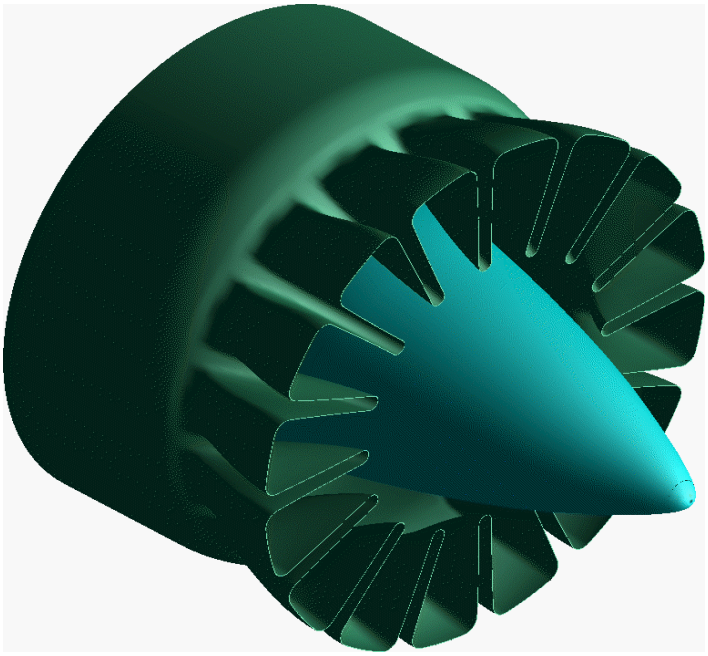

Figure 55. Fan/Core Mixer Isometric View, Aft Looking Forward

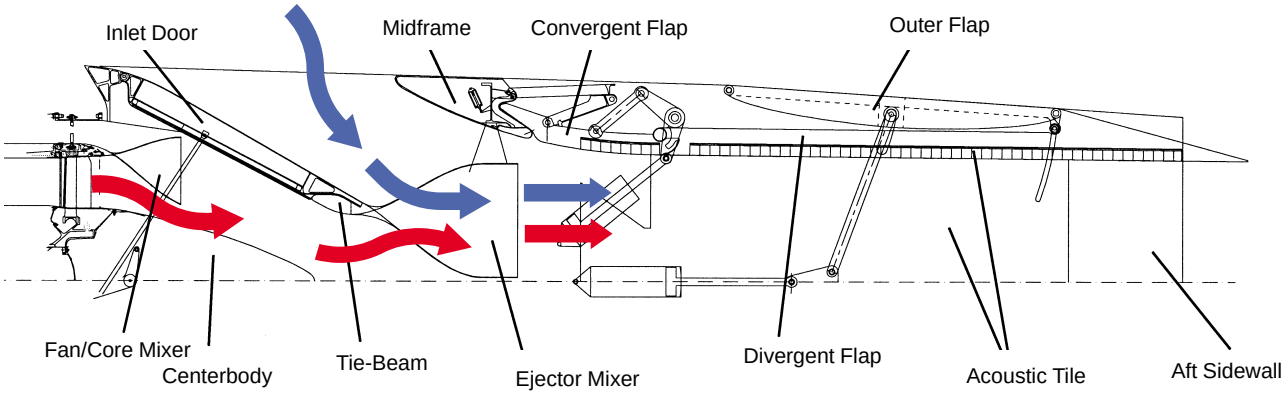

Figure 56. Nozzle in Noise-Suppression Mode

Noise-Suppression Mode

Forward Looking Aft

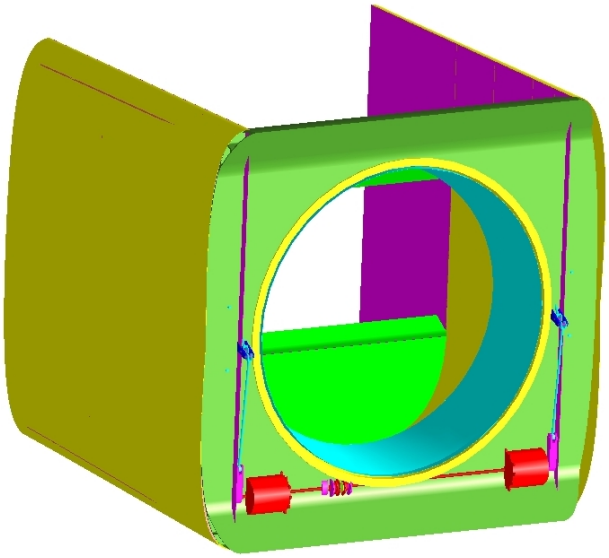

Aft Looking Forward

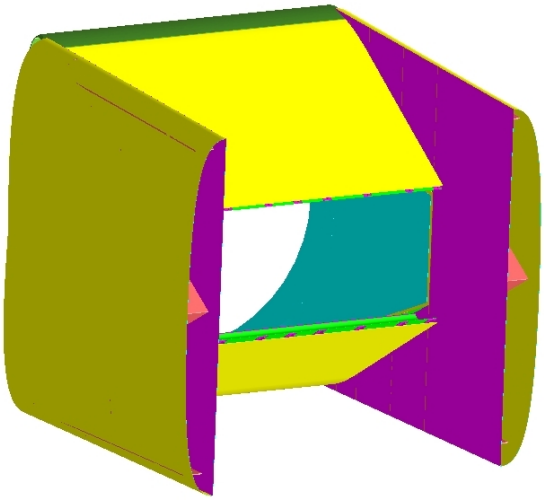

Cruise Mode

Forward Looking Aft

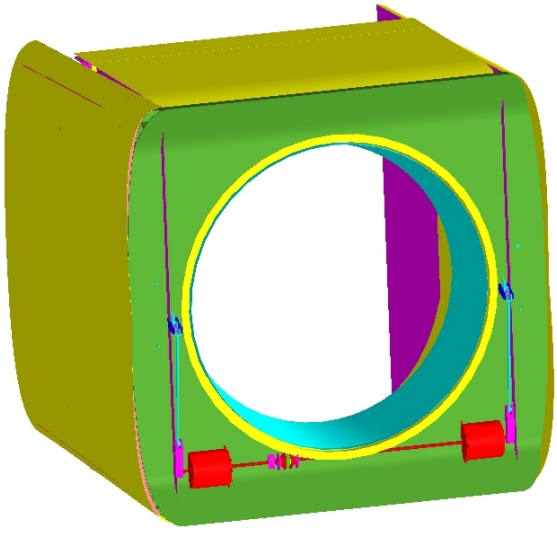

Aft Looking Forward

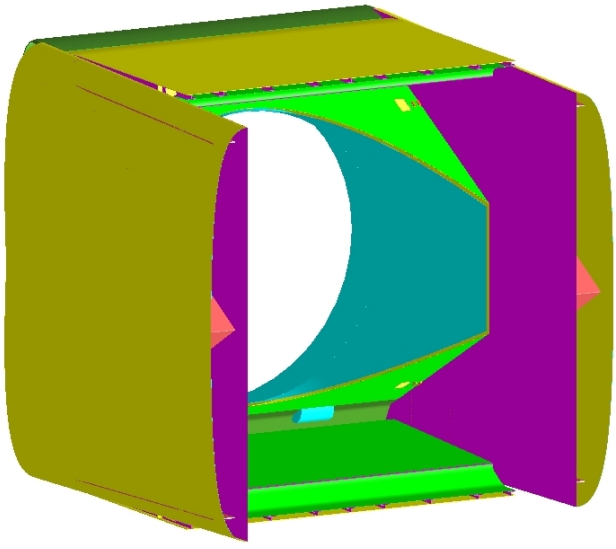

Figure 57. Transition Duct

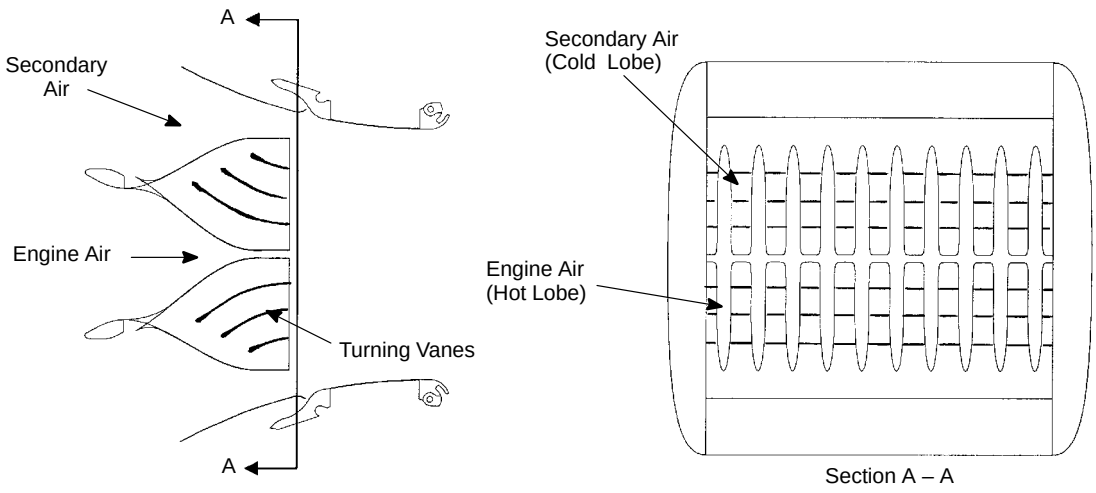

Figure 58. Ejector/Mixer

area on the secondary side contracts through the mixer from a Mach number of about 0.3 at the forward end to about 0.5 at the mixer exit.

The secondary inlet is shown in more detail in Figure 59. It is 2D throughout with both the forward shoulder and aft lip contours formed from a portion of a 2:1 ellipse with the major axes inclined parallel to the 30° inlet ramp. The forward-shoulder ellipse is sufficiently large to avoid any separation at the takeoff design point while minimizing drag at cruise due to the cusp formed with the inlet door in the closed position. The aft-lip ellipse is small to provide low drag at cruise with the inlet door closed while providing sufficient bluntness to avoid any flow separation at takeoff. The axial edges of the inlet opening running fore and aft are sharp edged to provide low drag at cruise. The aft flow guide is contoured with a cubic curve to provide separation-free secondary flow to the mixer/ejector.

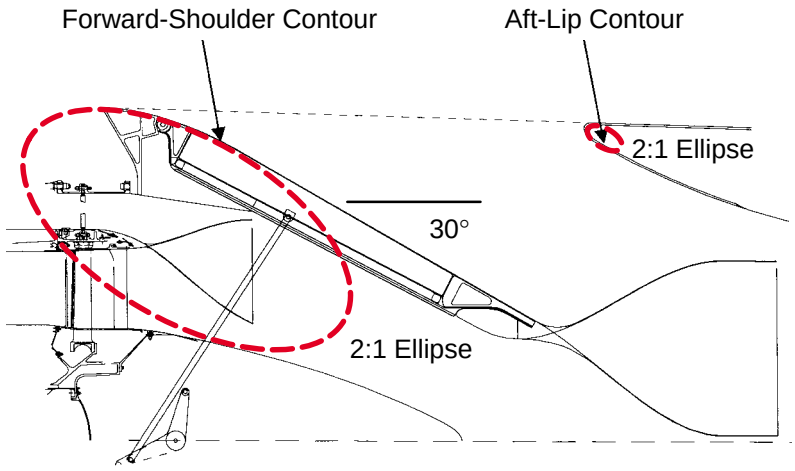

Figure 59. Ejector Inlet

The ejector is a rectangular box wherein mixing of the engine and secondary air occurs. The aft flow guide contour runs back to the station where the divergent flap hinge is located as shown in Figure 60. From this point aft, the upper and lower surfaces formed by the divergent flaps are flat. The sidewalls consist of flat, vertical walls and are parallel to each other. During the suppressed mode, the flaps can be actuated such that the nozzle exit area and thus the flow area within the ejector from the hinge point aft can be varied. The ejector area ratio is referred to as MAR (mixer area ratio) and is the ratio of the flow area at the ejector exit flaps to the duct area at the flap forward hinge point. This ratio is scheduled with nozzle pressure ratio to avoid any aerodynamic mode shifting (subsonic flow to supersonic flow) and can vary from a maximum of 0.975 down to about 0.85. At a MAR of 0.95, the aspect ratio of the ejector box (width to height) is 1.50 at the nozzle exit to enhance sideline-noise suppression. This combination of the MAR, ejector flow area, and aspect ratio set the nozzle internal flowpath width. Entrainment of secondary air to mix with the primary engine gas stream is necessary to reduce the jet exit velocity and therefore the noise of the exhaust jet. However, internal mixing of the supersonic engine air with the low-velocity entrained air generates high-frequency, internal noise. Thus, acoustic/liner treatment is installed on the divergent flaps and sidewalls to suppress the high-frequency noise and is specified from acoustic requirements. The noise-suppression treatment surface area (A_{treat}) in the ejector is about 6.1 times the cross-sectional flow area (A_{mix}). The sidewall trailing edge ends upstream of the flaps and is set by a combination of acoustic treatment requirements, envelope requirements for the actuation system, and external boattail closure angle guidelines from Boeing.

5.4.3 Cruise-Mode Operation

Side views of the exhaust system at three cruise mode operating conditions are shown in Figure 61, and the Mach 2.4 cruise point is shown with more detail in Figure 62. In the cruise mode, the ejector inlet doors are in the closed position, cleaning up the external nozzle flowpath, and a small cusp is formed at the leading edge of the door on the external nozzle surface. With the inlet door in this position, large openings in the upper and lower portions of the T-duct are exposed, and the engine air flows around both sides of the acoustic mixer at a relatively low Mach number, about 0.3. This effectively moves the nozzle throat area control from within the acoustic mixer to the convergent flaps. The convergent flaps are actuated down from the aft flow guide surface to form the nozzle throat for all cruise mode operation and are continuously variable in position during this mode to satisfy the changing area requirement set by the engine cycle. This contrasts with the takeoff mode wherein the engine sees a fixed throat area for all power settings. The throat has a 4.0-in radius connecting the convergent and divergent flaps to minimize the shock strength of the flow expanding

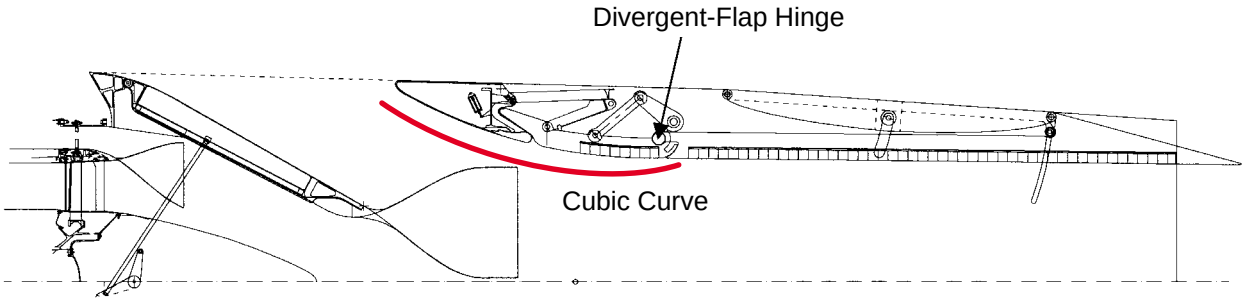

Figure 60. Divergent-Flap Hinge in Ejector Inlet

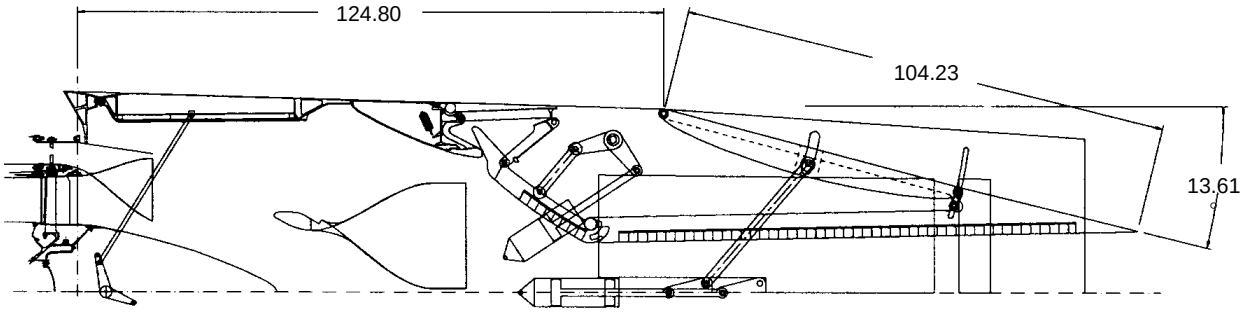

Subsonic Cruise (Mach 0.9/36,000-ft/Power Code 38)

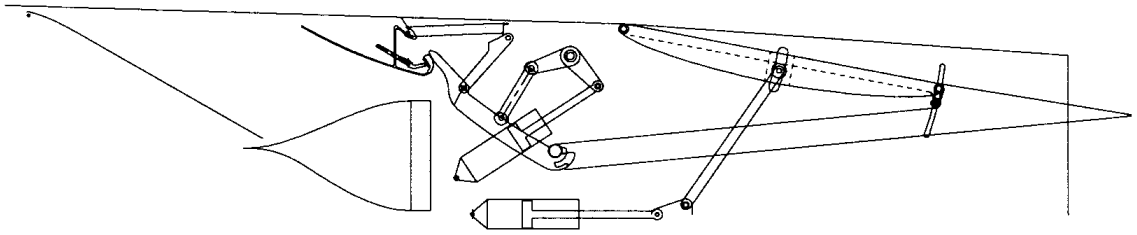

Transonic (Mach 1.6 Climb)

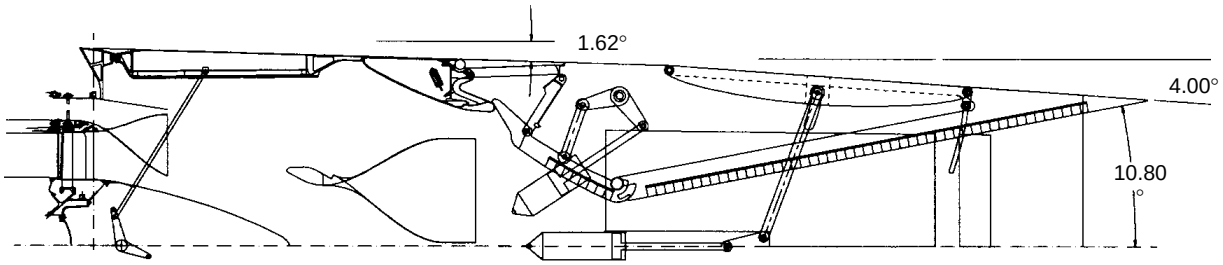

Supersonic Cruise (Mach 2.4/55,000-ft/Poser Code 50)

Figure 61. Nozzle in Cruise Operating Modes

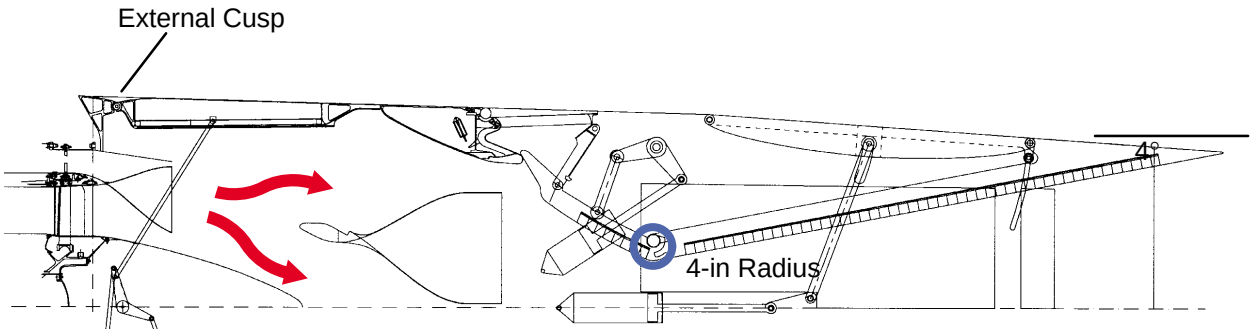

Figure 62. Nozzle in Supersonic Cruise Mode (Mach 2.4)

around the sonic throat at low area ratios. The divergent flap length is set to provide maximum internal performance at the Mach 2.4 design point at a fully expanded area ratio. This cruise design point for the nozzle sets the sidewall upper external mold line such that the flap external boattail angle and the sidewall upper mold line are coincident. The trailing edge of the sidewall at this condition ends upstream of the flap trailing edge (about 10% of the divergent flap length) and was considered to not affect cruise performance. A small slot (about ½ inch) at the trailing edge of the sidewall provides an exit for engine bay cooling air that is also used to cool the exhaust system.

A control system actuates the divergent flaps, varying the nozzle exit area independent of the convergent-flap position to achieve maximum internal performance across the flight regime according to a schedule based on fully expanded area ratios. An exception to this schedule occurs near the low end of the nozzle pressure ratio operation where control system accuracy prohibits an area ratio less than 1.23 in order to avoid the potential for an aeromechanical instability that would occur at an area ratio of 1.0. This compromises the performance at subcruise conditions (and lower pressure ratios).

The external-flap boattail angle is set at 4° at the Mach 2.4 design point, for low cruise drag. At all other flight conditions and power settings, the nozzle exit area is less than the Mach 2.4 cruise area, the external flap angles increase, and portions of the sidewall protrude beyond the flap external edge, to varying degrees, as shown in Figure 61. In the full end view shown in Figure 63, the nozzle exit for the cruise point is nearly a square, and the cross sections forward of the exit and near the turbine exit are consistent with low installed nacelle drag.

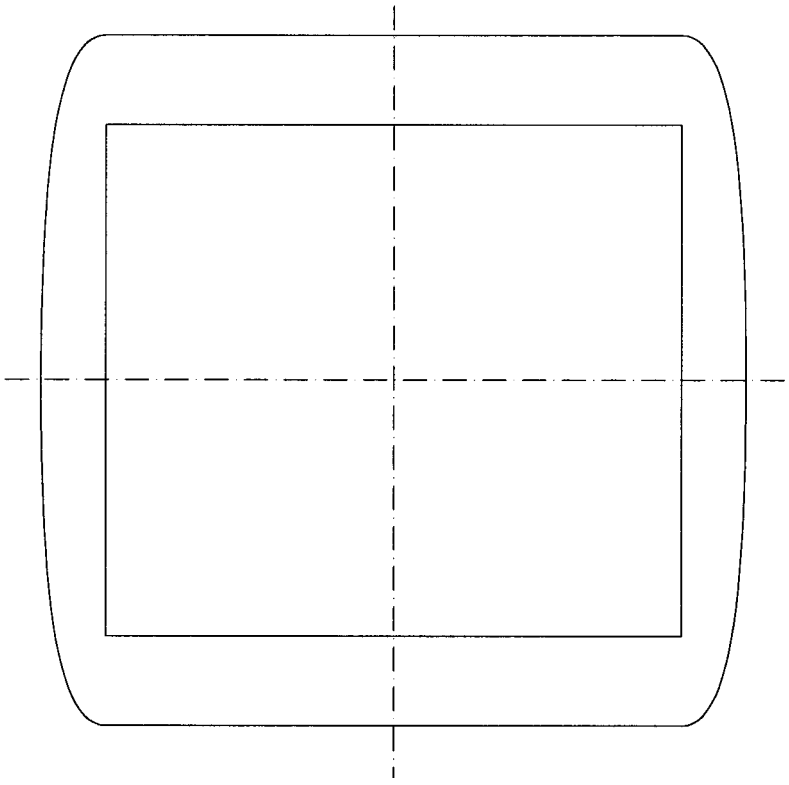

Figure 63. Supersonic Cruise End View, Aft Looking Forward

5.4.4 Reverse-Thrust Operation

In the reverse-thrust mode, Figure 64, the convergent flaps are rotated to the fully inward position to block the engine air and reverse it through cascade boxes located in ports on the top and bottom of the nozzle. The resulting clearance between the two flaps at the centerline is ½-in. The external doors are hinged at the forward end and are actively opened and closed via geneva mechanisms integrated with the kinematic motion of the convergent flaps. Interchangeable cascade boxes located in the upper and lower ports are designed to discharge the flow in the forward direction to produce reverse thrust and to splay the flow sideways for integration with aircraft efflux pattern requirements defined by Boeing in Figure 65. The boxes are sized to match the required engine discharge area while achieving the efflux patterns. The ejector inlet doors are sequenced during transition into reverse to the closed position to match the required engine effective area. These doors can be opened slightly, if necessary, during reverse-thrust mode to obtain additional exit area for the engine air.

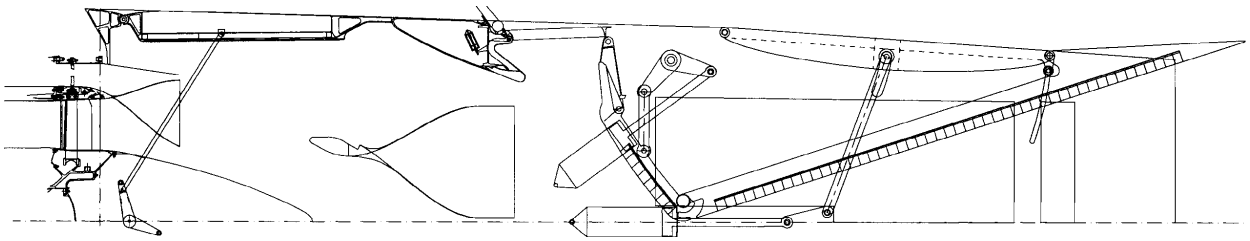

Figure 64. Nozzle in Reverse-Thrust Mode

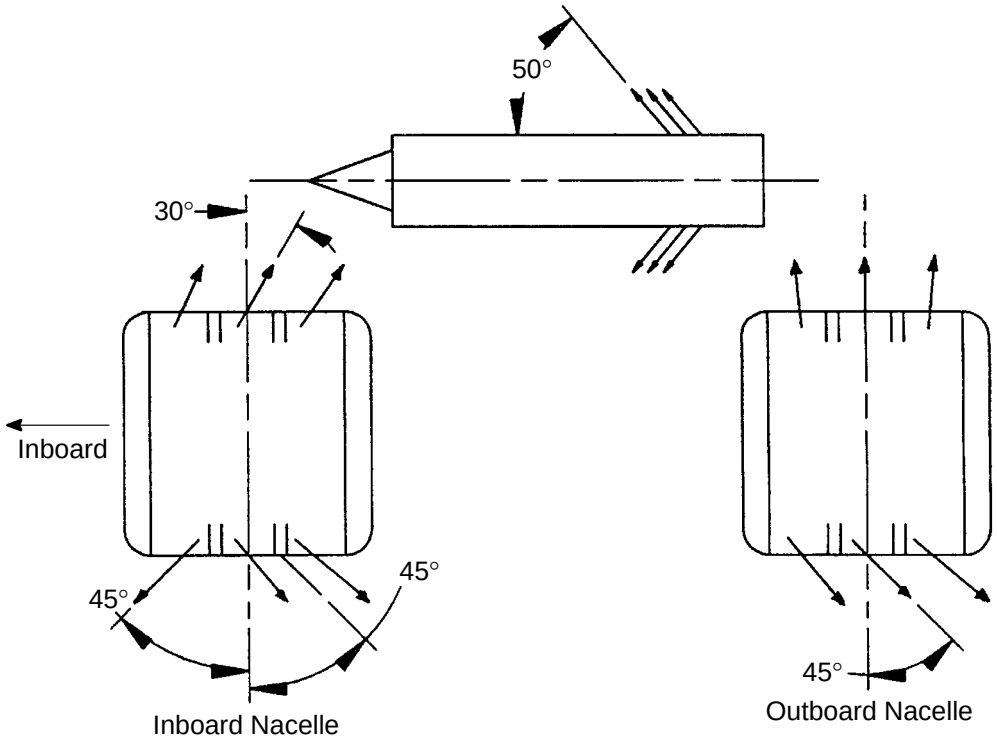

Figure 65. Reverser Splay and Efflux Pattern Requirements

5.4.5 Gas-Path Leakages

A cross section of the nozzle in cruise mode showing leakage paths and effective areas upstream of the nozzle throat is shown in Figure 66. Effective gaps heights and areas shown in the table are based on mechanical design studies and were used to estimate leakage losses included in the cycle deck performance models.

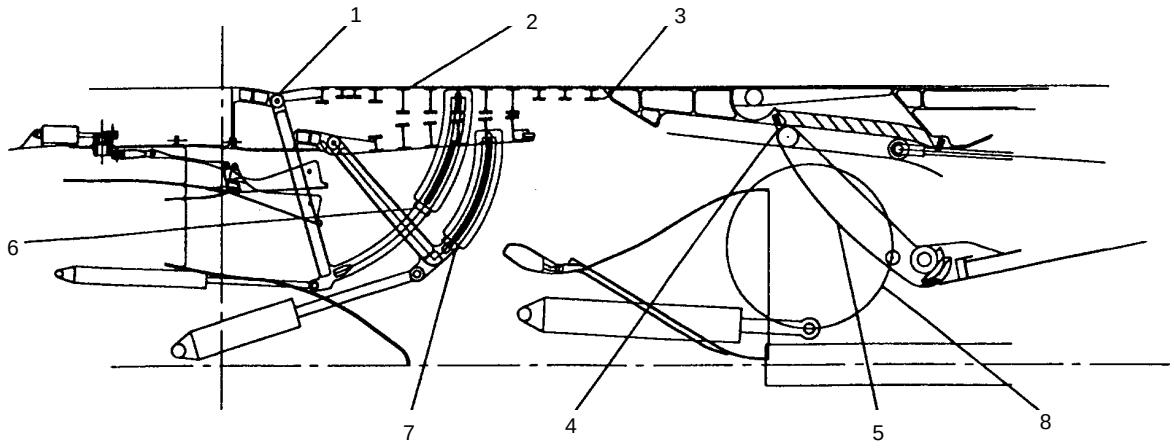

Region	Interface Description	Assumed Seal Type	Leakage Length (in)	Seal Gap (in)	Seal Leakage Area (in^2)	Corner Leakage Area (in^2)
1	Outer Door/T-Duct Hinge	Fixed Leaf Seal	$2 \times 60.84 = 122$	0.004	0.488	0.16 (1 and 2)
2	Outer Door/Sidewall Interface	E-Seal	$4 \times 50 = 200$	0.003	0.600	
3	Outer Door/Midframe Interface	Fixed Leaf Seal	$2 \times 60.84 = 122$	0.008	0.976	0.625 (2 and 3)
4	Convergent Flap/ Midframe Interface	Brush or Plunger Seal	$2 \times 60.84 = 122$	0.008	0.976	0.316 (4 and 5)
5	Convergent Flap/ Sidewall Interface	Plunger Seal	$4 \times 32 = 128$	0.008	1.024	
6	Outer Door Link/ Sidewall Interface	C-Seal	$4 \times \pi \times 2 = 25$	0.002	0.050	– – –
7	Inner Door Link/ Sidewall Interface	C-Seal	$4 \times \pi \times 2 = 25$	0.002	0.050	– – –
8	Convergent Disk/ Sidewall Interface	Brush Seal	$4 \times 57.2 = 229$	0.002	0.458	– – –
Total	**– – –**	**– – –**	**973**	**– – –**	**4.622**	**1.101**

Figure 66. Estimated Seal Leakage Forward of A_8 at Cruise

5.5 Full-Scale, Fixed-Chute Nozzle

5.5.1 Aeroacoustic Design Considerations and Criteria

This section focuses on the genesis of the aeroacoustic design for the full-scale, fixed-chute nozzle and provides a rationale for the recommended aeroacoustic design criteria. These design recommendations have been continually updated as new information became available through testing, analyses, aircraft/engine system trade studies, mechanical design development, and material research (EPM).

A significant factor in revising/updating the aeroacoustic design recommendations has been the need to meet the noise regulations anticipated for the time of introduction of the HSCT into service. In the first phases of the HSR program (early 1990's), meeting FAR36 Stage III noise rules, Reference 1 (with a nominal design margin of 1 EPNdB at each certification point), was considered adequate and was the program goal. However, in the later 1990's, there has been increased pressure to introduce more stringent Stage 4 noise regulations for subsonic transportation in the early part of the next century. It is anticipated that the HSCT, at introduction, will have to meet the then-prevailing noise regulations for commercial subsonic transportation; hence, during HSR Phase II, the noise goals for the HSCT were revised to be compatible with anticipated future subsonic noise rules. This in turn required revisions to the aeroacoustic design criteria.

In the early phases of the HSR program several cycle/nozzle combinations were assessed for environmental acceptability (nominally meet FAR36 Stage III, Reference 1) and economic viability (expressed as TOGW). Configurations studied covered a wide range of specific thrust (ideal jet velocity) from about 3000 ft/s (turbine bypass engine, requiring a mixer/ejector nozzle with 120%+ entrainment ratio) to about 1300 ft/s (mid-tandem fan engine with a mechanically simpler nozzle). This resulted in selecting a moderate-bypass-ratio (0.6 to 0.8), mixed-flow turbofan with a moderate-entrainment mixer/ejector (about 60 to 70% entrainment ratio). This subsection is a summary of the aeroacoustic design considerations and design criteria for such a mixer/ejector nozzle.

The nozzle aeroacoustic design considerations listed below are broad guidelines. Selection of a particular configuration or aeroacoustic design approach needs to be made by evaluating the impact of such guideline(s) on a system TOGW basis. Aeroacoustic design considerations aimed at achieving significant noise reductions while maintaining high nozzle thrust coefficient are:

- Ejector inlets that induct the ambient air should have minimal aerodynamic losses.
- Chute designs need to have smooth flow paths (minimize sharp corners) that achieve continuous acceleration in the primary passage with a slight convergent/divergent section.
- Streamwise vorticity introduction by the chutes (in terms of angular mismatch between the primary and secondary streams) to enhance the mixing (and hence noise reduction) should be traded with associated thrust loss.
- Chute designs need to achieve rapid mixing of the primary and secondary streams so that acoustic liners close to the chute exit contribute to EPNL reductions.
- Mixing enhancement devices at the chute exit that improve the acoustic suppression of the liners and achieve a more uniformly mixed-out profile at the

ejector exit should have minimum thrust loss. Application of such devices at the chute exit should minimize disruption of the primary and secondary flow passages.

- Mixing-enhancement devices at the ejector exit that achieve noise reduction of premerged and merged components should have minimal thrust loss at takeoff as well as other mission segments.
- Liner designs and attachments that provide the needed acoustic impedance should minimize aerodynamic losses due to skin friction, steps, gaps, etc.
- Fan/core mixer design should achieve highly uniform mixing of core and fan streams entering the chute mixer (reduce the extent of hot streak — unmixed core stream) while meeting engine operational requirements at all mission conditions.

Table 18 shows the chronological development of the aeroacoustic design in terms of selected geometric parameters, status, and goals for noise and takeoff thrust performance, and the databases that were heavily utilized in the assessment of status as well as in the generation of technology projections. For the sake of brevity, not all parameters are listed. The principal factor that emerges from this table is: **The noise status numbers have shown significant improvement since the Dec 95 PDR with minimal reduction in the takeoff thrust coefficient.**

Table 18. Nozzle Aeroacoustic Design Evolution

Parameter		Milestone		
		12/95 PDR	8/96 AA PDR	9/99 Final
Cycle		3570.80	3770.60	3770.60
Noise Goals	dB Re: Stage 3	–1, –3, –1	–1, –3, –1	–1, –3, –1
	Status Re: Goals	+4.9, +2.8	+1.9, +2.0	+0.2, –1.9
C_{fn}	Goal	0.945	0.945	0.960
	Status	0.938	0.938	0.949
SAR		2.5	2.9	2.9
Mixing Length, Inches		120	140	138.4
A_t/A_{mix}		4.0	5.3	6.1
Aspect Ratio		1.2	1.5	1.5
Number of Chutes	Hot	18	20	20
	Cold	20	20	20
Sidewall Chute		Full-Width Cold	Full-Width Cold	Half-Width Cold
Mixing Enhancer		None	Chevrons	None
Database		Gen 1, 1.5, DSM	Gen 2 (HAM)	Gen 2.5, 3.0, 3.5

The design refinements and increased noise suppression are attributable to continued aeroacoustic technology development coupled with nozzle mechanical design and aircraft system trade studies.

Three major changes followed the December 1995 PDR. The suppressor area ratio (SAR) was increased from 2.5 to 2.9, and the nozzle aspect ratio (defined at the nozzle exit under takeoff

conditions) was increased from 1.2 to 1.5. In addition, the mixing length of the ejector (measured from the chute exit to the midpoint of the flaps and sidewalls at the nozzle exit) was increased from 120 to 140 inches. These changes resulted in an increase in the ratio of acoustic treatment area to mixing area (A_t/A_{mix}) from 4.0 to 5.3.

The change in SAR resulted from the change to higher fan pressure ratio cycles (which lead to higher nozzle pressure ratios at takeoff) and the need to reduce the mixed velocity of the jet at the ejector exit (and hence the level of externally generated noise). This was achieved at the cost of increasing the internal mixing noise component, resulting in the need for more treatment area — and length. It should be mentioned, however, that nozzle length is not driven solely by acoustic considerations. In many cases the limiting criterion has been the aerodynamic requirement for reducing cruise drag by keeping boattail angles less than or equal to 5°.

The increase in nozzle aspect ratio was also driven by sideline-noise considerations. It was made practicable by a more efficient nacelle design that enabled a reduction in cruise drag with a minimal impact on nozzle weight.

The final element contributing to the noise reductions between the December 1995 and August 1996 PDR's was the employment of chevrons at the nozzle exit. These had been shown to provide slight noise reductions over a broad range of frequencies and angles, with little to no performance penalty at takeoff. Integration of these devices at cruise presents a problem however, and — should they be deemed necessary — further work is needed to establish the optimum configuration.

Following the August 1996 aeroacoustic PDR, the chute configuration at the sidewall was changed from full-width cold to one-half-width hot. This reversion to the earlier (Gen 1.0) configuration was prompted by the velocity profiles at the ejector exit — first experimentally, later with CFD. It was noted that the secondary fluid entrained by the full-width cold chute at the sidewall failed to mix with the adjacent primary stream, resulting in a "cold hole" at the ejector exit. This behaviour was not seen with the half-width, hot-chute sidewall configuration of the earlier mixers, and it was felt that the exit velocity profile nonuniformity (inadequate mixing) was a contributing factor to the increased noise levels of the later designs. The configuration change achieved the desired result as far as the exit profile was concerned, but this was accompanied by a loss in thrust relative to the full-width cold-chute design that was attributed to the scrubbing of the hot, primary, fluid along the sidewall. In consequence, and also because it was believed that the acoustic treatment within the ejector would be more effective with cooler flow along the face sheet, the final configuration was selected to have a one-half-width cold chute at the sidewalls. This configuration should preserve the improved mixing, performance, and treatment effectiveness.

Since the December 1995 PDR, reductions of 4.7 EPNdB have been demonstrated at the sideline and cutback conditions defined in the nozzle P5 and P6 metrics. The reductions were demonstrated with acceptable thrust performance and must be regarded as remarkable achievements.

One further design option that has yet to be exercised (except under the heading of *Technology Projections*) is the use of rapid-mixing devices at the trailing edges of the chutes. These have potential for further acoustic improvements (about 1.5 to 2.0 EPNdB) at reasonable thrust loss but require work for optimization.

5.5.2 Mechanical System Design

The objective for the mechanical design of full-scale, fixed-chute nozzle development program was to provide mechanical characterization of high-performance, noise-suppression, exhaust nozzle

technologies that enable an economically viable supersonic aircraft. The exhaust nozzle system requirements constituted the basis of the nozzle mechanical design development program, and they are listed as follows:

- FAR 36 Stage III Noise Goals: –1-dB Sideline, –3-dB Cutback, –1-dB Approach
- Nozzle thrust goals: $C_{fn} > 0.96$ at takeoff; $C_{fg} > 0.982$ at supercruise
- Nozzle weight < 7830 lbm (MTOW < 750,000 lbm)
- Life goals:
  - 18,000 hr at supersonic cruise (9,000 hr for acoustic liner and ejector/mixer)
  - Cycles dependent on mission times
- Supercruise boattail angle less than or equal to 4° degrees (external aerodynamic performance)
- Subcruise boattail angle less than or equal to 15° (external aerodynamic performance)
- Reverse transition time: 2 seconds
- Capable of achieving all selected mission points
- Kinematic ability to meet required cycle areas
- Capable of meeting defined structural envelope
- Capable of achieving reverse area requirements
- Fail-safe operation throughout defined mission profile
- Nozzle bay purge flow through W_2 inlet bleed
- Thermal protection system (TPS) to be used where feasible

The exhaust nozzle mechanical design was developed on the basis of the requirements specified above, as described in Section 5.2.

The final baseline exhaust nozzle configuration was the linear-actuation system concept derived from the alternate kinematics downselect, as described in Section 5.2.6, and is shown in the suppressed takeoff mode in Figure 67. This nozzle configuration reflects the MFTF3770.60, 800 lbm/s engine cycle: fan pressure ratio of 3.7, thrust lapse rate of 70%, and bypass ratio of 0.6. The nozzle has a 2.9 SAR with a 1.5 aspect ratio and 0.95 MAR for suppressed takeoff (these values have been the standard for the nozzle development over the last two years of the program). The mixing area (A_{mix}) value of 3570.3 in^2 is based on the cycle area and acoustic requirements. The mixing length is 138.4 inches and represents the distance between the exit plane of the ejector mixer and the average between the trailing edges of the aft sidewalls and divergent flaps, for the suppressed takeoff condition. The nozzle internal flowpath width, within the two-dimensional region, is 71.33 inches and is derived from the cycle and acoustic parameters associated with the suppressed takeoff condition. The acoustic treatment area to mixing area ratio (A_{trt}/A_{mix}) is 6.1, based on the requirement of the acoustic treatment starting at five hot-lobe widths aft of the ejector mixer exit plane. The remaining acoustic parameters are consistent with the requirements as stipulated by the Acoustic Team and are as follows:

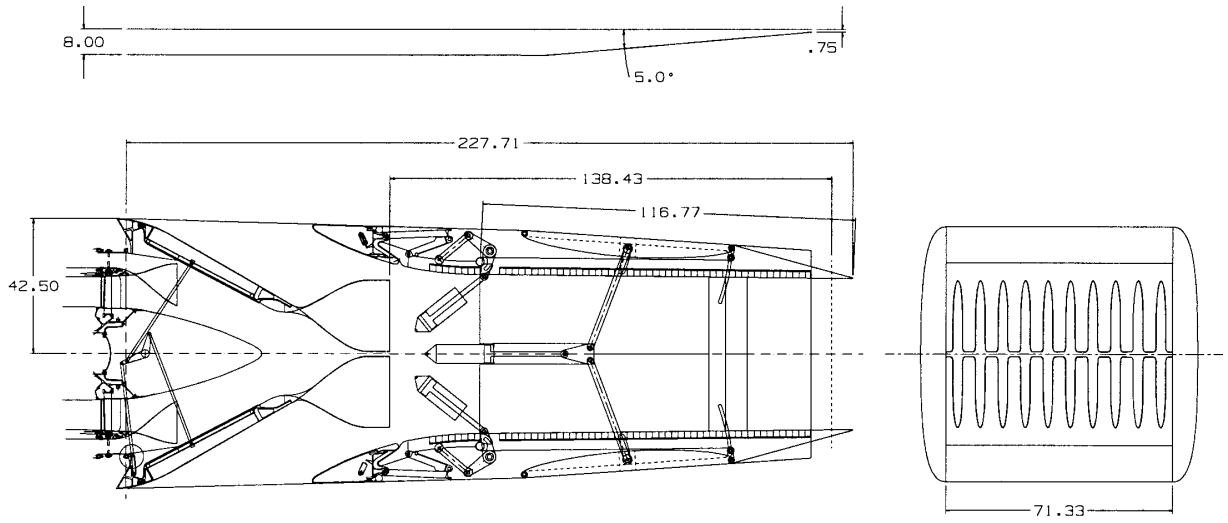

Figure 67. Final Baseline Configuration for Exhaust Nozzle

- Chute penetration = 0.925
- Ejector mixer cold lobes = 20 per nozzle
  (18 full lobes, with 4 half lobes at sidewalls)
- Ejector mixer hot lobes = 20 per nozzle (20 full lobes)
- Chute expansion ratio (CER) = 1.05

The width of each ejector mixer hot lobe is 2.76 inches at the mixer exit plane, as calculated from the previously specified nozzle characteristics. The lengths of the divergent flaps are each 116.7 inches and are consistent with the goal of optimum internal aerodynamic performance at the Mach 2.4 supercruise condition. The overall nozzle length is 227.7 in. The nozzle fore/flange half of 42.5 inches is based on the requirements for integration between the propulsion system and aircraft. and results in a maximum nozzle nacelle area (A_{max}) of 7220 in^2. The resulting boattail angles for subsonic cruise and supersonic cruise conditions meet the system requirements at values of 13.6° and 4° respectively. The sidewall boattail angle was improved to 5° as a result of the ability of the linear-actuation system to more efficiently "package" the divergent flap actuation system with the absence of the disks.

The three-dimensional definition and nomenclature of the nozzle are illustrated in Figure 68 (two pages). The nozzle is shown in its various operating modes in Figures 69 through 73. Figure 74 indicates the material and maximum temperatures for the nozzle components. The integration between the exhaust nozzle, aircraft, and remaining propulsion system modules is shown in Figure 75. Finally, Figure 76 shows the status and detail breakdown of the nozzle weight.

5.5.2.1 Nozzle Aerodynamic Loading

Aerodynamic loads for the nozzle components were developed using the 3770.60 cycle model. Flight conditions and flap loads are summarized in Table 19.

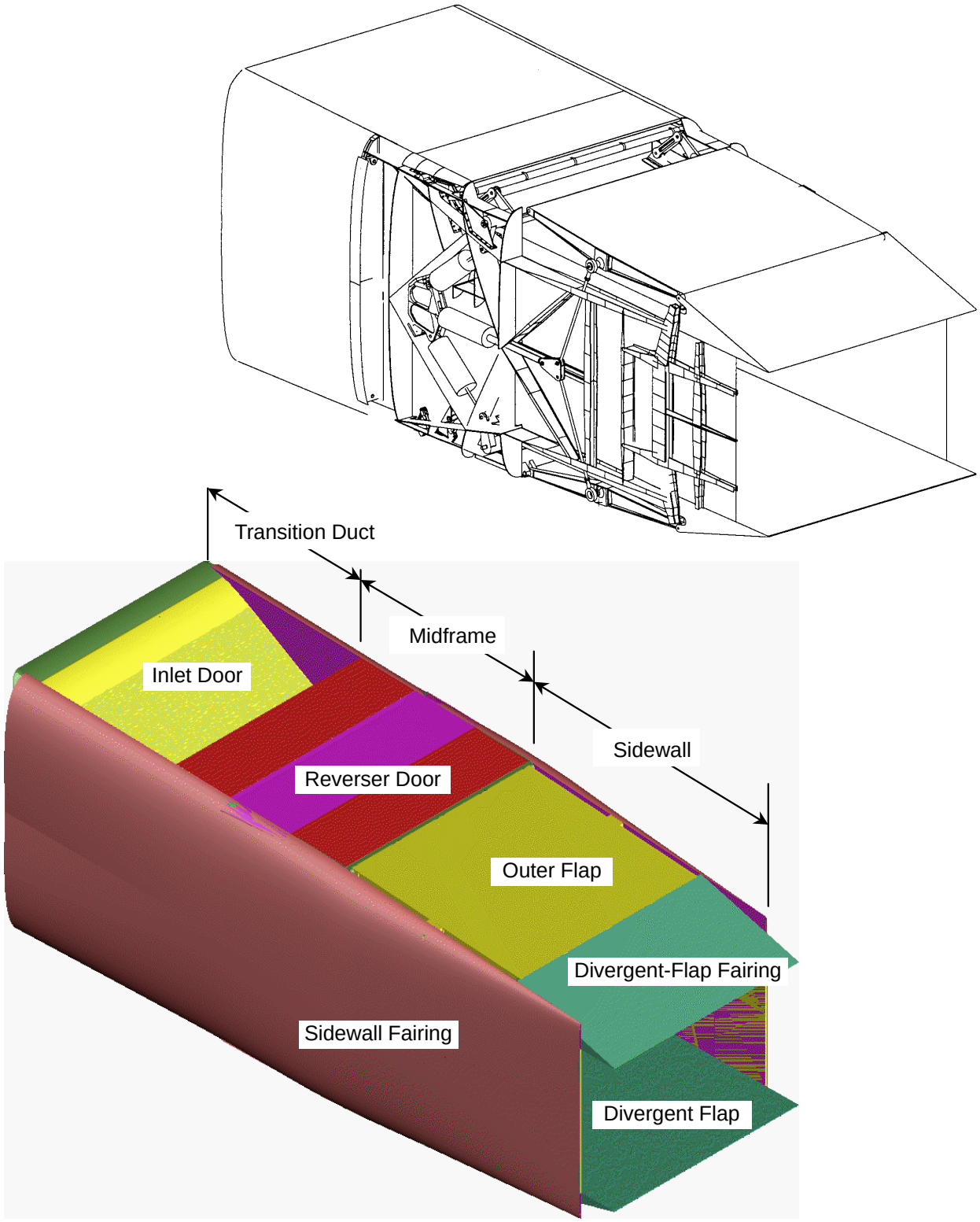

Figure 68. Three-Dimensional Definition and Nomenclature of Final Baseline Exhaust Nozzle Configuration

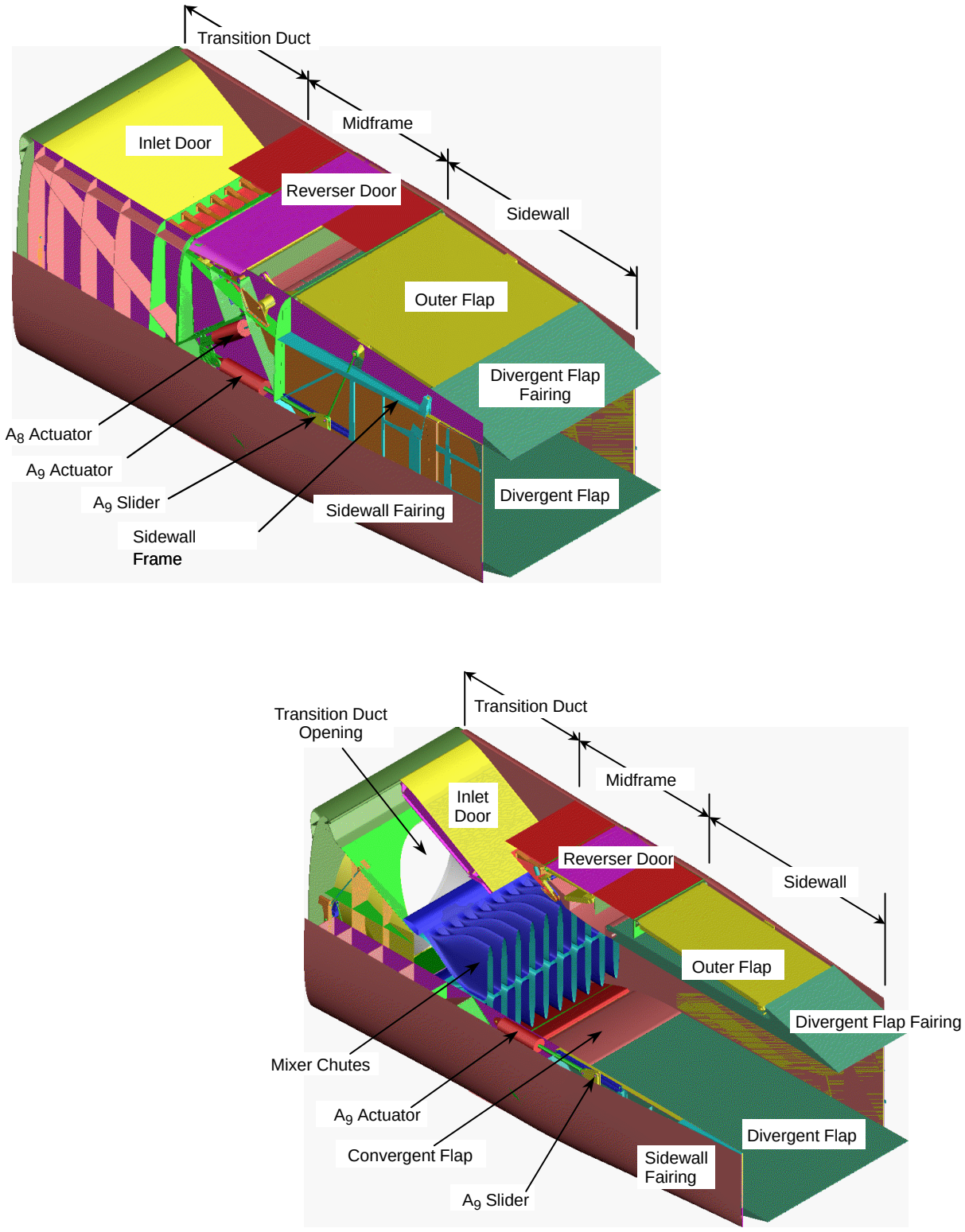

Figure 68. Three-Dimensional Definition and Nomenclature of Final Baseline Exhaust Nozzle Configuration (Concluded)

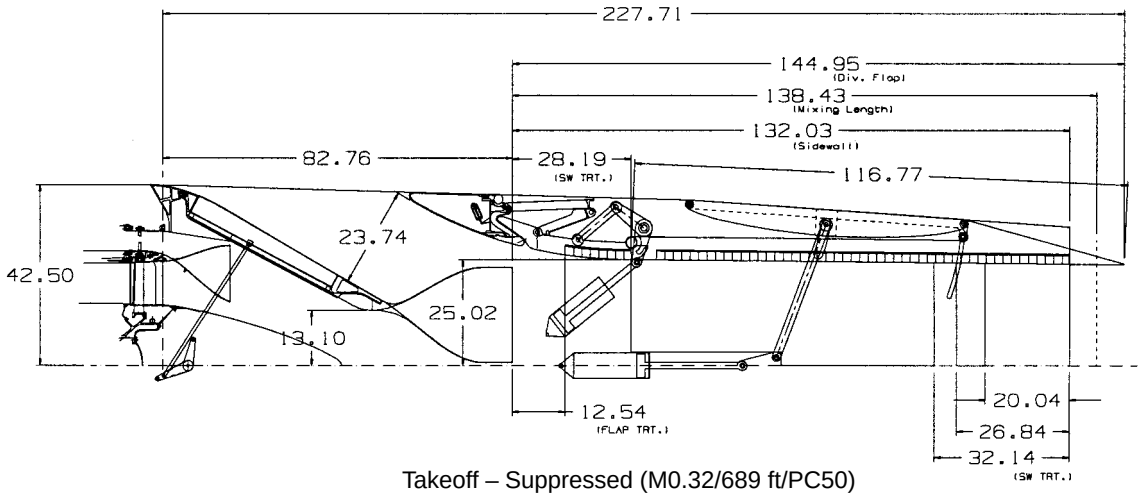

Takeoff – Suppressed (M0.32/689 ft/PC50)

3770.60 Cycle
SAR = 2.9, Aspect Ratio = 1.5
MAR = 0.95, Width = 71.33 in (Flowpath)
A_8 = 1230.6 in^2

Figure 69. Suppressed Takeoff Condition for the Final Baseline Exhaust Nozzle Configuration

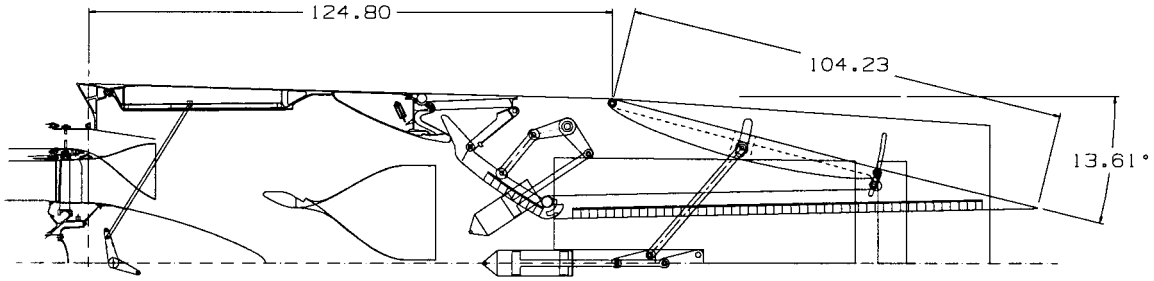

Subsonic Cruise (M0.9/36,000 ft/PC38)

3770.60 Cycle
SAR = 2.9, Aspect Ratio = 1.5
Width = 71.33 in (Flowpath)
A_8 = 1505.5 in^2, A_9 = 1851.8 in^2

Figure 70. Subsonic Cruise Condition for the Final Baseline Exhaust Nozzle Configuration

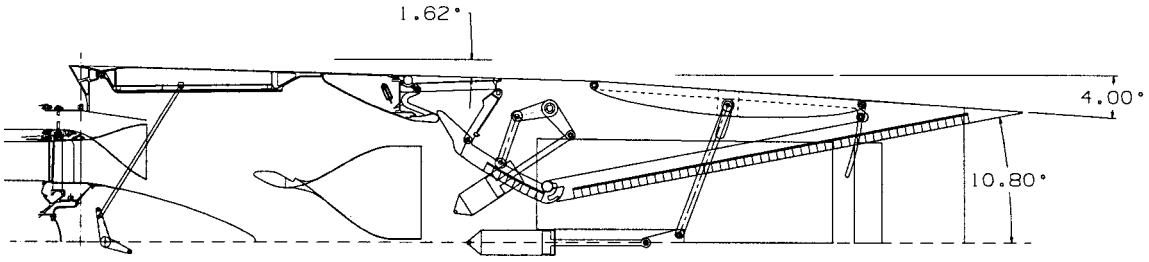

Supersonic Cruise (M2.4/55,000 ft/PC50)

3770.60 Cycle
SAR = 2.9, Aspect Ratio = 1.5
Width = 71.33 in (Flowpath)
A_8 = 1360.8 in^2, A_9 = 4487.1 in^2

Figure 71. Supersonic Cruise Condition for the Final Baseline Exhaust Nozzle Configuration

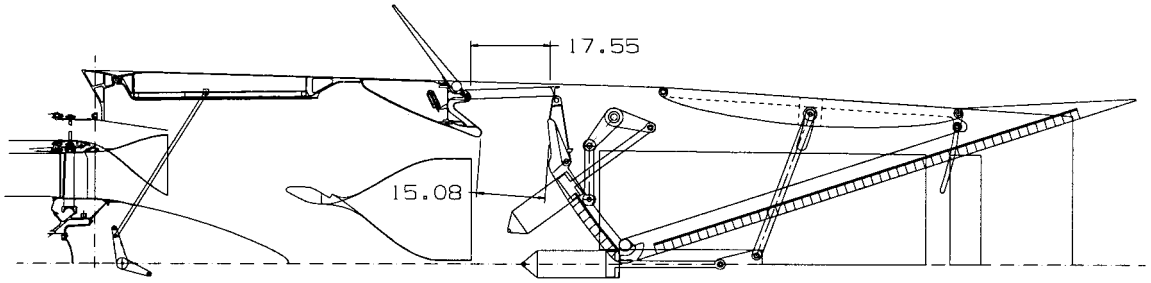

Reverse (M0.2/0 ft)

3770.60 Cycle
SAR = 2.9, Aspect Ratio = 1.5
Width = 71.33 in (Flowpath)

Figure 72. Reverse Thrust Condition for the Final Baseline Exhaust Nozzle Configuration

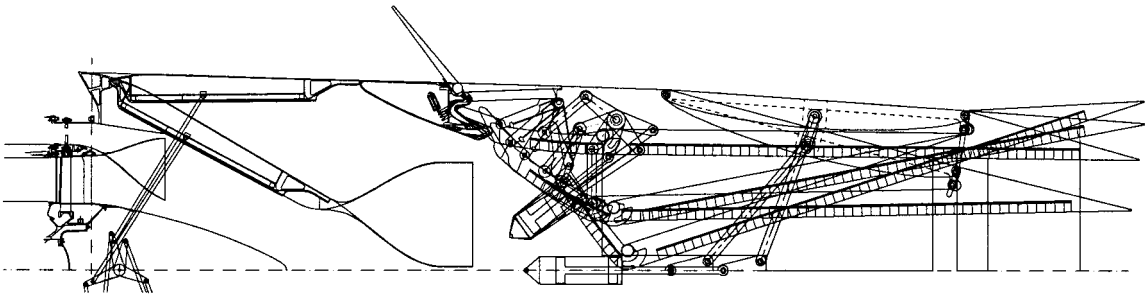

Takeoff (Suppressed)
Subsonic Cruise
Supersonic Cruise
Reverse

Figure 73. Overlay of Four Conditions for the Final Baseline Exhaust Nozzle Configuration

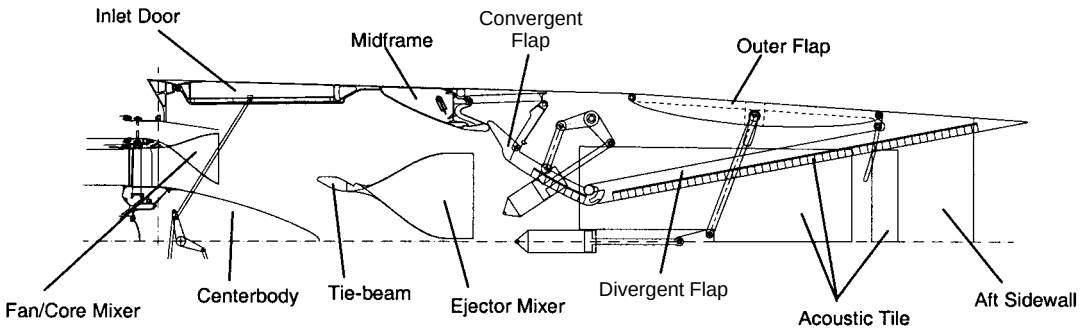

Component	Material	Maximum Temperature (F) *
Centerbody	CMC	1800
Fan/Core Mixer	Inco 718	1200
Inlet Doors	Inco 718	950
Ejector Mixer	R108	1670
Transition Duct	Ti6242/Inco 718	1000
Midframe	Inco 718	900
Aft Sidewalls	TiAl	800
Convergent Flaps	Inco 718	1200
Divergent Flaps	TiAl	1000
Outer Flaps	Ti 6242	600
Rev. Doors & Cascades	Wasp./Advanced Ti	1200
Acoustic Liner	CMC/Bulk	** 1400

* Bulk temperature of structure
** Temperature of flowpath facesheet

Figure 74. Component Temperatures and Materials for the Final Baseline Exhaust Nozzle Configuration

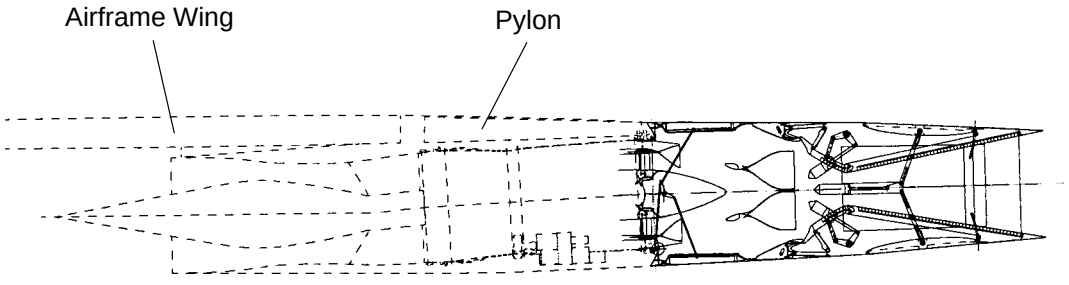

Nozzle Centerline:
Vertically offset from engine centerline (about 0.2 inch)
Rotated from engine centerline (about 2° cw)

Figure 75. Integration of the Final Baseline Exhaust Nozzle Configuration

Component	Status Weight
Centerbody	68
Fan/Core Mixer	175
Inlet Doors	550
Ejector Mixer	813
Transition Duct	1030
Midframe	801
Aft Sidewalls	403
Convergent Flaps	561
Divergent Flaps	599
Outer Flaps	361
Rev. Doors & Cascades	190
Acoustic Liner	700
Subtotal	625 1
Controls & Actuation	1355
Miscellaneous	408
Nozzle Total	**8015**

Linear System Nozzle:

- Alternate kinematics (linear actuation system)
- Single Inlet Door (total 2 per nozzle)
- R108 Uncooled Mixer (Gen 3.6 – product scale)
- TiAl Divergent Flaps
- TiAl Aft Sidewalls (Noncantilevered)
- Lower density bulk
- 2 second Rev. Trans. Time
- Fixed Fan/Core mixer
- Advanced material control system

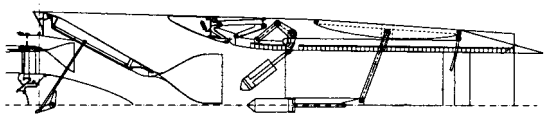

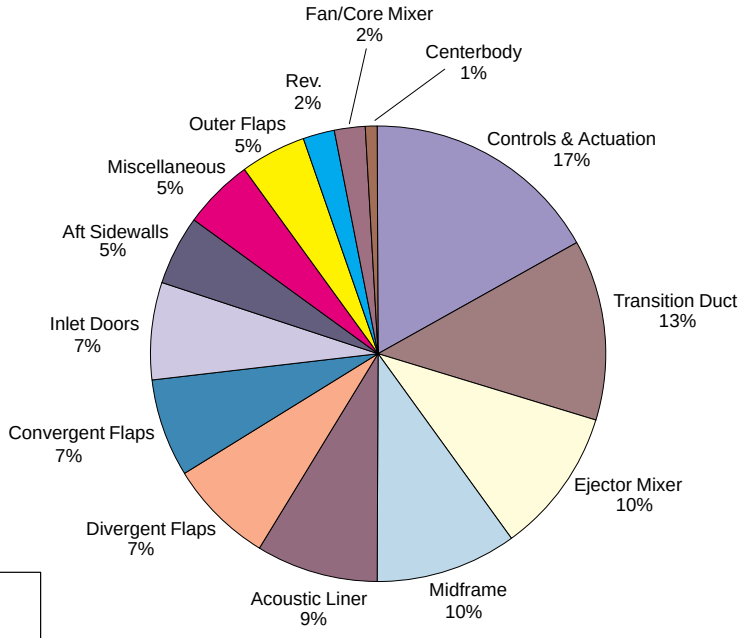

Figure 76. Weight Breakdown of the Final Baseline Exhaust Nozzle Configuration

Table 19. Flap Loads

Flight Point	Cycle Data (3770.60)			Convergent Flap		Divergent Flap	
	NPR	P_{T8}	Mach	Load, lbf	Cp. (in)	Load, lbf	Cp. (in)
Takeoff Suppressed	3.38	49.8	0.32	–2,021	–14.3	23,454	67.4
Takeoff Unsuppressed	3.38	49.8	0.32	–6,685	–12.8	–35,923	62.2
Subsonic climb	4.15	50.77	0.6	79,622	–17.3	50,276	42.1
Subsonic Cruise	3.7	12.15	0.9	17,813	–17.3	9,089	36.8
Supersonic climb	13	42.79	1.6	86,477	–17.7	35,867	28.8
Supersonic Cruise	4.5	32.4	2.4	69,570	–18.3	24,763	27.1

The nozzle aerodynamic lines were evaluated through a combination of analytical studies, computational fluid dynamics studies, and subscale model tests. Extensive CFD studies were performed to assess various aspects of the exhaust system aerodynamics in the cruise and noise-suppression modes as well as the fan/core (F/C) mixer. Limited full Navier–Stokes (FNS) CFD evaluations of the F/C mixer in combination with the downstream nozzle were performed in both the cruise mode and the noise-suppression mode. These were 90° quadrant studies intended to also capture the effects of flowpath transition from round to rectangular. Two-dimensional CFD studies of the converging/diverging portion of the nozzle in the cruise mode were conducted using Euler and FNS codes to assess performance and provide a basis for cycle deck predictions. Studies included assessment of flap length as well as contoured divergent flaps aimed at improving cruise performance.

Mixer/ejector design was optimized through a series of 1/7-scale-model tests. The tests varied mixer lobe shape, penetration, and area ratio to achieve a design that maximized thrust while minimizing jet noise. A large scale model (LSM) test of the exhaust system in the suppressed mode was conducted at the P&W C11 acoustic engine test facility in West Palm Beach behind an F100 engine. This model was approximately 56% scale and provided key acoustic and aerodynamic performance information related to scaling effects of the 1/7-scale models to the product. Lessons learned during the LSM test were applied to the design of the HSCT nozzle. LSM testing demonstrated a need for better mixing of the fan and core engine flows and also demonstrated a reduction in the suppressed mode nozzle flap loads.

Five series of tests were conducted with the chute aerodynamic stereolithography rig. This was a simple flow stand using stereolithography and plexiglass models to obtain flowfield diagnostic data at very low cost and rapid turnaround time. Variations on mixer design and integration were evaluated with these test series.

5.5.2.2 Nozzle Thermal Condition

A review of the HCST nozzle purge flow was performed. System parameters of flows, pressures, and gas temperatures were predicted for a variety of cases covering a wide range of possibilities. The cases selected show the effects on system parameters of purge flow level, split percentage, engine operating condition, flap-cavity exit area, and seal coverage.

The flow model is a simple network of 23 flow restrictions. The primary airflow is the nozzle purge. The air supply is assumed to originate from the engine inlet case, as a quantity of air is required to purge the engine compartment. It is assumed that this flow can be brought through the transition duct bulkhead and through the sidewall to purge and bathe various components in the HSCT nozzle. The estimated flow area of the engine compartment is an order of magnitude larger than flow areas in the nozzle; therefore, it can be assumed that negligible head loss occurs through this region.

In consideration of the purge flow design, other sources for the purge flow were considered. Any exterior air source would begin at the same initial condition due to the resultant ram pressure. Therefore, the results presented here would be applicable because a similar analysis would be performed. Bypass fan air was considered; however, such a source would come at higher cost to the cycle. The additional work performed on this air would be wasted because the purge pressures in the nozzle are low. The high pressure associated with the fan air would be lost as the flow is dumped into the low-pressure regions such as the flap cavity.

A second factor that influenced the design was the availability of hardware. Hardware and flow passages for a minimum purge required for the engine compartment bay must exist. By deriving the

nozzle purge from the engine compartment purge, the added flow can simply be attained by increasing the system size. If additional flow is required for the nozzle, then the system can just grow accordingly to accommodate the need. A purge system originating from another source would require all the associated hardware and passages to deliver the flow. The cost and penalty should be less from a derived system.

Flow area sizing was performed to deliver the purge with adequate pressure head. Table 20 lists the flow areas and a brief description of each restriction.

Table 20. Flow Model Restrictions

Restriction	Area (in^2)	Description
R30	1064	Flow area through the engine bay compartment
R39	40	Leakage areas prior to flow entrance into nozzle
R40	60*	T-duct bulkhead entrance holes
R42	60*	Additional T-duct restriction/blockage
R44	60*	Additional T-duct restriction/blockage
R51	60*	Additional sidewall restriction/blockage due to structural supports
R52	60*	Additional sidewall restriction/blockage
R53	60*	Additional sidewall restriction/blockage
R54	60*	Additional sidewall restriction/blockage
R55	60*	Additional sidewall restriction/blockage
R56	60*	Additional sidewall restriction/blockage
R57	60*	Additional sidewall restriction/blockage
R1	19*	sidewall to flap-train cavity split holes
R59	19*	sidewall downstream effective restriction
R4	1.14	Convergent flap to midframe hinge gap
R45	0.316	Convergent flap sidewall and midframe corner areas
R5	0.224	Convergent flap to sidewall sealed gap
R10	1.14	Divergent flap/convergent flap hinge gap
R11	0.72	Divergent flap to sidewall seal (1st quarter)
R12	0.72	Divergent flap to sidewall seal (2nd quarter)
R13	3.73**	Divergent flap to sidewall gap (3rd quarter)
R14	3.73**	Divergent flap to sidewall gap (4th quarter)
R20	150	Flap-train cavity exit to ambient conditions
* Nominal sizing; see Table 21 for specific sizing at various purges and flow splits.		
** Unsealed gap; see “Seal Study” discussion for details of seals and seal gaps on the divergent flap.		

Purge Level and Flap Cavity Split – The first parametric study examined purge level and flow split. the purge flows were chosen as 0.5%, 1.0%, and 2.0% of engine flow. The airframer requirement for the engine compartment bay was specified as six air changes per minute, which is approximately 1.5 lbm/s. The 0.5% to 2.0% range was selected to address the thermal requirements in the nozzle and equates to 2.75 to 11.0 lbm/s at supersonic cruise flight conditions.

Purge split between the flap-train compartment and sidewall static structure was reviewed at 25, 50, and 75%. For each of these splits and purge levels, geometric sizing was performed. Table 21 lists the resultant restriction areas to attain the various split and purge values. Sizing was performed at Mach number 2.4 supersonic cruise conditions at 55,000-ft altitude.

Figures cited in the following discussions represent the nine cases listed in Table 21. The figures include flow, temperature, and pressure results.

Table 21. Design Parameters for Purge and Sidewall/Flap-Cavity Split Levels

Split (%)	Purge (%)	Sidewall Areas		Flap-Cavity Areas	
		Restriction	Downstream Restriction	Purge Entrance	Exit
25	0.5	30	14.2	4.8	150
25	1.0	60	27.0	9.0	150
25	2.0	120	56.3	18.9	150
50	0.5	30	9.9	9.9	150
50	1.0	60	19.0	19.0	150
50	2.0	120	37.0	37.0	150
75	0.5	30	4.8	14.2	150
75	1.0	60	9.0	27.0	150
75	2.0	120	18.7	56.5	150

Cycle Point Evaluation – To perform heat transfer analysis at a variety of cycle points, the nozzle purge and leakage flows must be defined at those points. Additionally, the performance of the purge at low Mach number cycle conditions was in question. The purge flow relies on ram pressure, and at low Mach number flight points the ratio of inlet to exhaust pressure is significantly lower than at supersonic flight points. The evaluation was concerned with any flow reversal or an excessive leakage-to-purge flow ratio that would result in hot mixed bay temperatures.

To address these concerns, the purge system was modeled at several cycle points. These included the baseline condition of supersonic cruise, with 2.4 Mach number, at 55,000-ft altitude. Flow-restriction sizing was performed at this cycle point. The majority of parametric studies were also performed at this flight condition.

The other flight points evaluated included a suppressed takeoff condition, a low Mach number and altitude point immediately following suppressed mode, a supersonic climb point at 36,000-ft altitude, and a second supersonic cruise point at 62,000 ft. The Mach numbers for the climb and cruise points were 1.6 and 2.4 respectively.

The results for the four additional flight points evaluated are described in the following discussions. For all the reported runs, nominal sizing was employed. See Table 21 for this restriction sizing information. Each case was evaluated with 1% and 2% purge. Divergent flap sealing was set to 50% of the flap length. (See discussion of seal study.) The results show that purge flow does drop off as a percentage of engine flow at lower Mach number flight. However, flow reversal did not occur at any flight point evaluated. Although the percentage purge supply to the bay is reduced, the flow enters at a colder temperature. Therefore, the flap bay temperature stays at a reasonable working

temperature. For Design Table case 13, the predicted bay temperatures were 827° and 671°F for 1% and 2% sizing, respectively. This is in a workable range for nozzle flap thermals.

Flap Cavity Exit Area Study – A study was performed to examine the effect of the flap cavity downstream exit area on the cavity environment. When large flow percentages are brought into the flap cavity, the resultant higher pressure can lead to reverse flow into the flowpath at the aft portion of the divergent flap. In the majority of cases, the cavity exit area was specified at 150 in^2. This is generally adequate to evacuate the flap cavity. For 2% purge level, with cavity split at 50% or greater, the aft 50% section of the divergent-flap/sidewall interface exhibits reverse flow into the gas path.

Purge levels of 1% and 2% were examined, but 0.5% purge was not investigated because the 150 in^2 exit area is adequate for this level of purge. Figures 77 and 78 summarize the results found in this study. The modeled exit area has a large effect on the flap cavity pressure. When flap cavity overpressurization occurs, the flow leaks back to the gas path. Proper system sizing should account for system pressure and bay leakage to the gas path due to overpressurization.

Seal Study – A seal study was performed to determine the amount of sealing required along the divergent flap. The effect of sealing on leakage and flap cavity resultant temperature was calculated. The study involved several parameters. The amount of sealing along the divergent flap was varied for different purge levels. Two cycle points, supersonic cruise and takeoff, were examined. These covered the two main modes of nozzle operation, suppressed and unsuppressed. All unsuppressed cycle points should exhibit similar sealing characteristics to the supersonic cruise point. The same holds true for suppressed cycle points with the evaluated takeoff point. Along with the purge level and mode of operation, the effect of unsealed gap size was investigated because expected operational clearances have not yet been determined. The sum effects of thermal growths, initial fits, and part tolerances have yet to be calculated for the flap-train and sidewall.

Seal study results are shown in Figures 79 through 81. Figure 79 shows the resultant flap cavity temperatures for various purge levels at supersonic cruise conditions. The amount of sealing along the divergent flap was varied from 0% to 100% in 25% increments. The seal is assumed to hold a

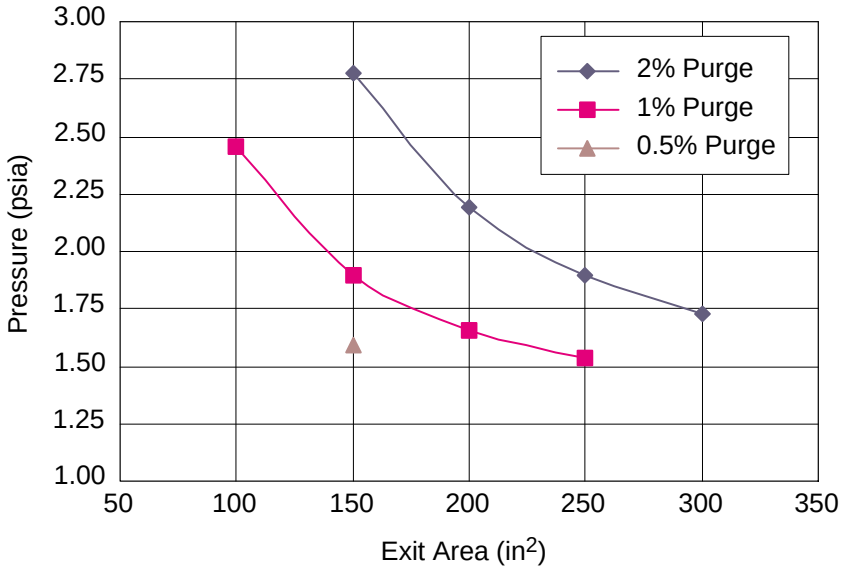

Figure 77. Flap Cavity Exit Area Influence on Cavity Pressure

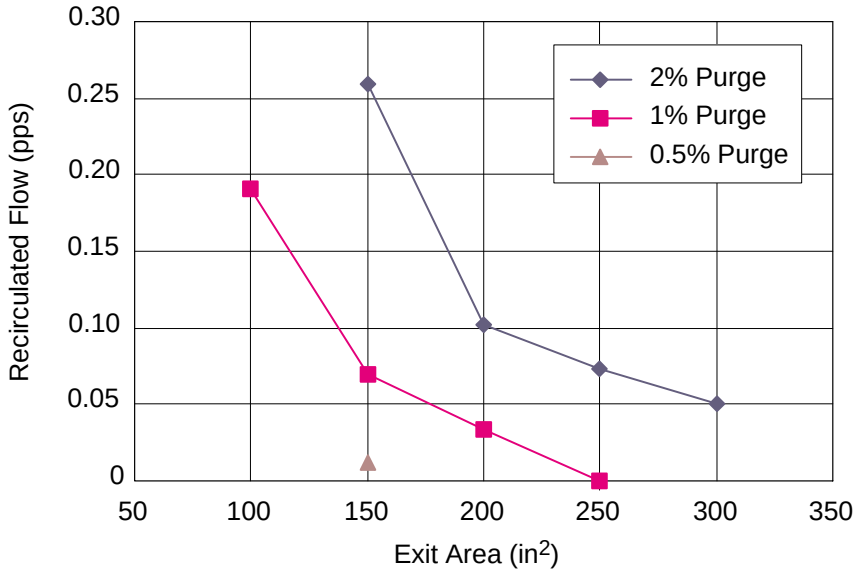

Figure 78. Effect of Exit Area on Leakage from Flap Cavity to Gas Path

0.008-in gap. The results show a 70° to 100°F reduction in flap cavity temperature by sealing to 50%. The benefits for sealing beyond 50% are small, as evident by the flattening of the curves from 50% to 100% sealing. For the predictions shown in Figure 79, a gap of 0.050-in was assumed for the unsealed sections of the divergent flap/sidewall interface.

The results of the unsealed-gap study are presented on Figure 80. Flap cavity temperatures were predicted for various unseal gap sizes at supersonic cruise operation condition. The unsealed gap size was varied at 0.05, 0.1, and 0.2 in. The open gap size demonstrates a large effect on the predicted temperature when the sealing is not performed near the throat where gas-path pressure is significantly above the bay pressure. As the pressure declines through the diverging section of the nozzle, the assumed gap size loses effect on the resultant flap cavity temperature. Again, the 50% seal coverage position appears to represent a good approximate cutoff where additional sealing provides diminishing returns against variation in unsealed gaps. Sealing less than 50% would make the design less robust, as variation in gap will lead to variation in the heat transfer environment in the flap cavity. The predictions of Figure 80 are for nominal purge flow sizing (1%).

Figure 81 shows the results for takeoff cycle. In this case, only one purge flow is examined. Two cases were considered: (1) complete seal and (2) deflections open. Even under sealed conditions, the expected sidewall deflections due to thermal and pressure loads were incorporated in the gap size for the restriction. The predictions were obtained from the sidewall deflection model. The added sealing does not significantly increase protection from the gas path leak. This is due to the flat pressure profile in the nozzle. Because the nozzle is not choked at the convergent/divergent hinge location, the static pressure does not drastically reduce through the nozzle. Thus, large gaps in the aft section of the divergent flap will leak equally with gaps in the forward section.

In the second case, the seals are assumed capable of spanning the deflections. Therefore, the deflections are neglected and the standard 0.008-in gap is assumed for a sealed section. The results show a dramatic reduction in bay temperature by sealing beyond 50%. These takeoff results present the only argument to extend the sealing beyond 50%.

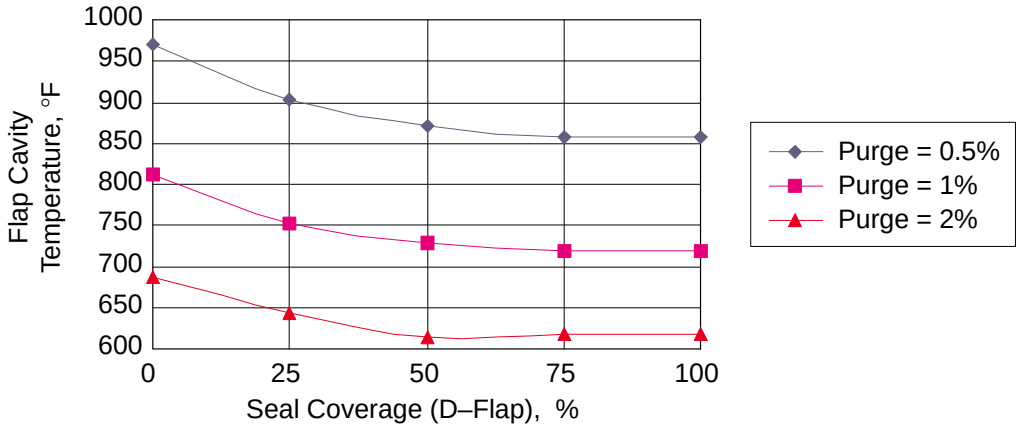

Figure 79. Effect of Purge Level on Flap Cavity Temperature Vs Divergent Flap Seal Coverage

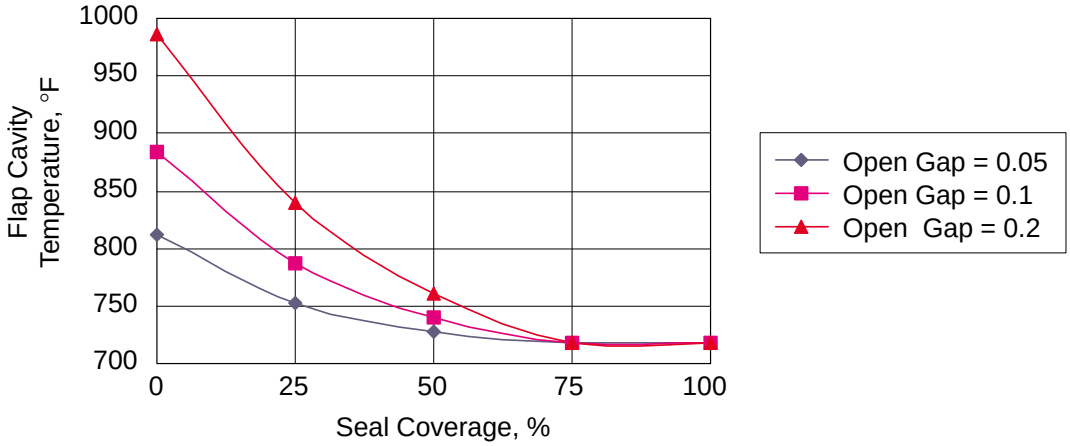

Figure 80. Effect of Unsealed Gap Size on Flap Cavity temperature Vs Divergent Flap Seal Coverage

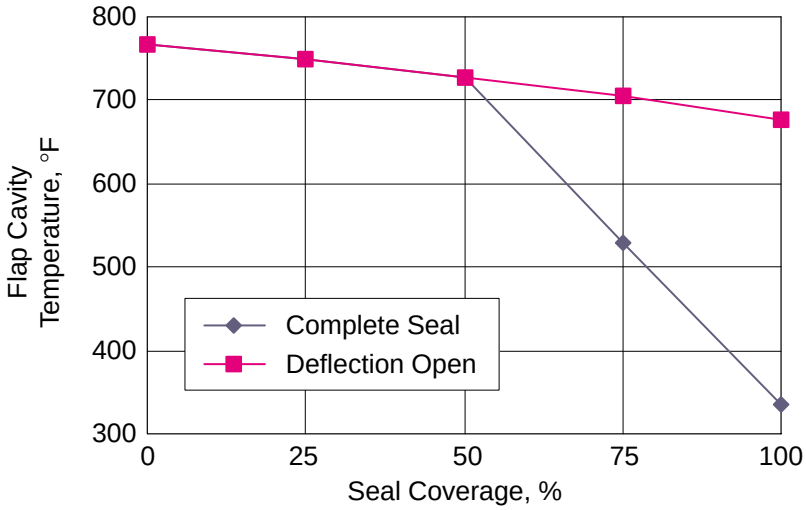

Figure 81. Flap Cavity Temperature Vs Seal Coverage at Takeoff (Nominal Sizing)

The as-designed purge system appears capable of addressing heat transfer concerns in the nozzle flap and sidewall regions under most cycle condition. The data should enable the designer to properly size key system components and establish a basis for length of sealing along the divergent flap.

Purge Air Needed to Satisfy Static Structure and Flap-Cavity Requirements – To aid the nozzle designer in product design, a series of graphs are shown that summarize the purge flow thermal effect on various nozzle components. Nozzle designers are familiar with the temperature requirements for the various materials under consideration. To make the material selection for a component, the designer will need to know the predicted maximum metal temperature that the component will experience. The maximum component temperature will occur at the extreme boundary condition of supersonic cruise flight. All analyses of this report were performed at this flight condition for consistency.

Several factors influence the expected metal temperatures of the nozzle components. The gas path and exterior boundary conditions have the largest influence on resultant temperatures. Another influencing factor is the nozzle purge temperature and flow environment.

Figures 82 through 85 illustrate the effect of purge temperature on individual component maximum temperatures. In these figures, the necessary flap cavity temperature can be determined based on each flap component thermal requirement. Once the approximate flap cavity temperature is found, Figures 86 and 87 can be consulted to determine the purge flow level and split necessary to produce this flap cavity temperature. Finally, with the purge flow level and split determined in a manner similar to the flap-train region, the sidewall and transition duct thermal environment is presented. In these regions, the purge flow is not exposed to any leakages from the gas path; therefore, the purge air temperature is modeled only as the result of thermal heat-up. Figures 88 through 92 can be consulted to determine the purge temperature needed based on the flap-train actuators or actual sidewall thermal requirements. With the purge temperature determined, Figures 93 and 94 relate purge flow amount to purge flow heat addition from the walls.

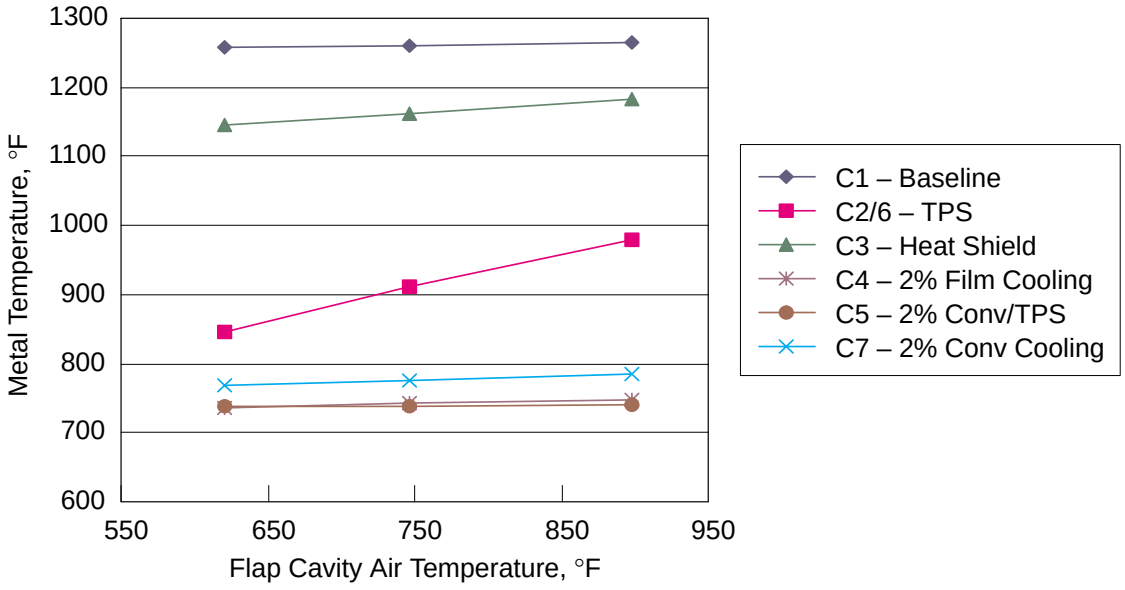

Figure 82. Convergent Flap Maximum Structural Temperatures

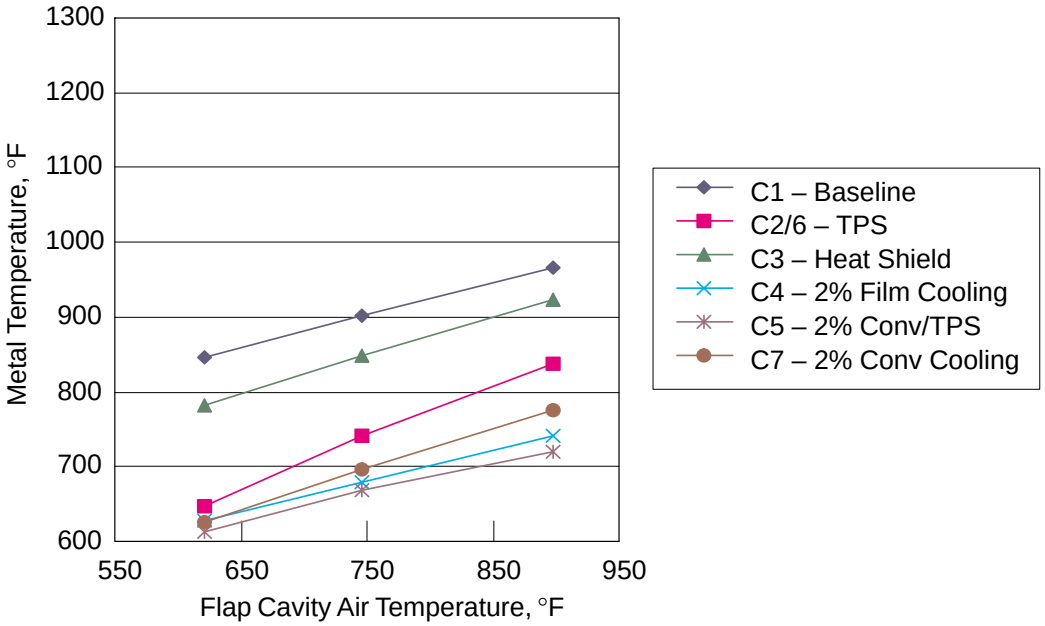

Figure 83. Convergent Flap Minimum Structural Temperatures

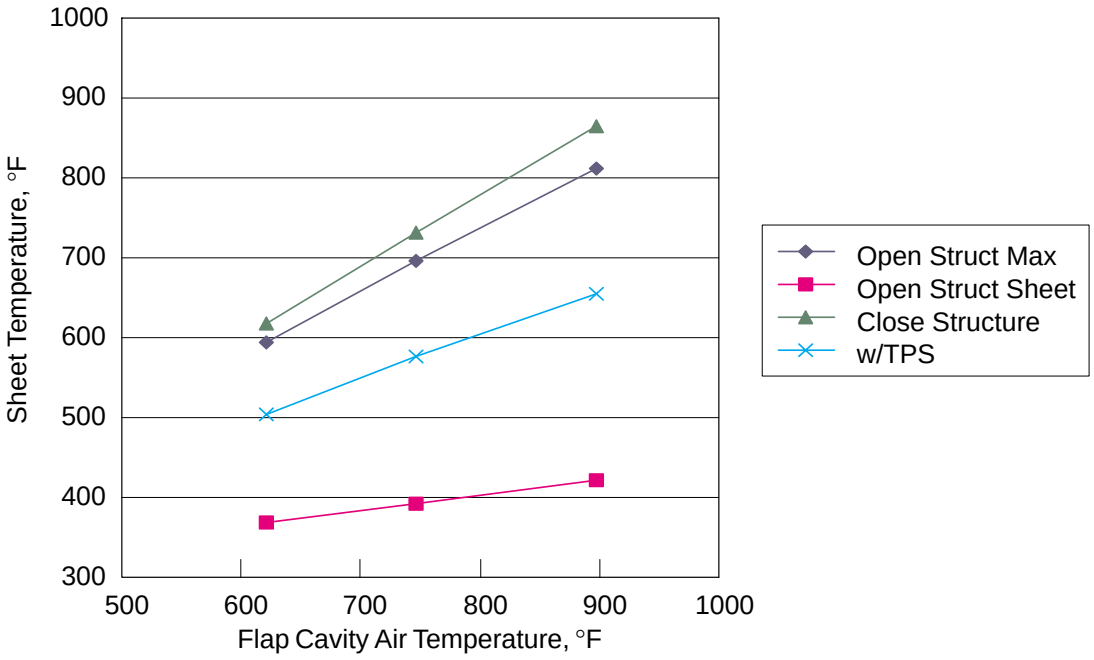

Figure 84. External Flap Temperatures at Various Flap Cavity Air Temperature Conditions

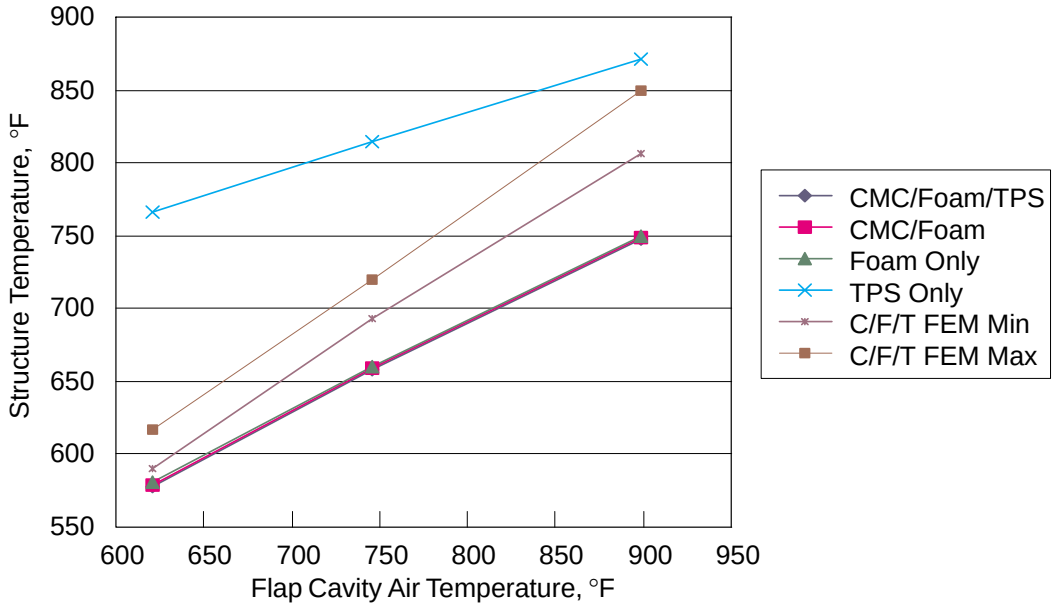

Figure 85. Divergent Flap Metal Temperatures at Various Flap Cavity Air Temperature Conditions

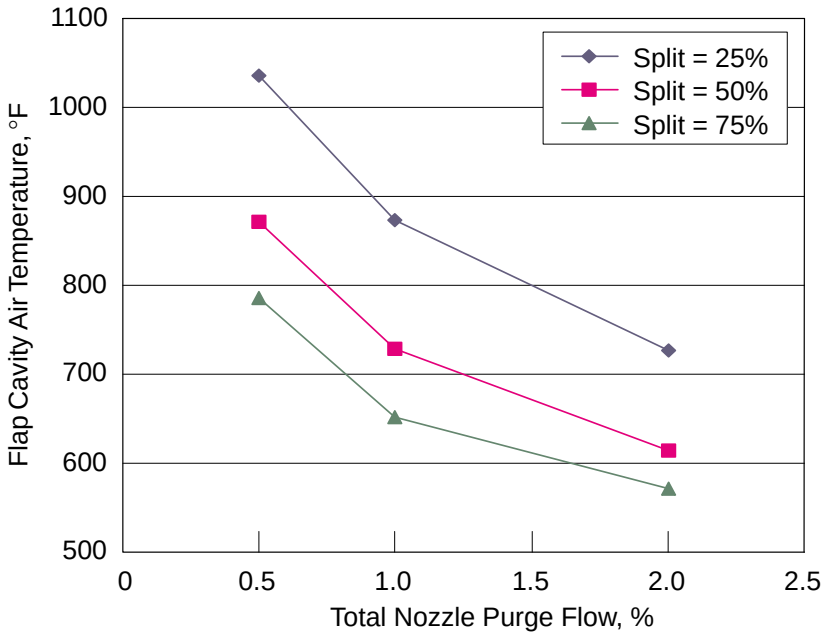

Figure 86. Flap Cavity Air Temperatures at Different Purge Supply Levels

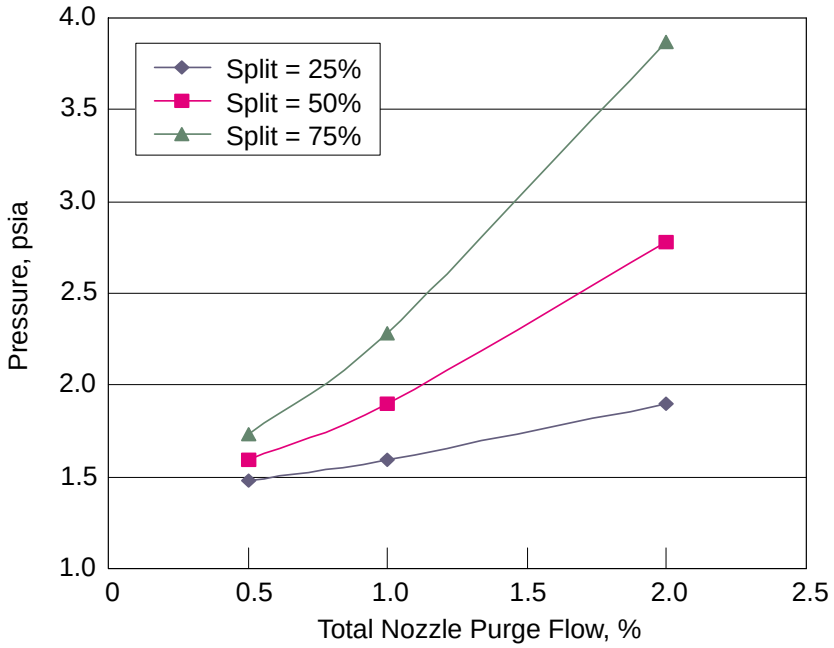

Figure 87. Flap Cavity Air Pressures at Different Purge Supply Levels

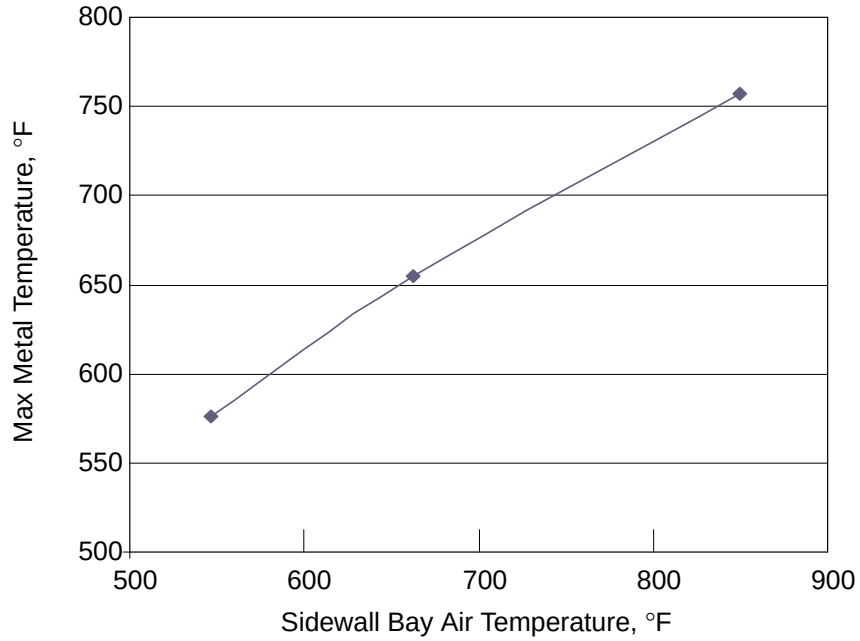

Figure 88. Flap-Train Actuator Maximum Temperatures at Various Sidewall Bay Air Conditions

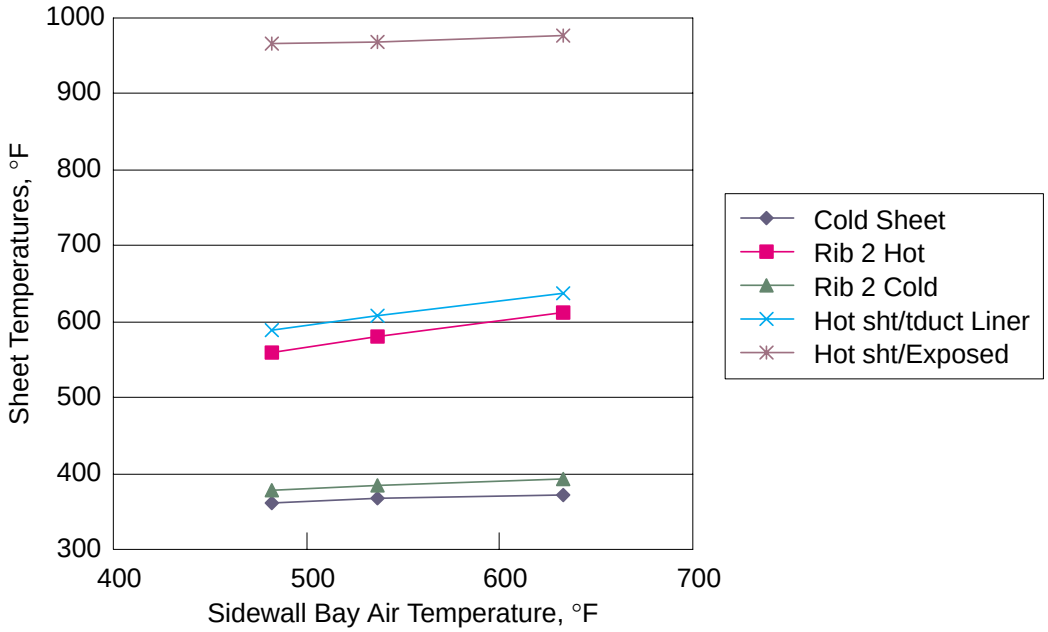

Figure 89. Compartment 2 Sidewall (at T Duct) Metal Temperatures at Various Sidewall Bay Air Conditions

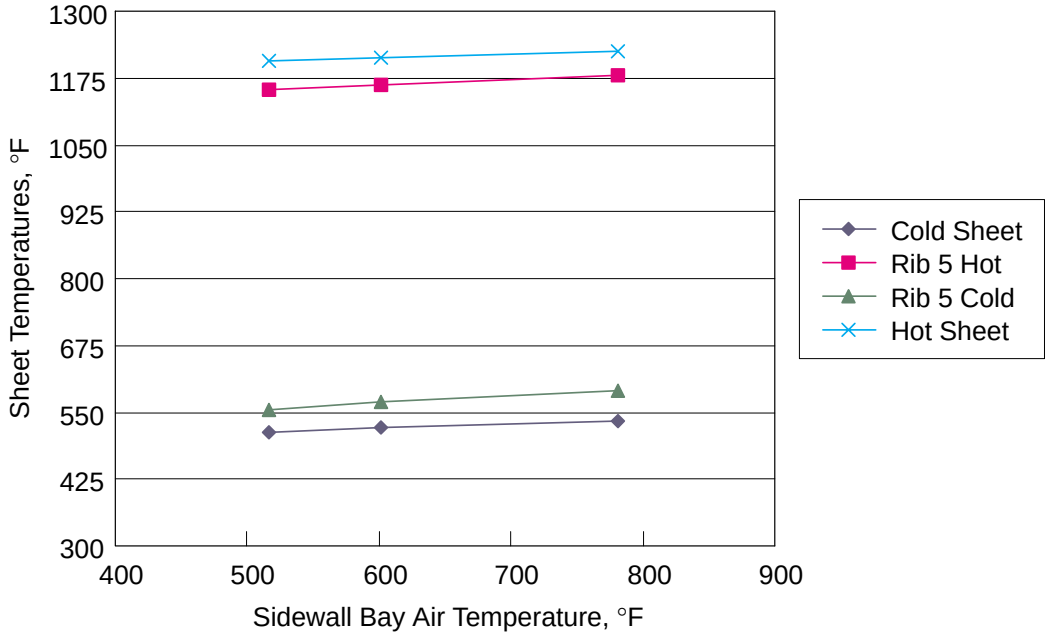

Figure 90. Compartment 5 Sidewall Metal Temperatures at Various Sidewall Bay Air Conditions

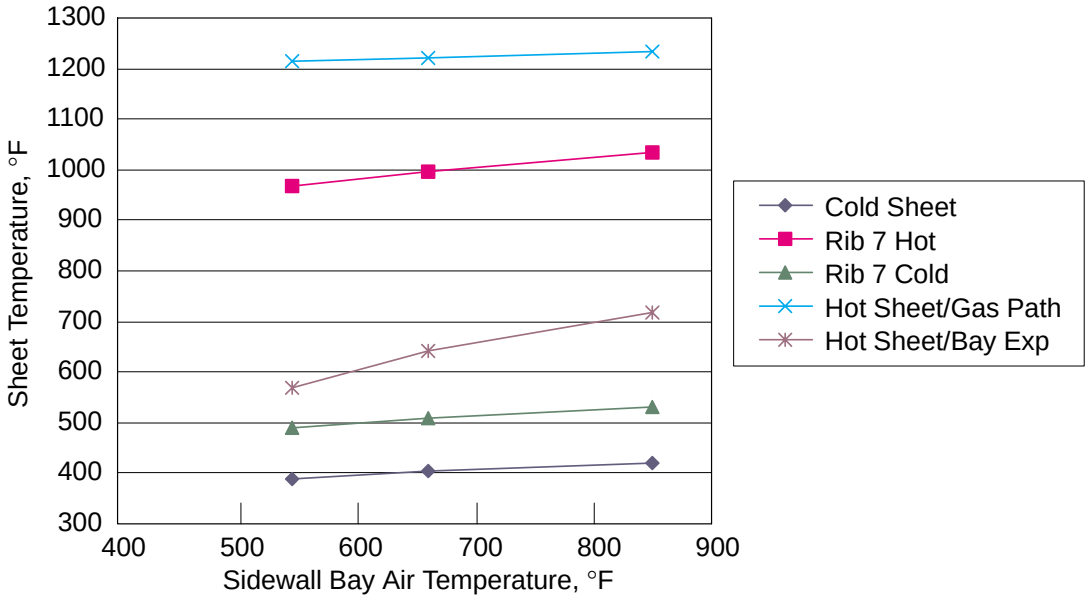

Figure 91. Compartment 7 Sidewall Metal Temperatures at Various Sidewall Bay Air Conditions

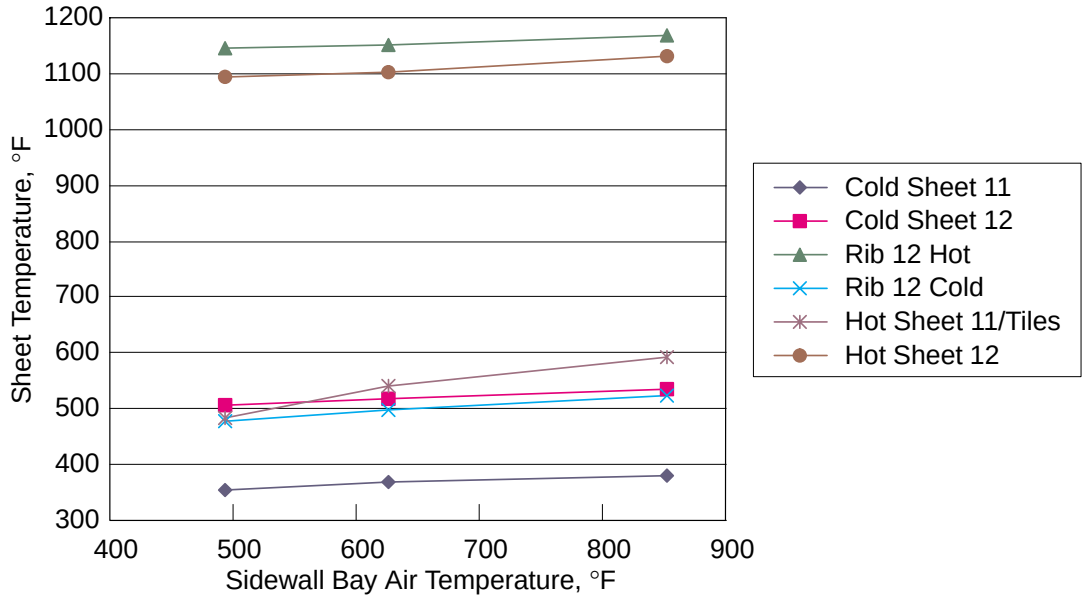

Figure 92. Compartment 11/12 Sidewall Metal Temperatures at Various Sidewall Bay Air Conditions

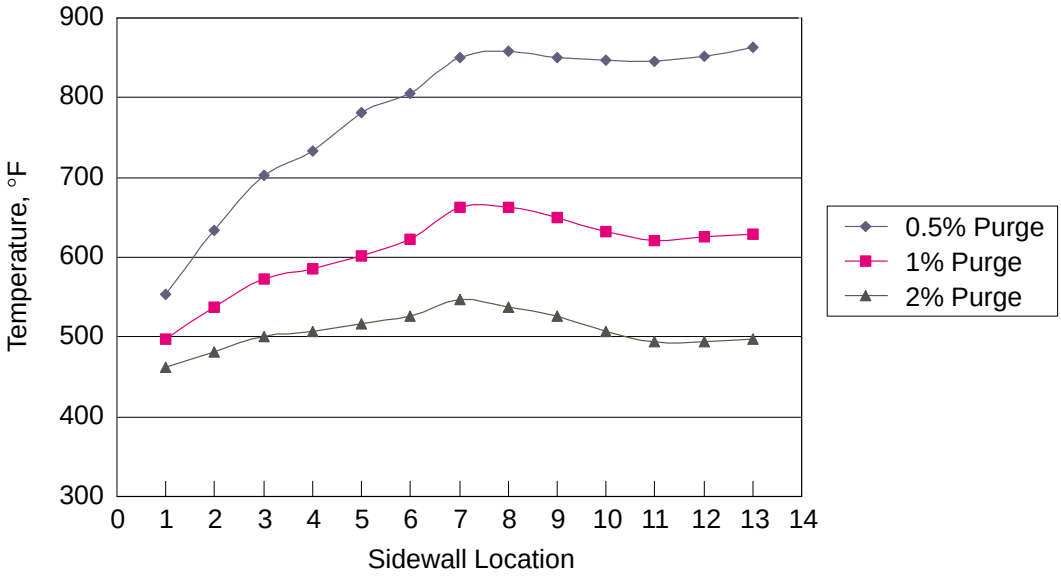

Figure 93. Heat Addition/Subtraction Sidewall Bay Air Temperature Profile (No TPS on T Duct)

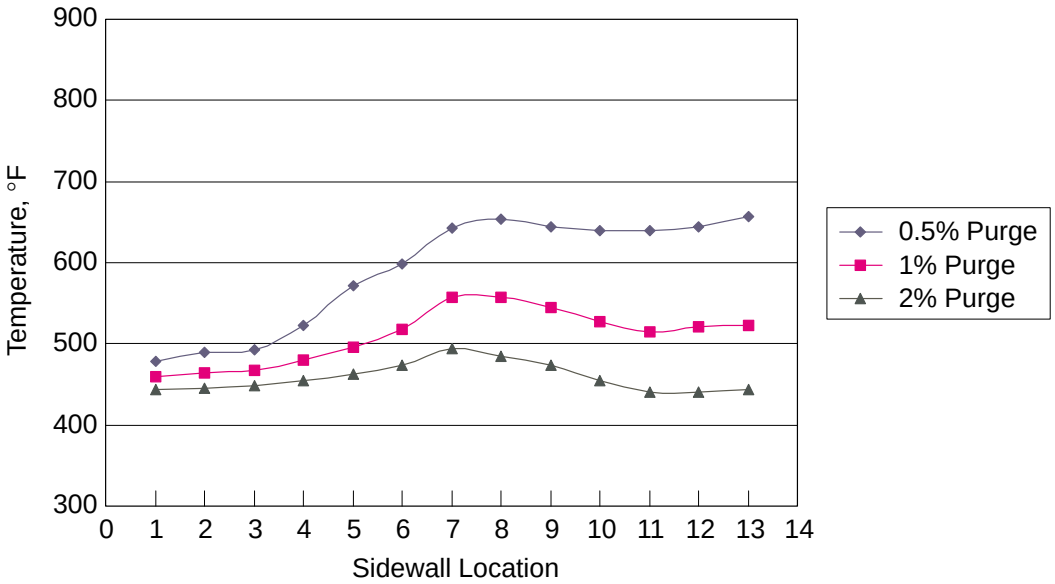

Figure 94. Heat Addition/Subtraction Sidewall Bay Air Temperature Profile (TPS on T Duct)

The figures cited in the foregoing paragraph summarize the thermal conditions of the nozzle. All results are shown for supersonic cruise conditions unless otherwise noted. The results are separated into two sections. The first section is for flap cavity conditions. In this region the air temperature is the result of mixing between the purge flow and leakages. The metal temperatures for each individual nozzle flap-train component are shown in Figures 82 through 85. Figure 82 shows the convergent flap maximum metal temperature for several considered designs. The graph shows that some design options exhibit minimal thermal influence from the flap cavity air temperature. The convergent flap design incorporating a thermal protection system (TPS) demonstrates the strongest flap cavity air temperature influence. Figure 84 shows the external flap maximum temperatures. In this study, three external flap designs were considered: an open sheet and stringer design, a closed structure like a honeycomb or superplastic-formed/diffusion-bonded structure, or a thermally protected design. Figure 85 shows similar results for the divergent flap. Here, results from the finite-element model and the one-dimensional analysis are shown. The FEM calculated a temperature range for the corrugations. (See FEM max and min values.) Several cases with different hot-side protection were also presented for the divergent flap on this figure.

Figures 86 and 87 graph some flow model results. Figure 86 shows the expected mixed flap cavity air temperature at three different purge flow-split conditions between the flap cavity and the sidewall bay were considered. Figure 87 plots the flow model results for the flap cavity air pressure.

The second section is for transition duct and sidewall conditions. For this section, the purge flow is not exposed to hot gas leakages. Figure 88 shows the predicted flpa train actuator temperatures in the convective and radiation environment under various purge flow temperatures. In this case, the sidewall bay air temperature has some influence on the resultant actuator temperature. Figures 89 through 92 show the effect of sidewall bay air temperature on sidewall temperatures. For the actual sidewall hardware, the large influence from the gas path and exterior thermal conditions can be seen. The purge flow does not exhibit a strong affect on the resultant temperature. The flatness of the hot- and cold-sheet temperature curves demonstrates this fact. The sidewall bay air temperature cannot be relied on to drive the sheet temperatures hotter or colder.

Figure 89 graphs temperatures for the sidewall section at compartment 2. See Figure 95 for compartment locations within the sidewall. In this compartment, a portion of the sidewall is located within the actual transition duct hardware and is protected by the liner. Unlike the exposed cold or hot sheets, these sheet temperatures do exhibit a thermal response to the sidewall bay air temperature. Figure 90 shows the temperatures for compartment 5. Nodal positions were selected in central locations on the compartment sheets. Temperature curves for these nodes are graphed. In order to show rib thermal gradients, maximum and minimum temperatures off the rib are also graphed. These nodal temperatures do not exhibit much response to the sidewall bay air temperature. Figure 91 shows selected sidewall compartment 7 nodal temperatures. In this compartment, two distinct boundary conditions exist on the hot side: nozzle gas path and flap cavity conditions. The flap cavity exposed conditions with ramped down temperature and lower film coefficient results in a more sidewall-bay-air-influenced sheet temperature. Figure 92 presents selected nodal temperatures for compartment 11 and 12. Here, a tile-shielded sheet temperature is presented along with fully exposed sheets.

Finally, the sidewall bay flow temperature profiles are shown on Figures 93 and 94. These profiles result from heat addition and subtraction from the hot and cold sheets, respectively. The only difference between the two profiles is within the transition duct. For Figure 93, the transition duct

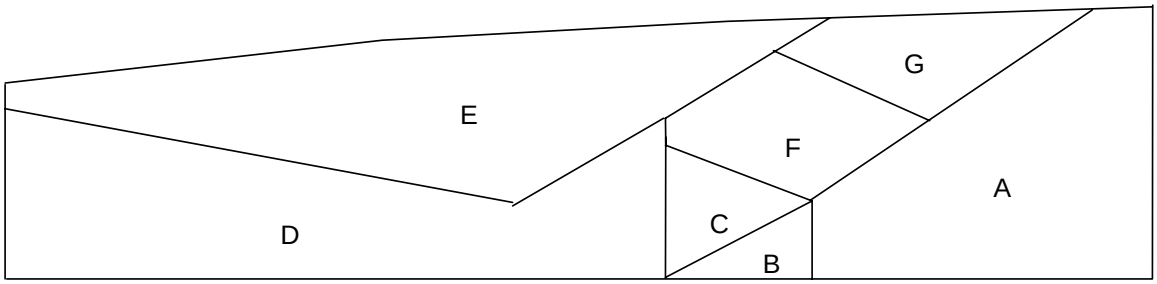

(a) Hot Sheet Exposure

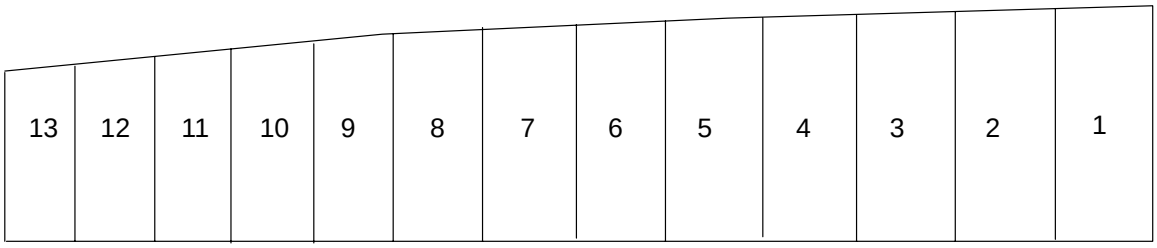

(b) Internal Section Compartments

Figure 95. Sidewall Compartment Layout

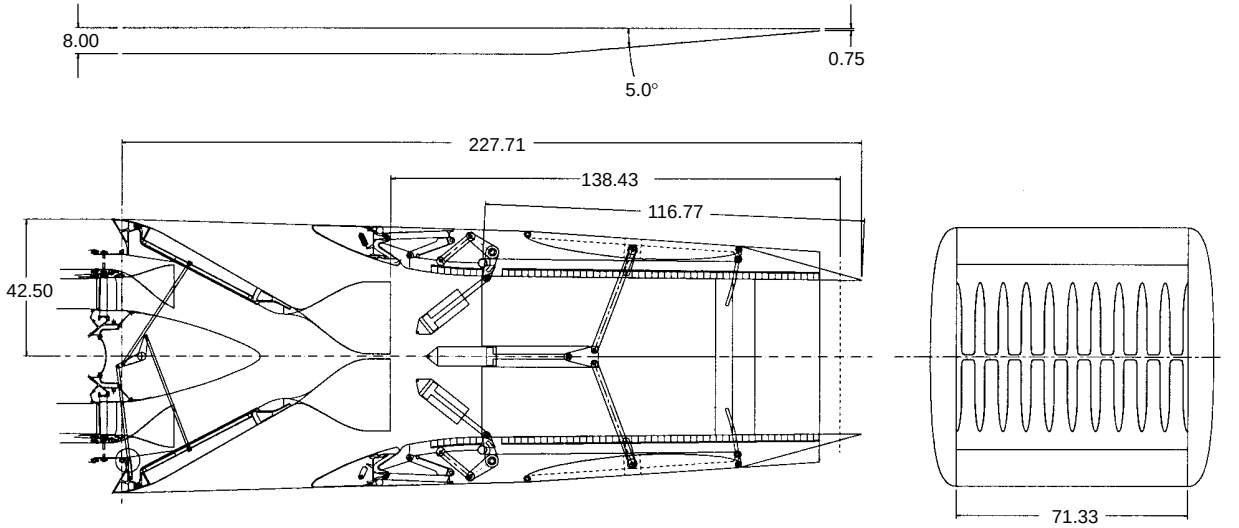

Cycle	Flow Rate (pps)	A_{mix} (in^2)	SAR	MAR	Aspect Ratio	Mixing Length (in.)	Nozzle Width (in.)	A_{trt}/A_{mix}
3770.60 (April 22, 96)	800	3570.3	2.9	0.95	1.5	138.4	71.33	6.1

Chute Penetration (in.)	No. of Cold Lobes (per nozzle)	No. of Hot Lobes (per nozzle)	CER	Hot Lobe Width at A_8 (in.)	Hot Lobe Width at Exit (in.)
0.925	20	20	1.10	2.509	2.76

Nozzle Length at Takeoff (in.)	Div. Flap Length (in.)	Nozzle Fore–Flange Half Ht. (in.)	A_{max} (in^2)	Forward Boattail (deg.)	Supercruise Boattail (deg.)	Subcruise Boattail (deg.)	Sidewall Boattail (deg.)	Nozzle Weight (lb/nozzle)	Nozzle c.g. (in.)
227.7	116.7	42.5	7220	1.62	4.0	13.61	5.0	8015	TBD

Figure 96. Nozzle Definition Summary

is modeled without a thermal-protection system. Therefore, it picks up significantly more heat than a T duct with TPS. The profile for this second configuration is shown in Figure 94.

To conclude, Figures 82 through 94 summarize the thermal influence of the sidewall bay and flap cavity air system on the nozzle static structure and flap or sidewall hardware located in these regions. With this information, the designer can assess the thermal environment effects on nozzle hardware located in these regions.

5.5.2.3 Nozzle Geometry Summary

Key Aerodynamic Geometry and Dimensions – The final geometry and key dimensions for the fixed-chute nozzle are defined in Figure 96. This nozzle was designed for the 3770.60 engine cycle with a flow rate of 800 lbm/s and an A_{mix} of 3570.3 in^2. In the takeoff mode, the MAR is 0.95 with a mixing length of 138.4 in. This length is the distance between the mixer exit and the nozzle exit, which is the average of the end of the divergent flaps and sidewalls. The critical boattail angles are as follows: supercruise is 4.0°, subcruise is 13.6°, and the sidewall is 5.0° relative to the engine centerline.

Key Mechanical Nozzle Geometry and Dimensions – There are several key mechanical features of interest. The final nozzle has an 8.0-in sidewall envelope with a 5.0° sidewall boattail angle. Each mixer rack contains 10 hot lobes and 10 cold lobes, for a total of 20 hot and 20 cold lobes per nozzle. The final mixer design incorporates a half hot lobe along each sidewall. This nozzle has optimized the use of acoustic tile coverage by eliminating the disks previously used to actuate the divergent flap. However, there are two areas that required less than the optimum 2.0-in thickness of the acoustic absorbing bulk. The area near the nozzle centerline where the divergent flap actuator sweeps fore and aft uses 1.0 inch of bulk to make room for the actuator trolley in each sidewall. The other location is the vertical sidewall area between the divergent flap actuator linkage slots. This area also uses 1.0-in bulk. The divergent flap slots in the gas path are unique; however, preliminary aerodynamic performance analysis indicates that these slots trade favorably compared to the excessive sidewall deflection without the use of the aft tie rod. The tie rod passes through the divergent flap and ties the sidewalls together to limit deflection. The convergent flap is actuated through the linkage located in the sidewalls and requires the addition of a convergent flap seal at the forward end of the flap. This flap seal is driven by a series of helicoil springs located in the forward bulkhead along the width of the nozzle. The inlet doors are synchronized by the use of geared rotary actuators (GRA's) tied together with a drive shaft. The actuators are located near the bottom of the nozzle. These GRAs drive a link that ties to a crank in each sidewall, which link to both doors. The final nozzle weight is calculated to be 8015 lbm.

As the nozzle design evolved into this final configuration, many improvements were made to the overall design. The latest flap actuation scheme reduces nozzle weight and improves structural efficiency, safety, and system performance. The previous disk scheme used cantilevered rollers on the disks; the disks extended into a divergent flap roller track that did not offer a positive retention feature. From a safety standpoint, the tie rod holds the sidewalls together and provides positive retention of the divergent flaps. This latest actuation scheme also enhances system performance. By incorporating the tie rod design, sidewall tip deflection is held to a minimum, which reduces boattail drag and improves performance. In addition, the external flap, which actuates the divergent flap, deflects during operation in a manner that improves aerodynamic performance during the subcruise and supercruise flight points.

SAVE Event

Background – In 1996 following the December 1995 Preliminary Design Review, the P&W and GEAE mechanical design teams focused on improving the mechanical configuration on a full-scale size nozzle rather than the ½-scale design that was presented at the design review. During this process, several configurations were assessed under the "parallel effort" phase with the objective of going forward with the best configuration into the FSD design, fabrication, and test effort. The selected concept to go forward was the separate reverse port (SRP) nozzle, which consisted of sidewall, disk-mounted, actuated-flap-train components as illustrated in Figure 36 (page 35).

SAVE Event – Further definition of the mechanical components continued following the parallel effort decision. Total nozzle weight was estimated and rolled up to 9986 lbm. This was deemed unacceptable since it did not meet the strategic target maximum takeoff gross weight goal of 7830 lbm, missing the target by over 2000 lbm. The viability of the HSCT program was impacted by inability to meet this requirement. A review indicated the current status weight was reasonable with the added concern that, as the design matured, the weight had the potential to increase further. Figure 97 illustrates the total nozzle weight break-up.

Component	Status Weight
Centerbody	68
Fan/Core Mixer (VABI)	271
Inlet and Duct Doors	830
Ejector Mixer	867
Transition Duct	1063
Midframe	1275
Aft Sidewalls	934
Convergent Flaps	634
Divergent Flaps	920
Outer Flaps	310
Rev. Doors and Cascades	190
Acoustic Liner	788
Heat Shields	
Subtotal	8051
Controls and Actuation	1428
Misc.	408
Nozzle Total	9986

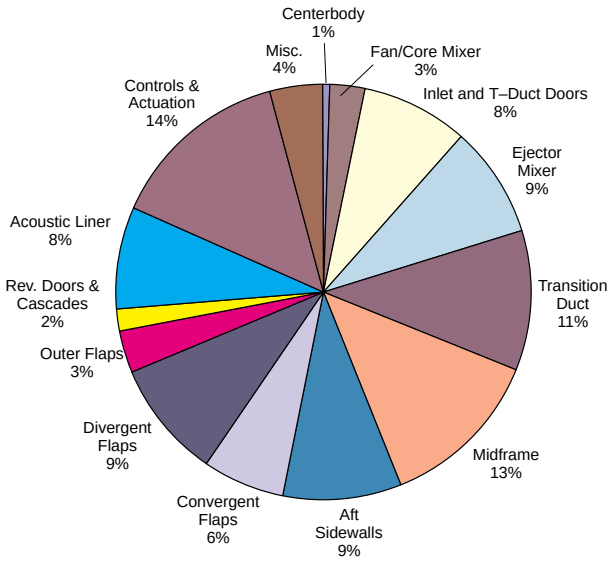

Figure 97. Pre-SAVE Nozzle Weight Summary

In December 1997, the SAVE event was held with the goal of assessing all nozzle components in terms of weight and contribution to the main goals of the HSCT program. Weight attributes were generated and compared to overall weight, noise, aerodynamic performance, life, fabricability, and reliability; then a product performance profile was generated. Figure 98 summarizes the projected nozzle weight resulting from the SAVE event.

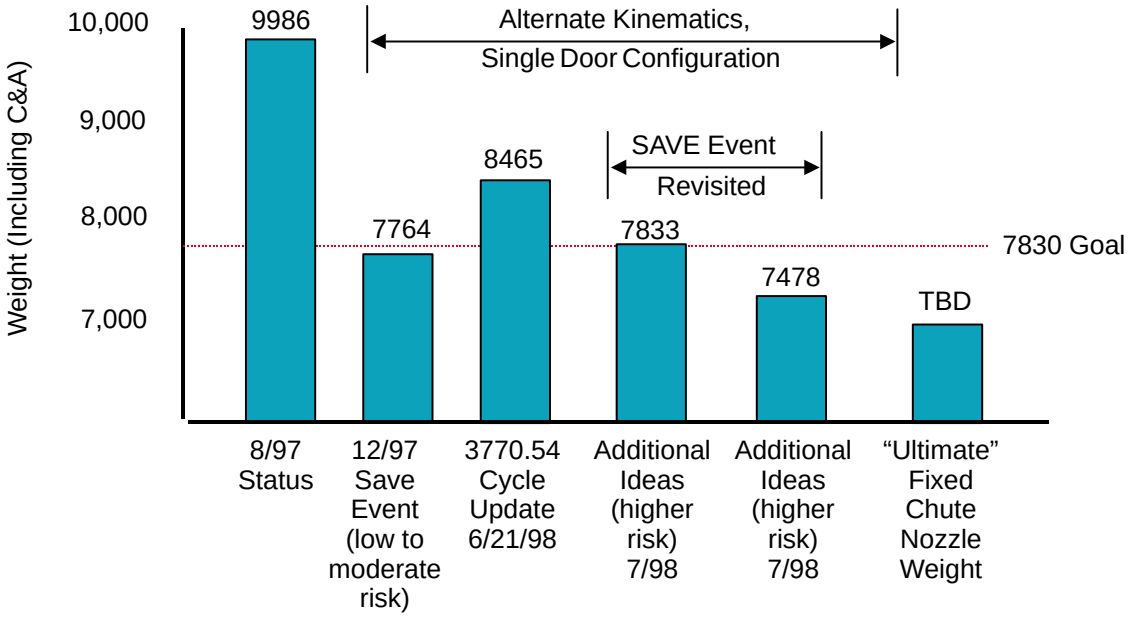

Figure 98. Nozzle Weight Estimates

SAVE Event Results – The SAVE event identified 16 items that were critical in bringing the total nozzle weight within program goals. The alternate kinematics task was identified as the single most contributors to weight reduction. Table 22 summarizes the 16 items identified.

Table 22. SAVE Event Results

Idea	Weight Savings (lbm)
1. Single-door ejector	364
2. Honeycomb in outer skins, transition duct, midframe, sidewalls	123
3. Sidewall crossbeam	170
4. Titanium transition duct, aft flap, sidewalls	223
5. Composite outer fairing	64
6. Fan/core mixer	60
7. Increase structural envelope	330
8. Alternate kinematics	457
9. Composite outer flaps	51
10. Composite cascades	26
11. Optimized door kinematics (inlet)	85
12. CMC chute vanes	51
13. Increase suppressed/unsuppressed transition time	43
14. Low-density bulk absorber	88
15. Minimum liner attachments	34
16. Reduced liner face sheet wall	55

Comparison To SAVE Event Goals

In August 1997, the nozzle team estimated the nozzle weight to be 9986 lbm. This was a 50% increase from the previous estimate. This new weight indicated the nozzle was approximately 2000 lbm over the 7830-lbm system target weight. In December 1997, the team decided to hold a *Systematic Approach to Value Engineering* event with the hope of reducing nozzle weight. This event was used to identify the key component drivers for weight and function of the nozzle. The results were used to identify the areas of the nozzle that could be targeted for redesign to provide a significant weight savings. After the SAVE event, the weight-saving ideas were grouped into three proposals: "A," "B," and "C." The team chose to target the items identified in proposal "C." Due to funding and time limitations, the team chose six areas of focus to reduce the weight of the nozzle. Table 23 is the itemized list of proposal "C" along with the actual weight savings capitalized on during the post-SAVE-event design efforts. The total weight savings realized was 1971 lbm, which reduced the nozzle weight from 9986 to 8015 lbm. If time and money allowed the design effort to continue, the team could have incorporated 10 more SAVE event items to potentially save an additional 1042 lbm, thus dropping the nozzle total below 7000 lbm.

Task C5, *Incorporate Alternate Kinematics*, saved the most significant weight of all the tasks worked. It saved a total of 1454 lbm per nozzle which was above and beyond the predicted 457-lbm savings. Because this new actuation system incorporated the tie rod to reduce the sidewall deflection, task B33 was eliminated. This task was supposed to investigate increasing the sidewall structural envelope to reduce deflection, but this was taken care of with the addition of the tie rod. The next

Table 23. Latest Nozzle Weight Savings Compared to the Original SAVE Event Goals

Ref. No.	Weight Reduction Item	SAVE Goals Weight Reduction	Linear Actuation 05/99 Status Weight Reduction	Comment
A5	Single Door	364	**246 ***	**less than SAVE goal**
A4	Incorp. Honeycomb	123	– –	post CDR candidate
B17	Sidewall Cross Beam	170	– –	**part of alt. kinematics**
B23	Incorp. Ti	223	– –	post CDR candidate
B25	Composite Fairings	64	– –	post CDR candidate
B39	Fixed Fan/Core Mixer	60	**96**	**meets SAVE goal**
B33	Increase Structural Envelope	330	– –	post CDR candidate
C5	Incorp. Alternate Kinematics	457	**1454 ****	**exceeds SAVE goal**
D9	Composite Outer Flap	51	– –	post CDR candidate
D11	Composite Cascades	26	– –	post CDR candidate
E13	Optimize Door Kinematics	85	– –	post CDR candidate
E38	CMC Vanes – Ejector Mixer	51	– –	post CDR candidate
E27	Increase Mode Transition Time	43	– –	**part of alt. kinematics**
F9	Lower Bulk Density	88	**88**	**meets SAVE goal**
F6	Minimize Attachments – Acoustic Liner	34	– –	post CDR candidate
B16, F10	Reduce Facesheet Thickness – Acoustic Liner	55	– –	post CDR candidate
N/A	Reduced Ejector Mixer Length	N/A	**54**	
N/A	T–Duct Further Design Development	N/A	**33**	
	Total	2222	1971	

Positive values represent weight reductions

* Inlet Door = 280; C&A = –34 (wt. adder)

** Midframe = 474; Aft Sidewall = 531; Flap C&A = –23(wt. adder); Pump C&A = 130; C_{flap} = 73; D_{flap} = 321; Outer Flap = –51(wt. adder)

- Current Baseline Linear System Meets or Exceeds Applicable SAVE Goals
- Achieved 89% of SAVE Event Total Goal
- 10 remaining SAVE weight reduction items representing potential for an additional 1042 lb/nozzle

most significant savings came from eliminating one set of inlet doors required to transition the nozzle from takeoff to cruise mode. This savings totaled 246 lbm compared to the predicted 364 lbm. The next largest savings came from task F9. Although this task did not offer large savings, it was already being worked through the EPM program. The lighter bulk was eventually incorporated to save 88 lbm, which was the same as the predicted weight savings. Task B39 saved 96 lbm by changing the VABI design to the fixed fan/core mixer. A new fan design was developed which eliminated the need for a VABI. Therefore, the Fixed Fan/Core Mixer offered a fixed-area mixer at a lighter weight and reduced complexity compared to the previous VABI design. This weight savings was more than the predicted 60 lbm.

Two other efforts were worked in parallel to the SAVE event tasks: the "Reduced Ejector Mixer Length" and the "T-Duct Further Design Development." The first, an ongoing task by the aerodynamic group to shorten the mixer, also shortened the nozzle. This task was completed because of the LSM, CASL, and Gen. 3.5 high-performance mixer results indicated that shortening the mixer provided a shorter nozzle without a performance loss. This task saved 54 lbm per nozzle. The other task was a redesign of the transition duct. The original nozzle had an Inconel 718 structure with no liner. By changing the back structure to Ti 6–2–4–2 and adding a hot-side liner, the transition duct saved 33 lbm.

5.5.2.4 Fan/Core Mixer

The fan/core mixer design was to serve multiple purposes. It was located just aft of the turbine exhaust case (Figure 99), and the basic functions were to:

1. Mix fan and core flows to reduce gas temperature, extending mixer/ejector life
2. Hold fan pressure ratio constant to operate at high efficiency
3. Increase stall margin
4. Improve specific fuel consumption
5. Suppress noise through improved hot/cold-stream mixing

Early in the CPC program, the fan/core mixer was to be designed such that it would aid in maintaining adequate fan stall margin. The fan/core mixer at that point was a variable-area concept that would allow different fan/core area ratios at different engine power settings.

Later in the program, the bypass fan was redesigned and consequently did not require assistance from the fan/core mixer for stall margin. This was followed by a performance study that examined the system impacts of a fixed-area fan/core mixer. Aside from performance, a fixed-area fan/core mixer would be much easier to design, due to the removal of moving parts, and offer the added benefit of weight reduction. These factors drove the design team to look at options other than a variable-area mixer (hence the study). The conclusions were that, with no need to add fan stall margin, a fixed-area fan/core mixer would not impose a significant performance loss and should be used. The study produced a recommended area ratio for the mixer and initial estimates of the performance losses. There was a small performance loss at subsonic cruise (about 3%) at 60% thrust setting. Takeoff performance differences between variable and fixed mixers were negligible. The design effort at that point was redirected to develop the fan/core mixer as a fixed-area concept (Figure 100).

Design Issues – The prominent design challenge to a fixed-area fan/core mixer is to keep the mixer lightweight while making it strong enough to overcome the vibratory characteristics of a large-panel

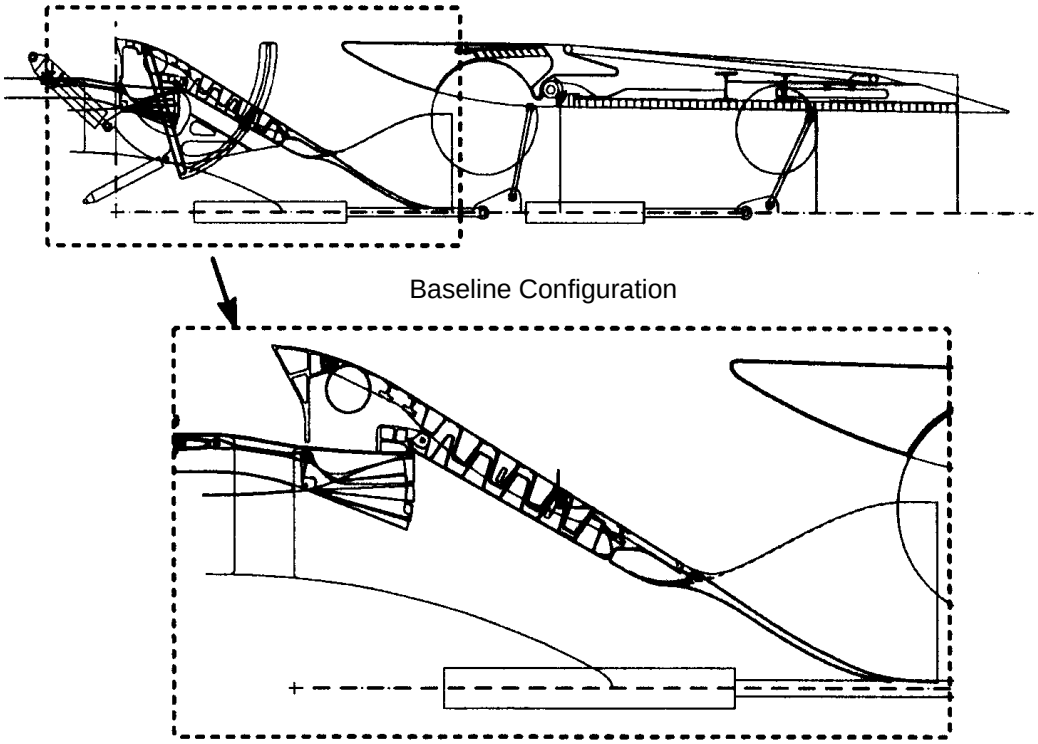

Figure 99. Fan/Core Mixer, Nozzle Integration

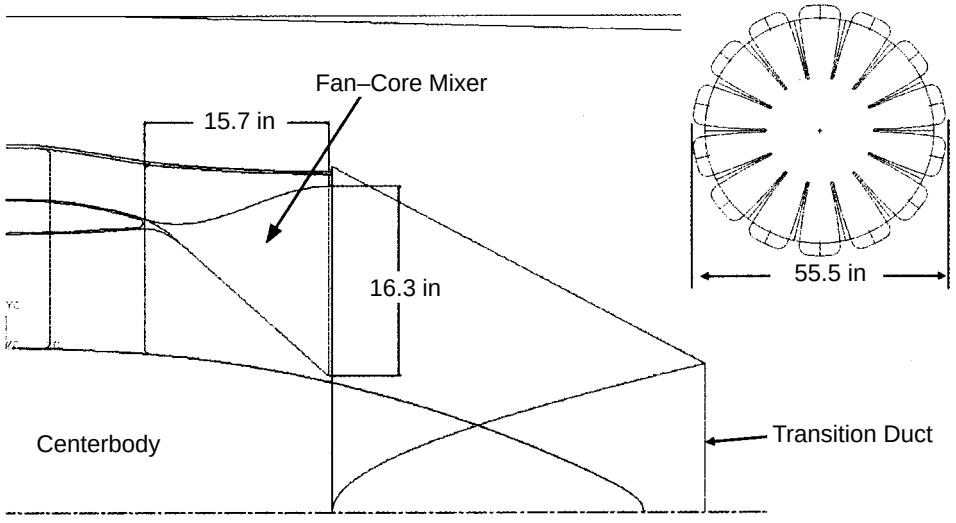

Area Ratio: 0.28 (A16/A56)
Assumptions: 80% Mixer Effectiveness, No Losses Through Mixer

Figure 100. Fixed-Area Fan/Core Mixer

body design. Without adding supports at the trailing edge on the ID and OD, as well as cold-side vanes, the natural frequency of this body was extremely low, about 50 to 200 Hz, due to the large areas of unsupported panels (vane sidewalls). This was seen in the initial design iterations of the mixer/ejector that is downstream.

The design team attempted to improve the penetration and mixing of the flow by adjusting the mixer lobes to facilitate deep penetration into the core stream, see Figure 101. The AACE team worked with the fixed-area fan/core mixer geometry to minimize pressure losses due to flow separations. The deep-lobed mixer had more separation on the core side. The optimized aerodynamic geometry was closer to the profile on the left of Figure 101.

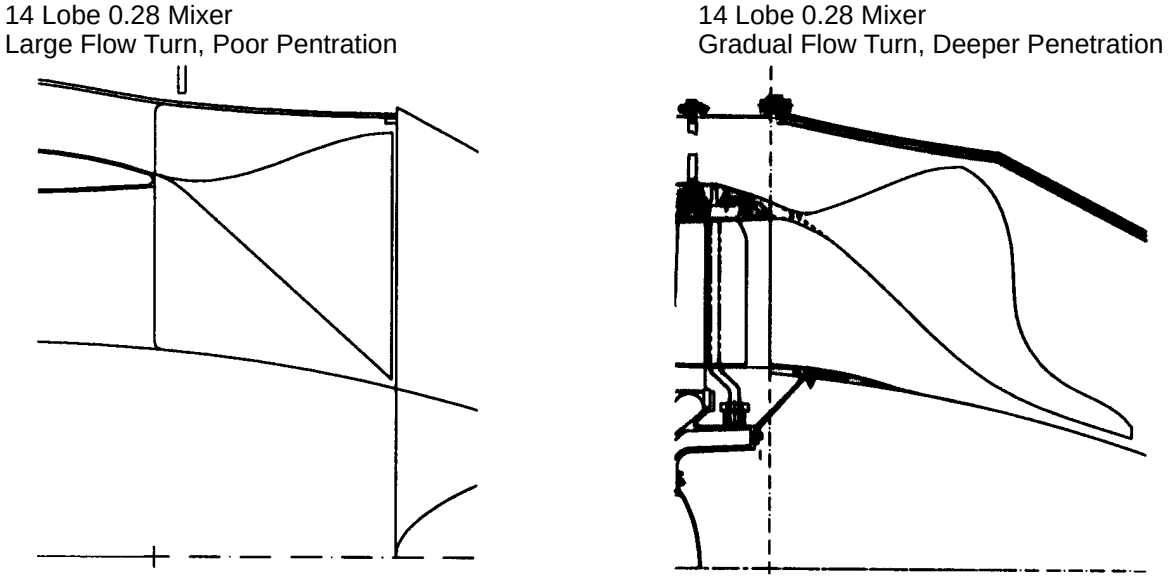

Figure 101. Normal and Deep-Lobed Fan/Core Mixers

Key issues that reflect the downstream system impacts need to be addressed with the new geometry:

- What is the engine performance impact with the new fixed-area fan/core mixer?
- How much acoustic detriment exists without a fan/core mixer? That is, with optimized suppression system, is the fan/core mixer needed?
- What is the actual mixing effectiveness and effects on downstream components (mixer/ejector temperature effects)?

5.5.2.5 Transition Duct

The transition duct changes the engine flowpath from annular to rectangular. The transition duct also provides the structure for connecting the nozzle to the engine.

Several nozzle systems are closely related to the transition duct. The fan/core mixer is located in the forward section of the transition duct. The ejector/mixer, a device that mixes outside air with the engine exhaust for noise reduction at takeoff, is located in the aft section of the transition duct. Air diverter doors are mounted in the transition duct. The diverter doors are on the top and bottom of the nozzle and swing inward to introduce outside air to the mixer/ejector.

The transition duct uses liners made of high-temperature materials such as composites and nickel alloys to transition the flowpath from annular to rectangular. The liners also isolate the structural members from the hot exhaust gases.

The basic structure of the transition duct comprises forward and aft bulkheads with structural sidewalls between the bulkheads, see Figure 102.

The axial station where the transition duct flowpath fairing becomes fully rectangular is where it mates with a noise-silencing mixer/ejector. The mixer/ejector introduces atmospheric air into the nozzle flow stream for the purpose of reducing noise during takeoff. Large air-diverter doors are mounted at the top and the bottom of the transition duct structure. The doors swing inward, aligning with the mixer/ejector, to introduce outside air into the mixer. The doors and the mixer/ejector are supported by the transition duct structure. The forward bulkhead serves several purposes. First, it provides a mount for the aft structure of the transition duct. Second, it provides a short section of the airframe/nozzle outer mold line fairing for the top and bottom of the nozzle immediately forward of the doors that open to divert outside air inwards to the mixer/ejector during the noise suppression mode during takeoff. Third, it provides support for the mounts for the right and left side outer mold line fairing panels.

The outer mold line fairings are the outer skin where the atmospheric air contacts the nozzle. These fairings are truss core panels that are bolted to the sidewalls. The panels are removable so that maintenance can be performed on the diverter door actuation system. The panels are rigidly mounted and are structural members of the nozzle in addition to serving as fairings.

Structural Function – In the context of viewing the nozzle as a long, rectangular box with a bottom, top, and sidewalls, the sidewalls are the principal structural members of the nozzle. The top and bottom walls of the nozzle are interrupted by openings for diverter doors, reverser doors, and the convergent/divergent flaps. The many interruptions preclude the possibility of upper and lower walls serving as primary structural members to carry the vertical G loads of the nozzle. Therefore, the sidewalls must be the primary load-carrying structure. These sidewalls are 2.5-in thick by approximately 80-in high and constructed of 6–2–4–2 titanium truss core.

The most significant load on the sidewalls is the downward G loading from a hard landing. The entire weight of the nozzle is cantilevered on the transition duct, inducing an overturning moment on the sidewalls. This load puts the upper portion of the sidewalls in tension and the lower in compression. The face sheets in the truss core structure carry these loads along with assistance from the rails and integral beams. Without the webs connecting the sheets together the face sheets would not stay in plane when subjected to this high bending load. A single face sheet without support would warp out of plane (due to shear lag) when subjected to large overturning bending loads. However, the square-grid pattern of the webs ties the sheets together and minimizes the distance over which the face sheets are unsupported.

Pressure-induced loads on the sidewalls tend to push them outward away from the engine centerline. These outward loads are resisted by the members of the fore and aft bulkheads that tie the sidewalls together. To resist bulging of the sidewalls from pressure-induced loads and to reduce stress, the sidewalls have integral structural beams to help carry the pressure loads and external G loads. In addition to the top and bottom rails each sidewall has four horizontal beams, two diagonal beams, and a vertical beam. The four horizontal beams reduce the length of unsupported span of the sidewalls and serve to transfer loads into the bulkheads. Reducing the length of unsupported span

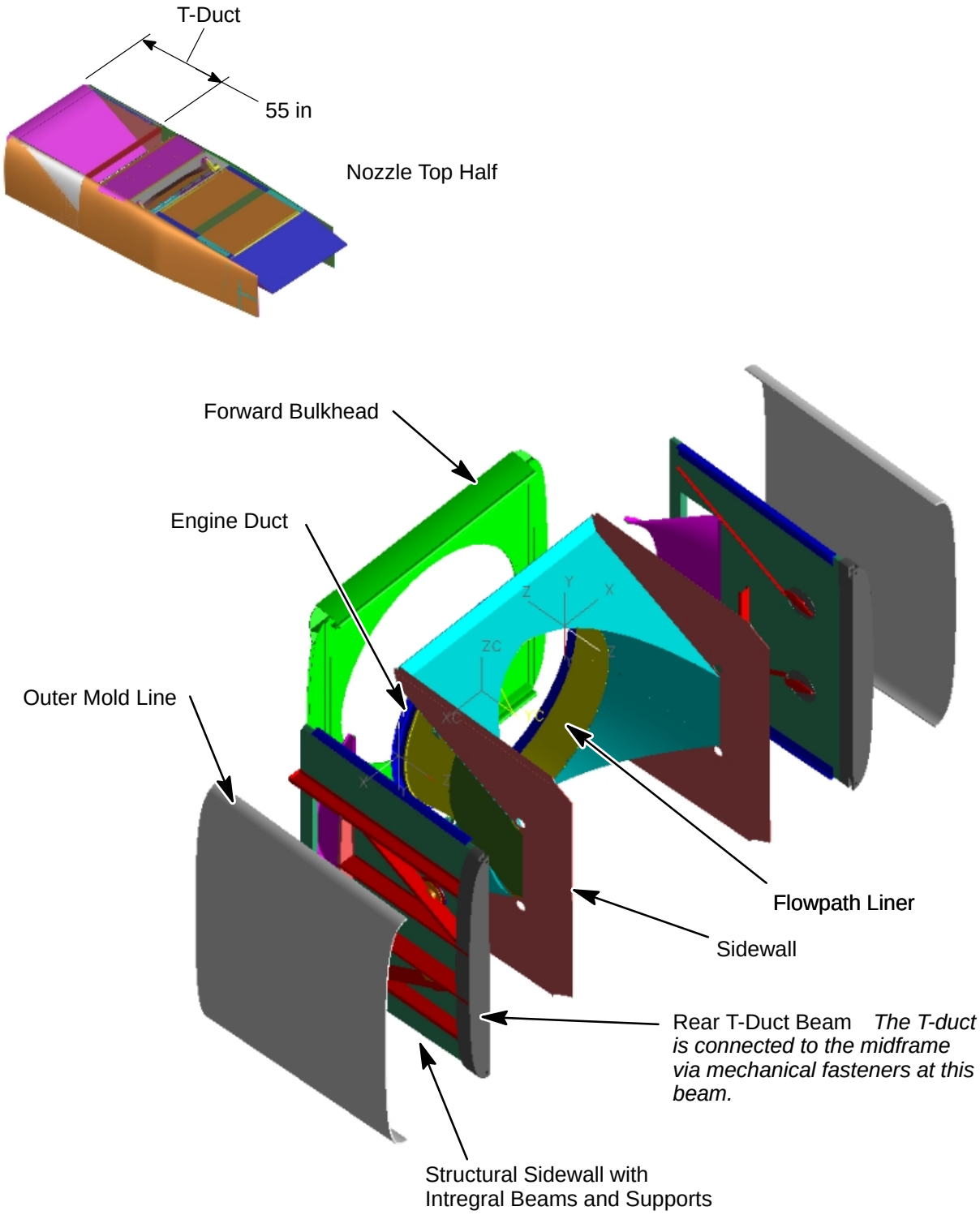

Figure 102. Transition Duct Exploded View

of the flat sidewalls allows reduced face-sheet thickness — the major factor influencing the weight of the sidewalls. Therefore, the extra weight of the integral beams is more than offset by the reduction in face-sheet weight. Note: the integral beams are formed 6–2–4–2 Ti sheet metal with a typical thickness ranging from 0.045 to 0.063 in.

Liners – All surfaces exposed to hot exhaust gases have liners. None of the liners are actively cooled with fan duct air, as in military exhaust systems. The flowpath downstream of the spool piece is subjected to hot gas flowing out of the fan/core mixer. At the highest temperature in the flight envelope, the temperature of the mixed gases leaving the fan/core mixer is predicted to be 1288°F. Along the length of the fan/core mixer, the flowpath duct is bathed in fan duct air (because of the geometry of the mixer) that has a maximum temperature of 500°F. Several inches forward of the fan/core mixer discharge there is a joint connecting the titanium flowpath duct to the nickel liner. This connection is a slip joint that will accommodate the difference in thermal growths between the hotter flowpath liner and the cooler sidewall/forward bulkhead/spool-piece components.

With the doors deployed, the flowpath converges inward and aligns with the mixer/ejector. The doors lay on top of a section of the liner called the "incline." The incline is not part of the flowpath but is subjected to hot gas when the doors are swung outward, so the incline must be made of a liner material (nickel or ceramic tile). With the doors outward, the gaspath air recirculates and fills the entire rectangular cross section of the nozzle, necessitating the use of liners on the sidewalls.

The flowpath liner is bolted to the sidewalls at the aft end of the liner. The flowpath liners have a higher thermal growth than the sidewalls. The liners have slip joints at the forward ends, where they mate with the spool piece, to prevent a thermal fight.

An alternate configuration for the sidewall liners is ceramic tile.

Conclusion – The conceptual design of the transition duct provides a configuration that meets the weight goals and satisfies the structural requirements. In a follow-on effort, this baseline design could be enhanced with new materials, such as composites, to achieve further weight savings.

5.5.2.6 Convergent Flap

The conceptual design of the HSCT convergent flap evolved from the alternate kinematics mechanical and structural design efforts leading to a kinematics concept downselect. HSCT nozzle requirements allowed no fan air for cooling the nozzle components. Purge air from the engine nacelle is the only source allowed for cooling nozzle components.

Openings in the sidewall adjacent to the flap train allow purge flow to enter the flap cavity, as the only means of temperature control within the cavity and adjacent components — particularly the nozzle flap train. Figure 103 Illustrates the flap train general arrangement and nomenclature. Figure 104 illustrates the physical configuration of the convergent flap. The flap is approximately 34-in long and 71-in wide to fit within the nozzle sidewalls.

Thermal Protection Systems and Structural Arrangements – A key objective was to evaluate the trade of flap system weight versus cooling air required. DOC + I factors were used to aid in evaluating cooling flow requirements. The trade between nozzle weight and cooling flow is:

$$17.1\ \textit{lbm of Nozzle Weight} = 0.1\%\ \textit{(DOC+I Factor)} = 1\%\ W_8\ \textit{(Cooling Air)}$$

Figure 105 summarizes the proposed structural and cooling concepts to be evaluated for various purge and fan flow rates. The trade studies were performed to aid in downselecting a cooling

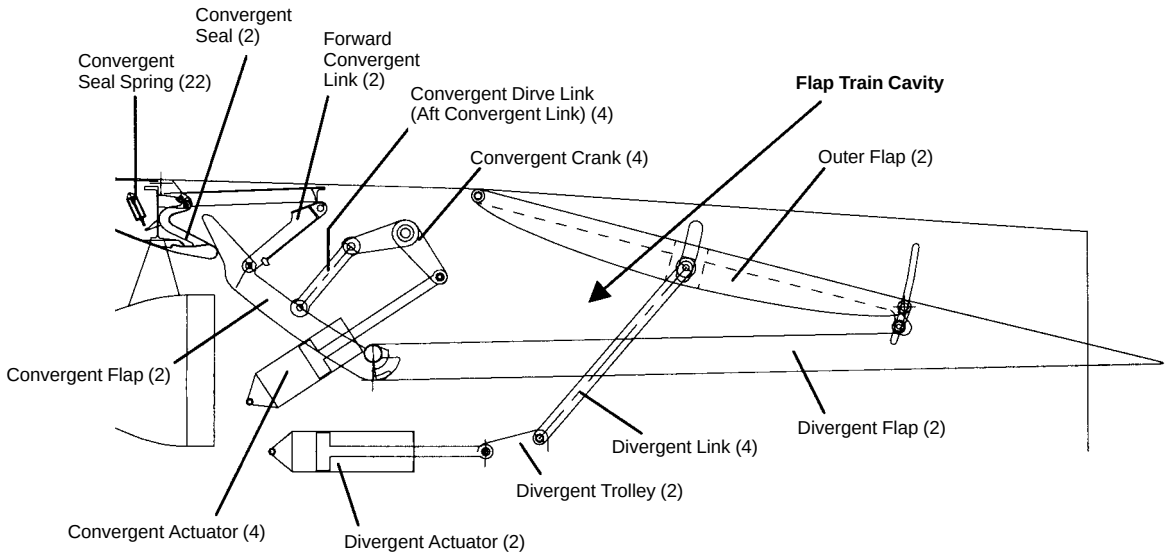

Figure 103. Flap Train Arrangement and Nomenclature

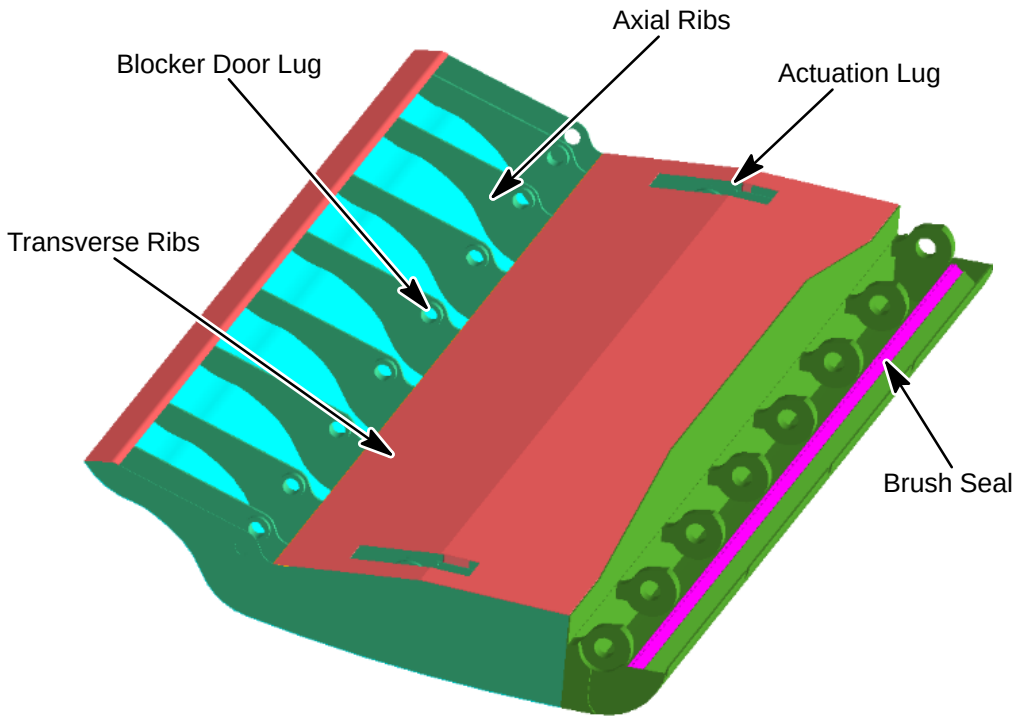

Figure 104. HSCT Convergent Flap Sheet and Stringer Design

arrangement that will allow the use of titanium in the back structure. The weight of the convergent flap as it was presented in the June 2, 1999 conceptual design review is 435 lbm and includes 75 lbm for the forward seal. Figure 106 illustrates the forward seal arrangement.

Concept Features – Salient features of the concepts are as follows.

Concept 1 – Baseline Configuration

- Sheet and Stringer Construction
- No Thermal Protection
- Proposed Cooling: Back-Side Purge Flow = 0.5%, 1%, 2% W_8
- Material Candidates:
  - C–263 (AMS 5872), Max Use Temp 1500°F, 0.302 lbm/in^3
  - IN718 (AMS 5596), Max Use Temp 1200°F, 0.297 lbm/in^3
  - Waspaloy (AMS 5544), Max Use Temp 1500°F, 0.298 lbm/in^3
  - IN939, Max Use Temp 1450°F, 0.295 lbm/in^3
  - Thermo–Span Alloy, Max Use Temp 1400°F, 0.297 lbm/in^3

Concept 2 – Sheet and Stringer with Thermal Blanket on Hot Side

- Proposed Cooling: Back-Side Purge Flow = 0.5%, 1%, 2% W_8
- Material Candidates (Back Structure):
  - Ti 6–2–4–2 (Back Structure), Max Use Temp 1000°F, 0.302 lbm/in^3
  - C–263 (AMS 5872), Max Use Temp 1500°F, 0.302 lbm/in^3
  - Waspaloy (AMS 5544), Max Use Temp 1500°F, 0.298 lbm/in^3
  - IN718 (AMS 5596), Max Use Temp 1200°F, 0.297 lbm/in^3
  - IN939, Max Use Temp 1450°F, 0.295 lbm/in^3
  - Thermo–Span Alloy, Max Use Temp 1400°F, 0.297 lbm/in^3

Concept 3 – Sheet and Stringer with Heat Shield, No Thermal-Barrier Coating

- Proposed Cooling: Back-Side Purge Flow = 0.5%, 1%, 2% W_8
- Back Structure Material Candidates:
  - IN 625, Max Use Temp 1800°F, 0.305 lbm/in^3
  - C–263 (AMS 5872), Max Use Temp 1500°F, 0.302 lbm/in^3
  - Waspaloy (AMS 5544), Max Use Temp 1500°F, 0.298 lbm/in^3
  - IN718 (AMS 5596), Max Use Temp 1200°F, 0.297 lbm/in^3
  - Thermo–Span Alloy, Max Use Temp 1400°F, 0.297 lbm/in^3
- Heat Shield Material Candidates:
  - Waspaloy (AMS 5544), Max Use Temp 1500°F, 0.298 lbm/in^3
  - C–263 (AMS 5872), Max Use Temp 1500°F, 0.302 lbm/in^3

Concept 4 – Sheet and Stringer with Truss Core Sandwich Hot Face

- Proposed Cooling: Back-Side Purge Flow, Fan-Air Film Cooling in Sandwich Structure
- Sheet and Stringer Back Structure

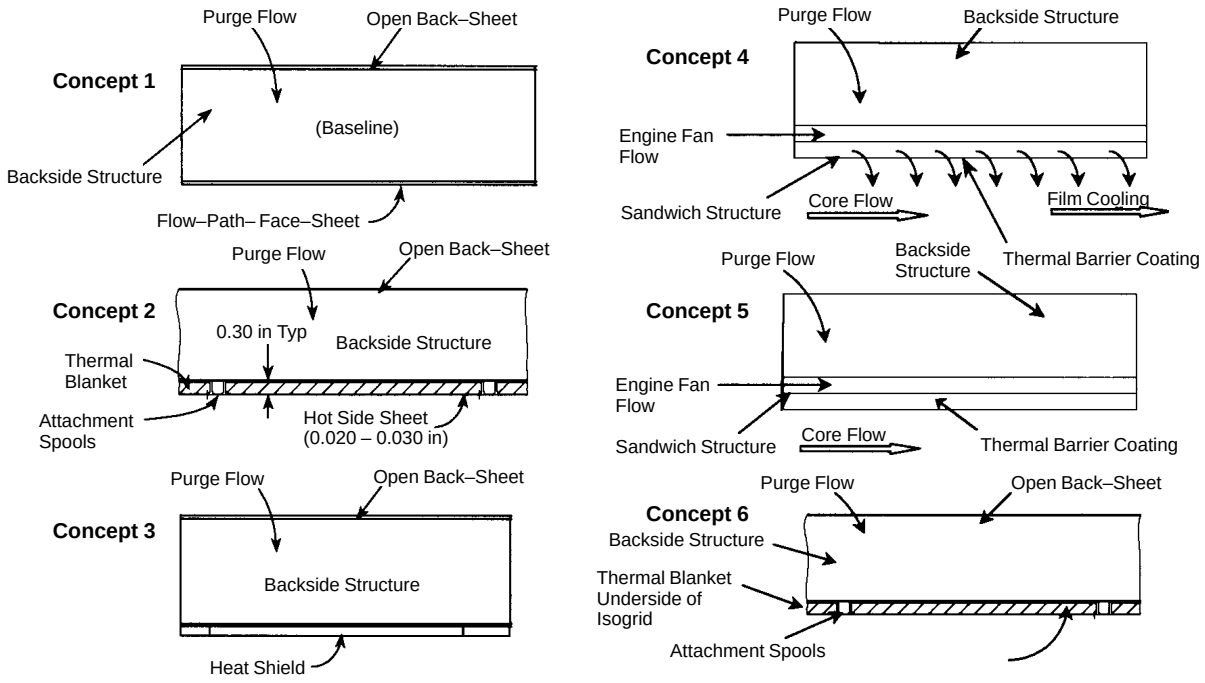

Figure 105. Proposed Forward Flap Cooling Concepts

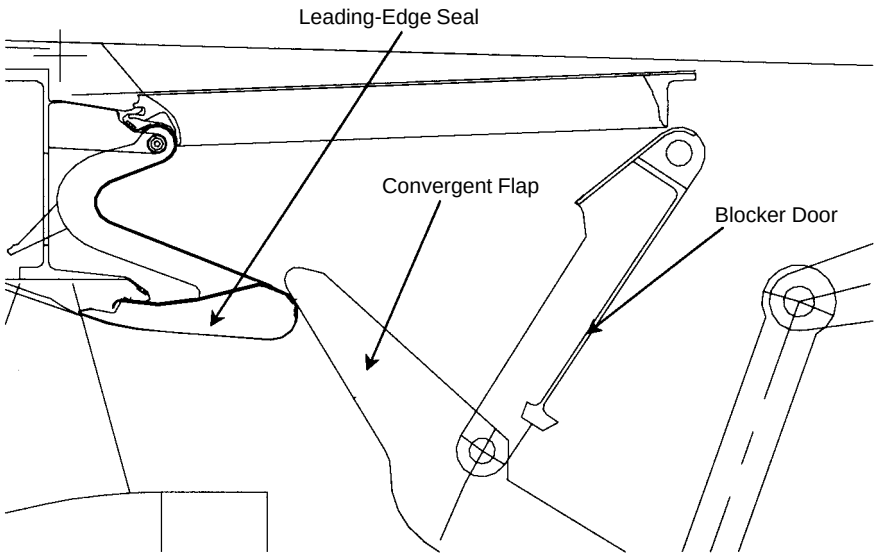

Figure 106. Convergent Flap Leading-Edge Seal Arrangement

- Flowpath Face: SPFDB Sandwich Structure, Waffle Truss Core Sandwich
- Back Structure Material Candidates:
  - Ti 6–2–4–2, Max Use Temp 1000°F, 0.302 lbm/in^3
  - Alloy "C," Max Use Temp 1000°F
  - Thermo–Span Alloy, Max Use Temp 1400°F, 0.297 lbm/in^3

Concept 5 – Sheet and Stringer with Truss Core and Thermal Blanket

- Proposed Cooling: Back-Side Purge Flow, Fan Air in Sandwich Structure
- Sheet and Stringer Back Structure
- Flowpath Face Structure: SPFDB Sandwich Structure, Waffle
- Back Structure Material Candidates:
  - Ti 6–2–4–2, Max Use Temp 1000°F, 0.302 lbm/in^3
  - Alloy "C," Max Use Temp 1000°F
  - Thermo–Span Alloy, Max Use Temp 1400°F, 0.297 lbm/in^3

Concept 6 – Sheet and Stringer, Isogrid and Thermal Blanket

- Proposed Cooling: Back-Side Purge Flow = 0.5%, 1%, 2% W_8
- Back Structure Material Candidates:
  - Ti 6–2–4–2, Max Use Temp 1000°F, 0.302 lbm/in^3
  - Waspaloy (AMS 5544), Max Use Temp 1500°F, 0.298 lbm/in^3
  - Thermo–Span Alloy, Max Use Temp 1400°F, 0.297 lbm/in^3

Heat Transfer Analysis – The study found that Concepts 2 and 6, employing a thermal blanket provided, adequate temperatures for purge flow ranges from 1% to 2% total engine flow. This allows the use of titanium and provides further weight savings.

Sealing Concepts: Convergent Flap to Sidewall and Convergent/Divergent Hinge Interface The hinge design consists of a brush seal assembly housed within the hinge structure and attached to the convergent flap. The opposite end, where the brushes are located, contacts the divergent flap creating the seal. The estimated weight for the seal portion of the baseline design is 24 lbm for the convergent flap and 34 lbm for the divergent flap. The brush seal is illustrated in Figure 104.

The "E" seal, an alternate approach, employs a groove and seal assembly located on the outer rim of the hinge assembly as shown in Figure 107.

Conclusion – Results from the heat transfer study identified Concepts 2 and 6 as the best alternatives capable of bringing the back-side temperature within titanium alloy range. Basic structural arrangement for these concepts consist of sheet and stringer construction connected to a continuous face sheet on the flowpath side and a perforated sheet on the opposite side. Temperature control on the back side is achieved with the use of a thermal blanket on the hot side in combination with purge air entering the flap back side through the perforated sheet. Openings in the sidewall adjacent to the flap train allow purge flow to enter the flap cavity. Figure 108 summarizes the temperature distribution from the flowpath side to the back-side sheet.

5.5.2.7 Divergent Flap

The main function of the divergent flap is to control aerodynamic expansion of the exhaust flow aft of the nozzle throat. Another major function is to contain acoustic tiles to provide acoustic damping

Figure 107. Alternate “E” Seals

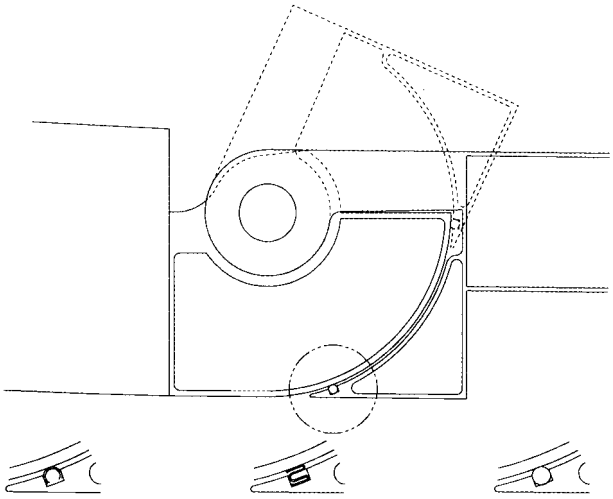

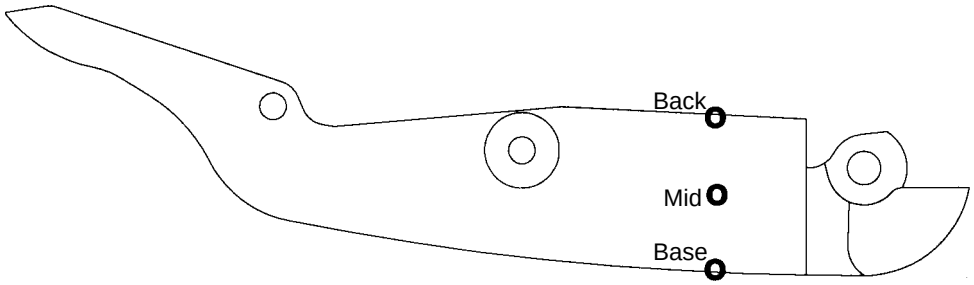

	Concept	Temperature Base	Temperature Mid	Temperature Back
	1	1145	964	858
Preferred →	2 and 6	896	830	767
	3	1082	927	832
	4	841	567	629
	5	494	554	623
	7	522	682	684

Figure 108. Temperature Summary – HSCT Convergent Flap

and reduce the overall noise emanating from the nozzle. Noise suppression is one of the most important goals of the HSCT program.

Conclusions – A design using gamma titanium aluminide (γ) material showed a favorable trade in terms of weight when compared to the conventional Inco 718 sheet metal divergent flap that was the CPC baseline when the HSCT program began. The DOC+I evaluation process was used to make

system level trades comparing material, weight, cost, cycle, configuration, etc. This process indicated that γ offers a favorable trade in the nozzle divergent flap.

The design went through an evolutionary process. The initial intent was to cast the divergent flap from γ (Figure 109). Due to manufacturing limitations, the design evolved into a component with γ sheet metal construction (Figure 110). This final construction method eventually became the baseline because it was even lighter than the cast γ.

Design History – The EPM program initially considered γ because it offered a potential enabling technology. This material has a temperature limit and an elastic modulus equivalent to those of Inco 718 but has density and strength less than or equal to those of Ti 6–2–4–2. Therefore, the material has a potential for saving weight in deflection-limited parts such as divergent flaps. In deflection-limited designs, the designer typically must add material to increase stiffness and thus reduce deflections, which also reduces stresses. In this case, a material that has a low density, lower strength, and high elastic modulus is a good candidate. However, the downside to γ material is relatively low ductility — an order of magnitude lower relative to most conventional nozzle materials.

When γ was initially considered for the EPM program, it was only available in cast form. Even though it could be cast, a considerable amount of time and effort was put into casting trials to advance the technology. Several options were studied for making an efficient load-carrying structure. Through iterations with the casting vendor, rib shapes were developed to give the grid-type structure some structural stiffness. The grid structure was optimized to consider the effects of pressure, temperature and HCF on the flat panels between the ribs. Other major features were acoustic tile attachments and a roller track for the disk nozzle that used rollers for actuating the aft end of the divergent flap to control expansion and nozzle exit area.

As mentioned earlier, the HSCT/EPM program used a method called DOC+I to make design decisions on a systems level concerning cost, manufacturing, design, weight, etc. Because the casting development was not advancing as well as planned, the EPM program decided to pursue the sheet metal version of γ for use in the divergent flap. In addition, the design team was struggling to get weight out of the flap based on the casting limitations of efficient load-carrying structures (parallel face sheets or something similar) and large minimum thickness requirements (greater than 0.100 in). Although only one company in the world, Plansee in Austria, made γ in sheet, the technology offered many benefits. Sheet metal could allow much thinner designs than castings and offered the use of more efficient sheet metal type structures.

The materials group began by developing material characteristics and properties through coupon testing. Early samples were formed to determine bending limits and allowable bend radii. It was shown that the material could be formed into a 0.25-in bend radius, it could be brazed successfully, it could be superplastically formed under the right conditions, and it could be diffusion bonded. However, this was done on a very limited number of coupons and certainly was not optimized. For the sake of time, money, and schedule, the engineering team decided to limit the design to 0.25-in bend radii and use brazing as the method of attachment. The brazing trials showed that the bond was inherently stronger than the parent material. In addition, knowledge about the limited ductility of this material caused design to rely heavily on brazing for attachments in general to properly distribute attachment-point loading.

With this initial manufacturing information, design began developing concepts that could effectively use this material and manufacturing method. After evaluating different concepts, a two-sheet and

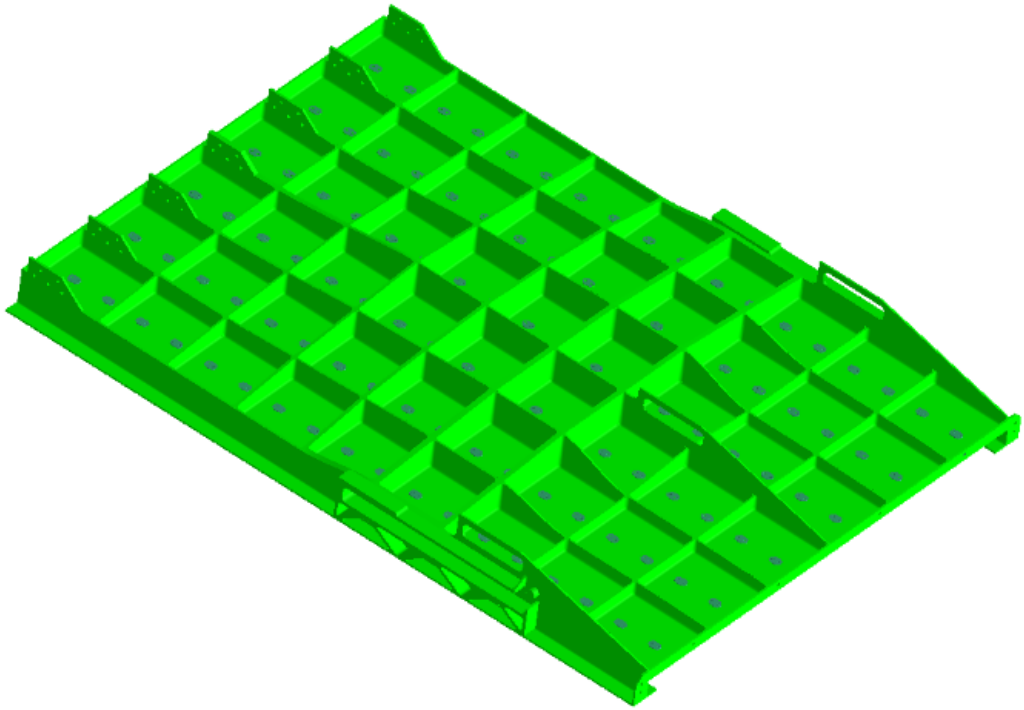

Figure 109. Gamma (TiAl) Cast Divergent Flap

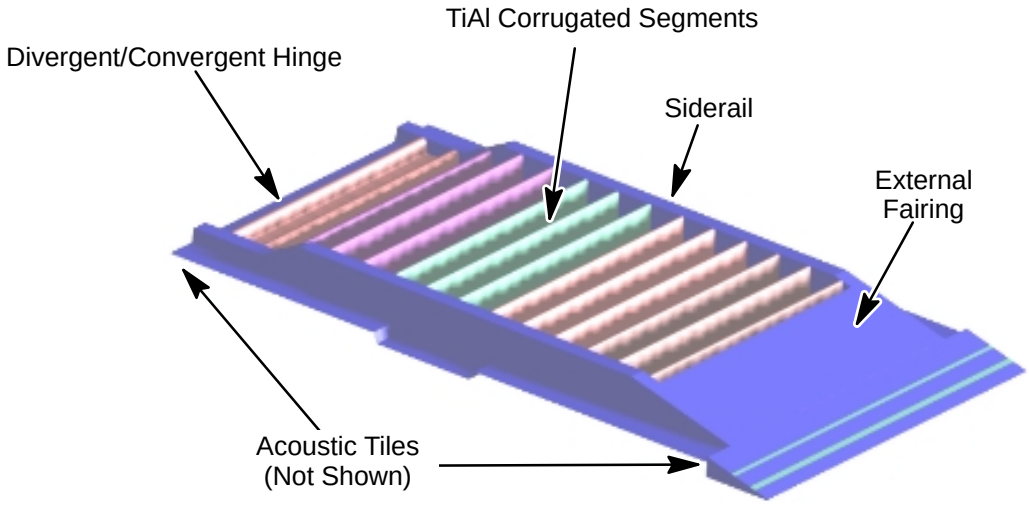

Figure 110. Sheet Metal Gamma (TiAl) Divergent Flap

three-sheet corrugated truss core construction was chosen as the concept to pursue. A study was done to compare the baseline conventional sheet metal Inco 718 design, Improved sheet metal Inco 718 design, SPF Inco 718 sheet metal (two sheet) design, and SPF γ sheet metal (two sheet) design. The SPF designs attempted to evaluate the benefit of contouring the corrugations to allow taller, stiffer corrugations in the center of the flap and shorter, lighter corrugations near the outer edges. Another key criteria for this flap design required the flap to have an open back structure to allow access to acoustic tile attachments which needed back-side access. The results of this study showed that the SPF γ sheet metal (two sheet) design was the lightest flap design that met the criteria of acoustic tile compatibility, panel HCF, and overall flap deflection.

After this analysis, attention again focused on optimizing the flap design further. A study of a two-sheet versus a three-sheet design was conducted to determine the benefit of adding a third sheet to the two-sheet SPF design in terms of additional stiffness and weight. The study concluded that for a subscale flap, the addition of a third sheet added 6 lbm and reduced the critical tip deflection by 24%. By strategically increasing the weight of the two-sheet flap by 6 lbm, it was determined that the two-sheet design offered lower risk manufacturing, easier assembly, and deflections with 15% of the three-sheet flap of equivalent weight. It was decided to pursue the two-sheet design until the fabrication method was more mature, assembly could be improved, and/or the aerodynamic performance demanded less deflection from the divergent flap. If these concerns about manufacturing and assembly can be eliminated, a three-sheet design could provide a lighter, stiffer flap.

Near the end of the HSCT program a SAVE event was performed to determine the best area to work to lower the nozzle weight of the baseline disk nozzle. The final weight roll-up showed the nozzle desperate for weight savings. It was at this time that the higher risk γ became the new baseline divergent flap design in place of the conventional Inco 718 sheet metal. This was primarily decided because of the weight savings it offered despite the high risk of an untested and partially characterized material. In order to further reduce risk on this design, a hot acoustic rig test (HART) was performed. A simplified subelement was designed and rig tested to evaluate durability in an acoustic, engine-like environment. This is a good step in evaluating the durability of this relatively "brittle" material in a harsh vibratory environment. The next step is to get a demonstration piece in a hot, real engine environment that would further reduce the risk and unknowns to this material.

The HSCT program concluded with an alternate kinematics study. This study also originated from the SAVE event as offering a large potential weight savings. Two nozzle actuation concepts were studied: linear and rotary. The studies were done on a system level and attempted to make design changes based on the overall system impacts. When the two-sheet divergent flap design was created, it was designed around the disk-actuated nozzle. It is important to note that the actuation study compared only no-disk-actuated nozzles. This could potentially have an impact on the divergent flap design. It was assumed for the sake of this study that the two-sheet design applied equally well to the nondisk nozzle as the disk nozzle. If this nozzle design is pursued further, it is advisable to revisit the conventional Inco 718 sheet metal design to ensure that the best overall divergent flap design is being used.

The major difference concerning the divergent flap in the two nozzle actuation concepts is how it is actuated to control nozzle exit area. In the Linear concept, a link ties directly to the top center of the siderail box beam (Figure 111). The rotary concept (Figure 112) needs a link box on the outsides of the siderails to actuate the flap. The integration of the divergent flap linkages to the siderails in this concept is more difficult and creates an offset moment that causes additional twisting of the both

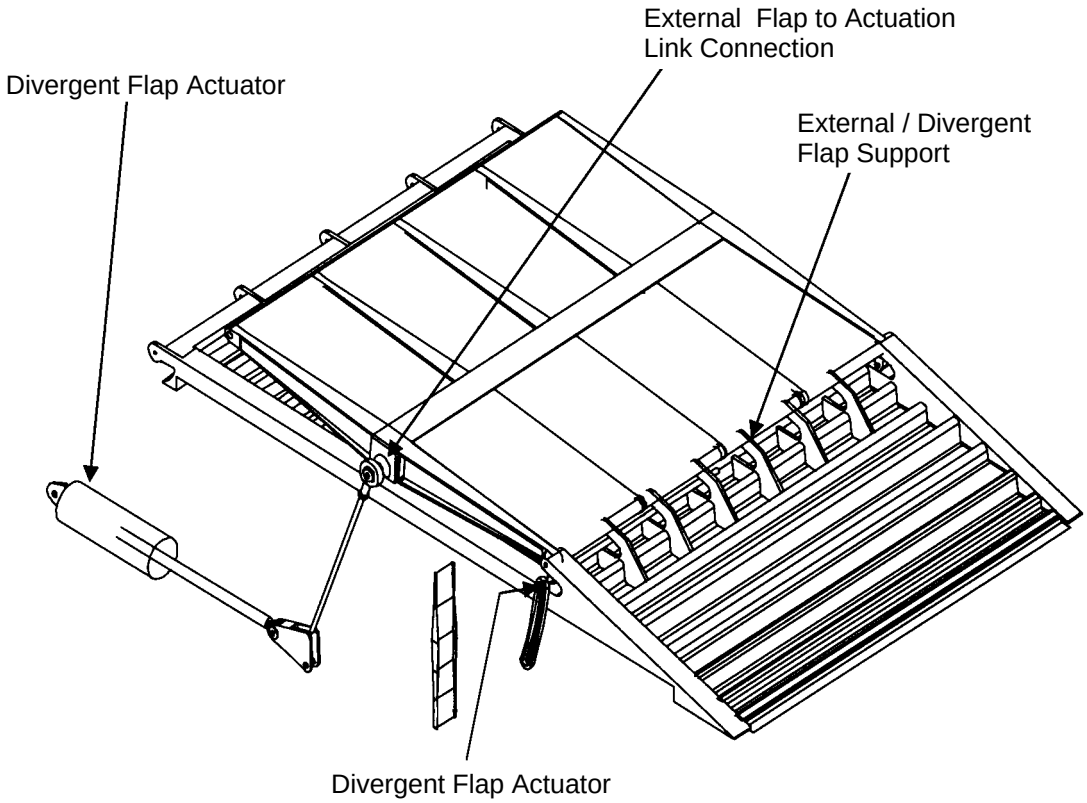

Figure 111. Linear-Actuated Divergent Flap

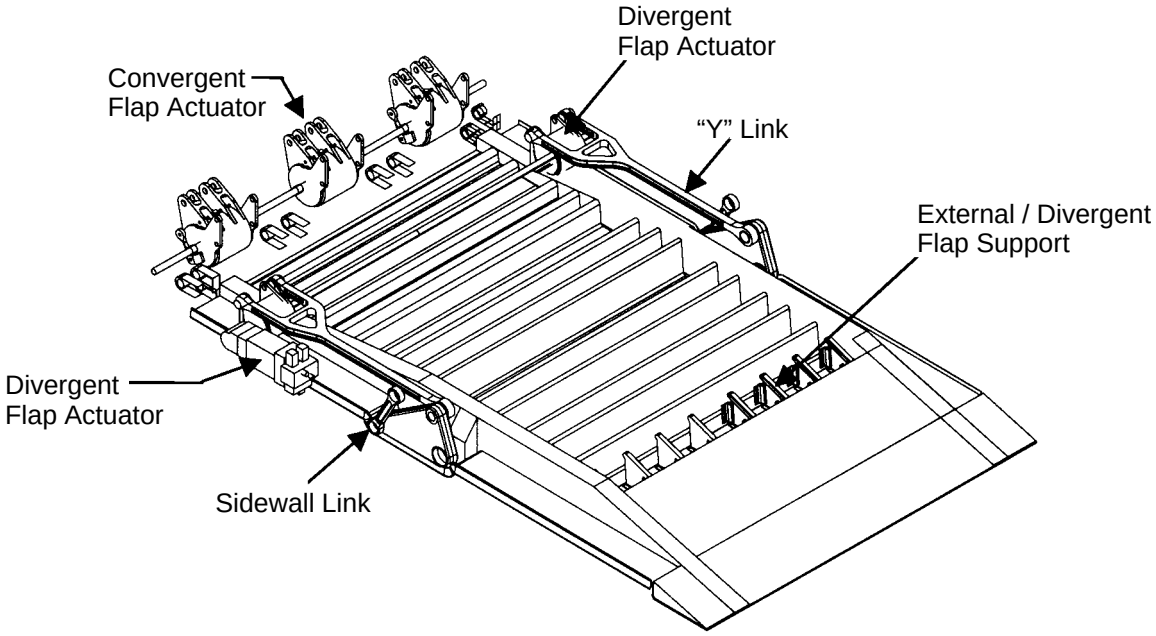

Figure 112. Rotary-Actuated Divergent Flap

siderails. Although designing around these integration issues is possible, it is an additional design task that is not required of the linear system.

5.5.2.8 Nozzle External Flap

The proposed HSCT engine has a 2D convergent/divergent nozzle. The flap train in the proposed design consists of pairs of convergent, divergent, and external flaps. There were two proposed kinematic concepts to actuate the flaps. The first of these used rotary actuators, and the second used linear actuators. In the rotary actuation scheme, the external flap serves primarily as a fairing to reduce aerodynamic drag. In the linear actuation scheme, the external flap is connected to the divergent actuator and positions the divergent flap as well as serving as a fairing. This discussion summarizes the design efforts undertaken for the external flaps for both kinematic concepts.

The initial design phase consisted of trade studies to determine the lightest flap construction and material combination. The following construction methods were considered: truss core, sheet/stringer, and honeycomb. The following materials were considered: organic-matrix composite, ceramic-matrix composite, titanium 6–2–4–2, γ titanium, and Inconel 718. The trade studies were performed by using hand calculations and spreadsheets to size the external flap. Based on the required sizing, the flap weights were estimated and the lowest that met structural criteria was selected. The structural criteria used for these estimates were those deemed most critical and included strength, deflection, and acoustic HCF. The results are listed in Tables 24 through 26.

Table 24. Rotary System External Flap Trade Study Summary

Construction	Material	Flap Weight, lbm	Limiting Factor
Truss Core	SiC/SiNC	129	HCF
	Ti 6–2–4–2	104	HCF
	Graphite Polyimide	74	Shear Stress
Sheet/Stringer	Ti 6–2–4–2	122	Deflection
Honeycomb	Ti 6–2–4–2	98	Deflection

Table 25. Linear System External Flap Trade Study Summary

Construction	Material	Panel Weight, lbm	Limiting Factor
Truss Core	SiC/SiNC	109	HCF
	Ti 6–2–4–2	84	HCF
	Graphite Polyimide	54	Shear Stress
Sheet/Stringer	Ti 6–2–4–2	102	Deflection
Honeycomb	Ti 6–2–4–2	78	Deflection

Table 26. Linear System External Flap H-Beam Trade Study Summary

Construction	Material	H-Beam Weight, lbm	Limiting Factor
I-Beam/Box Beam	Gamma Titanium	81	Stress
	Inco 718	103	Deflection (A_9)
	Ti 6–2–4–2	78	Deflection (A_9)

Based on the weight estimates shown above, the panel portion of the flaps was chosen to be Ti 6–2–4–2 honeycomb. The graphite polyimide truss core had the lowest weight but was not chosen because, even at the highest purge levels, the flap temperature was near the 600°F limit for this material. For the linear system external flap, the H-beam was chosen to be an I-beam and box beam made of Ti 6–2–4–2.

In the rotary system, Figure 113, the external flap consisted of a 2-in thick panel that was 70.7-in wide by 73.9-in long. The leading edge of the flap attaches to the nozzle bulkhead with a clevis style hinge. The trailing edge of the flap attaches to the divergent flap with a sliding hinge system consisting of roller bearings (attached to the flap) that ride in tracks in the divergent flap. A follower flap provides a seal between the aft of the external flap and the top surface of the divergent flap.

In the linear system, Figure 114, the external flap consisted of a 2-in thick panel that was 70.7-in wide by 65.1-in long. The panel was attached to an H-shaped skeleton that consisted of two tapered I-section side rails and one box-section beam connecting them. The leading and trailing edges of the flap both attach to the nozzle bulkhead with a clevis style hinge. A linkage, driven by the divergent actuator, connects to an outboard lug on the side rails and serves to position the external flap and the divergent flap.

The lightest construction for the HSCT nozzle external flap panels is Ti 6–2–4–2 honeycomb. The weight of the rotary system external flap is 98 lbm. The weight of the linear system flap is 158 lbm. There is a possible weight savings by using graphite polyimide for the external flap. Based on the current thermal analysis, the temperatures are marginal for this material. A more detailed thermal analysis may reveal that the temperatures are not as high as currently predicted. In addition, further development of this composite may allow it to endure higher temperatures.

5.5.2.9 Acoustic Tiles

An enabling, ceramic-matrix-composite, acoustic-tile design could allow the HSCT to use a higher temperature capability and/or lighter acoustic liner relative to the baseline CPC metallic liner.

The acoustic tile was designed specifically for noise suppression. The HSCT program focused on two distinct methods of using tiles for noise suppression. The first was a SDOF sandwich structure consisting of two face sheets with a honeycomb core. The top (or cold) sheet is solid, but the bottom sheet is perforated. Typically, the porosity is on the order of 10 to 12%. This style of suppression is tuned to reduce a specific frequency. Although it does a good job for a specific frequency and is a proven design, it offers little suppression for other frequencies. In addition, this design is conventional for metallic liners; however, it is very difficult to fabricate from CMC. The EPM program chose not to pursue fabrication of this design from CMC.

The broad-band design offers much more benefit in terms of design and fabrication flexibility. It is easier to design with because it allows suppression for a wide range of frequencies as well as allowing more room for error when defining the specific frequency band of interest. This design consists mainly of a single, high-porosity face sheet with a porous foam absorber backing. This particular design also has a thermal-protection system that does not assist in noise suppression but protects the back structure from hot exhaust gas. This design varies significantly from typical 2D nozzles that have cooled liners. The acoustic liners allow hot exhaust gas to pulse in and out through the holes in the porous face sheet in order to suppress noise. This air infiltrates the porous foam and comes into contact with the back structure. The TPS provides a thermal insulation between foam-penetrating hot air and the back structure.

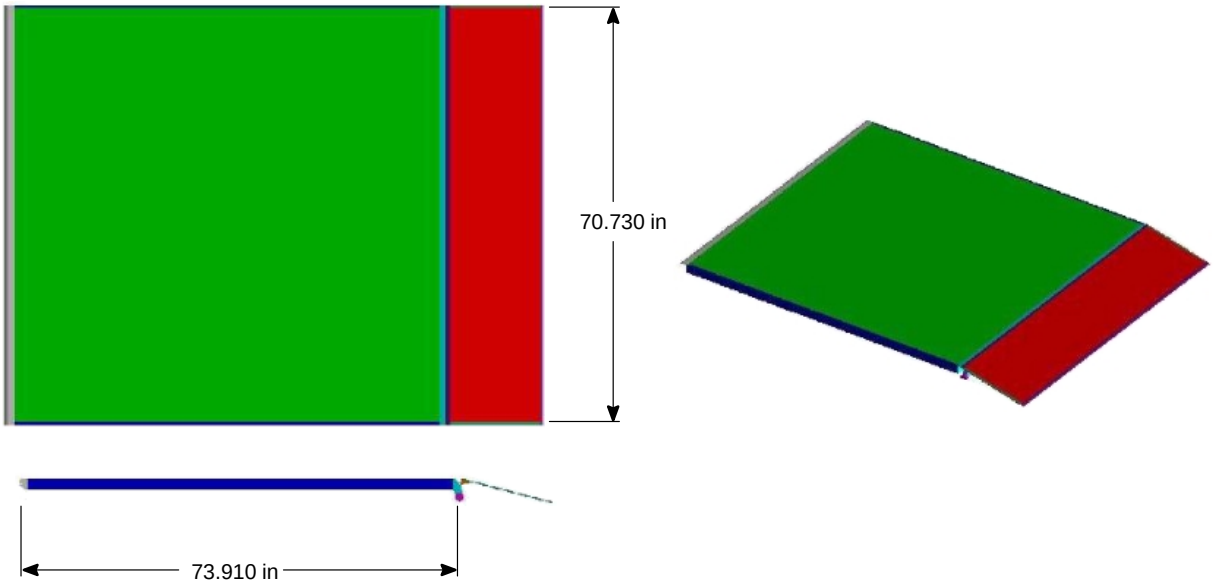

Figure 113. Rotary System External Flap

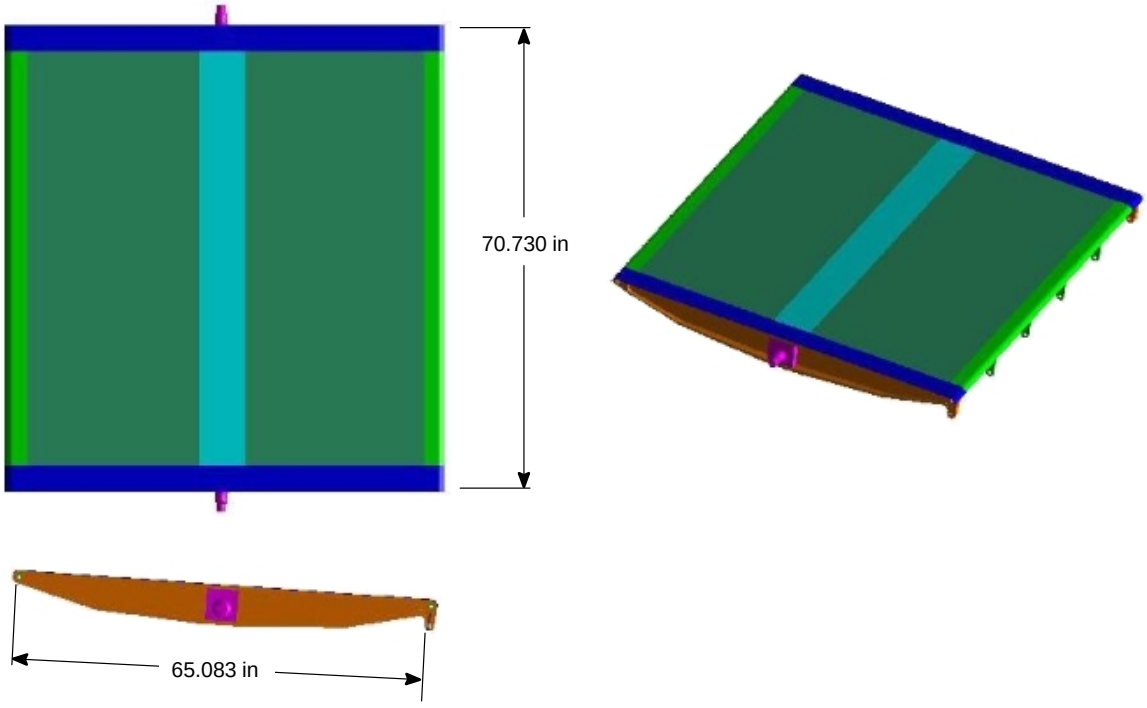

Figure 114. Linear System External Flap

This broad-band design is relatively simple; therefore, fabrication options are more diverse. Generally, CMC designs offer higher temperature capabilities as well as lighter weight options. The mixer/ejector effectively reduces engine noise by efficiently reducing gas velocity. However, the mixer itself creates mixing noise, and this is the noise targeted by the acoustic liner tiles on the nozzle divergent flaps and sidewalls aft of the mixer.

Summary – CMC acoustic tiles are the baseline design for the HSCT nozzle. They are located primarily on the nozzle divergent flaps and sidewalls (Figure 115). The CMC acoustic liner tile design uses a series of components to suppress nozzle noise and thermally protect the back structure. The design consists of a porous face sheet, tile attachments, noise-absorbing "foam," and a thermal-protection system (Figure 116).

The CMC design traded favorably against metal designs consisting of both the SDOF and broad-band designs based on system level trades. The HSCT program used DOC+I projections to make these trades by comparing material, weight, cost, engine cycle, configuration, etc.

Design Features – The acoustic tile is only one component of the noise suppression system referred to as a broad-band absorber. This noise-suppression device comprises a highly porous face sheet and a broad-band absorbing foam. To make this device mechanically feasible, other features must be added. Figure 116 shows the complete CMC acoustic tile with all of the necessary features. The total package consists of a highly porous CMC face sheet, various components for attachments, bulk absorbing foam, and TPS.

The face sheet has local buildups around the fasteners to reduce localized fastener stresses. The attachment consists of a CMC lug, bushing, threaded sleeve, pin, spring and self-locking nut. This attachment requires back-side access for assembly. The CMC lug is a unique design that eliminates the interlaminar shear stresses inherent with a standard, integral rib made from a 2D laminated plate (Figure 117). The lug is inserted through the hot side of the tile plate until the chamfered edge mates with the chamfer in the tile plate. The lug passes through the bushing and is inserted through the back structure and then into the threaded sleeve. The threaded sleeve is pinned to the CMC lug. A key to this fastener is the threaded sleeve because it essentially allows threads to become an integral part of the CMC fastener. After the threaded sleeve is pinned, the spring is dropped over the top of the CMC lug/threaded sleeve, and then the self-locking nut tightened to attach the tile to the back structure. When the nut is tightened it pulls the lug in tension, and the bushing goes into compression between the tile and the back structure. This accomplishes two things. First, the chamfer on the lug and chamfered hole in the plate mate (similar to a countersunk fastener in a countersunk hole). Second, the plys in the tile plate are compressed between the lug and the bushing — which increase the strength of the fastener joint significantly.

Design Tradeoffs – The first trade for the acoustic tiles was to use either SDOF or broad-band noise absorption material. It was concluded early in the program that SDOF absorber could not be made from CMC because of the manufacturing complexity. The three options left were metallic tile designs for both the SDOF and broad-band and the CMC for the broad-band. Based on the DOC+I projections and the cycle temperatures, the CMC broad-band absorber was chosen as the baseline.

When CMC broad-band designs were chosen as the baseline, two CMC designs systems were considered. One design consisted of an entirely 2D laminated structure (Figure 118) with integrally laid-up stiffening ribs that formed into "T" attachments. It was fabricated from the GE oxide/oxide system. The other design was the 2D laminated flat panel with "Miller" fasteners for attachments

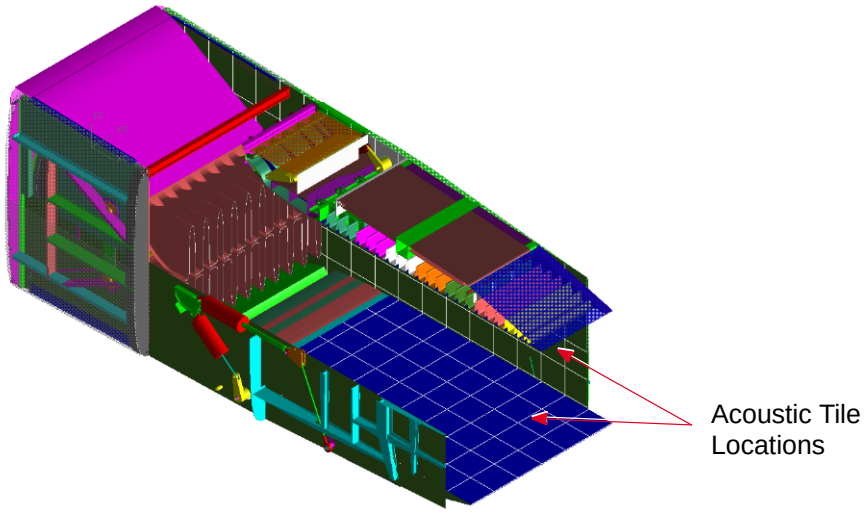

Figure 115. Acoustic Tile Placement

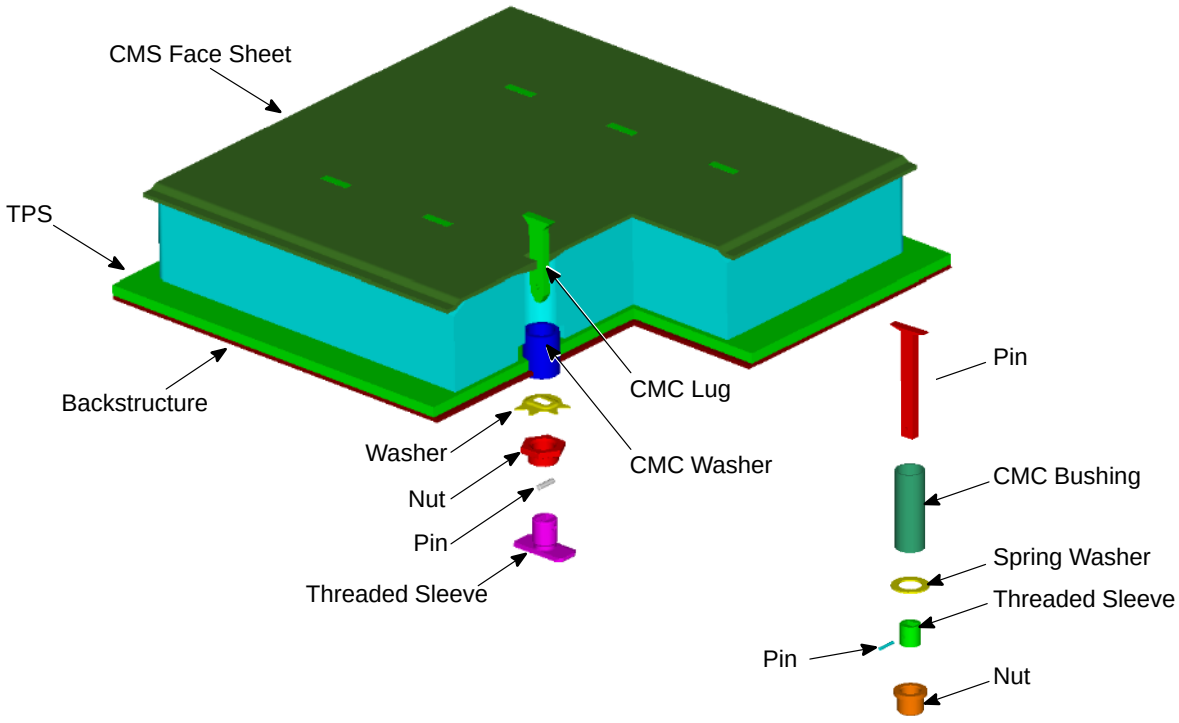

Figure 116. CMC Acoustic Tile Design

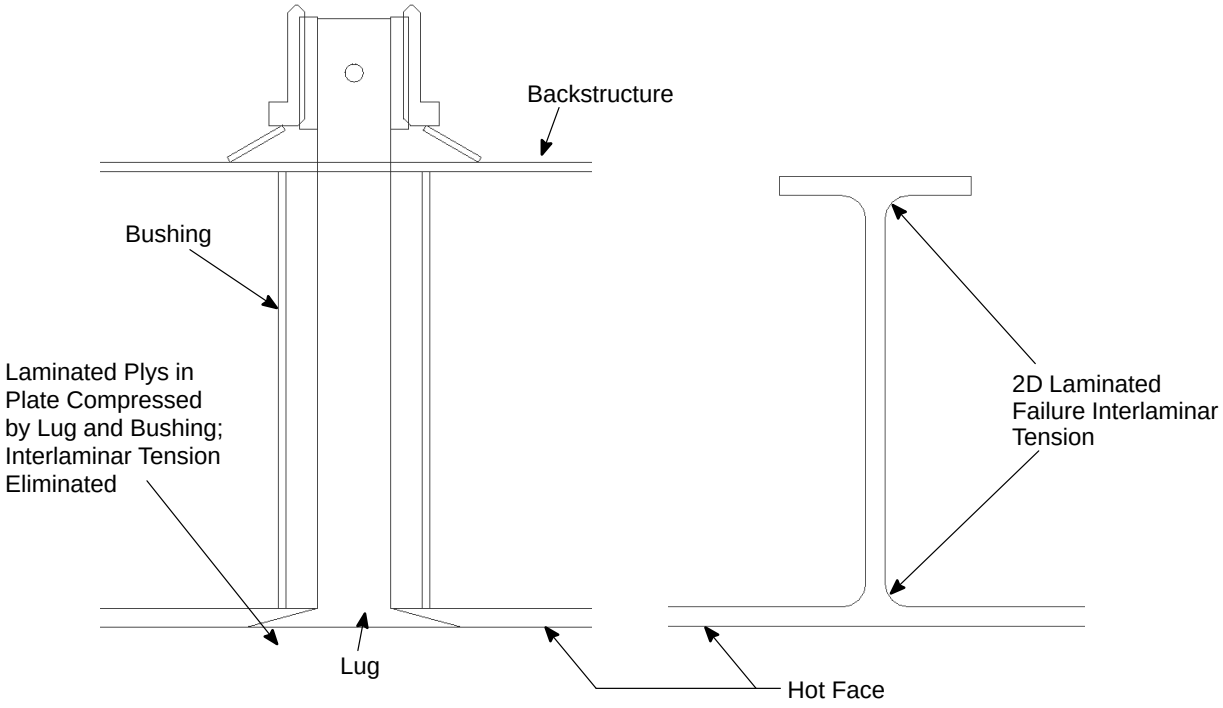

Figure 117. CMC Acoustic Tile Lug

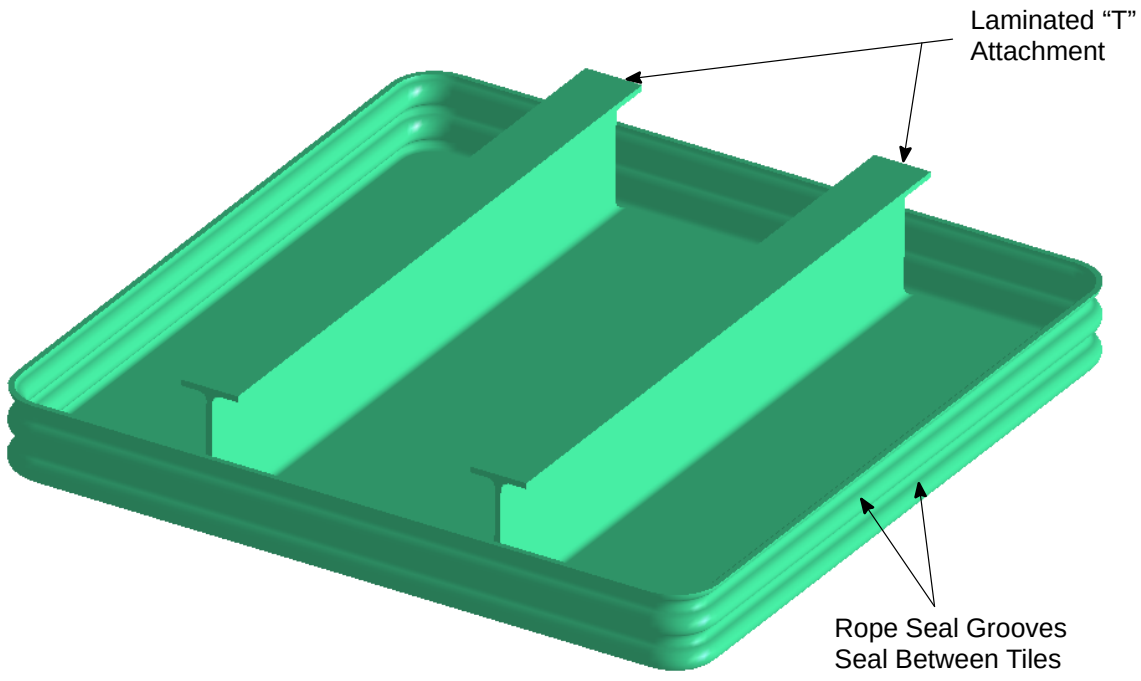

Figure 118. CMC Acoustic Tile 2D Laminated Structure

(Figure 119). It was fabricated from the Dow Corning SiC/SiNC system. Both designs were analyzed by the DOC+I process — under tremendous scrutiny because the systems were relatively close. However, when the two designs were run head-to-head in a hot acoustic rig test the Dow Corning material and the flat-panel design come out the winner. The T-stiffened design had significant failures in both the T attachments and the face sheet. The flat-panel design endured the entire test without any failures. Therefore, that design was selected as the new baseline.

The next trade was using T fasteners that were thermally free and hot-side removeable compared with the bolt-through fasteners that were thermally free but not hot-side removeable (Figure 120). HSCT chose the bolt-through design because it allowed the use of a belleville or spring washer to reduce panel and lug loads during thermal bowing. The divergent flap has relatively easy back-side access where the sidewalls do not. This particular issue had not been totally resolved when the program ended.

The number of fasteners was also traded. The first design had nine fasteners per 12-by-12-in tile; the second iteration had six fasteners, and the final iteration had only four. The number of fasteners was reduced primarily because the spacing was driven by acoustic stresses. In reality, the tiles had so much damping that the spacing could be drastically increased with no significant increase in acoustic stresses. It is believed that this damping is driven mainly from the support from the bulk absorber. The issue between four and six fasteners is a question of redundency. If one fastener is lost in the four-attachment configuration, the tile will probably depart from the back structure. Six fasteners give the design redundency at increased part count, added complexity, and added weight. This trade needs to be addressed on a design-specific basis in future design efforts.

Another trade evaluated a six-ply laminated tile plate versus an eight-ply plate. The DOC+I projection showed a very small weight benefit, but the risk of changing the ply design and generating new material properties drove the decision to stay with eight plys.

Review of Stress and Deflection – Stress is generated from two main sources. First, the thermal gradients across the flat plate liner cause thermal bowing. The panel itself could withstand a gradient up to 600°F; however, the design was limited by local, fastener-induced stresses in the panel caused by the panel bowing away from the structure. This tensile load could be lessened in two ways. Strategically spacing the fastener near the outer edges of the panel and away from the center allows the panel to bow without putting excessive tension in the attachments. To further reduce the lug tension load, springs were added to the attachments. This allowed the attachments to pull away from the back structure and thus relieve the tension load. However, designing these springs for long-term durability is difficult. Much consideration must be given to the spring design for any future acoustic tile design efforts.

5.5.2.10 Mixer Concepts

The mixer is a static structure within the two-dimensional portion of the exhaust nozzle flowpath, just aft of the transition duct. It serves as an integral part of the noise-suppression system within the mixer/ejector exhaust nozzle for the MFTF propulsion system. The full-scale ejector/mixer design was analyzed at two flight conditions/configurations to determine the thermal and pressure loads and the relative “life” capability of the materials. Manufacturing feasibility was also evaluated. Several concepts were studies. The final design was a cast superalloy (René 108) structure.

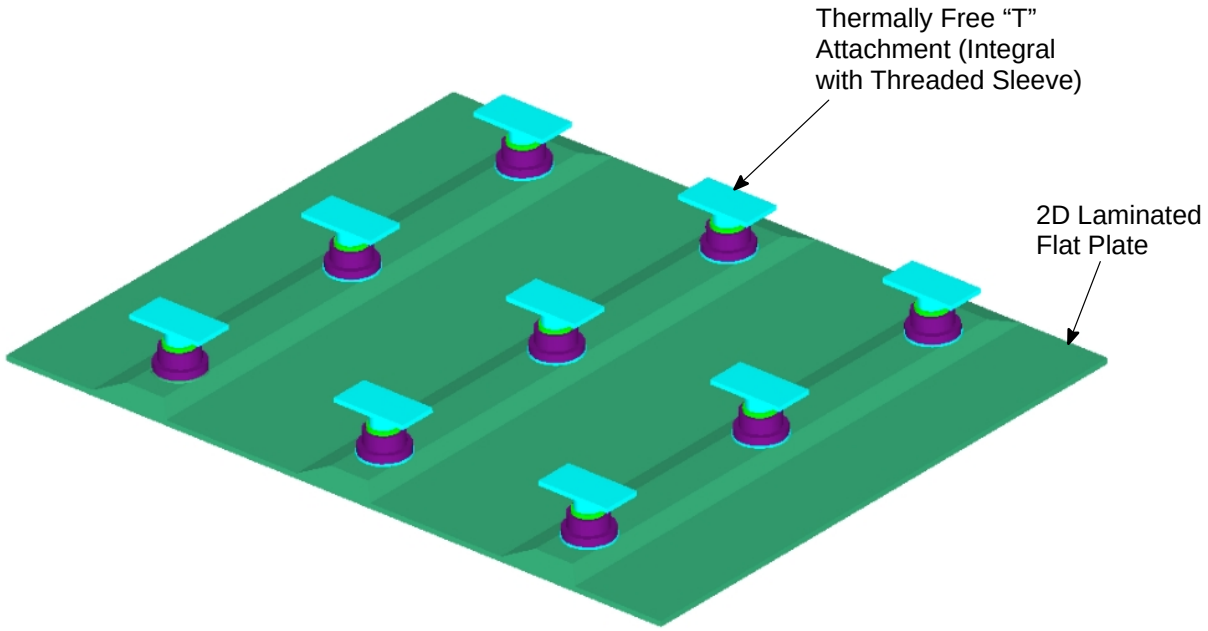

Figure 119. CMC Acoustic Tile Flat Panel

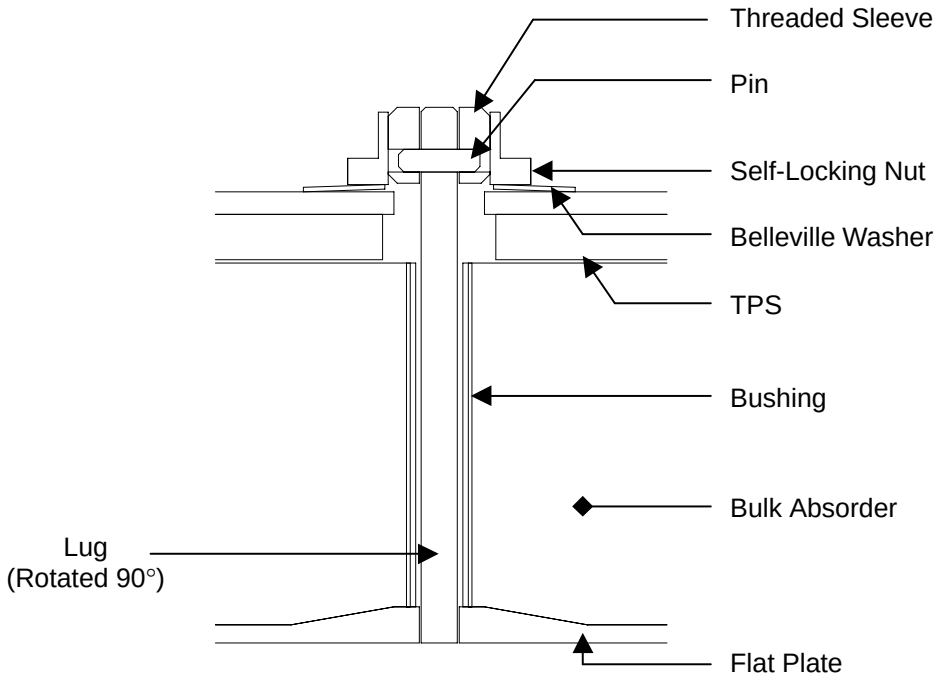

Figure 120. CMC Acoustic Tile “T” Fastener Design

René 108 Mixer

The René 108 design met material yield-strength requirements and has the potential to meet low-cycle fatigue (LCF) requirements. Further design work is required on the attachment features. Additionally, further analysis using 1999 deep lobe fan/core mixer CFD data should assist in bounding the impact of upstream fan/core mixer geometry design changes.

Geometry – The mixer, as shown in Figure 121, sits transversely across the downstream end of the transition duct. It comprises two sets or racks of 10 secondary (cold) and 10 primary (hot) lobes, located above and below the nozzle horizontal centerline. For each rack, the 10 secondary lobes consist of 2 half lobes at each sidewall and 9 full lobes located transversely across the nozzle.

Each secondary lobe contains three curved vanes held in position by a "floating" joint between the edges of the vanes and rails in the sides of the lobes. Each lobe is supported at the upstream end by a tie-beam attachment and at the downstream end by a strut. The individual lobes are joined at the inner, axial edges by a keyed slot and clip. These details are shown in Figure 122.

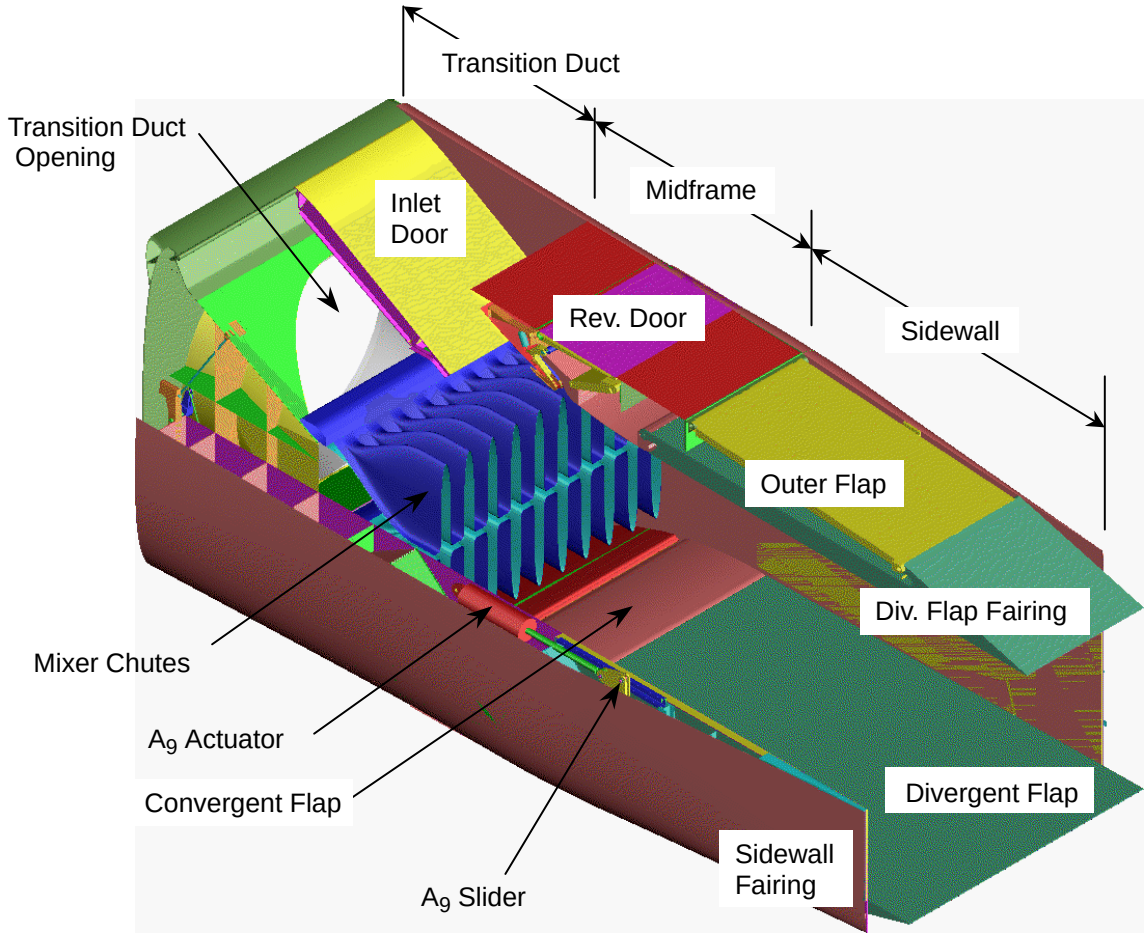

Figure 121. Ejector Mixer Within Exhaust Nozzle System

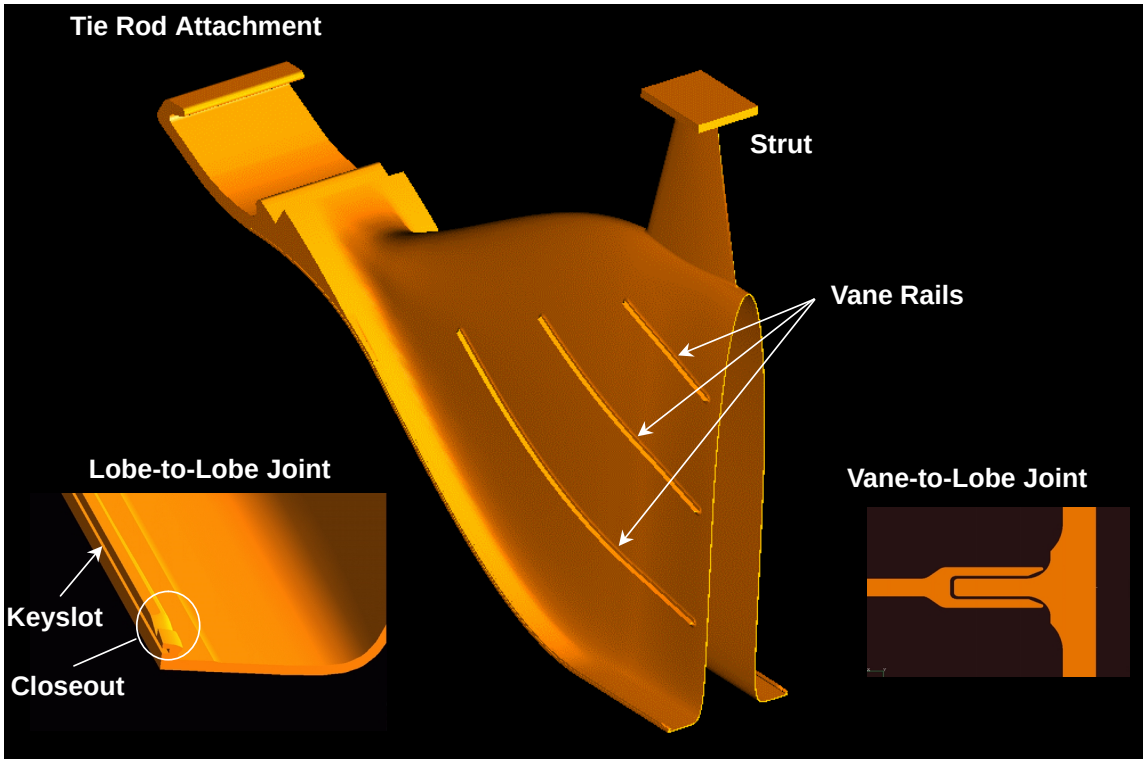

Figure 122. Ejector Mixer Lobe Features

The mixer shape is defined by the aerodynamic requirements for minimum pressure losses and flow separation. The primary side of the lobes consist of a convergent/divergent profile that defines the engine throat area during the suppressed modes of operation, as shown in Figure 123.

Function – The ejector mixer serves two main functions within the exhaust nozzle, during the suppressed modes of operation. It defines the throat area of the engine and simultaneously mixes entrained external air with the engine exhaust flow to reduce the exit jet velocity and thereby reduce the jet noise. The throat area is established by the primary side geometry of the ejector mixer, as shown in Figures 123, 124, and 125. The engine core flow is guided outward by the primary lobes of the mixer, and the entrained external air is guided inward toward the nozzle horizontal centerline by the secondary lobes of the mixer. Mixing occurs at the exit plane of the ejector mixer by way of transversely alternating streams of engine gas flow and entrained (ejected) external air, as shown in Figures 123 and 126.

For the unsuppressed modes of operation, the ejector inlet openings are closed, and the ejector mixer becomes fully bathed in the engine gas flow, as shown in Figures 127 and 128.

Material – The chute materials and weights are listed in Table 27.

Thermal and Pressure Loads – The ejector mixer loads were analyzed for two flight conditions/ configurations for the 3770.60 engine cycle. CFD analyses were conducted for takeoff/suppressed and cruise/unsuppressed operations. Thermal boundary conditions and static pressure loads were mapped from these analyses. Temperature adders to account for turbine radial profile and engine deterioration were applied for the maximum-temperature analysis.

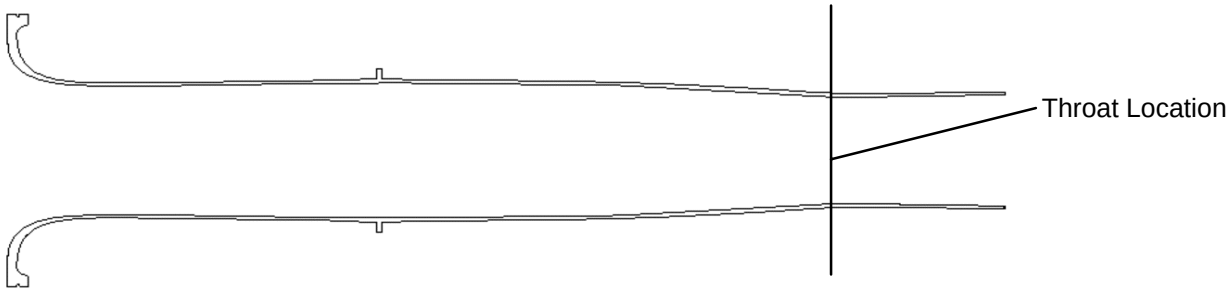

Figure 123. Waterline Section-Cut of Ejector Mixer

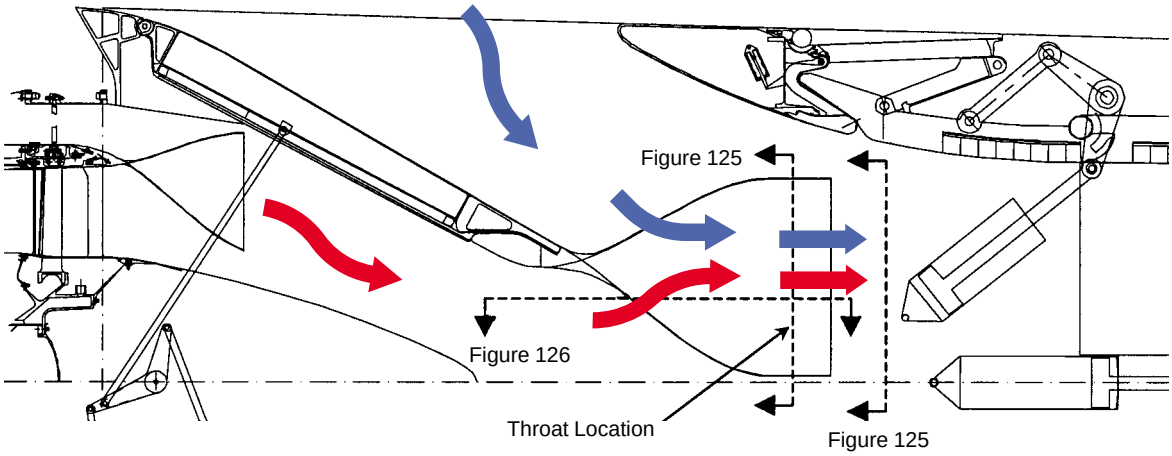

Figure 124. Buttline Section-Cut of Nozzle (During Suppressed Mode of Operation)

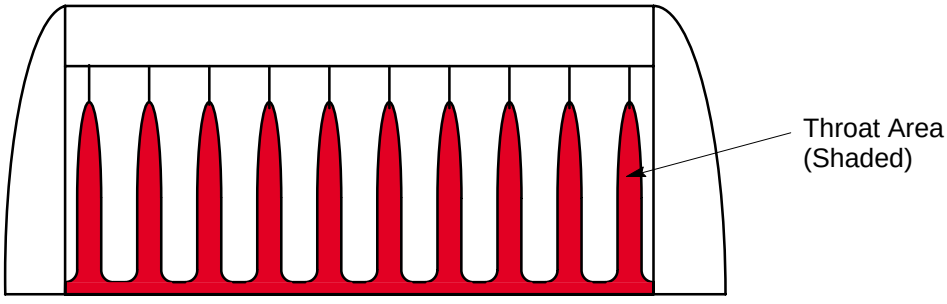

Figure 125. Aft Looking Forward Section-Cut of Ejector/Mixer (From Figure 124)

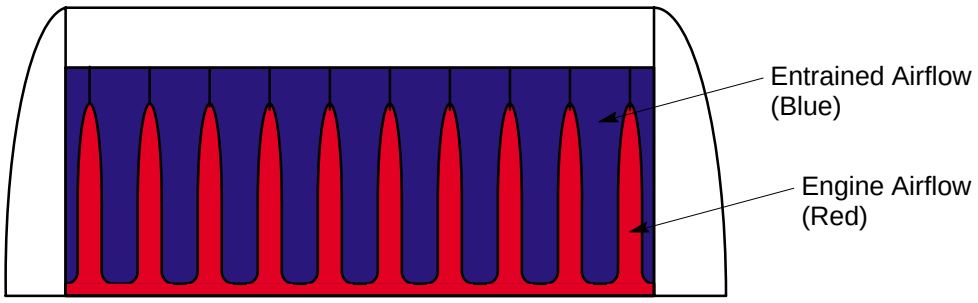

Figure 126. Aft Looking Forward View (From Figure 124)

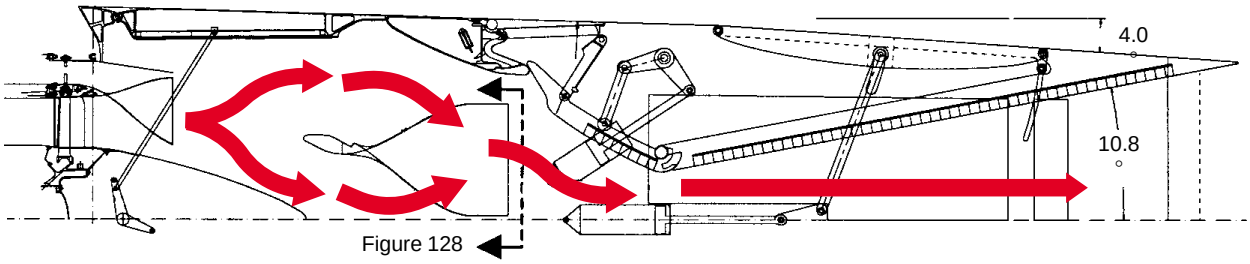

Figure 127. Buttline Section-Cut of Ejector Mixer (During Unsuppressed Mode of Operation)

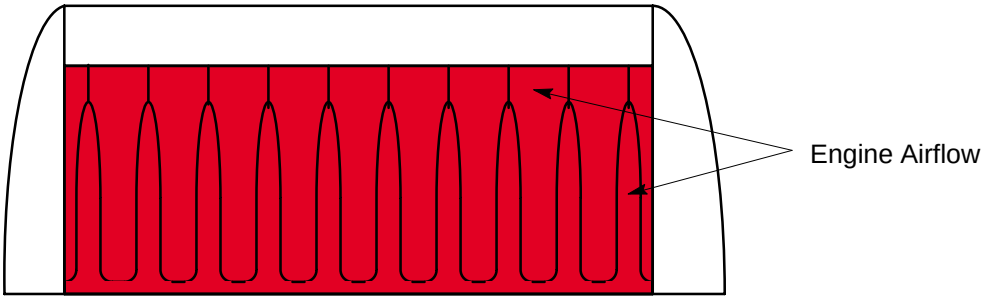

Figure 128. Aft Looking Forward View (From Figure 127)

Table 27. Chute Materials and Weights

Part	Material	Weight, lbm
Chute Lobes	René 108	436
Vanes	HS188	118
Struts	René 108	50
Forward Attachment	René 108	129
Lobe Flanges*	René 108	42
Coating	VPA	31
Bolts	Waspaloy	5
Seal	Waspaloy	2
	Total Weight	813
* Includes key and C-clamp.		

The resulting stress levels at takeoff and cruise are illustrated in Figures 129 and 130. Overall stress levels in the mixer lobe were found to be acceptable, as shown in Figure 131. Lobe joint and vane joint stresses were also found to be acceptable for an LSM2 size mixer under takeoff conditions. Stress levels under LSM2 loads were greater than would be desired for the HS–188 C-clamp, thereby requiring a material change or an increase in thickness. Further analysis would be required to refine the design of the lobe-to-lobe and vane-to-lobe joints under full-scale loads.

Life – A comparative analysis of LCF was performed for equiaxed and directionally solidified (DS) René 108 ejector materials. Thermal and pressure loads from CFD analysis were used. The LCF cycle included shutdown, takeoff, and cruise. The contribution of cruise to LCF was found to be negligible. The calculated lives for both materials were shorter than desired in very localized areas. However, the minimum LCF life for the DS mixer was conservatively 5× better than for equiaxed, and the rupture life of DS was at least 2.5× that of equiaxed René 108.

Manufacture – Manufacturing feasibility of the ejector mixer was evaluated under the CPC as well as the EPM programs. A 56% scale casting trial was completed at Precision Castparts (PCC) for equiaxed René 108 and at HOWMET for DS René 108 for LSM Build 2. Both suppliers demonstrated 100% fill castings and wall thicknesses from 0.115 to 0.180 in. GEAE, NASA, and PCC also demonstrated weld-repair capability of both equiaxed and DS René 108 castings in the NASA substrate welding at elevated temperature (SWET) facility.

Lessons learned were that an 0.080-in nominal wall thickness is still a challenge. However, it is believed to be achievable with higher temperature/strength shell systems. Improved grain structure would also result from continued manufacturing development. Finally, full-scale casting technology can build on the 56% scale experience but will require significant development.

Summary – The Generation 3.6 ejector mixer design meets requirements for yield strength and has the potential to meet LCF requirements with refinements to local features and analysis techniques. Further design work is required on the attachment features such as tie rod, strut, vanes, and side seals. Changes to the fan/core mixer or other upstream geometry may impact the ejector/mixer design because of the resulting temperature distribution on the ejector mixer. Further analysis using the 1999 deep lobe fan/core mixer CFD data should bound the impact of fan/core mixer design changes.

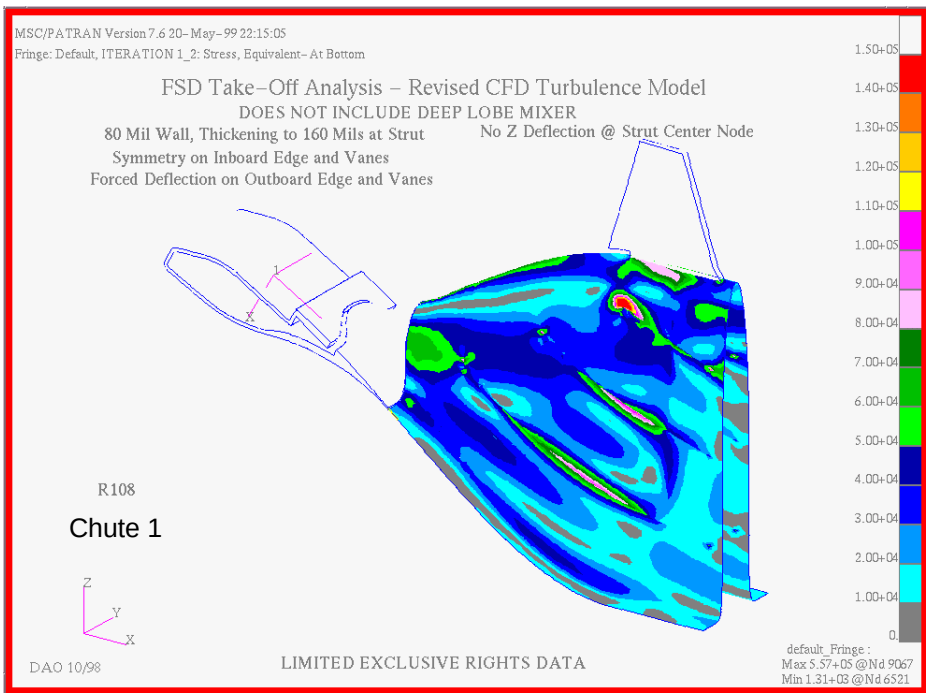

Figure 129. Ejector Mixer Stress Levels at Takeoff

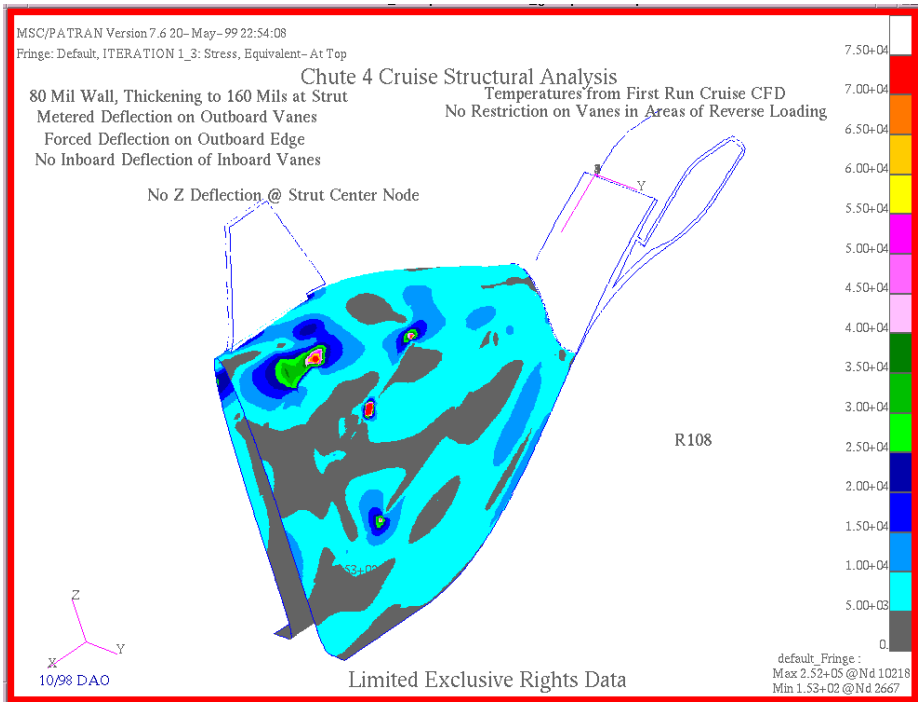

Figure 130. Ejector Mixer Stress Levels at Cruise

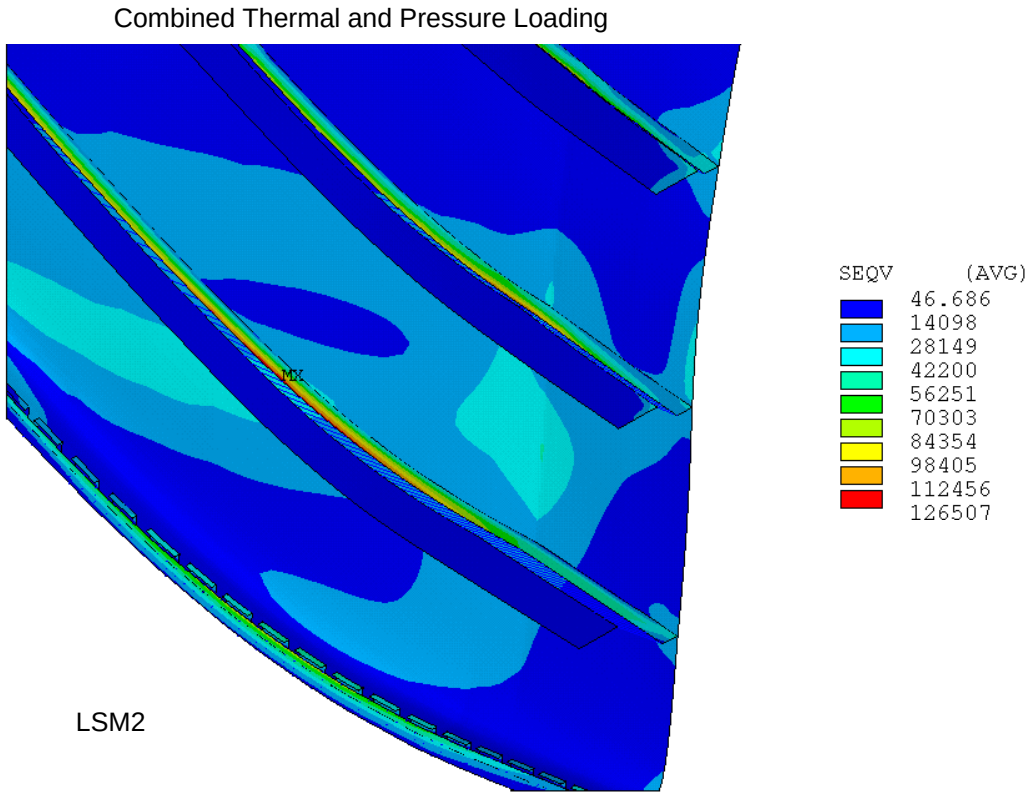

Figure 131. Ejector Mixer Von-Mises Stress *Overall stress levels in mixer lobe are acceptable.*

CMC Mixer Concept

The HSCT mixer conceptual design effort involved a feasibility study of a mixer made from a ceramic-matrix composite (CMC). The mixer, which spans the 71.33-in width of the nozzle (Figure 132), is a large contributor to the nozzle weight. P&W currently uses CMC's in the design of acoustic tiles and liners for nozzle applications because they offer high-temperature capability and low density. In an attempt to save nozzle weight, a CMC feasibility study for the mixer/ejector was conducted for the HSCT conceptual design.

The mixer environment is harsh, with large temperature and pressure gradients. For the current cycle, 3770.60, the mixer is exposed to gas-path temperatures of 1500°F and higher (with ambient air flowing on the secondary side in suppressed mode). The complicated contour is a challenge in manufacturing, and the large pressure gradient (35 psi) poses challenges in structural design.

Design and analyses were conducted for two CMC materials, SiCSiNC and SiCSiC. The advantage of fabricating the mixer out of CMC is in potential weight savings, since the density of CMC is about 1/3 that of a Ni-based alloy. CMC's also have good resistance to creep, crack growth, and wear, and they maintain strength at high temperatures, which means the engine could run at hotter cycles with a CMC mixer. However, CMC's are sensitive to moisture and salt fog exposure, and they can be expensive and difficult to manufacture depending on the geometry.

Typically, SiCSiNC is used for nozzle applications and SiCSiC for combustor applications. However, both materials were evaluated for this study. The primary differences between the two are as

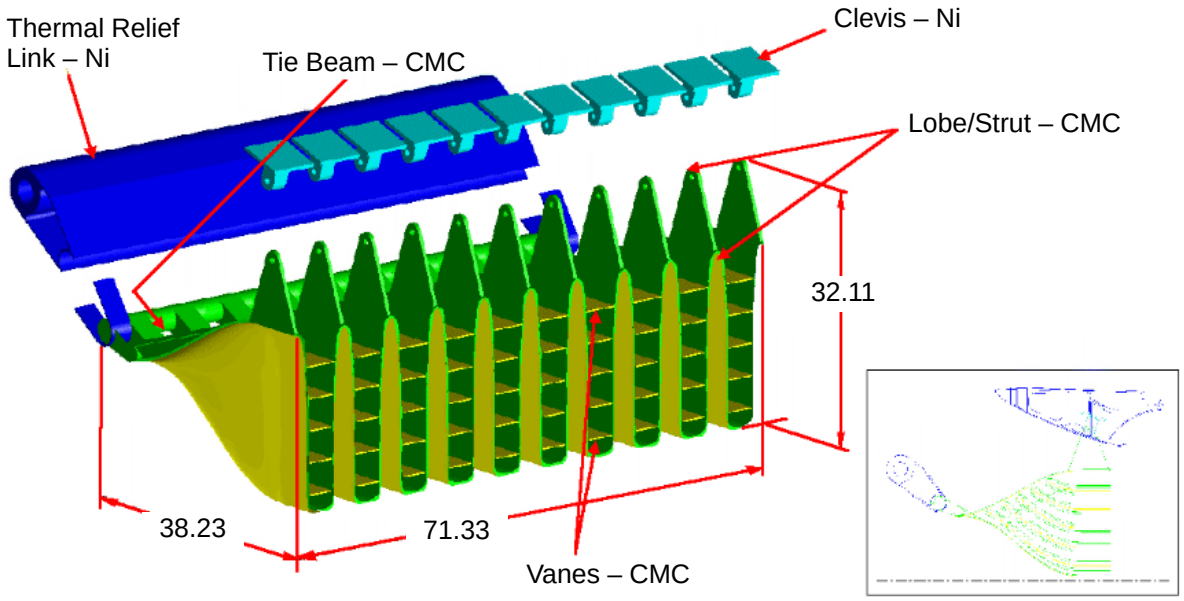

Figure 132. Exploded CMC Assembly Showing Attachments to Static Structure

follows. SiCSiC has a high conductivity (similar to a metal); SiCSiC is currently about 5 times the cost of SiCSiNC; and SiCSiC has higher strength allowables than SiCSiNC. Application of SiC-SiNC in nozzles has been limited to very hot, but generally nonstructural, parts such as liners and acoustic tiles. Due to the nature of a nozzle mixer/ejector, subject to a large pressure load with cold flow on one side and hot on the other (inducing a thermal stress), both materials were evaluated as possible candidates; see Table 28. The low thermal conductivity of SiCSiNC makes it vulnerable to large thermal gradients. Techniques such as a thermal-barrier coating or a radiation blanket are options for addressing this issue. Table 29 is a list of comparisons.

Although CMC's have a high strength-to-weight ratio, the estimated weight of the mixer will change marginally. Since CMC's have a surface roughness greater than that of sheetmetal, the gross takeoff weight will increase to anywhere from 1,394 to 12,054 lbm, depending on the surface roughness. The wall of this CMC mixer would be as much as 0.25-in thick at locations of high stress, in the region of secondary vanes and in the curved region transitioning from a secondary to a primary lobe. To meet aerodynamic performance criteria, the final mixer design will have a different geometry

Table 28. Properties/Allowables Comparison Between CMC and Ni Alloys

Properties at 1200°F	SiCSiNC	SiCSiC	Inco 625	Haynes 230
Tensile Stress (FS=1), ksi	——	——	28.5	38.5
Interlaminar Tension (Allowable), psi	500	1360	——	——
Density, lbm/in^3	0.08	0.10	0.305	0.324
In-Plane Conductivity, Btu/ft^2–hr–°F	10.092	160.20	130	130
Interply Conductivity, Btu/ft^2–hr–°F	14.04	204	130	130
Coefficient of Thermal Expansion, 10^{-6}/°F	1.68	2.25	10.3	7.8

Table 29. Thermal Gradients Through CMC SiCSiNC Mixer *Gradients for mixer alone, with a TBC, and with a radiation blanket. The gradient shown is through the CMC material only.*

Parameter		Mixer Alone	With TBC	With Radiation Blanket
Heat Flux (Btu/in/ft^2/hr/°F)		14	5	10
Thickness (in)		0.25	0.0125	0.08
ΔT – Thermal Gradient, °F	Point 4	647	598	514
	Point 3	282	261	224
	Point 2	591	551	479
	Point 1	559	529	475

than that of the current metal design. Based on this study, a CMC mixer design can meet the requirements for SAR and optimum mixing even though material thickness will increase in specific areas.

This feasibility study showed that the best candidate for a CMC mixer is SiCSiC because it offers high conductivity and strength compared to SiCSiNC. The high conductivity of SiCSiC dramatically reduces the thermal gradient through the mixer wall and therefore reduces the interlaminar tension (ILT) stress. In addition, because of the higher allowables of SiCSiC, there is a very comfortable margin of safety. Table 30 summarizes the results discussed above. The large thermal gradient across the mixer wall in the SiCSiNC design causes the stresses to exceed current allowables for this material. However, more extensive analysis is needed to determine the cost compatibility versus weight with respect to a metal mixer.

Table 30. Strucutural Analysis Results *The location of maximum ILT is in the curved region of the lobe as it transitions from secondary to primary.*

Parameter	SiCSiNC	SiCSiC
Temperature Gradient, °F	600	80
Maximum Interlaminar Tension, psi	777	96
Maximum Shear, psi	–0.36	13.17
Maximum Deflection, in	0.022	0.014

There is currently a lack of property data to design to. The current CMC database is really only suitable for flat-panel, fast-fracture designs. These databases account for environmental degradation but are incomplete for fatigue/life. A 3σ knockdown is used to determine what allowables the designers should use. Even with the knockdown, there is still the issue of properties being affected by the geometry of a CMC part (due to the microcracking of the fibers). Leakage will contribute to the performance of the nozzle, so sealing at the joint interface between lobes and at the sidewall needs to be more thoroughly addressed, primarily through rig testing.

Areas that should be investigated are: (1) weave architecture and (2) rig testing for structural and aerodynamic/performance assessments. It is suggested that this work include analyzing both SiC-SiC and SiCSiNC materials. The structural analysis and material properties used for the feasibility study were for a 2D weave and layup. If a 3D weave were used, the ILT and interlaminar shear

allowables would increase by 50% to 100%, but the in-plane properties would decrease by that same amount. This work consisted of a 3D FEM of the curved mixer section where ILT was limiting. A series of design curves was generated to assist in the design of similar applications. The design curves were of radius as a function of pressure and/or temperature. This model can be also modified to reflect a 3D weave for future analysis.

CMC material properties are dependent on the part geometry. Documented properties (used for design allowables) are for flat panels. When CMC's are formed into complex shapes, such as a mixer, the allowables are affected. Although FEA is a good tool to aid in the design of a part, a test should be run to confirm the findings. A full-lobe rig test would give a better picture of the stresses induced in the mixer and could also serve to validate the 3D FEA. This rig test could include 2D and/or 3D weave architecture. All of this work is essential to take advantage of the potential weight savings that CMC materials in complex geometric parts can provide.

Sheet Metal Mixer Concept

The feasibility of a conventional uncooled, sheet metal alloy (versus cast superalloy) ejector/mixer for the HSCT engine noise-suppressing nozzle was also investigated. The impetus for this study grew out of difficulties associated with manufacturing thin-walled superalloy mixers (baseline) experienced in the Enabling Propulsion Materials program. Superalloys are very difficult to weld, braze, and machine. An alternative approach to cast superalloys for the mixer is a wrought, high-temperature, sheet metal alloy, Figure 133.

A sheet metal mixer fabricated from Haynes 230 sheet with a cast/welded Haynes 230 nosepiece and centerline strut was shown to be feasible. Preliminary finite-element stress analysis shows acceptable stress levels at the critical design condition (takeoff). Nozzle temperatures may mandate the use of thermal-barrier coatings. Creep rupture at the takeoff condition was determined to be the primary design driver.

5.5.2.11 Inlet Door

The exhaust nozzle configuration contains two ejector inlet doors near the forward end, above and below the horizontal centerline of the nozzle. These two doors serve as integral parts of the noise-suppression system within the mixer/ejector exhaust nozzle for the MFTF propulsion system.

The ejector inlet door structural design was analyzed for single versus double door effects on engine operability and cooling effects on engine weight and tolerance for temperature variations. Operability was examined for transitions from suppressed to unsuppressed and suppressed to reverse operation. Temperature variations were examined for loading conditions during takeoff/suppressed and climb-out and supersonic cruise, unsuppressed operation. It was determined that a single, uncooled honeycomb door design would provide the lowest weight and range of maximum temperature.

Function – The ejector inlet doors serve two main functions within the exhaust nozzle. They provide for the opening and closing of the ejector inlets and form a portion of the subsequent flowpath for the external free-stream air and the engine flow.

During suppressed modes of operation, the doors provide for the opening of the ejector inlets and the corresponding inner bound to the flowpath of entrained free-stream flow leading into the cold lobes of the ejector mixer. Simultaneously, they form an external bound to the flowpath of the engine

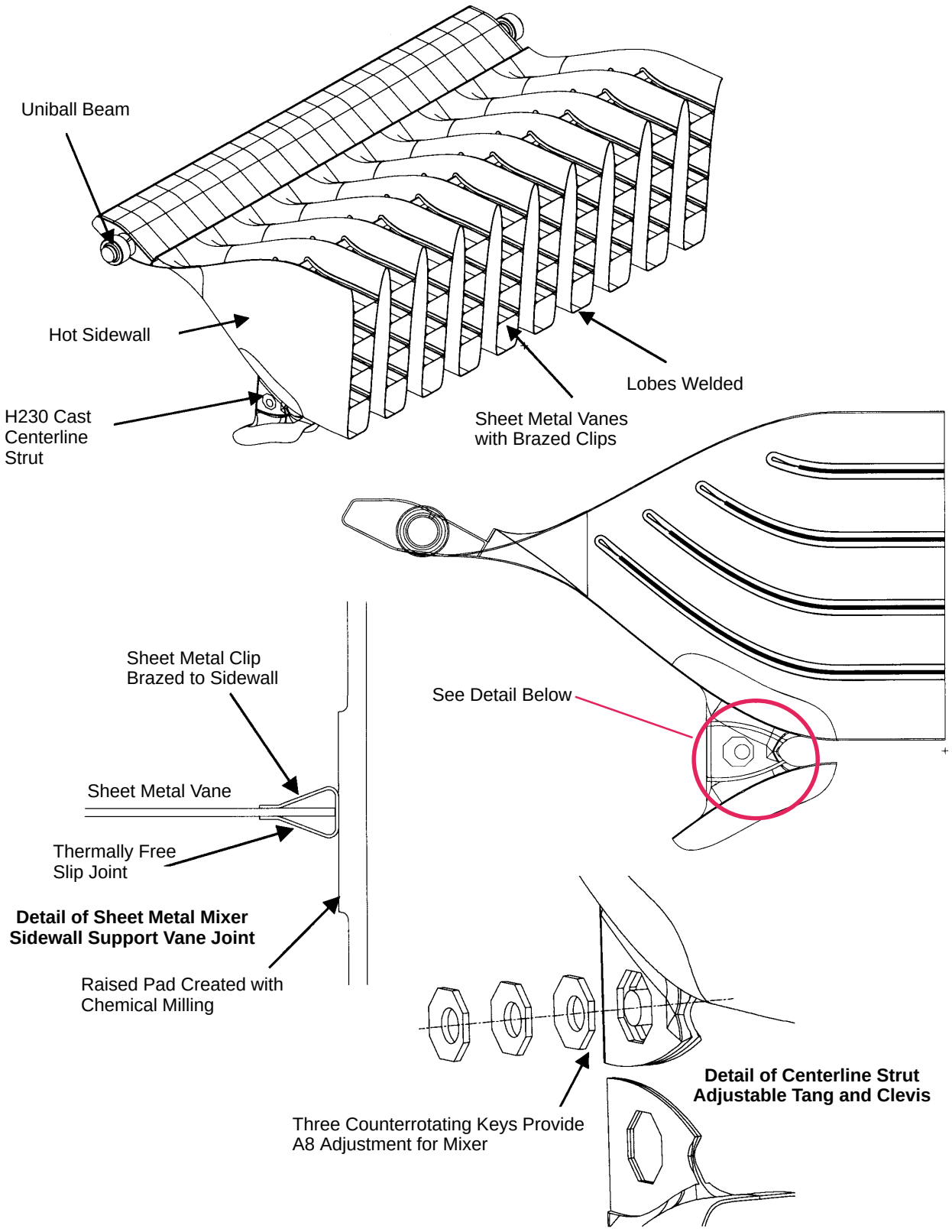

Figure 133. Haynes 230 Sheet Metal Mixer

fan/core gas leading into the hot lobes of the ejector mixer by forming a portion of the outboard surface of the transition duct (see Figure 135).

Conversely, during unsuppressed modes of operation, the doors close the ejector inlets and correspondingly form a portion of the outer mold line (OML) for the nozzle and an outer bound to the flowpath of the fan/core engine flow. The transition from suppressed to unsuppressed modes, that is the opening and closing of the ejector inlets, affects engine operability by increasing the effective throat area (A_{e8}) and reducing the fan stall margin. Also as a result of these transitions, the changing thermal and pressure loads imposed by the gas flow must be accommodated by the structural and material design of the door.

The use of a single door per ejector inlet versus a double door was evaluated, and it was determined that the single-door concept provided a weight savings and benefited from a simplified control system logic.

Geometry – The ejector inlet door is integrated with the actuators to provide positioning of the door, as shown in Figure 134. Each ejector inlet door consists of axial support beams integrated between an inner and outer honycomb sandwich panel. A typical cross section through a door beam is shown in Figure 136. The outer panel is honeycomb followed by a support beams, structural honeycomb panel, thermal insulation, and a radiation shield.

Material Selection – The selection of the door materials was based on a two-part trade study. First it was determined that it was not necessary to cool the door to meet the design criteria. These criteria stated that the temperature gradient through the honeycomb panel was to be less than 300°F, and the maximum temperature for a titanium design was to be below 800°F

It was found that the uncooled design maximum temperature range was 200°F versus 350°F for the cooled design. Also, the uncooled design ΔT was within the specification limit.

A study was also made of the door and engine weights for metal and CMC designs. The weight was less for metal.

Material – The materials and the weights of the door components are listed in Table 31.

Summary – The uncooled Inco 718 single-door design was the recommended baseline for the ejector inlet doors. Further recommended analyses would include effects of thermal profile imposed by the fan/core mixer, deflections of mating structure and door, sealing, detailed FEM, and natural frequencies.

5.5.2.12 Midframe

The midframe, along with the transition duct, makes up the main load-carrying static structure of the mixer/ejector exhaust nozzle.

Function – The function of the midframe is to extend the static structure aft from the transition duct, guide the ejected airflow, contain gas pressure, resist maneuver and blade-out dynamic loading, and provide support for various other nozzle components. These other components include the inlet doors, ejector mixer chutes, reverser cascades, reverser doors, convergent flaps, divergent flaps, outer (external) flaps, convergent flap actuators, divergent flap actuators, aft sidewalls, and a portion of the acoustic treatment.

Geometry – The midframe extends from the aft end of the transition duct to the outer flap forward hinge as shown in Figure 137. The components that makeup the midframe are shown in Figure 138.

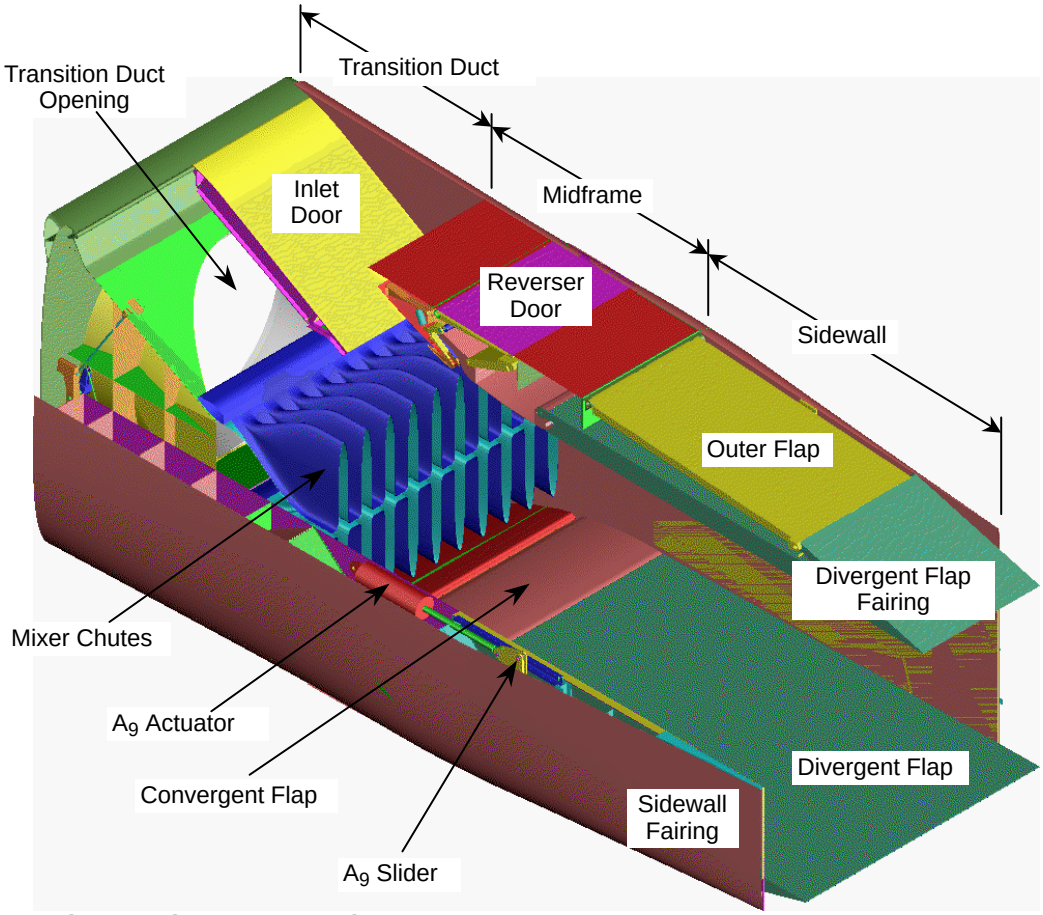

Figure 135. Ejector Inlet Door Location

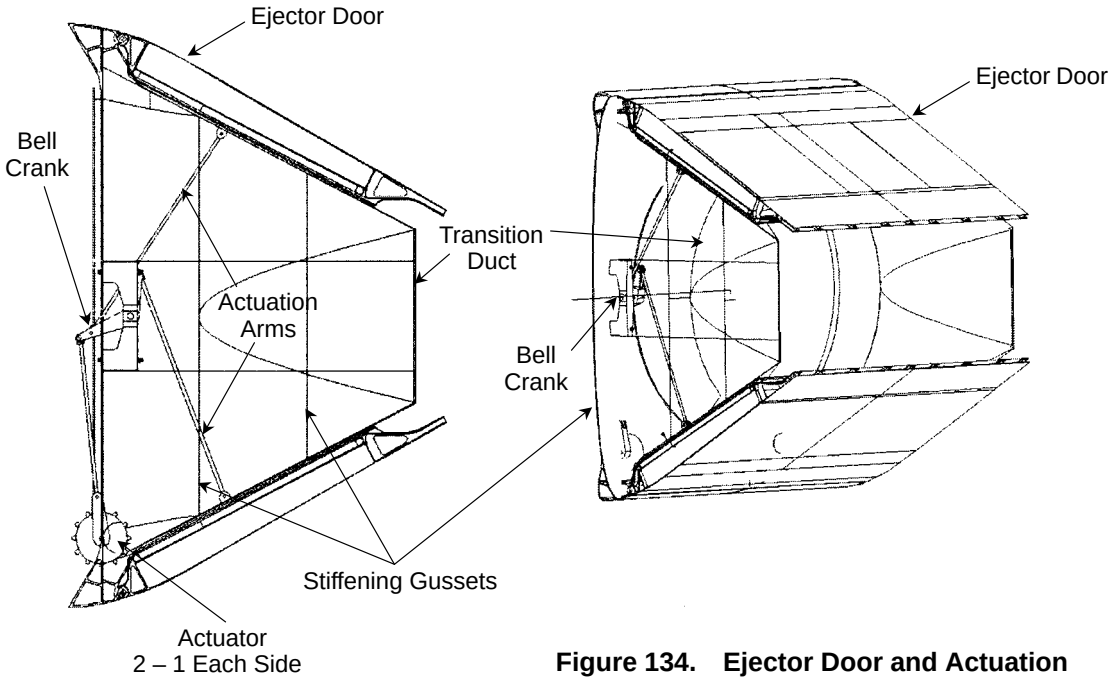

Figure 134. Ejector Door and Actuation

Table 31. Uncooled Door Structural Design

	Outer Panel	Honeycomb Panel	Support Stringers	Side Beam	Close Outs	Radiation Shield	Thermal Protection	Actuation Linkage	Total
Wt. (lbs/noz.) % Total	37.8 0.07	113.2 0.21	68.4 0.12	55.2 0.10	68.6 0.12	33 0.06	98 0.18	76 0.14	550
Material Density Sizing Criteria Criteria Value Bulk Temperature (°F) Δ Temperature (°F) Loading	Inco 718 0.297 Fty.2% 119 ksi 260 256 –	Inco 718 0.297 Fty.2% 119 ksi 912 274 36.4 psid	Inco 718 0.297 Fty.2% 119 ksi 580 387 440 in–lb	Inco 718 0.297 Fty.2% 119 ksi 580 387 500 in–lb		Hast X 1424 0 –	EPM Mat. 0.054 – – 1295 258 –	Inco 718 0.297 Fty.2% 119 ksi	
Manufur.	Honeycomb	Honeycomb	Beam	Beam		Sheet	Blanket		

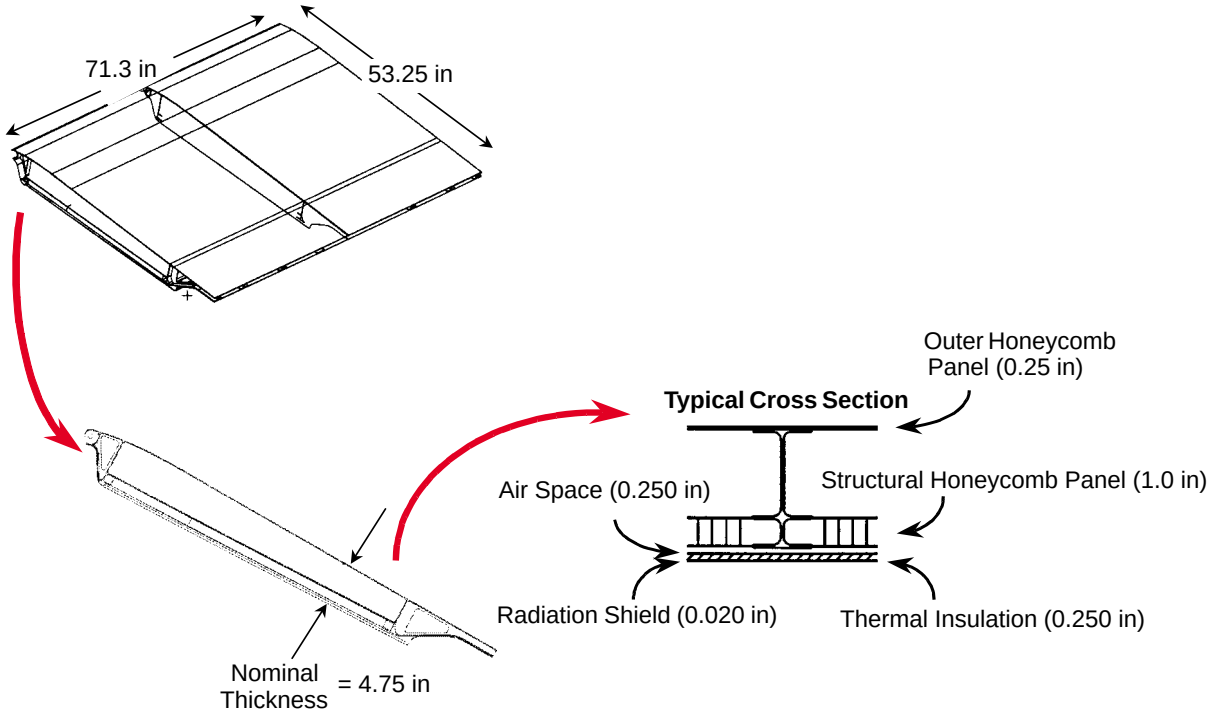

Figure 136. Ejector Inlet Door Cross Section

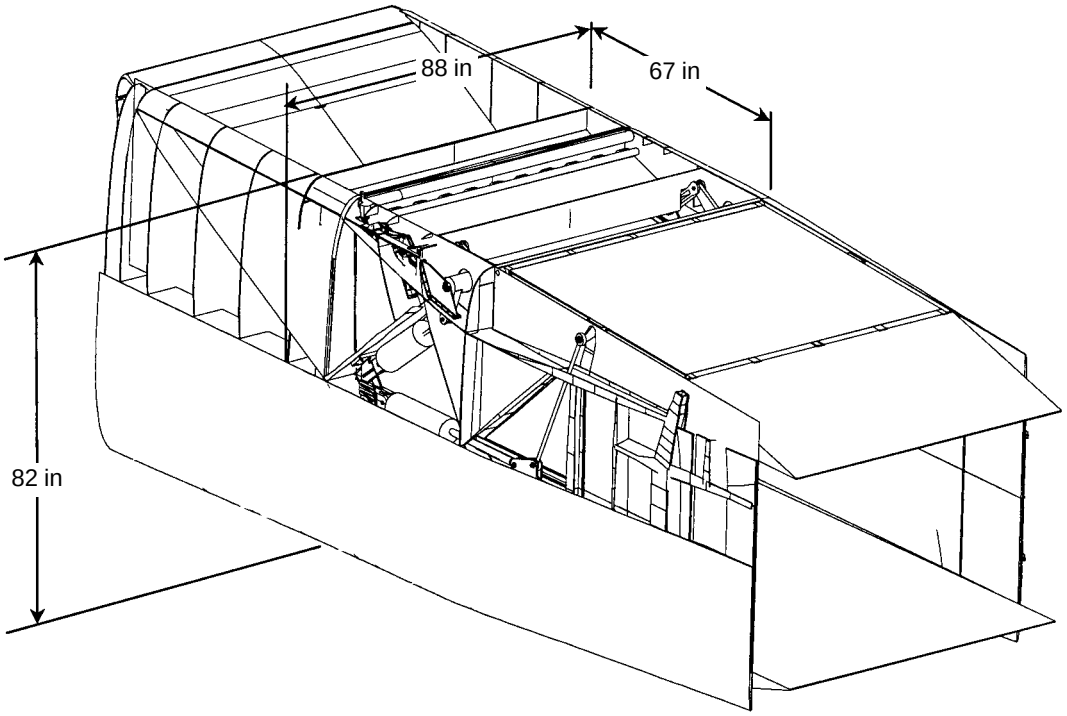

Figure 137. Midframe Location within Nozzle System

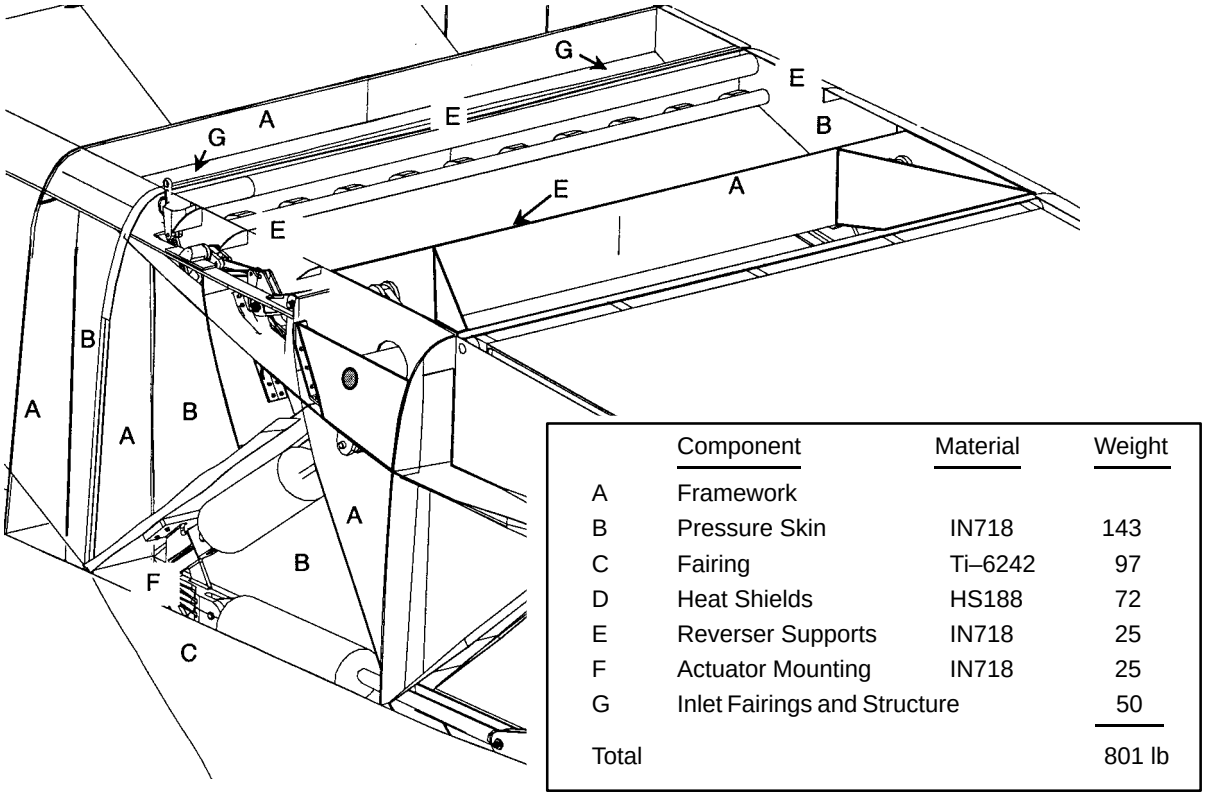

	Component	Material	Weight
A	Framework		
B	Pressure Skin	IN718	143
C	Fairing	Ti–6242	97
D	Heat Shields	HS188	72
E	Reverser Supports	IN718	25
F	Actuator Mounting	IN718	25
G	Inlet Fairings and Structure		50
Total			801 lb

Figure 138. Midframe Components

The dimensions of the I-beam cross sections were sized to satisfy stress and deflection criteria. These criteria were based on the yield strength of the material for stress and maximum deflection limited by flap train system requirements. Components supported by the midframe are shown in Figure 139.

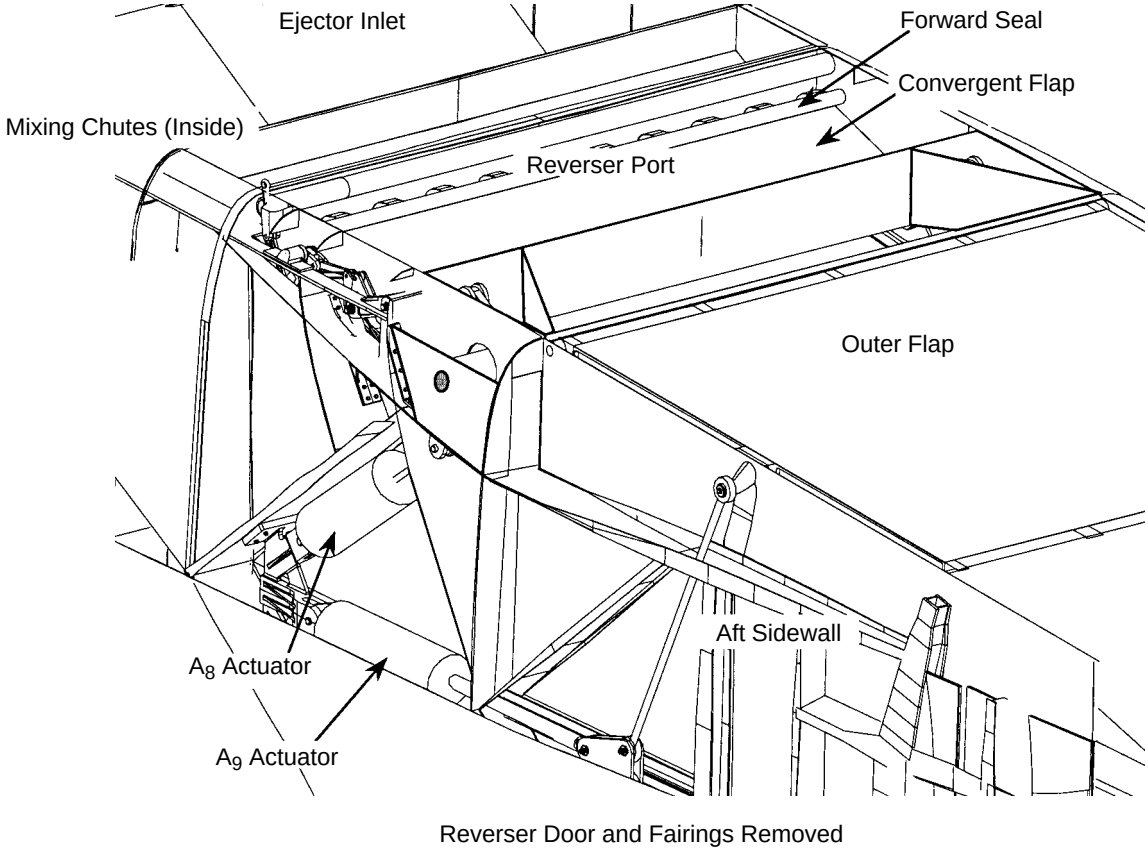

Figure 139. Components Supported By the Midframe *The midframe supports numerous other components.*

Material – The materials and weights of the midframe components that resulted from the structural analysis are listed in Figure 138

Loads – The structural design of the midframe was based on satisfying stress and deflection criteria for pre–defined loading conditions. These load cases are listed in Table 32.

Table 32. Load Cases for Midframe Analysis

Case	Flight Point	Midframe Sizing Region
1	Mach 0, 600-ft, PC50	Convergent Crank, Outer Flap Hinge
2	Suppressed Takeoff (Mach 0.32, 689-ft, PC50)	Divergent Flap Actuator, Outer Flap Hinge, Forward Convergent Link
3	Mach 1.6 Climb (Mach 1.6, 36,000-ft, PC50)	Convergent Actuator
4	Supersonic Cruise (Mach 2.4, 55,000-ft, PC50)	Forward Convergent Link

Loading for structural analysis of the midframe included:

- surface pressure loading applied directly on the pressure skins of the midframe and
- reaction loads from the various components supported by the midframe.

Component surface pressure loading definitions were derived from Gen 2.0 subscale model test data for the suppressed operating modes and from 1D aerodynamic analyses for the unsuppressed operating modes. Reaction loads from the flap train components were derived from the kinematics analysis of the exhaust nozzle (*Mechanica*, a mechanisms analysis computer program, was used for the kinematics analysis). Reaction loads from the ejector mixer were derived from the finite-element model (FEM) analysis of the mixer, using CFD predictions for the surface pressure loading on the mixer.

Analysis – The midframe structural framework was sized using an iterative analysis method that used both ANSYS (GEAE design-analysis software) and an Excel spreadsheet model to optimize midframe beam geometry. This approach involved the use of simple beam elements and thereby provided an efficient method of quickly establishing the correct structural configuration and sizing of the midframe. Four load cases were applied to an ANSYS model of the midframe to establish and size the configuration. Comparison of the resulting beam stress and deflection to the design criteria showed that the midframe was structurally adequate to react loading from pressure and from the components it supports at critical operating conditions.

Summary – Preliminary analysis has shown that the midframe is structurally adequate to react loading from the flowpath pressure and the components it supports at critical operating conditions. Further analysis of the midframe would include effects of thermal gradients and dynamic effects such as maneuver loading and engine blade-out events. Further refinement of the FEM would involve modeling the midframe beams and panels using shell and brick elements.

5.5.2.13 Aft Sidewall

The aft sidewalls are structurally adequate to react loading from pressure at the critical operating conditions.

Function – The functions of the aft sidewalls are to:

- Contain the exhaust gas as it moves from the midframe to the exhaust nozzle exit.
- Provide a place for the installation of acoustic treatment panel
- Provide a clean (smooth and low boattail angle) aerodynamic outer fairing to close the sides of the exhaust nozzle.
- Provide a passage for engine-bay purge air and exhaust nozzle cavity purge air to bleed through to the sidewall trailing “edge.”
- Provide support for the A_9 slider track (part of the divergent flap actuation system).

Geometry – The aft sidewall is located at the aft end of the midframe and bounds the transverse extent of the exiting exhaust gas with a planar, vertical pressure panel as shown in Figures 140 and 141. This pressure panel is in turn supported by the sidewall frame, which is composed of I-beams and shear webs. The sidewall transverse pressure loads are reacted into the midstructure and into two

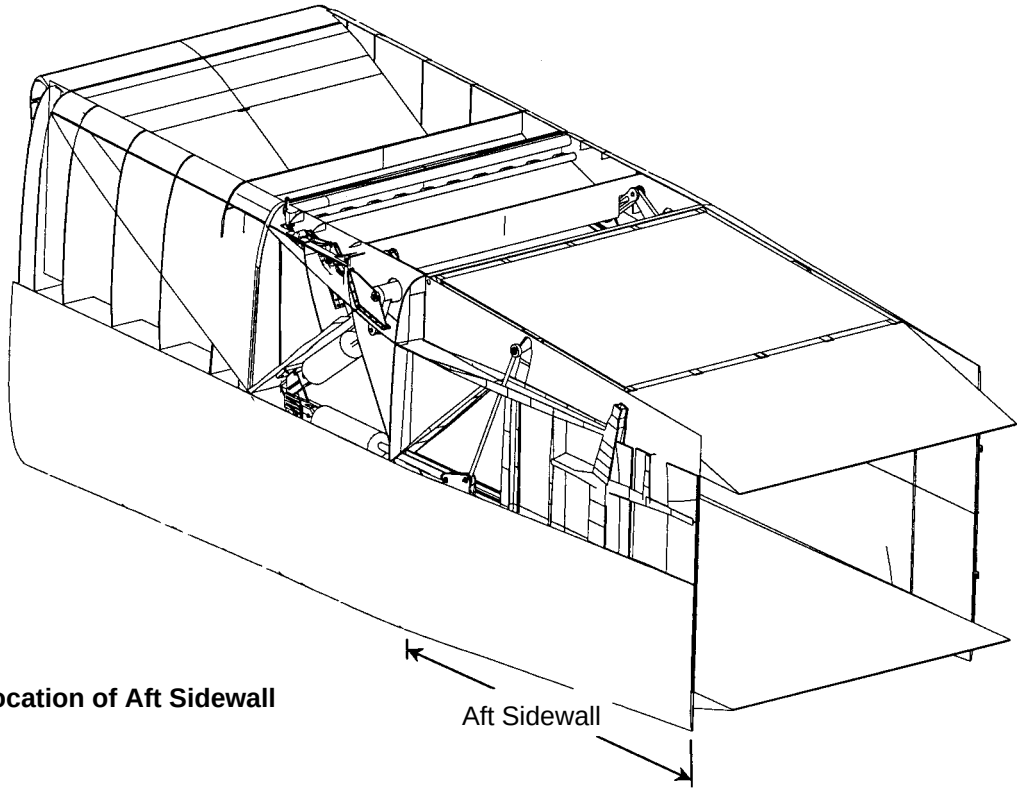

Figure 140. Location of Aft Sidewall

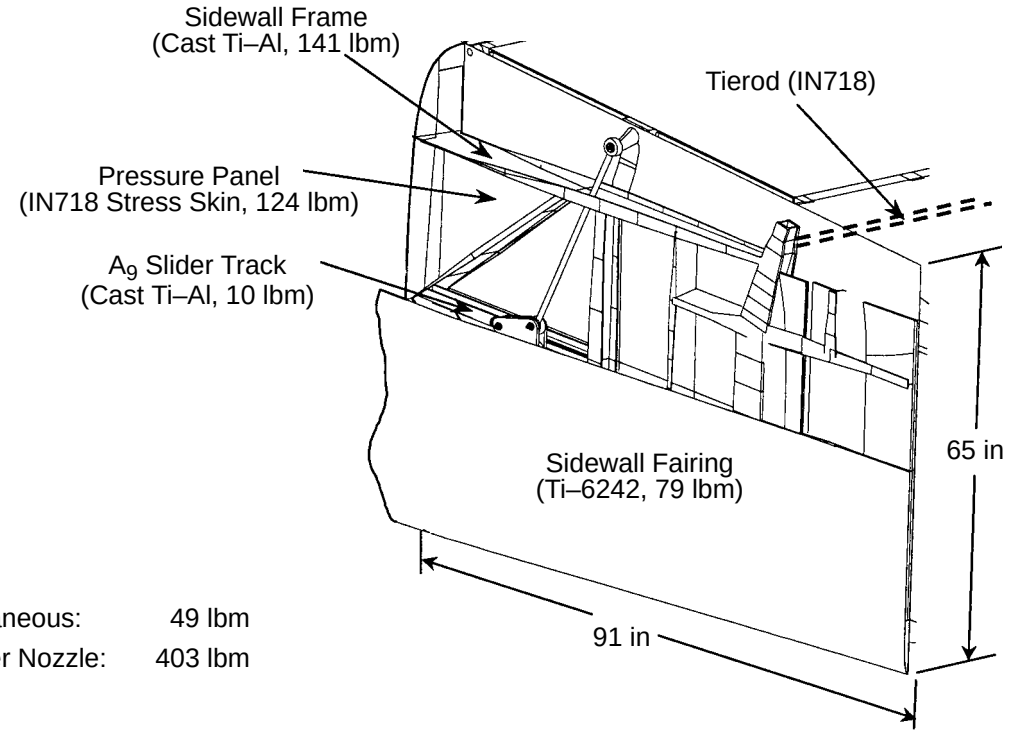

Miscellaneous:	49 lbm
Total Per Nozzle:	403 lbm

Figure 141. Aft Sidewall Components and Materials

tie rods that transversely span the exhaust nozzle. These tie rods react a portion of the transverse load from one sidewall to the other sidewall. The tie rods are included, one each, in the upper and lower external flaps. Because the external flaps move up and down between the sidewalls and the tie rods follow the flaps, it is necessary for the ends of the tie rods to be attached to the sidewall frames through the use of sliding joints. It is envisioned that this sliding attachment could be accomplished by attaching each end of the tie rods, to a "slider block" that would slide in a track, of C-shaped cross section, that would be part of the sidewall frame.

Material – The nomenclature, materials, and weights for the sidewall components are called-out in Figure 141.

Loads – The structural design of the aft sidewall was based on satisfying stress and deflection criteria for the predefined loading conditions shown in Figure 142. These represent surface pressure loading on the pressure panels for the suppressed takeoff conditions, for both the subsonic and supersonic flow solutions. The surface pressure loading definitions were derived from Gen 2.0 subscale model test data. The dimensions of the sidewall beams were defined using an iterative procedure with ANSYS and Excel. ANSYS modeling consisted of beam and shell elements, along with the surface pressure loadings as stated above.

Analysis – The sidewall frame was sized using an iterative method that used ANSYS and an Excel spreadsheet model to optimize sidewall frame beam geometry to satisfy stress and deflection criteria. This approach involved the use of simple beam elements and thereby provided an efficient method of quickly establishing the correct structural configuration and sizing of the sidewall frame The maximum allowable design stress for the titanium aluminide sidewall frame was 22,000 psi (fatigue crack growth, FCG, allowable for cast Ti–Al at 800°F for an effective life of 18,000 hours). Final stress and deflection results from the ANSYS FEM showed that the aft sidewall structure met the design criteria

Summary – Preliminary analysis has shown that the aft sidewall is structurally adequate to react loads from pressure at critical operating conditions. Further analysis should include optimization of

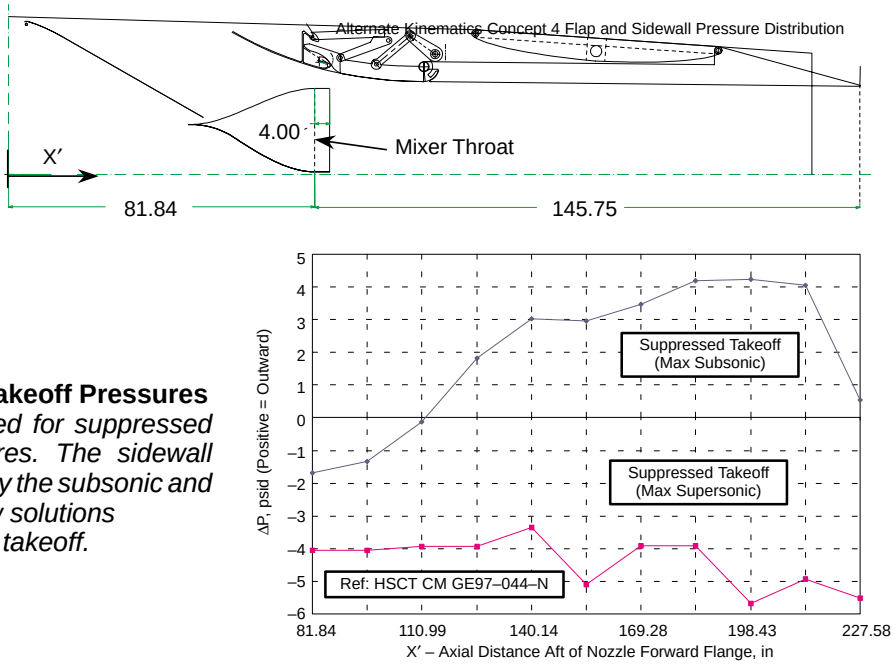

Figure 142. Suppressed Takeoff Pressures
Sidewall is sized for suppressed takeoff pressures. The sidewall frame is sized by the subsonic and supersonic flow solutions for suppressed takeoff.

the framework and tie rod position, effects of thermal gradients, flight dynamics, and aerodynamic instabilities. Further refinement of the FEM would involve modeling the sidewall frame and panels using shell and brick elements.

5.5.2.14 Forward Seal – Convergent Flap

The forward seal for the convergent flap is a fabricated, nonstatic structure and contains the internal gas pressure for the gap between the midframe beam and convergent flap. The exhaust nozzle contains two forward seals that correspond to the upper and lower convergent flaps. The seal accommodates the rotary and translational movement of the convergent flap for all modes of operation.

Function – The function of the forward seal is to contain the internal gas pressure within the existing region between the midframe beam and the forward end of the convergent flap. It must accomplish this by accommodating the movement of the convergent flap during all modes of operation. As a result, the forward seal defines a portion of the internal flowpath, aft of the ejector inlet aft lip.

Geometry – The forward seal is located between the aft surface of the midframe beam and the forward edge of the convergent flap, as shown in Figure 143. A primary pressure panel seals between the beam and the flap for nonreverse flows and a secondary panel seals for reverse flow operation as shown in Figures 144 through 146. The forward seal is mounted to the midframe at the forward end of the reverser port, by a hinge. The forward seal rotates about the hinge and is held against the convergent flap sealing surface by the internal gas pressure, for all of the unsuppressed and nonreversing modes of operation. During the suppressed modes, aerodynamic analysis has shown that it is possible for the ΔP loading on the forward seal to be in the inboard direction, thus tending to force the forward seal away from the sealing surface of the convergent flap. Therefore, during these modes of operation, the forward seal will be held against the convergent flap sealing surface by a series of 11 helical springs. During the reverse mode, the forward seal is rotated into the most forward position by the internal gas pressure and thus defines the forward portion of the reverser port flowpath.

Material – The materials and weights for the components of the seal are given in Figure 144. IN718 and HS188 are used for the seal to maintain functionality while exposed to hot engine gases. Most of the weight is in the seal assemblies.

Summary – The convergent flap forward seal was defined to prevent gas leakage and to accommodate convergent flap positions by means of a metal-to-metal seal. Seal materials were selected to maintain functionality in the exhaust gas environment.

5.5.2.15 Engine and Exhaust Nozzle Mounting and Installation

Proper installation of the HSCT engine and exhaust nozzle onto the wing is critical for the overall success of the HSCT. The installation must provide:

- Low drag
- Efficient operation of the ejector in suppressed mode
- Proper engine bay purge
- Accessibility for inspection, maintenance and removal
- A mounting system of sufficient strength and stiffness

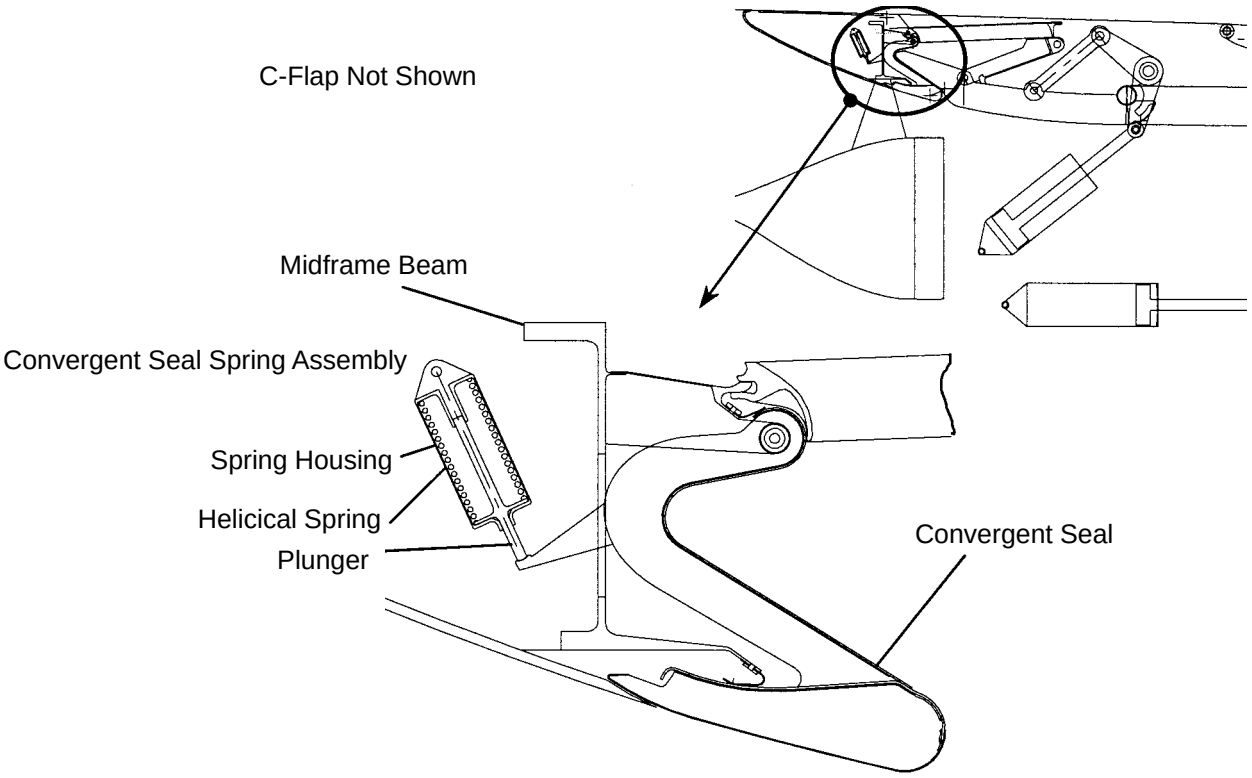

Figure 143. Midframe C-Flap Forward Seal Location

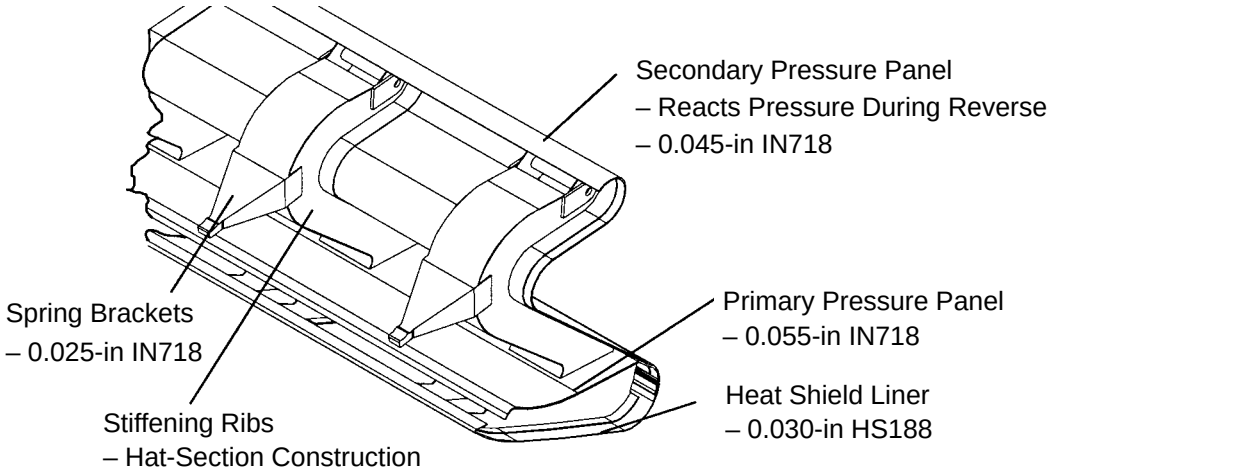

Weight Rollup for C-Flap Forward Seals and Springs	
22 Spring Assemblies (0.32 x 22)	7 lbm
2 Seal Assemblies (33.9 x 2)	68 lbm
	75 lbm Total

Figure 144. Forward Seal Pressure Panels

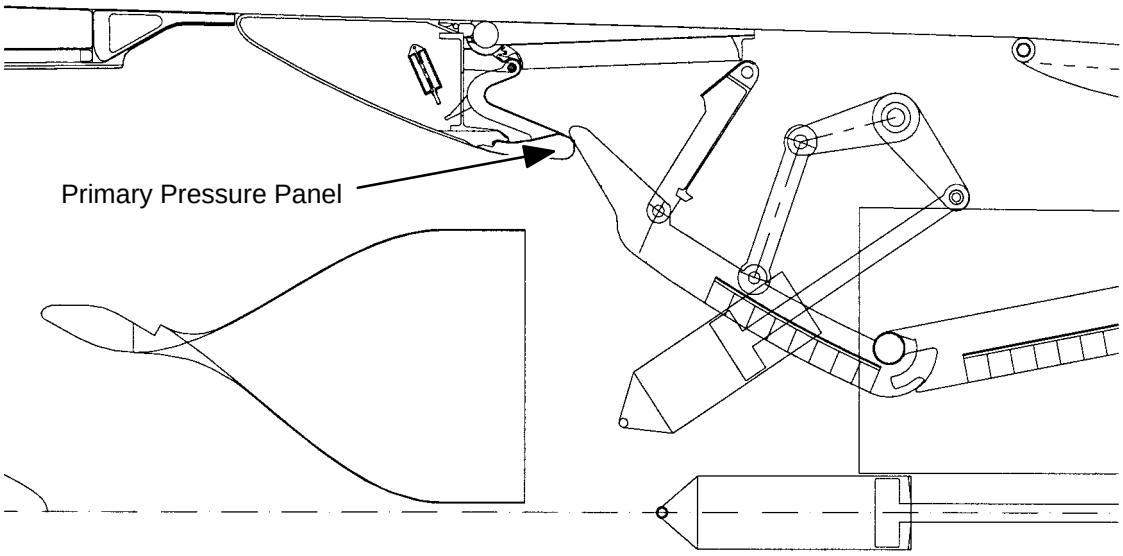

Figure 145. Forward Seal, Nonreversing Mode, Sealing Regions

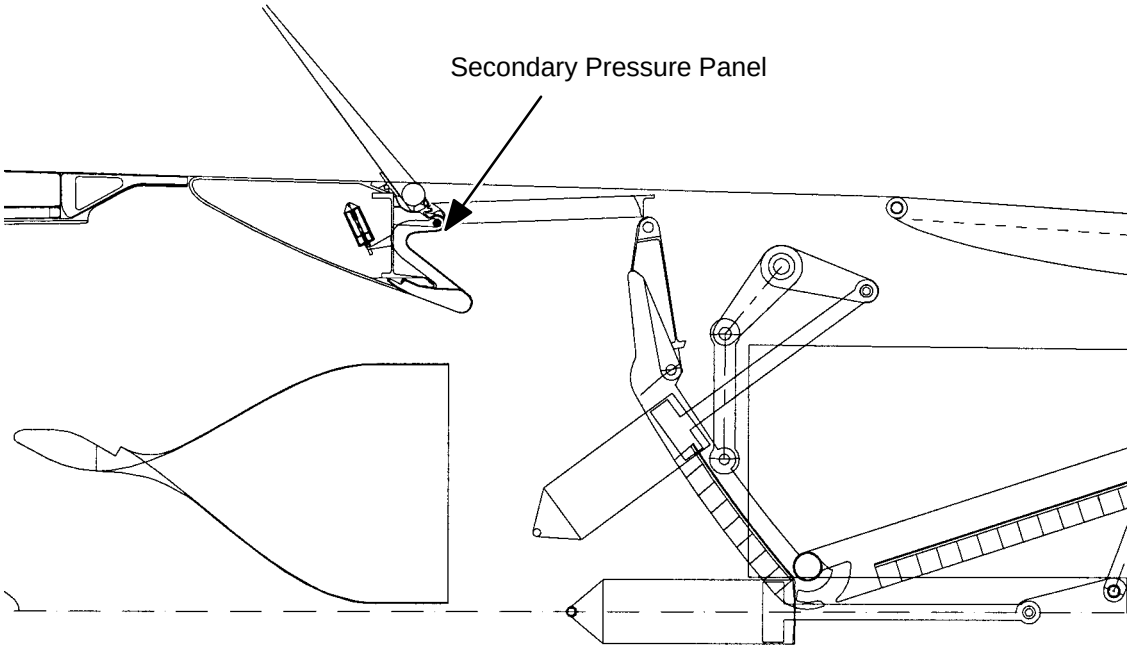

Figure 146. Forward Seal, Reversing Mode, Sealing Regions

- Correct position of the engine relative to critical airframe structure so that, in the unlikely event of an uncontained engine failure, the wing main spars are unlikely to be critically damaged

Installation of the engine and exhaust nozzle, on the wing, is unlike any installation currently used for subsonic aircraft. Instead of being forward and below the wing, as is typical for subsonic aircraft, the engine on the HSCT is mounted aft on the wing with the exhaust nozzle extending aft beyond the tailing edge of the wing. Figure 147 shows the HSCT wing with exhaust nozzles extending aft.

Figure 148 is another view of the installation — with the wing not shown. This view shows the basic propulsion "pod." The inlet and engine nacelle would be mounted to the wing directly; the engine would be hung from the pylon attached to the wing aft spar. The exhaust nozzle cantilevers off the aft end of the engine.

Figure 149 is another view, with the inlet and engine nacelle removed. The engine is mounted to the pylon at forward and aft mount locations. The forward engine mount assembly will react thrust (fore/aft), vertical and lateral loads, and torque about the engine axis. The aft mount will react vertical and lateral loads.

The mounting system structure, including the wing and engine attachment points, must be able to support the ultimate loads shown in Table 33 without failure and 2/3 of the ultimate loads in Table 33 (that is, limit loads) without permanent deformation. The engine shall be designed to operate satisfactorily under 2/3 of the vertical, side, and thrust loads of Table 33 and a pitch and yaw rate of 1rad/s and 0.5 rad/s, respectively.

Initial analysis of the pylon and engine mounts indicated the design to be acceptable in terms of stress criteria. There has been concern whether the stiffness of the overall mounting system is acceptable, but no clear criteria for stiffness was developed. Dynamic loading conditions such as wing flutter and engine dynamics considerations such as blade-out also need further evaluation.

Summary – Initial analysis indicates the mount system to be acceptable, but further analysis will certainly be required.

5.5.2.16 Controls Technology – Linear Actuation Only

Lightweight Actuator and Hot Seals Development

This development effort was led by P&W and supported by Hamilton Sundstrand (HS, formerly Hamilton Standard) and Triton Systems Inc. (TSI). The approach was to develop technology for critical actuator subcomponents instead of a complete prototype actuator. This approach was deemed much more cost effective and productive than developing a complete actuator prototype, which would have included noncritical-technology subcomponents. The objectives, strategies, and accomplishments prior to contract termination are described below.

Lightweight, Hot Actuator – The objective of this task was to develop the technology and database for an advanced lightweight nozzle actuator housing fabricated using 3M Nextel 610 continuous fiber reinforced aluminum metal matrix composite (ALMMC) material. The actuator housing was to be designed and fabricated by TSI using the pressure-infiltration casting (PIC) process with input from HS on hydraulic line feed through, end fittings, and high-strength mounting bosses. The housing subcomponent was to be tested by HS. In addition, flat plates were to be fabricated using the PIC process. They were then to be cut into test specimens and shipped to HS for mechanical-

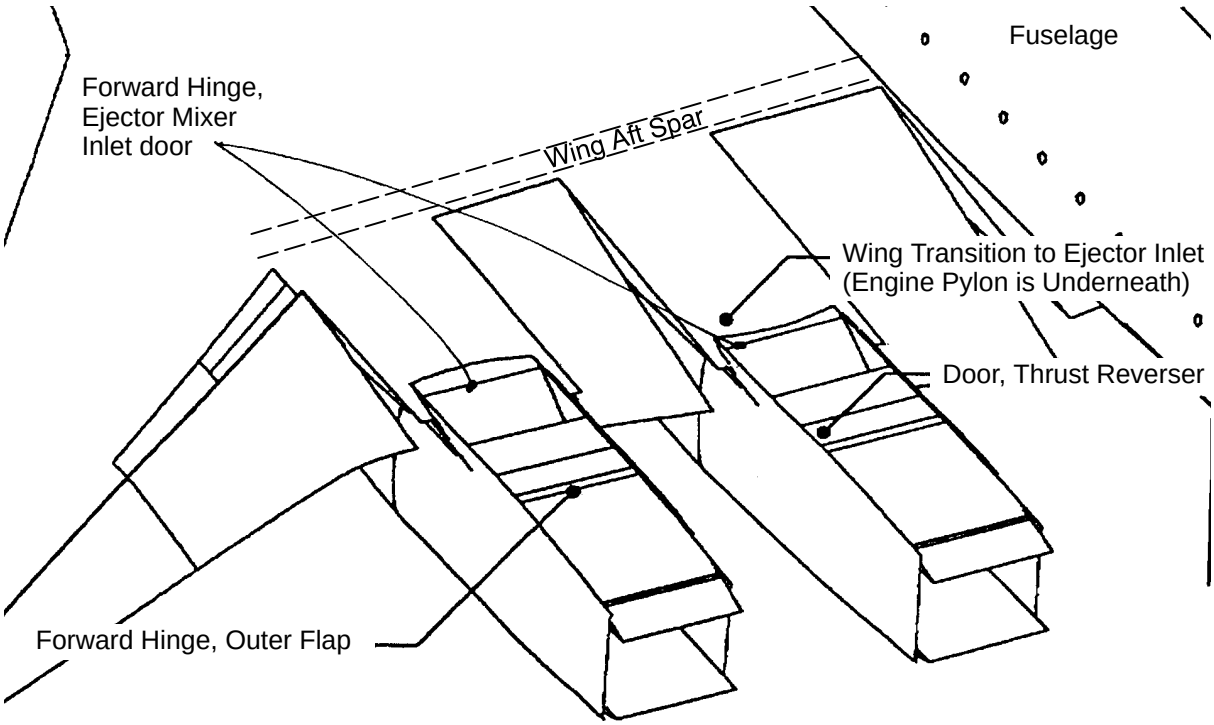

Figure 147. Exhaust Nozzles Extending Aft of HSCT Wing

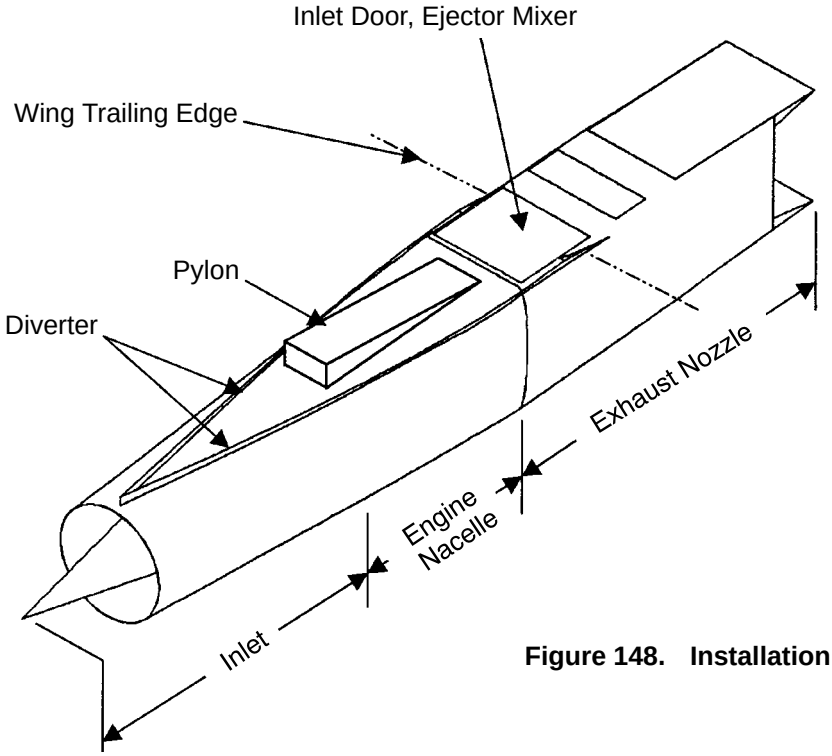

Figure 148. Installation with Wing Not Shown

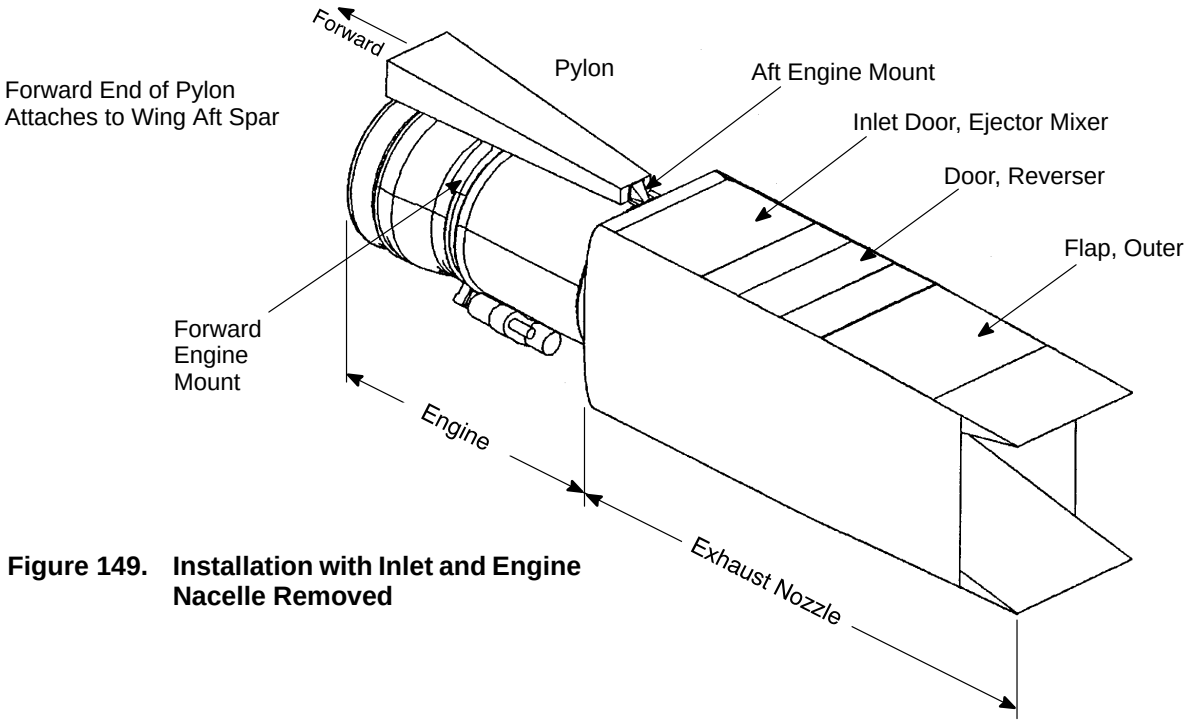

Figure 149. Installation with Inlet and Engine Nacelle Removed

Table 33. Strut Structural Design Envelope Load Conditions

Definitions:

M_{BO}	=	Ultimate engine torque
M_{RS}	=	Limit engine torque
S	=	Side force of nacelle dead weight
S_{BO}	=	Side force blade out
T_c	=	Cruise thrust
T_{max}	=	Maximum Thrust
T_R	=	Reverse Thrust
V	=	Vertical force of nacelle dead weight

Condition	Ultimate Load Factors
Vertical Inertia	7.0 V (Down) 7.0 V + 1.5 T_c –4.0 V (Up) –4.0 V + 1.5 T_c
Side Inertia	3.5 S, –3.5S Boeing 5.0S, –5.0S M_{DA}
Thrust	1.5 T_{MAX} 1.5 T_{MAX} + 3.0 V
Reverse Thrust	1.5 T_R 1.5 T_R + 3.0V
Gyroscopic	±1.5 V + 1.5 T_C + 2.25 Rad/Sec Yaw ±3.75 V + 1.5 T_C + 2.25 Rad/Sec Pitch
Blade Out	1.0 M_{BO} + 1.0V_{BO} + 1.0S_{BO} + 1.0V + 1.0T_{MAX}
Engine Seizure	1.5 M_{RS}
Gust and Maneuver	Not Available

property testing. The testing was to include tensile, creep, fatigue, and coefficient of thermal expansion from room temperature to 700°F. In addition, the titanium/aluminum MMC (Ti/ALMMC) interface was to be evaluated for reaction kinetics and interface shear properties. The following were accomplished:

- Completed winding six flat panels using Nextel 610 fiber
- Completed fabrication of flat-panel graphite mold tooling for PIC processing of the flat panels
- Completed Ti/ALMMC interface shear test specimen mold tooling design
- Initiated fabrication of Ti/ALMMC shear test specimen mold and winding tool
- Established test setup for determining Ti/ALMMC interface shear properties
- Started design process for actuator housing

Hot-Seal Development – Hot seals, necessary for hot actuators, have been designed by industry. However, long-term durability has not been satisfactorily demonstrated. The strategy for this effort was to select several promising seal designs and to perform long-term durability testing. Several promising seal designs were selected. Test fixtures were fabricated, and a testing laboratory contracted. However, testing was cancelled due to Contract termination.

High-Temperature Hydraulic Fluids

Background – Due to the high-temperature environment of the HSCT engine nozzle, a hydraulic fluid capable of withstanding sustained exposure at temperatures from 500° to 600°F is required for the exhaust-nozzle actuation system. The Air Force Research Laboratory, Materials and Manufacturing Directorate (AFRL–MMD) had previously explored a number of fluid classes that could meet this environmental temperature requirement, but these fluids are generally flammable — an especially significant concern for a commercial aircraft application. However, one high-temperature candidate fluid class has been shown to be absolutely nonflammable: perfluoropolyalkylether (PFPAE) based fluids. AFRL–MMD has performed development work on PFPAE-based fluids and additive packages in support of the DoD/NASA Integrated High Performance Turbine Engine Technology program, but these development efforts were oriented toward high-temperature turbine engine lubrication applications. In this earlier work, various commercially available PFPAE fluids were thoroughly characterized and the physical and chemical property tradeoffs were identified. In addition, effective additives with high-temperature stability and low volatility were synthesized, developed, and formulated into candidate fluids. This background provided the HSCT program the opportunity to leverage AFRL–MMD's earlier work and use their expertise in a new development and evaluation effort focused on the unique requirements of the HSCT exhaust nozzle actuation application.

Base Fluid Selection – For the HSCT exhaust nozzle hydraulic system application, maximum continuous fluid temperature was defined as 600°F and maximum intermittent temperature as 675°F. Originally, a pump test using this fluid at 350° to 400°F was planned. (This test was later cancelled, see the following discussion of the pump development program.) A low-temperature requirement of kinematic viscosity no greater than 1250 cSt at –40°F was also specified to ensure that the hydraulic fluid would flow during engine-start conditions in severely cold weather.

The various commercially available PFPAE fluids differ in carbon-to-oxygen ratio and in branching or lack of branching. These backbone differences affect viscosity/temperature range and high-tem-

perature stability. Various molecular weights of the different structures are available in each chemical class. The defined viscosity/temperature requirements ruled out the well-known DuPont Krytox fluids. Fluids that were considered potentially capable of meeting the viscosity/temperature requirements were Fomblin M–03, Fomblin M–15, Fomblin M–30, Fomblin M–60, Fomblin Z–04, (all produced by Ausimont) and Demnum S20 (produced by DAIKIN Industries). Fomblin Z–04 is the only one of these fluids not currently commercially available. Of the Fomblin "M" fluids, M–15 was selected as the best compromise of viscosity/temperature properties. Demnum S20 has the lowest molecular weight/viscosity grade and, hence, has the most suitable viscosity/temperature characteristic for this application. Since the PFPAE fluids are very expensive, (about $1000/gallon), fluid cost is also an important consideration. The Fomblin "M" fluids are less expensive than the Fomblin "Z" fluids, and the Demnum fluids are even lower cost (compared to other PFPAE fluids) because they take advantage of low-cost direct fluorination in the manufacturing process.

High-temperature thermal stability tests were first conducted on the base fluids, without additives. Fluid properties were measured following standard, 24-hour, -fluid evaluation tests. Based on these tests, Demnum S20 proved to be the most thermally stable base-stock fluid.

Formulated Fluid Selection – Two additives were initially evaluated in the Fomblin M–15, Fomblin Z–04, and Demnum S20 base fluids: a perfluoroalkyldiphenylether (DPE) and a tri-perfluoropolyalkylether-phenyl-phosphine (PH3). Later, an additive from Ausimont (DA–306) and an additive from DuPont (SP3) were formulated into the PFPAE fluids along with the DPE additive. DA–306 and SP3 are both antiwear and antirust additives. DA–306 was found thermally unstable above 500°F in earlier development work. The SP3 additive is stable at a much higher temperature than the DA–306 and so was carried further in testing.

GEAE realized that high-temperature material compatibility was critical to the hydraulic fluid application. During the evaluation, the following typical engine hydraulic system materials were identified, and coupons for the thermal stability test were obtained to evaluate compatibility:

- Up to 500°F:
  - 17–4PH,
  - 440C,
  - M–50,
  - CPM10V,
  - Aluminum bronze, and
  - WC
- Up to 675°F:
  - 17–4PH,
  - 440C,
  - WC,
  - Inconel 625, and
  - Ti6Al4V

The Fomblin Z–04 base fluid was not evaluated further because the Fomblin M–15 was found to be slightly more stable and is lower cost. In this phase of the effort, other properties besides thermal stability were considered as well. A final hydraulic fluid formulation would need to provide antirust protection and antiwear protection, so these capabilities was assessed.

Results of the thermal stability testing of fully formulated candidate fluids with the high-temperature materials listed above were as follows: With the materials to be used up to 500°F, both Demnum S20 and Fomblin M–15 formulated with 1% SP3 and 1% DPE were marginal at 500°F, with only a few metals over the corrosion limit. In the over 500°F material tests with the higher temperature metals, formulated Demnum S20 and Fomblin M–15 passed at 626°F but failed at 653°F. Since the maximum continuous temperature requirement was 600°F, with hot spot temperatures of up to 675°F, these formulations are believed to have adequate thermal stability for the HSCT application.

Based on these results, AFRL–MMD recommends base fluids Fomblin M–15 and Demnum S20 as the most viable candidate hydraulic fluids for the high-temperature HSCT exhaust nozzle actuation system. The selected base fluid must be formulated with additives to improve thermal stability, rusting protection, and component wear. A combination of 1% SP3 additive and 1% DPE additive was found to be effective up to the specified temperatures and with the materials anticipated in the HSCT exhaust nozzle hydraulic system.

Hydraulic Pump Technology

Background – During the control system design studies for the HSCT exhaust nozzle actuation system, it became apparent that, due to the high hydraulic system flows, temperatures, and pressures needed to handle the loads and slew rates of this very large exhaust nozzle, the hydraulic pump requirements were well beyond the capabilities of current technology. In addition, the planned use of a new, high-technology, nonflammable hydraulic fluid raised issues concerning hydraulic pump performance and life. Therefore, GEAE felt it was crucial to launch a development effort to reduce the risk to the HSCT program posed by inadequate hydraulic pump technology. The goal was to reduce risk to the HSCT program by advancing hydraulic pump technology to meet the high-flow, high-temperature pump requirements of the HSCT engine nozzle actuation system. The HSCT hydraulic pump design requirements defined for this technology program are shown in Table 34.

Table 34. HSCT Hydraulic Pump Requirements

Parameter		Range
Fluid Properties	Type	PFPAE
	Viscosity (cSt): at –65°F at 104°F at 212°F	1180 17.15 5.66
	Specific Gravity at 77°F	1.836
	Bulk Modulus (ksi), Isothermal Secant at 6000 psi/40°C	130
Pressure Rise (psid)	20% Duty Cycle	5000
	80% Duty Cycle	2500
Temperature (°F)	Pump Fluid Inlet: Normal Extreme	–40 to 450 –40 to 550
	Ambient	–65 to 500
Rated Pump Flow (gal/min)	Thrust Reverse Transient (64% Rated Speed)	130
	Normal Operation (100% Rated Speed)	70

Program Structure – The hydraulic pump technology program was structured into two phases:

- **Phase I:** Assessment of the capabilities of current hydraulic pump technology and determination of the development efforts needed to meet the high-flow, high-temperature HSCT requirements using an entirely new class of nonflammable PFPAE fluids. Following this evaluation, the primary deliverable of Phase I was a proposed pump technology development program for Phase II, consisting of individual detailed development efforts with ROM costs.
- **Phase II:** Implementation of a pump technology development program (based on the proposed program from Phase I) including design and fabrication of test

hardware and performance of development testing. The primary deliverable of Phase II was to be a report containing the results of the technology development effort including material recommendations, test results, specific design issues identified, and solutions implemented. (The Phase II portion of the hydraulic pump technology program was in the early stage when the CPC program was terminated.)

Phase I Program Results – Two hydraulic pump technologies from two suppliers were evaluated in Phase I: conventional rotary piston pump technology by Vickers, Inc. and variable-displacement vane pump (VDVP) technology by Chandler Evans Control Systems Division of Coltec Industries.

The primary outcome of the hydraulic piston pump technology assessment performed by Vickers was identification of the specific pump piece parts for an existing Vickers large piston pump design that would be subjected to temperature and/or stress limitations when used at the conditions defined in Table 34. The Phase II program proposed by Vickers consisted primarily of incorporation of material changes to this existing pump, followed by bench testing with PFPAE fluid to assess the impact on pump performance and life. Relatively little analytical attention was given to the unique fluid properties of PFPAE, and no attempt was made to predict the impact on pump design or performance parameters.

The VDVP technology assessment by Chandler Evans concluded that, while design requirements of Table 34 were outside of existing VDVP design experience, analytical assessment of the key VDVP design parameters indicated that a VDVP of this large size and high temperature and pressure is technically feasible. The impact of the PFPAE fluid on the design was also evaluated, and it was concluded that in the primary areas of concern (viscosity and lubricity) PFPAE is more benign than jet fuel for the vane pump application. The greater density of PFPAE fluid (approximately twice that of conventional oils) was identified as an area requiring further evaluation and test. The relatively low bulk modulus of PFPAE results in better "fluid compliance" to absorb pressure shocks, but the higher density will adversely affect pump filling and increase the potential for "water hammer" pressure spikes. Chandler Evans' proposed Phase II program for the VDVP consisted of: (1) fabrication of a high-pressure evaluation pump followed by development testing of this pump on JP–5 fuel and PFPAE, (2) a high-temperature material evaluation and selection task to address the HSCT temperature requirements, (3) an analytical task to use computational fluid dynamics techniques to evaluate the design impacts of the very high-density PFPAE fluid, and (4) development of a VDVP preliminary design meeting the HSCT pump design requirements defined in Table 34.

Phase II Program Results – Based on the results of the Phase I hydraulic pump technology assessments and the very different proposed Phase II technology development programs from the two hydraulic pump suppliers, it was decided to proceed to the Phase II program for the VDVP approach, with Chandler Evans as the selected supplier. The VDVP technology approach offers size, weight, performance, and life advantages over conventional piston pump technology for the high flows, pressures, and temperatures and nontraditional PFPAE fluid specified for the HSCT application. A key difference in the two pump technologies is that the VDVP technology heritage is in fuel-pumping applications as opposed to the primary application of rotary piston pumps in oil systems. This gives the vane pump an inherent advantage: transitioning from a very severe fluid pumping application (jet fuel) to the more benign PFPAE. The piston pump, however, must transition from a very benign fluid to the less friendly PFPAE while also increasing flow capacity, temperature, and pressure.

The CPC program was terminated in the early stages of Chandler Evans' Phase II development work. Design, analysis, and fabrication of the high-pressure development VDVP was completed. A pump development test plan was defined, and testing of this pump on JP–5 fuel was in progress when the program was terminated. Pump testing had progressed to 100% pump speed and 1000-psi discharge pressure.

5.6 Design and Analysis Methods/Tools

5.6.1 Aerodynamic

5.6.1.1 HSR Nozzle CFD Methods

CFD tools were used extensively in the HSR nozzle program to analyze promising concepts, perform parametric studies of geometry variations, and to both extend and compliment experimental data obtained in wind tunnel tests. Nearly all of these CFD analyses were performed using Reynolds-averaged Navier–Stokes (RANS) solvers, employing eddy-viscosity-based turbulence models (typically two-equation turbulence models such as k–ε). As will be discussed further in this subsection, good qualitative results were obtained using these solvers, with quantitative accuracy largely limited by the turbulence models available in the codes of the HSR nozzle team members. This section provides summaries of some of the CFD approaches used and how they were applied to specific nozzle flow analyses.

At GEAE, sector analyses of mixer/ejector nozzle configurations provided an efficient method for evaluating mixer/ejector flowfield characteristics and performance for a given design modification. A design and analysis system was built around the PAB3D Navier–Stokes Solver (Reference 4). This system used a parametric modeling approach to generate a half-lobe geometry of the mixer primary and secondary flowpaths. This half-lobe mixer geometry was an input to an automated grid generator that generated the sector computational grid for the mixer/ejector configuration, including the secondary inlet and ejector nozzle flap. The computational grid was a structured, multiple-block topology designed to handle the complexities of the mixer/ejector configuration. The grid points were closely packed near the walls, sector sidewalls, and turbulent mixing regions to facilitate usage of the low Reynolds number, Jones–Launder two-equation k–ε turbulence model within the PAB3D code. Because the ejector nozzle sidewalls were not modeled in this system, symmetry boundary conditions are applied to model the sector sidewalls.

The sector analysis approach proved to be an extremely valuable screening and diagnostic tool during the maturation of the mixer design. Several design studies — including mixer chute cross-sectional shape, mixer axial profile shaping, mixer chute length, and secondary inlet ramp modifications — were conducted to evaluate the performance impact of design modifications. These studies identified several design improvements that were subsequently verified by scale-model testing. These improvements included mixer elliptical cross-sectional shapes of the Gen 2.0 mixer designs, reduced flow angularity of the Gen 3.5 mixer design, reduced chute length of the Gen 3.6 mixer design, and reduced shoulder ellipse on the secondary inlet forward ramp. Each of these improvements was incorporated into the product definition after system level trades showed an overall system benefit. These reference design studies should be consulted to understand the utility and limitations of the sector analysis.

Boeing Company – Seattle developed a secondary inlet analysis technique that was found to be an efficient method for incorporating structural vanes into the secondary inlet with minimal impact on

the nozzle performance. This analysis technique used the USM3D unstructured flow solver (Reference 5) to generate the inviscid flowfield and a Boeing-developed boundary layer code to assess the likelihood of boundary layer separation and reattachment.

The basic philosophy for incorporating these structural vanes was to align the vanes with the local flowfield. The flow-aligned philosophy minimizes the impact on total pressure recovery of the secondary inlet. To achieve this, the streamlines for the secondary inlet flowfield without the vanes were mapped using the unstructured Euler flow solver. The vane shapes were developed using these streamlines as the vane mean lines, then incorporated into the secondary inlet. This configuration was reevaluated with the Euler code to determine the vane pressure distributions. The boundary layer code used these pressure distributions to assess the vane boundary layer characteristics. The entire process was repeated as necessary to develop a vane set without flow separation. This design approach and philosophy was successfully used in the development of the vane geometries for the HAM8, LSM1, Gen 3.0, Gen 3.5, and Gen 3.6 mixers.

At the NASA–Glenn Research Center, nozzle sidewall effects on flow within the DSM Mixer 9 geometry were investigated with the NPARC RANS code (Reference 6), using the Chien k–ε turbulence model. In the HSR program, nozzle analyses were typically conducted for a sector of the overall geometry (as discussed previously) and neglected effects of the sidewall. In this study, a full quadrant of the overall nozzle geometry was analyzed, and the presence of a significant low-energy region near the mixer sidewall was predicted. This phenomenon was also observed in Boeing LSAF tests of the DSM Mixer 9 model. Solutions obtained from half-chute and full-quadrant simulations of the nozzle indicated that, away from the sidewall, the symmetry assumption of the sector approach appears to be valid. Comparison of axial velocity and total temperature contours at the mixing-duct exit plane exhibited good qualitative agreement with data.

Boeing St. Louis conducted several analyses of the HAM Mixer 8 nozzle flowpath. These analyses included comparisons of the sector and full-quadrant approaches. In addition, ideal-gas calculations were compared to calculations obtained with the equilibrium air method of Liu and Vinokur, and the effects of tab insertion to the primary stream were investigated. All calculations were obtained with the NASTD (Reference 7) RANS code, which is now known as WIND (Reference 8) using the Menter SST (hybrid k–ω/k–ε) turbulence model. Predictions of a low-energy region near the mixer sidewall were obtained for the HAM configuration with a full-cold sidewall. The calculated low-energy region was similar to that predicted using NPARC for the DSM configuration and compared well with experimental data. Additional calculations of the same geometry, one with a half-cold sidewall and another with a half-hot sidewall, eliminated this low-energy region. The equilibrium air calculations resulted in higher secondary air pumping and lower thrust levels than those obtained with the ideal-gas approach. Analyses that modeled tab insertion into the primary stream resulted in faster initial mixing (relative to no tabs) but less mixing further downstream in the mixer, due to segregation of the high-energy and low-energy regions.

In late 1994, a multiple-site team consisting of NASA–Langley, NASA–Glenn, and the former McDonnell–Douglas groups in St. Louis and Long Beach (now the Boeing Company) conducted an investigation of transonic boattail drag using each site's primary RANS solver (PAB, NPARC, and NASTD respectively). After validating these three flow solvers using data established by the AGARD Working Group Number 17, parametric studies of nozzle area ratio (nozzle exit area divided by maximum nozzle cross-sectional area), boattail angle, and free-stream Mach number effects on nozzle boattail drag were conducted for configurations with a mixed-flow turbofan cycle

and the DSM nozzle geometry (Reference 9). Results for common cases run by all team members indicated generally good agreement using the different sites' codes, except for cases with free-stream Mach numbers very near to unity. Grid sensitivity and turbulence model limitations were believed to be the causes for discrepancies. Following comparison of the code predictions for the common cases, each of the sites performed individual calculations to complete the parametric study. The boattail drag predictions from these calculations were used to construct a new database for rectangular nozzle boattail drag at transonic conditions.

The discrepancies in code predictions for these cases and for calculations investigating nozzle mixing and thrust performance led to another multiple-team effort investigating the prediction of fundamental nozzle and mixing layer cases. This *Nozzle CFD Enhancement Team* consisted of the members of the previously mentioned boattail drag study as well as GEAE, P&W, UTRC (using the NASTAR RANS solver), and The Boeing Company – Seattle (using the GIFS RANS solver). The codes from each of the sites were compared for a supersonic round nozzle, planar mixing layer, and the Boeing single-lobe configuration (Reference 10). The codes were able to provide similar predictions of nozzle mixing, when using a common grid, turbulence model (two-equation k–ε based models were used with each code), and boundary conditions. Deficiencies in predicting compressible jets at high temperatures were found with all codes and were attributed to the turbulence models available in production-use RANS codes, like those of the HSR nozzle team members.

CFD was effectively used as a tool for mixer/ejector nozzle analyses, particularly when the goal of the analysis was determining qualitative flow behavior, helping to interpret experimental data, or performing parametric studies on nozzle geometry variations or flow conditions. The quantitative accuracy of the RANS solvers typically employed, however, were limited by the fidelity of physical models available, particularly turbulence models. Construction of the computational grids was also a limiting factor, both in terms of the effort needed to construct grids for use with the RANS codes and in inaccuracy introduced by the computational grids. Continuing research into developing better physical models such as turbulence models, and the continual improvement of computational power will hopefully result in improved-fidelity CFD tools in the future.

5.6.1.2 One-Dimensional Ejector Code

The 1D ejector code has been written to define nozzle geometry and predict the effect of nozzle geometry on performance and entrainment. This code was originally developed for use in the National Cycle Program (NCP) and has been enhanced for use in correlating trends in the HSCT performance and entrainment data. The code is valuable for predicting trends and sensitivities due to changes in nozzle geometry. Since it has been shown to predict available data accurately, it is also useful for extrapolating into regions where no data are available. In addition, the code is a significant time saver, allowing vast numbers of geometries to be analyzed in a very short time.

Takeoff Mode – Mixer/Ejector Nozzle

Mixer/ejector nozzle performance and entrainment levels can be predicted using the 1D ejector code that solves the continuity, momentum, and energy equations formulated with a control-volume approach for the nozzle mixing duct downstream of the primary nozzle exit plane. Characteristic curves of performance and entrainment can be determined for parameters such as NPR, SAR, and MAR based on the 1D code solutions for no losses in the nozzle (C_{sp} = 1.00 η_s = 1.00, f = 0.00). Real nozzle losses are handled by additional curves that map performance and entrainment sensitivities

relative to changes in primary stream thrust coefficient (C_{sp}), secondary total pressure recovery (η_s), and friction coefficient (f). While secondary total pressure recovery and wall friction coefficient are user-defined inputs, the primary stream thrust coefficient is determined from curves that map trends observed in previous Gen 1.5 and Gen 2.0 data.

Characteristic Curves

Figure 150 illustrates the basic form of the characteristic curves that are derived from the 1D code predictions. These curves are read to provide performance (C_{fg}) and entrainment ($\varpi\sqrt{\tau}$) as functions of ASAR, MAR, and NPR. Performance and entrainment are then adjusted to account for losses based on the characteristic sensitivities. These curves were derived assuming the L1M cycle relationship between NPR and T_{T8}, a CER of 1.07 (A/A* = 1.10), and C_d = 0.97. At the current time, no correction is provided to account for nonuniformities in the exhaust system exit velocity profiles.

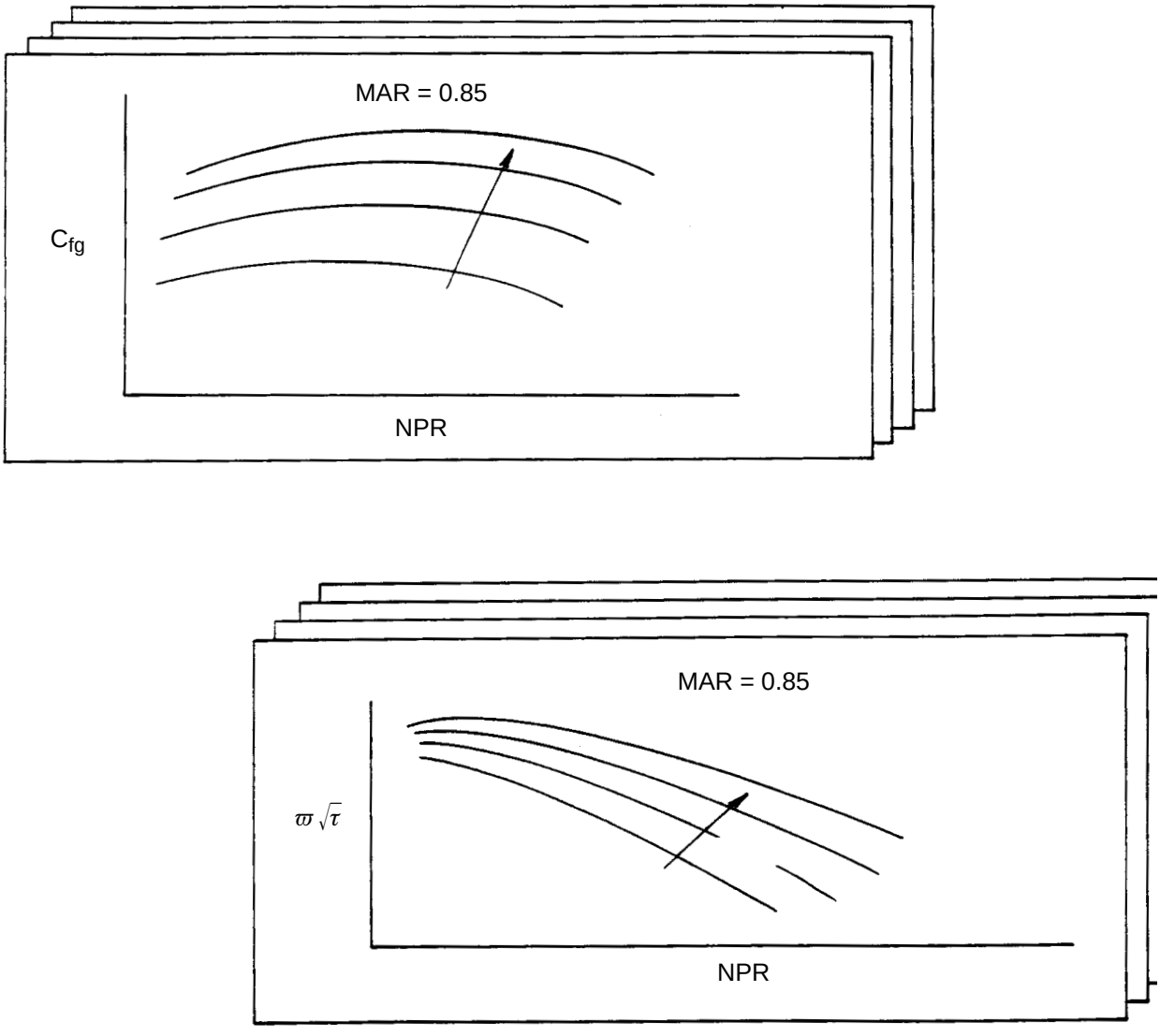

Figure 150. Mixer/Ejector Nozzle Characteristic Performance Curves

Losses

As mentioned, the major loss mechanisms are included in the primary stream thrust coefficient (C_{sp}), secondary inlet total pressure recovery ($\eta_{s)}$, and mixing duct friction coefficient (f). The losses are incorporated into the table reads for the baseline performance. Although technically not a loss, the ram drag of the entrained secondary flow must also be subtracted from the overall thrust.

Stream Thrust Coefficient – The primary nozzle stream thrust coefficient (C_{sp}) for the mixer without mixing duct sidewalls and flaps has been correlated as a function of the ratio of hydraulic diameter (D_H) over equivalent diameter (D_E) at the mixer throat, defined as follows:

$$D_{HE} = \frac{D_H}{D_E} = \frac{4A_8/P}{\sqrt{4A_8/\pi)}} = \frac{\sqrt{(4A_8/\pi)}}{P}$$

By including this curve in the performance calculation, C_{sp} takes into consideration variations in aspect ratio, lobe count, and penetration. These variables have not been considered in previous 1D estimates of mixer performance. Perimeter is estimated using the assumptions that went into the design of the Gen 1.5 chutes. The Gen 1.5 chute geometry assumes vertical lobes with semicircular peaks and troughs and an equal number of hot and cold lobes. This estimate seems to work well, even for the Gen 2 “best aero” chutes.

Secondary Inlet Total Pressure Recovery – Secondary inlet total pressure loss between the free-stream condition and the mixing plane must be known and input as inlet recovery, defined by:

$$\eta_s = \frac{P_{ts_{mixingplane}}}{P_{ts_{freestream}}}$$

where P_{ts} is the secondary total pressure.

In past analyses, the secondary inlet recovery has been treated as a constant with respect to the secondary Mach number at the mixing plane. This code, however, does not make that assumption. Rather, it is assumed that the inlet recovery (η_s) and the reference Mach number at which it occurs (typically, reference M_n = 0.4). The code then iterates on entrainment and recovery until a solution is reached. The use of this variation in inlet recovery has improved the shape of the performance curves to be much more consistent with data.

Mixing Duct Wall Friction – The wall friction for the mixing duct, used in the equation fL/D, must be input. Based on Gen 2 HSCT data, it has been determined that typical values for the friction coefficient are f = 0.020 for HSCT product-sized liners and f = 0.040 for HSCT 1/7-scale model liners.

Ram Drag – Ram drag is defined as the momentum of the entrained secondary flow at the free-stream velocity. It is calculated by:

$$F_{ram} = \frac{W_s V_\infty}{32.174}$$

Nozzle performance is calculated according to:

$$C_{fn} = C_{fg} - \frac{F_{ram}}{F_{id_p}}$$

External Data Interface – Inputs and outputs are as follows:

Input	Nozzle Primary Flow	T_{Tp}	Primary total temperature (T_{T8}, °R)
		γ_p	Primary ratio of specific heats
		NPR	Nozzle pressure ratio (P_{T8}/P_{amb})
		C_d	Flow coefficient (assumed 0.97)
	Secondary Flow	P_a	Ambient pressure (psia)
		Mn_{fs}	Free-stream Mach number
		T_{Ts}	Secondary total temperature (°R)
		γ_s	Secondary ratio of specific heats
	Nozzle Geometry	A_8	Primary nozzle throat area (in^2)
		AR	Nozzle aspect ratio at the mixing plane
		SAR	Suppressor area ratio (A_{mix}/A_8)
		MAR	Mixing duct area ratio (A_g/A_{mix}) — If 0.0 is input, then code will optimize at critical MAR
		CER	Chute expansion ratio (A_{pe}/A_8)
		PEN	Mixer penetration
		NLOBE	Number of lobes on mixer
		t	Mixer lobe thickness (in)
		L_{mix}	Mixing duct length (in)
	Losses	η_s	Secondary total pressure recovery at the mixing plane
		Mn_{ref}	Reference Mach number that corresponds to η_s
		f	Friction coefficient as used in the equation fL/D
Output	Performance	$\varpi\sqrt{\tau}$	Secondary-to-primary, temperature-corrected entrainment ratio
		C_{fg}	Gross thrust coefficient
		C_{fn}	Net thrust coefficient (thrust minus ram drag)
		C_{sp}	Primary stream thrust coefficient

Predictions Compared with Data

Figure 151 shows typical performance and pumping predictions using this code compared with Gen 1.5 and Gen 2 data. Figure 151 compares variations in SAR and aspect ratio MAR; liner and free-stream Mach number can also be compared. The 1D code from which the performance curves were derived exhibits a larger error when operating in the supersonic mode; some of the performance curves show a slightly larger error at high NPR's when the nozzle switches to the supersonic mode of operation. However, in all cases the predicted entrainment matches the data extremely well.

5.6.1.3 Massachusetts Institute of Technology Compound Flow Analysis

The Massachusetts Institute of Technology Compound Flow Analysis (MITCFA) code (References 11, 12, and 13) couples a discrete-vortex method (DVM) with classical compound-flow, differential-

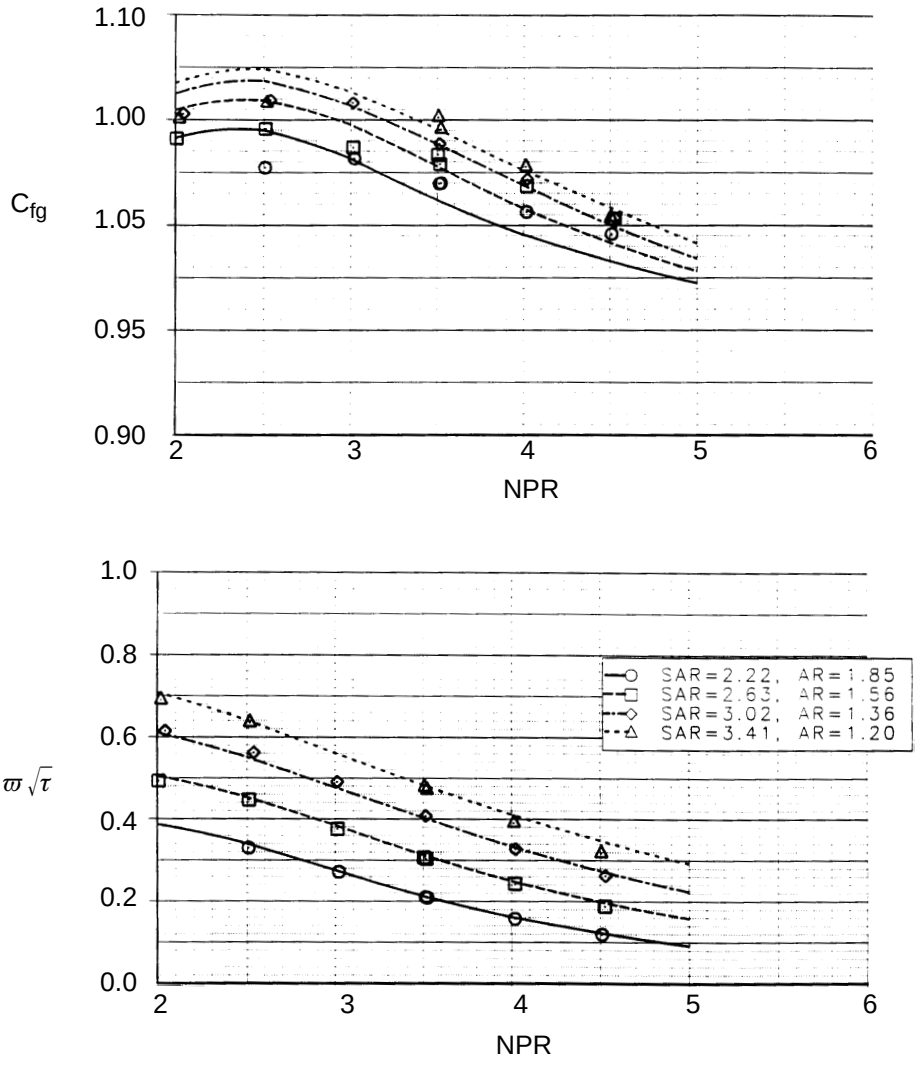

Figure 151. Comparison of Performance and Entrainment for Variations in SAR and Aspect Ratio, Gen 1.5 Data

control-volume analysis to determine the aerodynamic performance of a planar mixer/ejector combination. The DVM is used to represent the evolution of the distorted shear layer and model the stretching of the interface between the primary and secondary flows in the compound-flow analysis. The differential control volume approach then solves a system of seven coupled nonlinear differential equations in the streamwise direction to determine the evolution of the primary and secondary flow areas, fluid dynamic properties, and thermodynamic properties. These two approaches are coupled through the size of the shear layer, which scales the interface shear stress and the heat transfer across the shear layer. Iteration is performed on the secondary mass flow to force the pressure at the end of the ejector to match ambient conditions. Determination of this mass flow helps specify the aerodynamic performance of the mixer/ejector combination. Additionally, the combination of the streamwise flow evolution with the DVM results provides insight into the underlying fluid dynamics and an inference of the acoustic performance of the mixer/ejector.

Whereas more detailed 3D flowfield information is available through CFD, the MITCFA code provides reasonable predictions (within 5% of thrust coefficient and 10% of pumping According to Reference 12 in a much shorter time. While a CFD solution can require weeks to set up and converge, the MITCFA code can be set up and run in a matter of minutes, making it much more amenable for initial design and optimization. The inputs for the MITCFA code consist of 7 fluid-dynamic variables, 14 geometric-design variables, and specification of the mixer-lobe geometry and circulation distribution. While determination of the circulation distribution is difficult without an existing CFD solution, the solution is not strongly dependent on the circulation distribution for high Reynolds number, high-lobe-aspect-ratio, low-circulation mixers such as have been proposed for the HSR program.

Validation and Results

Initial validation of this approach was obtained from David Tew's experiments with convoluted mixers at UTRC (Reference 11) in which several basic mixer configurations were tested and compared to the output from the MITCFA code. As illustrated in Figure 152, good qualitative agreement is obtained between experimental flow visualization and the DVM predictions. Additional validation comparisons were made with the Boeing single-lobe experiments under this program. These comparisons help establish the accuracy of the code and also demonstrate that proper physical trends are predicted by the code. While initial simulations agreed with experiments to within 5% on thrust coefficient, subsequent simulations with a slightly modified empirical loss model improved the agreement by a factor of 2. To further demonstrate the ability of the code to capture flow phenomenon, comparisons were made with existing CFD simulations of an early design eight–lobe mixer. Not only had these CFD solutions compared well with experimental results, they also provided detailed comparisons of the flow with and without vortex-generator tabs. MITCFA simulations compared favorably to the CFD results; the largest difference was in the location of the compound shock predicted in the ejector. Additionally, the DVM prediction of the shear layer demonstrated reasonable agreement with the full 3D CFD. In general, the DVM prediction appeared to slightly exaggerate the shear-layer dynamics. This was particularly true of the case with vortex-generator tabs, which were modeled solely as a perturbation to the circulation.

Additionally, several trade studies were performed with the MITCFA code, either alone or in conjunction with other tools. A simulation of the LSM build 1 lobe at sideline conditions was performed and compared to CFD simulations. The CFD runs were obtained using NASTD, a flow solver developed at McDonnell–Douglas that has evolved into the WIND code. Not only did the pumping ratio and thrust coefficient compare well with the NASTD results from which the initial conditions were obtained, the streamwise evolution of thermodynamic quantities and mixedness parameters were also well captured. Initial shocks associated with the mixing between the primary and secondary flows were not predicted because the MITCFA code assumes that the pressure difference between the primary and secondary flow fields equilibrates over an infinitesimally short streamwise distance. However, agreement between CFD and MITCFA improves with increasing streamwise distance as transverse gradients decrease (Figure 153) and the inherent assumptions of the compound flow analysis become more appropriate. For this case, the pumping ratio and thrust coefficient agree with CFD to within 2% and 1%, respectively. The mixedness based on total temperature is off because the standard postprocessing of the MITCFA code output does not properly account for the mixing that occurs within the shear layer. Including this concept in the analysis results in a 5% difference in mixing parameter between CFD and MITCFA. Sensitivities of the

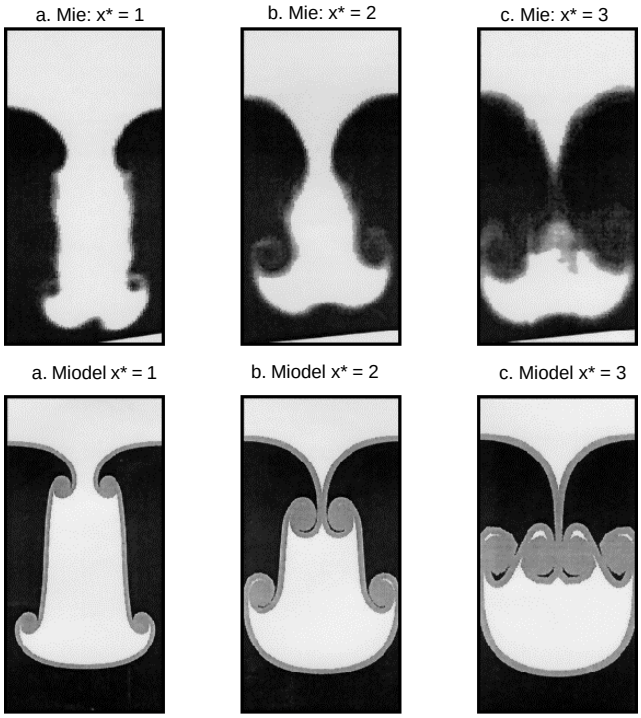

Figure 152. Shear Layer Evolution Comparison Between Experimental Mie Scattering and a Discrete-Vortex Method Similar to the Implementation in the MITCFA Code

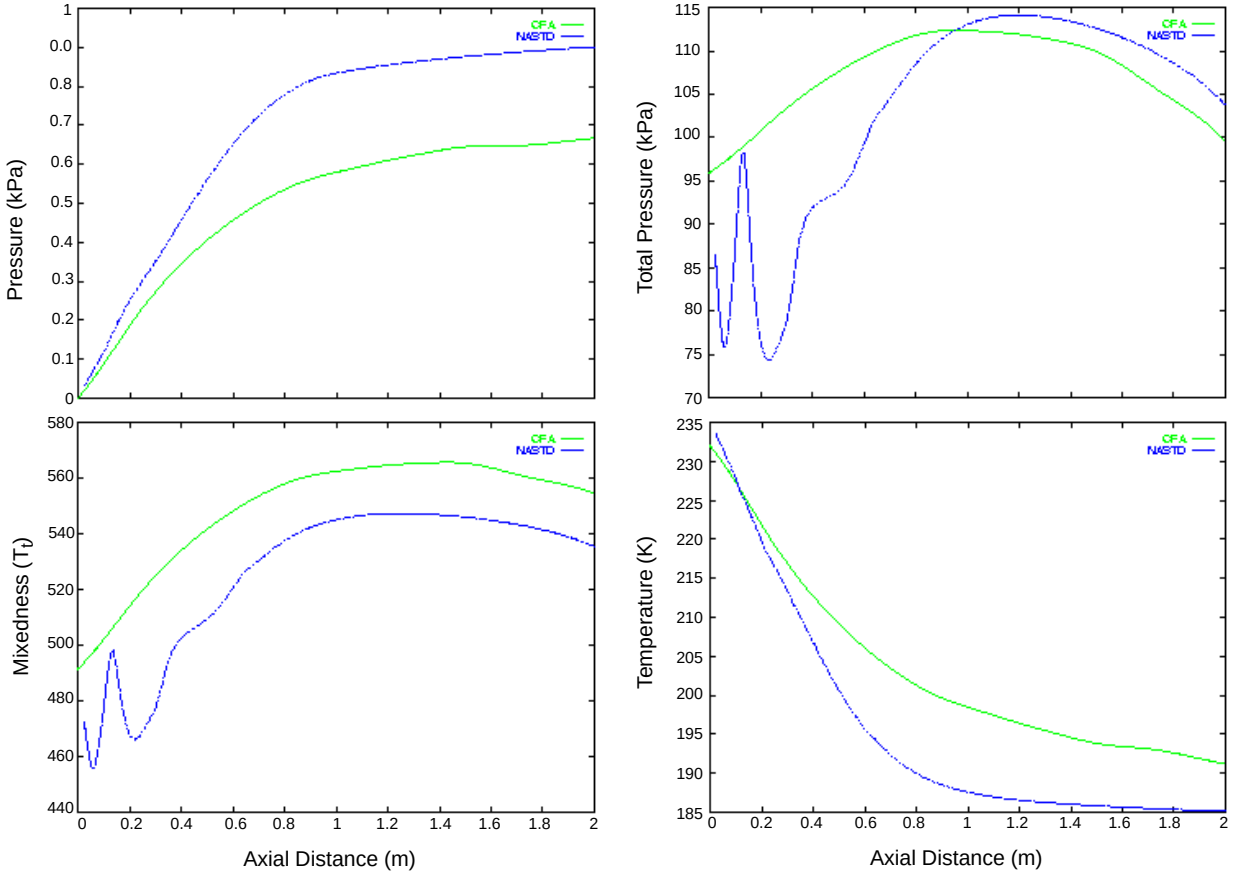

Figure 153. Streamwise Flow Property Evolution Comparison Between NASTD and MITCFA for LSM Build 1 at Sideline Conditions

pumping ratio, thrust coefficient, and scalar mixing parameter to variations in the code inputs were examined to assess the ability of the code to perform design optimizations. This study indicated that the code could be used for basic optimization and that the greatest benefits in terms of mixing could be obtained by increasing the circulation and decreasing the lobe length scales. This work culminated in the development of a user's manual describing how to operate the code, as well as summarizing both the underlying theory and the cumulative experience with the code.

As part of his doctoral research, Teeple (Reference 12) performed a formal optimization using the MITCFA code to model the mixer/ejector and empirical correlations to determine the nozzle weight and EPNL. This study indicated that, if noise considerations outweigh aerodynamic performance, the nozzle design should have greater flow angularity, larger mixer perimeters, and longer ducts. If thrust is emphasized, fewer low-penetration lobes were determined to be preferable. Additionally, multiple-variable optimization yielded a different solution than single-variable optimizations, indicating that parametric studies alone will not yield optimal designs. Finally, the primary drivers for the optimization were the SAR, the MAR, and the average angle of the primary flow as it leaves the mixer.

The MITCFA code also complemented a CFD parametric study on the effect of flow angularity on aerodynamic efficiency. In this case, the analysis indicated that a minimal primary flow angle is important for maintaining flow efficiency. Because of the relatively smaller momentum, angularity in the secondary flow is of lesser importance.

The code was also used to examine potential vortex-generator tab placement and sizing for increasing the vortical mixing that occurs within the ejector, where acoustic liners can effectively absorb the generated noise. However, lobe resolution studies indicated a sensitivity of the mixing parameters to the details of the lobe representation. The inability to obtain a consistent solution for refined lobe geometries using from 5 to 1000 vortices establishes a level of precision of about 7% in mixing parameters for the code with regard to variations in the circulation distribution. Although code predictions for aerodynamic performance are much more consistent, attempts to model oversized idealized vortex-generator tabs produced mixing parameter variations within the established level of precision of the code. Thus, it was determined that optimization of circulation distribution using tabs could not be modeled by the present version of the code due to inability to obtain reliable sensitivity information. Since LDV results with the HAM mixer (Gen 2.5) demonstrate that B tabs can have a significant influence on the ejector flow field, there appears to be a modeling limitation with representing tabs within the MITCFA code. This may be a difficulty in the slender-body approximation with the DVM not being able to represent continuum vorticity effects, especially in the transverse plane. However, as demonstrated by prior studies, gross aerodynamic performance appears to be predicted accurately.

Summary

The MITCFA code represents an enhancement to the basic compound flow analysis by including the shear-layer evolution that is important in properly modeling convoluted mixer/ejector systems. This addition provides a higher level of fidelity in the analysis while maintaining a very rapid cycle time for design evaluation and system trade studies. While the present capability generates reliable predictions for aerodynamic performance parameters, predictions of detailed shear-layer evolution could be improved.

This tool has been validated in a number of applications through comparison with experiments and CFD analyses and has been applied to a number of trade studies including parameter sensitivities and optimizations. This tool has provided insights for improving aerodynamic performance, and fundamental questions regarding the interactions between primary and secondary flows have been examined.

5.6.1.4 Aerodynamics Scaling Methodology

The scaling of aerodynamic performance of the subscale mixer ejectors to product scale has evolved significantly during the HSR program. The original procedure, presented in PDR 1996, used the test results from the $1/7^{th}$ scale model test incrementally adjusted to full scale. The LSM test ($1/2^{th}$ scale) and the subsequent Gen 3.0 test ($1/7^{th}$ scale) using geometrically similar mixer ejectors provided additional databases to enhance and standardize the PDR procedure. This standardized procedure is referred to as the LSM/Gen 3.0 approach. At the conclusion of the HSR program, a scaling subteam was formed to conduct a thorough review of the LSM/Gen 3.0 scaling. The primary tasks of the subteam were to understand the limitations of the current scaling process and to recommend a revised scaling process that provides consistent results independent of the user. The original PDR procedure, the LSM/Gen 3.0 approach, and the revised scaling process are discussed below.

PDR Approach

The aero performance from the 1/7-scale model test is projected to product using a three-step approach as follows.

1. Define the performance input parameters of the 1D ejector code to match $1/7^{th}$ scale-model test data
2. Define the adjustments to the performance parameters due to scaling effects
3. Project $1/7^{th}$ scale test data to product size with 1D code using the adjusted performance parameters

Step 1 – Matching $1/7^{th}$ Scale Data with 1D Code: The main objective in Step 1 is to define the nozzle/mixer performance parameters: C_s (stream thrust coefficient) for the primary flow and η_s (pressure recovery factor) for the secondary. Input parameters for the 1D code consist of cycle information, chute geometry definition, and the nozzle performance inputs. The cycle information and chute geometry definition are specific to the test conditions and model and are set at the start of Step 1. The performance parameters, on the other hand, can be varied to match the test data. The performance parameters are C_s, η_s, and the mixing duct friction (f) factor.

It should be noted that for ejectors treated with acoustic liners, the f factor used in the 1D code represents all the loss mechanisms associated with liners and not just the wall friction. Examples of these loss mechanisms are flow pulsating in and out of holes, additional friction due to porosity, effects of gaps and steps, etc.

The process of matching the data in Step 1 starts with assuming a value for f based on historical data. The values of C_s and η_s are then iterated until the 1D code output (C_{fn}, mixer/ejector net thrust coefficient) matches the test data. The number of iterations to define C_s and η_s is highly dependent on the initial values of these parameters. Since, the values of C_s for these types of mixers are rather well predicted (based on prior tests and CFD analyses), the bulk of the iteration is performed to define η_s.

Step 2 – Defining Scaling Adjustments: Three adjustments associated with loss mechanisms in the mixer ejector were identified in PDR '96:

1. Reynolds number effects on friction; the scaling of friction affects the performance of primary nozzle (C_S), inlet (η_S), and mixing duct (f).
2. Mixer base drag; scaling mixer base drag will only affect inlet performance (η_S).

Pin support; the earlier mixer designs included pins in the secondary inlet for structural support. Subsequently vanes replaced the pins in the inlet. Therefore, an adjustment due to differences between the pin in the subscale test and the vanes in product was calculated. This adjustment is applied only to the inlet performance (η_S).

The performance input parameters are then modified based on the above adjustments and used in Step 3 for prediction of the product performance.

Step 3 – Projection of 1/7th Scale Test Data to Product Size: The values of performance parameters defined in Step 1 are adjusted with increments obtained in Step 2. The aero performance of the product nozzle is then predicted using the 1D code with the new values of the performance parameters and appropriate cycle and chute geometry information.

LSM/Gen 3.0 Approach

This approach builds on the PDR approach and attempts to take advantage of testing at LSM scale. The advantage is that the LSM model has more geometrical similarities to product compared with 1/7th scale model. The aero performance from both model scales is projected to product using a five-step approach. Similar to the PDR approach, each step is made up of number of assumptions, adjustments, and reiterations. The steps are as follows:

1. Matching LSM and GEN3.0 data for hardwall/static free stream (bellmouth) with 1D code
2. Matching LSM data for treated/static free stream (bellmouth) with 1D code
3. Matching Gen 3.0 data for treated/static free stream (bellmouth) with 1D code
4. Matching Gen 3.0 data for treated/forward flight with 1D code and then projection of the data to product using 1D code
5. Projection of LSM data for treated/static free stream to product with 1D code and adjustments obtained using Gen 3.0 treated/forward flight data

Step 1 – Matching LSM and Gen 3.0 data for Hard Wall/Static Free Stream (Bellmouth) with 1D Code: The main objective in Step 1 is to define the nozzle-mixer performance parameters C_S and η_S. The process of matching the data in Step 1 is similar to the PDR approach (Step 1) except this procedure is performed at LSM scale. It is also performed at sideline and cutback conditions, and the aim is to satisfy both conditions with one set of nozzle performance input parameters.

After matching the 1D results with the test data at LSM scale, the procedure is then repeated for Gen 3.0 at sideline and cutback conditions. The performance parameters are scaled according to the procedure established in the PDR approach. The changes in values are based on Reynolds number corrections at different scales. The correction of η_S also includes the adjustment due to changes in the base area. The correction for mixing duct f factor involves changes in wall roughness in addition

to the Reynolds number correction. If the 1D code output with the adjusted values of C_s and η_s does not match the Gen 3.0 data, then the procedure shifts back to matching the data at the LSM scale. This time a new input value for C_s and η_s is used to match the test data. It should be noted that the value of *f* factor remains constant for each given scale throughout Step 1.

It should be emphasized that the goal in Step 1 is to match the data at both scales and at both sideline and cutback conditions. When the 1D code matches all four data sets with one set of nozzle performance input parameters (C_s, η_s, and *f* factor) then the process is advanced to Step 2. The Step 1 procedure is graphically illustrated in Figure 154.

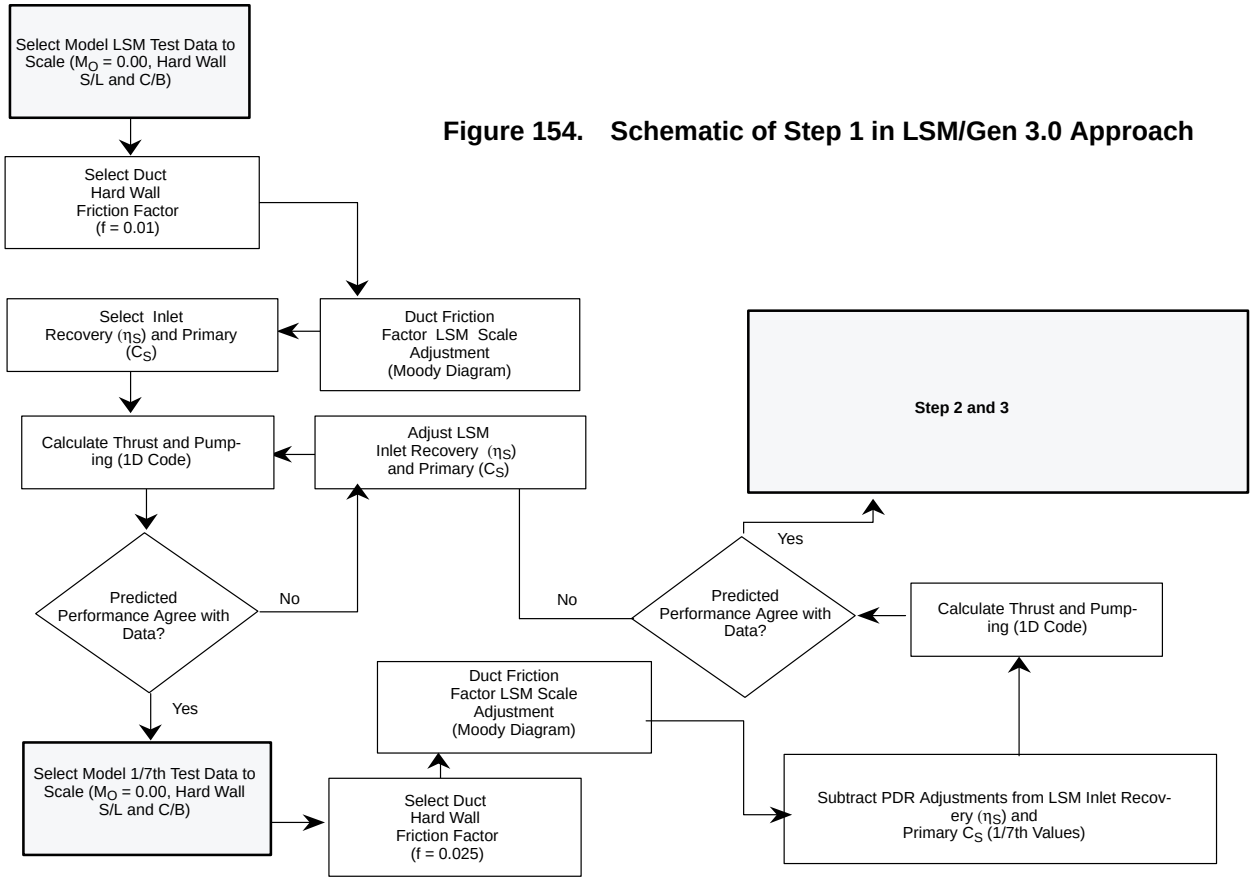

Figure 154. Schematic of Step 1 in LSM/Gen 3.0 Approach

Step 2 – Matching LSM Data for Treated/Static Free Stream (Bellmouth) with 1D Code: The main objective in Step 2 is to define the *f* factor for the acoustically treated ejector shroud. This is accomplished by carrying over the mixer performance parameters (C_s and η_s) from Step 1 and then iterating on the *f* factor to match the data at sideline and cutback conditions.

Step 3 – Matching Gen 3.0 data for treated, static (Bellmouth) with 1D Code: The main objective for Step 3 is to determine the *f* factor for the acoustically treated ejector shroud of Gen 3.0 model. Step 3 is similar to Step 2 and is performed in parallel with Step 2. Step 3 uses the mixer performance parameters (C_s and η_s) from Step 1 and iterates upon the *f* factor to match the data at sideline and cutback conditions. It is important to note that if the *f* factor were scaled down to Gen 3.0 scale solely due to wall roughness changes, then the value would be much smaller. This is mainly

due to other loss mechanisms associated with the acoustic liner which may be more exaggerated at subscale compared to large-scale.

Step 4 – Matching Gen 3.0 Data for Treated/Forward Flight with 1D Code and Projection of the Data to Product using 1D Code: The main objective of Step 4 is to project the performance of Gen 3.0 mixer ejector measured at $1/7^{th}$ scale to full scale. To accomplish this, one needs to determine a secondary pressure recovery factor (η_s) for the mixer ejector with flight inlet (not the bellmouth) and at forward-flight conditions prior to projection. Therefore, in the first substep, 1D output is matched with the test data (C_{fn}, net thrust coefficient) by iterating on the value of η_s. This substep uses the C_s and f values from Step 3. After completing the initial substep, the performance value measured at $1/7^{th}$ scale is projected to full scale by scaling the values of C_s, η_s and f.

Step 5 – Projection of LSM Data for Treated/Static Free Stream to Product with 1D Code and Adjustments using Gen 3.0 Treated/Forward-Flight Data: Step 5 takes a slightly different approach compared to Step 4 since the LSM data were measured at static condition (with a bellmouth) and there was no test for a LSM model with flight inlet at forward-flight condition. In this step, the performance of a hypothetical LSM model with flight inlet at forward flight is first estimated using information from Steps 3 and 4. Then, this performance is projected to full scale. The value of C_s and f of an LSM model (treated) is obtained from Step 3. The η_s value is, however, estimated by scaling the η_s value of the Gen 3.0 model with flight inlet at forward flight (Step 4) to LSM scale. The scaling is performed similar to PDR approach.

The performance of a hypothetical LSM model with flight inlet at flight condition is projected to product by scaling the f factor. It is assumed that the values of C_s and η_s do not change when scaled from LSM scale to product scale.

Revised Scaling Process

Two basic functions are recommended for the revised scaling process. The first is a basic Reynolds number scaling for correcting model test data to product scale. This function would not adjust the 1D code input parameters for size-dependent features, for example: lower friction losses because product scale liners have relatively smaller face-sheet hole size. The second function is a prediction that utilizes all available information for projecting model test data to product scale.

The basic architecture for the revised scaling process is very similar to the LSM/Gen 3.0 approach as shown in Figure 155. The 1D code remains the backbone of the process. The basic difference lies in the determination the 1D code input parameters. The philosophy of the revised process is to use all available information to calculate the well-known parameters, for example stream thrust coefficient (C_s), then iterating on the least known parameter, for example, secondary pressure recovery factor (η_s). This philosophy simplifies the iteration process during Step 1 of the LSM/Gen 3.0 approach where the initial matching of the scale-model test data occurs. The liner f factor is calculated from correlations to existing data, for example flat plate and liner scaling correlations. These direct calculations eliminate interpretation of the Moody diagram that can lead to variation in the final results.

Concluding Remarks

Three approaches to scale the aero performance of model test data to product have been established. First is the PDR procedure that was presented in PDR ’96. Second is the LSM/Gen 3.0 approach that

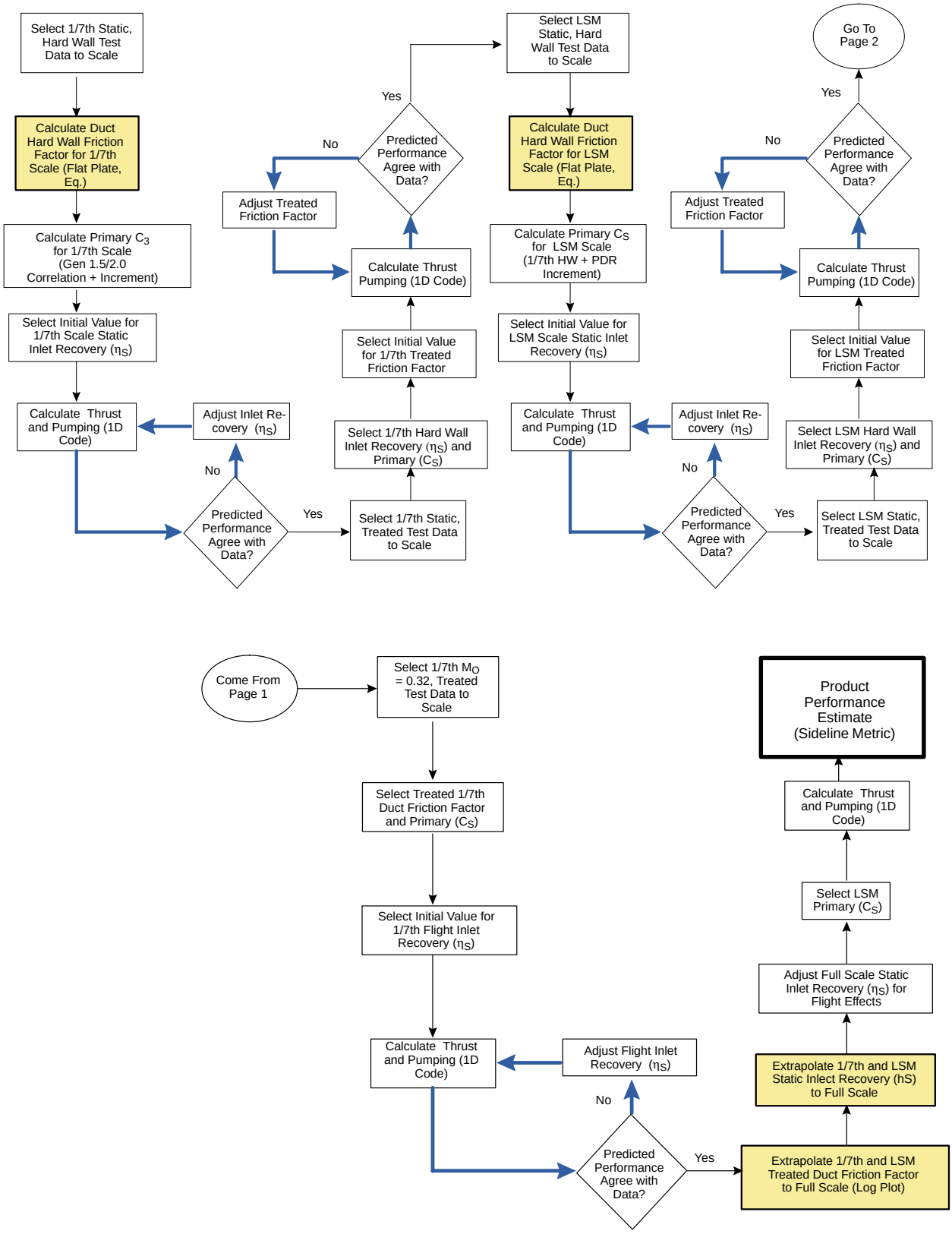

Figure 155. Schematic for the Revised Scaling Process

is a refinement of the first method as it takes advantage of testing at LSM scale and reduces the uncertainty associated with the projection of data at $1/7^{th}$ scale to full scale. Third is the revised scale process that is evolving from the LSM/Gen 3.0 approach. Initial comparisons with the LSM/Gen 3.0 scaling results show promise, but more development is necessary before implementation. Specifically, the friction factor correlations should be updated to reflect the liner scaling test results. Moreover, the process ought to be exercised by several users to ensure consistent results. Finally, an accuracy assessment is needed to verify that the process has improved the thrust prediction capability.

5.6.2 Acoustic

5.6.2.1 Semiempirical Mixer/Ejector Noise Models

The noise of a mixer/ejector nozzle results from the complex flow field generated within the ejector box by the mixing of the primary (engine airflow) and secondary (entrained external air) streams. While the noise generation process is, of course, a continuum, it has been found convenient to envisage it as having three distinct regimes, as shown in Figure 156. Each source region can then be thought of as having different characteristics, in terms of frequency and amplitude, that can be associated with different aspects of the nozzle and flowfield.

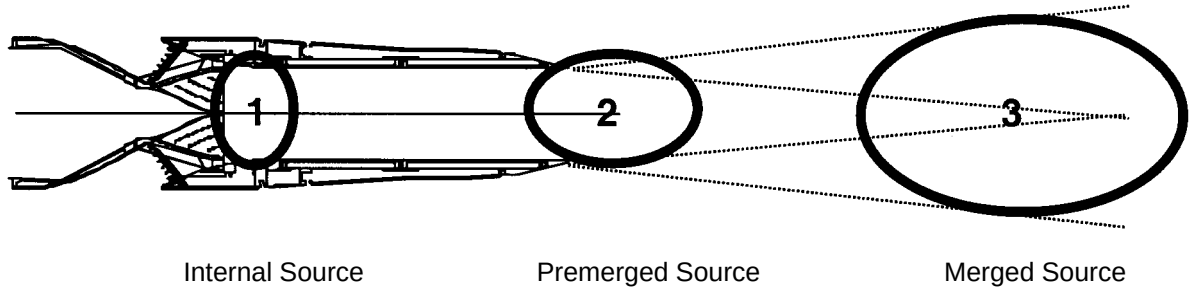

Figure 156. Mixer/Ejector Noise Generation Regions

Region 1 – The Internal Mixing Source

Just downstream of the mixer, the primary and secondary streams encounter each other in a highly turbulent environment characterized by small length scales and shock structures resulting from the mixer chute geometry. Noise generated in this region tends to provide the higher frequency components of the spectrum, which are amenable to attenuation by acoustic treatment located in the flaps and sidewalls of the ejector box. Development of methodology for design of these acoustic liners is covered in Subsection 5.8.1 of this report.

Region 2 – The Premerged Mixing Source

In the vicinity of the trailing edge of the nozzle, the mixing of the primary and secondary streams evolves with distance downstream of the mixer. The turbulence length scales become longer, and the layering between hot (primary) and cold (secondary) streams is less apparent. The two streams are not fully mixed in this region however — in the interest of saving weight for the nozzle as a whole, the length of the ejector precludes that — and thus this region can be regarded as a transitional

stage between the more easily defined “internal“ and “merged“ source regions. Noise is generated through the initial mixing of the plume with the ambient air outside the nozzle and also from the continued mixing of the primary and secondary streams (hence the descriptor “premerged” source). Noise generated in this region provides the midfrequency portion of the exhaust nozzle spectrum.

It should be noted that the premerged region is the least well-defined of the three; the methodologies outlined in the following discussions, for example, differ in the definition of the presumed location of this region — whether totally external to the ejector or partially within but mostly external to it.

Region 3 – The Merged Mixing Source

Far downstream of the nozzle, merging of the primary and secondary flows is complete, with the noise generation process resembling that of a simple nozzle operating at conditions corresponding to this fully mixed stream. The low-frequency portions of the spectrum are generated in this region.

Figure 157 illustrates the three source regions in terms of frequency content. The figure also demonstrates the relative importance of the sources in terms of annoyance parameter (Noy) which is used in the estimation of perceived noise level. As can be seen in the figure, the penalty for suppression of the merged component lies in the high Noy values of the internally generated noise.

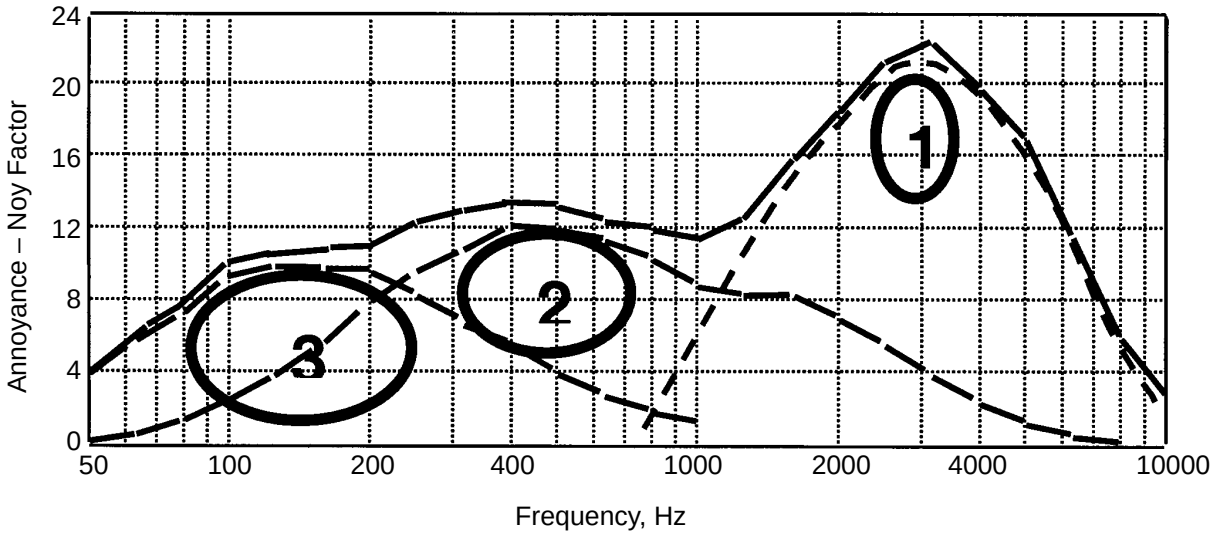

Figure 157. Illustration of the Noise Generated in the Three Regions in Terms of Annoyance (Noy Factor)

In addition to the mixing noise sources described above, the convergent/divergent chute design ensures that under certain flow conditions shocks (and hence shock-associated noise) will be present within the ejector. At high nozzle pressure ratios, shocks (and associated noise) will also be present external to the ejector. These sources must also be considered in the prediction of noise from mixer/ejector nozzles.

Two methods have been developed for prediction of mixer/ejector noise (hence “source-separation of data” using this three-source paradigm for mixing noise with the two shock noise sources included. They are described in the following discussions.

Stone Model

Nomenclature used in the following equations and discussions is defined in Table 35. No particular effort has been made to reconcile Table 35 nomenclature with the rest of this report or include it in the *Lexicon* listed in the front (roman numeral) pages.

The objective of the development of the semiempirical "Stone" (for J.R. Stone, the developer of the methodology) mixer/ejector noise-prediction model has been to provide a tool for the assessment of the impact of changes in flowfield characteristics on radiated noise.

The model can be described as a semiempirical representation of the acoustic far field of a 2D mixer/ejector nozzle in terms of aerodynamic parameters by analogy to the extensively investigated circular nozzle case. Continuous improvement is a key feature of the methodology development; improving the model for one noise generation process leads to subsequent improvements in other elements of the model. The same basic approach is employed for each of the sources described in Subsection 5.6.2.1, namely:

- Predict overall level (UOL) at the directivity angle (Θ) of interest;
- Compute SPL from predictions of (SPL–UOL) as a function of directivity angle Θ and Strouhal Number $S_t = S_t$ (fL/V).

As an example, for premerged mixing noise:

$$UOL_{Pre,mx} = C_{Pre,mx} + 10\log\left[\left(\frac{\rho_a}{\rho_{ISA}}\right)^2\left(\frac{c_a}{c_{ISA}}\right)^4\right] + 10\log\left(\frac{A_{Pre}}{R^2}\right) + 10\omega_{Pre}\log\left(\frac{\rho_{Pre}}{\rho_a}\right)$$

$$+ N_{Pre,mx}\log\left(\frac{V_{e,Pre}}{c_a}\right) - 10\log(1 - M_0\cos\psi) + Fcn_{Pre,mx}(\phi, \theta'_{Pre}, AR)$$

$$+ 15\log[(1 + M_{c,Pre}\cos\theta)^2 + 0.04M_{c,Pre}^2]$$

where the corrected angle θ'_{Pre} correlates the effects of refraction, and the appropriate Strouhal Number is:

$$S_{Pre,mx} = [GF(\phi,AR)]\left(\frac{fD_{Pre}}{V_{e,Pre}}\right)\left(\frac{T_{Pre}}{T_a}\right)^{0.4(1+\cos\theta'_{Pre})}(1 - M_0\cos\psi)$$

Use of Strouhal number entails the determination of a characteristic length and velocity for each source component. Likewise, computation of the overall level requires definition of a characteristic area. In the development of the model, the following have been found to give the best fit to the available data.

Internal mixing component:

- Characteristic Area = A_P … the primary throat area
- Characteristic Length = D_{hP} … the hydraulic diameter of the primary stream
  = $4A_P$/Perimeter
- Characteristic Velocity = V_P … the velocity obtained by ideal expansion of the primary flow into the conditions pertaining at the chute exit

Table 35. Symbol Definitions

A	Flow cross-sectional area or surface area (indicated by subscripts), ft^2
AR	Ejector exit aspect ratio (H_{exit}/W_{exit}), dimensionless
c	Speed of sound, ft/s
C_{source}	Coefficient in *UOL* or OASPL relations for various noise sources, dB
D	Diameter, ft
D_{eq}	Equivalent diameter ($\sqrt{4A/\pi}$), ft
D_h	Hydraulic diameter ($4A/Perimeter$), ft
DM	Degree of mixing, dimensionless
f	One-third-octave-band center frequency, dimensionless
Fcn_{source}	Mixing noise component azimuthal directivity term, dB
$GF(\phi, AR)$	Geometric factor, dimensionless
M	Mach number, V/c
N_{source}	Mixing noise component velocity relation slope, dB
R	Source-to-observer distance, ft
S	Strouhal number, dimensionless
SPL	One-third-octave-band sound pressure level, dB
T	Total temperature, °R
UOL_{source}	Mixing noise component OASPL uncorrected for refraction or convection, dB re: 2×10^{-5} N/m^2
$V_{e,\ source}$	Mixing noise component effective velocity, ft/s
V_{fe}	Fully expanded jet velocity, ft/s
V_{mix}	Mixed jet velocity, ft/s
θ	Directivity angle of observer to source (relative to engine inlet axis), degrees
θ'_{source}	Directivity angle corrected for source positioning and refraction effects, degrees
ρ	Density, lbm/ft^3
σ	Standard deviation
ϕ	Azimuthal angle of observer to source (relative to plane of ground), degrees
ψ	Directivity angle modified for angle of attack, degrees
ω_{source}	Mixing noise component density exponent, dimensionless

Other Subscripts	
0	Free jet stream
a	Ambient condition or property
c	Convection
ISA	Evaluated at Standard Atmosphere conditions
mx	Mixing
P	Primay stream
Pre	Premerged region
rms	Root mean square
x	Axial component

Merged mixing component:

- Characteristic Area = $A_{E,exit}$ … the ejector exit area
- Characteristic Length = $D_{E,eq}$ … the equivalent diameter of the ejector exit
- Characteristic Velocity = V_{mix} … result of mixed primary and secondary streams

Premerged mixing component:

- Characteristic Area = A_{Pre} … defined as $(1 - DM)A_P/MAR + (DM)A_{E,exit}$
- Characteristic Length = $D_{P,eq}$ … the equivalent diameter of the primary stream.
- Characteristic Velocity = V_{Pre} … defined as $(1 - DM)V_{fe,P} + (DM)V_{mix}$

DM used in the above represents the "degree of mixing" of the flow at the ejector exit. Numerically, it locates the characteristic velocity for the premerged region on a scale having the fully expanded primary velocity $V_{fe,P}$ as an upper limit and the fully mixed jet velocity V_{mix} as a lower limit.

The prediction methodology was developed using data from testing in GEAE Cell 41 as a primary source (see Subsection 5.7), taking due account of extraneous (non-jet-related) noise sources. Velocity profile data obtained by laser velocimetry (LV) were analyzed in detail to identify quantifiable flowfield characteristics that relate to noise generation, particularly in the difficult premerged region. It was found that the statistical spatial variation of axial velocity as well as average axial velocity at the ejector exit were important in determining the premerged noise. It was empirically determined that the characteristic velocity for the premerged region could be calculated as follows:

$$V_{Pre} = V_{x,rms} + 1.00\sigma)V_{x,rms})$$

Where $V_{x,rms}$ is the area-weighted root mean square axial velocity at the ejector exit plane and σ $(V_{x,rms})$ is the standard deviation from that average value. From this, a correlation has been developed for the DM in terms of mixer physical characteristics, as shown in Figure 158.

The data used in the development of the prediction model cover a broad range of configurations, both in regard to the geometric characteristics of the mixers and the type of acoustic treatment employed within the ejector. "True" hard wall, "perforated" hard wall, and "treated" (perforated plus bulk) are variations, together with the treatment area (which can be envisaged in terms of length). As the robustness of the prediction model has increased, it has become possible to investigate these effects more closely and incorporate them into the model. Conclusions can be summarized as follows.

- Source location is of great importance. Treatment effectiveness, even at a fixed angle and frequency, can differ for mixing noise and shock noise because they are generated at different locations. For example, shock noise is usually generated closer to the mixing plane than mixing noise; a longer effective treatment length is available for attenuation.
- Separate treatment effectiveness of perforate alone and bulk absorber with perforated face sheet must be established. It is assumed that the components affected by the treatment are the internal mixing and internal shock noise only. Given this, four simultaneous effects must be separated sufficiently to produce the model:
    1. Perforate effect on shock noise
    2. Perforate effect on mixing noise
    3. Bulk absorber effect on shock noise
    4. Bulk absorber effect mixing noise

Correlation: $DM=0.93[(Pen)^3(SAR)(L_E/D_{h,p})/(NPR)^{1.5}]/[2.3+((Pen)^3(SAR)(L_E/D_{h,p})/(NPR)^{1.5})]$
where $DM=(V_{p,fe}-V_{Pre})/(V_{p,fe}-V_{j,m})$ and $V_{Pre}=V_{x,ms}+1.0$ from LVσ Profile Data

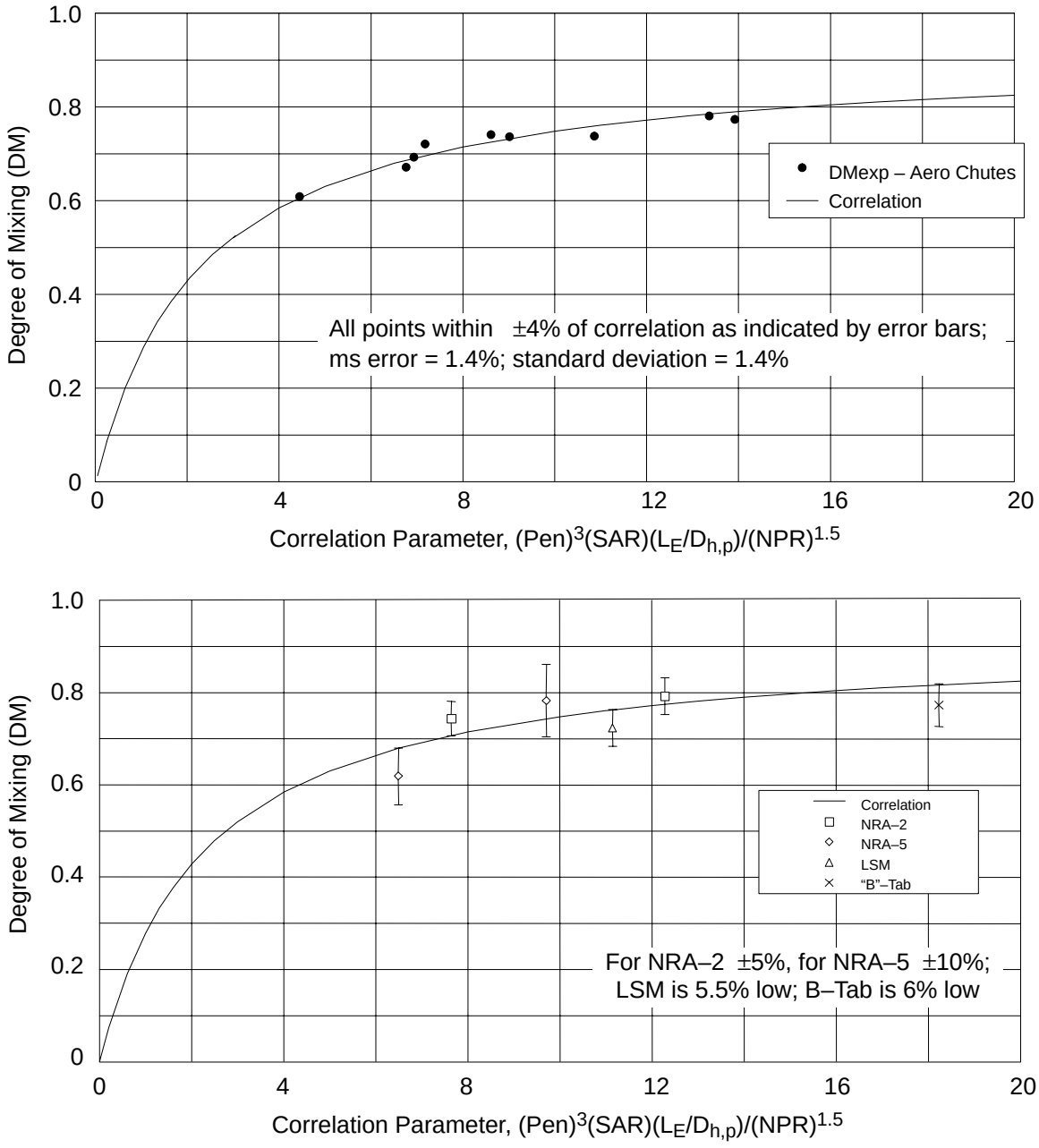

Figure 158. Degree of Mixing Correlation with Geometric and Operational Parameters

Given the problems with noise from extraneous sources, it is impossible to quantify accuracy. However, it is clear that overall levels, spectra, and directivity characteristics agree very well with experimental data where "clean" experimental data are available. The sample shown in Figure 159 (a–c) is for typical takeoff conditions with NPR = 3.43, M_0 = 0.32 at the sideline orientation (ϕ = 25°) for the partially treated Configuration 411.1. Not only are the predicted total noise spectra in good agreement with the experimental data, the individual noise components agree well over the appropriate ranges.

Jet-Noise Prediction Model (JN8)

JN8 is an empirical jet noise model developed for the prediction of noise from multilobed mixers inside a rectangular ejector. The family of JN8 codes has been extensively used in system-noise studies and for aircraft sizing throughout the HSR program. The latest version is based on a larger database that includes recent noise measurements from improved mixer designs.

The input parameters needed for this prediction model are flow quantities — such as primary and secondary mass flows, temperatures, and velocities — and geometric quantities — such as flow areas, number of lobes, ejector length, acoustic treatment area, penetration, etc. Predictions with this model show very good agreement with measured data and observed trends. Computed EPNL's from the predicted spectra are within ±0.5 EPNdB of the full-scale extrapolated data for most cases.

To illustrate the relative importance of each component and the accuracy of the prediction procedure, Figure 160 compares a predicted noise spectrum with data for the mixer/ejector nozzle at a typical takeoff power setting. The Noy-weighted spectrum is at the peak polar angle of 110° and at an azimuthal angle of 25° (representing a sideline location). The polar angle is measured from the engine inlet axis and the azimuthal angle from the major axis of the rectangular ejector. The internal noise, which includes mainly the high-frequency portion of the mixing noise (most heavily Noy weighted), is dominant over the range of angles important in PNL directivity. At lower NPR's, this trend is even more pronounced as the external noise (represented by the premerged hump) is much lower. Any future improvement in noise suppression should concentrate on reducing the internal noise. The development of advanced liners and more efficient acoustic treatment for the ejector are essential for achieving significant noise reduction. Figure 161 is a comparison of predicted and measured PNL directivity. There is very good agreement.

5.6.2.2 Penn State Mixer/Ejector Noise Model

Description/Methodology

The MENOISE code was developed by Phil Morris and Tony Pilon at Penn State University. It was designed to estimate the noise generated inside the ejector and radiated to the far field. An effort was made to keep the computations simple enough that a MENOISE run could be executed in under an hour. While MENOISE was designed to use the output of the MITCFA code as an input, it was designed with enough flexibility to use CFD information as input as well. In its present form, the code is applicable to 2D mixer ejector configurations, but it could be modified to handle axisymmetric geometries with little effort.

MENOISE is based on a semianalytical methodology developed in the 1970's by Morfey and Szewczyk (References 14 and 15). Based on the inputs from the CFA or CFD codes, acoustic sources are generated using the Morfey and Szewczyk model. The source properties are calculated from the

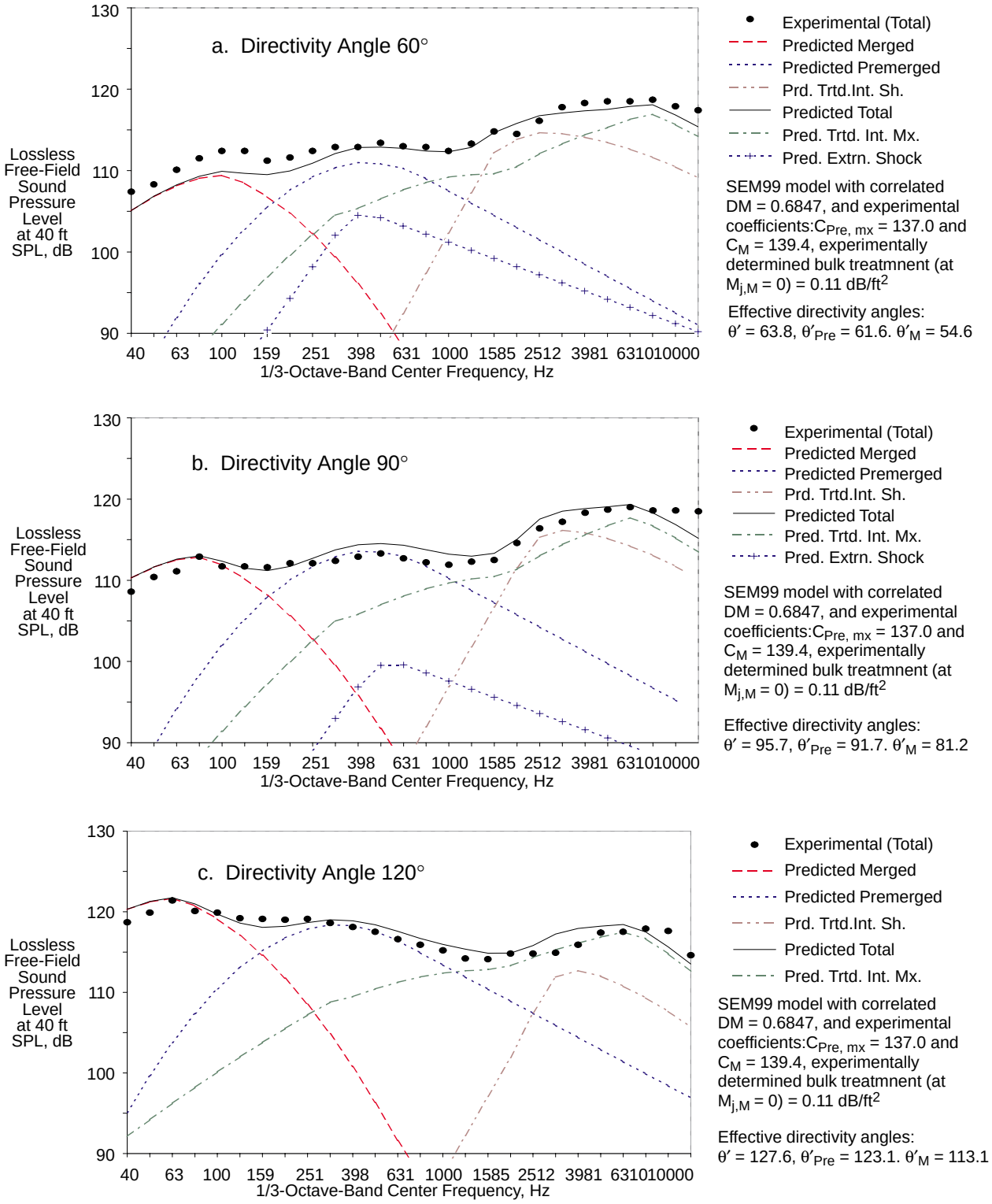

Figure 159. Comparisons Between Stone-Model Predictions and Measured Data for 60º, 90º, and 120º Directivity Angles

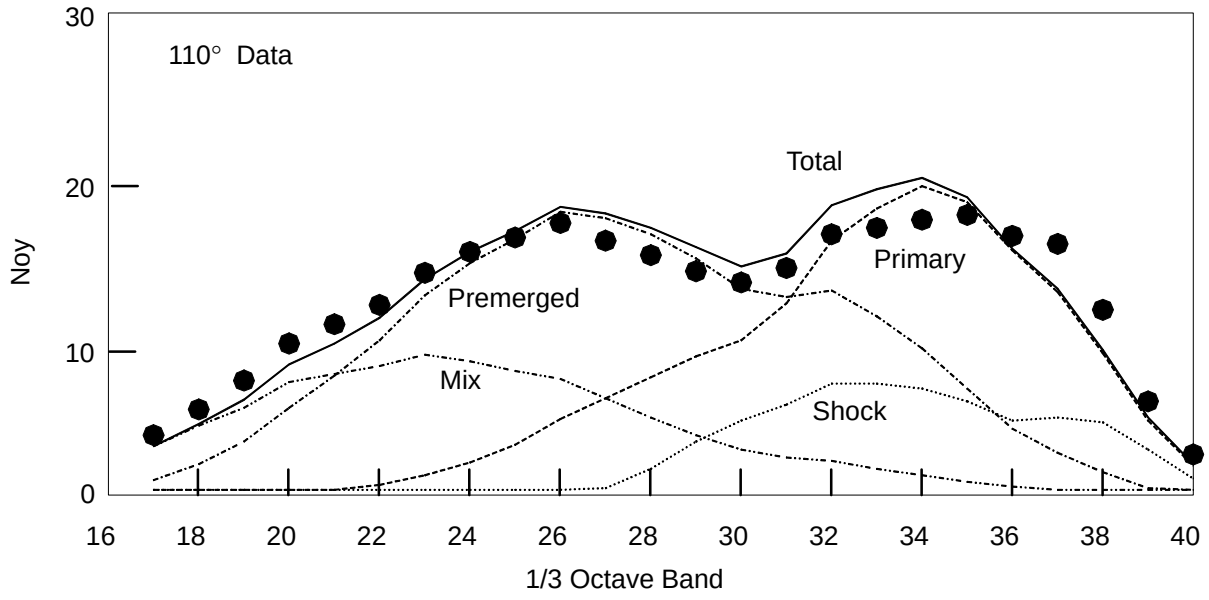

Figure 160. Comparison of JN8 Prediction with Data: Gen 3.0 Mixer, NPR = 3.6, T = 1600ºR, Distance = 1629 ft, Ttreated Ejector, M_t = 0.32

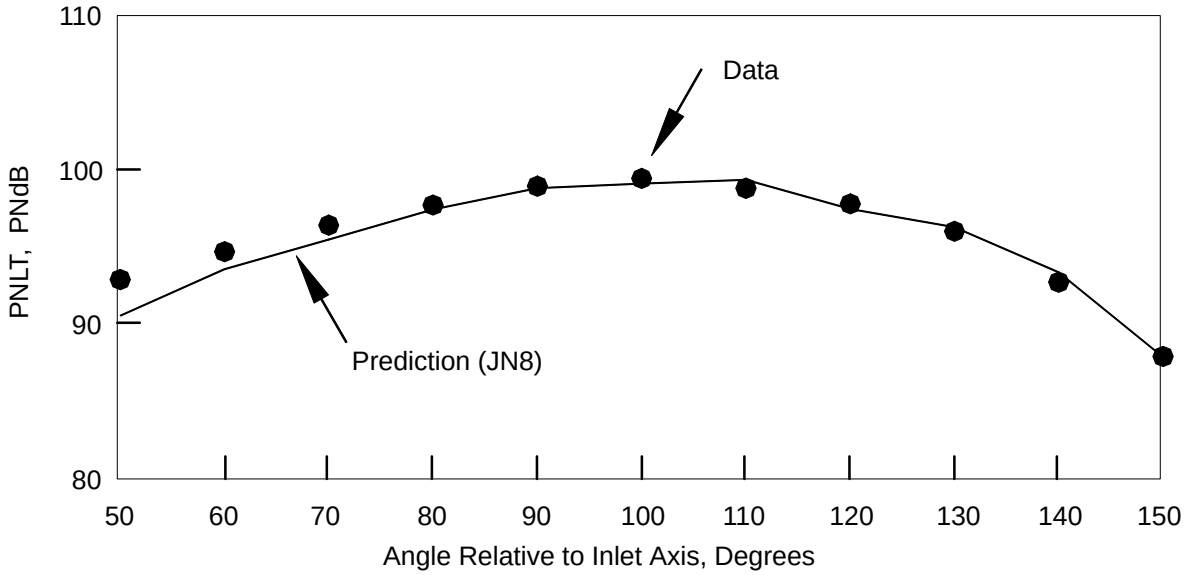

Figure 161. Comparison of Predicted and Measured PNL Directivity: Gen 3.0 Mixer, NPR = 3.6, T = 1600ºR, Distance = 1629 ft, Treated Ejector, M_t = 0.32

vorticity information, (k and ε from a RANS code) taken from the input data. The acoustic sources are calculated for various planes in the streamwise direction. Symmetry assumptions are used to construct source planes that span the entire ejector box. Using this methodology, a series of planes are constructed in the ejector box that have acoustic sources. Each of these sources has a strength, frequency content, and directivity associated with it. The method is considered semianalytical because it is not actually calculating the acoustic pressures from the turbulence but modeling the effects of this turbulence through these acoustic sources.

To find acoustic pressures in the farfield, it is first necessary to specify the locations at which one wishes to know the sound pressure levels. From each of these locations a series of rays are generated that travel from the measurement point and enter the ejector. One important consideration is the fact that there are line-of-sight rays and rays that are diffracted around the lip of the ejector exit. The diffracted rays are referred to as "creeping" rays. If a ray travels from the measurement location and enters the ejector, it will strike one or more source planes. When the ray intersects a source plane, acoustic energy is added based on the acoustic source located at that point in space. The amount of acoustic energy added will depend upon the angle at which the ray strikes the source plane (directivity of the source) and the source strength. The ray is then allowed to propagate further until it strikes another plane or a wall of the ejector. If the ray intersects another source plane, the acoustic energy from that source is added to the sum of the energy from the previous intersections. If the ray strikes a wall, it undergoes specular reflection, and the acoustic energy is unchanged for the hard-wall case. For the case where the wall is lined, a portion of the acoustic energy is subtracted as it is assumed to be absorbed by the liner. This process of intersecting source planes and bouncing off walls is allowed to continue until the mixer exit plane where the ray terminates.

MENOISE demonstrated good comparisons between predicted and measured noise for high frequency only. A second routine to predict the external jet noise, called JNOISE, uses the same Morfey and Szewczyk approach of basing acoustic sources on the flow information. This routine has also been added to MENOISE. For the JNOISE routine, noise is directly predicted in the far field, and the ray-tracing methodology is not used.

Application

The principal investigators for the MENOISE routine used experimental data from the LSM test as a baseline for comparison. Figure 162 shows a comparison between each of the MENOISE components and measured data. The high-frequency noise from the ray-tracing method for the internal noise matches the data fairly well. At other angles, it is found that the prediction matches well in terms of peak frequency and matches nearly as well in terms of level. Figure 162 also shows that the jet noise model captures some of the low-frequency merged noise, but improvements are needed. The JNOISE prediction for this case assumes that the merged noise is equivalent to a conic nozzle of the same exit area at a velocity and temperature equal to the fully mixed velocity. Modifying this assumption could improve the results. It is also seen from Figure 162 that there is a range of frequencies for which noise is not predicted accurately. This midfrequency range is due to what has been termed the "premerged" noise. The MENOISE code currently does not have capability to predict this noise.

Future work on MENOISE should focus on improving the prediction at other azimuthal angles, as the code presently underpredicts noise at azimuthal angles other than 90°. It is thought that this is due to a three-dimensional diffraction effect at the corners of the ejector in the ray-tracing routine.

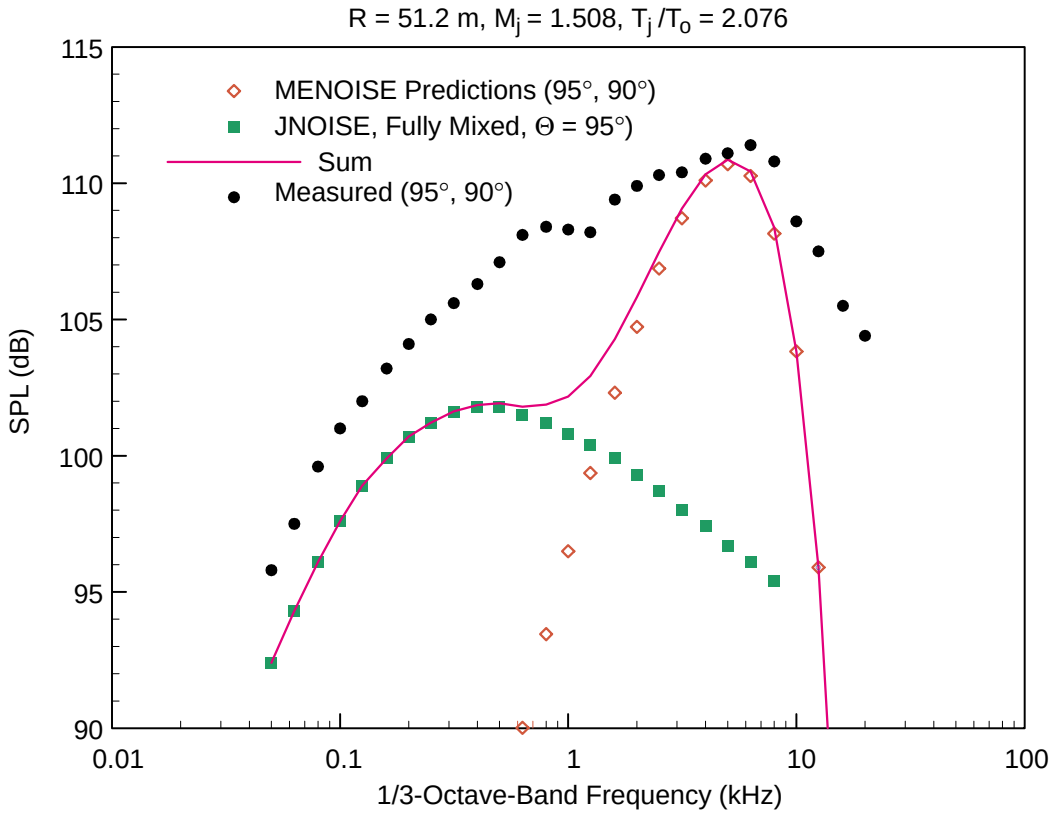

Figure 162. Predicted and Measured Spectral Levels at 95 to the LSM Upstream Axis

It was also found that changing the length of the ejector did not produce the expected trends, which leads one to believe that additional investigation may be needed into the effect of the density of the acoustic source planes. The code should be further evaluated with comparisons to mixer ejectors other than the LSM and with the addition of liners in the ejector.

In summary, it is found that the MENOISE code promises to be a valuable tool for the rapid design of mixer ejectors. Further evaluation and development work will no doubt enhance this tool.

5.6.2.3 GEAE Duct Modal Analysis

A model for the internal noise generated by a mixer/ejector, using as input the results of a 3D k–ε based CFD simulation, has been developed and implemented. The key idea behind the model is a simplified view of the complex, 3D flowfield predicted by CFD. The CFD results are decomposed into a two-dimensional, multilayer flow consisting of alternating layers of hot and cold fluid separated by vortex sheets. This simplification makes it is possible to calculate the acoustic modes (duct modes) that exist in the ejector and to use these modes as a basis for a noise-prediction model.

Computation of noise proceeds by first calculating the active acoustic modes in the ejector. This is done under the assumption that the flow is locally parallel; however, some of the effects of the nonparallel flow are accounted for using an *ad hoc* method motivated by workers in the field of jet-stability theory. Numerically, computation of the acoustic modes is the most challenging aspect of implementing the model; the form of the dispersion relationship requires a numerical evaluation

of a (sparse) matrix determinant. As a practical matter, all of the numerical work had to be performed using complex, double-precision arithmetic.

Determination of the amplitude of the acoustic modes required development of a Green's function for the 2D, multilayer flow. Given the Green's function, the modal amplitudes can be computed in a manner closely coupled to the calculation of the acoustic modes. In brief, the acoustic modes are calculated at the exit of the mixer and then propagated through the ejector. As they move downstream, they interact with the acoustic sources and increase in amplitude. The acoustic sources are characterized by a strength, a volume, and integral length and time scales. These quantities are all estimated from the CFD simulation.

Predictions based on this model for the NRA (NASA Research Announcement) and Gen 2 mixers showed that the roll-off of the sound at higher frequencies occurred at a higher frequency than was observed in experiments. To improve the model, future work should focus on the calculation of 3D acoustic modes, on upgrading the acoustic source model (perhaps along the lines now used in NASA's MGB code), and on including the effect of acoustic liners.

5.6.2.4 Computational Based Aeroacoustics – MGBK Code

Background

A computational-based method was developed that combines Reynolds-averaged Navier–Stokes (RANS) solutions with appropriate expressions for sources of fine-scale turbulence to predict jet mixing noise. The resulting algorithm predicts the small-scale turbulence noise in the far field for subsonic as well as supersonic jets.

The methodology is based on derivatives of the acoustic analogy. The original algorithm (the MGB code as developed by GE) is a unified aeroacoustics code whereby the mean flow and turbulence information are derived from semiempirical relations known as Reichardt method. In the present format, the improved MGB code (MGBK) is essentially a postprocessing algorithm that predicts the far-field jet noise due to convecting multipole type sources external to the nozzle exit plane. Mean flow and turbulence information are usually provided through a RANS solution. A stochastic model suggested by C. Tam is included that predicts shock-associated noise for imperfectly expanded jets.

In the MGBK code, exit conditions are provided as part of flowfield solution by defining the nozzle boundary conditions well upstream of the exit plane. Predictions do not account for internal noise generation, which could be another important source of jet noise. Various time and length scales needed for modeling small-scale noise sources are derived from turbulence kinetic energy and dissipation rate. Far-field noise predictions are usually given as one-third-octave spectra and sound pressure level directivity on an arc or a sideline.

Recent Advances

It is well known that sources of fine-scale turbulence noise are associated with two-point, time-delayed, fourth-order, space/time correlation. With proper assumptions and appropriate modeling, one may find closed-form integration to various source terms and thus reduce the computational barriers: computer processing time and memory requirements. Removal of simplifying assumptions, however, may make it increasingly difficult to derive closed-form solutions to source terms.

Significant improvements have been made in the source modeling without sacrificing the robustness of computations.

1. Shear noise was included in the predictions in addition to the existing self-noise source term.
2. Nonisotropy of turbulence was modeled into the sources of fine-scale turbulence. The existing isotropic turbulence model of Batchelor as formulated in the original MGB code was replaced with an axisymmetric turbulence model.

In addition to the usual quadrupole-type sources, new sources due to mean-density gradient were modeled into both self- and shear-noise predictions. These sources are of dipole and monopole type. Predictions indicate that contributions from these new sources arise primarily from dipole terms of the self noise.

In all these predictions, interaction of the mean flow with the radiated sound is accounted for as a closed-form solution to Lilley's equation for an axisymmetric jet (Balsa's solution). Although this Green's function limits the predictions to an axisymmetric geometry, a quasi-3D method may be applied to predict noise from 3D jets. In this approach, the flow is assumed to be locally axisymmetric, and additional volume integration is carried on the source strength in an azimuthal direction. The final result, however, provides only a polar distribution for overall sound pressure level and spectra.

Introduction of nonisotropy into the source requires more detailed knowledge of turbulence parameters than those obtained from a Reynolds-averaged solution. In an axisymmetric turbulence model, the small difference in turbulence intensities of u_2 and u_3 is neglected. If u_1 denotes the streamwise turbulence velocity component, an empirical parameter $(u_2/u_1)^2$ may be defined to divide the bulk of turbulence kinetic energy among various components. An additional length-scale ratio ($\Delta = l_2/l_1$) is defined similarly to relate turbulence length scales in stream- and spanwise directions. Noise prediction is usually sensitive to the selection of these parameters.

Sample supersonic jet noise prediction is shown in Figure 163 for a round convergent/divergent nozzle operating at a design pressure ratio of 3.14 and Mach number of 1.4.

The predictions include density gradient terms and use an axisymmetric turbulence model with:

$$u_2^2/u_1^2 = 0.60, \qquad \Delta = 0.84$$

5.6.2.5 Acoustic Scaling Methodology

Projecting model-scale acoustic data to full-scale requires several steps — although conceptually there are only four:

- Frequency Scaling
- Amplitude Scaling
- Extrapolation to the appropriate distance
- Conversion to Flyover

These are necessary in order to present information in terms of the psychoacoustic parameters defined in, for example, FAR36 (Reference 1).

Frequency scaling is achieved via the Strouhal number: *(frequency × length) ÷ velocity = constant*. (All other things being equal.)

Acoustic predictions include density-gradient terms.

Angle θ is from nozzle inlet.

R/C = 89
NPR = 3.12
M = 1.4
T_0 = 1716°R
U_j = 2409 ft/s
U_∞ = 400 ft/s

Nonisotropy parameters are:

$u_2^2/u_1^2 = 0.60, \quad \Delta = 0.84$

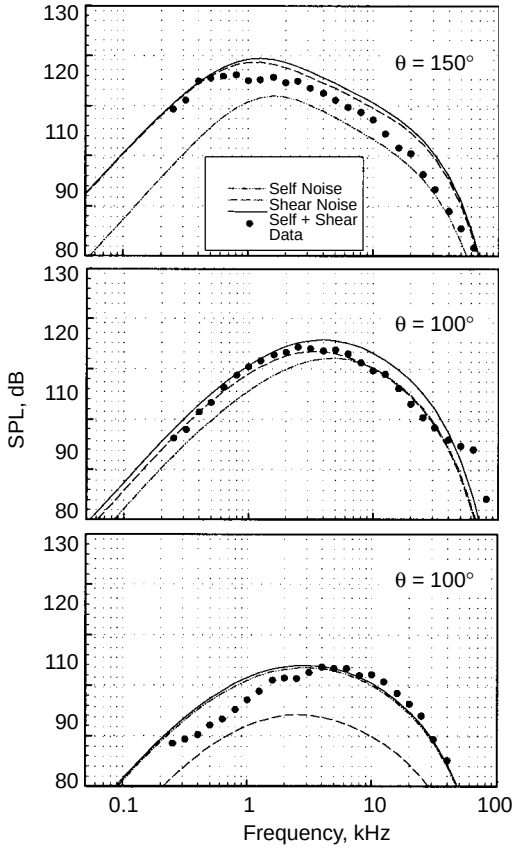

Figure 163. Predicted Spectra for Round, Convergent/Divergent Nozzle

In small-scale model acoustic testing, emphasis is placed on emulating the cycle conditions (temperature and pressure) of the full-scale nozzle. Velocities are thus held constant and we are concerned solely with keeping frequency proportional to the inverse of the characteristic dimension. From a practical standpoint, the scaling parameter used is the square root of the ratio of model area to full-scale area. In general, for jet noise, we are dealing with one-third-octave band data. The scaling parameter is used to determine the band shift required to convert the data to full-scale frequencies.

Amplitude scaling follows the work of Lighthill (Reference 16) who postulated that, for jet noise, the source intensity is related to the area, density, and velocity of the jet.

$$I \propto \rho^{\omega} A_j V_j^n$$

For the same jet conditions

$$I \propto A_j, \qquad 10\log(I) \propto 10\log(A_j)$$

or

$$SPL_{full-scale} = SPL_{model-scale} + 10\log\left[\frac{A_{full-scale}}{A_{model-scale}}\right]$$

In addition to the conversion from model-scale to full-scale quantities, consideration must be given to the conditions being simulated by the model-scale test. If the intent is to acquire data for direct comparison with, say, an engine on a static test stand, then the data are acquired and scaled as described above (giving due consideration to the effects of the absorption of sound by the atmosphere as a function of frequency). If, on the other hand, the intent is to simulate a flyover, it is

necessary to account for the effects of forward flight on the noise generation — and also for the fact that in these circumstances the source (jet) is in motion relative to the stationary observer (microphones).

Forward-flight effects on jet noise generation are complex and not well defined analytically. In consequence, they are included in the test data by immersing the jet plume in a stream of air moving at the flight velocity of interest. This can be achieved by means of a free jet or wind tunnel. In the former case, microphones are mounted in the acoustic far field of the jet plume, usually external to the free jet, whereas in the wind tunnel the microphones — while (hopefully) positioned in the acoustic far field — are also immersed in the tunnel flow. Each approach presents problems, ranging from the self-noise generated by the flow of air over the microphones in the wind tunnel environment (as encountered in the HEAT test, Subsection 5.7.4) to the need to account for the effects of the free-jet shear layer in the transformation from the test environment to the full-scale flyover. There are two approaches that have been used during the CPC program to account for the effects of the free jet, derived from the work of Mani (Reference 17) and of Amiet (Reference 18).

The final adjustment that must be made to the data is to take into account the frequency shift that results from the motion of the source relative to the observer during the flyover (Doppler effect).

Following the transformation to the flyover scenario, the scaling for frequency and for amplitude, the extrapolation to the desired altitude and observer location, taking due consideration of the effects of atmospheric attenuation on both the model (Reference 19) and the full-scale data (Reference 20), the result is a series of one-third-octave spectra over a range of observer angles. These spectra represent the physics of the problem.

For evaluation of a particular configuration relative to the requirements of the CPC program — FAR36 Stage III (Reference 1) minus *x* (where *x* has been variable), the spectra must be converted to "tone-corrected perceived noise level" (PNLT) via the procedures laid out in FAR36. The PNLT directivity as a function of angle is converted to a function of time using the flight speed of the (assumed) aircraft, and the effective perceived noise level (EPNL) is computed according to FAR36 requirements.

5.6.3 Mechanical

5.6.3.1 Exhaust Nozzle Geometry and Weight Prediction Tool

The engineering effort for the HSCT exhaust nozzle involved development of a large number and variety of nozzle geometries and associated weights in support of trade studies. The trade studies ultimately determined the impact of the nozzle geometry and weight on the overall aircraft system, relative to HSCT program requirements. These trade studies were performed at all levels, which included overall aircraft system, exhaust system, and nozzle component levels. The trade studies involved the relationship between the nozzle geometry and weight and aircraft/nozzle nacelle integration, acoustics, aerodynamics, and mechanical functionality and complexity. A prediction tool, for nozzle geometry and weight, was created to assist in the development and evaluation of nozzles as described above.

Objective

The objective for this prediction tool was to provide a relatively easy, quick, consistent, and reasonably accurate method of estimation for the geometry and weight of different-sized mixer/ejector exhaust nozzles.

Overview

The nozzle geometry and weight prediction tool was created as an Excel spreadsheet program. The product-scale version of the fixed-chute nozzle configuration, as presented in the December 1995 PDR, forms the basis for the geometry and weight calculations within this program. The geometry and weight calculations are based on equations consistent with the acoustic, aerodynamic, aircraft integration, and kinematic requirements of the FCN configuration.

The Excel spreadsheet consists of five basic calculation modules or worksheets. An additional worksheet, which consists of an iteration macro, is included to support these five calculation worksheets. The function of each worksheet is described below.

"noz_geom" Worksheet – This worksheet calculates the pertinent geometry parameters for generating the basic outer mould lines of the exhaust nozzle. The geometry equations reflect the kinematics of the FCN and, with certain exceptions, involve linear scaling of the dimensions based on the ratio of A_{mix} values. The forward flowpath dimensions are scaled according to the requirements of the turbomachinery interfaces. The nozzle forward flange height is established according to the requirements of the airframe wing/nozzle nacelle interface. Finally, the fan/core mixer and transition duct geometries are stipulated according to aerodynamic requirements.

Additionally, calculations are made for intermediate weight values of the exhaust nozzle components. The equations reflect a baseline weight for each component. These baseline values were established using fundamental methodologies for the sizing of structural beam and plate elements. The values are then scaled based on the following engine cycle data:

- ratio of A_{mix} values,
- ratio of flowpath gas pressure values, and
- ratio of material strength values corresponding to associated flowpath temperature values.

The calculation is automated by the use of an iteration macro ("Iterate Macro" worksheet) that iterates to the shortest possible exhaust nozzle.

This worksheet requires direct user input for specific cycle, acoustic, and engine interface parameters. Also, it references cells from the "p_t_scaling" worksheet and uses the "Iterate Macro" worksheet.

"noz_proj_wt" Worksheet – This worksheet generates the weight and center of gravity values for the exhaust nozzle components as well as for the total nozzle system. The final (that is, projected) weight values are calculated by scaling the intermediate weight values obtained from the "noz_geom" worksheet, based on further refinements in the weight estimations using preliminary-level, finite-element results.

The only exceptions to this are the weight values for the acoustic liner, the controls and actuation, and the miscellaneous. The acoustic liner and controls and actuation weight values are calculated by scaling values from the "acoustic_liner_wt" and "controls_wt" worksheets, respectively. The miscelllaneous weight value is set as a percentage of the nozzle component subtotal.

This worksheet does not require any direct user input but does references cells from the "noz_geom," "controls_wt," and "acoustic_liner_wt" worksheets.

"acoustic_liner_wt" Worksheet – This worksheet generates the weight and center of gravity values for the acoustic treatment as established by the calculations from the "noz_geom" worksheet.

This worksheet does not require any direct user input but does references cells from the “noz_geom” worksheets.

“controls_wt” Worksheet – This worksheet generates the weight and center of gravity values for the nozzle controls and actuation components and system. The weight equations reflect a baseline weight value established by the controls system team. These baseline weight values are then scaled based on the following engine cycle data:

- ratio of A_{mix} values and
- ratio of flowpath gas pressure values

This worksheet does not require any direct user input but does references cells from the “noz_geom,” noz_proj_wt,” and “p_t_scaling” worksheets.

“p_t_scaling” Worksheet – This worksheet generates weight scaling factors based on cycle pressure and temperature values. The scaling factors are used in the weight calculations for the inlet doors, ejector mixer, transition duct, midframe, and convergent flap nozzle components.

This worksheet requires direct user input for specific cycle pressures and temperatures.

5.6.3.2 Common Materials Properties Data

Several material systems were considered for nozzle applications on the HSR/CPC/EPM Program. The materials investigated were René 108, Ti–48–2–2, IN 939, Cast XD gamma titanium aluminide (γ), sheet γ, UT 22, N720/AS, and SiC/SiNC. The superalloys — Cast René 108, Ti–48–2–2, and IN 939 — were considered for the HSCT mixer in the nozzle. The selected material for mixer application was Cast René 108. The γ applications were in the sidewall, the aft close-out axial beam, and the corner beam. These applications required both cast and sheet γ. The three ceramic matrix composites — UT 22, N720/AS, and SiC/SiNC — were considered for the acoustic liner application. The selected material for the liner application was SiC/SiNC.

All the materials went through an extensive characterization. The mechanical and physical properties characterized were tensile (ultimate, yield, ductility, modulus), thermal (expansion, conductivity), high-cycle fatigue, low-cycle fatigue, stress-rupture, and creep. The design properties were determined by debiting the average properties for design considerations. Additional work was done for fatigue crack growth for some initial life considerations based on predicted product flaw sizes.

5.7 Scale-Model Testing

5.7.1 Small-Scale Mixer/Ejector Suppressed Aero/Acoustic Tests

5.7.1.1 Ejector Inlet Test at NASA Langley

In December 1994, P&W tested a 9.63% scale 2D mixer/ejector nozzle secondary inlet performance model at the NASA–Langley 16-foot transonic wind tunnel (16TT). The wind tunnel model was designed to use multilobed mixers from the NASA Gen 1.5 HSCT exhaust nozzle program. The model fit to an existing NASA–Langley 16TT isolated nacelle with a thrust-minus-drag balance.

This was a nozzle auxiliary inlet screening test, providing data to help downselect to the inlet concept to be pursued in the CPC program. An isolated ejector (no wing) test setup, the same as used for the GEAE NRA model at NASA–Langley, was used to supply the cold primary flow to the four-lobed

mixers. Secondary mass flow was entrained from the wind tunnel free stream and mixed with the nozzle primary flow. Secondary mass flow was not directly measured but was inferred from total and static pressure measurements within the inlet. Two four-lobe mixers previously tested in the Gen 1.5 mixer/ejector static performance assessment were used in this test.

Objective

The test objective was to develop an ejector inlet database for mixer/ejector nozzles operated in the sea level takeoff, noise-suppression mode. The model design includes parametrics on 2D-inlet geometry (ramp angles, edge radii, and inlet flow blockage), mixers, mixer area ratio, and external and internal aerodynamics (M_∞, NPR, respectively). The testing was conducted at ambient total temperature conditions (cold primary and cold secondary flow, $M_\infty = 0.0$ to 0.6) and from jet-off to a maximum primary total pressure of 75 psia ($NPR_{max} \simeq 5.0$).

For each configuration, the test determined the inlet geometric effects on ejector system performance of thrust minus drag (C_{f-drag}), mixer pumping ($\varpi\sqrt{\tau}$), secondary inlet performance as total pressure recovery (η), and internal and external pressure distributions. The results of this test improved our ability to optimize auxiliary inlet effects on mixer/ejector takeoff performance and estimate loads for this class of noise-suppression nozzles.

Facility

The test was conducted at the NASA–Langley 16TT facility located in Building 1146, Hampton, VA. The facility is a closed-circuit, single-return, continuous-flow atmospheric tunnel. The test medium is air with an air exchange for cooling. The normal testing range of the facility consists of Mach numbers from 0.30 to 1.3, angles of attack from –10° to 25°, and yaw capability from 0° to 5° (yaw support sting). The facility is equipped with a high-pressure (HP) air source that can supply a continuous mass flow rate of up to 15 lbm/s at 90°F. HP air is routed through the support system to the model by use of a flexible air line and bellows arrangement to minimize metric model tares.

Test Hardware – General

The NASA single isolated nacelle model that was modified to accommodate the GEAE NRA model was also used for this test. Model hardware forward of the instrumentation/transition section interface was supplied by NASA; model hardware aft of this station was supplied by P&W. Figure 164 is a schematic cross section of the P&W model hardware.

The test facility supplied the necessary instrumentation to record jet total pressure and temperature as well as mass-flow rate for the primary flow and total pressure and temperature in the wind tunnel test section. In addition, thrust minus drag, nozzle static pressures, and auxiliary inlet static and total pressures were measured.

Significant Results

HSCT mixer/ejector inlet performance (pumping and inlet recovery) and effects on 2D nozzle thrust minus drag has, in previous tests, been a major factor in the design of this family of exhaust systems. The ejector inlet parametric model configurations bounded the current auxiliary inlet concepts being considered for the HSCT Demo and product-scale designs.

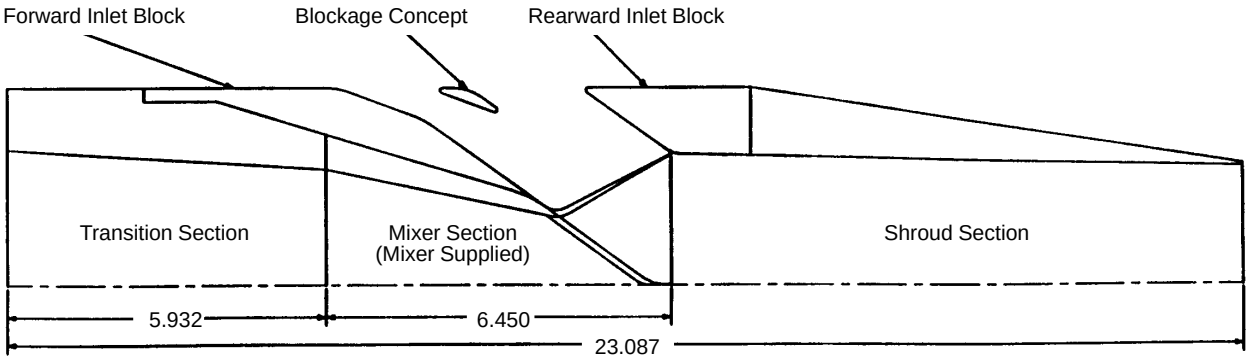

Figure 164. P&W Ejector/Mixer Model

Figure 165 shows thrust-minus-drag data for all configurations tested as design conditions of a forward-flight Mach number (M_∞) of 0.32 and an NPR of 3.5. Note: the following discussion does not consider configuration impact on jet noise.

Clean-Flowing Inlet – Data reduction emphasis was on configurations representing clean-flowing inlet geometries (no-blockage inlets) with Mixer 8 (short mixer length and lower lobe penetration) at a MAR of 0.9. The range of thrust-minus-drag performance realized over the variable-inlet

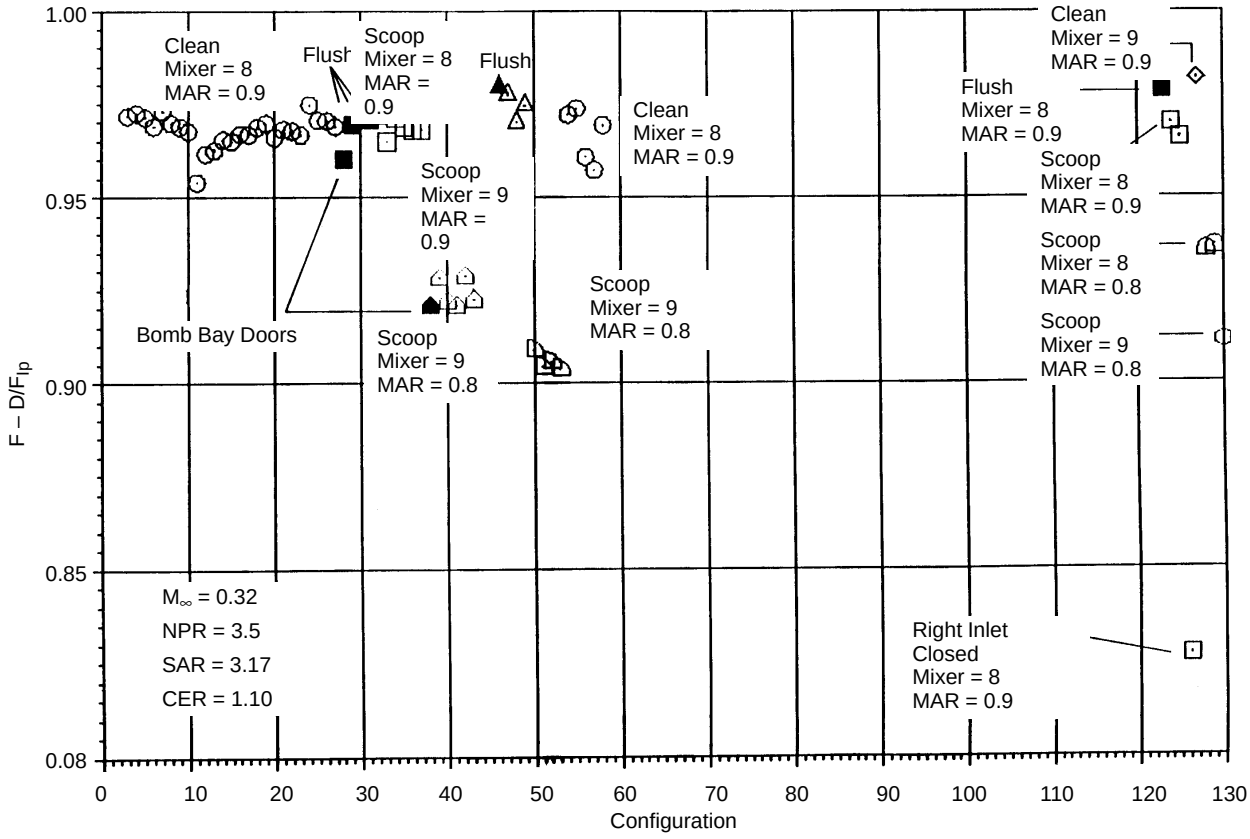

Figure 165. Thrust Minus Drag Coefficient, All Model Configurations

geometry was from 0.95 to 0.98 (C_{f-drag}) at design conditions. Ejector pumping and inlet recovery were determined from static and total pressure measurements at the leading edge of the chutes in the secondary flowpath. Typical pumping ratios and inlet recoveries of 0.40 and 0.97, respectively, were observed. These levels remained relatively constant over the range of inlet geometry variations tested, indicating that performance sensitivity to the inlet design is not critical, provided that the selected design maintains inlet recoveries in the range of about 0.97.

Effect of Inlet Ramp Angles – The clean-flowing inlet geometries indicate peak performance over the range of forward inlet angles up to 35° and rearward inlet angles up to 45° ($C_{f-drag} \approx 0.975$), indicating that maintaining a slightly contracting inlet is preferable. Also, as expected, the ramp angles have the highest effect on ejector performance, as compared with lip radii. Even though smaller forward inlet ramp angles provided the highest performance, inlet designs with forward ramp angles as high as 45° can achieve high performance (about 0.96), provided the forward lip radius is sized to minimize separations.

Effect of Inlet Lip Radii – Forward inlet lip radius has more of an impact on performance at high forward ramp angles (45°) than at low forward ramp angles (15°), but the least impact occurs at a forward ramp angle between about 37° and 43°. Rearward inlet lip radius had the least effect on performance, for varying rearward ramp angles.

Inlet Blockage – Three inlet Blockage concepts (flush-mounted inlet turning vanes, protruding scoop inlet turning vanes, and bomb bay doors incorporating a flush turning vane for lateral support of the doors) were tested. The inlet blockage configurations performed comparably to the clean-flowing inlet configurations and should be further analyzed at the systems level with trades on inlet length, mixer length (that is, nozzle length), and impact on weight and noise.

Specifically, the flush-mounted turning vane performed better, upwards of ½ to 1% compared to the clean-flowing inlet configuration at both forward flight speed and statically.

Effects of MAR and Mixer Variation – Two MAR's (0.8 and 0.9) and two mixer designs (Mixer 8 and Mixer 9 from the Gen 1.5 LET test) were varied during the test. MAR is the ratio of nozzle exit area to the mixing plane areas. Mixer 8 was the baseline mixer and had a mixer length of 0.6 and a lobe penetration of 80%. Mixer 9 has a mixer length of 1.0 and a lobe penetration of 90%. Both mixers were of the axial-flow design (turns the flow axial at the exit of the primary nozzle).

At the higher MAR, Mixer 9 performed better than Mixer 8 (approximately 4 to 5%), but at the lower MAR Mixer 8 performed better than Mixer 9 (approximately 2 to 3%). A significant difference in flap pressure distributions was shown for Mixer 9 as a function of MAR and NPR. It has been observed that when the primary nozzle lobe penetration is high and the MAR is low, flap pressurization occurs, resulting in higher internal drag, and should be avoided. The change in pressure integral can account for the decrease in thrust at high penetration and low MAR (as much as 4%).

Summary

Nozzle entrainment and performance remained relatively constant over the range of inlet geometry variations tested, indicating that current performance sensitivity to the inlet design is not as critical provided that the selected design maintains inlet recoveries in the range of 0.97.

Even though smaller forward inlet ramp angles provided the highest performance, inlet designs with forward ramp angles as high as 45° can achieve high performance (about 0.96) provided the forward lip radius is sized to minimize separations.

Inlet blockage configurations performed comparably to the clean-flowing inlet configurations and should be further analyzed at the systems level with trades on inlet length, mixer length (that is, nozzle length), and impact on weight and noise.

Flush-mounted turning vanes performed better, upwards of ½ to 1%, compared to the clean-flowing inlet configuration at both forward flight speed and statically.

It has been shown when the primary nozzle lobe penetration is high (Mixer 9 versus Mixer 8) and the MAR is low, flap pressurization occurs, resulting in higher internal drag, and should be avoided. The change in pressure integral can account for the decrease in thrust at high penetration and low MAR (as much as 4%).

5.7.1.2 Gen 1.5 Model Tests

Gen 1.5 Acoustics Test in Cell 41

The initial test of the NRA model system in the GEAE Cell 41 anechoic free-jet facility [see Subsection 5.7.5.4 – Gen 1 (NRA) at Cell 41] demonstrated the ability of the 2D mixer ejector nozzle concept to meet the then acoustic goals for a HSCT. The objectives of the Gen 1.5 acoustics test in Cell 41 were to investigate the noise of the 2D mixer ejector in more detail, in particular the effects of configurational variations. These included aligned versus staggered chutes, convergent versus convergent/divergent chutes, treatment variations (different bulk materials, different locations within the ejector, different treatment areas and different thickness bulk materials), secondary inlet shape and the effect of blockage of a "fin" across the inlet. In all, with the above variations, and the use of mixers of different SAR, 25 configurations were tested.

The GEAE Cell 41 anechoic free-jet facility is shown in Figures 166 through 168. The facility is a cylindrical chamber 43-ft in diameter and 72-ft tall. The inner surfaces are lined with anechoic wedges made from fiberglass wool to render the facility anechoic above 220 Hz. It can accommodate model configurations with throat areas up to 22 in^2 and 24 in^2 in the inner and outer streams, respectively. The two streams of heated flow are provided by separate natural gas burners and pass through silencers and plenum chambers before entering the test nozzle. Each stream can be heated to a maximum of 1960°R, with nozzle pressure ratios as high as 5.5, resulting in a maximum jet velocity of 3000 ft/s.

The tertiary, free-jet, air system is provided by a 250,000 scfm (at 50-in of water column static pressure) fan, driven by a 3500-hp electric motor. Transition ductwork and a silencer route the flow from the fan discharge through the 48-in diameter free-jet exhaust. The maximum flight simulation achievable with this system is approximately Mach 0.4. The combined model and free-jet flow exhausts through an acoustically treated T duct in the ceiling of the chamber.

The nonaxisymmetric nature of the two-dimensional ejector results in a sound field that varies in the Φ (azimuthal) direction. To accommodate this, a traversing tower mounted with an array of 13 microphones is installed in the cell. The range covered by the microphones and tower can be seen in Figures 166 and 167. The tower can be positioned at any point along a track, enabling detailed investigation of, for example, the sound field in the vicinity of the corner of the ejector exit.

Data from the microphone array are acquired and reduced on-line into one-third-octave bands (model scale) on a 40-ft radius arc (centered on the ejector exit) at standard day conditions (59°F, 70% relative humidity and 14.696 psi). This enables immediate comparisons at model scale and also

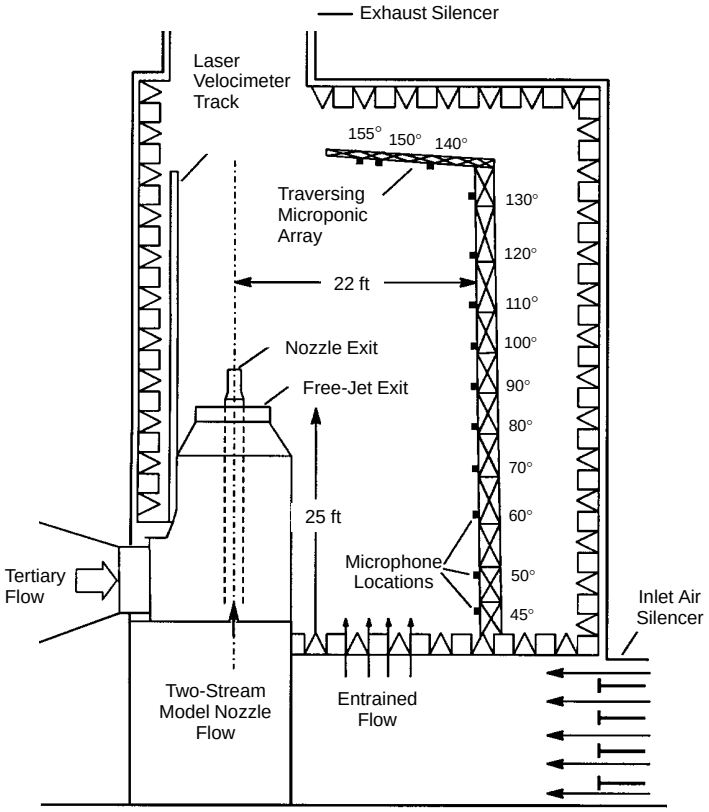

Figure 166. Schematic of GEAE Cell 41 Anechoic Free-Jet Facility Showing Microphone Locations

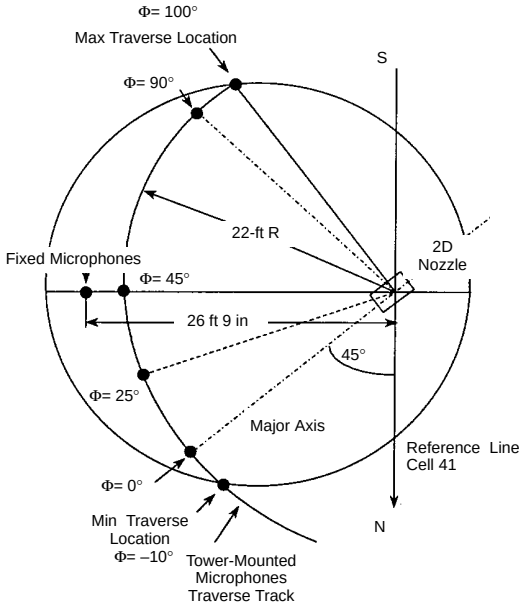

Figure 167. Overhead View of Traversing Microphone Tower Track Showing Extent of Traverse

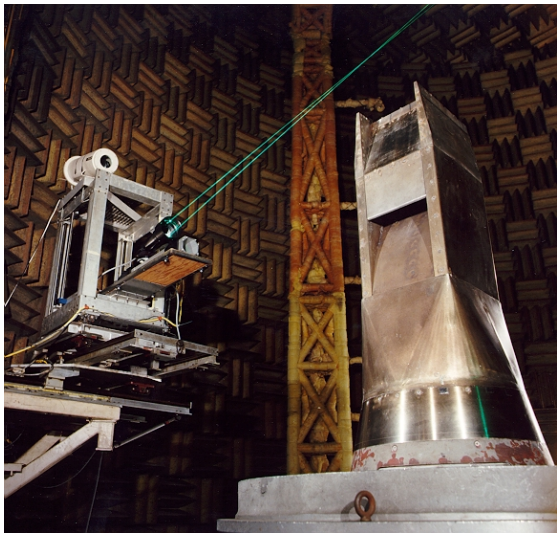

Figure 168. Photograph of Cell 41 Showing NRA Model, Acoustic Wedges, Traversing Tower, and LV System *LV system was not used in this test series.*

allows checks for data quality. For further analysis, the acoustic data are scaled and extrapolated to agreed-upon size and range following the procedures described in Subsection 5.6.2.5.

During this test the ejector length was varied between “80 in” and “120 in” full scale (for a full-scale throat area of 1086 in^2). Acoustic treatment material was varied from “astroquartz” fiber mat to nickel-based foam metal inserted in the tray segments shown in Figure 169. The effect of hard wall was achieved by forcing sheet metal against the underside of the treatment tray facesheet. (It should be noted that, following observations made during analysis of the HEAT data, Subsection 5.7.4, this practice was discontinued due to the suppression achieved by the face sheet alone.)

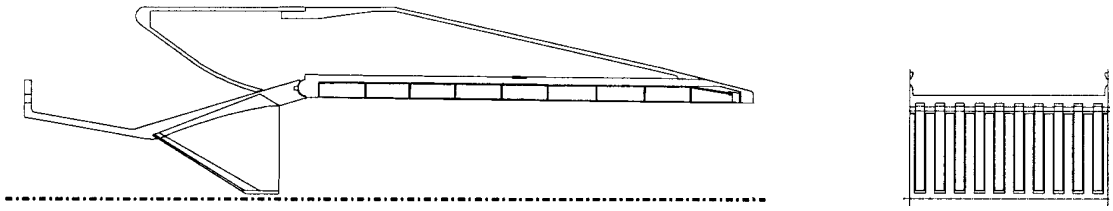

Figure 169. NRA “120 in” Nozzle Showing Treatment Tray Segmentation and Chute Shape

Five basic mixer configurations were tested: two aligned CD chute mixers of SAR = 2.8 and 3.3 respectively, an aligned convergent chute mixer with SAR = 2.8, and two staggered CD chute mixers with SAR = 2.8.

Repeatability of the data was established by comparing the 120-in fully treated configurations for both baseline mixers with data taken during the Gen 1 test of the same hardware in the same cell. In general, the repeatability of test results for both mixer/ejector configurations is very good. Small differences observed in the data could be due to uncertainty of exact duplication of ejector treatment, flight Mach number, and aerothermodynamic conditions.

The azimuthal variation of the acoustic field of the aligned CD-chute mixers with the 120-in ejector is significant and is much higher at lower ideal primary jet velocities (V_{JIP}). A variation of from 4 to 6 EPNdB is observed at jet velocities between 1147 and 1600 ft/s. Even at higher velocities, the azimuthal variation of noise levels is significant.

Substantial noise reduction was observed with flight simulation for the aligned CD-chute mixers with the 120-in. ejector. Significant SPL reduction due to flight simulation was observed at higher polar angles for the entire frequency range. Major noise reduction took place between flight Mach numbers of 0 and 0.24. Pumping (ratio of secondary flow to primary flow, W_s/W_p) increases with increasing flight Mach number. The transition (mode shift) from subsonic to supersonic seems to be slightly delayed with respect to NPR due to flight simulation.

A nickel-based foam metal was evaluated for use as acoustic treatment. The foam metal seems to be performing as well as and, in most cases, slightly better than astroquartz treatment. Consequently, this material was used in all subsequent testing.

Acoustically the staggered 10 and 9 full CD-chute mixer performed best compared to other configurations at ideal primary jet velocities above 1600 ft/s. At lower velocities the aligned convergent chute mixer was acoustically superior. The effect of mixer geometry on ramp static pressure distributions is insignificant. The static pressure distribution on the chute surface is more or less the same for the three CD chute mixers. However, it is significantly different for the convergent-chute mixer,

especially at lower nozzle pressure ratios. The ejector static pressure distributions indicate that the subsonic to supersonic mode switch, as a function of NPR, is delayed for the convergent-chute mixer and is relatively early for the nine and two half-staggered chute configuration — when compared to the baseline aligned-chute mixers.

Effects of cycle variation were investigated via the 10 and 9 full CD-chute staggered mixer with the fully treated 120-in ejector and 80-in, hard-wall ejector. Ideal primary jet velocities were held constant while the nozzle pressure ratio and total temperature were varied. With respect to aerothermodynamic conditions with velocity held constant, at higher jet velocities EPNL increases with increasing NPR and with decreasing nozzle total temperature. The trend reverses at lower jet velocities, especially with flight simulation. Based on EPNL contours, EPNL increases with increasing NPR and nozzle total temperature. However, it is interesting to note that a fixed EPNL can be achieved by lowering NPR and nozzle total temperature together at lower NPR conditions. With respect to increasing NPR, pumping decreases with decreasing total temperature.

Based on the dynamic pressure measurements made inside the ejector, acoustic treatment attenuates internal noise and is more effective at lower NPR (or jet velocity). Treatment closer to the mixer exit is also effective in flap dynamic pressure attenuation but relatively less so than a similar treatment area closer to the ejector exit, especially for very high NPR. Ejector treatment is especially important when the externally generated noise component is lower than or of the same magnitude as the internal noise component.

The best acoustically performing mixer/ejector configuration (the 10 and 9 full staggered CD-chute mixer with the 120-in ejector) was used to identify the acoustic benefits of treatment variation. It was found that the fully treated ejector performs the best. However, results of "7/9" treatment (in which the first and last treatment segments on the flap and first and last two segments on the sidewall had "perforated hard wall" rather than treatment in order to simulate the "real" nozzle more closely) are close to the full treatment configuration, especially at higher velocities. The 0.5-in-thick treatment is better in suppressing acoustic energy than the thinner treatments tested. Locating treatment closer to the ejector exit suppresses more acoustic energy than the further forward locations. The fully treated ejector is acoustically better than the flaps only treated configuration. Silicon carbide bulk material seems to have more potential in suppressing internal noise than other materials tested.

A high-gradient inlet ramp was "scabbed on" to investigate the influence of inlet geometry on radiated noise. Based on the tests, the effects were small on both the far-field acoustic characteristics and the flow- and performance-related parameters. Similar results were obtained with the use of a fin across the inlet to simulate a mounting pylon.

Further background and detail are available in Reference 21.

Mixer/Ejector Model Tests

Subscale model testing was conducted at Boeing's *Nozzle Test Facility* (NTF) in support of the Gen 1.5 HSCT Nozzle Program to develop a database for mixer/ejector nozzle performance and pumping in the noise-suppression operating mode.

Previous testing of mixer/ejector HSCT nozzles included individual nozzles supplied by P&W and GEAE without any common reference. As a result, conclusions were difficult, if not impossible, to derive from the existing database. Thus, it was obvious that a single parametric test was needed to incorporate all of the critical design concerns so direct comparisons could be made and conclusions drawn.

In support of this effort, various mixer/ejector model designs were provided by P&W and GEAE in a joint effort to optimize the performance that may be realized in the takeoff mode of operation. The testing was performed at hot-flow conditions with primary flow temperature of 700°F and maximum total pressure of 66 psia. The concepts were tested to measure thrust performance, pumping, and static pressure distributions.

In addition, the phenomenon of mode shift was examined. Mode shift is a condition observed in mixer/ejector nozzles when the flow in the mixing duct transitions from subsonic to supersonic. This occurrence is usually accompanied by a shift in shroud static pressures. For certain geometries, the shift can be quite drastic, causing a high dynamic load on the shrouds and sidewalls.

The data were used to evaluate the effects of temperature, mixing duct area ratio (MAR), suppressor area ratio (SAR), chute expansion ratio (CER), mixer lobe penetration at the mixing plane (PEN), mixing duct length, mixer length, and the number of mixer lobes (N).

Test Facility – Static testing was performed at the Boeing NTF, also known as the *Large Dual Flow Rig*, in Seattle, Washington. The primary and secondary flows are supplied by a common 300-psi source and are both limited to a pressure of 135 psia. The respective maximum flows based on cold flow temperatures are 35 lbm/s for the secondary and 25 lbm/s for the primary. Both supplies may be independently controlled and are measured using critical flow venturis accurate to ±0.25%.

The large dual-flow rig is mounted on a three-component strain gage thrust balance to measure axial and side forces up to 3000 and 600 lbf, respectively. The quoted accuracy of the thrust balance is ±0.25% of full scale. The test cell is ventilated to maintain ambient atmospheric pressure. A propane burner in the primary stream is capable of providing heated combustion products up to 1200°F.

Hardware – Each nozzle assembly consisted of a secondary flow plenum, a transition duct, a 2D convergent section, a mixer, a mixing duct comprising two ejector sidewalls and two ejector shrouds, and shroud brackets. This assembly is shown in Figure 170. In addition, a charging station duct with total pressure and temperature instrumentation and an adapter duct were supplied to the test facility. The primary choked area (A_j) was held constant at 10 in^2 for all test configurations.

The facility adapter duct served two functions. First, it reduced the flow areas from the facility to the levels required at the model inlet. Second, it added length to the overall model to align the nozzle exit with the Schlieren system. To allow thermal expansion of the primary duct relative to the secondary duct, a thermal-expansion joint was located at the interface between the adapter duct and the charging station. Originally, the model hardware was to be designed for testing at 1000°F. However, due to an error in the design of the thermal expansion joint, 700°F was determined to be the maximum temperature at which this test could be conducted. The transition duct is a circular-to-rectangular transition section designed to reduce the flow area by 10% at the 2D convergent section interface. The 2D convergence angle was limited to no more than 25°. A secondary flow inlet to the ejector was bellmouth shaped to minimize pressure losses and was integral with the mixing duct hardware.

Three sets of varying-length shrouds and sidewalls were tested to determine the effects of mixing duct length on performance and pumping. Of the three, the midlength shroud most closely represents the current mixer/ejector nozzle designs.

Text Matrix – The test matrix was set up to evaluate 16 mixer designs over a range of suppressor area ratios ($SAR = A_m/A_j$) that were sized to correspond to uncorrected secondary-to-primary flow

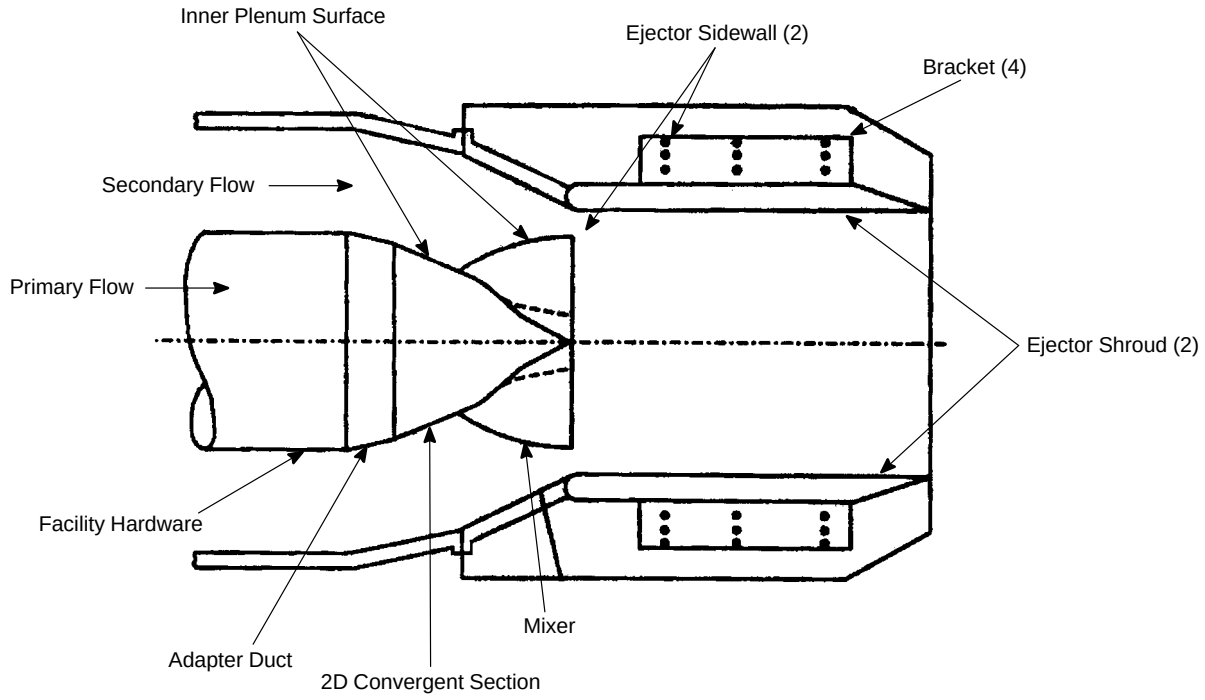

Figure 170. Nozzle Assembly

ratios (entrainment) of 40%, 60%, 80%, and 100%. These SAR's were based on engine conditions at the design point, a free-stream Mach number of 0.32, and an inlet recovery of 95%. The matrix of mixers used in this test is shown in Table 36.

Table 37 summarizes the test configurations and corresponding mixers. Mixers 1 through 11 represent the parametric portion of the test; Mixers 12 through 15 are specific geometries of interest for P&W and GEAE. The mixer designs included variations in lobe penetration, the Mach number of the flow exiting the mixer (A_p/A_j, or CER variations), the overall length of the mixer (L_{mix}/D), and the number of lobes (N). Design variations in the ejector include variations in ejector shroud length (L_{eject}/D), SAR, and MAR. The test matrix includes all of the configurations that were originally planned for this test. However, not all of these configurations were actually tested. Some were omitted due to hardware problems; others were omitted because of priorities within the allotted test period.

The baseline configuration (using Mixer 3) is defined for CER = 1.10, SAR = 3.0, 20 mixer lobes, and 80% penetration. (A mixer base area of 1.0 in^2 has been assumed for calculating the required mixing plane area.) The penetration for Mixers 1 through 8 is defined at the SAR that provides 80% entrainment (uncorrected flow ratio). Mixers 9, 10, and 11 were sized for 80% penetration at entrainment levels of 100%, 60%, and 40%, respectively. This corresponds to SAR levels of 3.4, 2.6, and 2.2. Additional SAR variations were achieved for Mixers 3, 6, 10, and 11 by translating the ejector shrouds away from the nozzle centerline. However, when SAR is varied in this manner, the mixer penetration also changes. The mixing duct area ratio ($MAR = A_9/A_m$) was varied by rotating the ejector shrouds while holding the mixing duct inlet area (A_m) constant. A baseline MAR of 0.95 was used for all configurations while MAR's of 0.8, 0.9, 0.95, and 1.2 were evaluated using Mixers 3 and 8.

Table 36. HSCT Generation 1.5 Mixer Summary

Lobe Penetration (%)	Mixer L/D	Lobe Count	Mixer Summary											
			SAR CER	2.2 1.00	2.6 1.00	3.0 1.00	3.4 1.00	2.2 1.10	2.6 1.10	3.0 1.10	3.4 1.10	2.2 1.25	2.6 1.25	3.0 1.25	3.4 1.25
60	1.0	20								1					
80	1.0	20				2				3				4	
100	1.0	20								5				7	
80	1.0	16								6					
80	0.6	20								8					
80	1.0	20									9				
80	1.0	20							10						
80	1.0	20						11							
P&W Mixer Concept															
100	0.6	20								12					
GE Mixer Concepts															
80	1.0	20				13									
88	0.6	20				14									
88	0.6	20				15									

As shown in the test matrix (Table 37), mixers were also evaluated without the mixing duct installed. This is denoted in the matrix as SAR = n/a since SAR has no physical significance for these configurations. This series of tests was run to determine a baseline performance level for each mixer.

Results/Conclusions – Of primary interest in the test are the effects of SAR, MAR, CER, PEN, mixer length, shroud length, number of lobes, and mixer chute shape on performance, pumping (entrainment), and mode shift. Performance is defined as the measured thrust normalized by the ideal thrust of the primary flow:

$$C_{fg} = \frac{F_{measured}}{F_{idp}}$$

In this manner, C_{fg} may be greater than 1.0. The pumping (entrainment) is the temperature-corrected, secondary-to-primary flow ratio scaled to a nominal effective primary choked flow area of 10 in^2

$$WTFLC = (\omega \sqrt{\tau}) \qquad \text{or} \qquad \frac{W_{s'}}{W_{p'}} \sqrt{\frac{T_{ts}}{T_{tp}}}$$

where $W_{s'}$ and $W_{p'}$ are the corrected primary and secondary flow rates. This scaled entrainment ratio allows comparisons of data obtained for various configurations by removing the minor shifts that resulted from mixer deflections.

The test successfully demonstrated the aerodynamic viability of a mixer/ejector nozzle for the HSCT program. The baseline geometry demonstrated gross thrust performance levels (normalized by the

Table 37. HSCT Generation 1.5 Test Configuration Matrix

	Mid–Length Shroud																Short Shroud			Long
Shroud L/D	3.00																2.20			6.00
	SAR	n/a	2.2	2.6	3.0	3.4	n/a	2.2	2.6	3.0	3.4	n/a	2.2	2.6	3.0	3.4	3.0	3.0	3.0	3.0
	CER	1.00	1.00	1.00	1.00	1.00	1.10	1.10	1.10	1.10	1.10	1.25	1.25	1.25	1.25	1.25	1.00	1.10	1.25	1.10
Mixer No.	MAR=0.95																			
1							24			25	26							30		
2		10			**11**	12											13			
3							**1**		**2**	**3**	**4**									
4												**14**			**15**	**16**			17	
5							31			32	33									
6							**37**			**38**	**39**							40		
7												48			49	50			51	
8							**52**			**53**								**8**		**9**
9							**18**				**19**									
10							**20**		**21**	**22**	**23**									
11							**41**	**42**		**44**	**45**									
12							46			**47**	62									
13		54			55															
14		56			**57**															
15		58			**59**															
16		60			61															
	MAR=0.80																			
1										27										
3										**5**										
5										34										
8										**63**										
	MAR=0.90																			
1										28										
3										**6**										
5										35										
8										**64**										
	MAR=1.20																			
1										29										
3										**7**										
5										36										
8										**65**										

Notes:

Mixer numbers are summarized in Figure 2.

Bold configurations represent those actually tested.

ideal thrust of the primary flow) of approximately 1.04 for secondary pressures near ambient and an NPR of 3.5. By using a 16-lobe mixer, this performance could be expected to go as high as 1.055 since the 16-lobe mixer has been shown to provide a thrust benefit of 1.5% over the baseline 20-lobe mixer. For the design point of NPR = 3.5 and secondary pressures near ambient, optimum performance was obtained at a MAR of 0.90. A long mixer was found to be effective in minimizing secondary losses. Although a short mixing duct may be beneficial to performance at lower NPR's, the mixing duct length is not a critical performance concern at and above the design nozzle pressure ratio. Since the data have shown that secondary losses are critical to the overall nozzle performance, it is important that these losses be minimized to provide the best aerodynamic design. Thus, the designs of the secondary inlets are critical to the actual levels of thrust attained for the HSCT nozzle.

Mode shift is a condition observed in mixer/ejector nozzles when the flow in the mixing duct transitions from subsonic to supersonic. This occurance is usually accompanied by a shift in shroud static pressures. For certain geometries, this shift can be quite drastic, causing a high dynamic load on the shrouds and sidewalls. Although the mode shift may not always be eliminated entirely, its effects may be greatly reduced by applying the results of this test. This test revealed the following trends:

- The tendency for mode shift was basically eliminated at MAR's less than 0.90.
- The tendency to mode shift was closely related to penetration. High penetrations (100%) caused severe mode shifts while lower penetrations reduced the severity of and the tendency to mode shift.
- The tendency for mode shift was related to shroud length (mixing duct length). The longer the shroud, the greater the severity of and the tendency to mode shift.

5.7.1.3 Gen 2.0 Mixer Test at LSAF

The Gen 2.0 1/7-scale model test was conducted at the Boeing Low Speed Aeroacoustic Facility (LSAF) from June 1995 through July 1996. The test actually comprised two separate model entries identified as LSAF 1032 and LSAF 1039. The LSAF 1032 entry tested the DSM concept model that was designed and built by P&W under NASA CPC contract. The second entry, LSAF 1039, tested the existing HAM, designed and built by GEAE, with new Gen 2.0 style mixers.

Test Objectives/Background

The Gen 2.0 mixer/ejector nozzle concept for the NASA CPC program had been developed using the knowledge gained from analysis and test of the previous concepts (Gen 1.0, 1.5). *Best Aero* concepts have aerodynamic shaping of the mixer lobes and an axial-flow design for improved thrust performance. Parametrics such as SAR and penetration were added. Mixers referred to as *DSM mixers* were designed to be compatible with the DSM concept. Also, the HAM model that had been designed and built by GEAE for the NASA–Ames Heat 1 test was available and had the positive attributes of better secondary inlet contours, longer ejector box, and higher aspect ratio nozzle. Best aero style mixers for use with the HAM were added to the Gen 2.0 test.

The objectives of the Gen 2.0 model test at LSAF (after the program redirection) were to acquire concurrent thrust and acoustic data for a series of parametric mixer models. The parameters evaluated included:

- Suppressor Area Ratio (SAR = 2.2, 2.5, 2.9)
- Penetration (0.85, 0.925, 1.00)
- Axial Versus Vortical Mixers
- Ejector Flap Length (120-in, 160-in full scale)
- Hardwall Versus Treated
- Free-Stream Mach Number (0 to 0.32)
- SiC Bulk Absorber versus Single Degree of Freedom (SDOF) with Felt Face Sheet
- Liner Depth (7 mm and 13 mm)
- MAR, Mixer Area Ratio
- Aspect Ratio, DSM = 1.17, HAM = 1.5 (at MAR=0.95)

Results from this vast database were used to develop later mixer concepts: Gen 3.0 and Gen 3.5.

Test Facility Description (LSAF)

The Boeing LSAF combines a large anechoic test chamber with a 9×12-ft free-jet wind tunnel. The tunnel size was modified during the test to 7×10 ft, which allowed for free-jet Mach Numbers up to 0.32. Acoustic instrumentation included a traversing azimuthal microphone array at a 15-ft sideline distance, with additional free-standing microphones to augment the array, and a traversing elliptical mirror for noise-source location. The test cell with the Gen 2.0 DSM model installed is shown in Figure 171. In the figure, the free-jet exit (without the Mach = 0.32 insert) and the elliptical mirror are visible. Figure 172 shows the wind tunnel with the original and Mach 0.32 inserts. Figures 173 and 174 show the layout of the test cell in plan view and end view respectively.

Hot primary airflow is provided to the model through the NLT3800 *Jet Flow Simulator.* This simulator is capable of providing up to 30 lbm/s of high-pressure cold flow and can heat the primary flow up to 1700°R. The airflow is provided to the simulator from a 300-psi supply system. Airflow to the simulator is measured through choked calibrated venturis. A propane burner, downstream of the venturi, provides the heat source to obtain the hot-gas conditions.

The facility charging station is located downstream of the primary flow venturis and the propane burner — about six feet upstream of the mixer model. The charging station is composed of a six-arm rake: three arms for total pressure and three arms for total temperature. Each arm has five measurement probes located in centers of equal area for a total of 15 total-pressure measurements and 15 total-temperature measurements. The location of the charging station rake is in an 8-in ID duct where the local velocity is low.

Forces acting on the model are measured with a six-component external balance system. The design loads for this system are 2,500-lbf axial force, 6,000-lbf side force, 6,000-lbf normal force, 125,000-in–lb roll and pitch moments, and 175,000-in–lb for yaw moment. The balance sits on a frame located below the propane burner. Airflow crosses the balance in a direction perpendicular to the thrust with a bellows system to absorb any air-supply-induced loads.

Facility and nozzle drag tare measurements were done prior to running the Gen 2.0 model hardware. These drag tares remove the drag of the model support system from the balance readings.

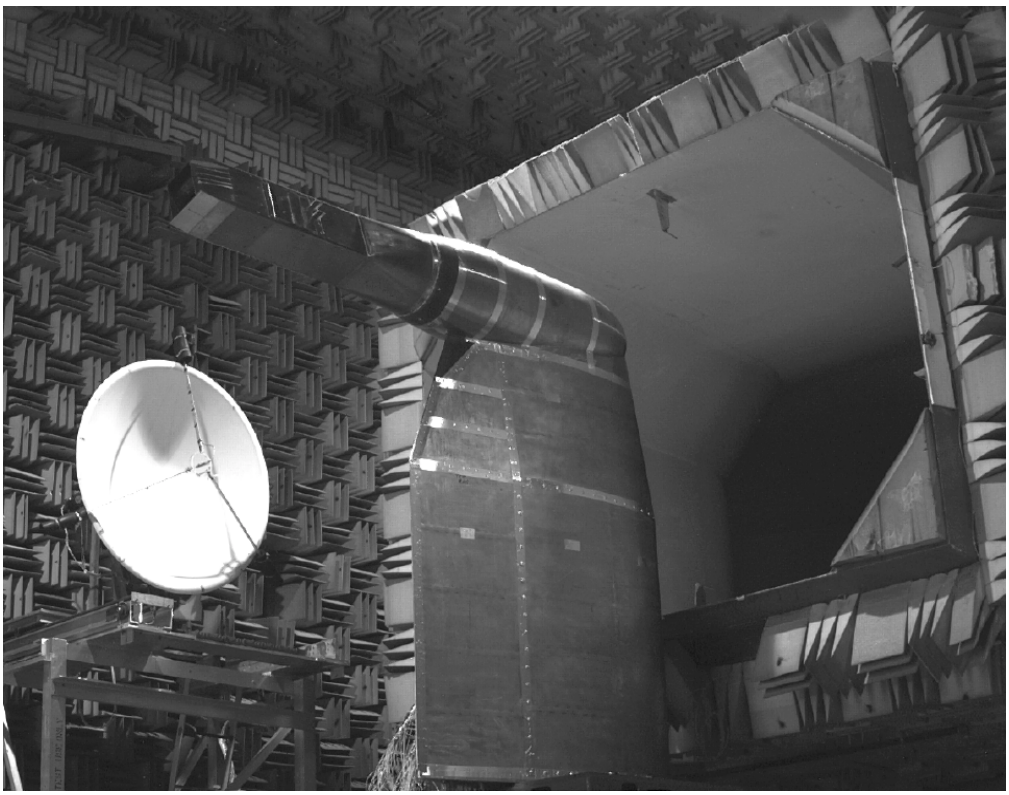

Figure 171. Photo of LSAF Test Cell with Gen 2.0 DSM Installed

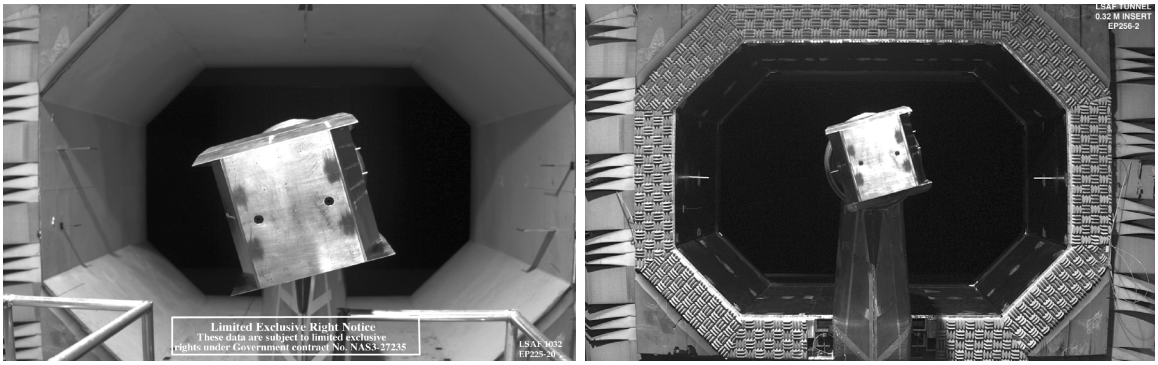

Original Mach=0.32 Insert

Figure 172. Wind Tunnel Photo Comparison of Original and Mach 0.32 Inserts

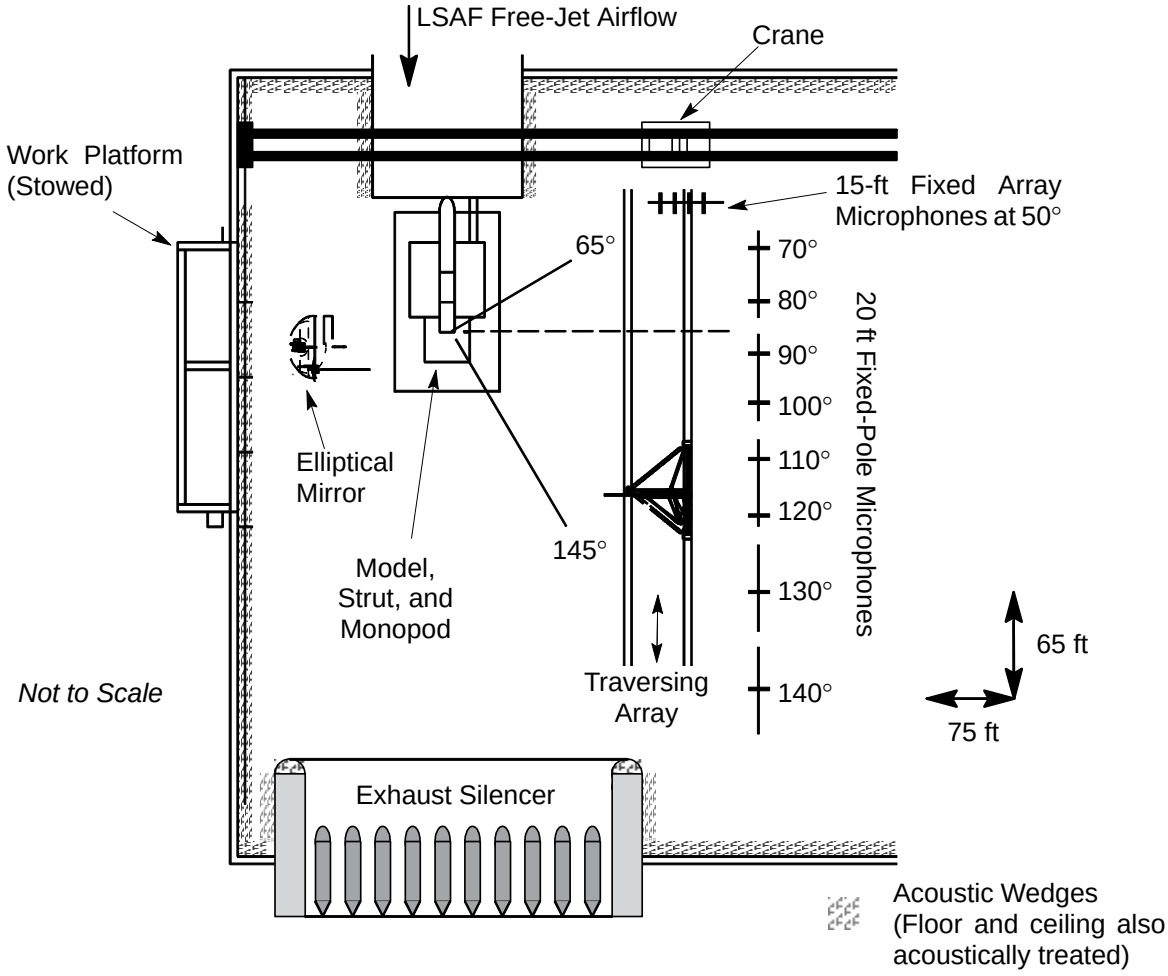

Figure 173. Boeing Low-Speed Aeroacoustic Facility – Plan View

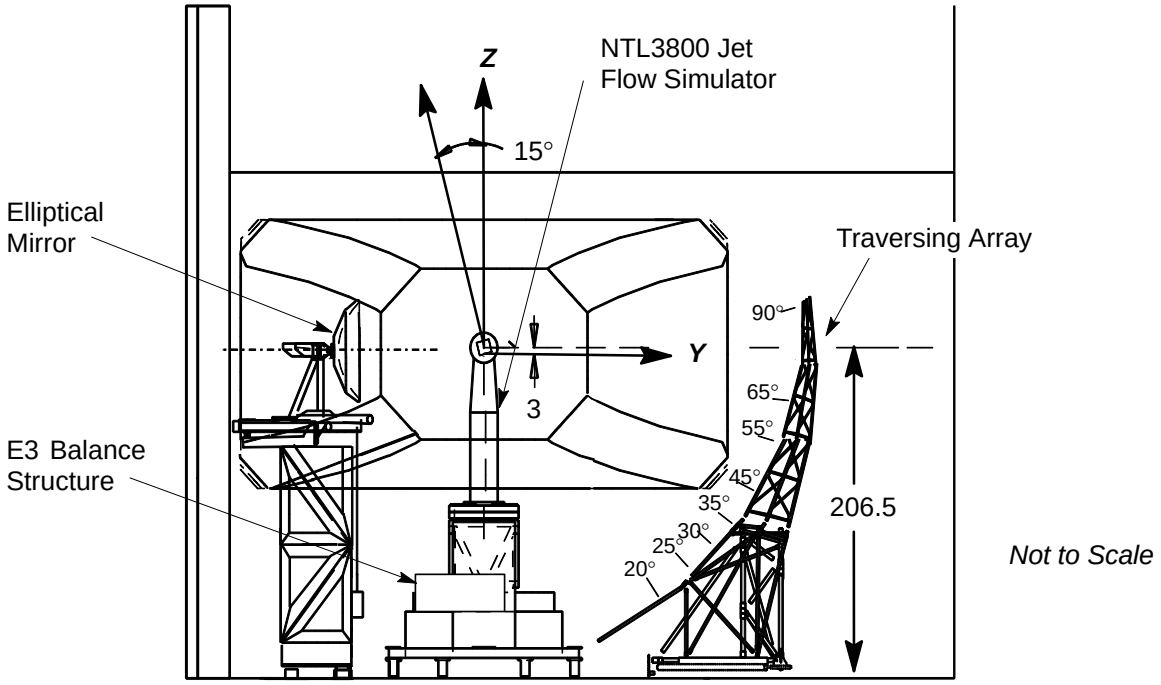

Figure 174. Low-Speed Aeroacoustic Facility – End View

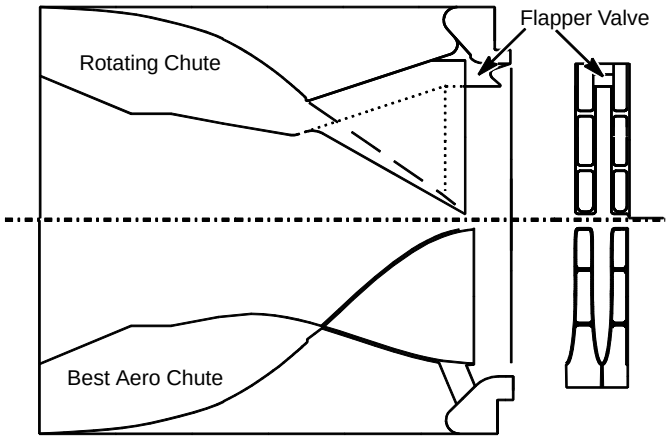

Figure 175. DSM Cross Section

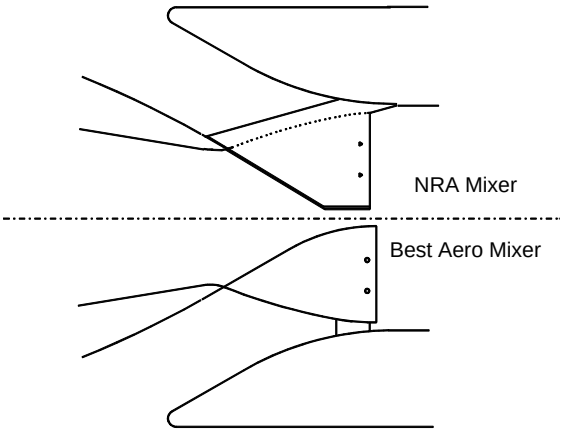

Figure 176. HAM Cross Section

The DSM model contains no total pressure rakes in the secondary inlets. The secondary flow for the DSM was calibrated using a flow tube mounted to the exit of the ejector. The flow tube has a total pressure and total temperature rake and was used to calculate the total flow, primary and secondary, through the nozzle. Subtracting the primary flow leaves the secondary flow. This calibrated secondary flow was then correlated with a static pressure in the mixer to obtain secondary flow rates during normal operation. The HAM model contained total pressure probes in the secondary inlet that were used to calculate the secondary flow rate.

Model Hardware

The Gen 2.0 LSAF test program used two basic mixer/ejector models: the DSM and the HAM. With the DSM model, two variants of mixers were tested: the vortical or rotating-chute mixer and the axial or best aero mixer.

Figure 175 illustrates the DSM models. All of the new HAM models were of the best aero type. However, as a check on the facility and to map to a previous known model, the Gen 1.5 NRA model was also tested. Figure 176 illustrates the HAM models. Differences of note between the DSM and HAM are the secondary inlet contours, aft inlet lip radius, and the mixer length. Pins were used in the secondary of both types of mixers to support the chute walls under pressure. Figures 177 and 178 show the Gen 2.0 DSM and HAM model hardware installed in LSAF.

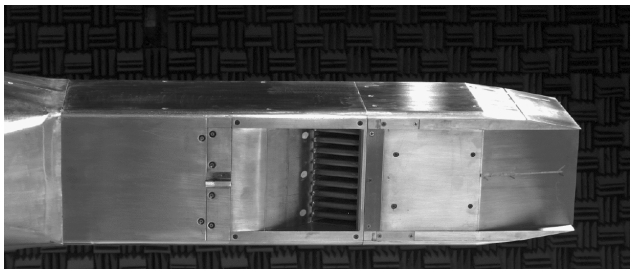

Figure 177. DSM Model Installed in LSAF

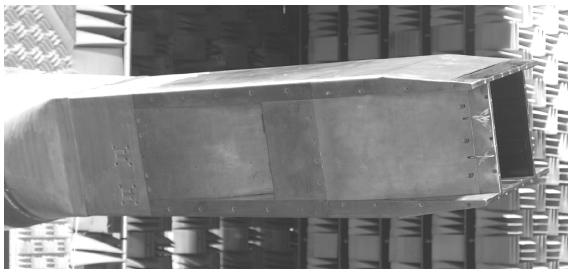

Figure 178. HAM Model Installed in LSAF

Table 38 is a list of the various mixers tested. A total of 12 mixers were evaluated during the Gen 2.0 test.

The DSM and HAM models were instrumented with static pressure ports throughout. Static pressure ports were installed on the inlet ramp and aft lip and down the mixer chutes on the secondary side. The DSM rotating chute mixer had additional static pressure probes located on the flapper valve. Static pressure ports were installed inside the nozzle ejector, with rows aligned with secondary and primary chutes and another row down the center of the sidewall. A few external static pressure ports were located near the exit of the nozzle ejector.

The HAM model secondary inlet was instrumented with three total pressure rakes, two in the upper and one in the lower inlet. Each rake contained 11 total pressure probes. These rakes combined with wall statics in-line with the rakes provided the means for calculating secondary airflow with the HAM model. The drag tare plates were instrumented with static pressure ports, 44 for the facility plate and 47 for the nozzle tare plate. These pressures were used to calculate a base drag force.

Table 38. Gen 2.0 Mixer Information

Mixer Type	Mixer	Type	SAR	ASAR	A_8	Model Scale	Penetration	Description
DSM A_{mix} = 58 in^2	1	Rotating	3.38	3.47	17.160	0.11489	0.85, 1.00	SAR Variation
	2	Rotating	2.5	2.49	23.200	0.13359	0.85, 0.925, 1.00	Baseline – Rotating
	4	Best Aero	2.5	2.67	23.200	0.13359	1.00	Pen Variation – Best Aero
	5	Best Aero	2.5	2.52	23.200	0.13359	0.925	Baseline Best Aero
	6	Best Aero	2.5	2.50	23.200	0.13359	0.85	Pen. Variation – Best Aero
	8	Best Aero	2.2	2.34	26.364	0.14241	0.925	SAR Variation – Best Aero
	9	Best Aero	2.9	2.89	20.00	0.12403	0.925	SAR Variation – Best Aero
HAM A_{mix} = 64.7 in^2	3	Best Aero	2.5	2.59	25.880	0.14110	1.00	Pen. Variation – Best Aero
	4	Best Aero	2.5	2.62	25.880	0.14110	0.925	Baseline Best Aero
	10	Best Aero	2.5	2.63	25.880	0.14110	0.85	Pen Variation – Best Aero
	8	Best Aero	2.9	3.06	22.310	0.13100	0.925	SAR Variation – Best Aero
	21	NRA	2.8	2.88	23.107	0.13332	1.00	Vortical Flow Style Mixer
* Note: Model scale is relative to full scale A_8 = 1300 in^2								

Significant Results and Conclusions

Figure 179 summarizes the results from the Gen 2.0 test. The figure shows thrust coefficient versus EPNL for the cutback (NPR = 2.48) and sideline (NPR = 3.43) operating conditions at Mach 0.32 for several of the key configurations. Best overall performance is plotted to the lower right side (low noise, high thrust) of the plots and worst toward the upper left (high noise, low thrust). Best overall performance was obtained with the HAM, Mixer 8 (SAR = 2.9, Penetration 0.925), treated, long flaps, and chevrons. The best aero shaped mixers performed similarly in thrust, with high thrust coefficients varying by about 2%, but varied considerably in noise suppression, with EPNL varying by 4 EPNdB depending on SAR and ejector length.

Figure 180 shows the measured velocity profiles at the exit of the DSM and HAM nozzles at the sideline condition for similar configurations. The figure only displays half of the exit plane in order to compare the two side by side. The figure shows that the HAM, with higher aspect ratio, is better mixed in the center of the duct. Both models show a large velocity hole at the center of the sidewall. The velocity hole for the HAM appears larger than for the DSM. The large size of this velocity hole convinced the nozzle team to move away from a full cold chute sidewall.

Figure 181 shows the effect of Mach number on noise, thrust, and pumping for the cutback and sideline test conditions. The figures show the expected trend of pumping improving, but thrust and noise decreasing, with increasing Mach number.

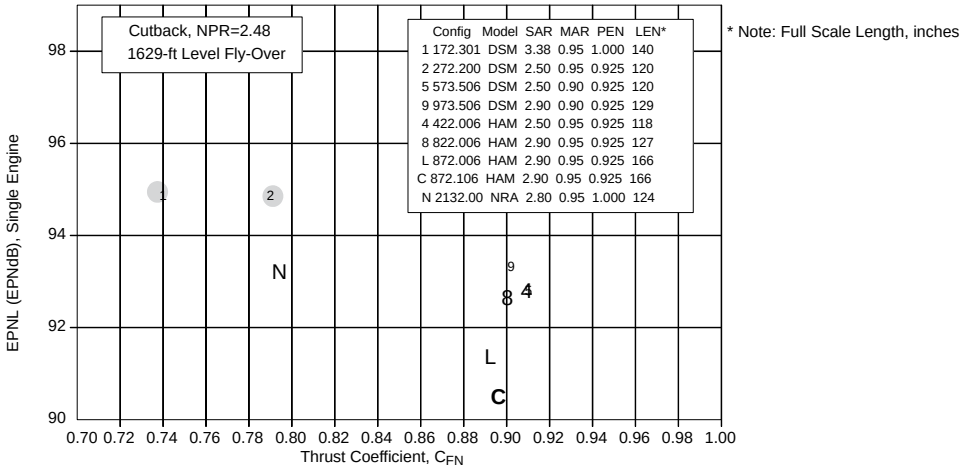

Figure 179. Overall Test Results, Mach 0.32, Hot Primary

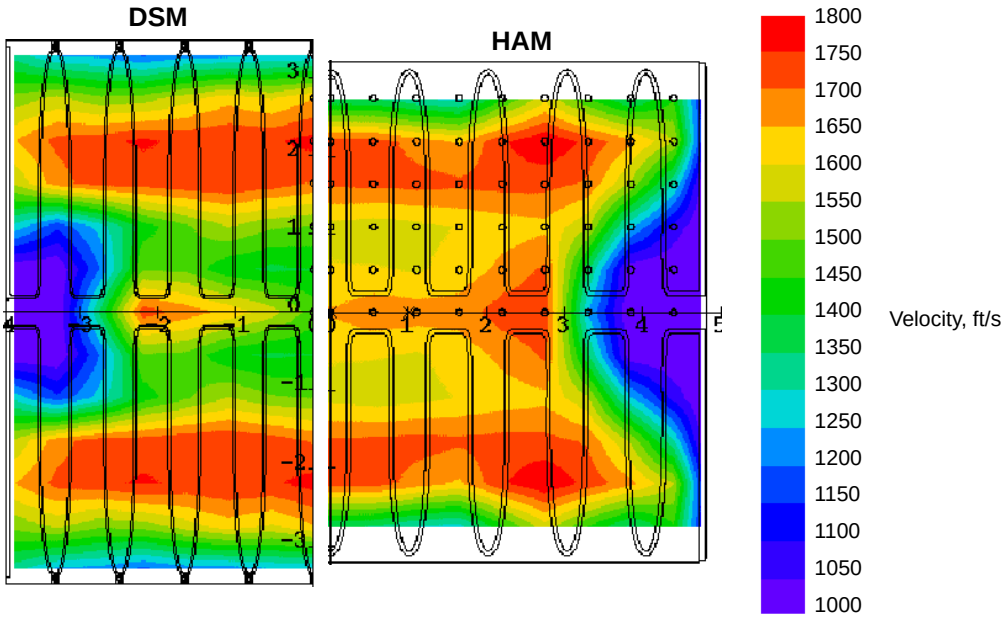

Figure 180. Exit Velocity Profile Comparison, DSM Mixer 9 versus HAM Mixer 8

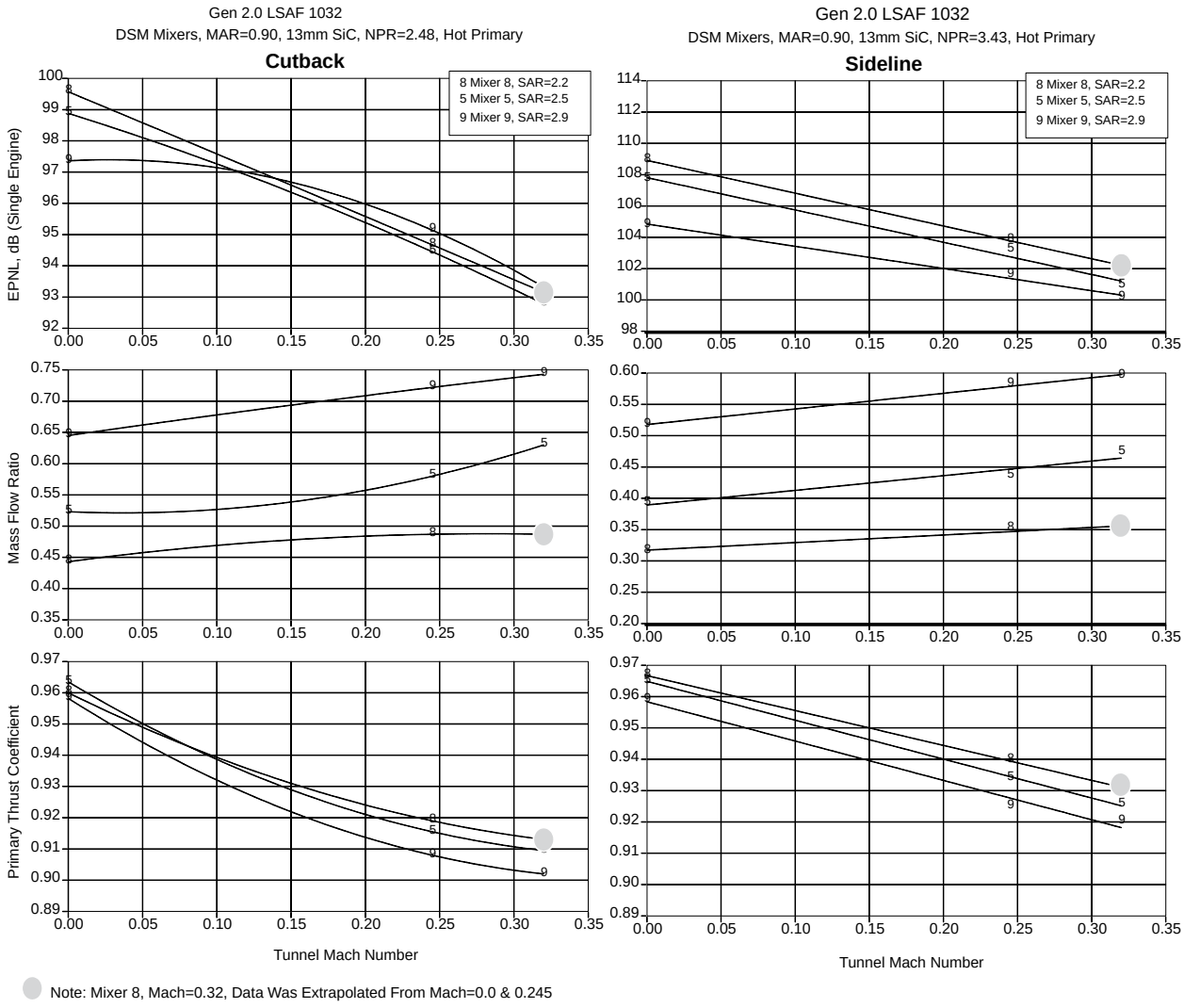

Figure 181. Effect of Mach Number for DSM, MAR = 0.90, Treated

Figure 182 shows the effect of changing ASAR (Aerodynamic Suppressor Area Ratio) on the DSM and HAM best aero configurations for noise, pumping and thrust. ASAR is used here rather than SAR since it properly accounts for the changes in the mixer throat due to pressure and temperature. The figure shows that for a constant ASAR, the two models have about the same thrust coefficient and pumping. At the sideline condition, the HAM model had better noise performance, particularly at the lower ASAR values. The noise at cutback was very similar between the two models

Figure 183 shows the effect of penetration on noise, pumping, and thrust at the cutback and sideline conditions. As penetration increases, noise and thrust decrease. Pumping is somewhat flat with changing penetration but shows a peak near 0.925 penetration.

Figure 184 shows the effect of MAR on noise, pumping, and thrust at the cutback and sideline conditions. Pumping increases with increasing MAR. Thrust and noise show optimum performance at about MAR=0.95.

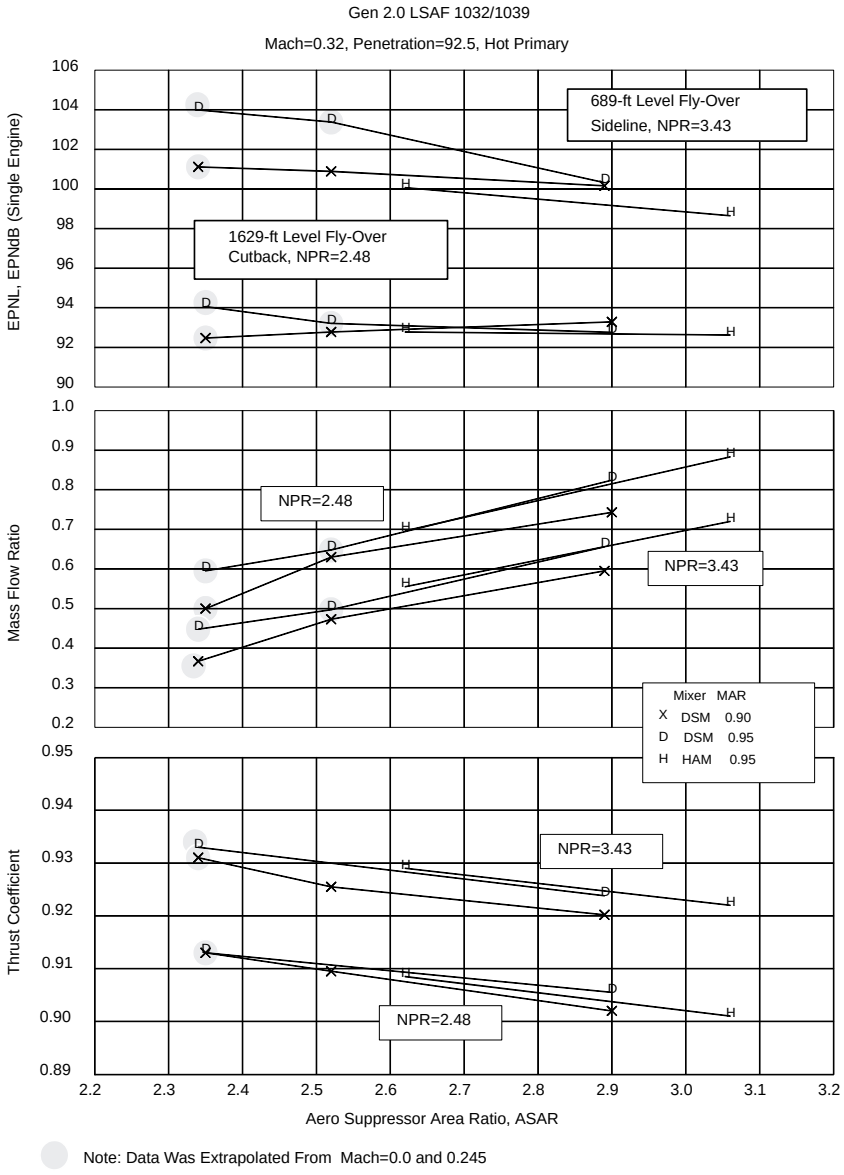

Figure 182. Effect of SAR, Mach 0.32, Treated

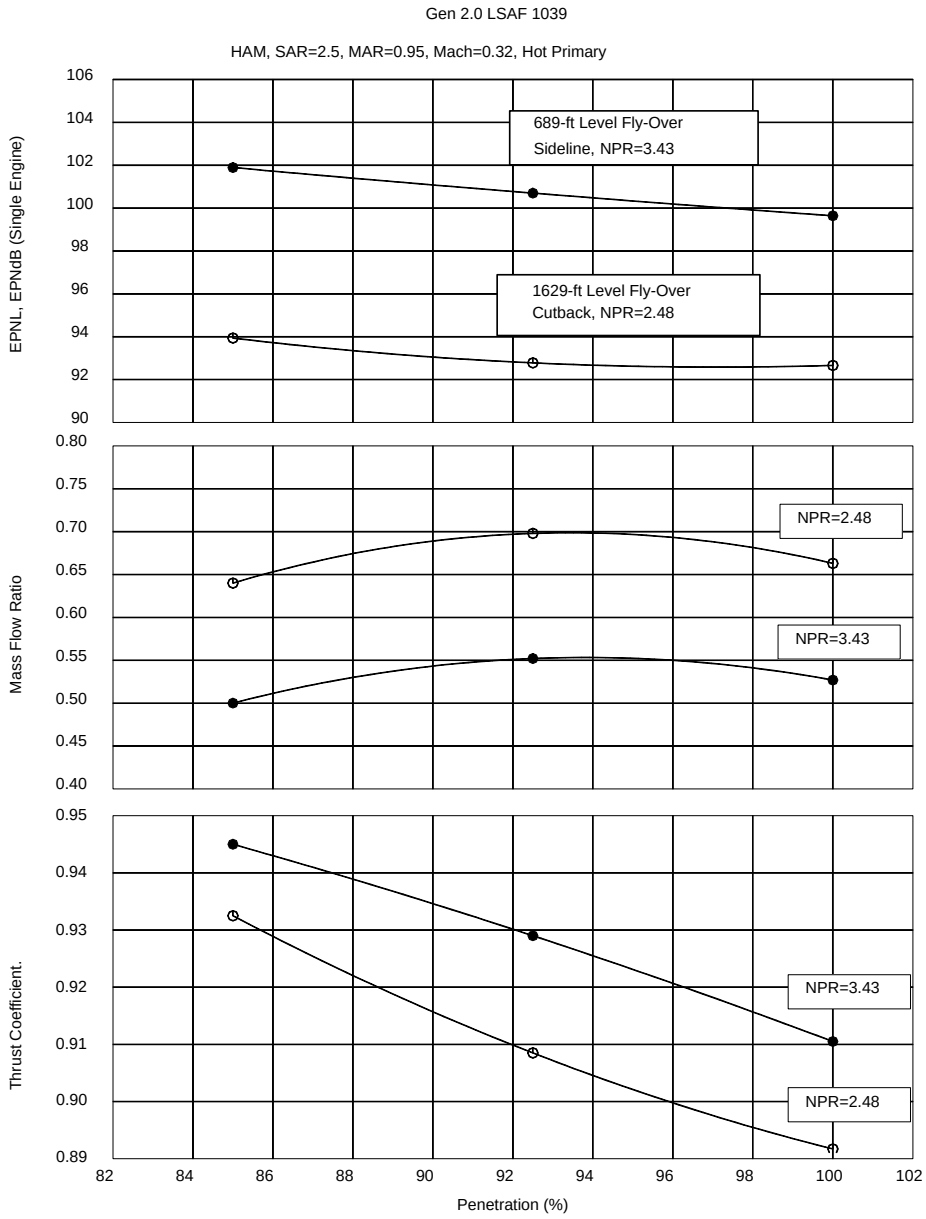

Figure 183. Effect of Penetration, Mach 0.32, Treated

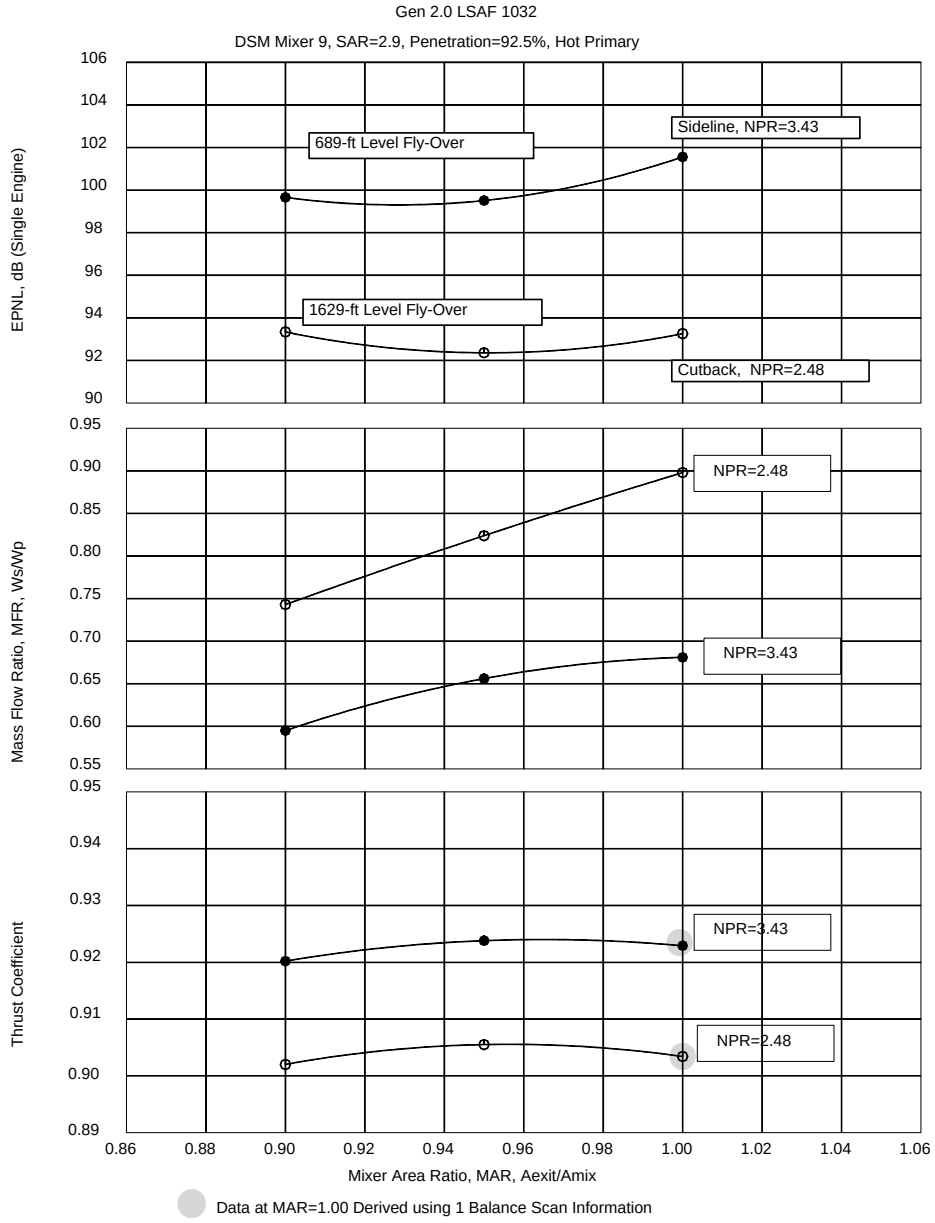

Figure 184. Effect of MAR, DSM, Mach 0.32, Treated

Figure 185 shows the effect of flap length on noise, pumping, and thrust at the cutback and sideline conditions. The added flap length was right after the mixer and was not treated. Treated area is the same for the two flap lengths. The figure shows that noise improves by 1 to 2 EPNdB with increase flap length, pumping is unaffected, and thrust is reduced by about 1%. Figure 186 shows the effect of the liner variations tested with the DSM model at cutback and sideline conditions. Best noise suppression is obtained with the 13-mm Sic bulk absorber material: about 6 EPNdB suppression at cutback and 2.5 EPNdB suppression at sideline relative to hard wall.

Best thrust and pumping performance was obtained with the 7-mm SDOF with felt metal face sheet: less than 1% thrust loss and little pumping loss. This chart suggests that the 13-mm bulk absorber with a smooth felt metal face sheet would provide the best model-scale performance. Friction losses caused by the porous face sheet are reduced and suppression levels maintained — thus reducing the model scale to full-scale correction that must be accounted for.

Figure 187 shows the effect of liner variations tested with the HAM model at cutback and sideline. The configuration labeled “hard wall, perf plate” consists of the baseline porous-hole-liner trays with a thin sheet of metal between the bulk absorber and the back side of the face sheet. The thin sheet of metal effectively blocks the bulk absorber from attenuating any of the acoustic energy. This method was used by the team at non-thrust-measuring facilities to simulate the hard-wall configuration. The data show that even though no absorber is present, the holes in the face sheet itself with the material thickness of the face sheet is enough to provide some suppression, about 2 EPNdB at cutback and 1 EPNdB at sideline. Additionally, the rough face-sheet surface caused over a 1% loss in thrust performance. The practice was cost effective, since only one set of trays was produced for a given model, but the results show that simulation of a true hard wall with a perforated plate backed by an unperforated sheet metal plate can lead to erroneous conclusions.

Figure 188 shows the effect of the DSM rotating, vortical, chute shape compared with the best aero, axial, chute shape at the cutback and sideline conditions. The two chute styles have similar noise suppression; at cutback the best aero chute is about 1 EPNdB quieter than the rotating chute and about the same at sideline. However, the best aero has substantially better thrust performance, with over 10% improvement at cutback and over 7% improvement at sideline. From an aeroacoustic point of view, the best aero chutes much improve performance compared to the rotating-chute design.

Figure 189 shows the effect of the HAM best aero chute compared with the older, Gen 1.5, NRA chute. The NRA SAR did not match any SAR tested with the best aero mixer, so an adjustment was made to the best aero chute performance, using data from Figure 182, for this comparison. The NRA provides similar noise suppression at cutback, but it provides about 3 EPNdB better noise suppression at sideline than the best aero chute. However, the best aero mixer provided substantial thrust improvement compared with the NRA mixer, about 11% at cutback and 9% at sideline. Again, from an aeroacoustic point of view, the best aero chutes provide much improved performance.

5.7.1.4 Gen 2/2.5 – NRA at GEAE

The GEAE Cell 41 anechoic free-jet facility and the NRA 2D mixer/ejector nozzle model are described in Subection 5.7.1.2, with an account of the Gen 1.5 acoustic test.

The early nozzle designs (Gen 1, Gen 1.5) demonstrated the ability to meet the noise goals — but at the expense of aerodynamic performance. The “aero” chutes designed for the second-generation mixers were intended to restore thrust without compromising noise. The design differences are illustrated in Figure 190.

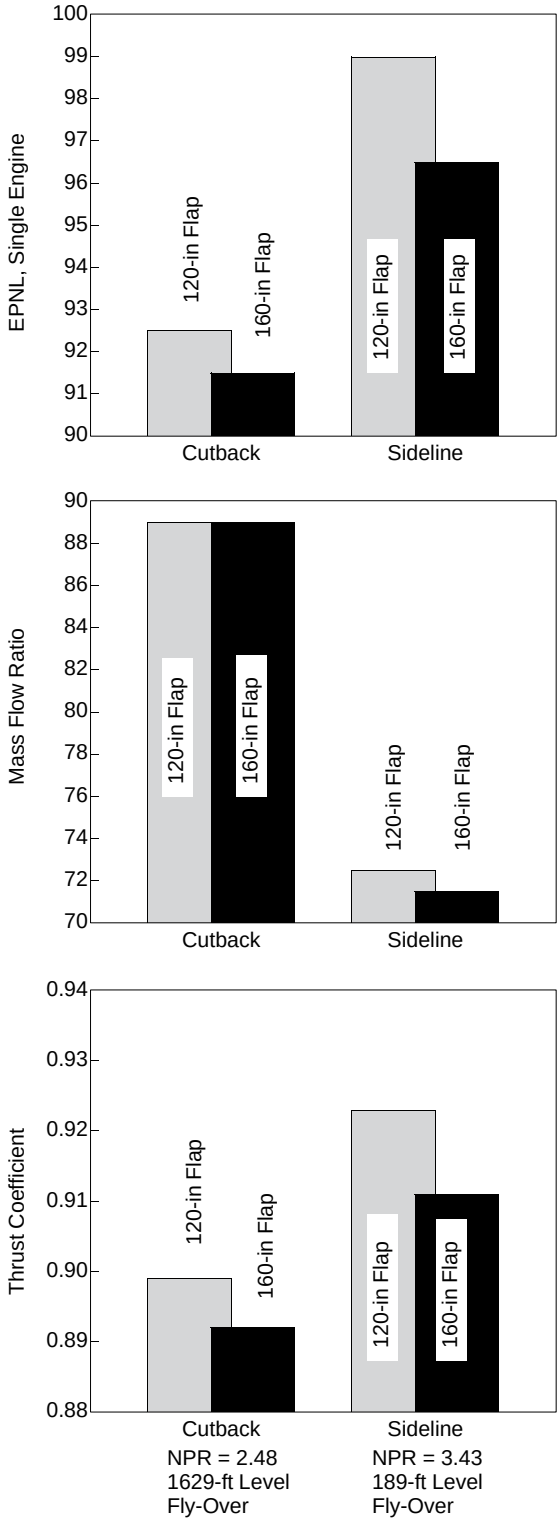

Figure 185. Effect of Flap Length: HAM, MAR 0.95, Mach 0.32

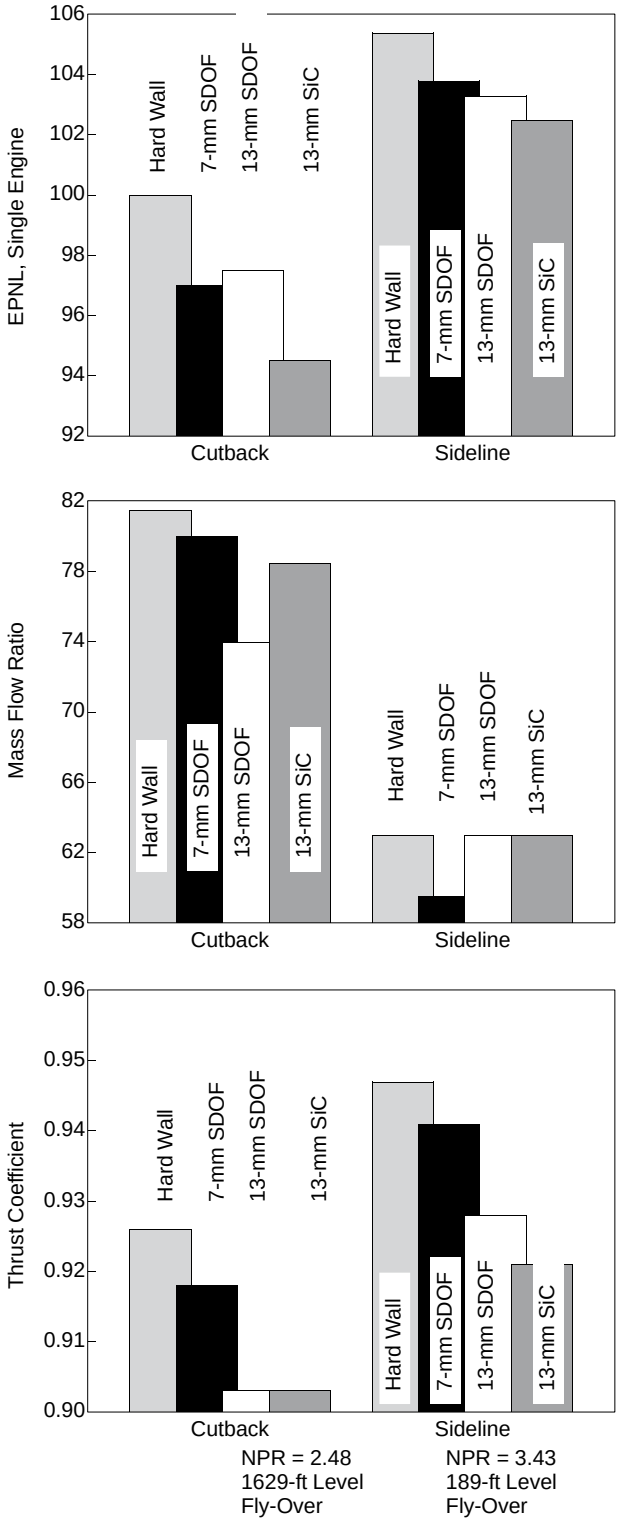

Figure 186. Effect of Liner: DSM, SAR 2.9, Mach 2.45, MAR 0.95

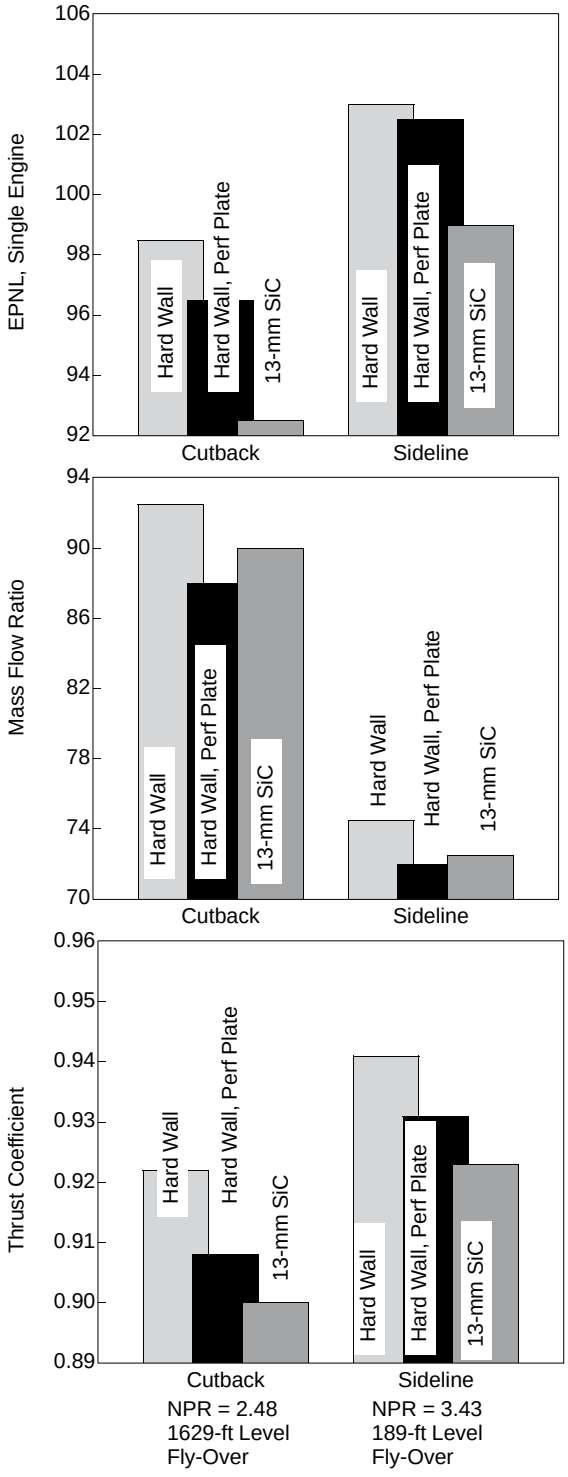

Figure 187. Effect of Liner on HAM: SAR 2.9, Mach 0.32, MAR 0.95

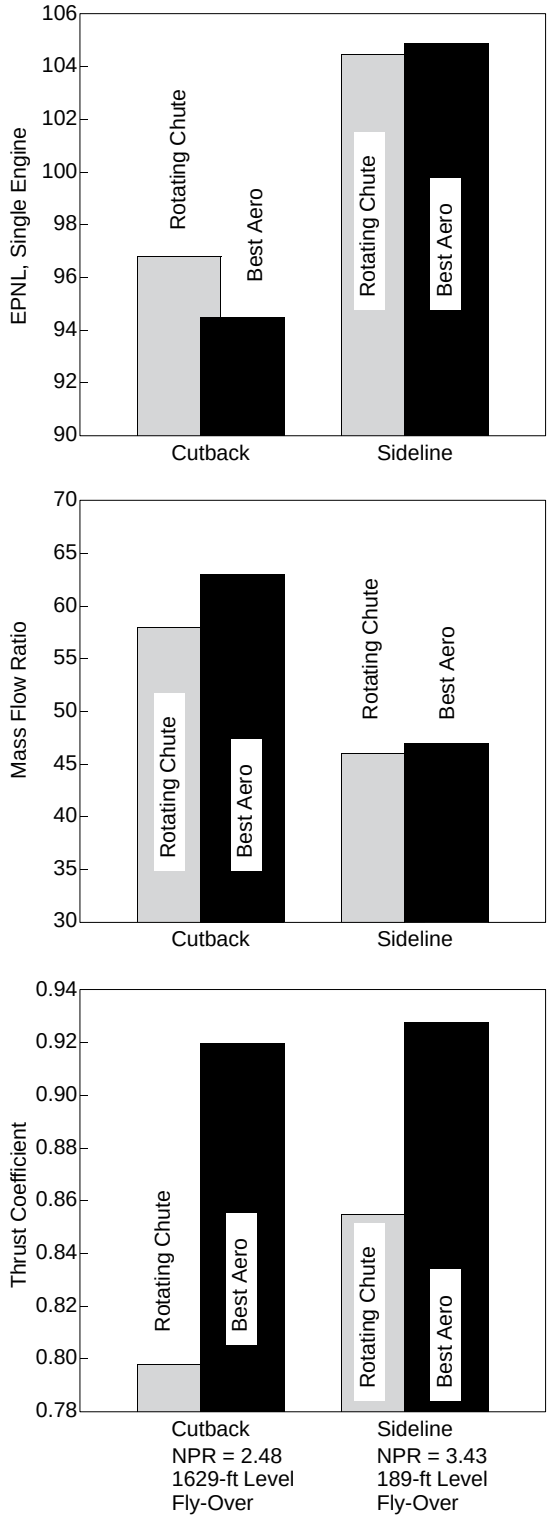

Figure 188. Effect of Chute Shape: DSM, Rotating versus Best Aero

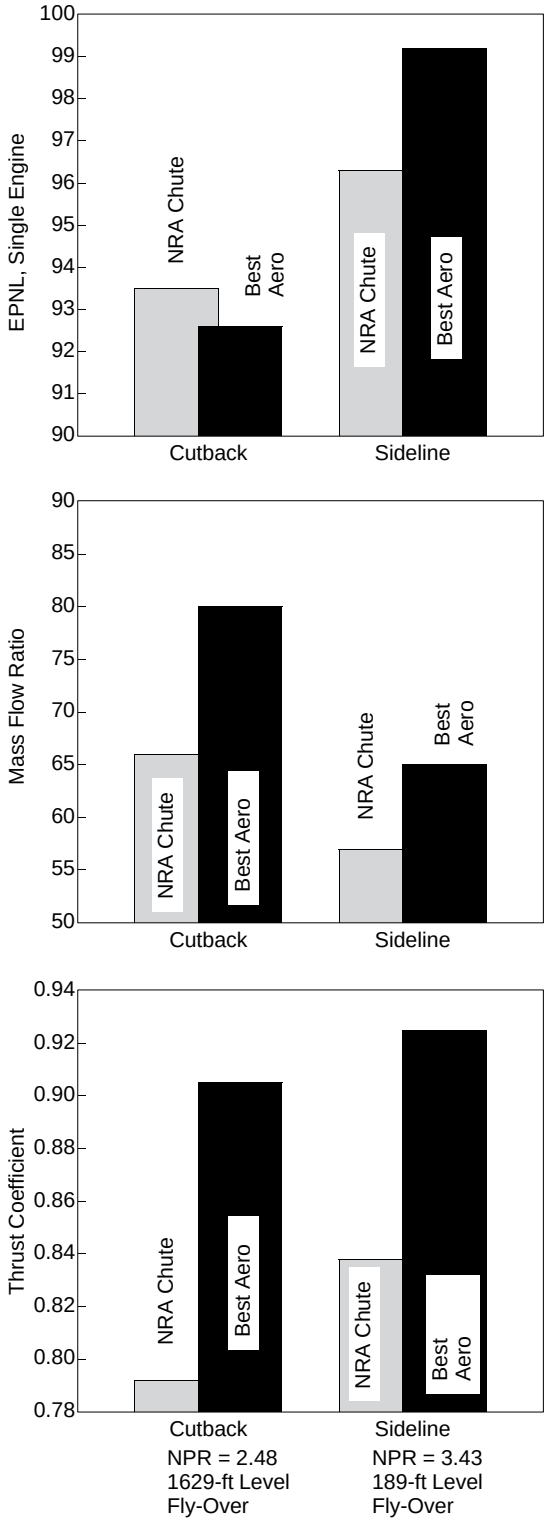

Figure 189. Effect of Chute Shape: HAM, NRA versus Best Aero

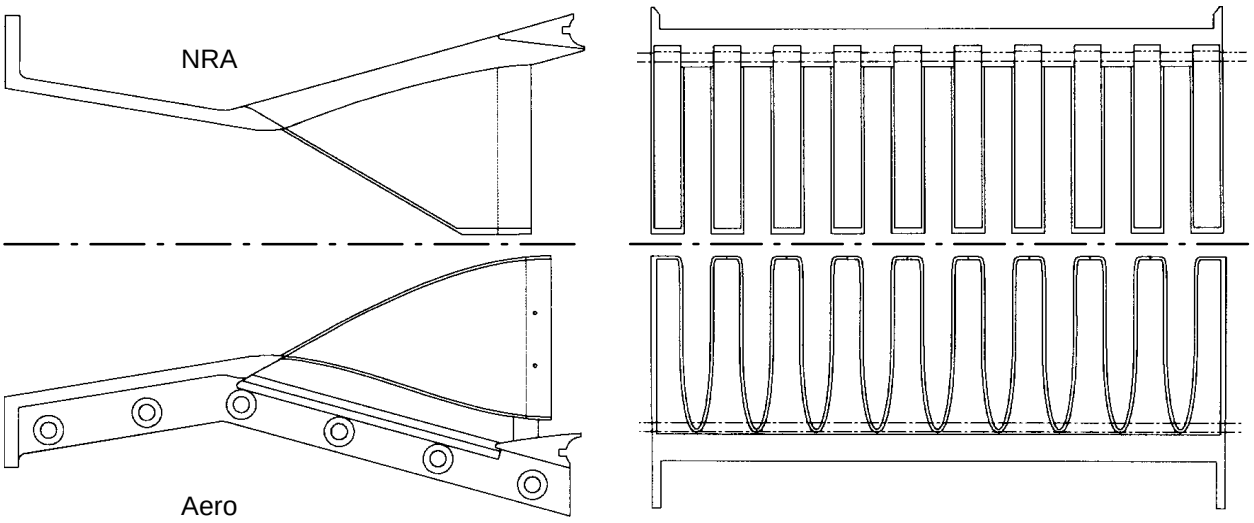

Figure 190. Comparison of NRA (Square Top) and "Aero" (Gothic Arch) Chute Shapes used in Gen 2.0 Testing

Distinct differences in the primary and secondary flowlines can be seen, as well as the most striking difference of the exit geometry. Two additional items should be noted. First, the vertical support strut connecting the crown of the aero chutes to the main structure gave rise to much concern during (and after) the tests. Second, the full-width cold passage adjacent to the sidewalls in these designs (in contrast to the ½-width hot chute of the Gen 1.0 and 1.5 NRA designs) likewise prompted much debate. The final change in the fundamental design of the chutes for the Gen 2 series of mixers (of both shapes) was to reduce the chute expansion ratio from about 1.43 to approximately 1.1 in the interest of improved takeoff performance.

Gen 2.0 Test Series

Test Objectives – The Gen 2.0 test series was planned to investigate the effects of parametric variations in mixer design. These included:

- Suppressor Area Ratio (SAR) – the ratio of mixing plane area (just downstream of the mixers) to primary stream throat area.
- Chute shape (see above).
- Chute penetration – for the "aero" chute, the height of the chute divided by the height of the passage at the chute exit. (In Figure 190, penetration = 100%).
- Chute number – for the same throat area, varying the chute number changes the width and shear perimeter of the individual lobes.
- Chute alignment – in the Gen 1.5 tests described in Subsection 5.7.1.2, the effects of staggered chutes (opposing chute tips offset rather than facing as shown in Figure 190) were tested to see if this benefit was repeated with the aero chute shape.
- Mixer Area Ratio (MAR) – the ratio of ejector exit area to mixing plane area. In Gen 1.0 testing it had been demonstrated that MAR effects could be significant, especially when the mode shift from subsonic to supersonic flow within the ejector occurred.

- Ejector Length – it had been demonstrated during the Gen 1.0 test that "longer was better" from the standpoint of acoustics. In terms of the trades between suppression, nozzle weight and boattail angle required for minimum drag, further investigation was appropriate.
- Ejector Exit Modifications – specifically chevrons. Very basic chevrons had been tested as a "scab on" part during the Gen 1.5 testing and had shown a benefit. A parametric series of configurations was derived for this test.
- Acoustic Treatment – bulk materials with different material properties and different porosity face sheets were tested. Treatment locations and quantities were varied and "true" hard-wall surfaces were used for the first time in the NRA model system.

Test Procedure – Table 39 summarizes the mixer designs that were tested in this series.

Table 39. Theoretical Design Intent and Measured Assembled Parameters for Gen 2.0 Mixers

Chute Type and Mixer No.	No. of Cold Chutes	No. of Hot Chutes	Theoretical			Measured / Assembled Dimensions				
			CER	Penetration	SAR	Avg. CER	Avg. Penetration	A_{mix} (in^2)	A8 (in^2)	SAR
NRA,#2	20	18	1.1	100%	2.5	1.088	N/A	62.689	25.324	2.476
								64.856*		2.561*
NRA,#5	16	14	1.1	100%	2.5	1.067	N/A	62.314	25.592	2.435
								64.527*		2.521*
NRA,#6	24	22	1.1	100%	2.5	1.098	N/A	63.276	25.364	2.495
								65.465*		2.581*
Aero,#3	20	18	1.1	100%	2.5	1.044	99.7	65.025	25.317	2.568
Aero,#4	20	18	1.1	92.5%	2.5	1.046	91.98	64.875	24.813	2.615
Aero,#7 (stagger)	9+2 halves top 10 10 bottom 9		1.1	100%	2.5	1.054	99.31	65.219	25.2161	2.586
Aero,#8	20	18	1.1	92.5%	2.9	1.0453	92.15	65.265	21.45	3.043
Aero,#9	20	18	1.1	92.5%	2.2	1.0682	91.01	64.149	27.764	2.347
Aero,#10	20	18	1.1	85%	2.5	1.0453	83.92	65.003	25.1794	2.582
* A_{mix} is calculated by the same method as for the aero mixers.										

Table 40 shows the cycle line used in the Gen 2.0 and subsequent test series. This was selected to ensure connectivity with the ongoing system studies.

It was believed at the start of the test series that points 13 and 16 would represent the cutback and sideline noise conditions. System studies, however, drove the engine to a higher fan pressure ratio; points 14 and 17 became more representative.

Data – In addition to the acoustic data taken during this test series, extensive measurements were made of the axial-velocity details at the ejector exit using nonintrusive laser doppler velocimetry (see Figure 168, page 182). Since jet noise is related to flowfield characteristics, it was hoped that these data would help in understanding the effects that changes in nozzle chute geometry had on the flowfield characteristics and hence on the noise. These data were used in the development of the "degree of mixing" parameter used in the Stone semiempirical prediction methodology described in Subsection 5.6.2.1.

Table 40. Cycle Points Set in Gen 2.0 Testing

Point	NPR	T_{T8}, °R	$V_{j\ ideal}$, ft/s	Cycle ID	Remarks
11	1.51	970	1133	NPF3765	PC26
12	1.99	1139	1559	NPF3765	PC32
13	2.37	1238	1813	3570.100	PC38, Community
14	2.48	1291	1883	NPF3765	PC38, Community
15	2.96	1416	2133	NPF3765	PC44
16	3.25	1482	2274	3570.100	PC50, Max Dry
17	3.43	1551	2359	NPF3765	PC50, Max Dry
18	4.00	1700	2598	NPF3765ext	Projected
19	2.14	1398	1813	“hot cycle”	To Match TP#13 V_{jIDEAL}
20	2.90	1610	2274	“hot cycle”	To Match TP#16 V_{jIDEAL}

Scaled/extrapolated acoustic data showing the variation in ejector exit velocity with penetration at test point 16 are presented in Figure 191. LV results for the same conditions and configurations are shown in Figure 192. The 85% penetration mixer is considerably noisier than the 92.5% and 100% designs. It can be seen that the average exit velocity for this mixer is considerably higher, resulting in the increase of the low-frequency noise seen in Figure 191. The midfrequencies are also elevated, which is believed to be a consequence of the profile characteristics (see Subsection 5.6.2.1). The 85% penetration mixer shown here gave the best aero performance of the Gen 2.0 mixer series, but the trade between thrust and acoustics was unfavourable from a system standpoint; thus, 92.5% penetration was selected as the best compromise.

Conclusions – Analysis of the data taken over the course of the Gen 2.0 test leads to the following conclusions.

SAR Effects

- Increasing the SAR increases the pumping of the ejector and in general leads to a lower ejector exit velocity and a more uniform velocity distribution.
- The lower ejector exit velocity from a higher SAR reduces the external jet noise component of the noise spectra but tends to increase the internally generated noise component due to the increased mixing.
- If the extra internally generated noise resulting from a higher SAR is not sufficiently attenuated by some mechanism, such as increased ejector length or extra treatment, the noise benefit resulting from reducing the jet exit velocity may be lost. A proper balance between internally and externally generated noise is extremely important.
- Increasing the SAR tends to delay the onset of supersonic operation and soften the transition to supersonic mode.

Chute-Shape Effects

- The NRA shaped chutes generate slightly lower EPNL values compared to the aero shaped chutes. Spectrally, there is little difference in the lower frequency noise and an increase in high-frequency noise for the aero chutes compared to the NRA chutes. The high-frequency noise increase leads to higher EPNL values due to the Noy weighting.

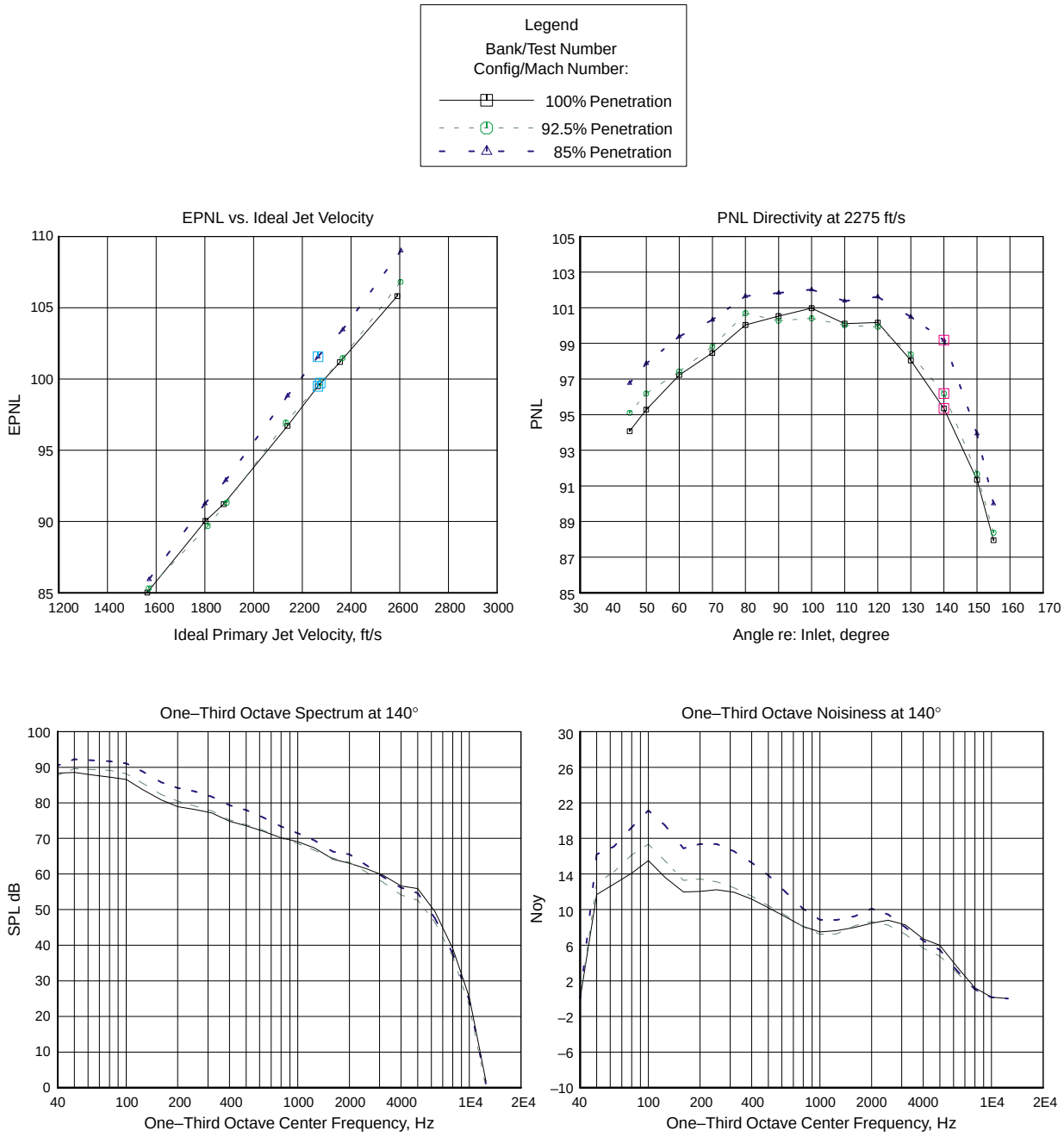

Figure 191. Variation of Acoustic Signature with Chute Penetration: MAR 0.95, 120-in Ejector, 5/9 Treatment

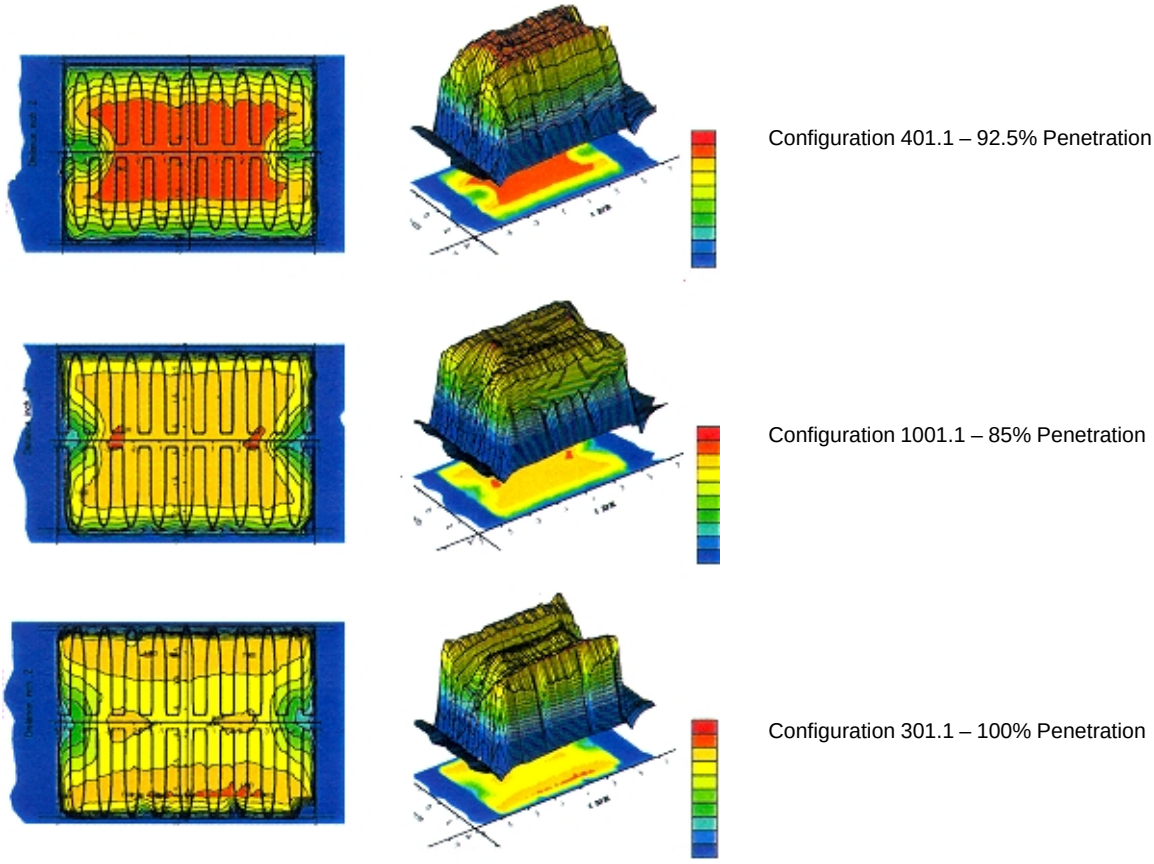

Figure 192. Variation of Ejector Exit Plane Axial Velocity with Chute Penetration: MAR 0.95, 120-in Ejector, TP 16

- Pumping for the aero shaped chutes is higher than the NRA shaped chutes. However, since the increased pumping is due to a higher efficiency chute design rather than an increase in SAR, the mixed exit velocity actually stays the same or increases slightly for the higher pumping mixer. As a result, no benefit in external noise generation is gained by the higher pumping. Internal noise increases due to the higher pumping.
- Increased pumping does not necessarily ensure a reduced exit velocity and a corresponding noise benefit. While increasing the pumping through a SAR increase shows a noise benefit, increasing the pumping through higher efficiency (such as chute shaping) does not show a noise benefit because of the increase in the mixed exit velocity for the higher efficiency chutes.

Penetration Effect

- The acoustic performance of the 100% penetration mixer is slightly better than that of the 92.5% penetration mixer due to decreased low-frequency noise resulting in a smaller duration correction for the EPNL calculation. The acoustic performance of the 85% penetration mixer is approximately 2 dB higher than the other comparative mixers.
- While the 100% penetration mixer shows reduced low-frequency noise, it also shows an increase in high-frequency noise that tends to increase the peak PNL values.

- The pumping of the 85% and 92.5% penetration mixers is approximately equal, with the 100% penetration mixer showing lower pumping levels.
- Velocity profiles show that the 85% penetration mixer has extremely poor mixing characteristics and has a large region of high-speed flow at the center of the ejector and a layer of low-speed flow next to the ejector boundaries. The 100% penetration mixer has the lowest exit velocity at the ejector center point but has more of an inverted profile with regions of high-speed flow along the ejector flaps.

Chute Number Effects

- For the three chute counts studied, the 20-lobe mixer is slightly quieter than the 24-lobe mixer, and the 16-lobe mixer is approximately 2 EPNdB higher than either of the higher lobe count mixers. The increased noise from the 16-lobe mixer is due to elevated midfrequency range noise usually attributed to premerged-type noise.
- For the range investigated, there is no discernable change in the characteristic frequency of the noise field as the lobe count is increased and the chute length scales are decreased.
- LDV data show that the 16-lobe mixer has poorer mixing characteristics than the 20-lobe mixer.
- Changing the lobe count from 16 to 24 appears to have little effect on the ejector pumping or axial flap static pressure distribution.

Chute Alignment Effects

- At 100% penetration and 5/9 treatment, there is only a small noise benefit observed from the staggered chutes. This is in contrast to early Gen 1.5 NRA staggered-chute data. The small noise reduction is attributed to reduced midrange frequency SPL providing a small beneficial duration correction. There is virtually no difference in corrected pumping for these configurations.
- At full treatment, the 100% penetration staggered chute shows more significant noise reduction compared to the 92.5% penetration aligned chute. Some of the noise reduction results from reduced low-frequency noise attributed to the difference in chute penetration. Additional noise reduction in the midrange frequencies is attributed to the chute stagger.
- Even though the 100% penetration staggered chute had less pumping compared to the 92.5% penetration aligned chute (presumably because of the penetration difference), there is still evidence of increased high-frequency noise due to the chute stagger.
- These data show a trend that the staggered chutes can reduce midfrequency noise — which can translate into a lower duration correction on the EPNL calculation.
- Minimal effects from the chute stagger are seen in the pumping and flap axial static pressure distribution when both the staggered and aligned chutes have 100% penetration.

MAR Effects

- For the SAR 2.5 NRA shaped chutes (Mixer 2) and the SAR 2.9 aero shaped chutes (Mixer 8) with a 5/9 treated ejector, decreasing the MAR from 0.95 to 0.90 generally reduces the EPNL. The effect was much stronger for the SAR 2.9 mixer than for the SAR 2.5 mixer.
- When the SAR 2.9 configuration was treated over the full ejector length, the additional treatment provided enough additional suppression for the MAR 0.95 case to make the EPNL approximately the same as for the MAR 0.90 case.

- Reducing the MAR from 0.95 to 0.90, due to the decreased exit area, reduces the pumping and slightly increases the mixed exit velocity relative to the ideal jet velocity.
- For Mixer 2 and Mixer 8, the reduced pumping and increased exit velocity serve to reduce the high-frequency (internally generated noise) at all power settings and increase the low-frequency (externally generated noise) at low power settings. It is possible to attenuate the additional internal noise generated by the higher MAR using additional acoustic lining.
- Data from the SAR 2.5 aero shaped chutes (Mixer 4) do not follow similar trends and show the MAR 0.90 EPNL to be slightly higher than the MAR 0.95. In general, the spectra levels for the MAR 0.90 setting are higher over most of the frequency range.
- As the MAR is decreased, the transition from subsonic ejector operation to supersonic ejector operation is shifted to higher pressure ratios.

Ejector Length Effects

- For the fully treated ejector case, increasing the ejector length from 120-in FS to 160-in FS decreases the EPNL by approximately 2 EPNdB over the whole velocity range.
- For the hard-wall ejector case, increasing the ejector length from 120-in FS to 160-in FS decreases the EPNL by 0.5 to 1.0 EPNdB.
- Increasing the ejector length decreased the nozzle pumping.
- Increasing the ejector length did not have a significant effect on the axial flap static pressure distribution.

Treatment Effects

- The true hard-wall lining has the highest EPNL of any of the liner configurations. The perforated hard-wall lining has levels 1 to 1.5 EPNdB below the true hard wall. Therefore, when analyzing the effect of treatment, it is important to know the details of the reference hard-wall geometry.
- All treatments show similar spectral levels at low frequencies. At mid to high frequencies, there are significant differences between the true hard wall, perforated hard wall, and open-cavity configurations. There is much less spread between the three bulk absorbers. Of the three bulk absorbers, the 200-ppi SiC showed the lowest SPL levels over the internal frequency range.
- The true hard wall had the highest pumping levels of any liner configuration, due to the smooth surface. The pumping of the perforated hard wall was several points lower than the true hard wall and explains the lower internal noise associated with the perforated hard wall. The bulks had similar levels of pumping, with the 200-ppi SiC pumping slightly more than the other two followed by the 100-ppi SiC and then the T–Foam.

Face-Sheet Porosity Effects

- The 37% POA face sheet shows lower EPNL levels by 0.5 to 0.75 EPNdB over the entire power range compared to the 21% POA facesheet.
- There was no significant difference in the corrected pumping values between the 37% POA face sheet and the 21% POA.

Azimuthal Effects

- Both for sideline and for cutback power settings, EPNL calculations show a maximum at $\Phi = 90°$ and a minimum around $\Phi = 30°$.
- At sideline, there is a 2.6-EPNdB difference between the maximum and minimum values.

In General – The Gen 2.0 test series in Cell 41 provided useful design information for future HSCT mixer/ejector nozzle designs. These data have shown the complexity of the noise issues related to the HSCT nozzle. Several noise sources combine to produce the overall EPNL, and changes in any one of the sources can significantly affect the final result. Isolating any single effect of a given design parameter is extremely difficult due to the complexity and integration of the nozzle subsystems. Changes in one parameter can produce subtle changes in other parameters that affect the aeroacoustic performance. As a result, evaluating a concept based solely on EPNL can be misleading since the EPNL gives no information as to how the noise is generated. Obtaining a proper balance between the internal and external noise sources is extremely important for the mixer/ejector system to provide the maximum possible noise suppression. As should be expected, the Gen 2.0 data show a strong correlation between the flowfield characteristics and the radiated sound field. For this reason, future tests should simultaneously evaluate both the flowfield and acoustics in order to understand fully how changes to the nozzle system affect both the aerodynamic and acoustic performance.

The Gen 2.5/2.5A Test Series

The Gen 2.5 and 2.5A Cell 41 test series were conducted to provide additional experimental data needed to assess the effects of different mixer design features such as hot or cold chute flow at the sidewalls and tabs attached to the chute trailing edges. Effects of external devices intended to reduce the externally generated jet noise were investigated, as was the effectiveness of different treatment areas. The test was divided between measurements to determine effects on the acoustic far field (including EPNL) and the acquisition of LV diagnostic data within the ejector (through glass sidewalls). The LV measurements provide mean and turbulent velocities throughout the ejector, starting near the exit of the mixer chutes and continuing to just downstream of the nozzle exit. In addition to the flowfield details, these measurements provide a means to determine the mixing effectiveness of the different mixer design features (via the “degree of mixing” parameter developed by Stone, for example, see Subsection 5.6.2.1).

Test Objectives – The following were the exit criteria for the Gen 2.5 and Gen 2.5A tests in Cell 41: determine far-field EPNL values and measure the flowfield of key mixer configurations for nozzle configuration development

- hot versus cold sidewalls — acoustics and internal LV
- vortex generators applied to the mixing chutes — acoustics and internal LV
- chevrons and vortex generator ramps applied to the ejector exit — acoustics
- treated versus hard-wall flaps — acoustics
- staggered chutes (using mixer racks with hot and cold side walls) — acoustics

Test Procedure – This series involved 61 tests. All but eight included acoustic measurements; nine included laser velocimeter measurements. Test configuration variations comprised hot or cold sidewalls, four different mixer exit devices (or none), turning vanes within the secondary chute passages, two different ejector lengths (also glass sidewalls for LV) with and without three different exit devices, and hard-wall or treated (10 variations) flaps.

In contrast to the Gen 2.0 test series, only one fundamental mixer design was tested: #8 from Table 39. This mixer has full-width cold chutes at the sidewalls (Figure 190) that were presumed to have caused the “cold holes” seen in the LV results of Figure 192. A variant of this mixer was built for

the Gen 2.5/2.5A tests, designed to the same SAR, penetration and cold-chute count but with ½-width hot chutes at the sidewalls for a total of "18 and four halves" hot chutes. (This is closer to the chutes used in the Gen 1.0 and Gen 1.5 tests.) These two mixers were then identified as #8c (the original) and #8h (the variant).

Two tab (vortex generator) designs were tested on the chutes. The first, "B" tabs, were larger than the "A" tabs shown in Figure 193. They were installed two to a chute, at about the midheight. They demonstrated that it was possible to affect the noise signature by some type of device at the chute exit, but the trade between noise and performance was not acceptable for this design.

(a) Location of "A" Tabs. "Reduced A Tabs" Shown by Circles

(b) Notches Cut in Chute Trailing Edge

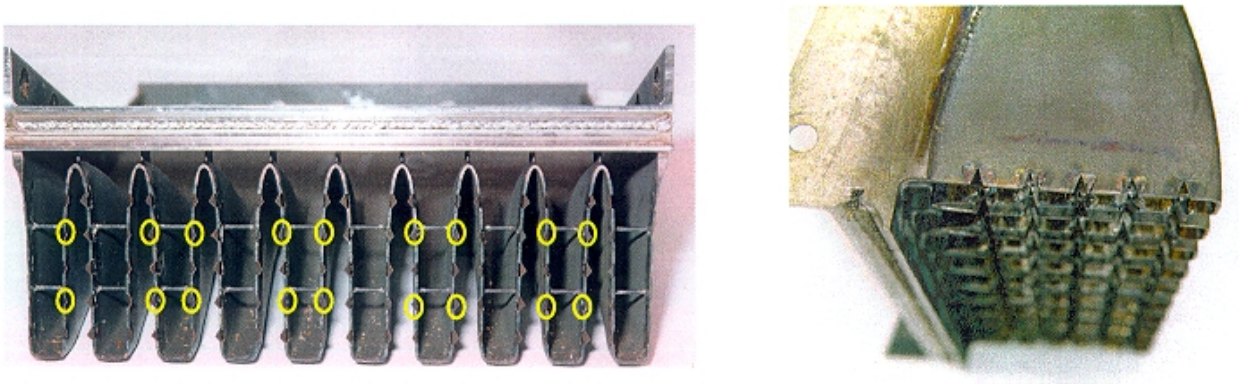

Figure 193. Examples of Modifications Made to Chute Trailing Edges to Promote Rapid Mixing While Minimizing Thrust Loss

Figure 193 also shows the three further modifications made to the chute trailing edges. "A" tabs — smaller than "B" tabs, with 10 tabs per chute — were located as shown in Figure 193(a), with "notches" — triangular cuts into the trailing edge at the same location as was previously occupied by the "A" tabs shown in Figure 193(b). A variation on the A tabs, the "reduced" A tabs, whose locations are shown by the yellow circles in Figure 193(a) was also tested (see Subsection 5.9.2.1).

Figure 194 illustrates the difficulties inherent in testing these rapid-mixing devices. Shown here are the effects on EPNL of installing and removing the A tabs — and in the process modifying the flowpath. It is believed that the benefit that remained after the tabs themselves were removed (by grinding them back to the trailing edge) was a result of the tack-weld process used in attachment. Some of this can be seen in Figure 193(b), where the presence of weld metal in the secondary passage is visible. It may well be that introducing disturbances into the secondary (cold) stream provides the most efficient means for enhancing the mixing process and reducing the noise.

Also shown in Figure 194 are results from testing the "reduced A tab" configuration, using only those tabs identified with circles in Figure 193. This configuration followed the second installation of "A" tabs, just prior to removal of all the tabs. It is hard to distinguish between "reduced A tabs" and "mixer after two sets of A tabs have been installed and removed" in Figure 194, but close inspection reveals a consistent benefit with the reduced A tabs — especially at 25° (Figure 194a).

Figure 195 shows two sets of data acquired with notches cut in the trailing edges of the mixer (8h) after both the first and second installation of the A tabs. The intent behind this test was to investigate use of a device other than tabs with which to generate a disturbance at the chute trailing edge,

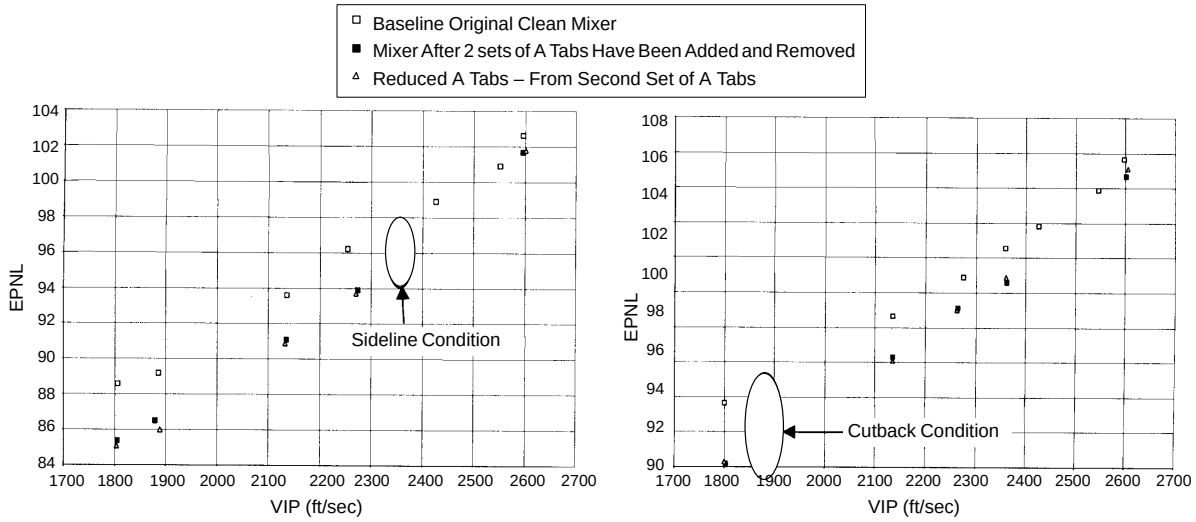

(a) Azimuthal Location (Φ) = 25° (b) Azimuthal Location (Φ) = 90°

Figure 194. Effect of A Tabs and Reduced A Tabs on EPNL at Sideline and Cutback Conditions

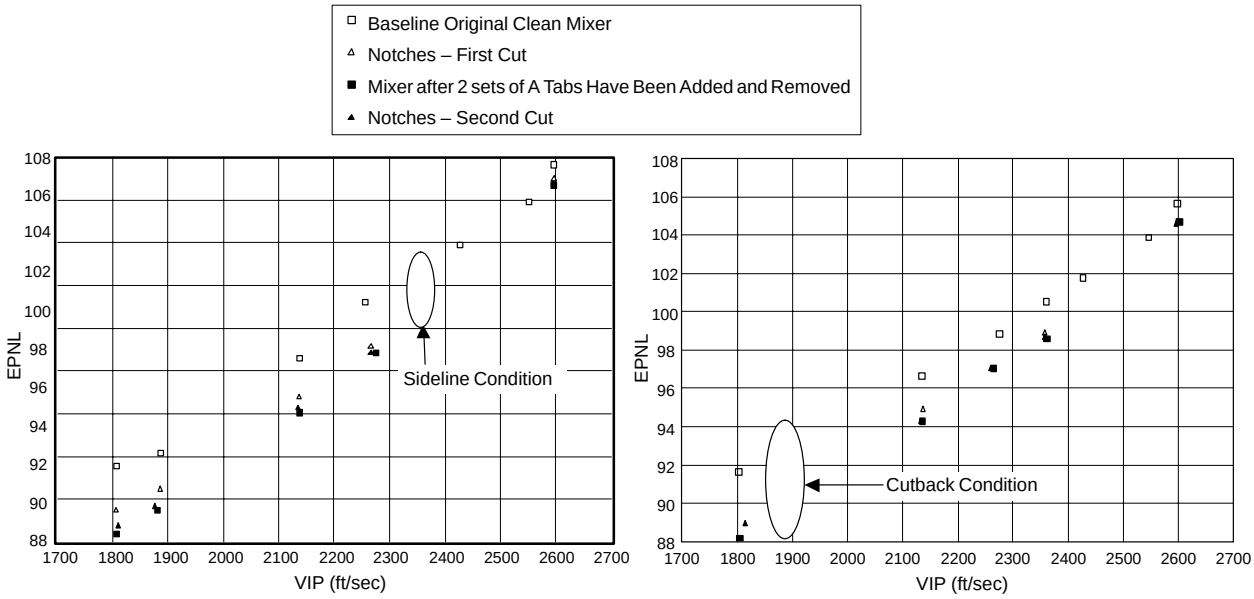

(a) Azimuthal Location (Φ) = 25° (b) Azimuthal Location (Φ) = 90°

Figure 195. Effect of Notches at the A Tab Locations

hopefully to provide a better trade in terms of thrust versus noise. Again, the effects of tab installation and removal complicate the results, leaving the tantalizing prospect of benefits that are unquantifiable due to the techniques employed. As a direct result of these observations, the methods employed in attaching tabs to the Gen 3.0 mixer (described in Subsection 5.7.1.6) were modified to ensure minimal undesired disturbance of the flow.

Figure 196 illustrates the complexity of the interdependence of thrust and noise at the P5 and P6 metric sideline and cutback conditions. Included on these plots are the PTC (vintage January 1998) airplane TOGW sensitivities to noise and performance. From these plots it is possible to gain an appreciation of which combination of noise benefit and performance degradation gives the best trade in terms of the airplane performance. It is shown here that reduced A tabs and notches show the most promise relative to the original clean (unmodified) mixer, while the resultant effects of tab installation and removal (identified as "Modified Mixer 8h Baseline) pose lingering questions. (For instance, why do we get this noise reduction? What are the mechanisms involved?) It should be mentioned that the performance information shown was inferred using the GEAE Cell 41 procedure, rather than measured directly.

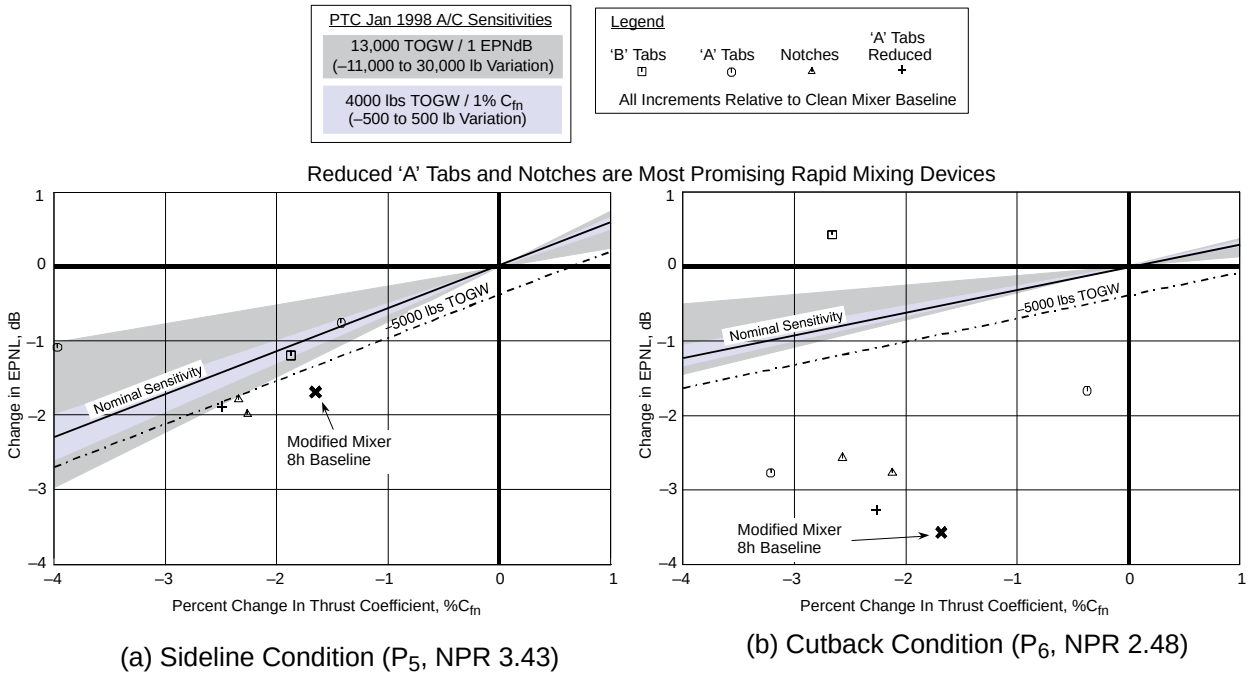

(a) Sideline Condition (P_5, NPR 3.43)

(b) Cutback Condition (P_6, NPR 2.48)

Figure 196. Noise versus Performance Trades with TOGW Impact

Flowfield Data – An important part of this test series was the acquisition of flowfield data. Given that the noise-generation process is related to the flowfield characteristics, any attempt to understand the effects of devices intended to change the noise through modification of the mixing must include measurements of that process. To this end, the sidewalls of the NRA model were replaced with laser-quality glass, the seeding system used for LV data acquisition was upgraded, and measurements were made within the ejector under normal operating conditions. Figure 197 shows the internal LV set-up. With this arrangement, it has been possible to take data in both the axial and transverse planes.

A good example of the flowfield information that has been obtained and its use in the analysis of the acoustic data is found in the data taken for the B tabs. Figure 196 shows that the B tabs gave just over 1 EPNdB benefit at sideline (25° azimuthal location) while increasing noise by about 0.5 EPNdB at cutback (90°). It can be seen from the contours of Figure 198 that the effect of the B tabs on the axial velocity has been to preserve a slug of fast-moving fluid in the central region of the ejector. The internal data (taken just downstream of the chute exit) show that the tabs have trapped the primary flow in the central region, and this persists to the ejector exit. At the exit, it can be seen that the tabs have forced the primary fluid towards the sidewalls — eliminating the "cold hole" that is otherwise a feature of these designs (see Figure 192). In terms of the acoustic data, both at sideline and at cutback, the effect of this central portion of hot, high-velocity fluid is to raise the low-frequency levels in the aft portion of the directivity pattern. At sideline, this increase is more than offset by a decrease in the high-frequency noise, leading to a net decrease in EPNL. At Cutback there is much less impact on the mid- to high-frequency portions of the spectrum, and the increase in low-frequency noise at the aft angles (and hence duration) leads to the increase in EPNL.

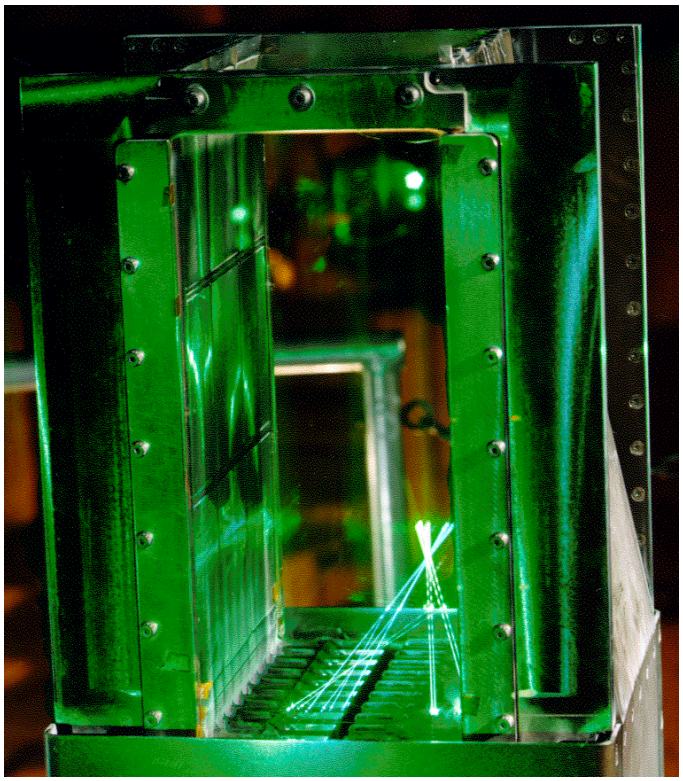

Figure 197. LV Setup showing Ejector with Glass Sidewalls

Further insight into the effect of the B tabs on the primary and secondary flow, and the mixing process, can be gained by looking at the velocity components in the transverse plane — the plane normal to the axial direction.

Figure 199 shows that without the B tabs (the clean mixer configuration), a large stirring motion is set up as a result of the secondary flow being directed inward and the primary outward. The tabs act as miniature delta wings; they generate their own vortex pattern, and the net result of the interaction of these two circulation systems can be seen in Figure 199. The impact of the tabs appears to be to reinforce mixing between the primary and secondary streams in the outer portions of the flow, while reducing it in the inner. As was seen in the axial velocity contours of Figure 198, the tabs act as a barrier, constraining the primary fluid to remain in the inner portion of the ejector.

Treatment Location Investigation – The penalty associated with reducing externally generated noise by means of a mixer/ejector nozzle is in the acoustic treatment required for the interior of the ejector. A major effort under the CPC program, in association with EPM, has been the development of a liner design methodology (Subsection 5.8.1) aimed at the design of a liner with material properties that: (1) will provide the acoustic attenuation required, (2) is capable of withstanding the

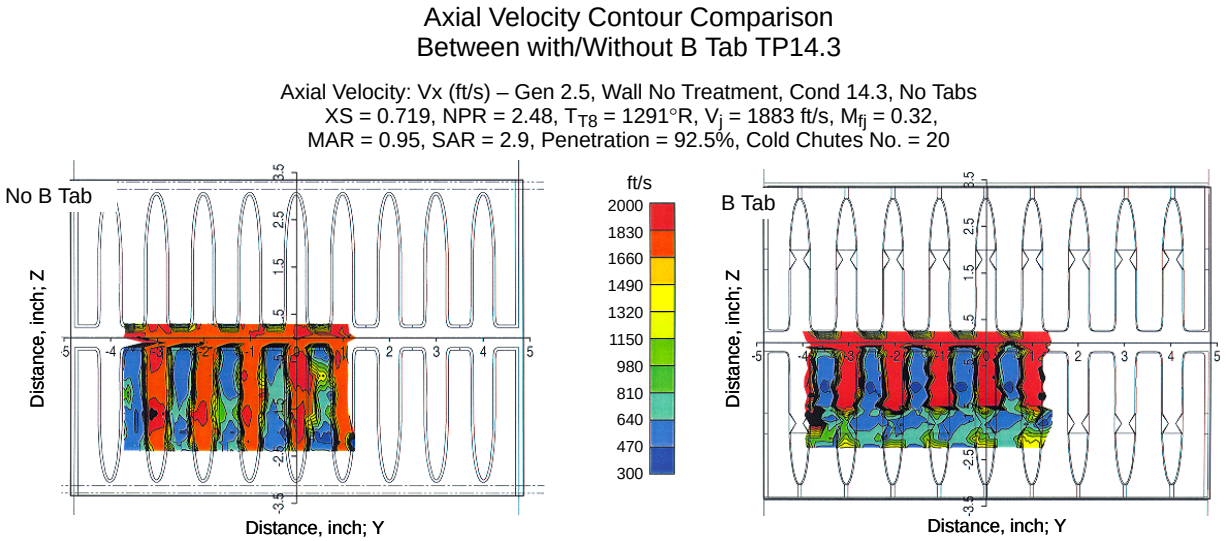

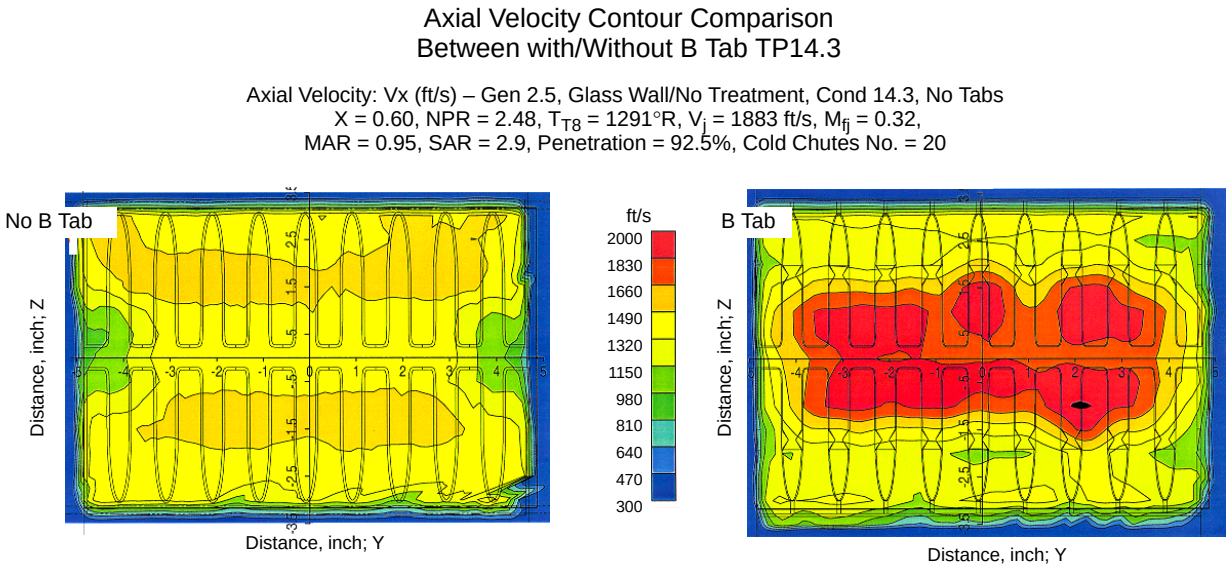

Figure 198. Axial Velocity Contours Showing the Effects of B Tabs on the Flowfield, External and Internal to the Ejector

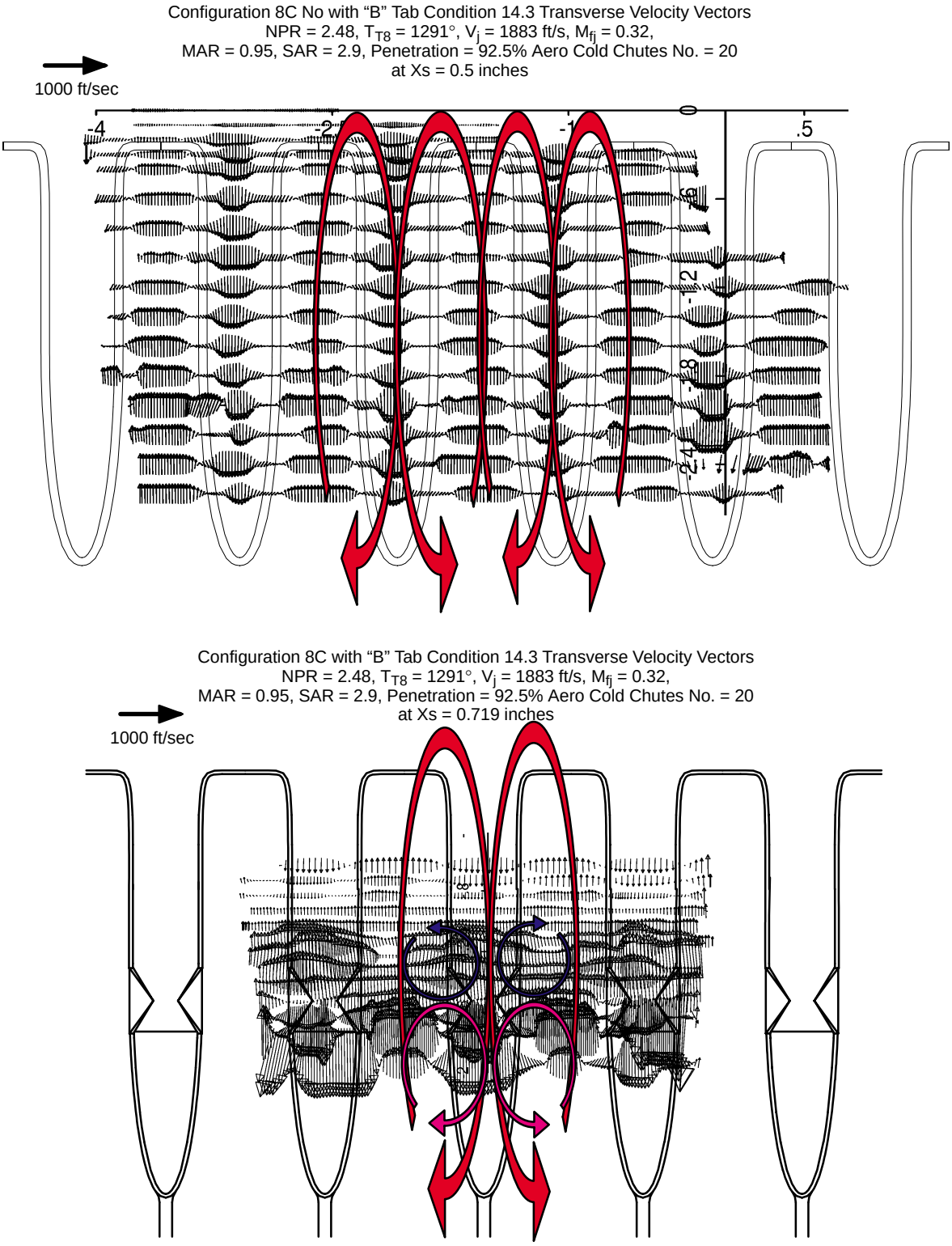

Figure 199. Velocity Vectors in the Transverse Plane just Downstream of the Chute Trailing Edge, Showing the Effects of B Tabs on the Circulation Patterns of the Mixing Process

environment within the ejector (not only at community noise conditions, but also at cruise), and (3) adds minimal weight.

Weight can also be reduced by judicious location of the liner. There is little use in going to great pains to install treatment in a region of the ejector where it is ineffective. Previous tests (Gen 1.5, Subsection 5.7.1.2, Gen 2.0, earlier in this subsection) attempted to simulate the "real" nozzle environment, by placing treatment only in areas that would be treatable in the full-scale design. In this test, the effects of treatment location were investigated systematically using the segmented treatment trays to adjust the location as shown in Figure 200.

	Mixer Exit					Ejector Exit		
Configuration	Tray 1	Tray 2			Tray 3	Tray 4		
		Sect. 1	Sect. 2	Sect. 3		Sect. 1	Sect. 2	Sect. 3
832.1	Treated							
832.999	Treated							PHW
832.99	Treated						PHW	
832.88	Treated					PWH		
832.77	Treated					Hard Wall		
832.11	Hard Wall	Treated						
832.33	Hard Wall	PHW	Treated					
832.55	Hard Wall	PHW			Treated			
832.66	Hard Wall					Treated		
842.1	Hard Wall							
832.101	Treated							
832.111	Hard Wall	Treated						
832.331	Hard Wall	PHW	Treated					
832.441	Hard Wall	PHW		Treated				
832.551	Hard Wall	PHW			Treated			
832.221	Hard Wall				Treated			
842.101	Hard Wall							

Figure 200. Schematic of Incremental Liner Configurations Tested

In Figure 200, PHW refers to "perforated hard wall." Sheet metal is held in place behind the perforate face sheet. It has been demonstrated that some attenuation is achieved by the face sheet alone. Hard wall refers to solid metal trays.

The results shown in Figure 201 are in terms of total EPNL. Based on this metric, it can be seen that, except for cutback with "B" tabs, there is little gain in attenuation by increasing the treatment from 80% to 100%. Previous tests had demonstrated that, on this basis, treatment near the mixer was ineffective. It will be recalled from Subsection 5.8.1.1 (and from earlier in this section) that the balance between internally and externally generated noise is of extreme importance. In Figure 201(b) for instance, it is tempting to conclude that treating the aft-most portion of the ejector gives very little additional benefit. What is needed here is to examine the noise components (Subsection 5.6.2.1) in detail to establish whether the treatment is ineffective or whether the external sources are masking additional treatment benefit. Again, it is currently assumed that the most forward treatment is ineffective. This may indeed be so or it may be that the effects are masked by other components.

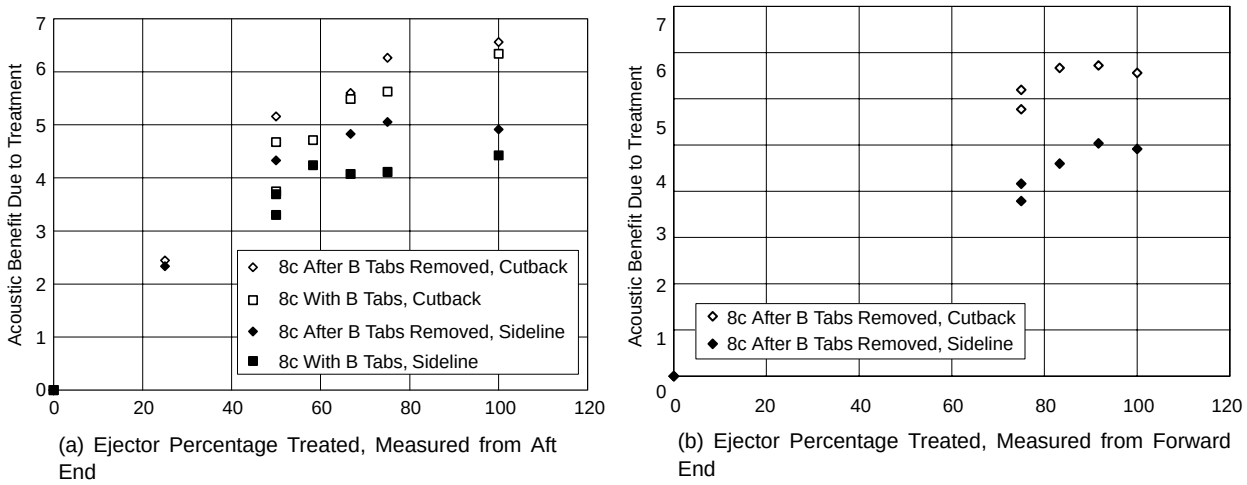

Figure 201. Results of Incremental Liner Testing in EPNdB Relative to Full Hard Wall for 160-in Ejector

One reason for conducting this test with B tabs installed was to investigate whether the presence of the rapid-mixing device would bring the effective start of the treatment further forward, as is assumed in the system study projections. (It will be recalled that B tabs did not appear to encourage mixing throughout the flow field however, so the above results are not necessarily surprising).

The final set of data collected was in support of the liner technology program (Subsection 5.8.1.1). The methodology is developed assuming an infinitely long duct treated on two facing sides. Here, two configurations were tested: treated flaps with hardwall sidewalls and vice versa.

Summary of Results – The main acoustic results are summarized below. Except where noted, these refer to the "160-in" ejector configuration.

- With the 120-in, fully treated ejector, the ½-width hot sidewalls of mixer 8h demonstrated about 1.2-EPNdB improvement over mixer 8c. At 160-in, on the other hand, 8h showed a slight increase in acoustic level relative to 8c.
- B tabs on mixer 8c provided 1 to 2 EPNdB noise reduction at sideline conditions, but very little at cutback conditions (Figure 196).
- A tabs on mixer 8h showed approximately 2 to 3 EPNdB noise reduction at cutback and 1 EPNdB reduction at sideline (Figure 196).
- Reduced A tabs on mixer 8h provided over 3 EPNdB noise reduction at cutback and almost 2 EPNdB noise reduction at sideline conditions (Figures 194 and 196).
- Notches on mixer 8h resulted in 2.5 EPNdB reduction at cutback and 2 EPNdB reduction at sideline conditions (Figures 195 and 196).
- Installation of the tabs resulted in disturbances in the secondary sides of the chutes and showed some inherent noise reduction and performance impact.
- Turning vanes installed in mixer 8c showed a modest acoustic benefit, likely due to less than precise installations and a decrease in pumping.
- Chevrons and vortex-generating ramps used separately at the exit of the ejector provided 1 to 1.5 EPNdB of noise reduction. Approximately half of the benefit has been shown to result from

the extra hard-wall shielding inherent in these deviceChevrons and ramps used together cancel out much of the benefit seen individually.

- Treatment on the flaps provides most of the suppression of noise radiated to the 90° microphone location. At 25°, sidewalls and flaps provide equal suppression.
- The first two treatment segments in the most forward tray do not appear to provide measurable noise suppression in terms of overall EPNL. Figure 201(a) is a plot of the acoustic benefit due to treatment as a function of treatment area location, with treatment removed from the forward end of the ejector (near the mixer exit). Figure 201(b) shows the same information with treatment removed from the aft end of the ejector.

The flowfield results are summarized below.

- Half-width hot sidewalls eliminated the cold holes seen with the full-cold-width sidewalls and resulted in a more uniform exit flowfield.
- Ejector length, 120-in versus 160-in (full scale) had very little influence on the ejector exit flowfield.
- B tabs on mixer 8c promoted mixing around the periphery of the jet plume and restricted mixing in the center of the plume, resulting in a hot, high-velocity slug of flow. Figure 198 compare the flowfield at the ejector exit with and without the B tabs.
- A tabs on mixer 8h resulted in a much smaller region of hot, high-velocity flow in the center of the jet plume.
- Reduced A tabs and notches on mixer 8h resulted in a much more mixed flowfield.

General Comments

- Mixer 8h with “reduced A tabs” and with notches has given the first two configurations tested during the CPC contract that have satisfied the nozzle P5 and P6 metrics, at sideline and cutback. This has been achieved with tolerable thrust loss and should be regarded as a major accomplishment.
- The Gen 2.0, 2.5 and 2.5A test series have given us considerable insight into the complex relationships between the flowfield and associated acoustics.
- Relative effects of SAR, ejector length, penetration, chute number, treatment type and location (to name a few) have been investigated.
- Preliminary investigations of rapid-mixing devices have demonstrated considerable potential for noise reduction and this can be achieved in a favourable trade (on a system basis) with performance.

5.7.1.5 Gen 2.5 HAM Acoustics and Aeroperformance Test in JNL

Previous mixer/ejector tests were performed with uniform flow provided to the mixer nozzle. In a real engine environment, the fan and core streams are mixed just upstream of mixer/ejector mixer; thus, flow entering the mixer/ejector mixer is not likely to be completely uniform. The main objective of this test series was to assess the effect of this nonuniformity on the acoustic and aerodynamic performance of a mixer/ejector nozzle.

The 1/7th scale hot acoustic model (HAM) was tested in the LSAWT of the NASA–Langley Jet Noise Laboratory (JNL) in the Spring of 1998 as part of the HSR Program CPC Gen 2.5 nozzle testing. The main objective of these tests was to assess the acoustic and aerodynamic performance of the HAM nozzle for mixed and unmixed fan/core flows.

The configuration of the HAM model tested in the LSAWT included a fan-to-core area ratio of 0.4, a mixer area ratio of 0.95, and an equivalent full-scale ejector length of 120 in. The standard configuration included mixer 8C and fully treated SiC ejector walls and was tested at a wind tunnel Mach number of 0.32. In addition to the standard configuration, testing was performed with mixer 4, a hard-walled ejector, and at a Mach number of 0.10. For simulating the actual engine flow, the separately controlled fan and core temperatures and pressures in the model were set at the appropriate cycle conditions. For simulating uniform, mixed-flow conditions in nearly all the HSCT related aero/acoustic testing, the fan and core streams in the model were both set to equivalent mixed total pressure and temperature conditions. The dual-stream jet engine simulator three axes force balance along with the LSAWT's 28-microphone sideline array allowed simultaneous thrust and acoustic measurements. Since the facility microphone array was fixed, different orientations for acoustic measurements were obtained by model rotation. Results given here are for orientations having angles between the nozzle major axis and the microphone direction of 40°, 25°, and 90°. Mixer 8C was tested at 40° followed by mixer 4 at 25°. Ejector inlet turning vanes were then installed in the model, and mixer 8C was tested at 25°, followed by both the treated and hard ejector walls at 90°.

The free-jet nozzle of the LSAWT has exit dimensions of 4.7×4.7 ft. It is shown in Figure 202 with the HAM model mounted vertically, which corresponds to the 40° acoustic orientation. The forward

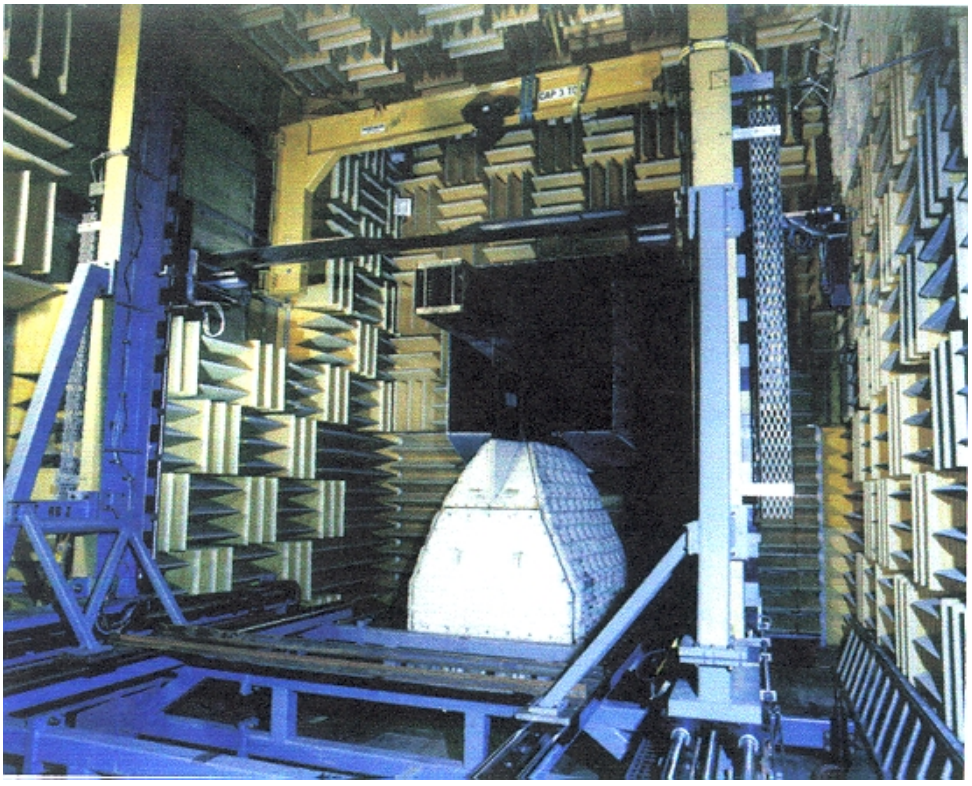

Figure 202. Photograph of HAM Nozzle Without Ejector Box in LSAWT

portion of the sideline acoustic array, positioned 11.5 ft from the tunnel centerline, can be seen in the top right of the photo. (In the photograph the ejector box has been removed from the model to permit pressure and temperature measurements close to the exit of the mixer using the large metal traverse seen in the photo. The traverse was removed from the test chamber, and all walls were covered with acoustic wedges for the data presented here.)

Note that for the 40° orientation shown in Figure 202, the major axes of the HAM nozzle and ejector inlets are parallel to the model support strut. However, for the 25° case, which represents the takeoff acoustic orientation, the model is tilted so the angle between the ejector inlet major axis and the vertical strut is changed from 0° to 15°. For the 90° case, representing the cutback orientation, the strut angle is 50°. Interference from the strut may be a strong influence on the orientation differences in the secondary airflow and nozzle performance discussed below.

Figures 203 through 207 present comparisons of six measured parameters for the 3770.60 engine cycle. These parameters are the effective perceived noise level (EPNL), the net thrust coefficient (C_{fnmix}), the ejector exit velocity (V_{mix}), the primary nozzle fuel and air mass flow (wpt), the ejector inlet secondary mass flow (ws), and the total ejector mass flow (wmix = wpt + ws). EPNL is plotted versus primary velocity (V_p), and is computed for standard day full-scale conditions at the certification sideline slant distance of 1634 ft at an aircraft Mach number of 0.32, with all appropriate acoustic corrections included except those for a distributed noise source. All other parameters are plotted versus primary nozzle pressure ratio (NPR). In all plots, darkened symbols represent unmixed fan/core flow and open symbols represent mixed flow.

Figure 203 compares results of different nozzle orientations for the mixed-flow conditions. Discussion of this and the following figures will concentrate on the region of the cycle line between 2.5 and 3.5 NPR, or 1900 to 2400 ft/s primary velocity, which is the region between cutback and takeoff operations. The EPNL in this region shows that the 90° data is as much as 2 EPNdB higher than the 25° and 40° data, indicating somewhat higher noise levels in the plane parallel to the major axis plane of the nozzle (that is, the cutback acoustic orientation). The C_{fnmix} results show a surprisingly significant decrease in nozzle performance as the orientation changes from 40° to 25° to 90°. As mentioned above, this decrease may be due to an increasing influence of the model strut on the flow into the ejector as the angle between the two increases, initiating a secondary flow degradation. This contention is supported in the lower plots, which show that although the primary nozzle mass is virtually the same for all orientations, there is a definite reduction in the secondary mass flow with increasing strut angle. The only physical difference in the model for the three orientations is the lack of ejector turning vanes in the 40° data. But since the inclusion of turning vanes would intuitively give the opposite result, that of higher thrust at the other two orientations, the influence of these vanes must be small.

Note that a similar behavior with nozzle orientation is seen for the unmixed flow data in Figure 204. Again, the cutback acoustic orientation is the noisiest, and the thrust coefficient decreases with increasing strut angle. However, at the 40° orientation there is no secondary mass flow increase over the 25° orientation, yet the thrust increase appears even higher than that for the mixed-flow case. This means that the computed mixed-flow velocity must be unusually high for this case, as is seen in the top right plot of Figure 204. The cause of these seemingly inconsistent data for unmixed flow at the 40° orientation is unknown.

The effect of mixed versus unmixed flows could be seen by overlaying Figures 203 and 204 but are best viewed from the remaining three figures. Figures 205 through 207 repeat both mixed and

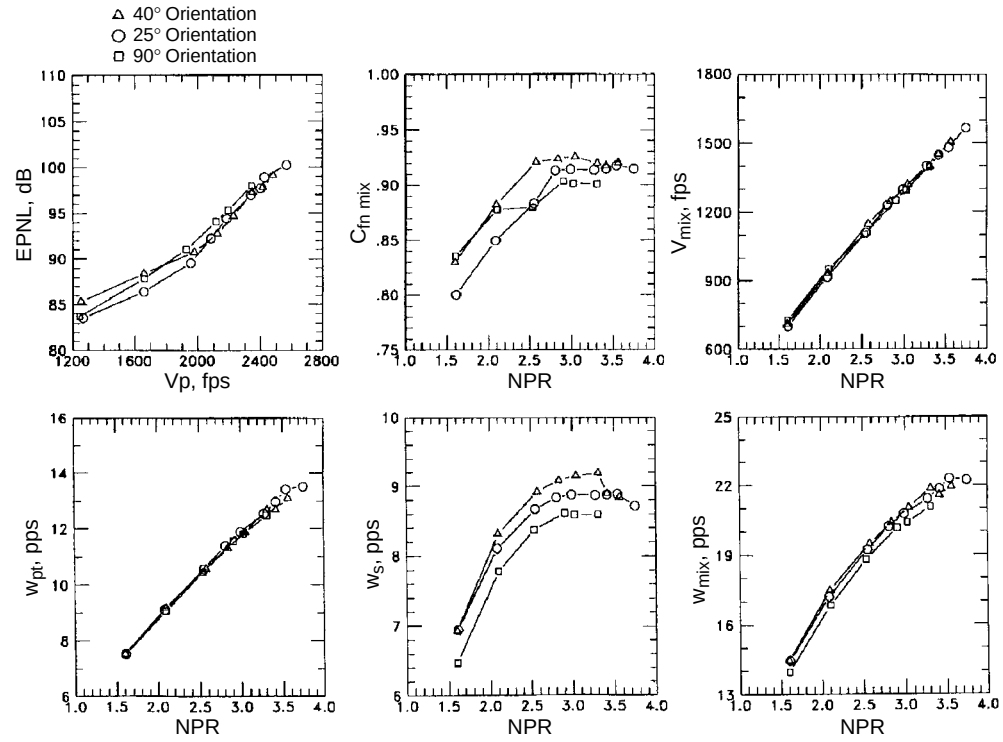

Figure 203. Mixed Fan/Core Flows for Acoustic Orientations of 40°, 25°, and 90° with Standard Configuration

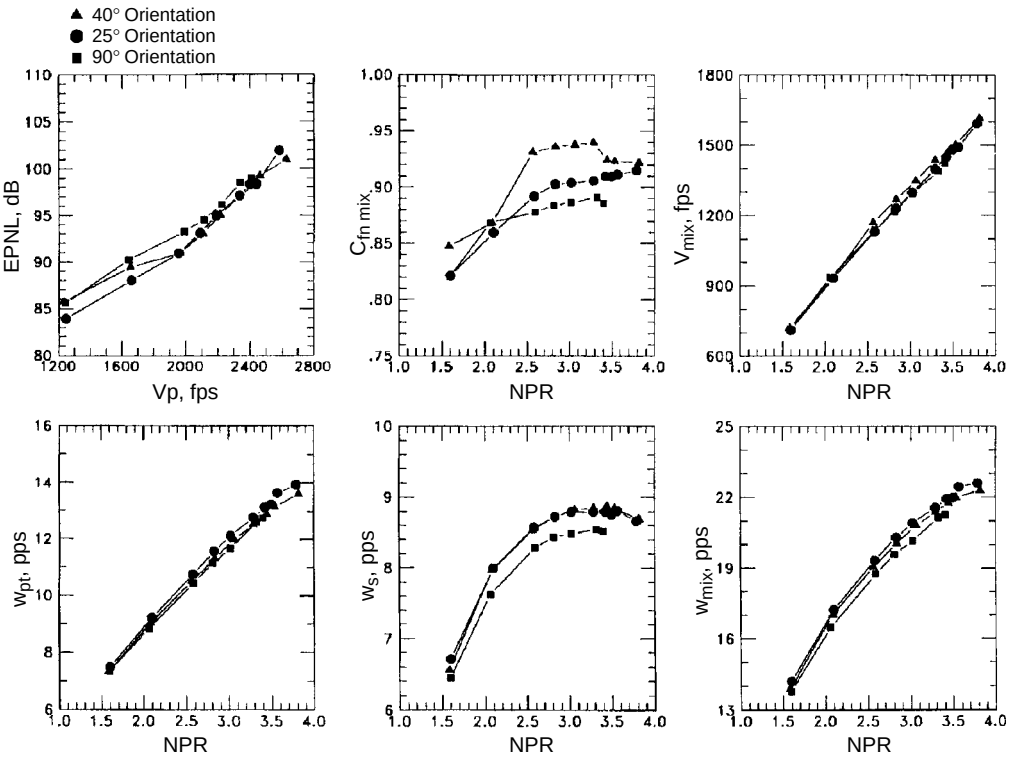

Figure 204. Unmixed Fan/Core Flows for Acoustic Orientations of 40°, 25°, and 90° with Standard Configuration

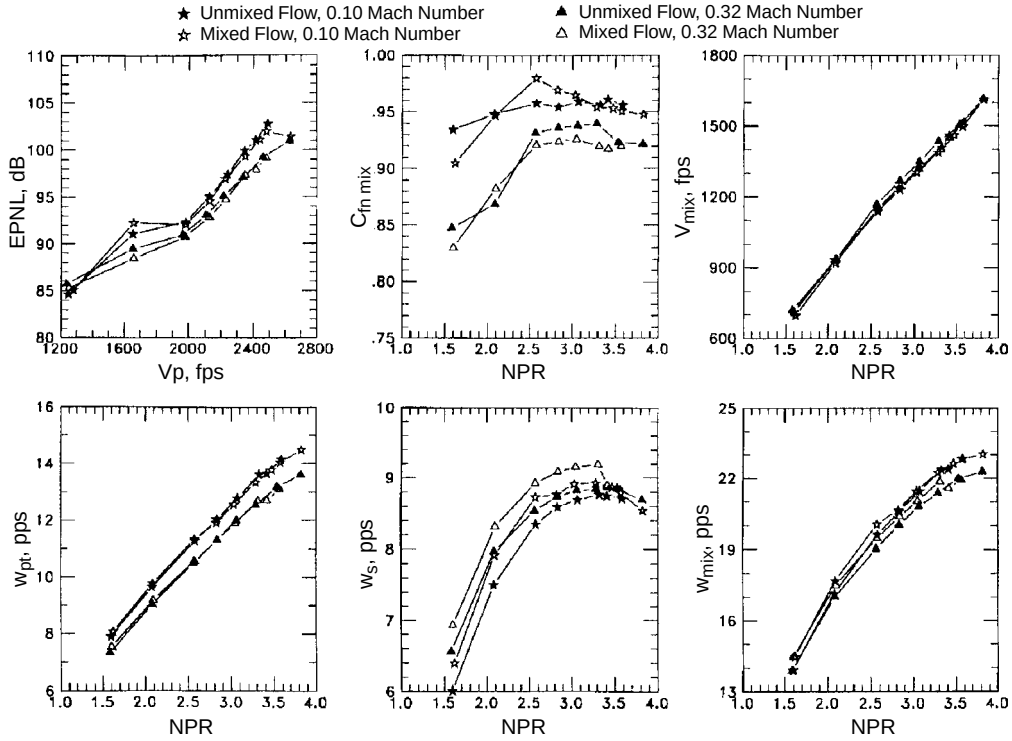

Figure 205. Mixed and Unmixed Fan/Core Flows at Mach Numbers of 0.10 and 0.32 and 40º Acoustic Orientation

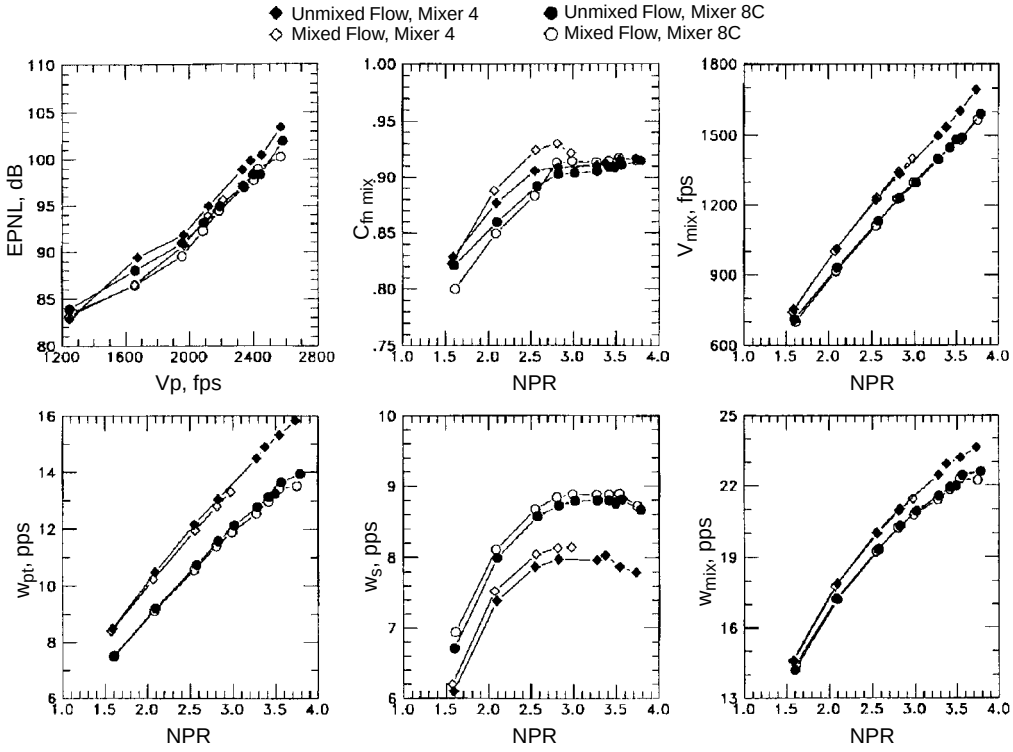

Figure 206. Mixed and Unmixed Fan/Core Flows for Mixers 4 and 8C at 25º Acoustic Orientation

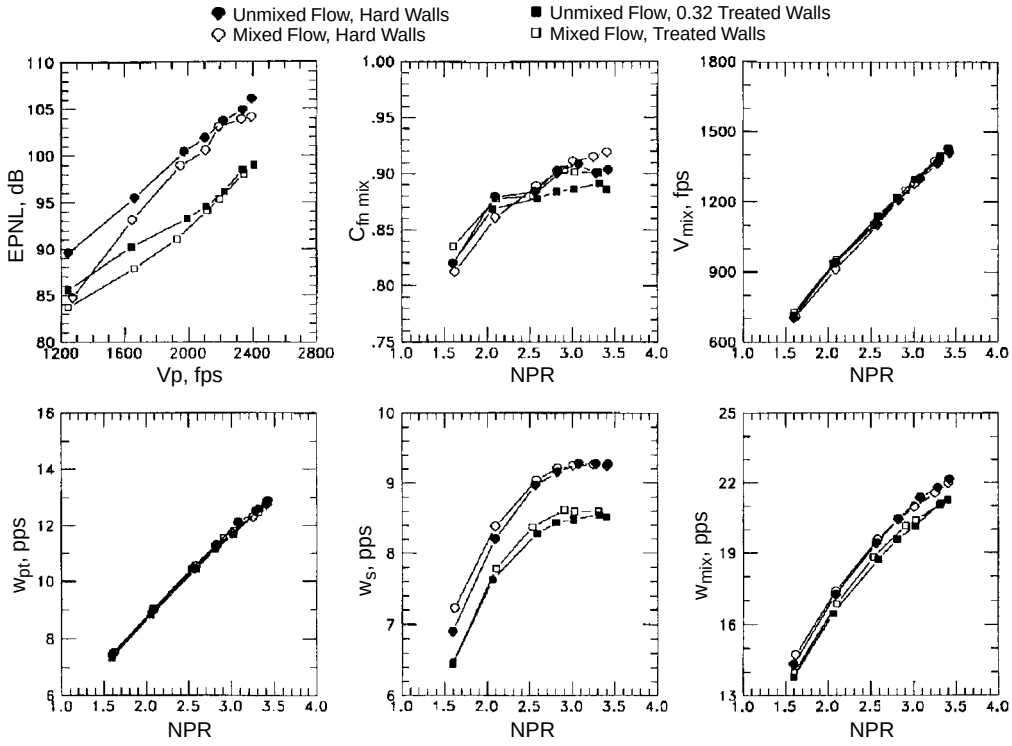

Figure 207. Mixed and Unmixed Fan/Core Flows for Hard and Fully Lined Ejector Walls at 90º Acoustic Orientation

unmixed data from Figures 203 and 204 at one of the three nozzle orientations. In addition, each of these three figures gives a comparison of either different tunnel Mach number, primary nozzle mixer, or ejector wall treatment. Figure 205 shows the 40° orientation data obtained at a tunnel Mach number of both 0.32 and 0.1, Figure 206 gives the 25° data for both mixers 8C and 4, and Figure 207 has the 90° data for both the treated and the hard-walled ejector. A discussion of the comparison of flow type will be given first, followed by a discussion of the other comparisons.

All the acoustic data in the region of interest for each of the six pairs of cycle line traverses given in Figures 205 through 207 show the unmixed flow (shaded symbols) to be between 0 and 2 EPNdB noisier than the corresponding mixed-flow (open symbols). Although (as per design) the primary mass flow are seen to be basically the same for both flow types, the mixed flow consistently induces a higher secondary mass flow than the unmixed flow. If, for a given primary mass flow, a higher secondary flow yields better C_{fnmix} (as expected from the physics and noted to be the case in the discussion of Figures 203 and 204), a higher thrust coefficient would be expected for the mixed flow. This is indeed the case for the data shown in Figures 205 through 207 for all but the one exception discussed previously.

The other comparison shown in Figure 205 is that of differing tunnel Mach number. The typical decrease of noise levels can be seen as the Mach number is increased from 0.10 to 0.32. Because the LSAWT is an in-draft facility, increasing tunnel Mach number results in the observed decrease in primary mass flow for a given NPR. However, because the thrust decrease measured by the force balance at the higher Mach number is larger than the thrust decrease due to lower mass flow, the net thrust coefficient shown in Figure 205 is larger at Mach 0.10 than at 0.32.

Figure 206 shows the effects of a larger mixer. Since mixer 4 is about 17% larger than mixer 8C, the larger proportion of hot primary air yields higher mixed mass flows and velocities. It also is about 2 EPNdB noisier than mixer 8C and has a somewhat higher thrust coefficient.

Figure 207 is a comparison of ejector wall treatment. As expected, the untreated walls give substantially higher noise levels, on the order of 7 EPNdB. However, the lower secondary mass flow induced by the treated-wall ejector yields lower values of net thrust coefficient.

In conclusion, testing of the HAM nozzle in the LSAWT shows that there can be a penalty of as much as 2 EPNdB due to incomplete mixing of the fan and core streams of a mixed-flow turbofan. There also appears to be a corresponding thrust loss, although one set of unmixed data indicates the opposite. Other results, all of which are in line with expectations, are that increasing either tunnel Mach number or ejector acoustic lining decreases both noise and nozzle performance, and that the larger area mixer 4 gives higher noise and better performance than mixer 8C.

5.7.1.6 Gen 3/3.5 LSMS at LSAF

The Gen 3.0 and 3.5 1/7-scale mixer concepts were tested at the Boeing Low Speed Aeroacoustic Facility. Two tests were conducted: LSAF 1057 from March 1998 through July 1998 and LSAF 1066 from April 1999 through July 1999.

Test Objectives and Background

The Gen 3.0 mixer ejector nozzle concept builds on knowledge gained from the Gen 2.0 series of testing. The suppressor area ratio, aspect ratio, penetration, nozzle length, and lobe shaping were optimized to provide best aeroacoustic performance based on the Gen 2.0 data. Additionally, the Gen 2.0 mixer had full-cold-sidewall lobes that produced a low-velocity region (velocity hole) at the exit of the nozzle near the middle of the sidewalls. Based on CFD, the Gen 3.0 was modified to have half-hot-sidewall lobes that eliminated the low-velocity area and provided more uniform flow. The 1998 test of the Gen 3.0 mixer (LSAF 1057) was a companion test to the large-scale model (56% scale) tested at the P&W C–11 test stand. The Gen 3.0 model with bellmouth inlets is a similitude model of the LSM. The Gen 3.5 mixer continued the evolution of the mixer design, with better aerodynamic shaping of the chutes for higher thrust while maintaining the same level of mixedness of the Gen 3.0 model. In addition, a half-cold chute at the sidewall was incorporated to make the acoustic liner more effective.

The objectives of the first model entry were to acquire concurrent thrust and acoustic data for the Gen 3.0 mixer ejector model and provide a basis for estimating scale effects. These objectives included:

- Scale effects through comparison with LSM.
- Forward flight effects (bellmouth inlet to flight inlet at forward speed)
- Liner performance.
- Effect of mixer area ratio

The objectives of the second Gen 3.0/Gen 3.5 model test were to assess the:

- Effect of half-cold (Gen 3.0) versus half-hot (Gen 3.5) chute at the sidewall.
- Effect of mixing enhancement devices: notches and tabs on the mixers and chevrons at the ejector trailing edge.

- Secondary inlet shaping effect – 200% inlet ellipse versus 100% inlet ellipse.
- Effect of liner area variations: incremental and segmented.
- Repeatability of data.

Test Facility Description (LSAF)

The Boeing Low Speed Aeroacoustic Facility is described in Section 5.7.1.3. In the first entry of the model, LSAF1057, the jet flow system was modified to reduce flow distortion and burner noise. Specially designed choke plates were installed downstream of the burner to achieve the desired effects. Additionally, the charging station was moved closer to the model. These design modifications resulted in very uniform flow with less than 1% distortion in pressure and temperature. The rig background noise was substantially reduced. In the 1998 test, acoustic data were acquired with an azimuthal array, and detailed azimuthal acoustic information was obtained. In the 1999 test, acoustic data were acquired at only two azimuthal angles: 25° and 90° (sideline and cutback). Figure 208 is an end view of the facility with the new microphone arrangement.

Model Hardware

The Gen 3.0 model was completely new, designed to match the HSCT baseline at the time (1997). One of the main objectives of the first Gen 3.0 model test was to provide scaling effects compared to a larger (56% scale) model referred to as the LSM. The LSM was tested on a static test stand and

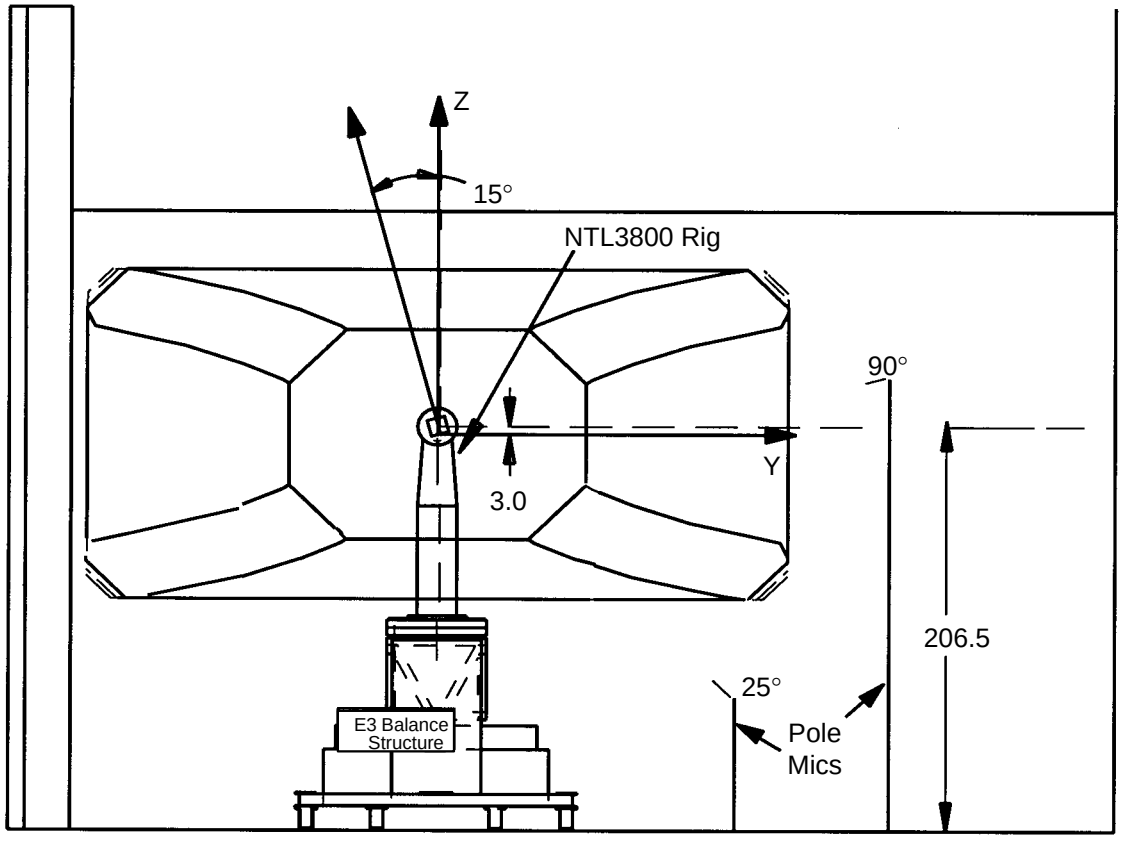

Figure 208. LSAF End View (Not to Scale)

had bellmouth inlets on the secondary to provide improved pumping. The Gen 3.0 model also had a bellmouth inlet, to match the LSM, and a flight inlet to obtain flight performance. Figure 209 illustrates the bellmouth and flight inlets.

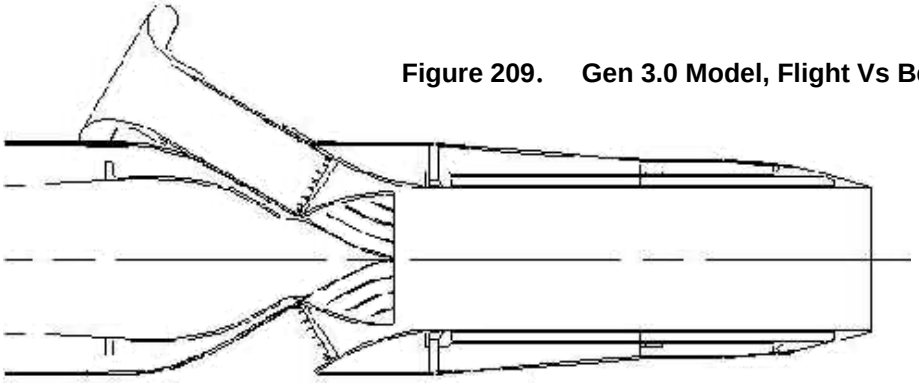

Figure 209. Gen 3.0 Model, Flight Vs Bellmouth Secondary Inlet

Two mixers were tested, Gen 3.0 and Gen 3.5. The primary difference between the two is the sidewall chute configuration. The Gen 3.0 mixer has a ½-hot sidewall chute while the Gen 3.5 has a ½-cold sidewall chute configuration. Other shaping changes were made to the Gen 3.5 to improve aerodynamic performance. Figure 210 illustrates the two mixers.

The Gen 3.0 mixer was modified during the second entry to evaluate mixing-enhancement devices. Considerable effort had gone into testing mixing enhancement devices at GEAE Cell 41 and at the P&W CASL test rig. However, difficulties with these test models and lack of thrust-measurement capability always clouded the results. The test entries at LSAF used the body of data that had been previously collected to determine a new configuration, dubbed the reduced notches and reduced A–tabs because of geometric similarities with other configurations, but with fewer devices. The reduced notches and reduced A–tabs are illustrated in Figure 211.

The Gen 3.0 model was tested with chevrons at the exit of the nozzle. These chevrons were tested with both the Gen 3.0 and 3.5 mixers. Figure 212 shows the Gen 3.0 model with chevrons installed.

The Gen 3.0 model had the usual hard-wall and treated liner configurations. Rather than the SiC material that was used in the Gen 2.0 liners, a new material referred to as T–foam was used. Incremental liner trays were also built for the Gen 3.0 to evaluate liner effectiveness. Figure 213 illustrates the liner configurations that were tested with the Gen 3.0 model.

The configurations tested with the Gen 3.0 model at the Boeing LSAF are summarized in Table 41.

Table 41. Configurations Tested with the Gen 3.0 Model at LSAF

Parametric		MAR	Liner	Description
Gen 3.5 Mixer	Baseline	0.90,0.93,0.95,0.98	HW, T–Foam. SiC	Flight Inlet, 200%, ½ hot SW mixer lobes
	Bellmouth Inlet	0.85,0.90,0.93,0.98	HW, T–Foam	Bellmouth Secondary Inlet
	Chevron	0.95	HW, T–Foam	Chevron end of nozzle
	Reduced Notches	0.95	HW, T–Foam	Notches cut into end of mixer
	Reduced A–Tabs	0.95	HW, T–Foam	A–Tabs welded into end of mixer
Gen 3.5 Mixer	Baseline	0.90, 0.95, 0.98	HW, T–Foam, Incremental Liner	Flight inlet, 200%, ½ cold SW mixer lobes
	Chevron	0.90, 0.95, 0.98	HW, T–Foam	Chevron end of nozzle
	Short Inlet	0.95	HW, T–Foam	100% Flight Inlet Ellipse

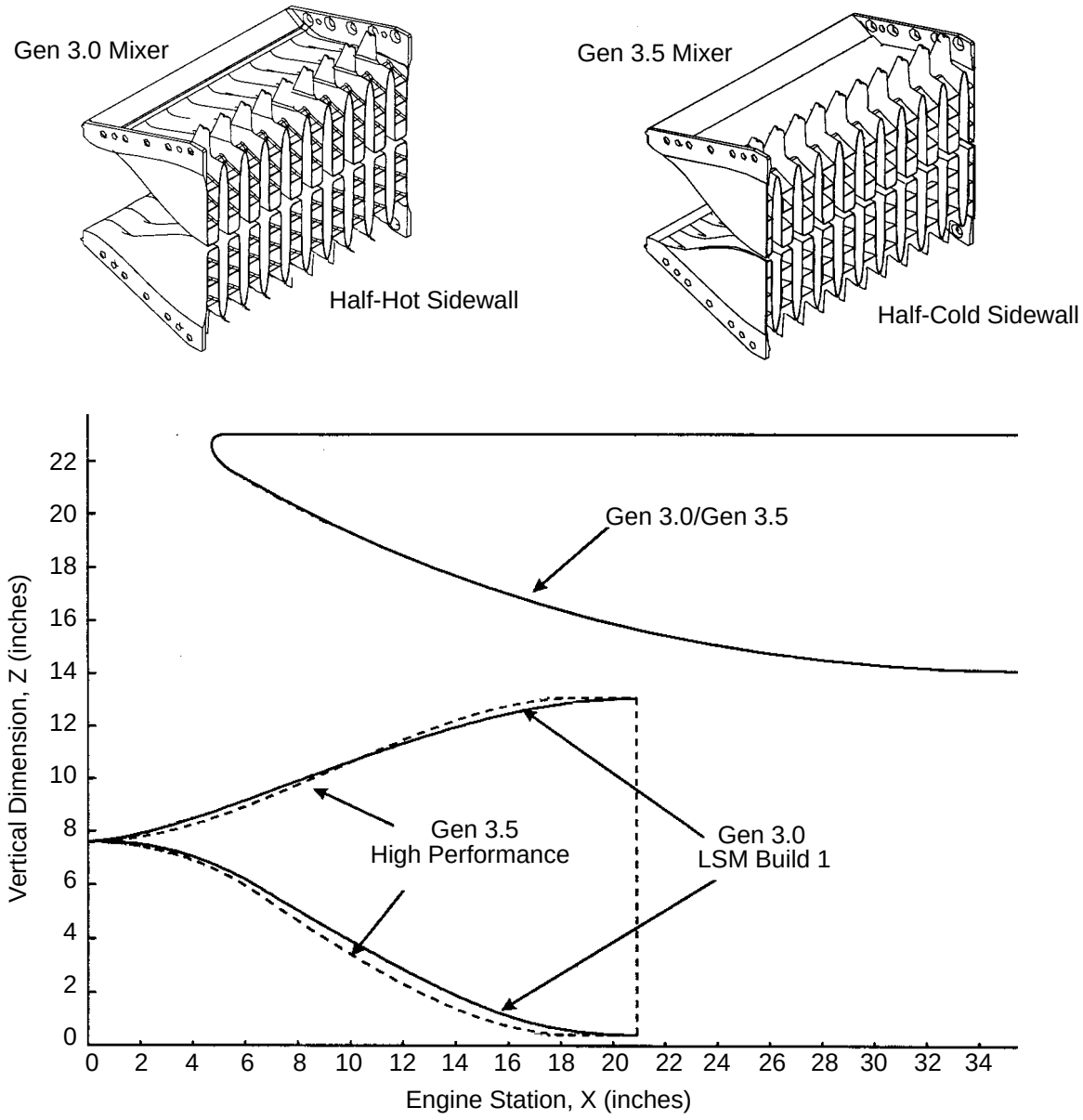

Figure 210. Gen 3.0 Vs Gen 3.5 Mixer

Reduced Notches

Reduced A–Tabs

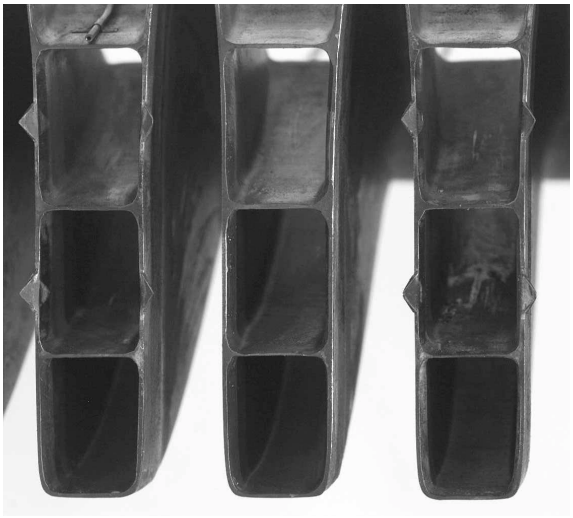

Figure 211. Gen 3.0 Mixer With Reduced Notches, Reduced A–Tabs

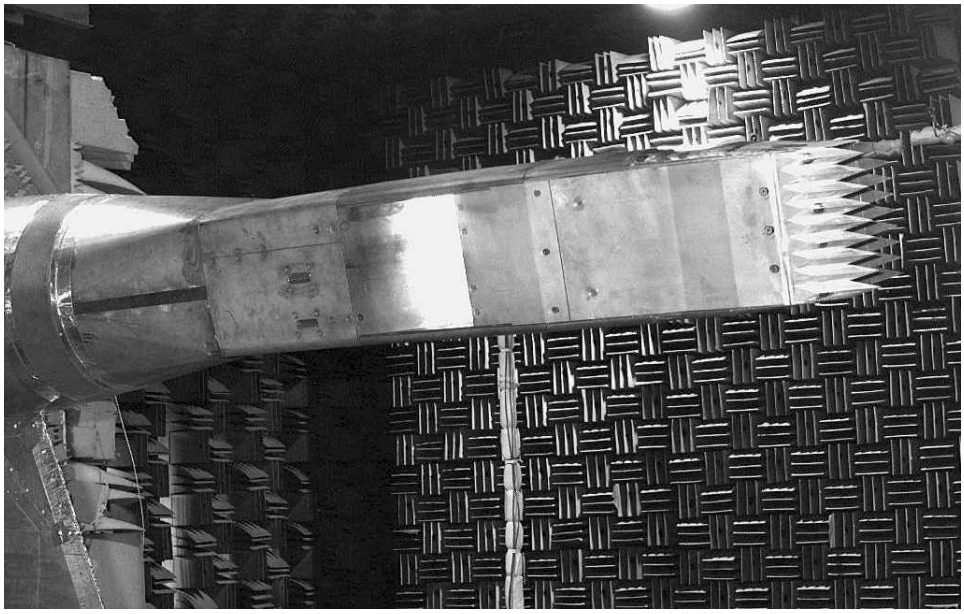

Figure 212. Gen 3.0 Model With Chevrons

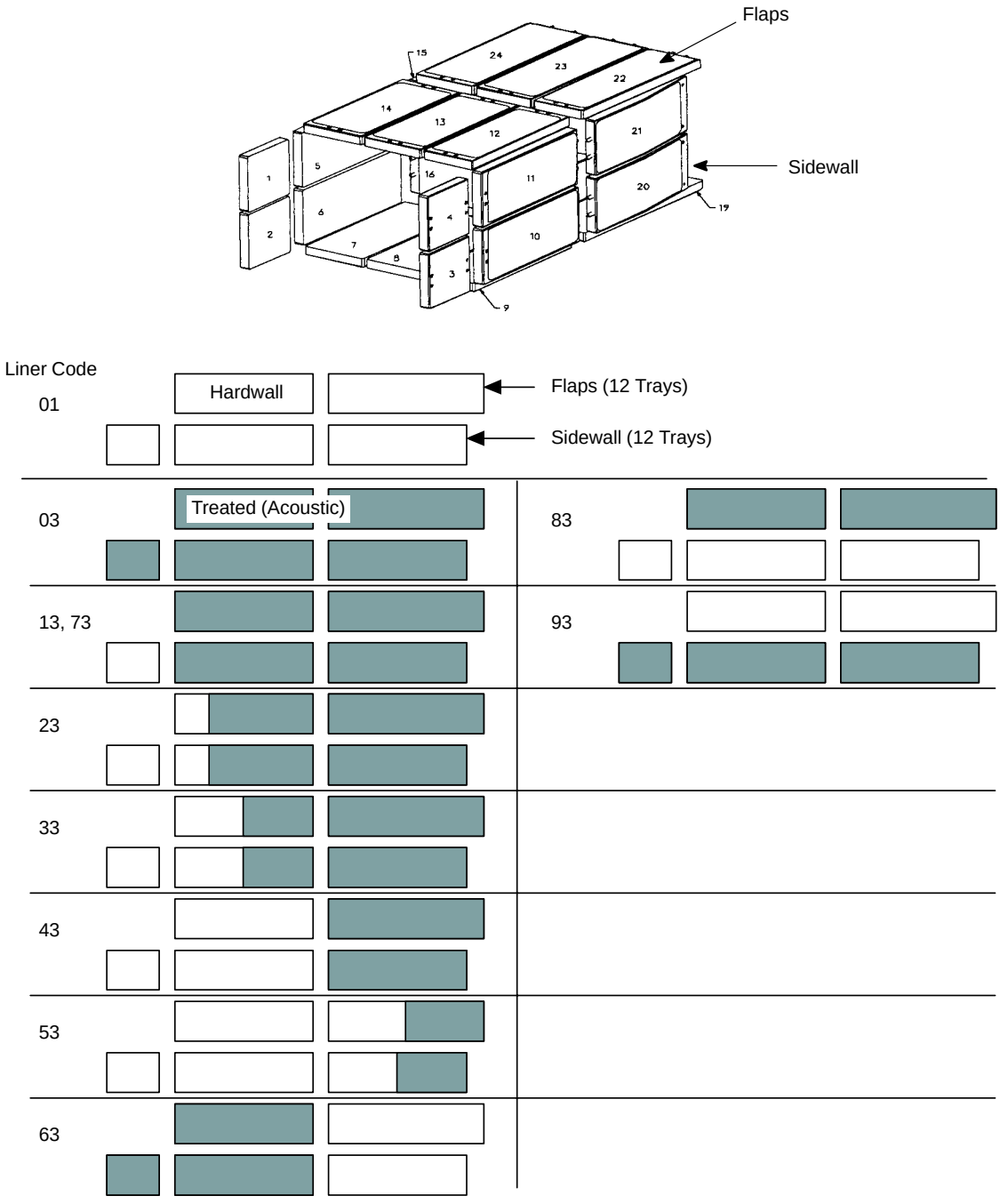

Figure 213. Gen 3.0 Model, Liner Configurations

Significant Results and Conclusions

Figure 214 shows the aerodynamic performance of the LSM and LSMS models. For hard-wall ejector, the scale effect is less than 1% on thrust. Pumping for the 1/7-scale model shows a considerable increase for the hard-wall case compared with the LSM. It is unclear (and unexpected) why the small model would pump better, but the increase is within the potential calculation error of the secondary airflow. For the treated ejector configurations, the difference in thrust is large, with the LSM about 4% higher than the 1/7-scale model. A major reason for this difference is the large hole size of the acoustic facesheet at the 1/7-scale. Material limitations make the hole size and depth for the 1/7-scale model far too large and deep. This increases friction drag beyond just simple Reynolds number. Additionally, the trays on the model are broken into two segments along the full length of the flaps and sidewalls. On the LSM the trays were broken into 12 segments. It is possible that flow transport inside the comparatively long 1/7-scale trays are contributing to the thrust loss. With treatment, pumping is about the same for the two models.

Figure 215 shows the effect of the bellmouth inlets on mixer/ejector performance. The bellmouth secondary inlets have a relatively small effect on noise and thrust performance. However, due to the improved in-flow conditions of the bellmouth inlet, pumping is considerably higher for the bellmouth compared with the flight inlet.

Figure 216 shows the flight effect on the mixer/ejector performance. Noise decreases by 5 EPNdB at cutback and by about 7 EPNdB at sideline, when the freestream Mach number is increased from 0.0 to 0.32. Thrust decreases sharply due to ram drag effects by about 6% at cutback and 4% at sideline. Pumping increases with increasing Mach number due to forward ram and increased total pressure.

Figure 217 is a summary chart comparing the performance of the baseline Gen 3.0 model with the baseline Gen 3.5 model and the modified Gen 3.0 model. The Gen 3.5 mixer shows a greatly improved thrust performance, about 1.5% at both cutback and sideline NPR compared with the Gen 3.0 mixer. Noise levels for the two mixers were nearly equal at the sideline NPR, but the Gen 3.5 mixer is quieter by about 1 EPNdB at the cutback NPR. Pumping also is higher for the Gen 3.5 mixer.

The reduced notches provided a noise benefit of about 0.9 EPNdB at sideline but no noise benefit at cutback, with no measurable loss in thrust. The reduced A–tabs yielded a significant noise benefit: about 2 EPNdB at both cutback and sideline NPR. The accompanying thrust loss was less than 0.5%, which is very favorable trade. The mixing enhancement concepts must be optimized in future tests.

Figure 217 shows that reducing the secondary inlet shape from the baseline 200% ellipse to a shorter 100% ellipse has no measurable effect on mixer/ejector performance at takeoff conditions. Hence, cruise considerations should dictate the design of this component. The effect of the chevrons mounted to the trailing edge of the nozzle had no measured effect on the mixer/ejector performance.

Figure 218 shows nozzle exit survey contour maps for the baseline Gen 3.0, Gen 3.0 mixer with reduced notches, with reduced A–tabs, and the Gen 3.5 mixer at the cutback and sideline conditions. The figure shows that the enhancement devices improved the mixing of the primary and secondary flows. The Gen 3.5 mixer shows an even large improvement in the mixedness of the flows. The enthalpy flux mixednesses (K) of the flow profiles are also shown on the figure.

Figure 219 and Figure 220 show the effect of varying the liner treatment area in the ejector. Thrust varies as a liner function of treatment area, with loss in thrust proportional to increasing area. The effectiveness of the liner depends on placement in the ejector. The liner in the downstream portion

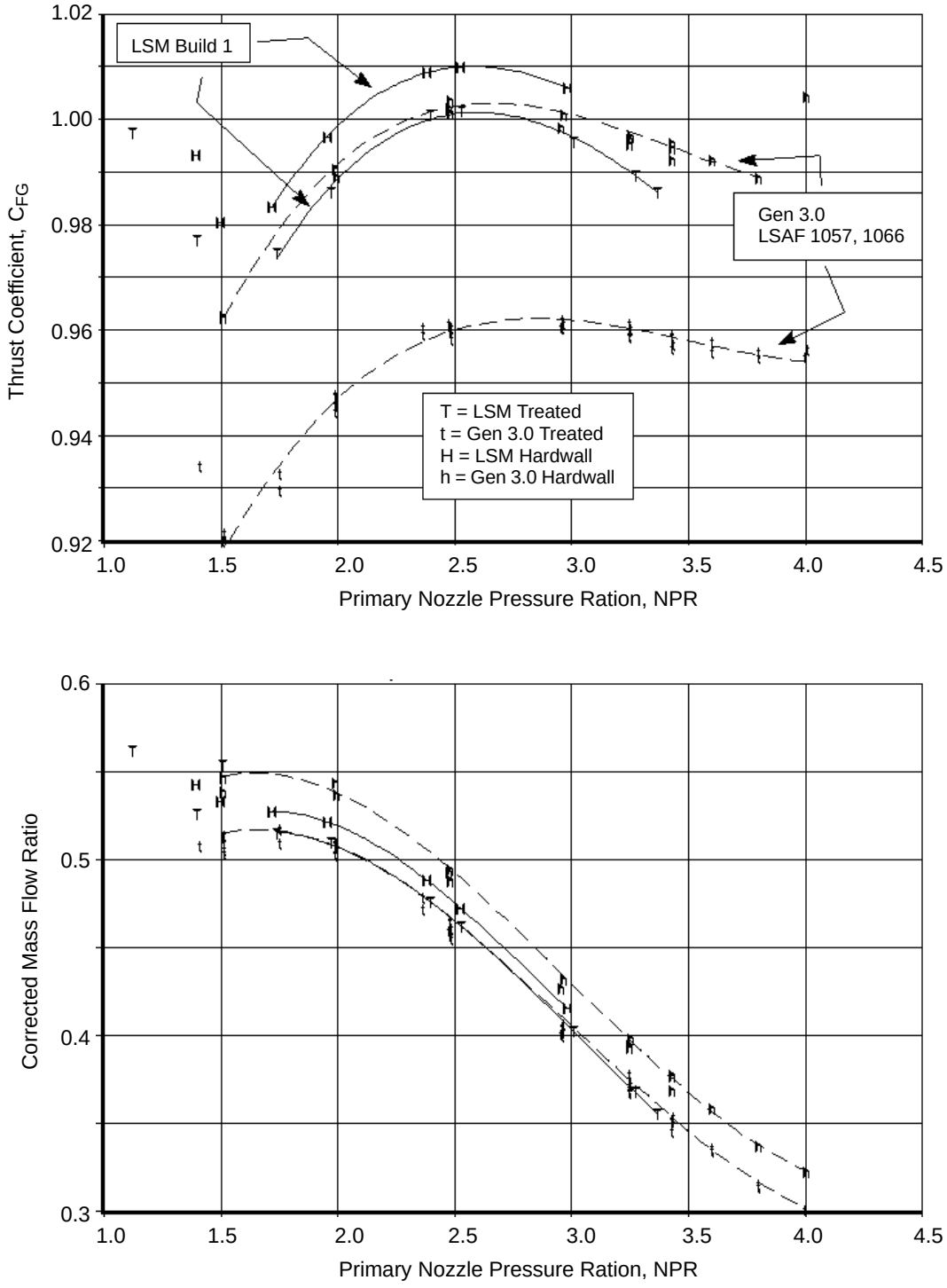

Figure 214. LSM versus Gen 3.0 (LSMS), Aero Performance, Bellmouth Inlet

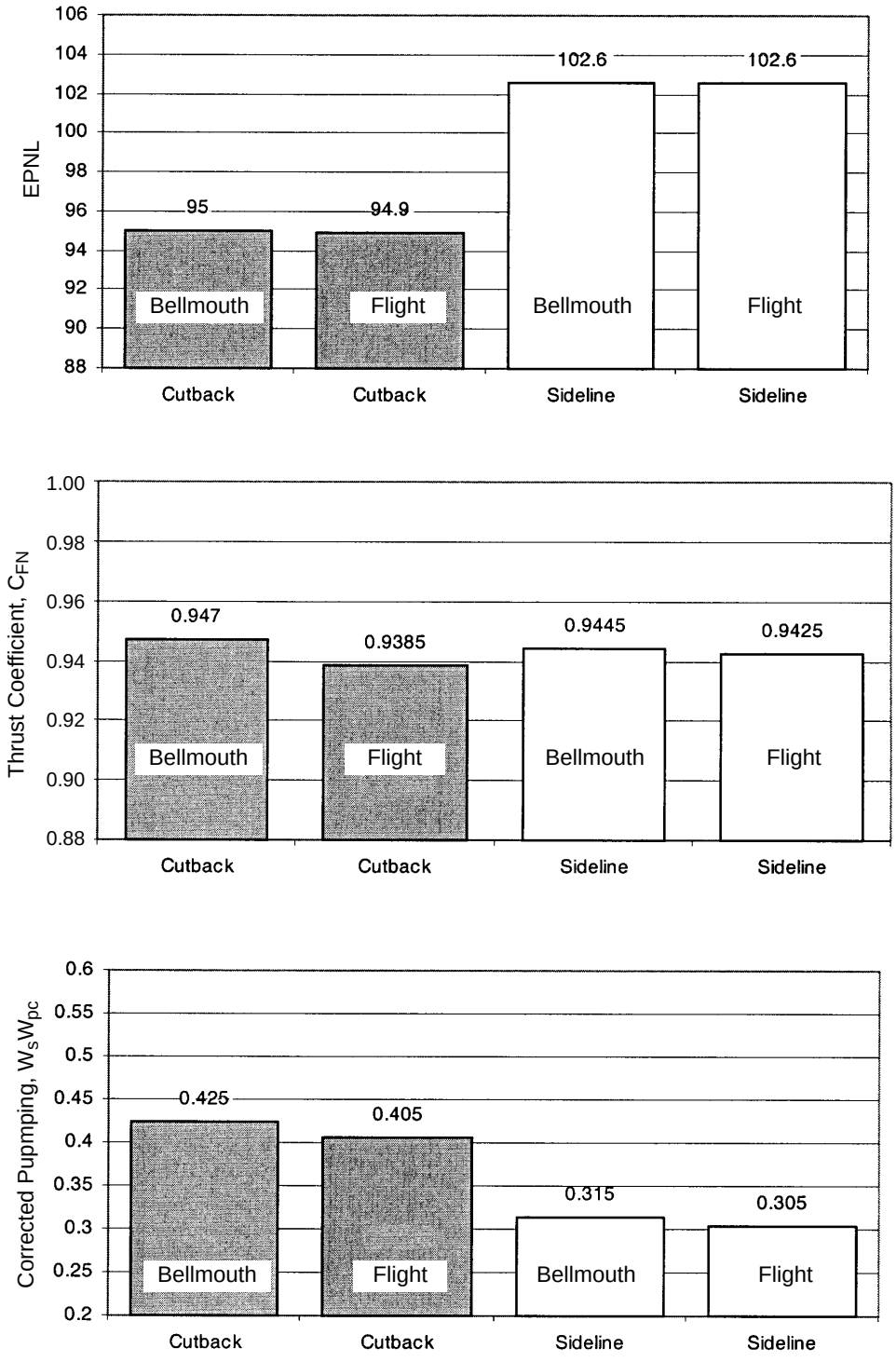

Figure 215. Effect of Bellmouth Inlet, MAR = 0.90, Treated, Mach = 0.0

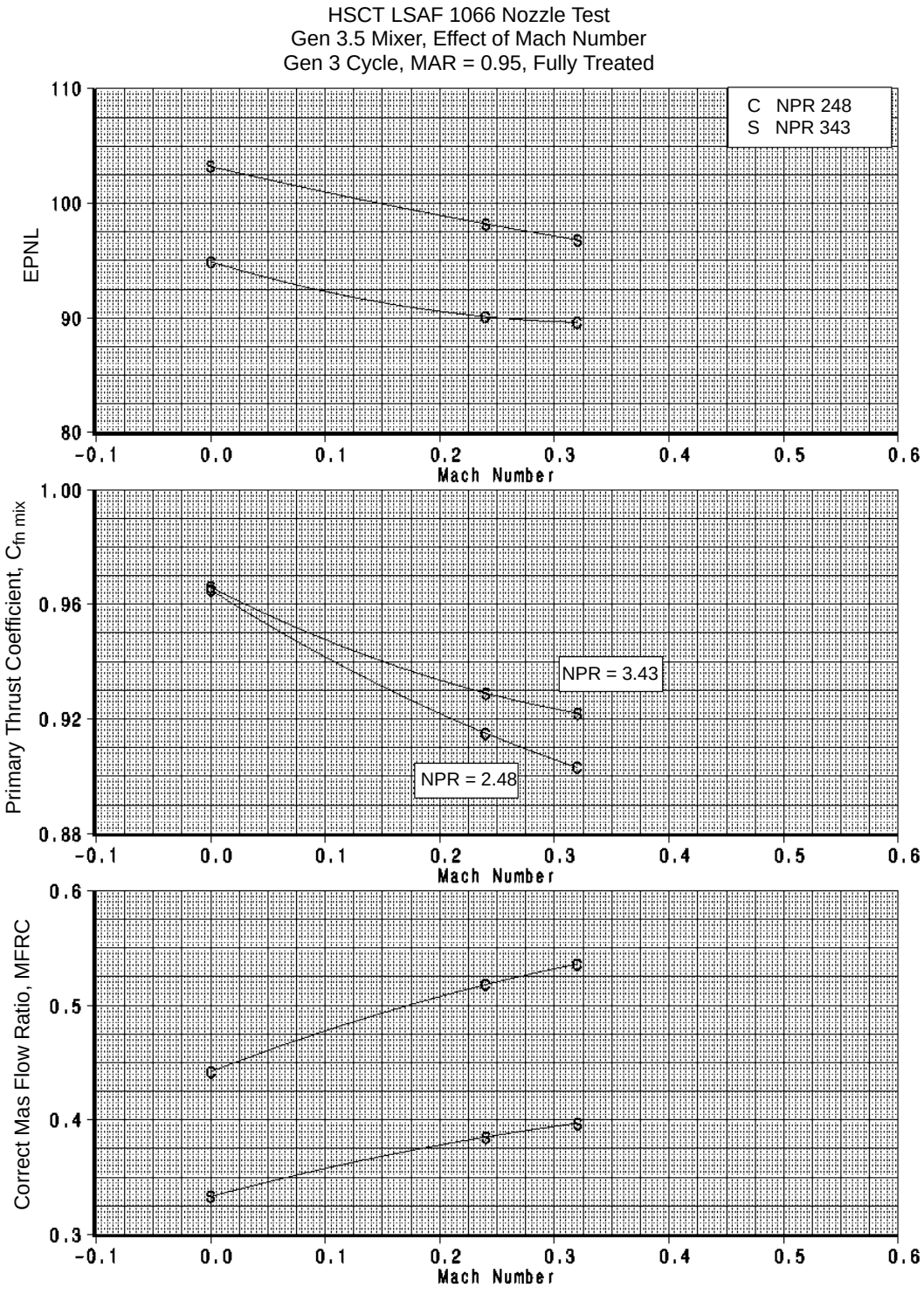

Figure 216. Flight Effects, Gen 3.5 Mixer, MAR = 0.95, Treated

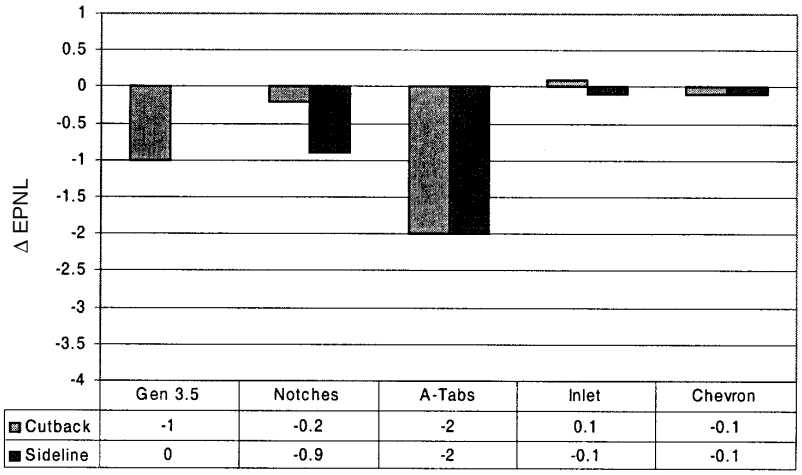

	Gen 3.5	Notches	A-Tabs	Inlet	Chevron
Cutback	-1	-0.2	-2	0.1	-0.1
Sideline	0	-0.9	-2	-0.1	-0.1

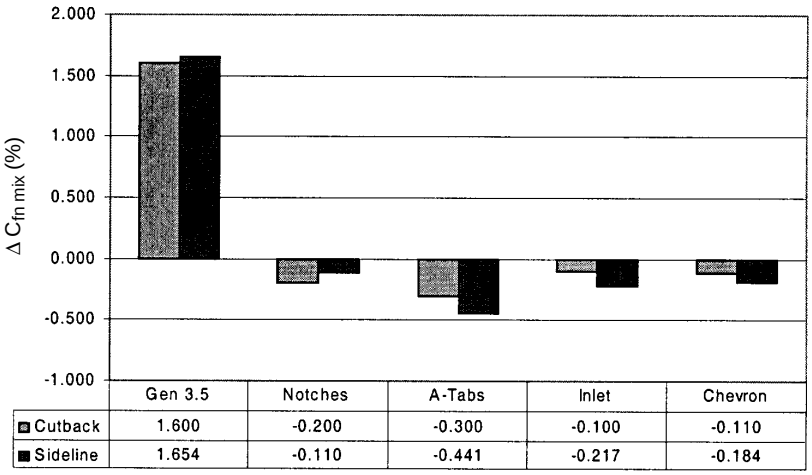

	Gen 3.5	Notches	A-Tabs	Inlet	Chevron
Cutback	1.600	-0.200	-0.300	-0.100	-0.110
Sideline	1.654	-0.110	-0.441	-0.217	-0.184

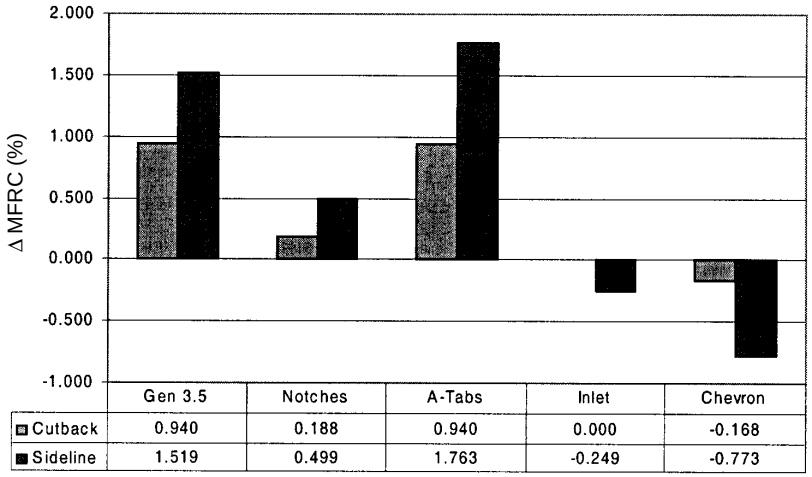

	Gen 3.5	Notches	A-Tabs	Inlet	Chevron
Cutback	0.940	0.188	0.940	0.000	-0.168
Sideline	1.519	0.499	1.763	-0.249	-0.773

Figure 217. Parametric Performance, MAR = 0.95, Mach = 0.32, Treated

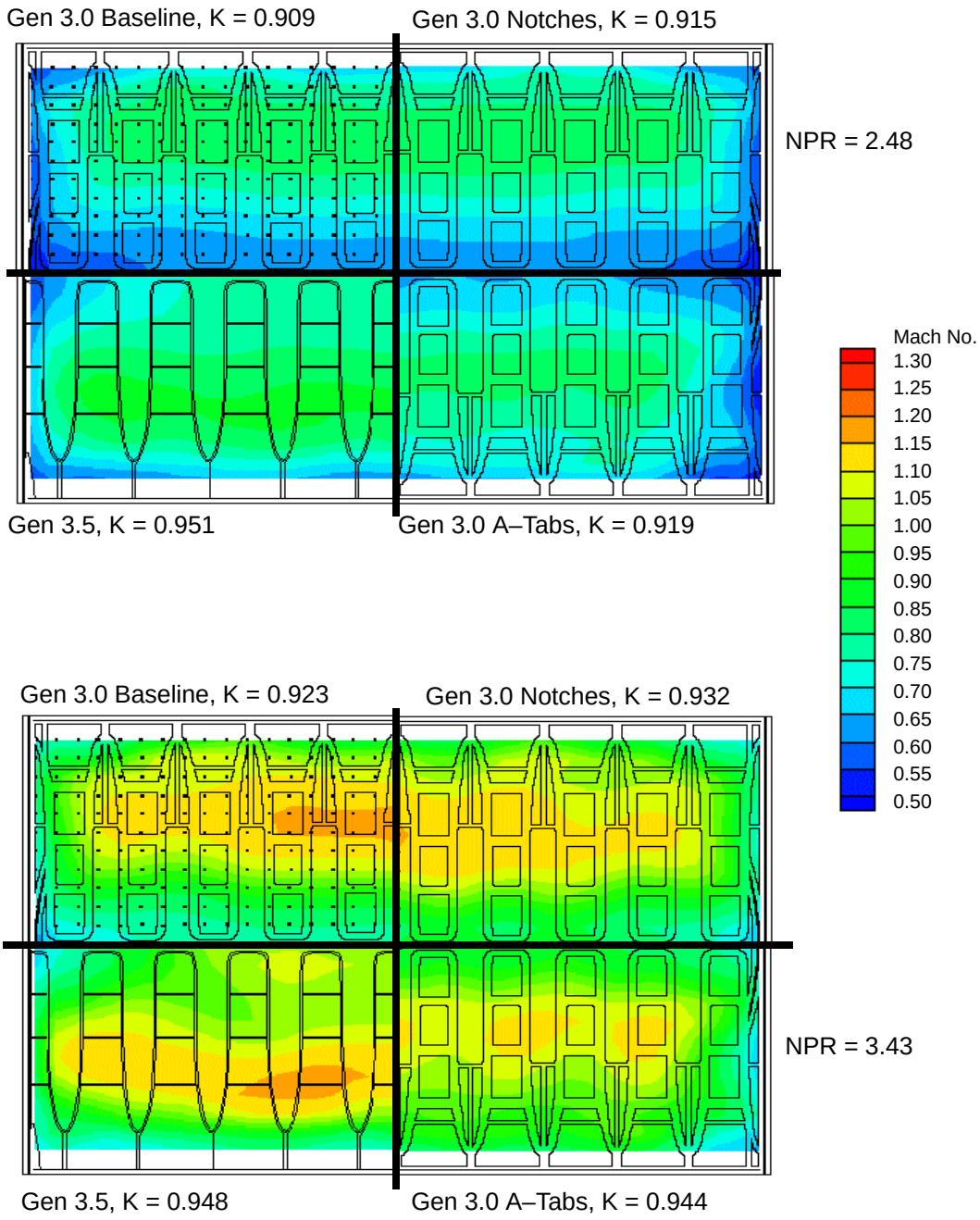

Figure 218. Exit Survey Comparisons, Mach Number, MAR=0.95, Mac=0.0, Treated, Flight Inlet

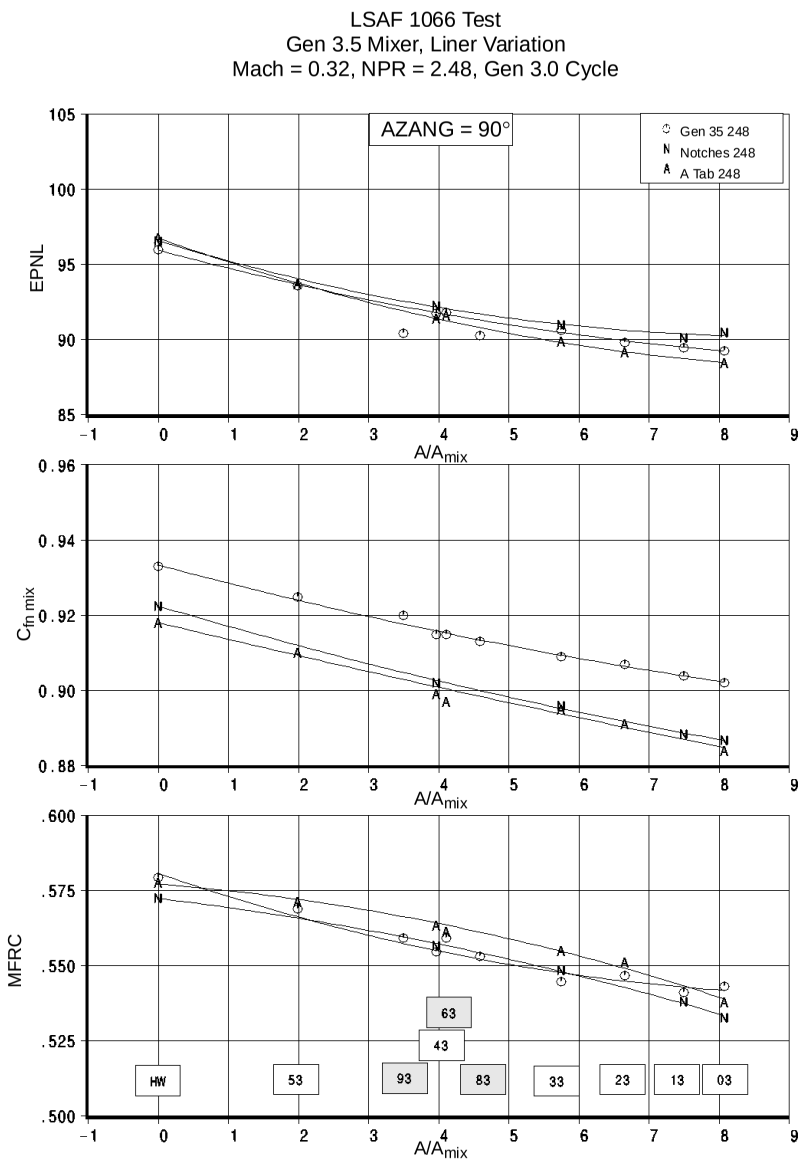

Figure 219. Gen 3.5, Liner Performance at Cutback, NPR = 2.48

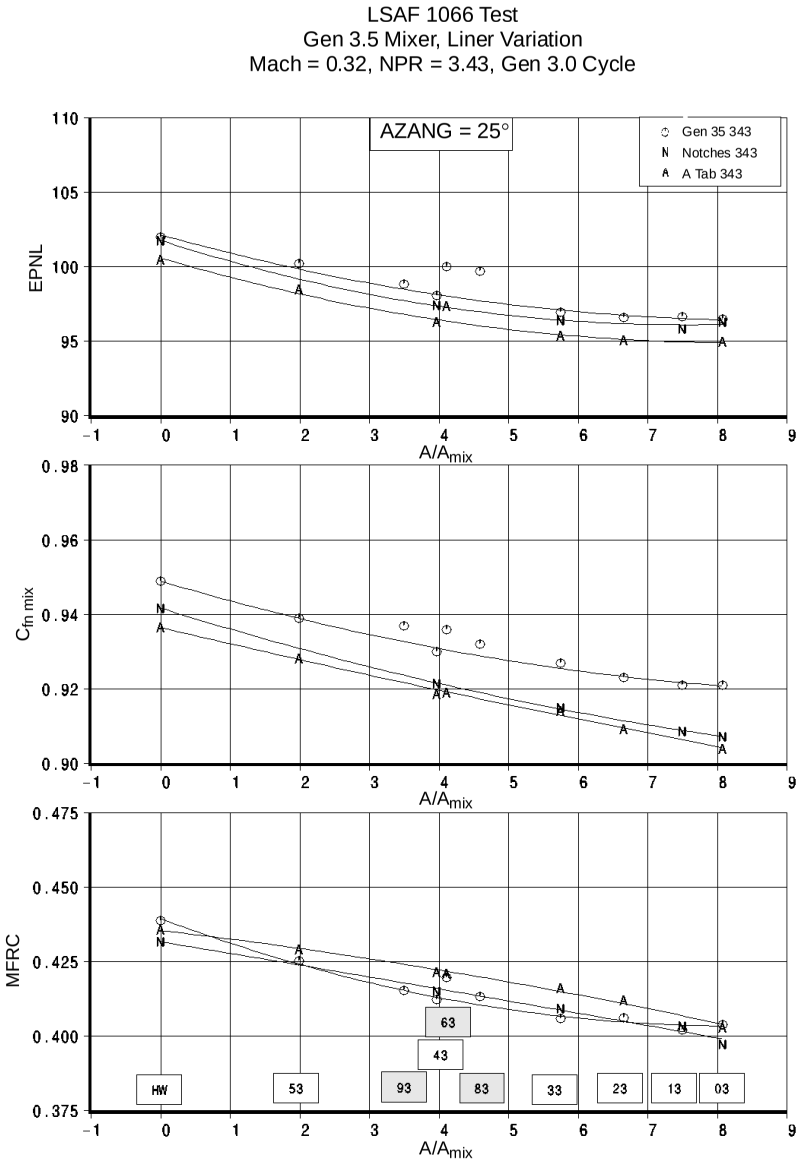

Figure 220. Gen 3.5, Liner Performance at Sideline, NPR = 3.43

of the mixer is very effective, while the liner in the upstream portion does not produce much noise suppression. The physics of the mixing-enhancement devices must be better understood to improve the effectiveness of the liner.

It is possible the results in Figure 220 are due to the benefit from increasing treatment area being limited by noise floors from sources other than internal noise. If that is the case, the last increment of treatment will produce the least benefit no matter where it is located.

5.7.2 LSM Test

5.7.2.1 LSM Test Objectives

The primary objective of Build 1 of the LSM nozzle was to confirm and reinforce current scaling techniques used to project from a subscale acoustic and thrust database to HSCT product size. The program was conducted as a static test; forward-velocity effects were not applied during testing. The specific objectives of this test program are listed below:

a. Measure jet noise levels at sideline, cutback, and approach conditions.

b. Measure absolute thrust levels at sideline, cutback, and approach conditions.

c. Measure noise attenuation and performance losses for treated and hard-wall acoustic liners. Treated acoustic liners are tiles with a 37% open area on the surface. Hard-wall acoustic liners are tiles with a solid surface (0% open area)

d. Quantify subsonic to supersonic mode-switch characteristics by measuring mixing-duct static pressure distributions.

e. Measure exhaust/ambient air mixing profiles at five mixing duct locations to quantify the mixed stream and determine the correlation with computational fluid dynamics.

f. Define the point at which the acoustic liners become effective by sequentially changing the treated tiles to hard-wall tiles.

A posttest objective is to compare acoustic and performance data from this test with that from the 1/7-scale LSM-similitude (LSMS) model. This comparison will verify scaling techniques used to predict product performance based on subscale data.

5.7.2.2 LSM Aeroline Definition

The LSM nozzle represents a 56.4% subscale model (with a nominal throat area of 2.7 ft^2) of an 800-lbm/s product size nozzle. A cross section of the nozzle that illustrates the dimensional characteristics is shown in Figure 221. The following parameters define the key characteristics of the LSM nozzle.

Nominal Throat Area, A_8	=	390.9 in^2
Mixing Plane Area, A_{mix}	=	1133.64 in^2
Suppressor Area Ratio, SAR	=	2.9
Chute Expansion Ratio, CER	=	1.1
Treatment Area, Atr	=	8682 in^2
Effective Treatment Area, Atr (eff)	=	7444.3 in^2
Atr (eff)/Amix	=	6.57

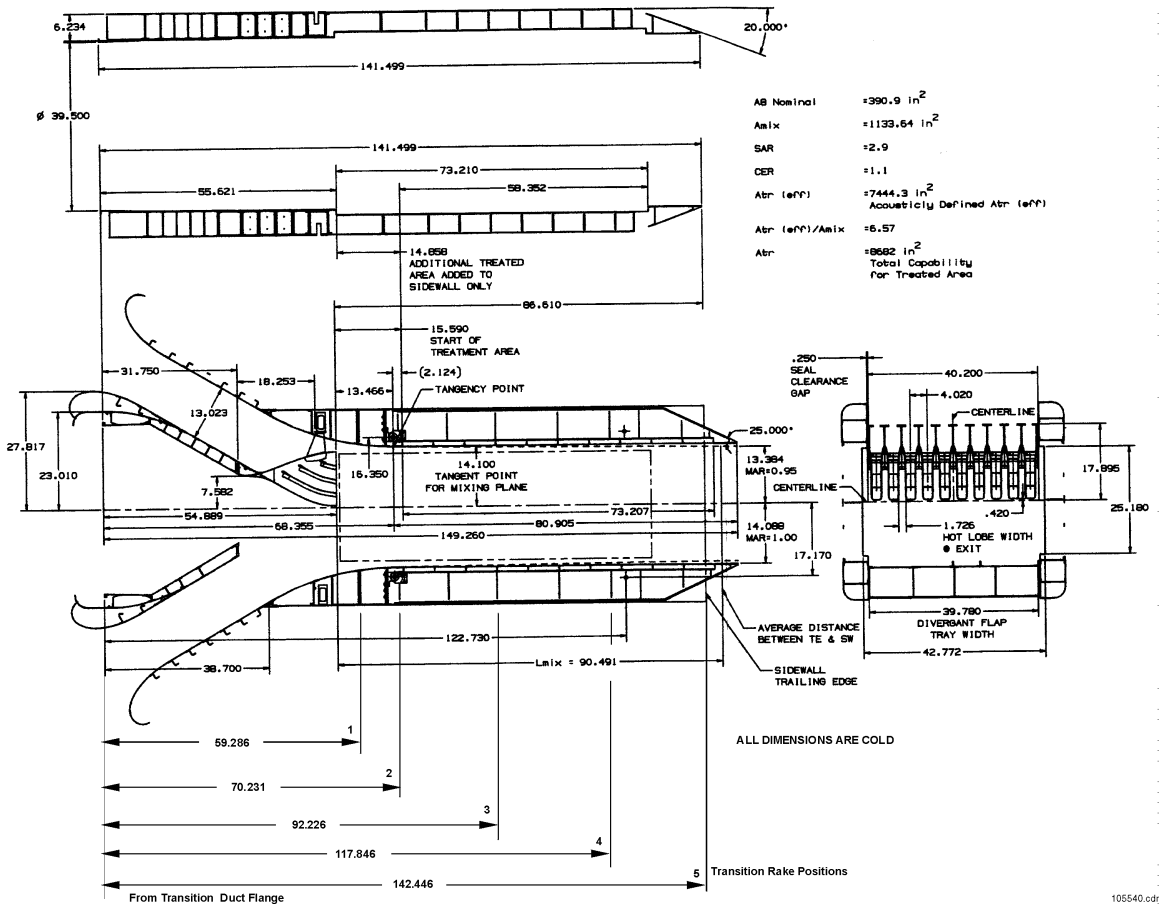

Figure 221. LSM Cross Section Dimensional Definition

5.7.2.3 LSM Aerodynamic Results

Aero Results Versus Predictions

LSM nozzle aerodynamic performance was predicted using a simplified 1D mixer/ejector code (E65R) developed at P&W for application to a variety of aircraft-propulsion-related ejector systems. E65R has been used in the HSCT nozzle program to predict aerodynamic performance for various mixer configurations. E65R was used to predict the performance of the LSM nozzle at static and forward flight conditions. The goal was to extrapolate aero performance from the static test data at sideline conditions to forward flight at the takeoff conditions as specified in the P7 aerodynamic-performance metric. One of the objectives of the LSM nozzle test was to validate and update the 1D prediction tool.

The first step was to predict the static performance of the nozzle as tested on the C–11 stand at P&W. Table 42 shows the flow properties used in the predictions for cutback and sideline conditions. Cutback and sideline conditions refer to NPR 2.5 and 3.25. Table 43 shows the corresponding geometric parameters used in these predictions. Table 44 shows the preliminary values of the parameters that account for thrust losses. The value of stream thrust coefficient (C_S), secondary pressure recovery (η_S), and duct friction factor (FRIC) has been obtained from Gen 1.5 and 2.0 test data. Table 45 shows the values of the performance numbers obtained for sideline and cutback

Table 42. Test Prediction Flow Properties

Flow Parameters	Cutback Conditions	Sideline Conditions
Altitude, ft	0	0
Ambient Pressure, psia	14.7	14.7
Ambient Temperature, °R	537	537
Primary Total Temperature, °R	1384.0	1590.5
Nozzle Pressure Ratio	2.51	3.257
Primary Total Pressure, psia	36.95	47.885
γp	1.3472	1.334

Table 43. Geometric Parameters

Parameters	Values
Mixing Area Ratio (MAR)	0.90
Suppressor Area Ratio (SAR)	2.95
Mixing Duct Length (L_{mix}), in.	90.5
Mixer Area (A mix), ft^2	7.87
Primary Throat Area, ft^2	2.69
Chute Expansion Ratio (CER)	1.10
Acoustic Tile Treatment	Rows 1–2 Hard Wall

Table 44. Parameters Contributing to Thrust Loss

Flow Parameters	Cutback Conditions	Sideline Conditions
Stream Thrust Coefficient (C_s)	0.976	0.976
Secondary pressure Recovery (η_s)	0.9664	0.9597
Duct Friction (FRIC)	0.02384	0.02384

Table 45. Aero Performance Prediction

	Cutback		Sideline	
Nozzle Performance Parameters	Prediction	Test Data	Prediction	Test Data
Gross Thrust Coefficient (C_{fg})	0.997	0.9975	0.991	0.9858
Net Thrust Coefficient (C_{fnet})	0.997	0.9975	0.991	0.9858
Pumping Ratio (Ws/Wp)	0.736	0.714	0.639	0.613

conditions. The prediction at the cutback condition agrees well with the test data. However, at sideline condition, the prediction is about 0.5% above test data.

The values of C_s, η_s, and FRIC can be adjusted to make the 1D prediction better match the LSM data. Table 46 shows values of C_s, η_s, and FRIC where η_s has been changed to get the 1D C_{fg} prediction to match the sideline LSM data as shown in Table 47. The updated values result in a good match at the sideline condition, but the prediction differs by 0.5% from cutback. Improving predictions of C_s, η_s, and FRIC based on LSM and Gen 3.0 test data is an objective of the CPC scaling-effects task.

Table 46. Updated Thrust Loss Values

Losses	Cutback Conditions	Sideline Conditions
Stream Thrust Coefficient (C_s)	0.9760	0.9760
Secondary Pressure Recovery (η_s)	0.9611	0.9520
Duct Friction (FRIC)	0.02384	0.02384

Table 47. Updated Aero Performance Predictions

	Cutback		Sideline	
Nozzle Performance Parameters	Prediction	Test Data	Prediction	Test Data
Gross Thrust Coefficient (C_{fg})	0.9920	0.9975	0.9860	0.9858
Net Thrust Coefficient (C_{fnet})	0.9920	0.9975	0.9860	0.9858
Pumping Ratio (Ws/Wp)	0.7290	0.7140	0.6240	0.6130

Static Data Extrapolated to Forward Flight

The LSM nozzle was installed behind an F100–PW–229 engine and tested at P&W on the C–11 test stand. This was a static test; therefore, no forward-velocity effects were applied. One objective of the test was to determine how well the model would perform in forward-flight sideline and cutback orientations. Static test data were extrapolated to predict performance at forward flight conditions specified in the P7 metric. The extrapolation of test data to forward-flight conditions was accomplished by using E65R.

The following steps were taken to extrapolate the test data at sideline orientation for a baseline (primary) test configuration to forward flight. The baseline configuration was tested at MAR 0.90 and SAR 2.95. The ejector treatment area was row 1 and 2 hard wall, other rows were treated (37% porosity) tiles.

The value of C_s and secondary pressure recovery (η_s) were determined from the LSM nozzle test. Duct friction factor was adjusted to reflect that row 1 and 2 are hard wall. The length to diameter ratio L/D (where D is the hydraulic diameter based on the wetted perimeter) at the mixing plane for the LSM nozzle is 2.721. The values of C_s, η_s, and FRIC act as the baseline values that correspond

to this particular configuration and model. Using the thrust loss coefficients in the ejector code provides predictions of C_{fg} and C_{fnet} consistent with the engine test.

5.7.2.4 LSM Acoustic Results

Nozzle acoustic data were recorded in order to support the test objectives discussed in Subsection 5.7.2.1.

Pretest predictions were generated among P&W, GEAE, and Boeing. Pretest predictions were based on either existing subscale model data or the respective organization's ejector nozzle jet noise prediction models used in conjunction with estimated nozzle performance. Projections were for specific jet HSCT/CPC noise metrics, specifically sideline (P5) and cutback (P6), established in January 1997. Noise goals at FAR36 (Reference 1) cutback and sideline conditions are expressed in terms of effective perceived noise level and are for an aircraft flyover. EPNL's relative to flyovers are highly dependent on airplane configuration, performance, and resulting engine thrust requirements. Analyses were conducted with single-engine, level-flight, free-field (no ground reflections or cancellations) flight projections selected to provide P&W, GEAE, Boeing, and NASA with a common analysis process. Adjustments to the more realistic four-engine flyovers, with real flight path and ground reflections, to the 4-ft-high pole microphones of FAR36 were jointly generated and agreed to by all parties. CPC nozzle noise goals and adjustments are listed in Table 48.

P5 and P6 metric conditions have been *frozen* for specified engine/nozzle cycle and aerodynamic performance conditions due to changes in the HSCT aircraft and cycle that provide a moving target for specific nozzle noise goals (Table 49).

Pretest noise projections for the LSM nozzle were generated individually by P&W, GEAE, and Boeing in February 1997. Flight EPNL projections, shown in Table 50, varied depending on the methodologies selected by each partner.

In October 1997, the partners added a static noise pretest projection. Static numbers are given in Table 50. Although EPNL is not really meaningful for static noise, a pseudo-EPNL number can be calculated by developing a projected time history based on the static data. The pseudo-EPNL does not account for the reduction in externally generated jet noise due to reduced relative shear between the jet and the ambient free stream. Note the difference in jet noise flight effect among the three estimates.

Acoustic Results Versus Predictions

A comparison of the October 1997 pretest prediction and the January 1998 LSM data requires some adjustments. The cycle throttle line from the F100–PW–229 engine differed from the nozzle inlet temperature and pressure ratio conditions specified in the P5 and P6 metrics used in the pretest noise projections. Also, the 3.43 NPR of the sideline metric was not achieved with the LSM nozzle only running up to NPR 3.34. From previous 1/7- to 1/8-subscale model tests, data have provided a correction to adjust for the cycle temperature and NPR differences.

Sufficient full- and partial-power line noise measurements were taken to provide adequate data for a statistical regression of projected EPNL versus NPR. The use of 24 repeat data points combined with regression analysis results in a noise power relationship accurate to ±0.4 EPNdB. Also, as LSM nozzle noise data were generally acquired at NPR 3.25 and below, this regression allows relatively accurate extrapolation to the NPR 3.43 of the sideline noise metric.

Table 48. P5 and P6 Noise Goal Adjustments

Orientation	Noise Goal Basis	Noise Goal	Adjustment*	Adjusted Noise Goal
Sideline Cutback	Stage 3 – 1 Stage 3 – 3	102.5 – 1.0 105.5 – 3.0	5.4 8.5	96.1 94.0
* Note: Flight Adjustment from single–engine, free–field, level flyover to four engines, 4–ft pole microphone over grass; nominal flight path.				

Table 49. P5 and P6 Noise Metrics (Goals)

Orientation	A_8 (in.^{2})	NPR	T_{t8} (°R)	V_{jj} (fps)	Altitude (ft)	Sideline (ft)	Flight M_0	Goal (EPNdB)
Sideline	1248	3.43	1550	2360	689	1476	0.32	96.1
Cutback	1248	2.5	1290	1880	1200	0	0.32	94.0

Table 50. LSM Pretest Noise Predictions (EPNdB)

		P&W	GEAE	Boeing	Average
Flight	Sideline	96.9	97.8	96.1	96.9
	Cutback	94.3	93.6	93.9	93.9
Static	Sideline	103.8	103.1	101.6	102.8
	Cutback	98	97.5	96.4	97.3
ΔFlight	Sideline	–6.9	–5.3	–5.5	–5.9
	Cutback	–3.7	–3.9	–2.5	–3.4

Pseudo-EPNL values for P5 and P6 metrics at MAR 0.90 with acoustic treatment are 105.0 and 100.9 EPNdB, respectively. As the actual metrics are not developed for static condition, further adjustments must be made to correct for the relative jet-noise flight effects. Adjustments are planned for subsequent analyses using the LSMS 1/7-scale *duplicate* model of the 56% scale nozzle. The nozzle currently being tested for noise and performance will provide consistent, back-to-back static noise versus anechoic wind tunnel in-flight noise data. Despite the variation in estimated flight effects from the three industry HSCT/CPC partners, current projections will be used until additional data are acquired and relevant analyses are conducted.

Cycle Throttle Line Differences – Another adjustment to the current data required in the assessment of the LSM nozzle against the P5 and P6 jet-noise metrics is cycle throttle line differences between the reference MFTF 3770.60 cycle specified in P5 and P6 and the F100–PW–229 engine used with the LSM nozzle. Data from the test shows a temperature difference of approximately 70°R. Previous model data from the HSCT/CPC Gen 2.0 and 2.5 nozzle model tests have shown

that reduced density of the jet, along with small differences in secondary to primary flow ratio, can amount to 0.2 and 0.4 EPNdB lower noise with the F100–PW–229 cycle at sideline and cutback, respectively. Therefore, the measured LSM nozzle noise must be increased by 0.2 and 0.4 EPNdB for the comparison. This adjustment will be measured in conjunction with the jet–noise flight effect during the LSMS model testing.

Fan Tone Contamination – Although the inlet antireingestion (AR) duct was installed to minimize contamination of the jet-noise spectra from the F100–PW–229 fan and other, nonjet sources, some fan tones were still present in the measured spectra. The contribution from these tones was minor, amounting to an EPNL increase of only 0.1 EPNdB at sideline and 0.2 EPNdB at cutback.

Engine Fan/Core Stream Unmixedness – Pretest noise predictions for the LSM nozzle were based on uniform 1D flow into the nozzle and did not account for radial pressure, temperature, or equivalent (fully expanded) jet-velocity distortion. By comparison, current airplane system trade studies have been assessing a 0.3-EPNdB jet noise penalty for incomplete fan/core stream mixing from the fan/core mixer of the product engine/nozzle design. The F100–PW–229 engine was not equipped with a fan/core stream forced mixer; therefore, a center-peaked profile was in evidence.

Although the absolute level of temperature measured at the charging-station rakes is in question, the averaged radial profile is a good indicator of radial temperature distortion at the primary stream inlet to the LSM nozzle. From total temperature and total pressure readings on the charging-station rakes, jet velocity can be calculated. The radial ideal velocity profile normalized to the respective average velocities is calculated from data recorded during the test. Also calculated is the anticipated pretest distortion level. The measured radial profiles for the LSM nozzle are estimated to increase internal nozzle mixing and thus reduce jet noise by 0.6 EPNdB at sideline (NPR 3.25) and 1.0 EPNdB at cutback (NPR 2.48). Therefore, pending results from follow-on subscale Gen 3.5 model testing, the current assessment of fan/core unmixedness penalty is that LSM nozzle jet noise is higher by at least 0.6 EPNdB at the sideline orientation and by at least 1.0 EPNdB at cutback.

Hot Versus Cold Sidewalls – When comparing the LSM nozzle calculated static pseudo-EPNL's calculated from flying a static PNL directivity at constant altitude and flight speed to pretest predictions, it is essential to recognize that the LSM nozzle is a two-year-old acoustic design. The nozzle sidewall can either have the mixer terminating with a hot (primary stream) or cold (secondary stream) lobe against the sidewalls. Previous 1/7- to 1/8-scale testing had indicated that a full-cold mixer lobe at the sidewall could introduce significant temperature distortions in the sidewall with attendant increase in moderate-scale premerged noise. The alternative would be either a half-cold or half-hot lobe at the sidewall. At the time of the LSM nozzle design, it appeared that a mixer with the hot lobes (half of a hot lobe) adjacent to the sidewall would be a safer approach, which was consistent with Gen 2 model testing.

The LSM test data indicate high local flow Mach numbers in the vicinity of the sidewalls, especially in the first half of the sidewall axial length. This can be seen in the wall static pressure data in Subsection 5.1.2.2. It is believed that the high local flow Mach number is a major cause of the shortfall in overall nozzle acoustic liner attenuation. The pretest noise levels did not account for this attenuation loss.

Flap/Treatment Length Differences – The LSM nozzle effective liner area, defined as A_t/A_m, is 6.7. Effective treated area (A_t) is the actual area of treatment with perforated plate covering bulk absorber material (excluding gaps) and solid metal at tile edges and regions of attachments. This is

nondimensionalized by the mixer area (A_m). The treated liner area of the current design with 135.5-in flap, yields an A_t/A_m of 5.6. In both cases, the acoustic liner forward of the 10-hot-lobe-width axial distance is not counted. The adjustment based on Gen 2.0 and 2.5 data, from LSM flap length to 135.5-in, would yield no adjustment in static EPNL at sideline power and indicates a potential increase in assessed cutback noise status of 0.2 EPNdB at NPR 2.5.

Summary: LSM Nozzle Noise Status Versus Pretest Predictions – Table 51 summarizes the status of the LSM nozzle measured and adjusted noise levels. Cycle throttle line differences, fan/core stream nozzle inlet unmixedness, hot versus cold sidewall noise generation and liner attenuation differences, and flap length liner effective area adjustments are studied further in the LSMS, Gen 3, and 3.5 subscale model tests.

Table 51. LSM Nozzle Measured and Adjusted Noise Level

	Sideline EPNL (NPR 3.43) 689-ft Altitude 1476-ft Sideline	**Cutback EPNL (NPR 2.5) 1200-ft Altitude/Overhead**
CPC Flight EPNL	96.1	94.0
CPC Noise Goal (Adjusted to Static)	103.0 P&W (102.0 Average)	97.7 P&W (97.4 Average)
LSM Static Pretest Projections	103.8 P&W (102.8 Average)	98.0 P&W (97.3 Average)
P&W's Adjusted LSM Status	104.1 EPNdB	99.7 EPNdB
Raw LSM EPNL *	105.0 EPNdB	100.9 EPNdB
Adjustments Based on Past Data		
Cycle Differences	+0.2	+0.4
F100–PW–229 Fan Tone Removal	–0.1	–0.2
Unmixed Fan/Core Flow Profile	–0.6	–1.0
Lost Attenuation ~ Hot Sidewall	–0.4	–0.6
Liner Area and Flap Length	0.0	+0.2

* Regressed from 0.90 MAR, treated data as discussed in Subsection 5.2.1.

Data Scaled to Product Size

Scaling from 56% LSM to product size involved a band shift of 2.5 one-third-octave bands. Data are corrected with microphone corrections and adjusted to a standard day. The data are then scaled from the microphone locations to a 1-ft radius using an air-attenuation model (Reference 19). The data were shifted two and three bands to account for area differences between the LSM and product size. A two-band shift adds 4.0 dB to the data, which was removed. Similarly, 6.0 dB would be added during the three-band shift, which was also removed. The difference in dB that would result from the correct 2.5 band shift was added. The amplitude difference in dB varied for each nozzle tested (RC and LSM) due to different nozzle areas. The two-band and three-band shift data are logarithmically added together, and 3.0 dB is subtracted from the sum. The result is then scaled to 150-ft radius using Society of Automotive Engineers (SAE) Aerospace Recommended Practice (ARP) 866 air-attenuation model.

5.7.2.5 LSM Conclusions

LSM nozzle noise and performance scaling data were successfully evaluated and assessed through static testing procedures conducted at P&W's test stand C–11 from December 1997 through January

1998. Tests demonstrated the highest level of noise suppression from actual engine testing at the lowest level of thrust loss ever achieved in history. Figure 222 illustrates the noise-suppression technology level demonstrated by the LSM test with respect to historical data. The LSM data point represents LSM sideline data scaled to full size with estimated forward-flight effects and adjusted to the HSCT cycle design point. There is a noise benefit of 15.7 EPNdB for the LSM nozzle when comparing LSM data (98.6 EPNdB) to round conic nozzle data (114.3 EPNdB). The corresponding net thrust coefficient from LSM data adjusted for forward flight is 0.938, which translates to a 6.2% thrust loss compared to an ideal nozzle efficiency of 1.0.

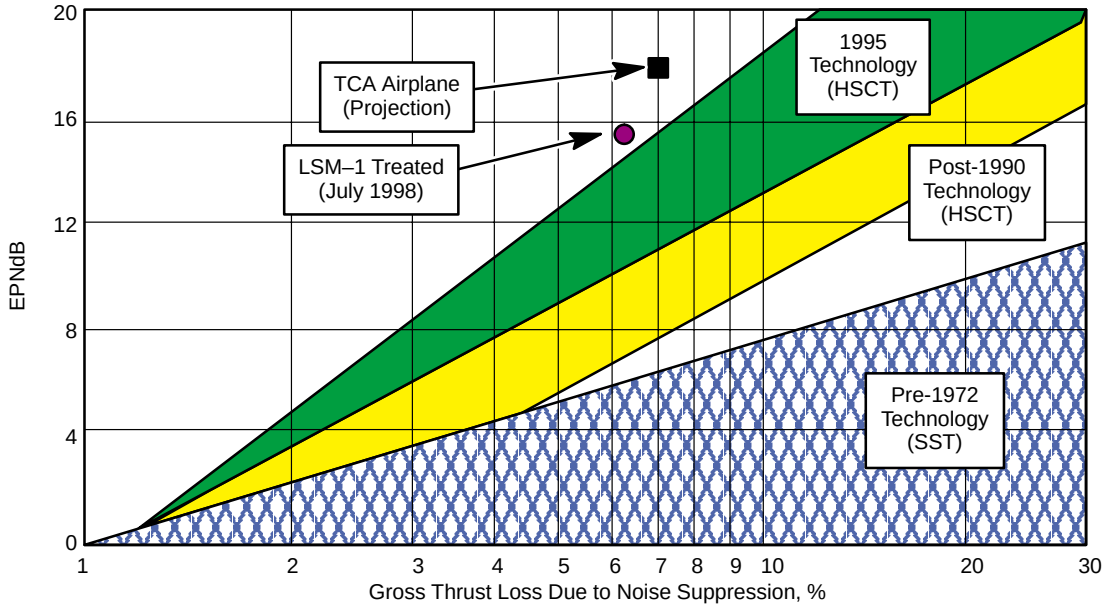

Figure 222. Thrust Loss Vs Noise Reduction

Performance results from the LSM test indicate a well-correlated prediction model at cutback power; however, an adjustment is needed at sideline power. The prediction for C_{fg} at cutback power was consistent with the test result of 0.997 (MAR =0.90, NPR =2.52, T_T =1383°R). The prediction for sideline power was 0.991 and the test result was 0.986. Treated sidewalls and flaps caused a 1% thrust loss compared to the all-hard-wall-tile configuration. There was a 1% C_{fnet} increase for each 0.05 MAR increase. Data analysis revealed that there was no mode shift from compound subsonic to compound supersonic at any of the MAR's tested (0.85, 0.90, 0.93, and 0.98). The best MAR for optimum aero and acoustic performance is between 0.90 and 0.93.

Preliminary assessments showed that noise measurements were about 1 EPNdB higher than predicted. This difference was evaluated as part of the subscale Gen 3.0 and 3.5 model tests. The 1/7-scale model program will provide forward-flight and cycle effects and subscale noise data to compare with the 56% LSM nozzle data.

Measured noise attenuation from the nozzle flap and sidewall acoustic liners was 1.5 to 2 EPNdB lower at static test conditions than the design intent of 2.5 to 5 EPNdB. The difference is partly being attributed to the selection of an ejector mixer with half hot chutes at the sidewalls (a design based on two-year-old technology), core flow hot streak from the F100–PW–229 engine fan and core streams, and nonoptimum attenuating bulk material. The half hot chute at the sidewalls provides localized supersonic flow at the acoustic liners as well as an unfavorable temperature profile

believed to adversely impact liner impedance and related noise attenuation capability. The unmixed fan/core flow hot streak increases midfrequency premerged noise, thereby masking attenuation measurements from the liners. Sequential testing of nozzle acoustic liners indicated that attenuation is ineffective (or not measurable) for the first half of the nozzle under static test conditions.

5.7.3 Small-Scale Mixer/Ejector Unsuppressed Aerodynamic Model Tests

5.7.3.1 High-Speed Model Tests

In developing the propulsion system for the HSCT, the need for a supersonic cruise database was identified. A subscale model test was planned to create this database for three current nozzle concepts with an objective to obtain this supercruise performance database for the three nozzle concepts. This database will be used to predict performance for the systems studies funded by NASA and will support ongoing design work.

Test Facility

Cold-flow aerodynamic performance was measured for each configuration at the NASA–Glenn CE22 nozzle thrust stand. This stand was calibrated using standard American Society of Mechanical Engineers (ASME) nozzles before testing. During the test, the ASME nozzle runs were repeated to detect any shifts or problems in the thrust and flow measurements. The thrust coefficient (C_{fg}) and flow coefficient (C_d) measurements are each accurate to within ±0.25%.

Hardware Description

Three 1/7-scale HSCT nozzle concepts were tested (Figure 223): a 2DCD, a 2D plug, and a 2D single-expansion-ramp nozzle (SERN). These models were fabricated and instrumented by Flui-Dyne Engineering Inc. of Minneapolis, NW. The circular-to-rectangular transition duct mates to NASA–Glenn hardware and was the same for all three nozzle concepts. The transition duct changes the flow from axisymmetric to two-dimensional flow.

2DCD Nozzle – Three 2DCD nozzles designed for the HSCT turbofan cycle were tested: baseline straight flaps, contoured flaps, and two-piece flaps. The baseline configuration had straight flaps with different divergent flap lengths and area ratios. Throat area (A_j) was 19.75 in^2 (for all models) with area ratios (A_e/A_j) ranging from 1.1 to 3.5 and divergent flap lengths of 10, 14, and 18 in. This 2DCD baseline was tested with smooth walls and with two degrees of rough (knurled) internal surfaces in an effort to determine the performance loss due to the acoustic liners at several area ratios.

A contoured and a two-piece flap design intended to provide the best possible performance at the supercruise design point were also tested at three area ratios ($A_{e/}A_j$ = 2.5, 3.0, and 3.5) and a divergent flap length of 10 in. The contoured flap was a truncated isentropic contour optimized for the supercruise area ratio and flap length. The two-piece flap was designed using the divergent flap leading- and trailing-edge angles from the truncated isentropic contour design. This design was similar to the supercruise position of the downstream-mixer nozzle concept. Both the contoured and the two-piece designs were intended to maximize supercruise performance at the expense of the lower pressure ratio, subcruise performance.

2D Plug Nozzle – The 2D plug nozzle was designed for the fluid-shield engine cycle. The 2D plug model baseline configuration used a plug surface with a supersonic cruise design point isentropic

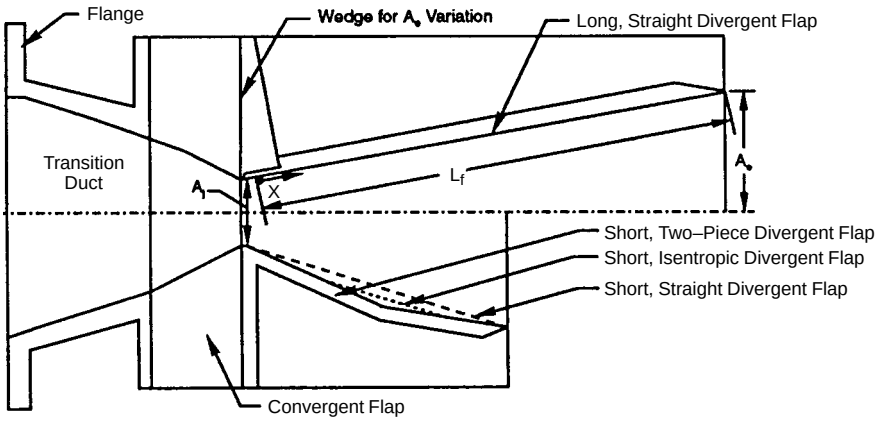

2DCD Model Configuration Geometry Variations

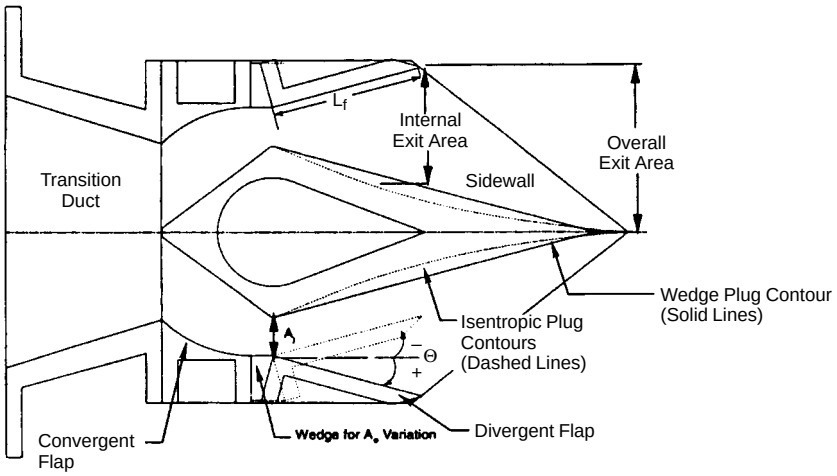

2D Plug Model Configuration Geometry Variations

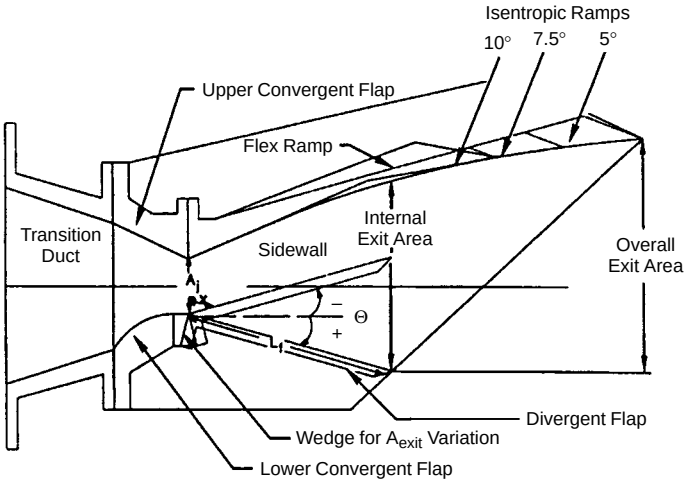

SERN Model Configuration Geometry Variations

Figure 223. Model Geometries

contour truncated such that the trailing edge was at a 5° angle. The flap had a straight surface with a length determined by wave cancellation for the complete isentropic plug contour. For consistency, the throat area was 19.75 in^2. Configuration variables included a plug with the isentropic contour truncated at a 10° angle and a straight plug (wedge) at a 15° angle. Flap length variations of 75% and 50% of the baseline length and flap angles of –15°, –10°, 0°, and 10° were tested. Flap length and angle variations covered the area ratio range from 1.7 to 4.0.

SERN – The SERN was also designed for the fluid-shield engine cycle. The SERN model baseline configuration used a ramp surface with a supersonic cruise design point isentropic contour truncated so that the trailing edge was at a 5° angle. The flap had a straight surface with a length determined by wave cancellation for the complete isentropic ramp contour. For consistency, the throat area was 19.75 in^2. Configuration variables included ramp truncation angle (and therefore length) for the isentropic contour of 7.5° and 10° and a ramp with a surface composed of two straight sections (flex ramp) using the leading-edge angle from the isentropic contour and a trailing-edge angle. Flap length variations of 75% and 50% of the baseline length and flap angles of –15°, –10°, 0°, 51°, 10°, and 15° were tested. Flap length and angle variations covered an area ratio range from 1.5 to 4.25.

Conclusions

Results of the high-speed performance tests showed that relatively long, straight-wall, CD nozzles could meet supersonic cruise thrust coefficient goals. The plug, ramp, and shorter CD nozzles required isentropic contours to reach the same level of performance. The effects of wall friction, even with simulated acoustic-liner roughness, were less than predicted.

2DCD Nozzle Performance Summary

- As expected, the isentropic contours provided the highest performance of the three flap types tested (C_{fg} = 0.992 at the 2.5 area ratio). The two-piece flap was about 0.002 lower, and the baseline straight flap was 0.007 lower than the isentropic design (Figure 224).

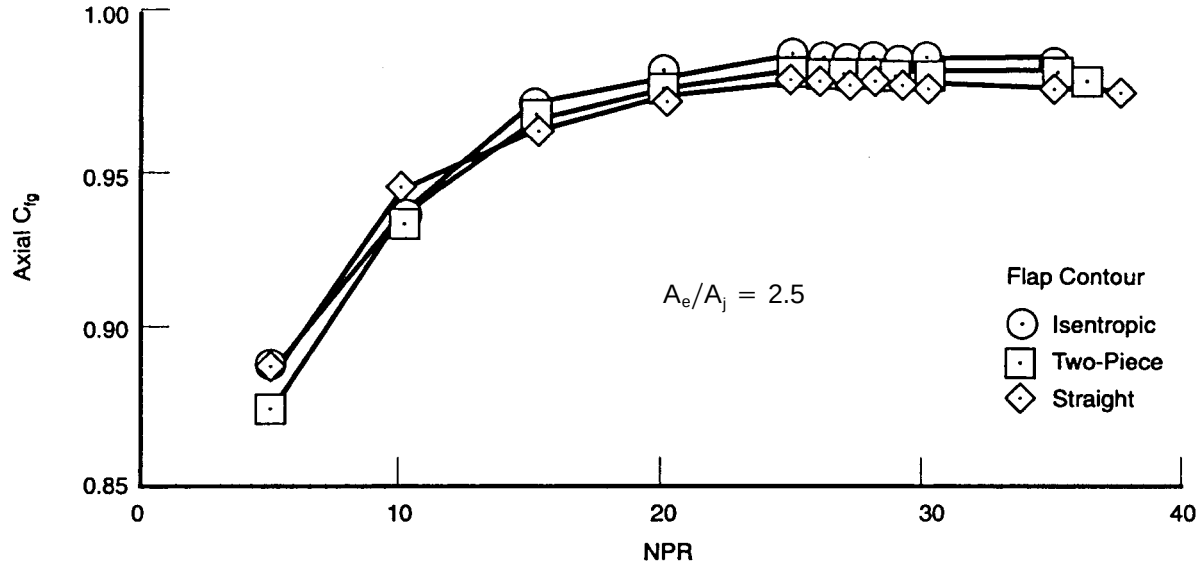

Figure 224. Performance of 2D/CD Nozzle

- Peak performance for the long flaps at an area ratio of 3.5 and an NPR of 27.5 was 0.988, or 0.8% higher than the short flaps due to the higher divergence losses of the shorter flap.
- The additional skin friction drag of the long flaps negates the decrease in divergence losses so that the performance for both the medium and long flaps is within 0.2% at an area ratio of 3.5 and a design pressure ratio of 27.5.
- Tests of the two degrees of roughness for the straight, long flap showed a 0.002 C_{fg} loss for area ratios between 2.5 and 3.5 but up to 0.0075 C_{fg} loss at 1.1 and 1.3 area ratios (Figure 225).
- The splitter configuration performed lower than the baseline configuration (0.5%) at an NPR greater than 15.

2D Plug Performance Summary

- The performance of the isentropic plugs was higher than the straight wedge at all of the flap angles and lengths. (Figure 226).
- For a 0° flap angle and a 4.598 flap length, the isentropic 5° plug had a peak C_{fg} of 0.987, higher than the 15° wedge and 0.5% higher than the isentropic 10° plug.
- The lower cowl angles perform better at the lower pressure ratios, while angles above 0° perform better at the higher area ratios.
- Even though the performance of the negative cowl angles (into the flow) is better at the lower NPR's, the flow tends to be less stable, and often the shock from the flap separates the flow off the end of the plug — creating further instabilities.
- At higher NPR's, flap length has little effect on the performance of the isentropic and wedge plugs with a flap angle of 0°.

SERN Performance Summary

- The isentropic ramps performed higher than the flex ramp (Figure 227).
- The 5° isentropic ramp performance (C_{fg} = 0.987) was 2% higher than that of the 7.5° ramp, 0.4% higher than that of the 10° ramp, and 0.9% higher than that of the flex ramp at a flap angle of 0° and a flap length of 7.379 in.
- Lower flap angles perform better at the lower pressure ratios (NPR less than 15).
- The 0° flap angle performs better than the higher angles at pressure ratios above 15. There is no performance benefit evident for flap angles greater than 0°.
- At a 0° flap angle and 10° isentropic ramp, only the longest flap length showed a slight decrease in peak C_{fg} from the 0.983 level of the two shorter flaps.
- Flap length had little effect on peak Cfg except for the 15° wedge/15° flap combinations — which showed a 1.5% loss for the shortest flap length.

5.7.3.2 Unsuppressed Model

Model Test Objectives

An unsuppressed model was designed and fabricated to determine the internal aerodynamic performance of the fixed-chute nozzle in the cruise mode in a cold-flow test. The model was designed to

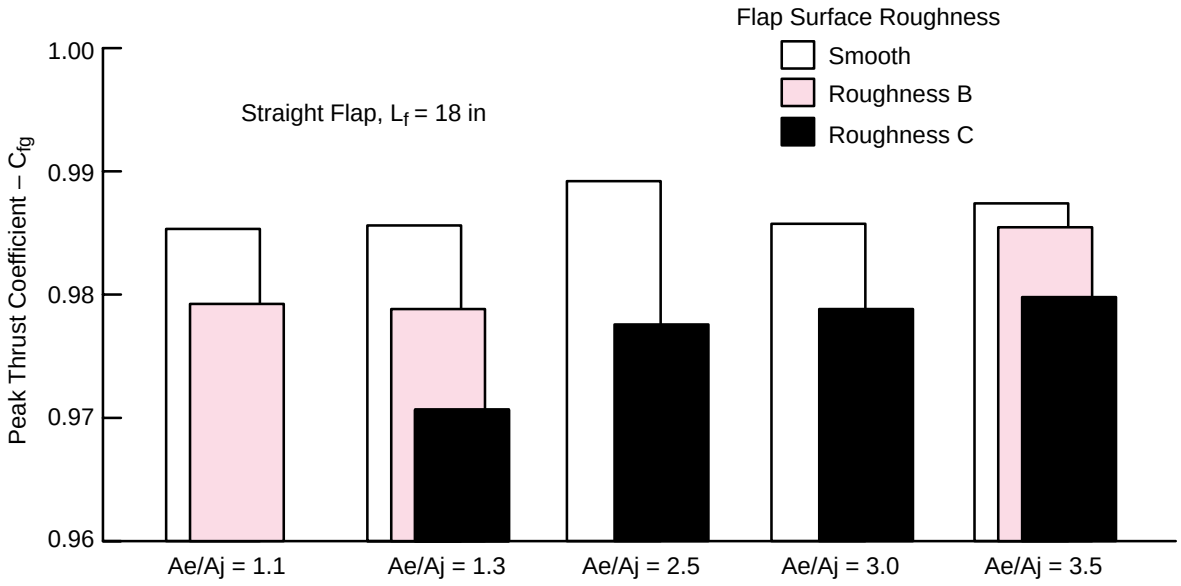

Figure 225. Effects of Flap Roughness on 2DCD Nozzle Performance

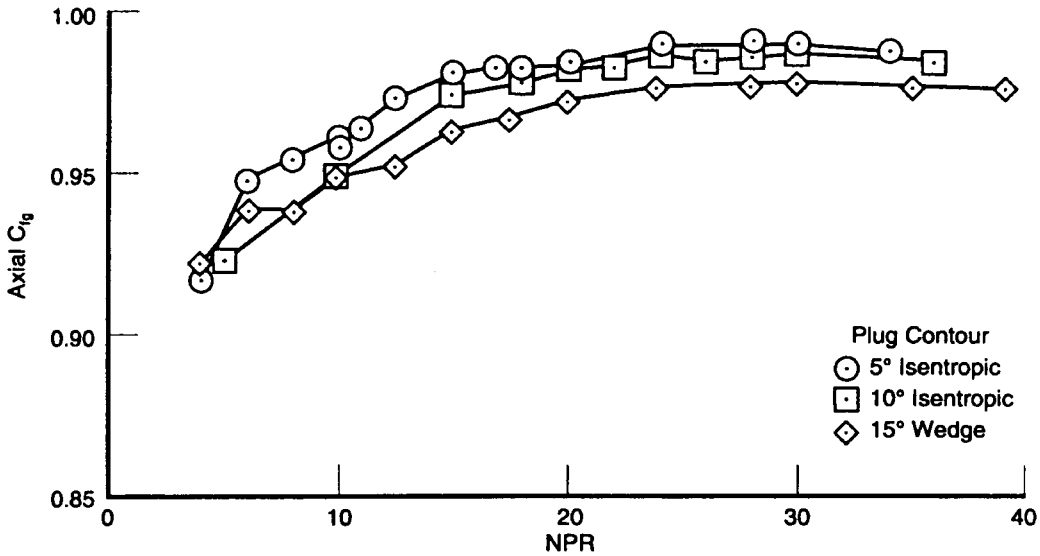

Effect of Plug Contour (L_f = 4.958 in, Flap Angle = 0°)

Figure 226. Plug Nozzle Performance

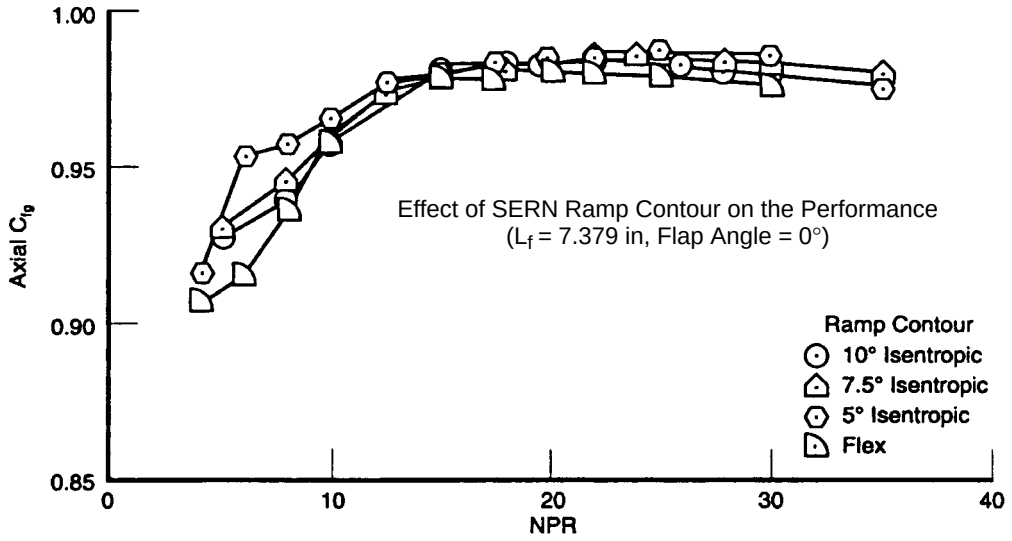

Figure 227. SERN Performance

be used in the NASA–Glenn Ce22 test stand, but the program was terminated before such testing was conducted. Objectives for this test follow.

1. Basic nozzle internal performance validation at subcruise, transonic and supersonic acceleration, and supercruise conditions.
2. Effects of treatment on thrust coefficient at subcruise, transonic acceleration, and supercruise.
3. Cruise-mode cycle duct pressure loss update (includes effects due to T-duct plenum dump loss and mixer chutes).
4. Low area ratio, nozzle aeromechanical stability design information and performance effects at subcruise conditions.
5. Sidewall length variation (relative to current product baseline) effects on subcruise, transonic acceleration, and supercruise thrust coefficient.
6. Gen 3.5 chevron impact on subcruise, transonic acceleration, and supercruise thrust coefficient.
7. Nozzle dynamic pressure frequency and amplitude characterization at subcruise, transonic acceleration, and supercruise conditions.
8. Mixer and T-duct pressure loading for mechanical loads.

Model Description

A cross section of the model in two different buildups is shown in Figure 229. The model flowpath simulation is10% of product size taken from the 3770.60 engine/nozzle design at 800-lbm/s size and includes the T-duct, upstream acoustic mixer, convergent and divergent flaps, sidewalls, and external nozzle flowpath surfaces. The fan/core mixer and centerbody are not part of this model simulation. The convergent and divergent flap positions can be varied such that three nozzle throat areas (A_8) and a wide range of area ratios (A_9/A_8) could be tested covering the complete cruise mode

operating regime. A plot showing the 3770.60 cycle A_9/A_8 versus A_8 points across the flight envelope and the corresponding available model geometries intended to cover those points is shown in Figure 228. The upstream T-duct and acoustic mixer are replaceable with a clean duct as shown in Figure 229 to enable the determination of the cruise mode pressures losses associated with that hardware. Sidewalls are also replaceable to determine the effect of sidewall length change and chevrons on nozzle performance. Another very important feature of the nozzle was the inclusion of both smooth sidewalls and divergent flaps and simulated acoustic treatment panels on these surfaces to determine the effects of treatment on cruise mode performance.

Model Instrumentation

The model will be instrumented with approximately 100 static pressure taps on the internal surfaces to obtain diagnostic aerodynamic data and to provide gas load information to support mechanical design analyses. Approximately 60 pressures would have been installed on the external flowpath surfaces had the model been compatible with the initially planned wind tunnel tests. Additionally, dynamic pressure sensors (Kulites) will be installed on the internal surfaces to obtain information related to high-frequency gas loading and acoustics.

5.7.4 High-Lift Engine Aeroacoustics Technology (HEAT) Model Test

Objectives

The primary goals of the NASA HEAT research program were to evaluate the first-order installation effects of the following:

- Noise: Integration of the mixer/ejector nozzle with the airframe.
- Propulsion: Impact of the airframe on nozzle performance.
- Aerodynamics: Influence of the nozzle secondary flow on wing aerodynamic performance.

Results from this test would be used to decide whether isolated nozzle testing in facilities such as GEAE's Cell 41 (described in Subsection 5.7.1.2) and Boeing's LSAF (Subsection 5.7.1.3) should continue or be abandoned as too unrepresentative.

Model Description

Testing was conducted at the NASA–Ames 40×80-ft wind tunnel during in mid-1994 and the first half of 1995. The first entry comprised an isolated nacelle test of the propulsion system for use as the reference or baseline for installation impacts. This test became known as HIN (HEAT isolated nacelle). For the second entry, the nozzle model was installed in a semispan representation of the airframe mounted on a reflection plane in the wind tunnel. This test was identified as HSS (HEAT semi-span).

Two new, approximately 1/7-scale, model nozzles were designed and built for these tests. The first, designated the HAM (for hot aeroacoustic model), replicated the fundamentals of the NRA model system used in Cell 41 but was designed with a square rather than rectangular inlet flange. This allowed installation in either of two orientations: with the secondary inlets "top to bottom" or "side to side" relative to the wing surfaces. The HAM model system uses the same mixer chute racks as

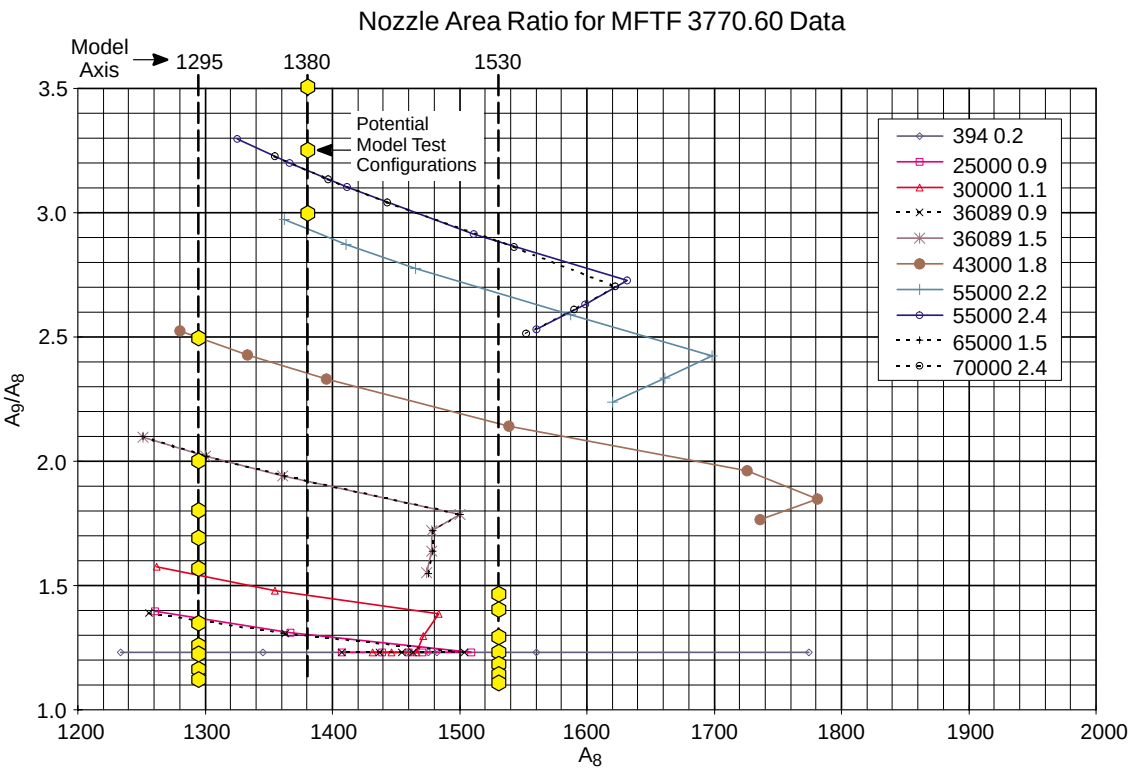

Figure 228. MTTF3770.60 Cycle A_9/A_8 versus A_8 Flight Envelope

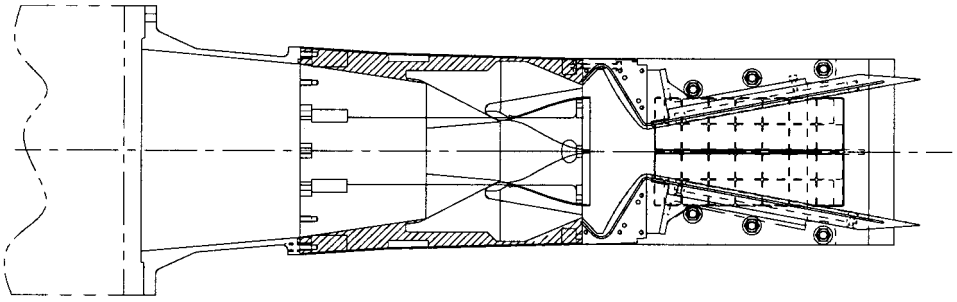

M 2.4 Cruise, Upstream Ducting and Mixer Simulated

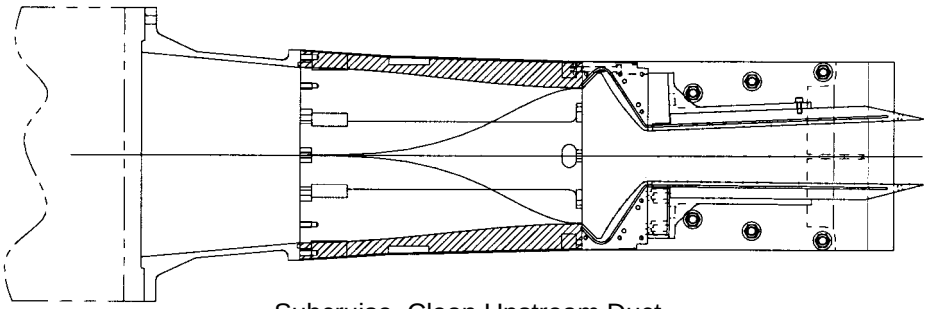

Subcruise, Clean Upstream Duct

Figure 229. Scale-Model Cross Section

the NRA system and has, since the HEAT test, been installed in Boeing's LSAF and NASA–Langley's JNL for further data acquisition as described in Subsection 5.7.1. Figure 230 shows a cut-away view of the HAM model.

The second system, designated the CAM (cold aeroperformance model), was designed strictly for cold-flow aerodynamic performance testing with the same flowpath as the HAM and was a typical, smooth-walled, highly instrumented, aeroperformance model.

The mixer designs used in these tests were those used in the Gen 1.0 and 1.5 test series in Cell 41 (Subsections 5.7.5.4 and 5.7.1.2). Configurations investigated for acoustics in the HIN test included:

- SAR 2.8 and 3.3: solid hardwall and with foam metal treatment.
- Inlet shape: "flight" (with a horizontal section upstream of the secondary inlets) for installation into the semispan model and "Cell 41" (with a "conical" section upstream) to simulate the large-diameter facility ducting upstream of the models in the Cell 41 environment.
- Inlet orientation: top to bottom, corresponding to Cell 41 90° location, and side to side, corresponding to Cell 41 0° location.

Nozzle acoustic configurations tested in the HSS test repeated the above — with the exception that, since the nozzle was installed on the wing, the "Cell 41" inlet shape was irrelevant.

The airframe model used in the HSS test was a 13.5% scale of an early HSCT wing configuration. The design was designated the Reference H wing configuration. Figure 231 is a schematic of the model installed in the NASA–Ames facility. The model semispan simulation included the wing, half fuselage, horizontal tail, and inboard and outboard engine/nacelle propulsion systems. The model

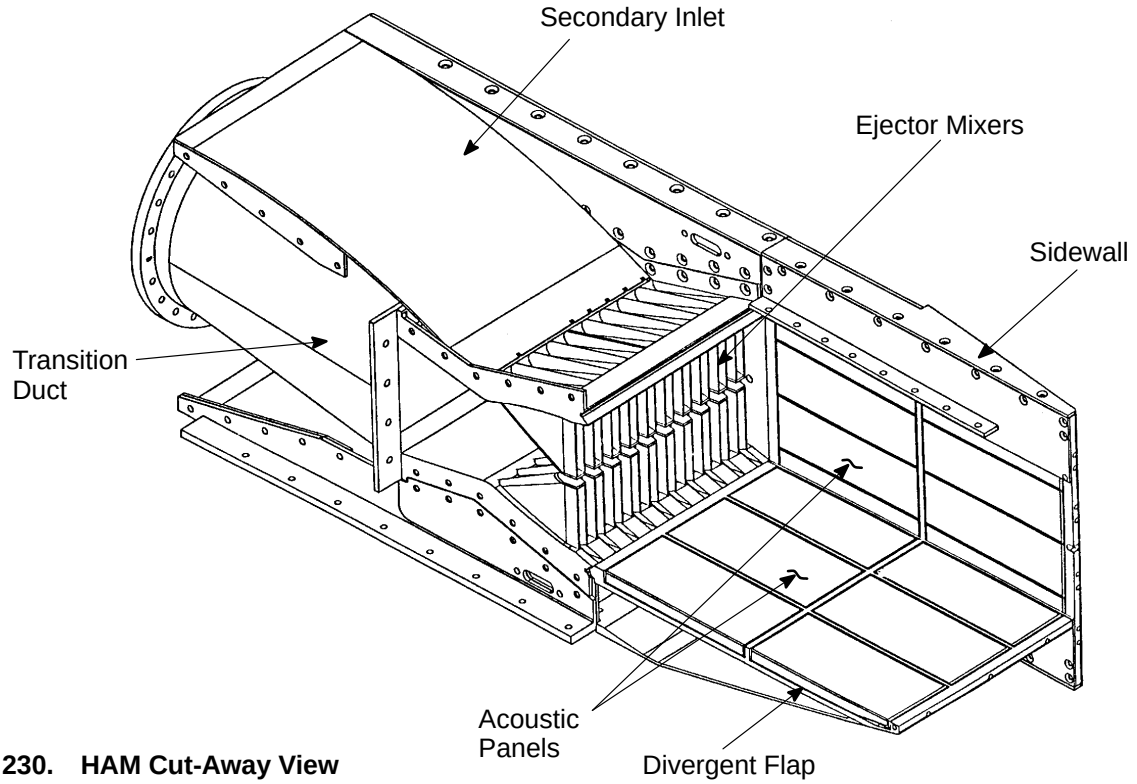

Figure 230. HAM Cut-Away View

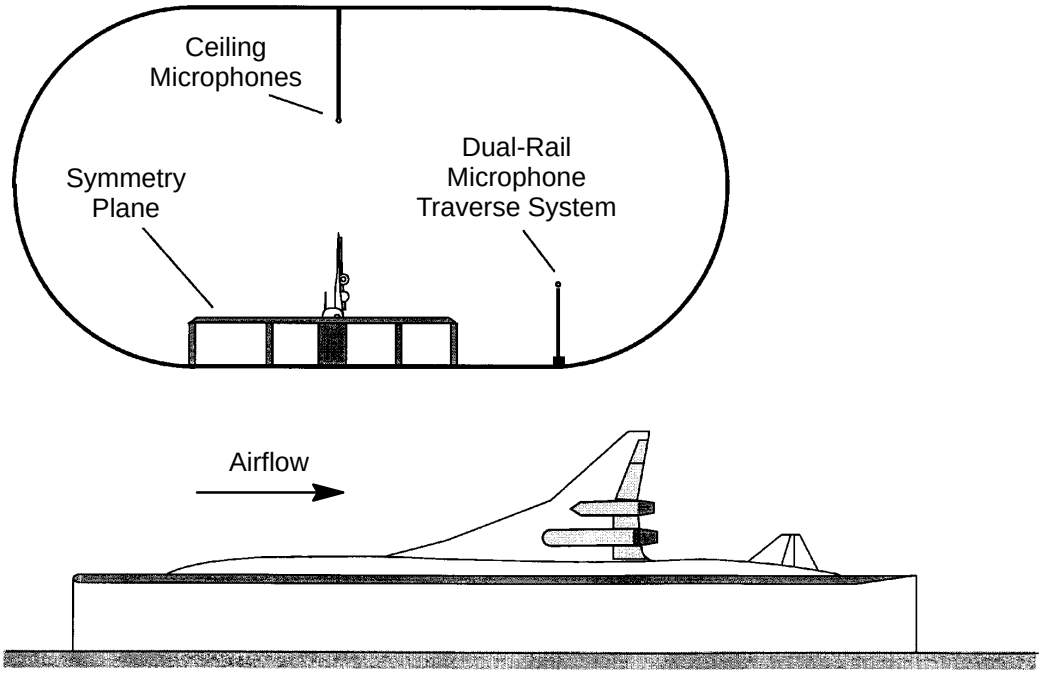

Figure 231. HEAT Model Installation in the NASA–Ames 40x80-ft Tunnel

was mounted on an acoustically treated reflection plane and could be rotated to obtain a range of aircraft angles of attack. Aircraft model variables included:

- 0° and 35° deflection leading-edge flaps
- 0°, 10°, and 20° trailing-edge flap deflections (each of four sections could be set independently)
- Trailing-edge flap configuration (simple hinged or slotted)
- Adjustable-incidence horizontal tail and elevators
- With or without nozzle support fins

Figure 232 is a planform view of the aircraft model with key geometric information noted.

The powered nozzle (HAM or CAM) was installed in the inboard location on the wing, with the presence of the outboard engine simulated by a flow-through nacelle.

Measurements and Test Conditions

Acoustic measurements were made with traversing microphones at the “cutback” location relative to the airplane (that is, directly under the flight path). In addition, three fixed microphones were mounted in the ceiling of the wind tunnel. For all test configurations, the microphones covered the full polar directivity range in the “cutback” location only. The specific vertical installation of the model in the facility did not allow proper placement of the microphones for valid “sideline” acoustic measurements.

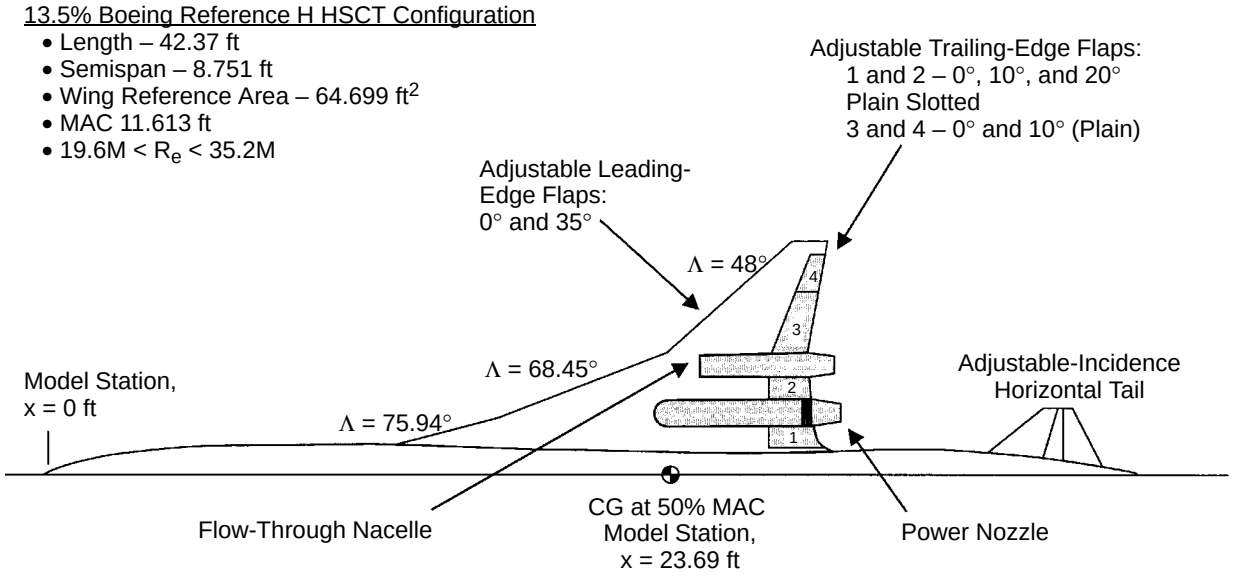

Figure 232. HEAT Model Geometry

A major concern prior to the test was the effect of background noise on the microphone signals. Acoustic testing in a wind tunnel removes the complications of shear layer corrections experienced in free-jet facilities, but flow over the microphones gives rise to a noise floor considerably higher than those of the free jets. Much effort has been expended on the design of nosecones for microphones immersed in the flow, which has alleviated some of the problems of earlier designs. Despite this, however, in order to extract the noise signature of the nozzle from the background, testing here was limited to the upper end of the cycle. Background noise problems were especially severe in the forward angles, leading to anomalies in establishing the 10-dB-down point for evaluation of EPNL. In consequence, comparison of configurations was made using the peak PNL levels calculated.

A second area of concern that was identified early was the potential problem of noise from the burner rig used to power the model. Much effort was spent in the attempt to ensure nondistorted temperature and pressure profiles at the charging station, but tones ascribed to the burner were still found in the spectra — more so for the HSS than for the HIN.

Total forces and moments on the wing/body/fuselage and the isolated nacelles were measured with the wind tunnel force-balance system. Numerous static pressures were recorded on the upper and lower surfaces of the wing/flap, on the external and internal surfaces of the HAM and CAM models, and on the reflection plane. During drag calibration tests, static pressures were also recorded on blank-off tare plates. Inlet boundary layer rakes were installed on the upper and lower surfaces of the wing/nacelle centered upstream of the ejector inlets, and total pressure rakes were installed in both ejector inlets. Internal pressures, temperatures, and metered flow rates of the propulsion models were recorded to determine the gross thrust. Wing/flap surface and off-body flowfield characteristics were obtained with flow-visualization techniques.

The wing/body model was tested at angles of attack from –2° to +16° over a Mach number range of 0 to 0.4. The inboard nacelle powered by the HAM was tested over a nozzle pressure ratio range of 2.0 to about 4.5 at hot-gas temperatures ranging from about 715° to 1400°F, corresponding to typical HSCT cycle conditions. The same gas conditions were also set for the isolated nacelle testing.

Significant Results and Conclusions

Acoustic Results – In general, comparison of the overall installed noise levels relative to the isolated values indicated the following

- At all conditions the forward angles (usually up to 90° or 100°, sometimes beyond) experience an increase in PNL due to installed testing.
- Spectral increases are generally broadband from very low frequency up to at least 1 to 2 kHz (full scale).
- At certain conditions, burner tones made interpretation of effects problematic.
- Background noise presented problems, particularly at the lower nozzle pressure ratios and higher tunnel speeds.

Preliminary analysis indicated the "flight" inlet may have had slightly higher noise levels (about 0.4 Peak PNL) than the "Cell 41" inlet shape. The details were unclear due to background noise and burner tone differences.

The jet-noise installation effect bookkept in aircraft system studies as a result of this test is +0.8 EPNdB at cutback only. The limited data at the sideline orientation provided no evidence that sideline noise increased due to installation effects.

Aerodynamic Results – No adverse effects on the aircraft force and moment performance were observed due to the presence of the inboard nacelle ejector inlet and nozzle flows. However, it is pointed out that, from this test, any effects could not absolutely be separated since the nozzle could not be mounted on a separate force balance. A slight propulsion-induced L/D improvement of about 0.2 was observed with the ejector inlets mounted top-to-bottom versus side-to-side. This improvement was also observed in the static pressure data on the wing and nacelle surfaces. No adverse effects due to the jet plume on the horizontal tail were observed; the worst case temperature rise measured on the tail leading edge was approximately 15°. Large spanwise flows were observed on the wing upper surface near the location of the outboard engine ejector inlet, primarily at higher angles of attack near 14° (nominal takeoff is near 10°). Since a powered nacelle was not placed at this location, the effect on ejector inlet recovery and nozzle performance could not be determined.

HIN CAM performance characteristics agreed reasonably well with data obtained on similar models tested at NASA–Langley. Performance characteristics of the HIN HAM with the acoustic treatment also agreed well with data taken in other tests. No appreciable integration effects on the ejector nozzle performance were observed. Total pressure recovery of the upper ejector inlet was about 1% below the lower inlet at the design point Mach number due to the wing flowfield. The wing boundary layer profiles could be directly seen in the rakes located within the upper ejector inlet. Likewise, no changes were observed in the wing boundary layer profiles between power on and power off conditions. Consistent with the profile data, little change in ejector pumping characteristics was measured between the HSS ands HIN tests. This lack of wing-flowfield/ejector-inlet characteristic interaction was also independent of trailing- or leading-edge flap positions. A reduction in ejector pumping ratio of about 5% for the side-to-side ejector inlet orientation relative to the baseline top-to-bottom orientation was measured, indicating an unfavorable effect; this was attributed to the 20° trailing-edge flap position at takeoff.

Overall Conclusions – Overall, the acoustic results showed minor effects of installation for the mixer/ejector nozzle designs tested. No appreciable aerodynamic interactions between the ejector

propulsion system and the aircraft were observed in this first installed, low-speed test of the HSCT aircraft/propulsion system. These conclusions lend confidence that, at least to first-order, the development of the HSCT technology could proceed with the isolated nacelle development test approach and not have any surprises with the integrated system.

Further detail and background are available in References 22 and 23.

5.7.5 Other Exhaust Nozzle Concept Tests

The concept tests are summarized below. Further detail and background are available in References 24 through 27.

5.7.5.1 Fluid Shield Nozzle

The FSN was considered as a potential suppressor for the FLADE engine. The aeroacoustics and aerodynamics of fluid-shield nozzles were investigated under the *Advanced Propulsion Technology* contract in a series of tests in GEAE's Cell 41 free-jet anechoic facility and *Aerodynamics Research Laboratory.* Essentially, the concept consists of an axisymmetric mixer plug nozzle around a portion of which is wrapped a second stream of air, providing an intermediate shear step between the core flow and ambient air (Figure 17, page 15).

Parameters varied during the acoustic testing included: shield thickness, shield wrap angle, mass flow and velocity ratios between core and shield flow at constant specific thrust (varying true thrust), hard-wall or porous plug, and super- or subsonic shield.

The acoustic tests used an axisymmetric, 36-chute, plug suppressor nozzle, tested as described in Subsection 5.7.1.2. The aerodynamic tests used a 2D representation of a sector of the acoustic model and were run using "warm" (about 400°F) conditions for the core stream.

Relative to a simple conic nozzle, at takeoff conditions, suppressions of approximately 8 EPNdB were achieved by the use of the suppressor nozzle alone. An additional 4 to 8 EPNdB were obtained with the fluid shield, depending on the particular geometry employed. Suppression increased with shield thickness and with increasing velocity ratio and/or mass flow ratio. As could be expected, noise benefits are at the expense of thrust. If the data are compared on a normalized-thrust basis, no additional benefit is found for the FSN over that obtained with a mixer alone.

The aerodynamic tests investigated chute design parameters as well as shield thickness and cycle effects. Shadowgraphs were used to screen the configurations prior to more intensive laser-velocimeter data acquisition and flow visualization using a planar laser sheet. The shadowgraphs provided insight into the highly complex 3D shock structures identified in the fluid shield and along the plug (simulated by a wedge here); the LV gave details of the flow within the shield and along the wedge, and the planar laser sheet allowed some insight to be gained into the mixing process.

5.7.5.2 Axisymmetric Mixer/Ejector Nozzle

An axisymmetric mixer/ejector nozzle (AMEN), designed and built as part of GEAE IR&D effort, was tested in GEAE's Cell 41 anechoic free-jet facility in 1993. (The same nozzle had previously been tested under IR&D funding in Boeing's LSAF and was later run in the NASA ARC 40×80-ft wind tunnel as a precursor to the HEAT test, Subsection 5.7.4).

The nozzle is shown in Figures 233 and 234. It has 24 convergent/divergent chutes and a suppressor area ratio (SAR) of 3.7. This large SAR and the short ejector length resulted in unacceptably high

Figure 233. AMEN in GEAE Cell 41 Ancehoic Facility

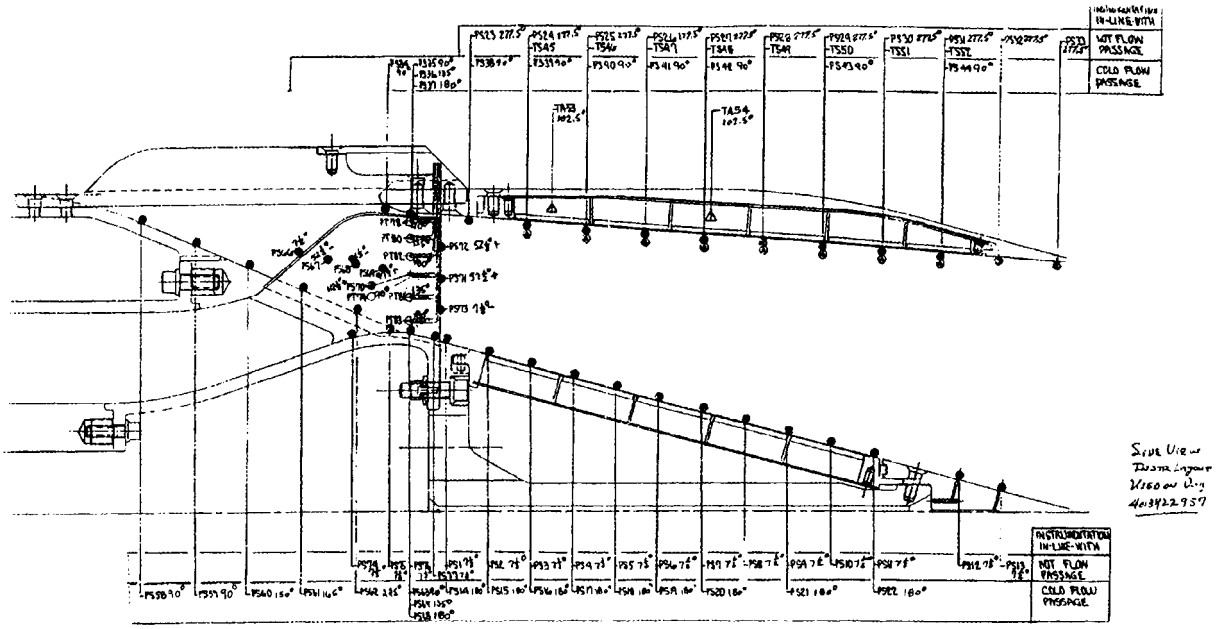

Figure 234. Side View of AMEN Showing Instrumentation

noise levels. (Suppression relative to a conic nozzle at sideline conditions was 13.7 EPNdB.) On the other hand, it had both ejector and plug surfaces available for a variety of treatment configurations, and it was also possible to run as a bare nozzle without the ejector.

Highlights of the test included the investigation of shock-cell noise (Figure 235) encountered while running cold with the hard-wall plug and no ejector and the logical progression of suppression from the bare nozzle with hard-wall plug through the treated plug, hard-wall ejector and plug to the fully treated ejector and plug (Figure 236).

5.7.5.3 P&W Gen 1

A high-area-ratio, 2D, shrouded, eight-lobe, mixer/ejector nozzle was tested in GEAE's Cell 41 anechoic free-jet noise facility. The tests evaluated two mixer designs — high-mixing vortical and aligned axial flow — along with variations in shroud internal mixing area ratios, shroud length, and shroud treatment. A total of 21 model configurations at 1:11.47 scale were tested over a range of

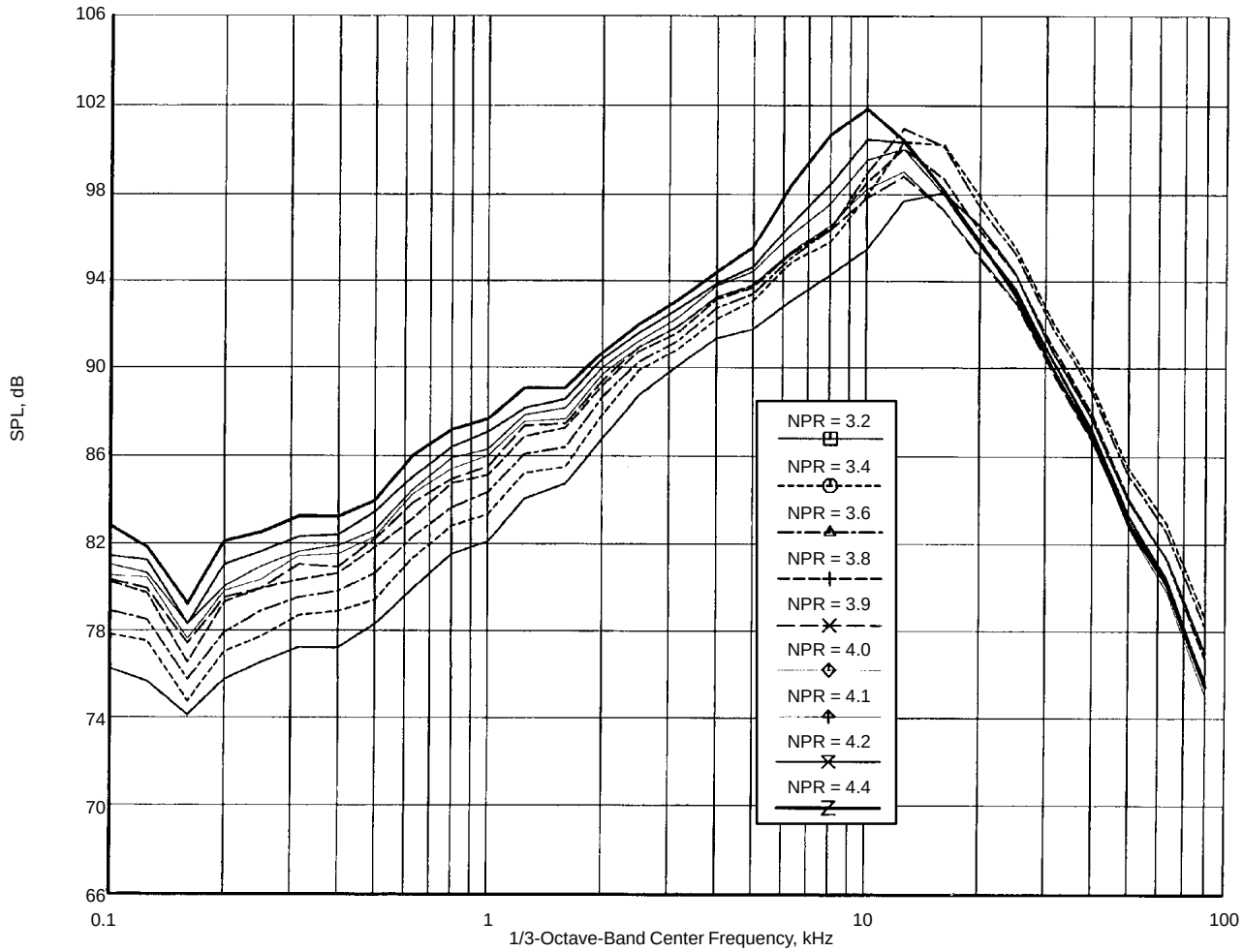

Figure 235. Shock-Noise Investigation: Hard-Wall Plug, Mixer Alone, 70°

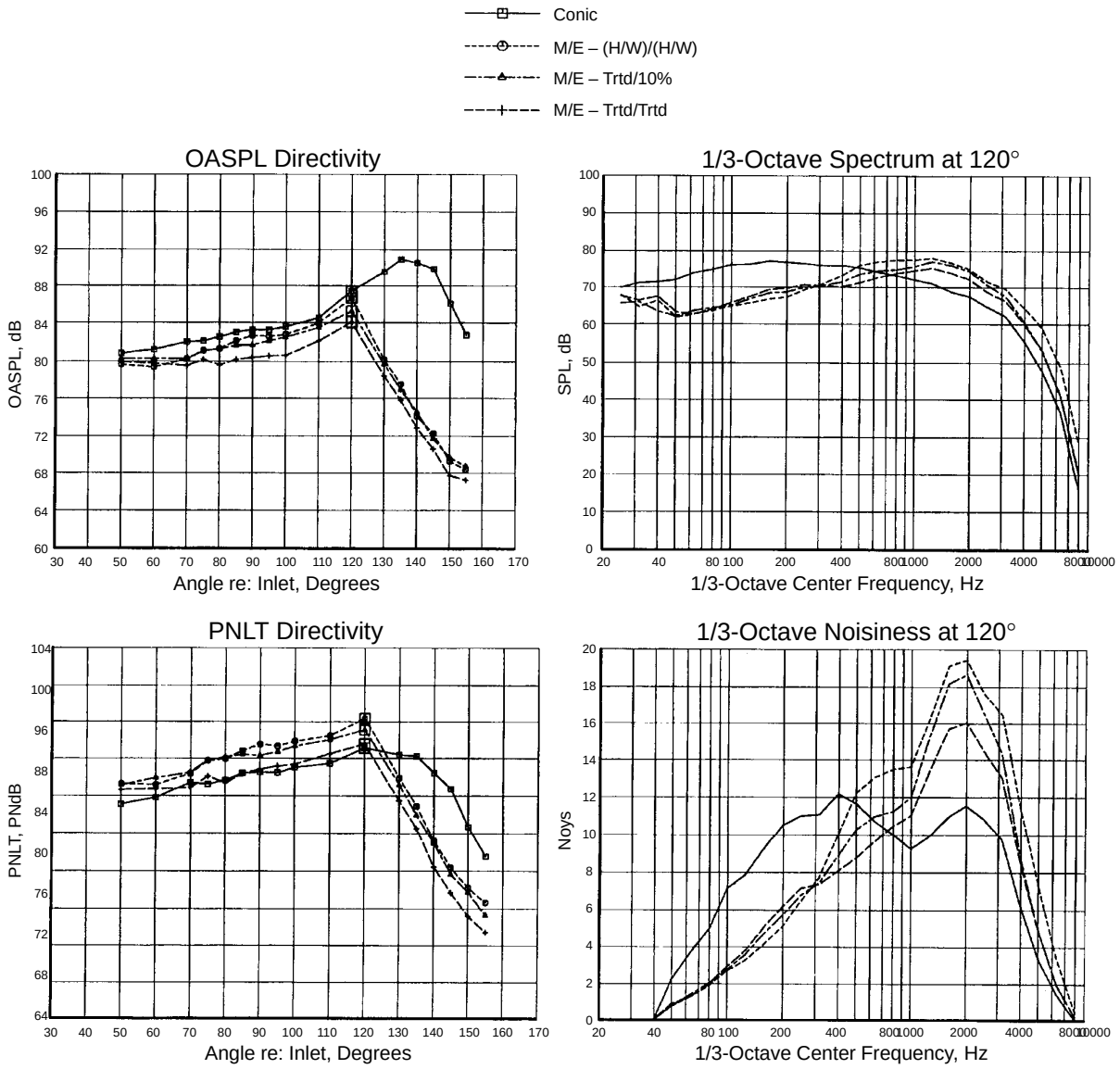

Figure 236. Effect of Treatment: M_{fj} = 0.32, V_j = 1600 ft/s

primary nozzle pressure ratios and temperatures representative of the HSCT engine cycle conditions. Two suppressor area ratios (4.9 and 4.4) were tested. A round convergent nozzle model was also tested to provide a baseline. Two-axis LV data were acquired and compared to CFD analyses using the P&W NASTAR Navier–Stokes code. A final report has been approved (Reference 28).

The two nozzle/mixer configurations tested are shown in Figures 237 and 238; Figure 239 shows the nozzle mounted in GEAE's Cell 41 facility. Favorable comparisons were made with previous results obtained with this hardware at the NASA–Lewis (now Glenn) 9×15ft LSWT. Significant reductions in exhaust noise were demonstrated with the high-suppressor-area-ratio, 2D nozzle designs.

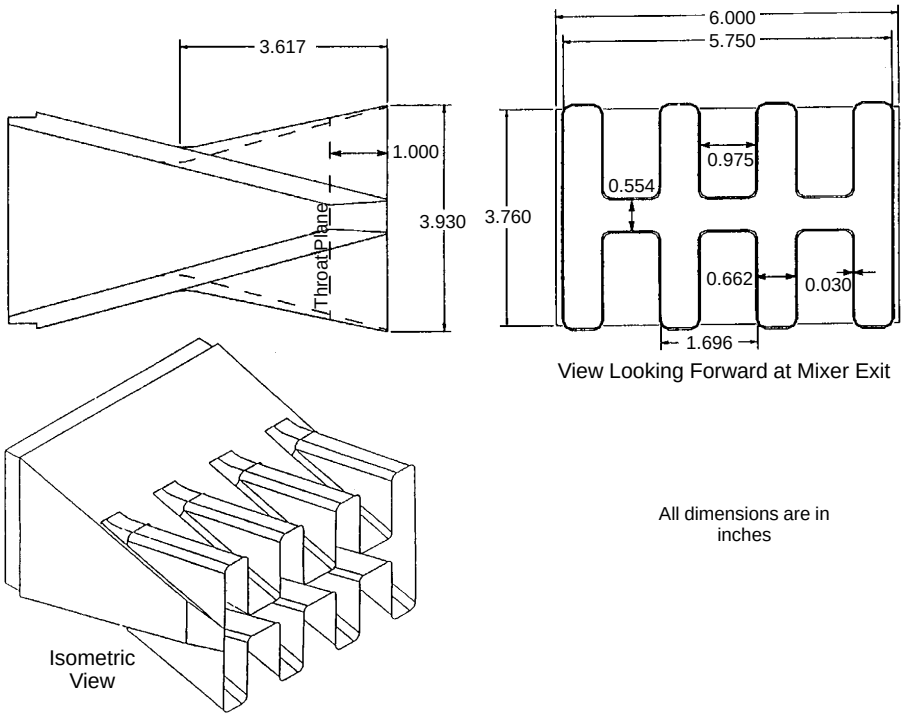

Figure 237. Geometry of 2D Vortical Mixer Nozzle

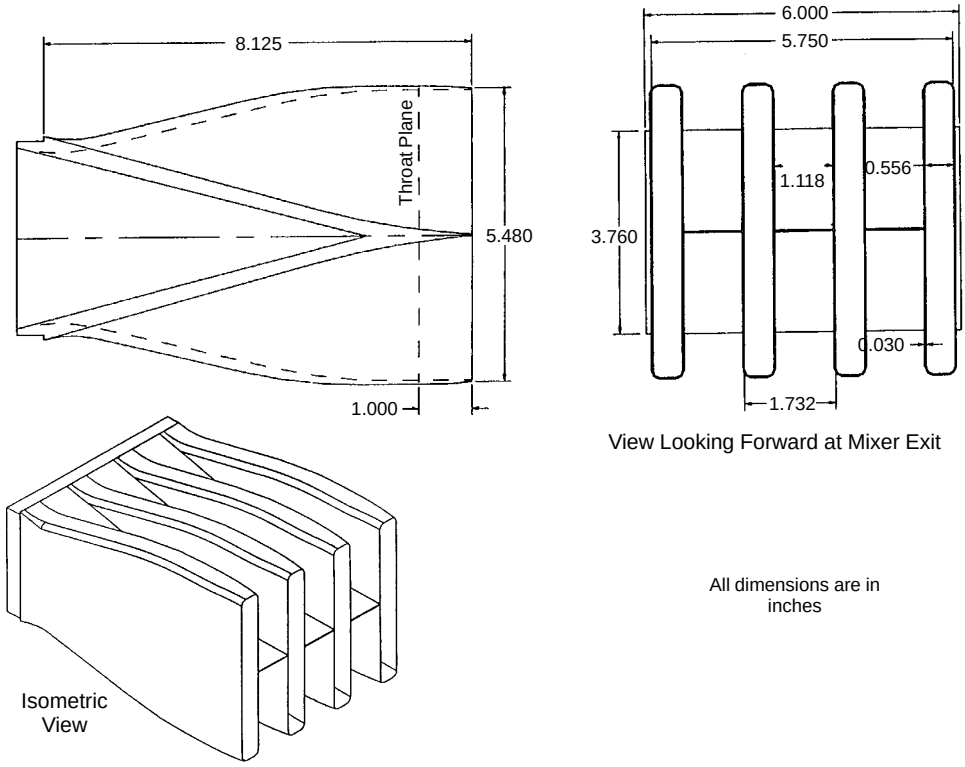

Figure 238. Geometry of 2D Axial Mixer Nozzle

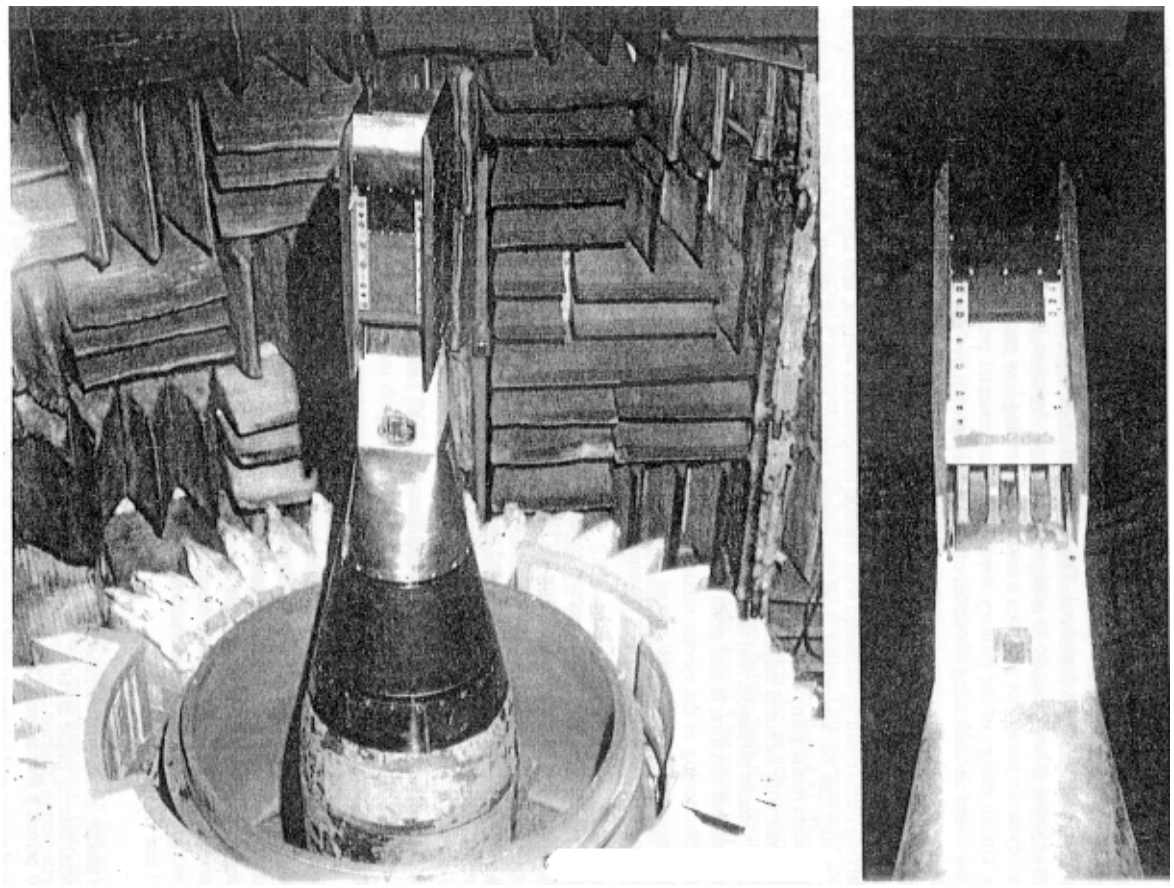

Figure 239. Mixer/Ejector Model Mounted in Acoustic Test Facility

5.7.5.4 Gen 1 NRA Tests

The NRA 2D mixer/ejector nozzle concept was developed as a precursor to the CPC program. Three models were designed, manufactured, and tested:

- The NRA acoustic model – used as a workhorse in Cell 41 over a seven-year period. The design met the then acoustic goals when it was first tested, achieving FAR36 Stage III noise levels (Reference 1) for ideal primary jet velocities of about 2400 ft/s. Unfortunately, this suppression was achieved at the expense of takeoff aeroperformance — the start of the continual compromise between performance and acoustics.
- The Langley model – tested in the NASA-Langley 16-ft transonic windtunnel to obtain ambient performance data at free-stream Mach numbers ranging from 0.0 (static) to 0.7.
- The ARL model – tested in GEAE's Aerodynamics Research Laboratory to evaluate the mixing characteristics of the 2D mixer/ejector model under warm conditions.

Two mixers were manufactured for the acoustic tests, each with 20 chutes and a ½-width hot chute at the sidewalls. SAR's were 2.8 and 3.3 with the "NRA" shape chute design described in Subsection 5.7.1.4. The ejector could be configured as "80 in" or "120 in" full scale, and the inner surface could hold treatment trays or the same trays with sheet metal forced against the underside of the perforated face sheet (the "pseudo" or "perforated" hard-wall configuration described in more detail in Subsections 5.7.1.2 and 5.7.1.4). In addition, a treated wedge, or splitter, could be installed at the midheight of the ejector, blocking the central gap between the chutes (and modifying the SAR) to increase the treatment area without increasing the length of the nozzle.

Of the many acoustic configurations tested along the "L1M" variable-cycle engine cycle line, both SAR 2.8 and SAR 3.3 mixers met the FAR36 Stage III sideline noise levels (Reference 1) at ideal primary jet velocities (V_{jiP}) ≤ 2400 ft/s with the "120 in" treated flap. For V_{jiP} < 2450 ft/s, SAR 2.8 proved slightly quieter than SAR 3.3, with the reverse effect at V_{jiP} > 2500 ft/s. Peak suppression achieved relative to a conic nozzle at sideline conditions (about 2400 ft/s) was 18.5 EPNdB, but this was achieved by sacrificing thrust. The corresponding C_{fg} was a disappointing 0.84 to 0.85.

Acoustic treatment yielded a benefit of approximately 3 EPNdB relative to the "perforated" hard-wall configurations at a nominal V_{jiP} = 2400 ft/s, increasing to about 4 EPNdB for V_{jiP} < 2000 ft/s.

Increasing flap length from the full-scale 80-inch (at a nozzle throat area of 1086 in^2) to 120 in resulted in an average benefit of 2.6 EPNdB in the V_{jiP} range of 1600 to 2800 ft/s, for treated configurations, and 1.7 EPNdB for "pseudo" hard-wall over the same V_{jiP} range.

For V_{jiP} > 2200ft/s, the mixer area ratio was identified as a highly significant parameter for both aerodynamic and acoustic performance. The MAR = 0.95 configuration was found to be approximately 3 EPNdB quieter than that with MAR = 1.2 (which entrained more secondary flow).

This test also demonstrated the transition from subsonic to supersonic mode of operation within the ejector, as a function of MAR and also of operating condition.

Scale-model tests of the NRA model in the NASA Langley 16-ft transonic wind tunnel were conducted in two phases. Twelve models were tested in the first phase, and ten models were tested in the second phase. Configuration variables for the tests included SAR, CER (chute expansion ratio), flap length, and MAR tested over a range of Mach numbers from 0 to 0.70 and nozzle pressure ratios from 1.5 to 6.5. These tests provided an initial data base from which to assess the effects of various key nozzle design parameters on mixer/ejector-nozzle performance in the noise-suppression mode at higher subsonic Mach numbers. Key results from the tests included the following.

- Nozzle installed performance (thrust minus drag coefficient) decreased with increasing Mach number, as expected, due to the inclusion of the external nozzle drag in the nozzle coefficients.
- Increasing SAR increased pumping and performance statically consistent with other testing, but the benefits were offset by external drag effects at higher Mach numbers.
- Increasing the flap length improved performance by about 1% at Mach 0.70.
- The convergent chutes with CER of 1.0 performed better than the convergent/divergent chutes (CER = 1.22 and 1.38) at nozzle pressures ratios less than 3.5, and the CD chutes performed better at higher pressure ratios, as expected, due to changes in expansion losses.

The ARL warm-flow mixing tests provided much insight into the mixing process. However, on comparing ejector exit survey data from ARL and Cell 41, it was found that the effect of operating temperature on the mixing process (mixing is more rapid at higher temperatures) was such as to make direct comparisons infeasible.

Finally, the acoustic effects quoted above are, in general, for the sideline azimuthal location. Similar effects were noted in the cutback location, but it was also noted that there was a sideline benefit relative to cutback of approximately 2 to 3 EPNdB. This has been ascribed to the two-dimensional characteristic of this nozzle system.

5.7.5.5 Near Fully Mixed Nozzle

The current near fully mixed (NFM) nozzle is an axisymmetric, ejector-suppressor nozzle having 10 full-penetration, aspirated-flow passages spaced circumferentially around the nacelle. A schematic of the NFM nozzle is shown in Figure 240. The inlets to the aspirated-flow passages are flush with the outer nacelle. The primary-flow exits resemble 10 rectangular plug nozzles. The ejector mixing section of the NFM nozzle can accommodate acoustic treatment both on the inner shroud

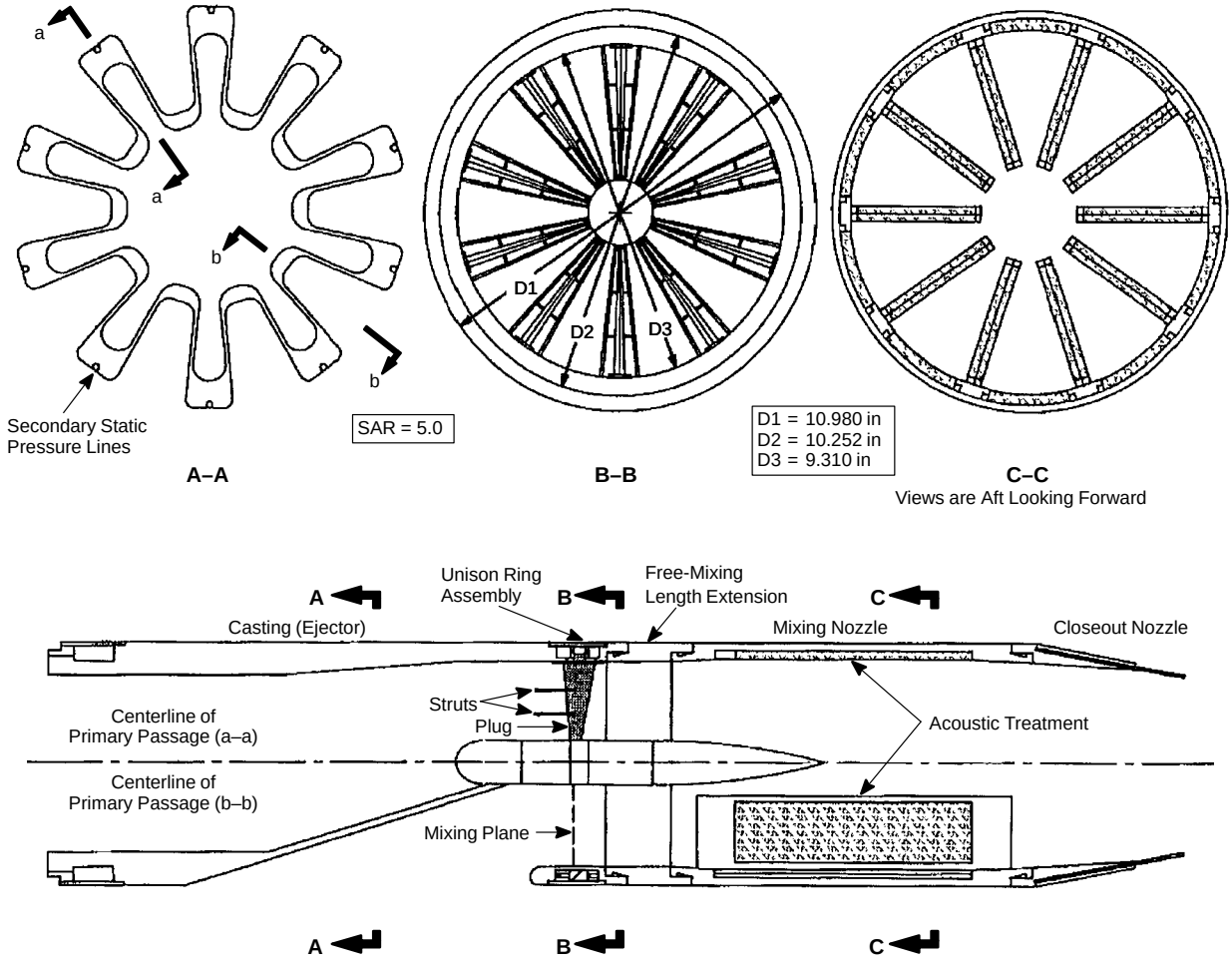

Figure 240. NFM Nozzle

surface and by means of panels extending radially into the flow (splitter plates). Newly designed acoustic treatment geometry was included in the nozzle test, as compared to previous NFM nozzle tests. The suppressor area ratio is 5. The final exit area of the closeout nozzle could be varied either by using one of several fixed-area closeout sections or by adjusting the position of the overlapping, translating leaves of one of the variable-area nozzles.

Testing was performed in the Boeing LSAF (described in Subsection 5.7.1.3) during the summer of 1993. The model conditions ranged up to an NPR of 5.5 and a temperature of just over 1800°R.

Further background and detail are available in References 29 and 30.

Objectives

The main acoustic test objectives were to evaluate the: (1) accuracy of the acoustic lining design process, (2) effectiveness of various designs and arrangements of acoustic panels, (3) effectiveness of various levels of aspiration, (4) benefit of a plug design for the primary nozzles in reducing shock-cell noise, (5) the EPNL suppression attainable, and (6) effect of MAR.

Aerodynamic Performance

NPR = 3.0 is representative of the 20% PLR (takeoff conditions) design point conditions for the GE21/Fl5–A5 engine cycle. At this NPR, a maximum C_{fg} of 0.9133 (hard-wall shroud with no splitter configuration, MAR = 0.99, static) was measured with an associated aspiration ratio of 1.5881. NPR = 4.0 is representative of the 20% PLR (takeoff conditions) design point conditions for the STJ989 cycle. At this NPR a maximum C_{fg} of 0.9223 (hard-wall shroud with no splitter configuration, MAR = 0.99, static) was measured with an associated aspiration ratio of 1.3631.

Comparison of the untreated and treated nozzle configurations produces the following findings. With the addition of the shroud treatment ($L/D \cong 1.0$) the thrust coefficient is reduced by about 4.0%. The treated splitters (total $L/D \cong 3.4$) reduces the thrust coefficient by an additional 2%. These losses are almost twice the levels observed in the previous NFM test (1992), where treatment impedance was higher. This suggests a strong relationship between treatment design and performance losses in the ejector mixing duct.

Acoustic Performance

For the three treatment configurations, at the peak directivity the perceived noise level of the shroud treatment results in about 2 to 3 PNDB attenuation, and the splitter treatment about 5 PNDB attenuation — roughly proportional to the amount of surface areas for shroud and splitter.

The sideline acoustic data (Mach 0.245) are summarized in Figure 241 at the NPR's of interest (3.2 and 3.8). This bar graphs show that the untreated NFM nozzle results in a benefit of approximately 9 to 11 EPNdB, relative to the RC nozzle. Acoustically treating the shroud results in additional attenuation of about 2 EPNdB. Installing treated splitters adds up to about 4 EPNdB additional attenuation.

Figure 242 is a plot of EPNL reduction as a function of thrust loss. No empirical corrections were applied to these noise data since no similar correction was derived for the thrust coefficient data. The effectiveness of the treated shroud and of the treated splitters is shown for the sideline condition for nozzle pressure ratios of 3.0 and 4.0. The values of both noise reduction and thrust are divided by

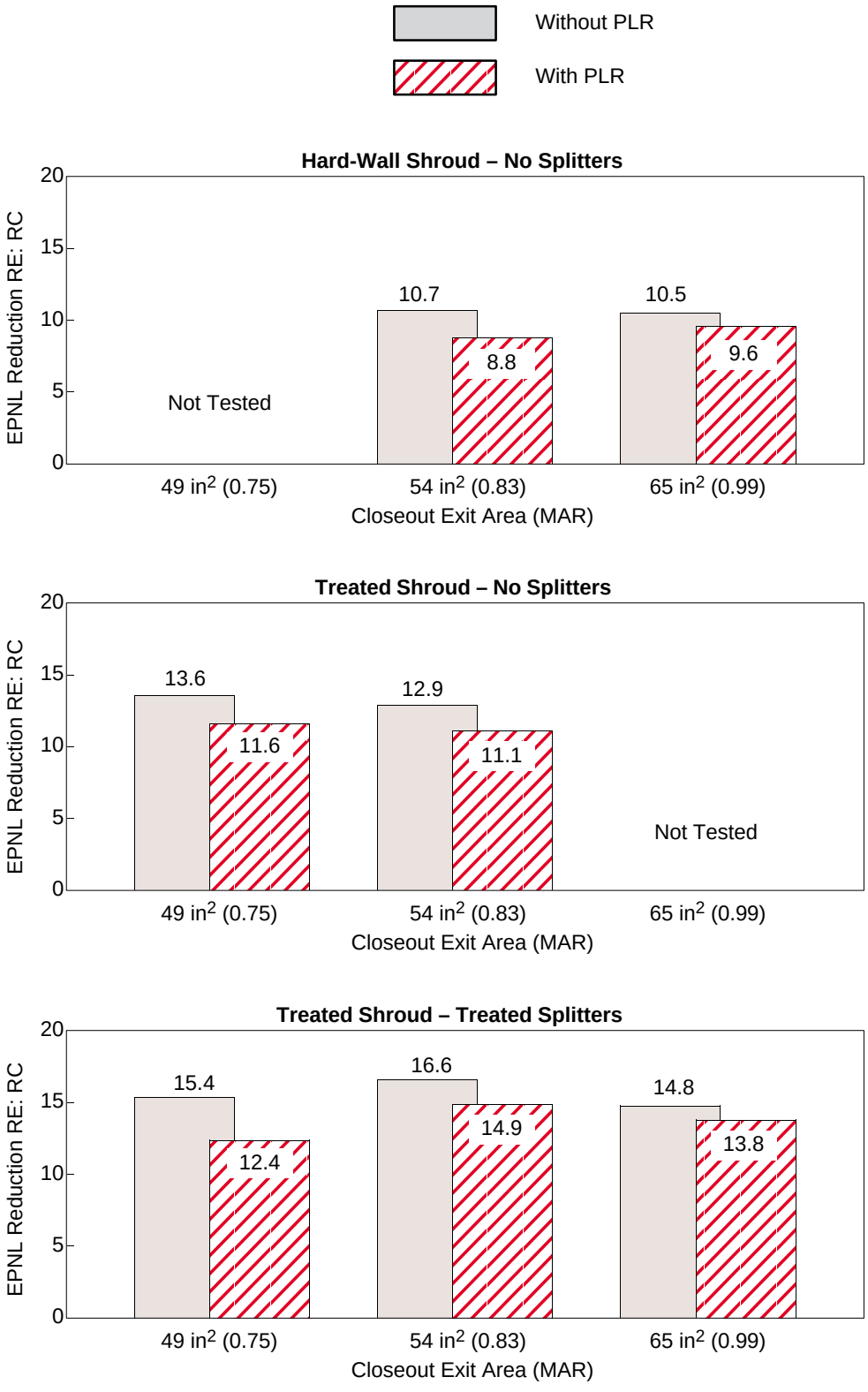

Figure 241. Summary of NFM EPNL Reduction at Sideline (Mach 0.245)

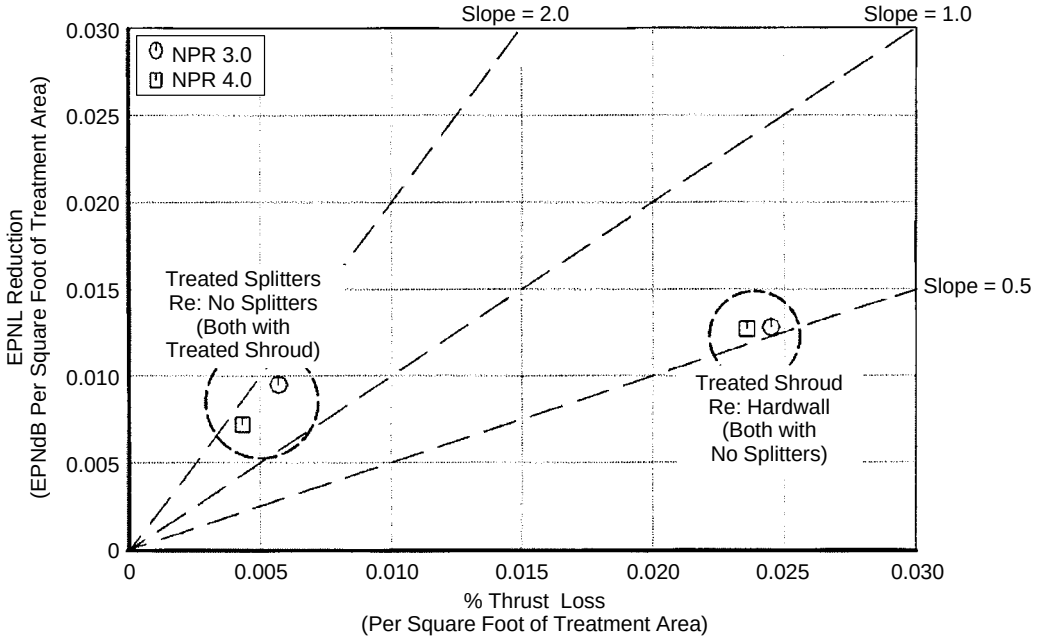

Figure 242. Attenuation versus Thrust Loss at Sideline Condition, MAR = 0.83, Tunnel Mach = 0.245, 4.7-ft Microphones

the appropriate treatment area in order to express the effectiveness of the particular treatment location on a "per unit area" basis. The plot shows that while the shroud treatment is about one and a half times more effective, it accounts for almost five times the thrust loss per unit area as the treated splitters. The splitter slope is about 1.7 EPNdB reduction per 1% thrust loss, while the shroud slope is about 0.5 EPNdB reduction per 1% thrust loss.

5.7.5.6 Axisymmetric Coannular Ejector (ACE) Nozzle

Model-scale acoustic and propulsion performance testing of the ACE nozzle was conducted in the Boeing LSAF free-jet wind tunnel test section in an anechoic chamber. The primary objective of the test was to obtain acoustic and performance data for the ACE nozzle with and without the ejector cowl. In addition, NASA–Langley supplied mixing-enhancement devices (micromanipulators) in the form of delta tabs, tone-injection rods, and wheeler ramps attached to the primary nozzle trailing edge and the ejector cowl trailing edge. Performance and noise were evaluated with and without the mixing-enhancement devices.

The ACE plug (boattail) nozzle has an ejector designed to provide aspiration of about 20% of the engine flow (Figure 15, page 14). The ACE concept produces higher performance by avoiding the use of lobes or chutes to force the aspirated and engine flows to mix using vorticity. In addition, ejector losses are reduced by the design point aspiration at 20% as compared to some suppressor systems that aspirate as much as 120%. A variety of enhancers were designed to promote mixing of the engine flow and the aspirated flow. These included delta tabs (Figure 16, page 15), tone-injection rods, and wheeler ramps.

Aerodynamic Performance – Several configurations of the ACE nozzle were tested for noise and performance at static and Mach 0.245 conditions. The configurations included the plug only without the ejector shroud and the baseline nozzle with ejector shroud. Various combinations of primary

nozzles and ejector cowls were tested with mixing enhancers designed to increase the mixing rate between the aspirated and primary streams and between the mixed stream and free stream. Plug-only thrust coefficients ranged from 0.9741 to 0.9773 depending on the primary nozzle mixing enhancers. Addition of the ejector cowl increased the performance of the baseline, wheeler ramps, and tone-rod mixing enhancers by approximately 0.5%. Combining the ejector cowl with the delta tab primary nozzle mixing enhancer resulted in a 2.4% thrust reduction relative to the baseline and the other primary nozzle mixing enhancers when combined with the ejector cowl. Aspiration ranged from 0.1925 to 0.2327 for the baseline configuration with mixing enhancers on the primary nozzle. With delta tabs placed on the ejector cowl, aspiration ranged from 0.1203 to 0.2204.

Acoustic Performance – Broadband shock-associated noise is seen for the ACE nozzle for nozzle pressure ratios of 3.0 and above. For the ACE nozzle without ejector, the delta tabs on the primary eliminated this shock-associated noise at NPR 4.0 and reduced it at other NPR's. None of the other mixing enhancers, either with or without ejectors, had any effect on the shock-associated noise. However, the contribution of the broadband shock-associated noise to the EPNL was small, at most 0.5 EPNdB, and the reductions that were achieved did not have any significant impact on the EPNL.

The effects of mixing enhancers on jet noise tend to follow certain characteristics. The delta tabs on the primary nozzle generally reduce the low- to mid-frequency (about 500 to 10 kHz model scale) jet-mixing noise by 2 to 4 dB and increase the high-frequency (over 10 kHz) jet–mixing noise by 5 dB or more, relative to the other three primary nozzle configurations (the baseline nozzle, the tone-injection rods, and the wheeler ramps) — which all give almost identical results. The high-frequency noise increase is not seen for the highest power settings (NPR's 3.5 and 4.0) or the highest noise emission angles (about 140°). These trends are generally seen for all three ejector shroud configurations (no ejector, baseline ejector, and ejector with tabs).

The model-scale measured data were extrapolated to sideline and cutback flight conditions. The results show that, plotted on an equal thrust basis, EPNL's for the various ACE nozzle configurations are all fairly close. The primary delta tabs with ejector shroud configurations generally have the lowest levels, while the baseline primary generally has the highest levels.

The greatest attenuations were achieved by the configuration of delta tabs on the primary nozzle with an ejector shroud installed — either the baseline or the tabbed ejector. The results show up to 2 EPNdB more attenuation with the primary delta tabs relative to the other three primary nozzle configurations (baseline nozzle, tone-injection rods, and wheeler ramps) when compared on an NPR basis. The exact benefit depends on the extrapolation condition and the power setting. The other three primary configurations give attenuation levels within an EPNdB of each other. Which of these other primary configurations gives the greatest attenuation depends on the shroud configuration, the extrapolation condition, and the power setting.

The round convergent (RC) nozzle was tested before and after the ACE nozzle. Comparisons to the RC nozzle at the sideline and cutback flight conditions and power settings follow. For sideline flight conditions and power settings, delta tabs on the primary nozzle (with either ejector installed) give the greatest attenuation: 5.3 EPNdB relative to the RC nozzle when compared on an NPR basis. Without an ejector, the primary tabs gave 4.7 EPNdB attenuation. The various other configurations (all those without primary tabs, including the baseline primary nozzle, the tone-injection rods, and the wheeler ramps) performed fairly similarly, achieving between 3.5 and 4.2 EPNdB attenuation. The effect of comparing ACE and RC nozzles on a thrust basis, accounting for the reduced thrust of the ACE nozzle relative to the RC at the same gas conditions, is to reduce the attenuation by

between 1.0 and 1.5 EPNdB. For cutback flight conditions and power settings, all the configurations tested performed fairly similarly, giving between 0.6 and 1.6 EPNdB attenuation relative to the RC nozzle when compared on an NPR basis. The effect of comparing ACE and RC nozzles cutback levels on a thrust basis is to reduce the attenuation levels by about 0.5 EPNdB.

5.8 Exhaust Nozzle Subcomponent Testing

5.8.1 Acoustic Liner Testing and Design Methodology

5.8.1.1 Acoustics

Objective and Approach

Development of acoustic liner technology has been a critical element of the HSCT program. The effort was aimed at designing, developing, and demonstrating promising acoustic liner concepts in scale-model aeroacoustic tests and developing an acoustic design methodology for large-scale tests. This activity has been coordinated with the EPM program, in terms of providing acoustic design specifications and testing liner material specimens being developed in that program.

The overall objective of the liner technology program was to develop a design methodology for both bulk absorber (with face sheet) and SDOF (honeycomb with face sheet) type liners to obtain needed acoustic suppression with minimum skin-friction loss. The liner design methodology consists of:

1. correlation of the steady-state flow resistance and physical properties of a liner at room temperature with normal impedance at a desired temperature and flow condition and
2. correlation between the normal impedance and the acoustic suppression of the liner accounting for liner scaling.

The first correlation relates the required properties of a liner design at room temperature to an established impedance goal for the liner at the actual flow and temperature conditions. If for some reason this impedance goal does not yield the desired or maximum acoustic suppression and needs to be revised, then the corresponding liner characteristics at room temperature can easily be determined without any additional test or analysis. The second correlation determines the acoustic suppression capability of a liner design with known normal impedance, accounting for liner scaling.

An important element in creating the liner design methodology was development of a liner-optimization model based solely on laboratory tests of liner samples, data correlation, and some analytical modeling. Ideally, in order to evaluate the liner acoustic properties, laboratory tests should be performed at frequency and temperature conditions corresponding to the appropriate-scale mixer/ejector internal environment (temperatures around 1000°F with frequencies up to the 10-kHz 1/3-octave band for full scale, the 80-kHz band for models). Laboratory tests, however, are limited to frequencies up to about 12 to 20 kHz, and high-temperature tests on liner designs are prohibitively costly. In this program, moderate-temperature DC-flow test results for face sheets and bulk materials, evaluated in the laboratory, have been used to predict the acoustic characteristics of liner designs at higher temperature conditions. Data taken in a flow duct running at Mach numbers up to approximately 0.8 with temperatures around 400°F have been used to validate the prediction methods.

Laboratory Tests, Data Analysis, and Typical Results

Laboratory tests consisted of high-frequency impedance tube tests, DC flow resistance tests, flow duct tests, and insertion-loss measurement tests. A high-frequency impedance tube was used to

measure normal impedance up to 20 kHz and to establish a procedure to measure *in situ* impedance of a bulk absorber. The flow duct tests were conducted to evaluate *in situ* impedance, DC flow resistance, and skin friction coefficient at different flow conditions. Insertion-loss measurement tests were conducted by Rohr Incorporation (currently, BF Goodrich Aerospace) under subcontract to GEAE.

Normal Impedance Tests

Two impedance tubes capable of measuring impedance spectra up to 6 kHz and 20 kHz, respectively, have been used to conduct these tests. Most tests were conducted in the high frequency impedance tube using bulk samples of 0.6-in diameter with and without face sheets of 0.94-in diameter. The low-frequency impedance tube was used for complex bulk samples of 1.25-in diameter. Three types of bulk samples of varying properties were tested: silicon carbide, T–Foam, and Feltmetal. The bulk samples of different depths (0.25 to 2.0 in) were tested for different scale liner application. A large number of face sheets with varying porosity, thickness, and hole diameter were tested for bulk absorber and SDOF type liners. Face sheets with triangular, square, and hexagonal shaped holes were also tested. All tests were conducted with broadband acoustic excitation at different OASPL levels. Typical normal impedance results showing the parametric effects of face-sheet properties are illustrated in Figures 243 through 245. The reactance and resistance increase with decreasing face-sheet porosity. The effect is significant on reactance. In general, the impedance levels increase with increasing face-sheet thickness, except for very thin face sheets. The effect of face-sheet hole diameter is insignificant on the resistance. However, the reactance decreases first and then increases with increasing face-sheet hole diameter.

DC Flow Resistance Tests

DC flow resistance at different heated conditions was measured for various bulk absorber samples and for several face sheets. The results have been used to develop the normal impedance correlation for the liner design methodology. A typical DC flow resistance with respect to approach velocity (velocity normal to the surface) for different T–Foam bulk samples is shown in Figure 246. The DC flow resistance increases with bulk density.

Flow Duct Tests

A new flow duct was designed and fabricated to evaluate the grazing-flow (flow parallel to the surface) effects on *in situ* impedance, DC flow resistance, and skin friction loss at heated flow conditions up to 400°F and Mach numbers up to 0.8. This duct was installed in the GEAE Aerodynamic Research Laboratory wind tunnel, which has the capability of providing heated flow. The 14-in long test section portion of the flow duct has two glass side walls, 12×4-in each, for LV measurements

Flow duct tests were conducted for bulk absorber and SDOF type liner panels, in the presence of grazing flow, up to a Mach number of 0.8, at temperatures up to about 400°F. A computer-controlled traverse system with total head pressure and temperature probe, installed on the upper wall of the test section, was used for flow and thermal boundary layer profile measurements at a single location. These data were used to evaluate the local skin friction loss of the panel.

Two panel trays of constant 0.5-in depth, one filled with honeycomb and the other capable of accommodating different bulk materials, were fabricated. Five cavities (of circular cross section)

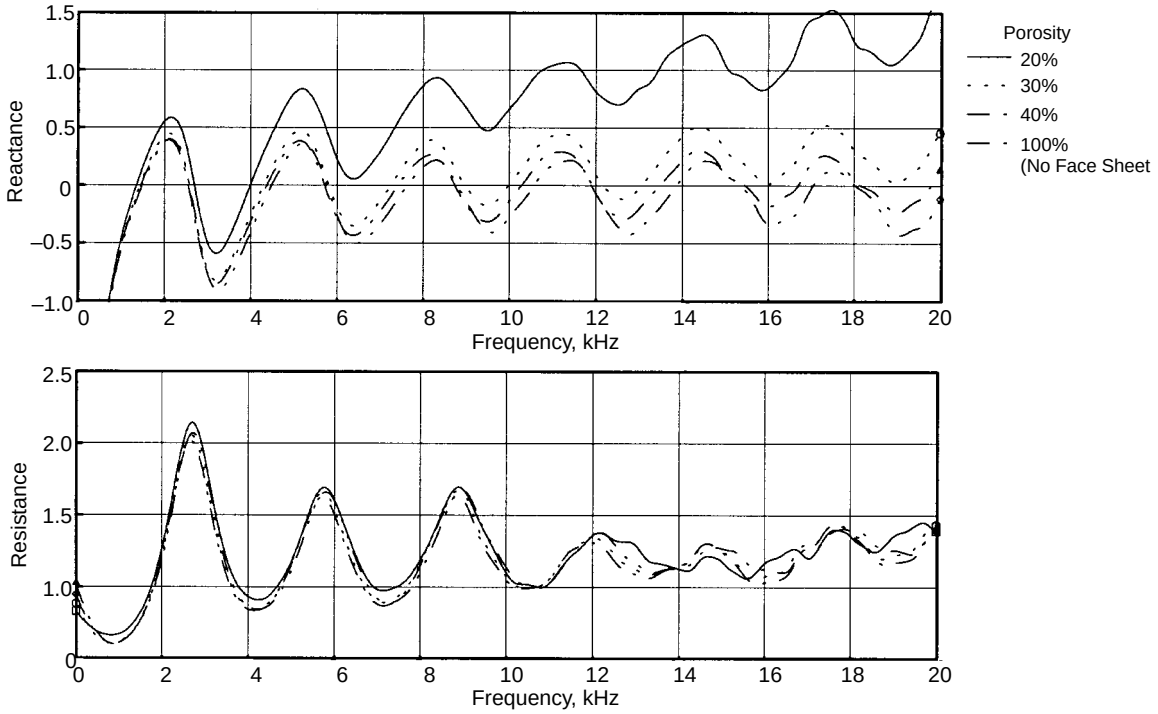

Figure 243. Effect of Face-Sheet Porosity on Normal Impedance for a 100-ppi, 2-in-Deep Silicon Carbide Bulk Sample with 0.025-in-Thick Face Sheets with 0.04-in-Diameter Holes; Excitation OASPL = 150 dB

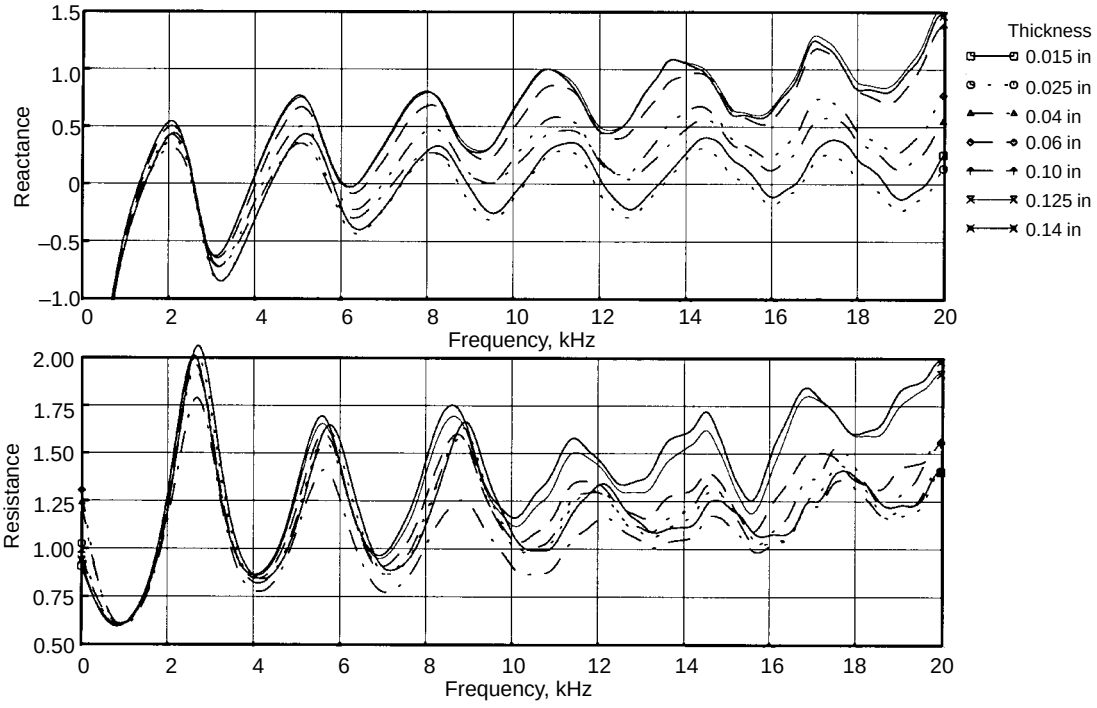

Figure 244. Effect of Face-Sheet Thickness on Normal Impedance for a 100-ppi, 2-in-Deep Silicon Carbide Bulk Sample with 40% Porous Face Sheets with 0.04-in-Diameter Holes; Excitation OASPL = 150 dB

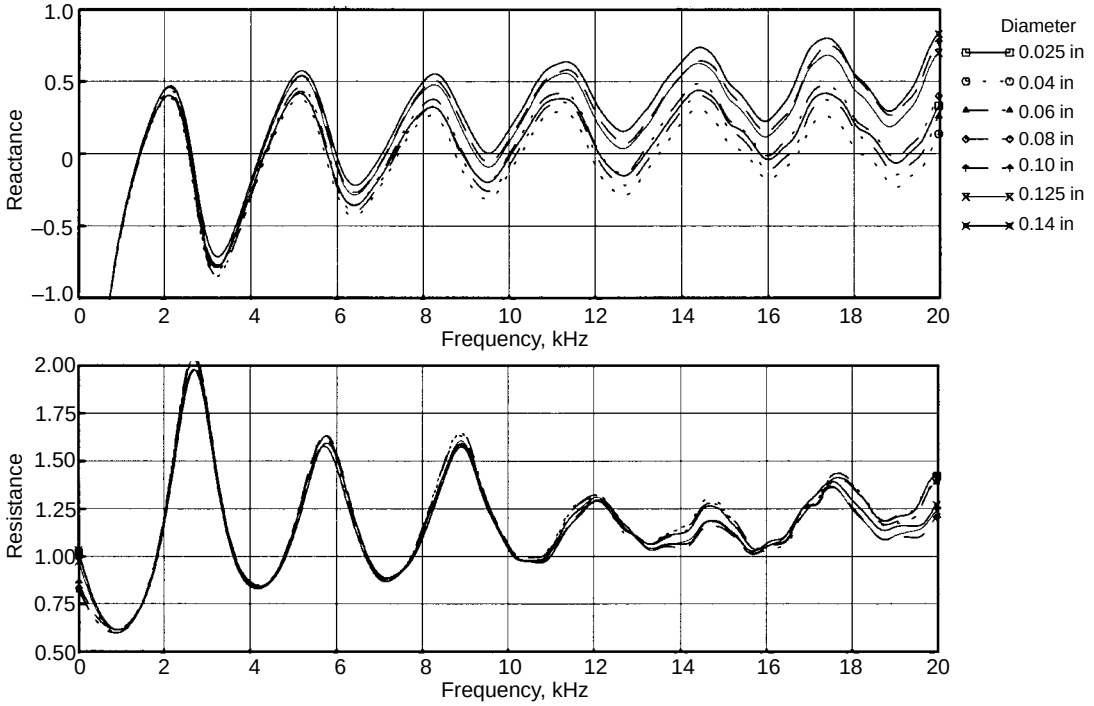

Figure 245. Effect of Face-Sheet Hole Diameter on Normal Impedance for a 100-ppi, 2-in-Deep Silicon Carbide Bulk Sample with 40% Porous 0.025-in-Thick Face Sheets; Excitation OASPL = 150 dB

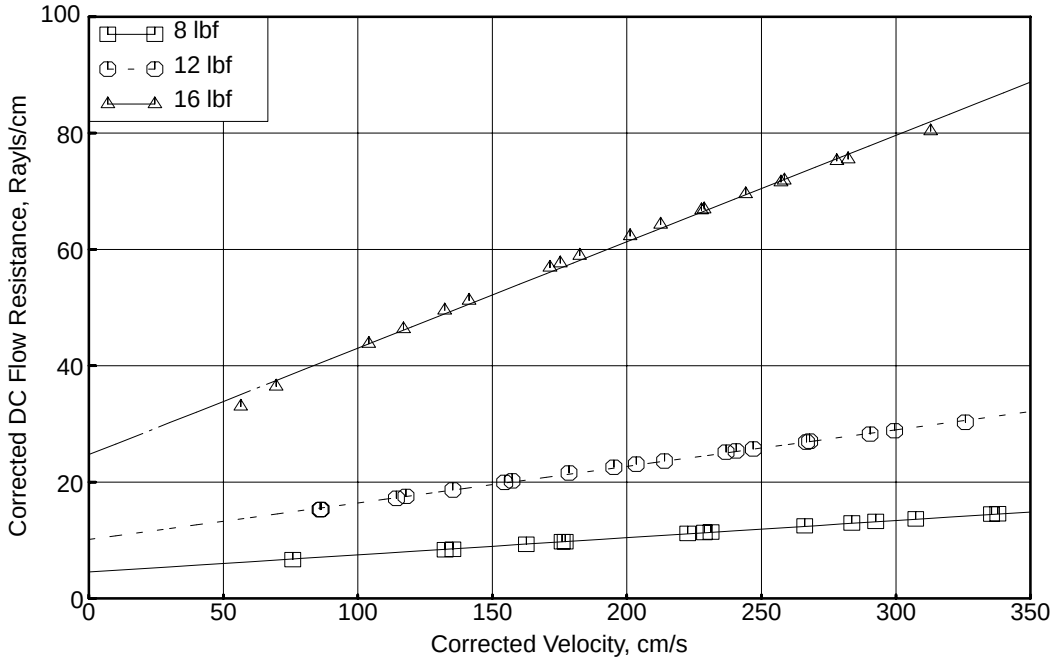

Figure 246. Effect of T–Foam Density on DC Flow Resistance at Standard Temperature (70°F) Conditions (for 0.5-in-Deep Samples)

with stiffened wall and different depths and diameters were inserted to each of the trays with appropriate transducer sleeves. Partition for DC flow port was also made in these trays. The design was such that different face sheets were easily installed on the panel trays. The face-sheet covers the entire tray surface, including the frame area, to accommodate face sheets of different thickness. All cavities were instrumented for acoustic measurement. The *in situ* results from all the cavities were obtained during a single test. DC flow resistance and skin friction coefficients in the presence of grazing flow were also evaluated.

***In Situ* Impedance:** Typical results showing the impact of grazing flow on in situ impedance are illustrated in Figure 247. The *in situ* impedance is strongly influenced at and around the antiresonance frequency of about 13 kHz for the 0.5-in-deep cavity. For deeper cavities, the antiresonance occurs more often within the same frequency range, thus influencing more data points. However, the relative *in situ* impedance (Δ relative to no-flow condition) at various grazing-flow Mach numbers is less influenced by antiresonance frequencies and the range of the influence is limited to a smaller band of frequencies on both sides of the antiresonance frequencies. Thus, the relative *in situ* impedance derived from each of the five cavities, ignoring the data at and close to the antiresonance frequencies, are used to derive a least squares fitted polynomial curve. Typical relative *in situ* impedance data for a bulk absorber with face sheet are shown in Figure 248. Such relative values can be added to the measured normal impedance of any desired panel design, and the normal impedance with grazing-flow effect can be derived. An example of normal impedance in the presence of grazing-flow derived for a 0.5-in-deep silicon carbide panel with face sheet is shown in Figure 249. Similar results are derived for panels of different depths.

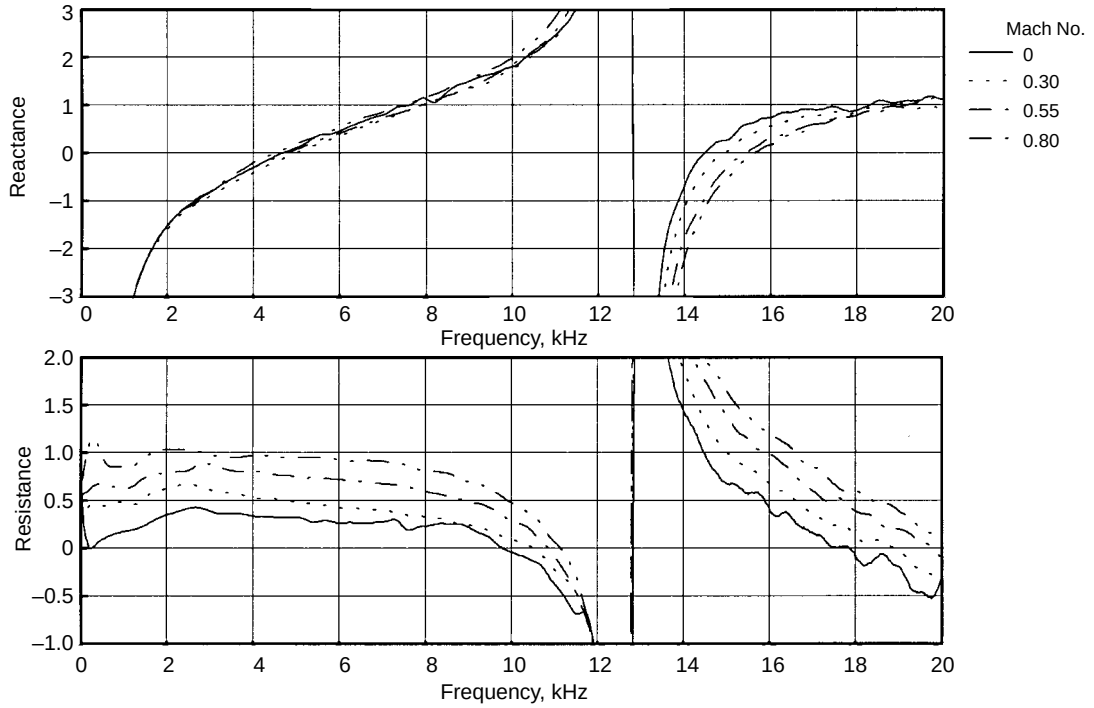

Figure 247. Effect of Grazing Flow on *In Situ* Impedance, Measured in a 0.5-in-Deep Cavity, for a 0.5-in-Deep, 100-ppi Silicon Carbide with a 20% Porous 0.025-in-Thick Face Sheet of 0.04-in Hole Diameter at Ambient Temperature

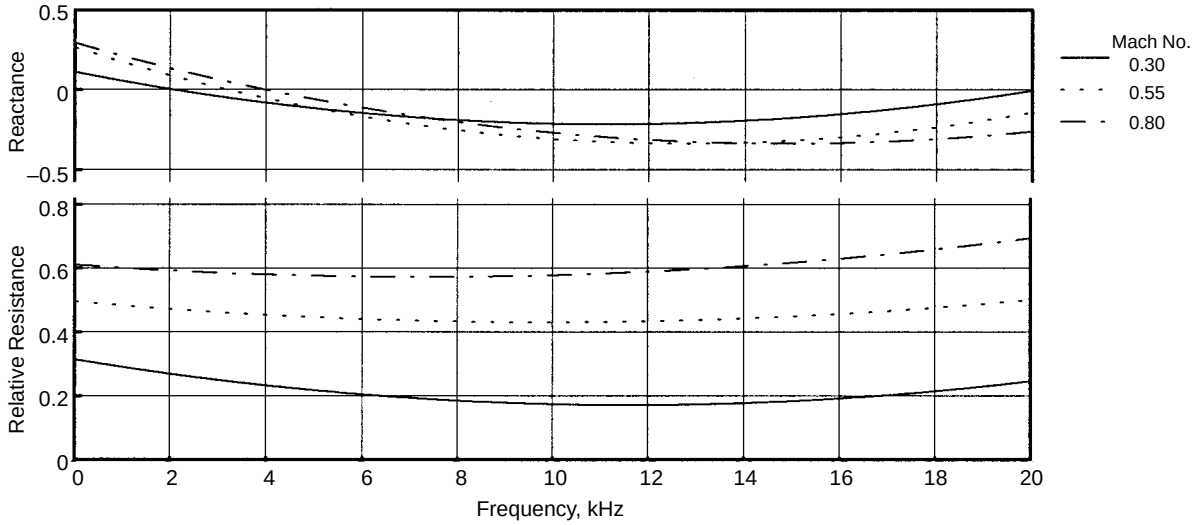

Figure 248. Effect of Grazing Flow on Relative *In Situ* Impedance, for a 0.5-in-Deep, 100-ppi Silicon Carbide Panel with a 20% Porous 0.025-in-Thick Face Sheet with 0.04-in-Diameter Holes at Ambient Temperature

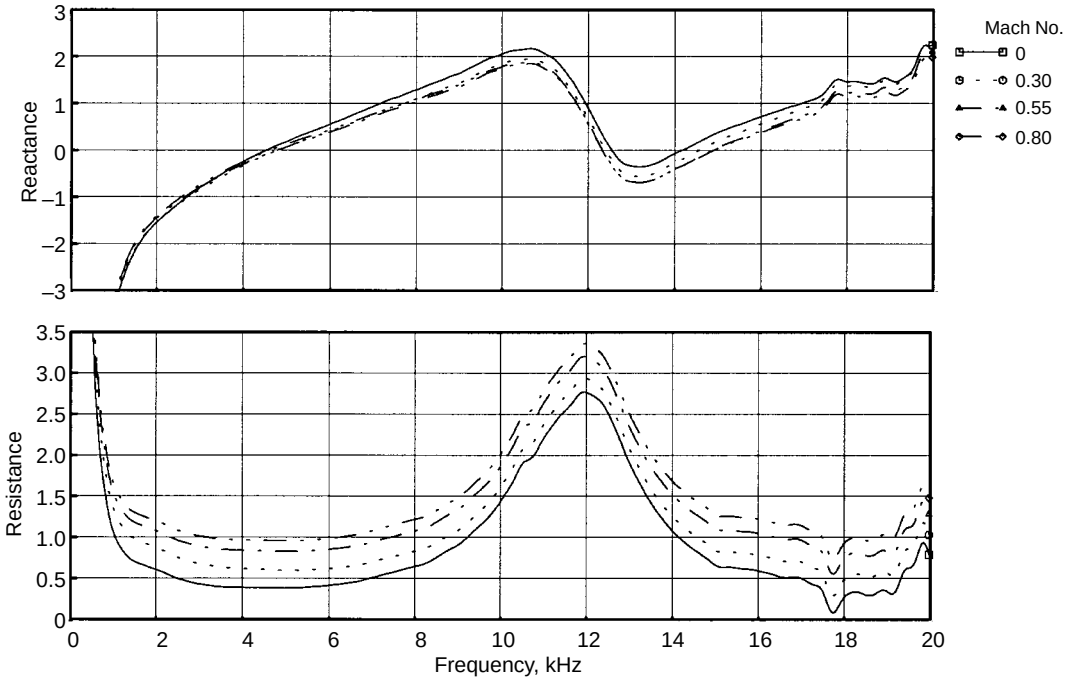

Figure 249. Effect of Grazing Flow on Normal Impedance for a 0.5-in-Deep, 100-ppi Silicon Carbide Panel with a 20% Porous, 0.025-in-Thick Face Sheet with 0.04-in-Diameter Holes, Derived from Measured Normal and *In Situ* Impedance Data at Ambient Temperature

The effect of temperature on normal impedance is derived in the same manner. In this case the relative *in situ* impedance for a heated condition is derived with respect to ambient data for the same grazing-flow Mach number, except that the frequency is normalized with respect to the square root of temperature ratio. With the addition of relative *in situ* impedance due to grazing flow and temperature to the measured normal impedance at ambient conditions, the actual normal impedance for a desired flow and temperature condition can be derived. It may be necessary to interpolate the relative *in situ* impedance data to a desired flow and temperature condition in order to compute the acoustic suppression for a particular configuration (a lined duct or ejector liner for example).

DC Flow Resistance: DC flow resistance, shown in Figure 250 for a typical panel, increases with increasing flow Mach number. This is indicative of normal acoustic resistance increase with grazing flow. Similar results for temperature, indicating a reduction of DC flow resistance with increasing flow temperature, were also obtained. These results can be used in the development of normal impedance correlation.

Boundary Layer Profiles and Local Skin Friction Coefficients: Typical boundary layer profiles for a bulk absorber panel at various grazing-flow Mach numbers are shown in Figure 251. The velocity profiles seem to be fully developed. These profiles are used to compute local skin friction coefficients (C_F), displacement thickness (δ^*), and momentum thickness (θ). While the skin friction coefficient is used to select a panel configuration with minimum friction loss, the momentum thickness is used in the correlation for normal impedance. Typical C_F and δ^* results for a panel compared to hard wall are shown in Figure 252. Unlike the hard-wall surface, the panel data for different flow and temperature do not collapse with respect to Reynolds number per unit length.

Insertion Loss at Ambient Condition: Insertion loss (acoustic suppression) for a number of liner panels was measured in a flow duct facility at BF Goodrich Aerospace (previously known as Rohr Inc.) up to a flow Mach number of 0.8. In this facility the insertion loss is evaluated by using a diffused acoustic field (generated by a reverberant chamber) in the flow duct. In this situation the identity of individual modes is highly diminished, and a more uniform sound field propagates through the flow duct. Measurements in this facility are, however, limited to ambient temperature only. The acoustic energy flux upstream and downstream of the panel was measured. The insertion loss is the difference between the two measurements. Measured insertion loss was further corrected relative to a hard-wall configuration. Typical results are shown in Figure 253. Insertion loss decreases with increasing flow Mach number. These results along with the normal impedance for the configuration were used for correlation development.

Mixer/Ejector Tests

A number of scale-model mixer/ejector nozzles with and without acoustic treatment have been tested under the HSCT program (see Subsection 5.7). The measured far-field noise data include two major components: internal and external noise (see Subsection 5.6.2). The internal noise, a high-frequency dominant noise, is generated by the mixer and the mixing process inside the ejector. The acoustic liners for the ejector are basically designed to suppress the internal noise component. For optimum liner design and for acoustic suppression/impedance correlation, it is necessary to extract the internal noise component from the overall acoustic signature. The Stone semiempirical mixer/ejector noise model described in Subsection 5.6.2.1 is capable of predicting the noise components for a mixer/ejector configuration, but the agreement between test data and prediction may not be exact for all conditions and configurations, especially at higher frequencies (internal noise domain).

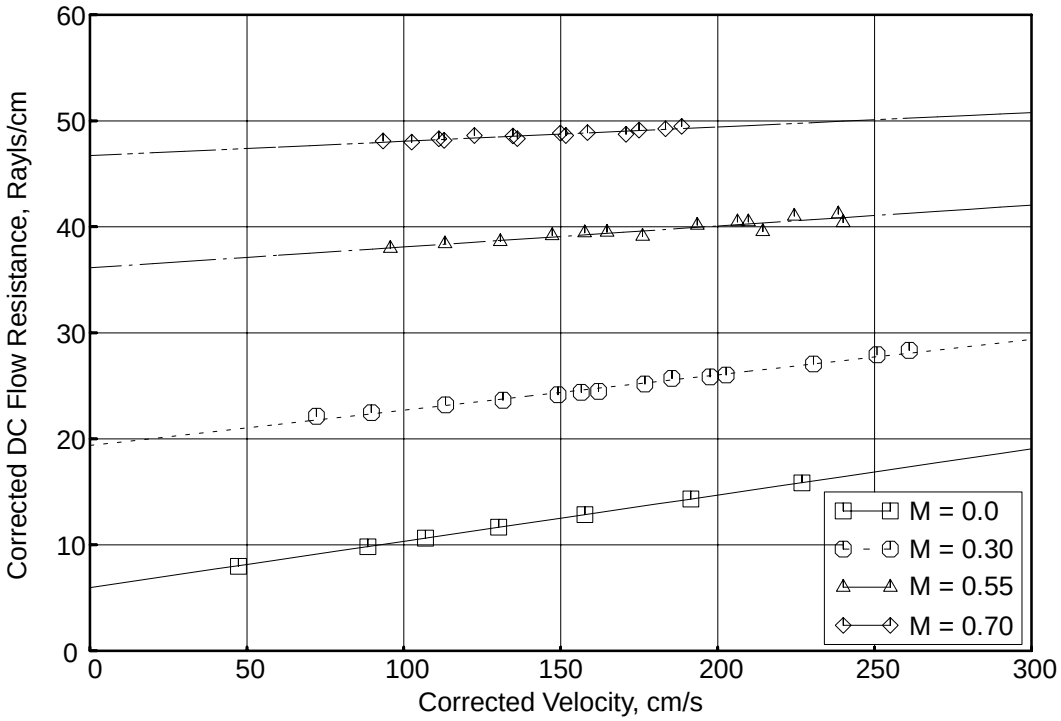

Figure 250. Effect of Grazing Flow on DC Flow Resistance for a 0.5-in-deep, 100-ppi Silicon Carbide Panel with a 30% Porous 0.025-in-Thick Face Sheet with 0.04-in-Diameter Holes at Ambient Temperature

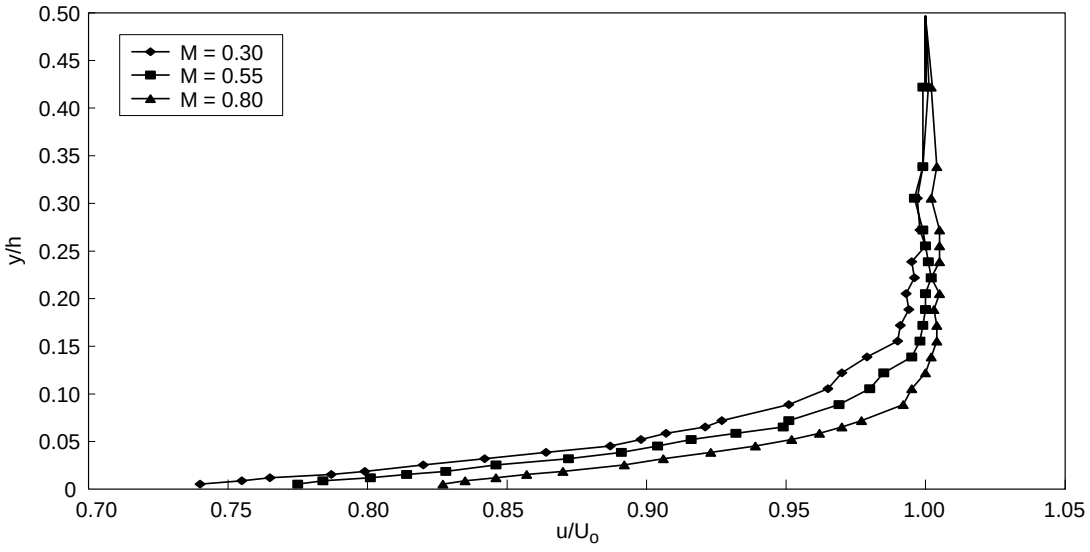

Figure 251. Effect of Grazing Flow on Boundary Layer Profile for a 0.5-in-Deep, 100-ppi Silicon Carbide Panel with a 20% Porous 0.025-in-Thick Face Sheet with 0.04-in-Diameter Holes at Ambient Temperature

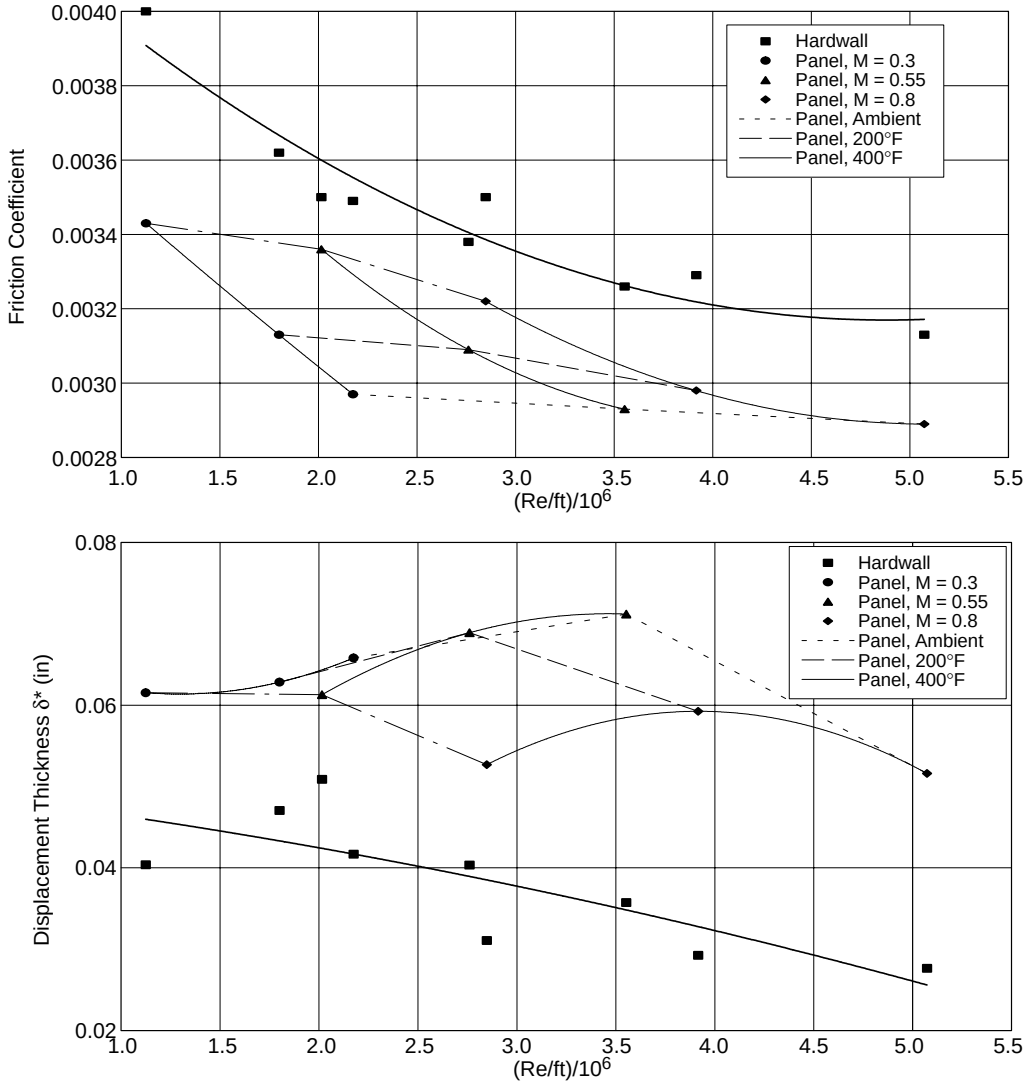

Figure 252. Local Skin Friction Coefficient and Displacement Thickness for a 0.5-in-Deep, 100-ppi, Silicon Carbide Panel with 30% Porous 0.025-in-thick Face Sheet with 0.04-in-Diameter Holes

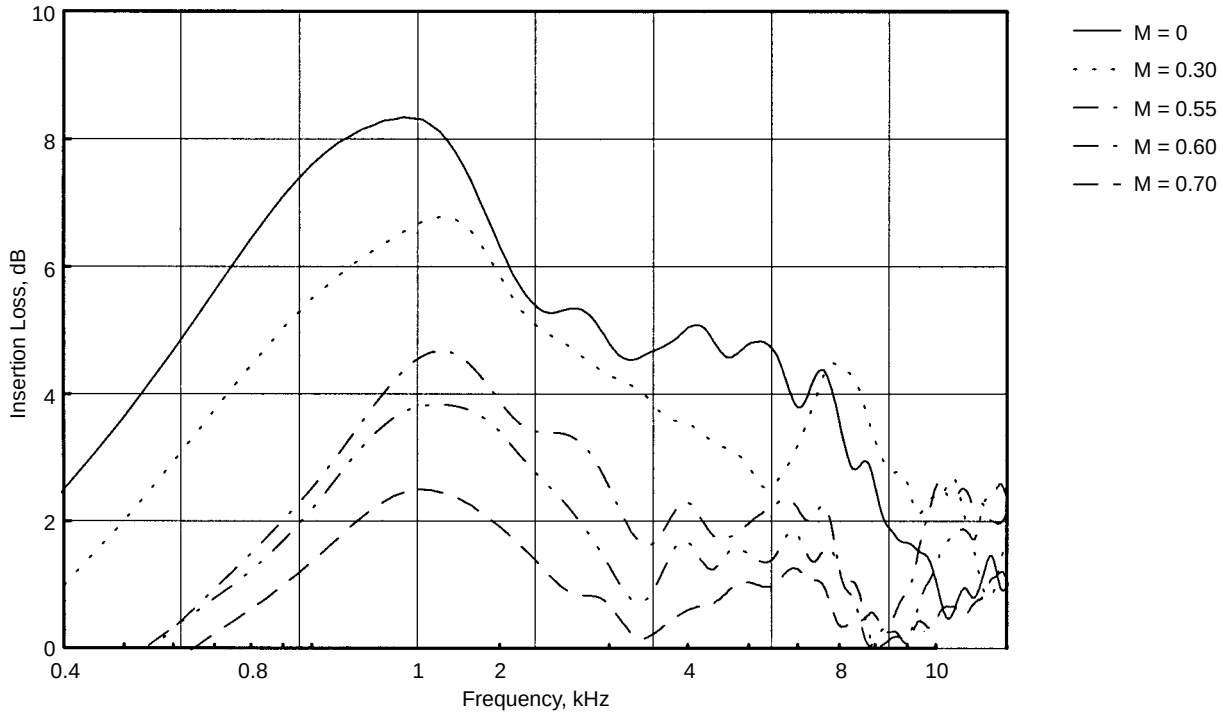

Figure 253. Effect of Grazing Flow on Insertion Loss for a 2-in-Deep, Three-Paper-Construction, 8-lb T–Foam Panel with a 40% Porous, 0.04-in-Thick Face Sheet with 0.04-in-Diameter Holes at Ambient Temperature

A “source extraction” code has been developed using the measured total noise data and the external noise component predicted by Stone’s code in order to extract the internal noise component for use in liner design development. Typical noise component results for hard wall and fully treated ejector are shown in Figure 254.

It should be noted in passing that the PWL spectra shown have been calculated assuming the noise field measured at the azimuthal angle $\phi = 25°$ is axisymmetric. The “true” PWL should, of course, account for the azimuthal noise variation.

The spectral differences (hard wall minus treated) of SPL at different polar angles and of PWL are the measures of the SPL and PWL suppression due to the acoustic treatment. Using the extracted internal noise, the acoustic suppression (PWL difference or ΔPWL) can be derived for different aerothermodynamic conditions and for different configurations. Figure 255 shows acoustic suppression for a fully treated ejector at different aerothermodynamic conditions. These results are used to develop the acoustic suppression/normal impedance correlation.

Data Correlation

Correlations, based on the laboratory test results, that will predict normal impedance for any desired acoustic treatment and acoustic suppression due to the treatment when applied to an ejector are important outputs of the liner technology program. The correlation to predict normal impedance accounts for flow, temperature, and acoustic field at which the treatment would be used. Measured normal impedance and DC flow resistance for various bulk materials of different depths with and

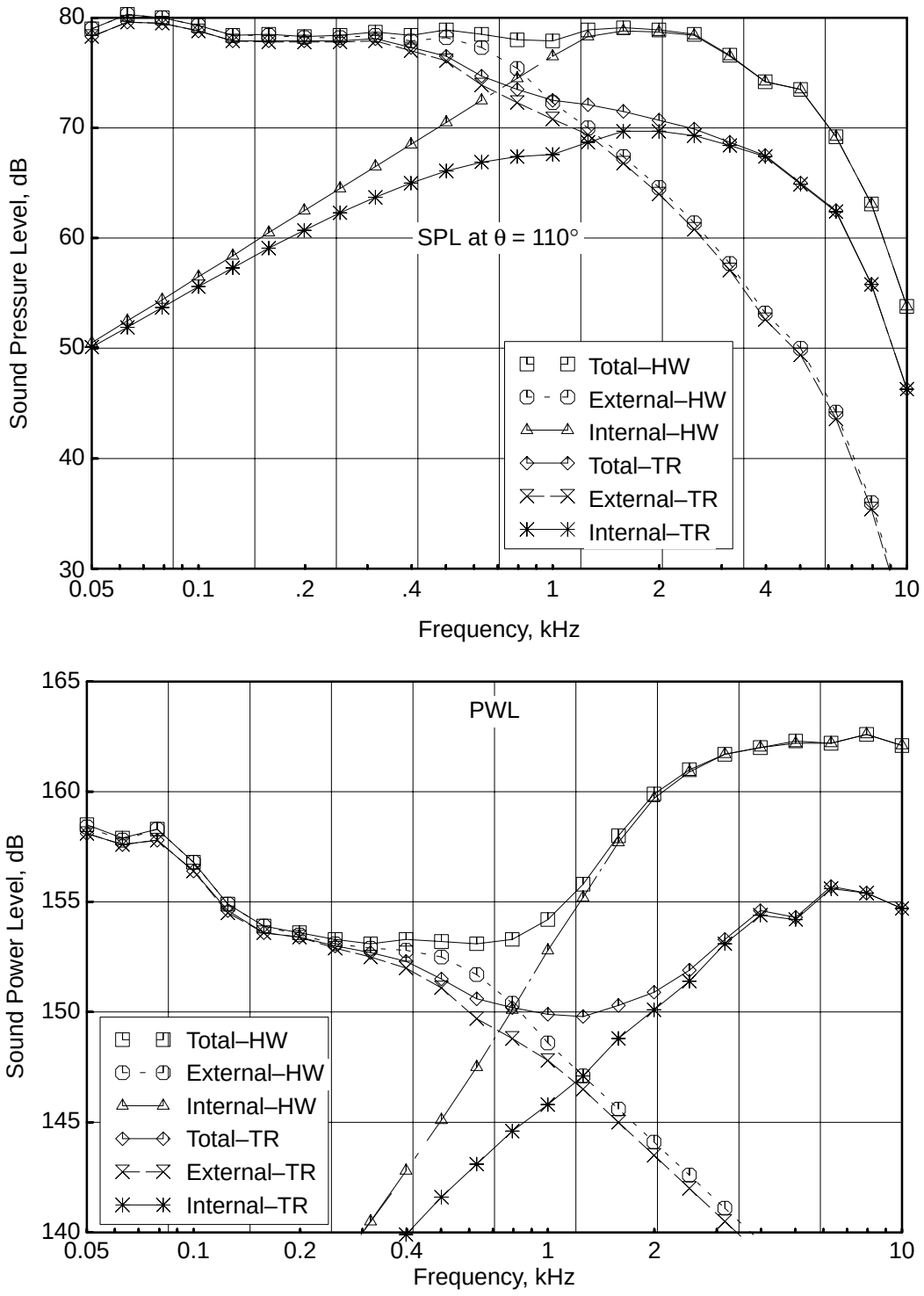

Figure 254. Measured SPL and PWL Spectra Compared with the Predicted External (Merged and Premerged) and Extracted Internal Components for Hard-Wall and Fully Treated 22.12-in (160-in Full Scale) Ejector for NRA Model with Mixer 8c; NPR = 3.43, T_8 = 1550°R, V_{mix} = 1430 ft/s, M = 0.32 {Takeoff}, ϕ = 25°

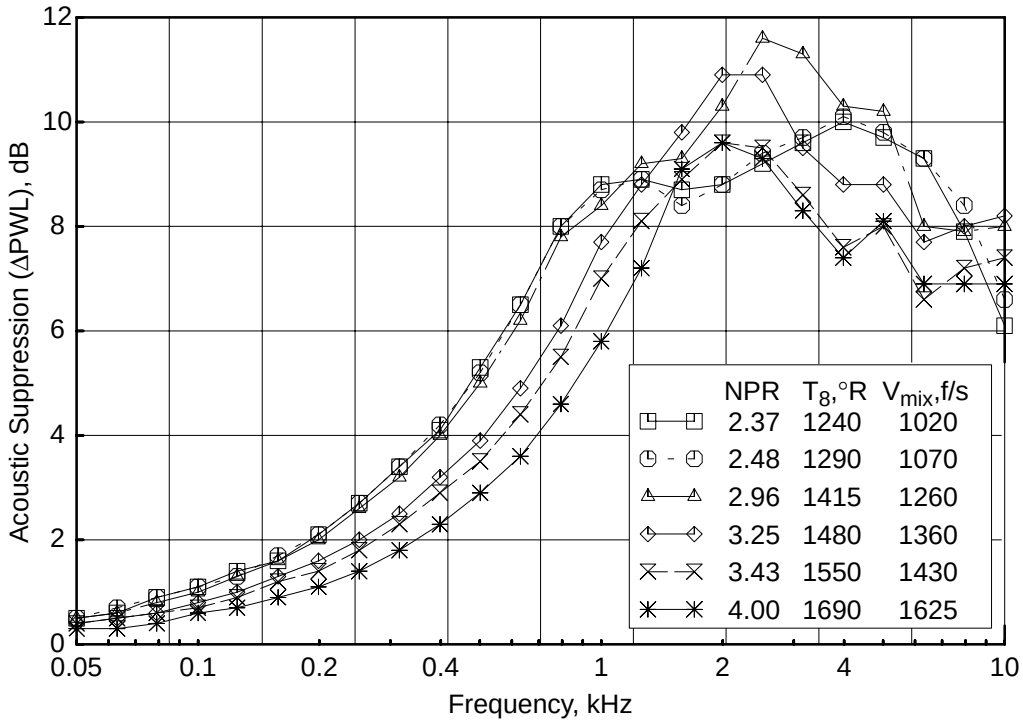

Figure 255. Extracted Acoustic Suppression Spectra for a Fully Treated 22.12-in (160-in Full Scale) Ejector for NRA Model with Mixer 8c at Different Aerothermodynamic Conditions, M = 0.32 {Takeoff}, ϕ = 25°

without face sheets of varying parameters, the relative *in situ* impedance due to flow and temperature for various panel configurations are used in this correlation.

The acoustic suppression/impedance correlation uses the extracted internal noise data from mixer/ejector tests, the insertion-loss data measured at ambient condition, and the measured and/or predicted normal impedance data. These correlations are used to develop the liner design methodology.

Liner Design Methodology

This methodology was needed to design an acoustic liner for a mixer/ejector nozzle (of any scale) in order to obtain maximum acoustic suppression at a desired aerothermodynamic condition. This complex process can be outlined in a stepwise manner. Components include a physical liner (either a bulk material with face sheet or honeycomb with face sheet) at a desired scale, prediction or experimental evaluation of normal impedance under operating conditions, prediction of acoustic suppression, and finally the prediction of far-field noise including EPNdB. An optimization process to minimize EPNL can be established by changing the liner physical parameters in steps.

Physical Liner: The depth of the liner and the physical properties of the material (bulk and/or the face sheet) are the parameters that are varied for the optimization process.

Normal Impedance: The normal impedance for the liner, accounting for flow, temperature, and acoustic field, is either derived by prediction methods or from experimental results.

Acoustic Suppression: The acoustic suppression is predicted either by semiempirical correlation or by using a modal analysis program. The dimensions of the ejector, the treatment area, and the

mean flow and temperature conditions are necessary for evaluation of acoustic suppression. A rectangular duct modal analysis is adapted to evaluate the acoustic suppression performance of treated ejectors. The analytical method is simplified by the assumption of equal modal energy distribution. Currently, the acoustic suppression due to the first 50 transverse modes along the two treated flaps (with hard sidewalls) is accounted for. Based on the size of the ejector and flow conditions, different modes are being cut-on (and hence propagate) at different frequencies. The first 50 modes, as considered in the current analysis, cover most frequencies. Several more modes must be included to cover the few remaining higher frequencies. The contribution from these additional modes may not change the peak suppression level and frequency but is expected to increase acoustic suppression at higher frequencies.

Farfield Noise (Including EPNL): The first step towards this objective is to develop a correlation between the internal noise component in the far field with the acoustic suppression or insertion loss (predicted or measured) due to treatment in the ejector.

The extracted internal components of PWL for takeoff or cutback conditions, for a mixer/ejector, are used to compute a ΔPWL between hard-wall and treated configurations (see Figure 255). For the same conditions, the acoustic suppression spectra are also predicted. The acoustic suppression spectrum should be the same as the internal component of ΔPWL at each condition if: the acoustic suppression prediction is accurate, the ΔPWL computation accounts for azimuthal variation due to nonaxisymmetry of the ejector, and the internal noise component extraction used for PWL calculation is accurate. However, significant differences are found to exist between predicted acoustic suppression and ΔPWL spectra.

To minimize the uncertainties associated with the above, a frequency dependent factor $\gamma(f)$, termed the "acoustic suppression transfer factor," has been developed to equalize the predicted acoustic suppression at each frequency with the extracted internal component of ΔPWL(f) at a particular cycle condition. This $\gamma(f)$ is then used (at that same condition) to calculate the internal component of ΔPWL(f) from the predicted acoustic suppression for various liner designs.

The next step is to develop a procedure to calculate the internal component of the SPL spectra at various polar angles using the internal component of the PWL spectrum. A factor $\delta(f)$ is derived from the internal PWL extracted from test data and the internal PWL predicted for the treated configuration of interest.

The assumption is then made that, at a given frequency, the internal component of SPL for this configuration will differ from the test data by the same factor $\delta(f)$ derived for the internal component of PWL. By applying this factor at all polar angles, the predicted internal component of the SPL spectrum for the configuration under consideration can be calculated.

The external component of far-field noise is assumed to be independent of treatment for a given aerothermodynamic condition and is derived from the data and extraction method described earlier. The total far-field noise is then constructed using the external and respective internal components of SPL spectra. These spectra are then used to compute PWL, OASPL, PNL, and EPNL. It should be noted that, in the absence of data with which to establish absolute levels, relative levels are all that can be predicted.

Liner Design Results

Using the liner design methodology described above, various liner parameters (bulk depth and resistivity; face-sheet porosity, thickness, and hole diameter) can be optimized to achieve the mini-

mum internal noise EPNL. As an example, Figure 256 shows the internal EPNL predicted for different scale mixer/ejectors as a function of liner depth. At higher liner depths the EPNL variation is insignificant. It will be seen that the liner depths selected for the full scale (2 in), LSM scale (1.2 in), and small-scale nozzles (0.485 in), while not optimal, are predicted to be close to the optimum. It should be noted that the optimum liner depth predicted for the approximately 1/7-scale models is much greater than would be computed solely on the basis of linear scale factor (0.27 in). Finally, Figure 256 shows that, while the slopes of EPNL with respect to liner depth are drastically different, the curves seem to collapse better when plotted against the ratio of liner depth to linear scale factor.

Figure 257 summarizes the variation of bulk resistivity, liner depth, and face-sheet properties with respect to linear scale factor for "optimum" ("optimum" is defined as the best that could be done in the real world with real materials) liner designs. Bulk resistivity increases considerably with decreasing linear scale factor for optimum design. A very high value of face-sheet porosity is always desirable; however, from practical considerations, some relaxation of this criterion is permitted. For instance, in a small-scale model, a very thin face sheet is most desirable to control the liner reactance at higher frequencies, but such a very thin face sheet is difficult to manufacture and is structurally undesirable.

Conclusions and Recommendations

A significant number of laboratory tests have been conducted, and a data base has been created of "traditional" normal impedance and DC flow resistance together with *in situ* impedance, DC flow resistance, and boundary layer profile in the presence of heated grazing flow. This database was used to develop a correlation to predict normal impedance for a liner design accounting for flow, temperature, and acoustic environment. Also, a correlation to predict acoustic suppression in an ejector environment was underway using the laboratory test data and scale-model mixer/ejector test data. Such a correlation can be used for acoustic suppression prediction for a treated ejector instead of the currently used modal analysis code.

A liner design methodology has been developed that is used to optimize a liner to give maximum acoustic suppression for a desired scale nozzle. This tool also identifies those physical parameters of a liner design which might need modification to meet the optimum requirement. While the liner technology achievements meet the goals of the program, the various elements are somewhat limited as to broader application.

Use of the acoustic transfer factor to construct ΔPWL from the predicted acoustic suppression minimizes uncertainties associated with the acoustic suppression prediction, internal noise extraction process, and azimuthal variation of far-field noise. If such a factor is not used, and the predicted acoustic suppression is presumed to give the ΔPWL for a liner design directly, the EPNL predicted will be much different and will depend on the number of modes and the assumptions used in the acoustic suppression prediction.

A process to predict the noise field interior to the ejector and in the far field for any arbitrary scale mixer/ejector nozzle liner design has been developed. However, a number of assumptions, not verified for the current application, and used in this process, introduce uncertainties in the final result.

The acoustic suppression prediction is based on the uniform flow and temperature conditions in a two-side-treated, constant-area, rectangular duct. In addition, assumptions of equal energy per mode

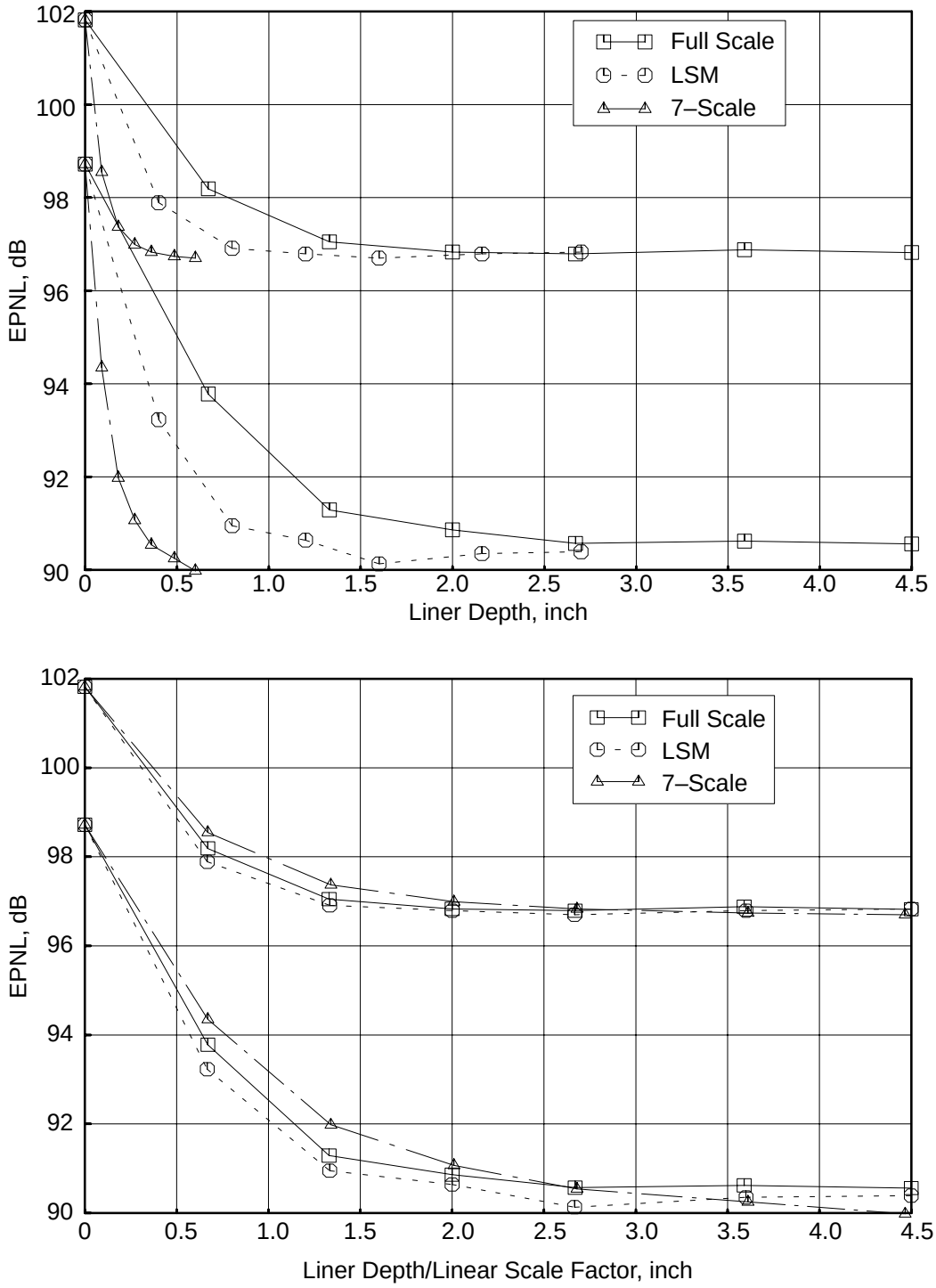

Figure 256. Effect of Liner Depth on Predicted Total and Internal Components of EPNL for Three Different Scale, Fully Treated, 22.12-in (160-in Full scale) Ejector; NPR = 3.43, T_8 = 1550°R, V_{mix} = 1430 ft/s, M = 0.32 {Takeoff}, ϕ = 25°

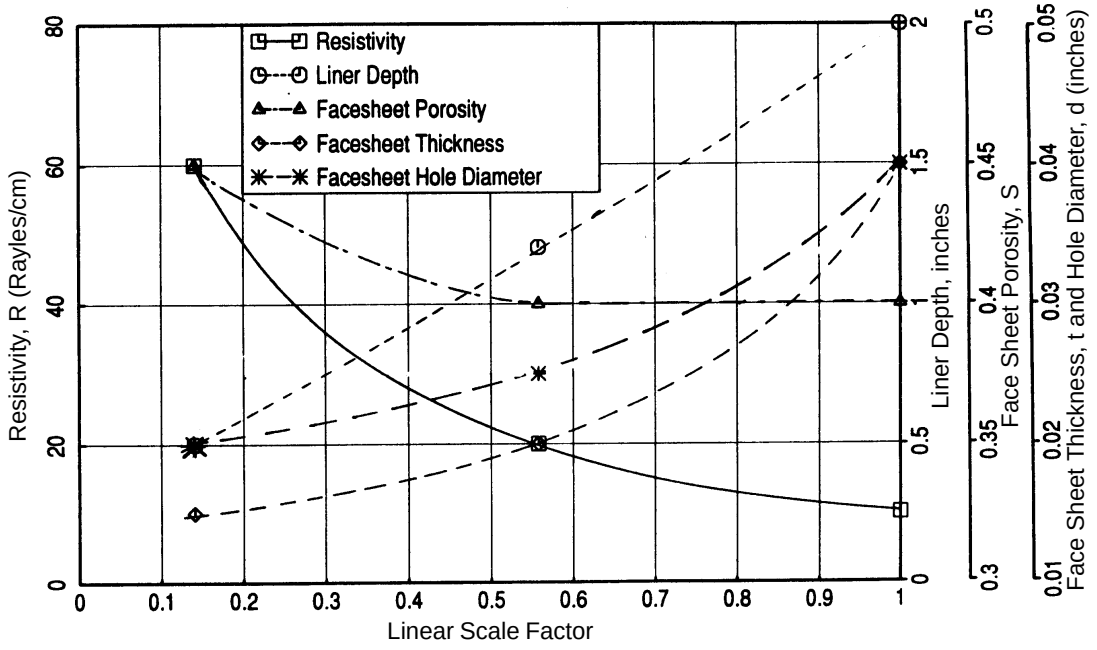

Figure 257. Variation of Bulk Resistivity, Liner Depth, and Face-Sheet Properties with Respect to Mixer/Ejector Linear Scale Factor for Optimum Liner Designs at Takeoff Conditions, M = 0.32

noise field and interaction of all frequencies with the treated surface for the entire ejector length may not be accurate. While the use of the acoustic transfer factor minimizes the inaccuracies associated with the prediction for a known test case, the assumption of the same factor for other liner designs and with different linear scale factor ejectors seems very optimistic.

The laboratory tests were initially planned for several bulk materials of varying properties coupled with a large number of face sheets of varying parameters. The normal impedance data were taken as intended. Due to time constraints, the grazing-flow effects were only studied for two bulk materials of fixed properties (100-ppi silicon carbide and 12-lb standard T–Foam). This puts limits on the use of the normal impedance correlation for materials of different type and of different properties.

Again, for the same reason, the acoustic suppression correlation, currently in progress, uses data from a limited number of 1/7-scale mixer/ejector nozzle configurations. The use of data from more configurations and models of a different scale (such as the LSM nozzle) would make this correlation more robust. It is highly recommended that future work include the laboratory tests for critical liner panels and more mixer/ejector data be used in the acoustic suppression correlation effort.

The internal components of EPNL for different liner designs are significant compared to the external component. In fact, for cutback, the internal component of EPNL is higher than the external component. Thus, we must find ways to reduce the internal noise component substantially to eliminate impact on total EPNL. If the current process of liner design does not suppress the desired amount of internal noise components, we need to redesign the liners with more innovative concepts.

5.8.1.2 Acoustic Liner Aerodynamic Testing

Aeroacoustic tests conducted on the Gen 3.0 1/7-scale models at the Boeing LSAF facility and the 56% scale LSM–1 on the F100–PW–129 engine in the PW C–11 test facility indicated substantially different nozzle thrust coefficient losses attributed to the acoustic liner: about 3.5% in LSAF as compared with approximately 1% in C–11. Normal scaling-effects approaches could not come close to resolving the differences. The actual face-sheet relative hole-size-to-metal-thickness ratio was different for the two tests, and a literature search of related topics strongly suggested this was a significant contributing factor to the difference in performance loss evaluation. Since the treatment loss was by far the least understood element of the nozzle performance losses, a plan was developed to address this issue.

Objectives

The objectives of the plan were to (1) understand the aerodynamic performance loss mechanisms related to the acoustic tiles, (2) develop an analytical model that would enable optimization of aerodynamic losses with acoustic requirements, and (3) explain the large difference in thrust loss observed between the LSM–1 and 1/7-scale tests.

Overall Approach

Four subtask were to be performed using a combination of analytical studies and acoustic liner component tests.

Subtask 1 – Liner Loss Analytical Modeling – An analytical model was to be developed by Boeing, using the FLUENT code, that would predict pressure losses and flow rates associated with flow recirculation within the acoustic tiles. The model was to be constructed using empirically derived curves for the relevant nondimensional parameters from a GEAE flow-duct rig test, a CE22 wind tunnel test, and historical data. The model, coupled with acoustic modeling, would then be used to optimize liner configurations for system integration. Due to delays in the GEAE flow-duct rig tests, this task could not effectively be conducted prior to completion of the CPC contract and was not performed.

Subtask 2 – Acoustic Line Pressure Loss Test in the GEAE Flow Duct Rig – The GEAE flow-duct test rig was to provide data needed to support Subtask 1. Flow and pressure-loss data for a range of acoustic liner face-sheet geometries and bulk absorbers were obtained.

Subtask 3 – Acoustic Liner Drag Test in NASA–Glenn CE22 Wind Tunnel – A small wind tunnel rig in the CE22 altitude chamber was used to directly measure the drag of a series of liner designs consistent with those tested in Subtask 2 to establish liner face-sheet design criteria and to support the analytical model in Subtask 1.

Subtask 4 – Historical Data/Literature Search and Analysis – A search of previous data related to acoustic liner designs was conducted to take full advantage of any previous tests or studies that may apply to the HSCT nozzle design and to support Subtask 1. This effort did not result in any relevant information; all previous work was directed at subsonic, commercial, nacelle applications and did not apply to the HSCT design and operating conditions.

GEAE Flow Duct Rig

Component testing of acoustic liners and bulk absorbers was conducted in the GEAE flow-duct rig during the HSR program to obtain data aimed at developing acoustic liner technology. This rig was

also used to support the liner aerodynamic-loss objectives previously outlined. A cross section of the rig is shown in Figure 258. For the aerodynamic performance loss tests, a duct Mach number was set and a vacuum pump could either suck air from the flow duct through the liner or pump it in the other direction and flow into the duct. Referring to Figure 258, test data provided pressure loss versus flow characteristics for the various test configurations using the measured flow, duct static pressure (P_{s1}), face-sheet back-side pressure (P_{s2}), and face-sheet back-side temperature (T_{s2}). A matrix of face sheets was tested to parametrically investigate porosity, hole-diameter-to-face-sheet-thickness ratio, face-sheet thickness, and hole alignment. Two bulk absorbers (100-ppi SiC and the T–Foam used on LSM–1) considered to be the leading candidates for the HSCT nozzle were also tested behind the face sheets to determine the interaction, if any, between the pressure-loss characteristics of the face sheets measured in the flow duct rig and the corresponding loss characteristics of the bulk absorbers from a DC flow rig described in the following paragraph. In addition to the flow duct rig, a DC flow rig (Figure 259) was used at GEAE to determine the pressure loss characteristics of four bulk absorbers: Sic 100 ppi, SiC 200 ppi, T–Foam LSM–1, and T–Foam three-layer paper.

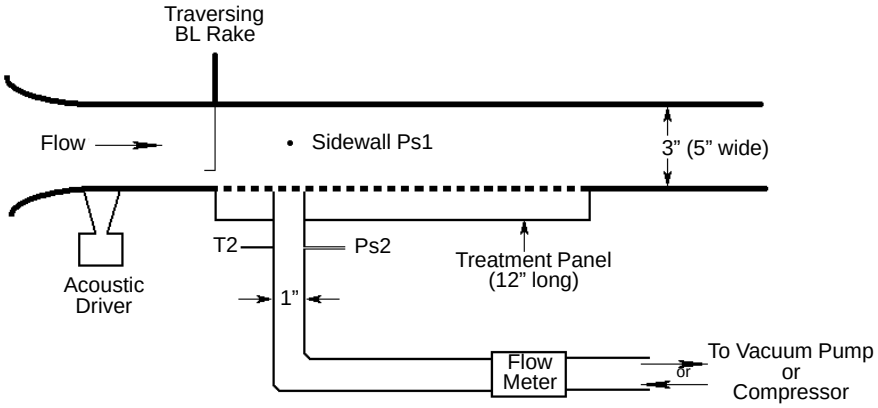

Figure 258. GEAE Flow-Duct Rig Cross Section

Typical results for one face-sheet test configuration in the flow duct rig are shown in Figure 260. Due to limitations in the suction capability of the test rig, some extrapolation of the data to higher Mach numbers and flow rates was required to create data in the expected operating range of the HSCT nozzle. Typical results for one bulk absorber test in the DC flow rig are shown in Figure 261.

NASA CE22 Wind Tunnel

Component testing of acoustic liners and bulk absorbers was also conducted in the NASA CE22 wind tunnel rig to support development of the analytical model and obtain directly the answer to the difference observed in the liner loss between the 1/7-scale and LSM–1 tests. A cross section of this test rig is shown in Figure 262. In this test, the drag of the test article (either a face sheet alone or a face sheet in combination with a bulk absorber as shown in Figure 262) was measured directly with a force balance over a range of Mach numbers. This installation represents the same tray-type installation used in the scale-model nozzle aeroacoustic tests. The exact same parametric family of face-sheet variables tested in the GEAE flow-duct rig was tested in this facility, as well as the two bulk absorbers. Variables included Mach number, inserts in the duct to vary the Mach number along the length of the face sheet (shown in Figure 262), and gap setting between the face sheet and the bulk absorber.

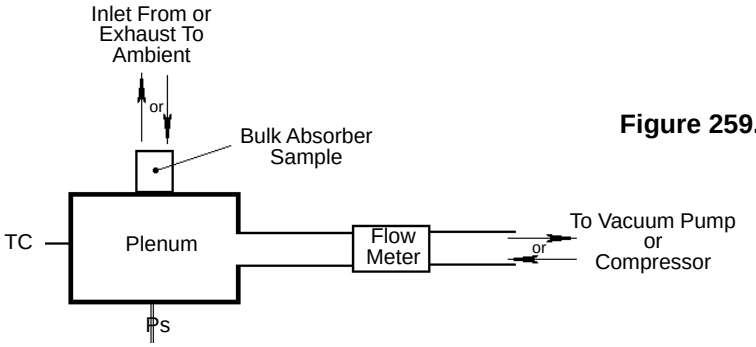

Figure 259. GEAE DC-Flow Rig Cross Section

Mn 0.0	$y = -21350.0983302742x^5 + 372.4492317118x^4 + 193.3382861501x^3 - 1.1721282813x^2$	$R^2 = 0.9995975762$
Mn 0.4	$y = 68.0054193317x^3 + 0.5274692801x^2 + 0.6313871159x + 0.0009834078$	$R^2 = 0.9994040471$
Mn 0.55	$y = 30.2297884867x^3 - 2.3853640700x^2 + 0.7257259220x + 0.0035906760$	$R^2 = 0.9993070353$
Mn 0.7	$y = -52.9699699513x^3 - 11.9686182384x^2 + 0.5781318983x + 0.0034995086$	$R^2 = 0.9996122965$
Mn 0.8	$y = 185.6786079067x^3 + 25.8090211717x^2 + 2.6644039259x + 0.0373778193$	$R^2 = 0.9985862565$

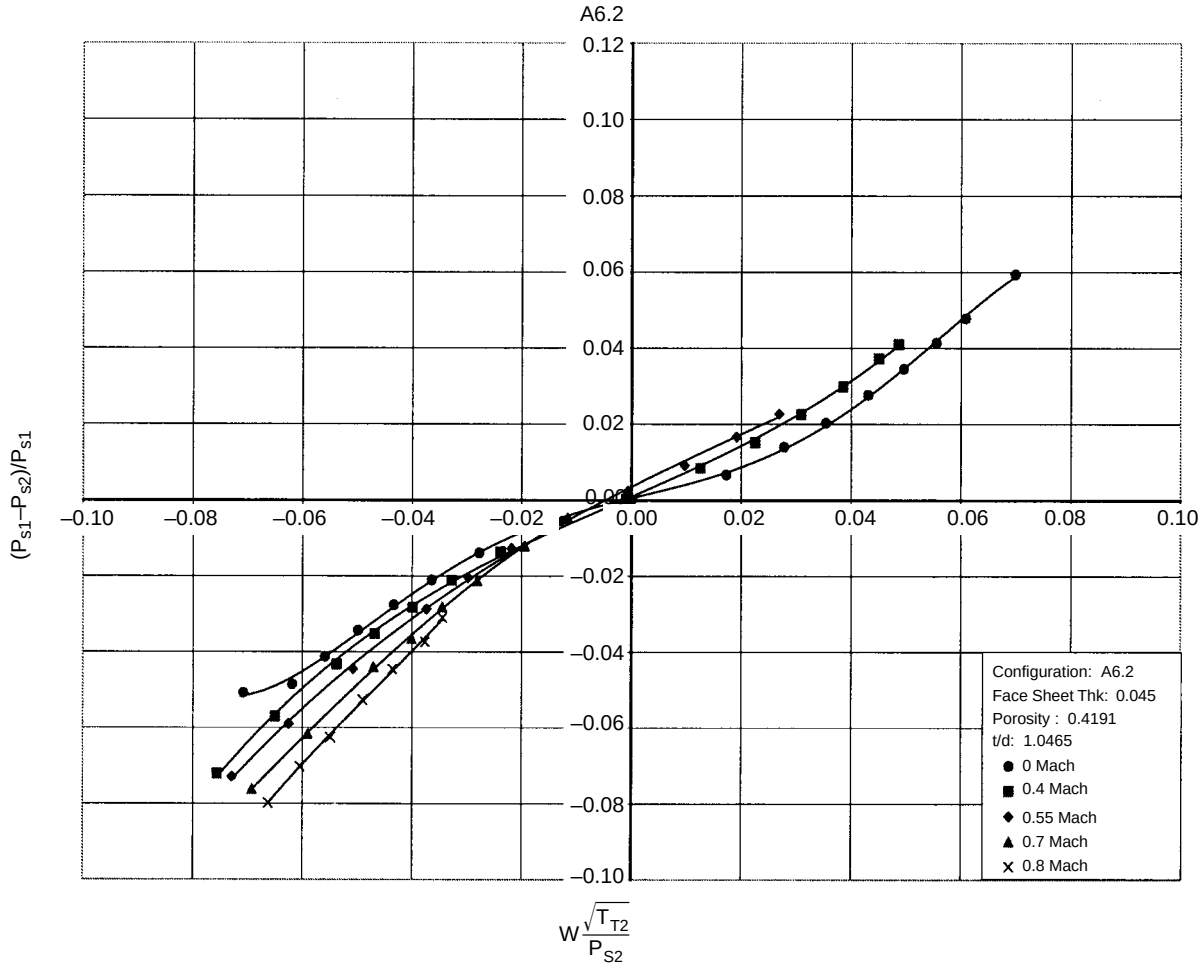

Figure 260. Plot of 40% Porosity, 1.0-t/d Face-Sheet Data

$y = -476557.5560684200x^5 + 5789.2933175954x^4 + 1746.9428099255x^3 + 4.4894839780x^2 + 0.6075516871x - 0.0000670247$
$R^2 = 0.9999581850$

$y = -4940416.7098083500x^5 - 12858.2045371488x^4 + 7258.9562714959x^3 + 11.6845418095x^2 + 1.3061730336x - 0.0001155152$
$R^2 = 0.9999419248$

$y = -19710033.4038696000x^5 + 50626.1358990035x^4 + 14287.1512799011x^3 + 4.6937411119x^2 + 1.9574107858x\ 0.0000255835$
$R^2 = 0.9999364165$

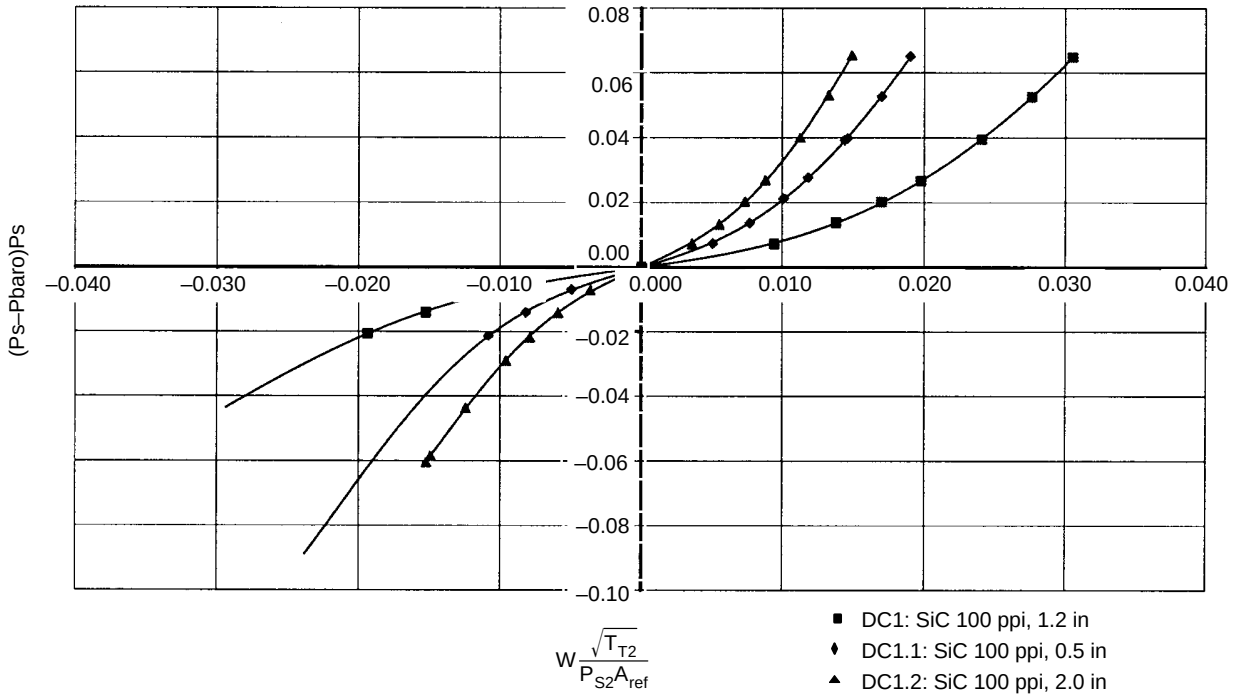

Figure 261. Plot of 100-ppi Sic Absorber Pressure Drop Data

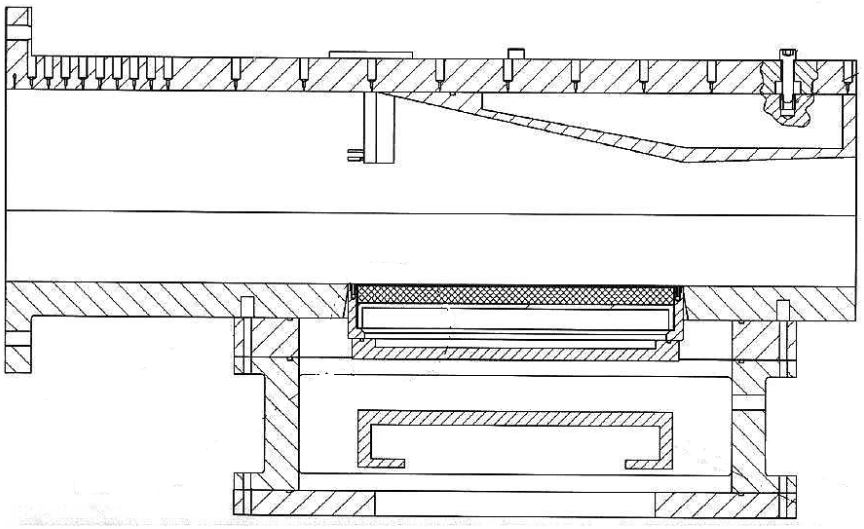

Figure 262. NASA CE22 Drag Rig Cross Section

Typical results for a family of hole-diameter-to-face-sheet-thickness ratios and porosities are shown in Figure 263 at a constant 0.60 Mach number.

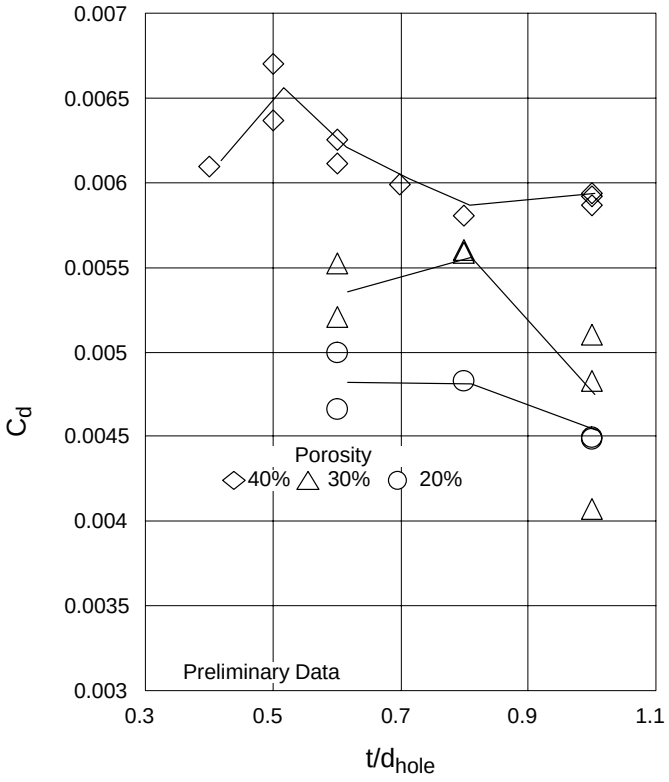

Figure 263. Drag Coefficient Variation with Porosity and t/d Hole

5.8.2 Chute Aerodynamics with Stereolithography Testing

Chute aerodynamics with stereolithography (CASL) testing provided a quick and relatively inexpensive way of studying a variety of design attributes and technologies for the HSCT program. By taking advantage of the "on demand" testing facility, the low cost of fabrication, and the ability to gather accurate empirical parametric data, the HSCT program was able to study a variety of nozzle flight conditions with the CASL test program.

5.8.2.1 CASL Testing Objectives

The objectives for each entry in CASL varied depending on the type of nozzle configuration investigated. Investigations using the CASL rig have concentrated in areas such as:

- Rapid-mixing devices: "a" tabs, chevrons, notches, etc.
- Cv_p test instrumentation/geometric approaches
- Techniques for reducing exit profile flow stratification
- Entrainment and mixing comparisons between HAM, LSM, and HPM
- Single-inlet-door concept
- Reverser mode analysis
- Forward ramp studies
- Frequency-shifted mixer secondary flow studies

5.8.2.2 Test Apparatus

D–37 Test Facility

All CASL testing was conducted at the P&W D–37 test facility in West Palm Beach, Florida. The D–37 facility is capable of supplying up to three regulated and metered gas flows simultaneously, with flows up to 3.5 lbm/s of dry nitrogen at 3,000 psia and 10 lbm/s of dry air at 200 psia. Automated data acquisition had the capability to record 88 channels of temperature and 32 channels of pressure. On-line computer data processing was available for test stand control, including calculated real-time parameters such as mass flow, Mach number, and transient probe position. Although it is not used in flow testing of SLA models, the test facility has the capability of providing heated air or air seeded with carbon dioxide for mixing studies. Finally, the facility was configured to provide two streams to the test rig: a high-pressure primary "engine" flow, and a near-ambient secondary flow.

CASL Rig and Test Model

The CASL rig, shown in Figure 264, provides primary and secondary flows to an ejector module. The ejector module is a removable section made of high-strength epoxy formed by the stereolithography process. A basic ejector module (Figure 265) incorporates the secondary inlet, mixer chutes, and primary-flow transition section.

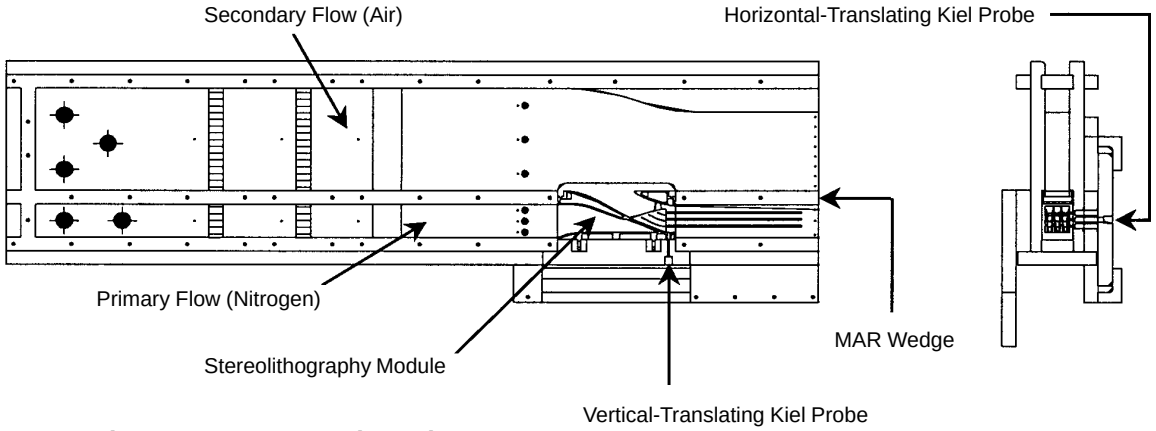

Figure 264. CASL Flow Rig

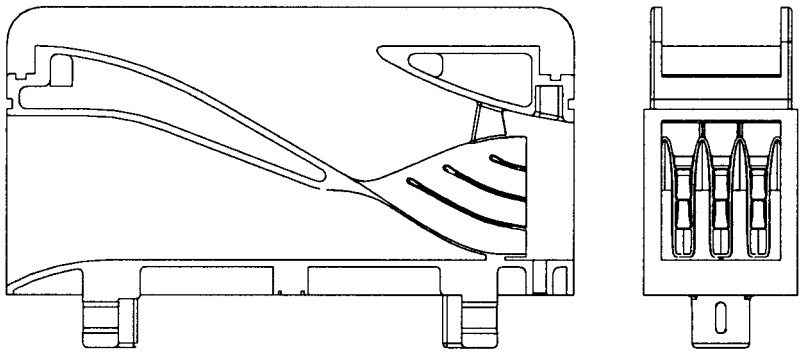

Figure 265. CASL Ejector Module

In addition, the module can be altered to model cruise mode, reverser mode, and other flight conditions for the nozzle. The rig is approximately 5-ft long and has a cross section about 16-in tall by 4-in wide. The rig is constructed of clear, 1-in thick Plexiglas. Primary and secondary flows both enter the rig through sidewall holes into plenums upstream of the mixer module. Each then passes through a series of restrictor plates to distribute the flow evenly through the passage. The removable ejector module is inserted through a slot in the bottom of the rig and then sealed with an O-ring plate. The downstream divergent flap is also removable to allow mixer area ratio (MAR) variations.

CASL Rig Instrumentation

The rig is instrumented for pressure and flow measurements to characterize the aerodynamics and assess detailed chute performance and flow quality. Instrumentation for the CASL rig is illustrated in Figure 266.

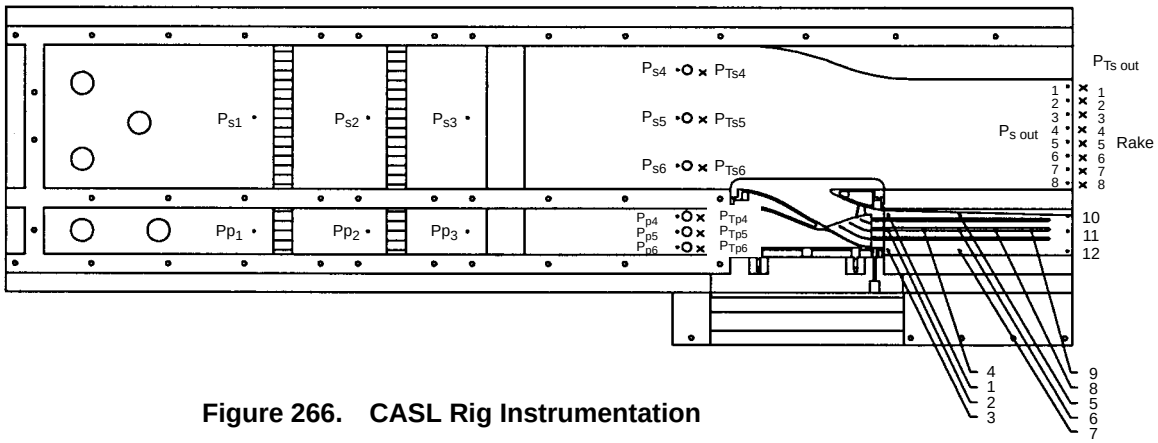

Figure 266. CASL Rig Instrumentation

Primary and secondary flow rates are both measured in the respective flow paths upstream of the mixer. The entrained secondary flow is calculated by taking the difference between the mass flow rate at the secondary exit of the rig (not entrained) and the mass flow rate entering the secondary side of the rig. The mass flow rate at the secondary exit is calculated from the total and static pressures measured from the eight total pressure ports at the secondary exit plane of the rig. A wedge was installed in the secondary duct to prevent the flow from diffusing as part of it is entrained through the mixer.

Total and static pressures are measured in the primary flowpath upstream of the mixer. This establishes total pressure, Mach number, and flow distribution in the upstream primary flow. The secondary total and static pressure are measured at three vertical locations upstream of the secondary inlet.

To characterize the mixing downstream of the chutes, the rig sidewall allows for transient data points at three vertical locations every 0.33 inches in the axial direction. Vertical dowel pins help position the horizontally translating Kiel probe at each of the axial locations.

Finally, a vertically translating Kiel probe is installed below the rig to characterize the pressure profile just behind the secondary exit of the mixer chutes. The actuator for this probe is installed in such a way that the mixer module can be removed or installed without removing the actuator.

5.8.2.3 Calculated Parameters

CASL testing provides several calculated aerodynamic parameters for the different modules, depending on the study of interest. One parameter calculated from the CASL test is mixing rate. Mixing rate is characterized by a parameter called "relative mixedness" (RM) defined by the equation:

$$RM = \frac{P_{Tdev}}{P_{Tavg}}$$

Where P_{Tdev} is the standard deviation in total pressure and P_{Tavg} is the average total pressure. The average total pressure can be calculated from:

$$P_{Tavg} = \frac{\sum_{i=1}^{n} P_{Ti}}{n}$$

Where P_{Ti} is the incremental total pressure and n is the total number of increments. The standard deviation in total pressure is calculated from:

$$P_{Tdev} = \sqrt{\frac{\sum_{i=1}^{n} (P_{Ti} - P_{Tavg,i})^2}{(n-1)}}$$

Knowing the average total pressure and the standard deviation of the total pressure, the relative mixedness of the flow can be calculated.

Another parameter of interest that can be calculated from this testing is the effect that the rapid mixing has on thrust performance. Thrust performance as it is affected by the mixing of the primary and the secondary flows can be calculated from the following relationship:

$$C_{Fn} = \frac{(W_{mix} \times V_{mix}) + (P_{s9} - P_0) \times A_9 - (W_s \times V_0)}{W^p \times V_{p,ideal}}$$

Where W_{mix} is the mixed mass flow rate, V_{mix} is the mixed-flow velocity, Ps_9 is the static pressure at the nozzle exit, P_0 is the ambient static pressure, A_9 is the nozzle exit area, W_s is the secondary mass flow rate, V_0 is the free-stream velocity, W_p is the primary mass flow rate, and $V_{p,ideal}$ is the ideal primary velocity.

The final aerodynamic parameter typically calculated in CASL testing is the secondary total pressure recovery. The pressure recovery ratio is defined as:

$$P_{Trec} = \frac{P_{Tmeasured}}{P_{Ts}}$$

Where P_{Ts} is the total pressure of the secondary flow and $P_{Tmeasured}$ is the total pressure measured by the vertically translating Kiel probe at the exit plane of the mixer chutes. In order to compare two different models, an area-averaged pressure recovery can also be calculated from:

$$A_{avg} P_{Trec} = \frac{\sum_{i=1}^{n} (A_i \times P_{Trec,i})}{A_{total}}$$

Where A_I is incremental area, A_{total} is the total secondary area, and n is the total number of increments.

5.8.2.4 Testing Accuracy

The CASL test program provided a quick and relatively inexpensive way of evaluating a variety of design attributes and technologies for the HSCT program. Because of the small scale and the intolerance of an SLA model sensitivity to high temperatures, CASL testing was never used as a means of obtaining acoustic data. Instead, it was used as a way of examining performance trends (flow separation, entrainment, etc.) as well as differences between design concepts (such as comparison between HAM8 to LSM and LSM to HPM, effects of rapid mixing, etc.) in a very timely manner. All CASL probe measurements were accurate to 1% of the maximum transducer limit. For this reason, CASL testing proved a vital tool in the design process of the nozzle for the HSCT engine.

5.8.3 Cv_p Testing

Subscale testing of the various lobed-mixer nozzles for the HSCT engine was an important tool in the design process of a product-scale nozzle. Cv_p testing (or primary-performance-only testing) of different mixer designs has been examined as a tool to assist in the understanding of the mixer/ejector nozzle primary flow performance. Thus, two series of Cv_p tests were performed under the HSCT CPC contract.

5.8.3.1 Objectives

There were two main goals for the Cv_p testing. The first was to determine the secondary-side configuration that provided the most accurate measurement of thrust by minimizing the base drag uncertainty. The second objective was to actually determine the Cv_p values for mixer designs such as the HAM8 (Gen 2.0), LSM (Gen 3.0), HPM (Gen 3.5), and 20/46 lobe-on-lobe (LOL).

5.8.3.2 Test Apparatus

Facility Description

Cv_p testing for the HSCT nozzle took place at two facilities: the NASA–Glenn CE22 and Channel 7 at ASE–FluiDyne's Plymouth Aerodynamic Laboratory. Both facilities are briefly described below.

NASA–Glenn CE22 – The NASA CE22 test cell is capable of providing 40 psig of primary combustion air at 40 lbm/s and secondary air at 40 psig (21 lbm/s), 125 psig (2 lbm/s), or 450 psig (8 lbm/s). The 40-psig primary air and the secondary air can be heated to 370° and 250°F respectively. Model exhaust can be supplied at atmospheric to a simulated 48,000-ft altitude condition. The model is installed in an altitude tank connected to the inlet and exhaust air piping (see Figure 267).

The facility can measure thrust in all three axes, providing axial, vertical, and lateral thrust measurements with a 3000-lbf limit in the axial direction and 1000-lbf limits in the vertical and lateral directions. Pressures can be measured with three different-range transducers. The facility records sixty-four 15-psi pressures, three hundred eighty-four 40-psi pressures, and thirty-two 500-psi pressures. In addition, a color Schlieron system is available for airflow analysis.

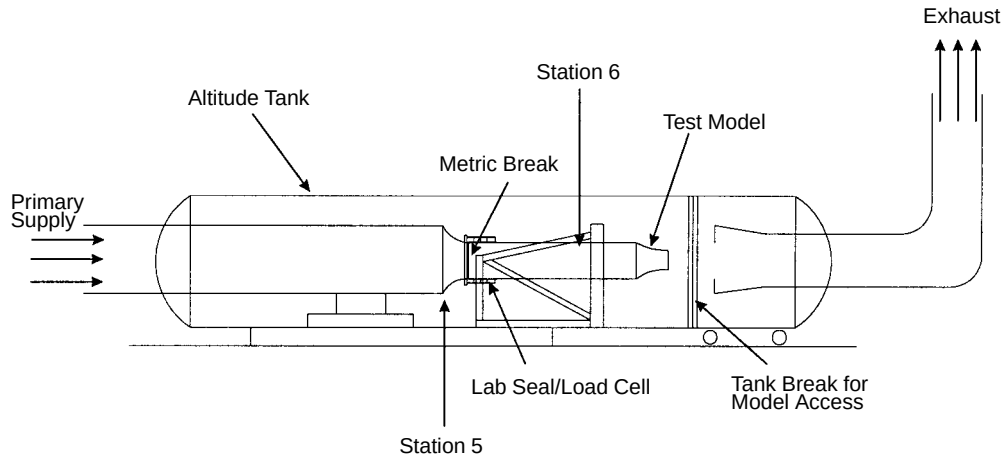

Figure 267. NASA CE22 Test Cell

Finally, this facility uses an electronically scanned pressure (ESP) system with rack-mounted pressure transducer modules. All facility pressures are measured with 0-to-15-psi transducers. All temperature measurements are made with K-type thermocouples.

Channel 7 at ASE–FluiDyne's Plymouth Aerodynamics Laboratory – The Channel 7 facility at FluiDyne's Plymoth Aerodynamics Laboratory is a cold-flow, high-pressure-ratio, static thrust stand with the ability to exhaust either to atmosphere or into a sealed cabin connected to a vacuum system. The basic arrangement of this facility is shown in Figure 268.

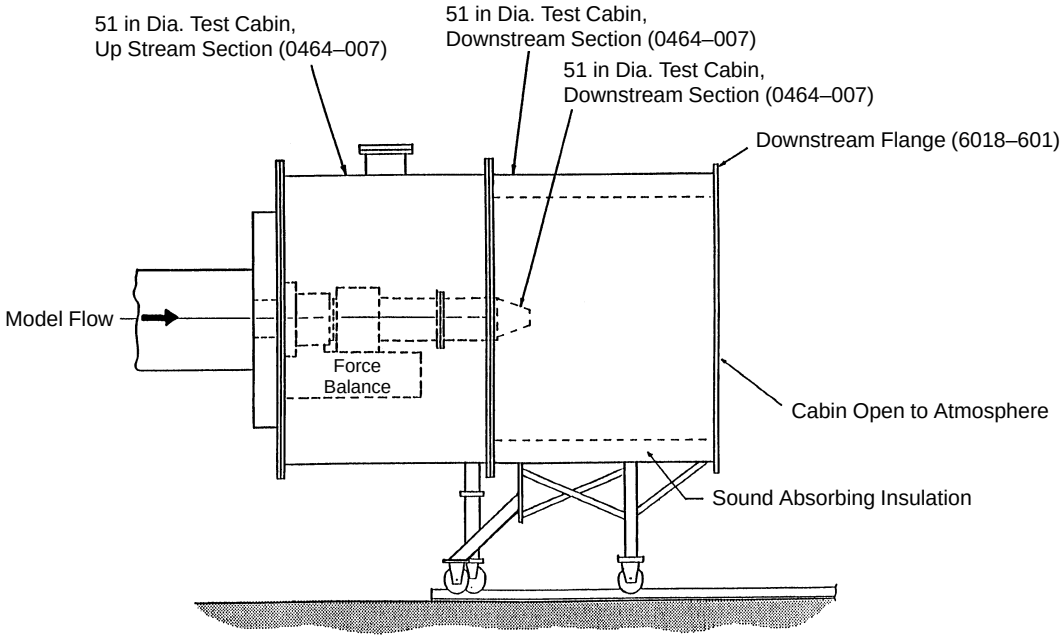

Figure 268. ASE–FluiDyne Channel 7 Test Facility

High-pressure dried air from the facility 500-psi storage system was throttled through an ASME long-radius metering nozzle and then discharged through the test model. The model assembly is supported by a three-component strain balance and isolated from facility piping by an elastic seal.

The test data from Channel 7 included measurements of axial and normal balance forces, model total and static pressures, ambient pressure, and the upstream ASME meter pressure and temperatures necessary to calculate the flow rate and stream thrust entering the metric portion of the model assembly. Pressures were measured with Pressure System Inc. (PSI) multiported transducers. Finally, the force balance and the temperature signals were recorded with an Analogic electronic digital data acquisition system.

Model Description

All models for the Cv_p testing were built out of cast aluminum with the primary flow line built exactly to design specifications. The HAM8, LSM, and HPM mixers were built to 1/7 of the product scale; the 20/46 LOL model was built to 1/4 the scale of the product. Figure 269 shows isometric views of the different types of models tested.

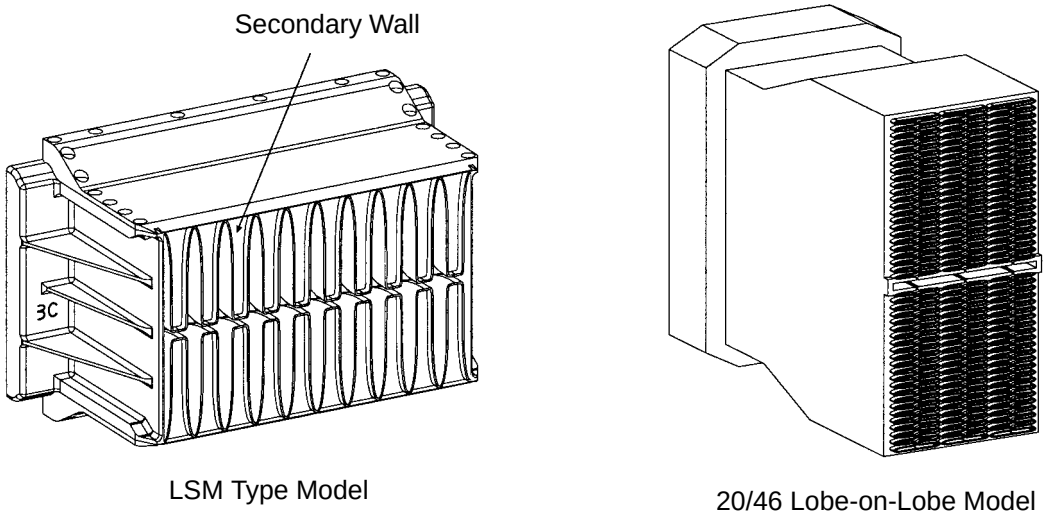

Figure 269. Example Cv_p Test Models

Model Instrumentation

All Cv_p test models were instrumented using 0.042-in diameter stainless steel tubing to measure static pressure. Figure 270 is a typical instrumentation sketch.

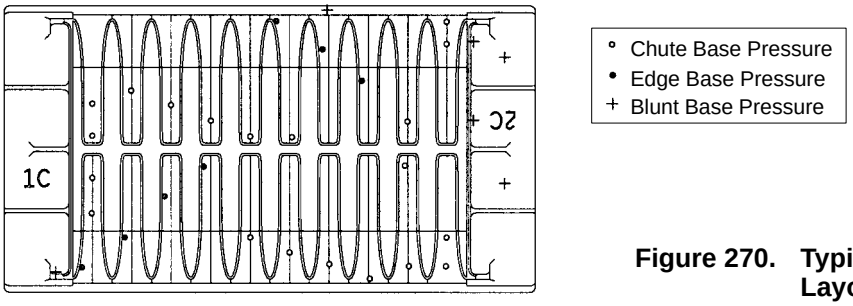

Figure 270. Typical Cv_p Model Instrumentation Layout

The base area is divided into three regions: the projected area of the secondary chutes called the "chute" region, the projected area of the wall between the primary and secondary called the "base" region, and the projected region that covers the flange called the "blunt base" region. Due to costs constraints, it was impossible to instrument the models with a large number of probes; therefore, the instrumentation was staggered over the entire base area and symmetry was assumed to obtain the total base drag.

5.8.3.3 Calculating Cv_p

The flow parameter of interest in this testing, Cv_p, can be calculated from the following equation:

$$C_{V_p} = \frac{F_{measured}}{F_{id}} + \frac{D_{base}}{F_{id}}$$

Where $F_{measured}$ is the measured thrust of the facility, D_{base} is the calculated base drag, and F_{id} is the ideal stream thrust. The base drag is calculated by:

$$D_{base} = \sum_{i=1}^{n} (A \times \Delta P)_i$$

Where n is the number of static probes on the model, A is the area of the region where the probe is located, and ΔP is the difference of the measured static pressure from the atmospheric static pressure. Finally, the ideal stream thrust can be calculated from:

$$F_{id} = P_T \times A_{8,design} \times C_{D,measured} \times \sqrt{3.282\left[1 - \left(\frac{1}{NPR}\right)^{0.28571}\right]}$$

Where P_T is the nozzle total pressure, $A_{8,design}$ is the design physical throat area, $C_{D,measured}$ is the measured discharge coefficient, and NPR is the nozzle pressure ratio. After calculating the values for D_{base} and F_{id}, the Cv_p can be calculated for a given test configuration.

5.8.3.4 Error Analysis and Testing Accuracy

A detailed error analysis was performed on both tests conducted during the Cv_p testing. At the worst case, the error for this type of primary flow testing is about ±1% of the calculated Cv_p. Based on the error analysis, it was determined that the Cv_p procedure described here is a good approach for studying the primary flow performance of mixer/ejector nozzles.

5.8.4 MIT Shock Tube Testing

A transient testing technique for the study of jet noise was investigated and assessed. A shock tunnel facility was used to produce short-duration (10 to 20 ms), supersonic, hot-air jets from a series of scaled test articles, including ASME conic nozzles and a large-scale-model-similitude mixer/ejector nozzle. The primary purpose of the facility is to investigate noise-suppressor nozzle concepts relevant to HSCT aircraft applications.

The shock tube has many strengths: it is mechanically simple, versatile, has low operating costs, and can generate jet conditions comparable to aircraft gas turbine engine exhausts. Further, as a result

of shock heating, the total temperature and pressure profiles at the nozzle inlet are uniform, eliminating the noise associated with entropy nonuniformities often present in steady-state, vitiated air facilities. The primary drawback to transient testing is the brief duration of useful test time. Sufficient time must be allowed for the nozzle flow and free jet to reach a quasi-steady state before acoustic measurements can be made. However, if this constraint is met, the short run times become advantageous. The test articles are only exposed to high-temperature flow for a fraction of a second and can be constructed of relatively inexpensive stereolithograpic apparatus or cast aluminum.

5.8.4.1 Testing Objectives

The objective of the research described herein is to assess whether or not a shock tunnel facility can be used to produce useful fluid mechanic and acoustic measurements of hot supersonic jets. It has been shown that the relevant fluid dynamic structures have sufficient time to reach a quasi-equilibrium state, that there is adequate test time to resolve the sound power spectrum levels, and therefore that useful far-field acoustic measurements can be acquired on scaled nozzles. Furthermore, a comparison between steady-state acoustic data obtained at Boeing's LSAF and transient shock tunnel noise data are presented for the nozzles described in Subsection 5.8.4.4.

5.8.4.2 Background, Test Facility, Apparatus, and Instrumentation

The fundamental purpose of a shock tube is to generate a reservoir of high-temperature, high-pressure fluid that is expanded through a nozzle to create a hot supersonic jet. Initially, the tube is separated into a driven section, denoted as region (1), and driver section, denoted as region (4), by two thin diaphragms, as shown in Figure 271a. The driven section contains the test gas, air for each test, and is typically evacuated to around 1/5 of an atmosphere. The driver section is evacuated and then filled with a mixture of helium and air to a pressure between 2 and 6 atmospheres, depending on the desired shock strength. When the section of the tube between the two diaphragms is evacuated, the pressure difference causes the diaphragms to press against knife blades and rupture. The driver gas acts like an impulsively started piston, initiating a series of converging compression waves and rapidly compressing the test gas. The compression fronts coalesce into a shock wave, propagating through the driven section, accelerating and heating the driven gas. Concurrently, a series of diverging expansion waves propagate through the driver gas mixture, decreasing the pressure and accelerating the fluid in the direction of the nozzle. The state of the gas traversed by the incident shock wave is denoted by region (2), and that of the gas traversed by the expansion fan is denoted as region (3), as depicted in Figure 271b. The test is initiated when the incident shock wave reaches the nozzle end of the tube, reflects from the end plate, and creates a region of stagnant, high-pressure, high-enthalpy fluid, denoted as region (5), which then ruptures a secondary diaphragm and expands through the nozzle to the desired conditions (Figure 271c).

The shock tube used at the MIT facility consists of a 7.3-m driven section and a 8.4-m driver, both constructed from 30-cm-diameter stainless steel pipe, as shown schematically in Figure 272.

The tube is suspended on rollers to provide access to diaphragms and allow repositioning of the nozzles with respect to the microphones. The nozzles exhaust into an 8.3×9.8×3.7-m anechoic test chamber treated with a 10-cm-thick fiberglass acoustic absorber that results in 10 to 20 dB reduction in reflected acoustic intensity for frequencies above 500 Hz.

Acoustic data were acquired using six Bruel & Kjaer 4135 ¼-in, free-field microphones positioned on a constant radius arc 3.7 m from the nozzle exit. The microphones were located at directivity

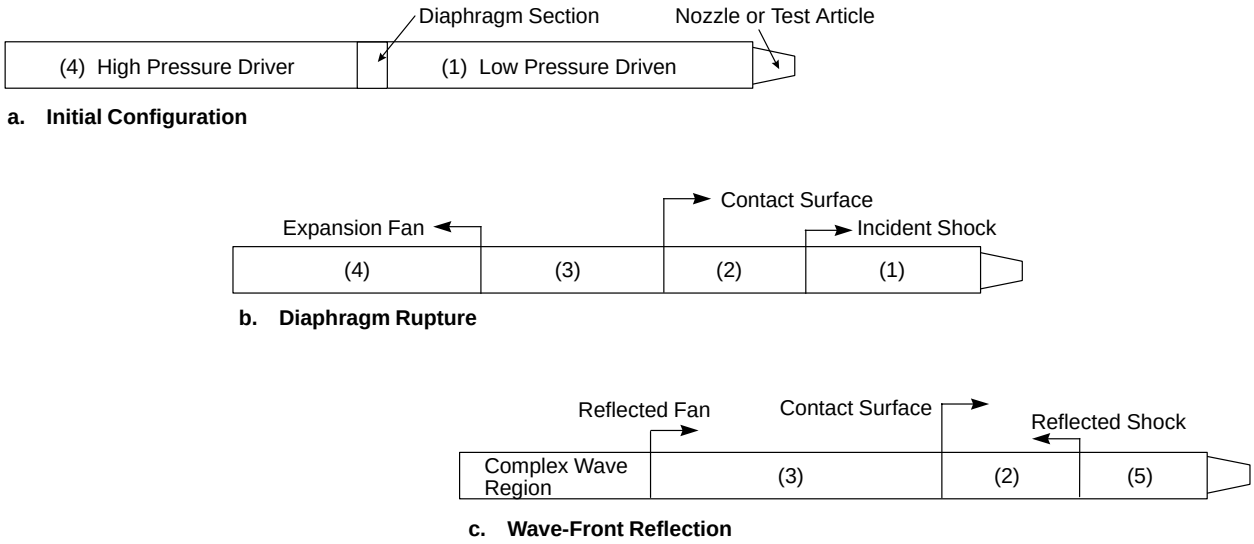

Figure 271. Shock Tube Notation and Wave Phenomena

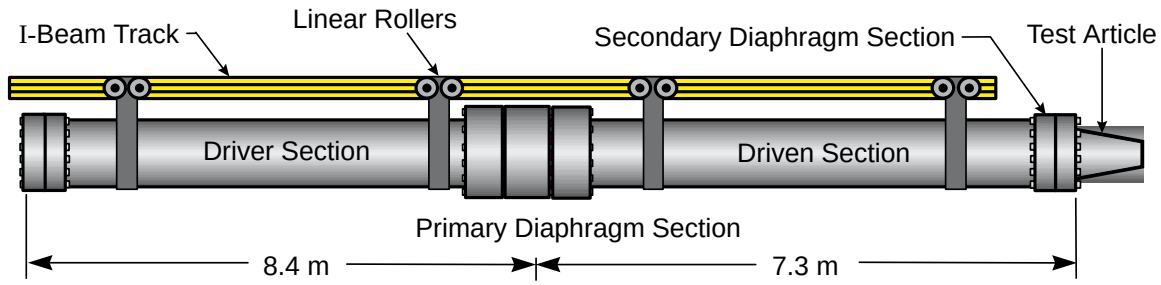

Figure 272. MIT Shock Tube Schematic

angles comparable to the steady-state facility: 70°, 110°, 120°, 130°, 140°, and 145°. Four Kulite XT–190 0–100-psia dynamic pressure transducers are flush mounted on the wall of the driven section of the shock tube. These four transducers are used to measure the primary nozzle pressure, shock speed, and test time (duration of the uniform-pressure region). Using this instrumentation, NPR can be determined with an uncertainty on the order of 0.1%. Total-temperature ratio (TTR) is determined with an uncertainty on the order of 0.1% through measurement of the incident shock speed and use of the shock tube equations. Two computers are used to control the operation of the facility and acquire the pressure, noise, and thrust data. The control computer is configured with National Instrument's LabView and the required cards to control the sequence of 13 solenoid valves and 2 mass flow controllers necessary to fill and fire the facility, as well as to acquire and save the dynamic pressure data obtained from four wall-mounted pressure transducers in the shock tunnel. The second computer is configured with two ADTEK AD830 high-speed, data-acquisition boards that enable it to simultaneously sample 16 channels at 12 bits, 330 Hz.

5.8.4.3 Models Tested

Four models were tested: three ASME axisymmetric nozzles and a 1/12-scale mixer/ejector model.The sizes of the three ASME standard axisymmetric nozzles used to assess facility performance, as well as the ASME nozzles used to acquire steady-state noise data at Boeing, are summarized in Table 52.

Table 52. Summary of ASME Conic Nozzle Geometry

Nozzle Description	Scale	Exit Diameter	Exit Area	Nozzle Length
Transient (Small)	1/20	2 in (5.1 cm)	3.14 in^2 (20.4 cm^2)	7.5 in (19.1 cm)
Transient (Medium)	1/15	2.67 in (6.8 cm)	5.6 in^2 (36.3 cm^2)	10 in (25.4 cm)
Transient (Large)	1/10	4 in (10.2 cm)	12.57 in^2 (81.7 cm^2)	14 in (35.6 cm)
Steady State	1/8	5 in (12.7 cm)	19.63 in^2 (126.7 cm^2)	17.5 in (44.5 cm)
Full-Scale Comparison	1	40 in (101.6 cm)	1248 in^2 (8052 cm^2)	140 in (355.6 cm)

Table 52 also shows the size that each of the nozzles is scaled up to when the full-scale acoustic performance assessment is made. The LSMS mixer/ejector model is shown in Figures 273 and 274.

The 1/12-scale model and the secondary diaphragm section are approximately 90-cm long. The chute racks tested in the model are made of either cast aluminum or plastic SLA. The aluminum chute rack was cast from an SLA model. The LSMS model also features a compliment of 13 Kulite pressure transducers located along the center line on both the top and bottom surfaces. The pressure measurements serve to confirm that the mixer/ejector model is operating at a quasi-steady mode by comparing to the pressure signatures from the full-size, steady-state model.

5.8.4.4 Significant Results and Testing Accuracy

The ASME conic nozzles were run at operating conditions relevant to the HSCT mixer/ejector development program. Nozzle pressure ratio varied from 1.51 to 3.43, and total temperature ratio varied from 1.82 to 2.91, as summarized in Table 53.

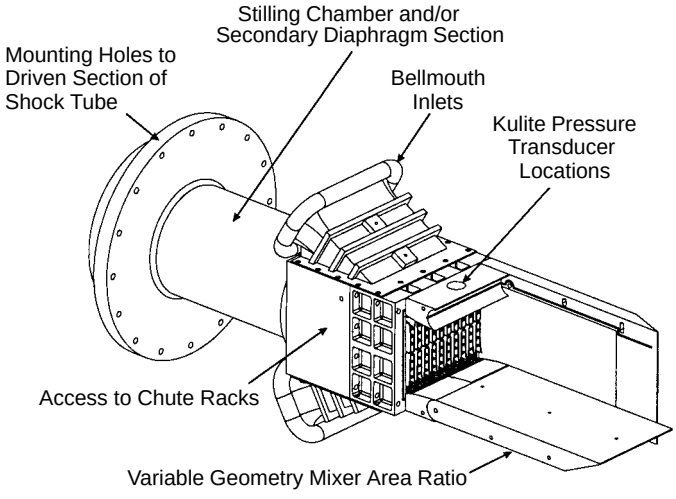

Figure 273. Isometric View of 1/12-Scale LSMS Model

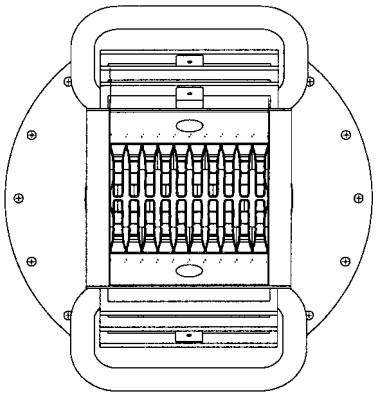

Figure 274. End View of Mixer

Table 53. Summary of ASME Conic Nozzle Acoustic Performance *One-third-cctave SPL*

Nozzle	Desired		Achieved		Comparison with Steady-State Assessment 250 to 4000 Hz Full-Scale Frequency Range
	NPR	TTR	NPR	TTR	
1/20	1.51	1.82	1.53	1.82	± 2dB on all directivity angles
	2.48	2.43	2.57	2.45	± 2 dB on 4 of 6 angles, ± 3–4 dB on 120♈and 130♈
	3.43	2.91	3.48	2.93	± 2 dB on 5 of 6 angles, ± 3dB on 130♈
1/15	2.48	2.43	2.50	2.44	± 2–3 dB on all directivity angles
	3.43	2.91	3.51	2.93	± 2 dB on 5 of 6 angles, ± 3 dB on 110♈
1/10	1.51	1.82	1.51	1.81	± 2–3 dB on 3 of 6 angles, ± 3–5 dB on 110♈, 120♈, and 130♈
	2.48	2.43	2.45	2.43	± 2–3 dB on all directivity angles
	3.43	2.91	3.45	2.96	± 2–3 dB on all directivity angles

Some typical results showing SPL versus full-scale 1/3-octave frequency and OASPL and PNL versus directivity angle are shown in Figures 275 through 278.

Figure 275 depicts a full-scale comparison between transient noise data taken from the 1/20-scale ASME nozzle and steady-state noise data acquired from the 1/8-scale version at an NPR and TTR of 1.51 and 1.82, respectively. The figure shows that the acoustic signature, as compared on a

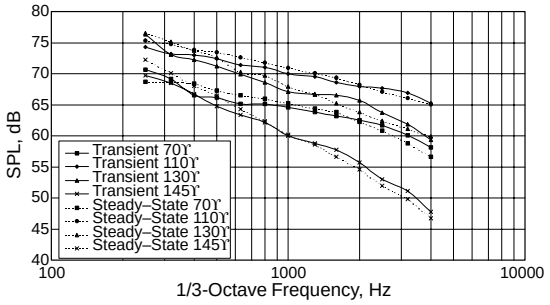

Figure 275. Comparison of 1/20-Scale ASME: NPR = 1.51, TTR = 1.82

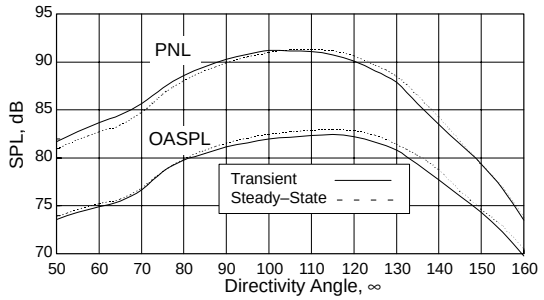

Figure 276. Comparison of 1/20-Scale ASME: OASPL and PNL Versus Directivity Angle

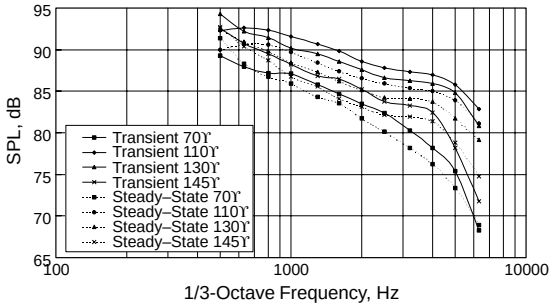

Figure 277. Comparison of 1/10-Scale ASME: NPR = 3.43, TTR = 2.91

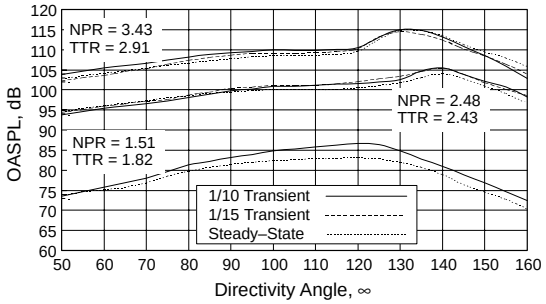

Figure 278. Comparison of 1/10 and 1/15 ASME: OASPL and PNL Versus Directivity Angle

full-scale standard day basis, agrees to within ±1 or 2 dB over a full-scale frequency range of 250 to 4000 Hz over all directivity angles examined.

Figure 276 shows the corresponding OASPL and PNL versus directivity angles plots for the transient versus steady-state noise data. The plot shows that the two sets of data display agreement to around 1 dB in magnitude and have similar behavior with directivity.

Figure 277 shows the same type of comparison as presented in Figure 275 but using the 1/10-scale nozzle at the highest NPR and TTR combination tested. The two data sets show agreement to within ±2 or 3 dB over all directivity angles.

Finally, Figure 278 shows OASPL and PNL versus directivity angle comparisons for the 1/10- and 1/15-scale ASME nozzles over the three NPR and TTR combinations tested. The figure shows that, in general, each of the nozzles exhibit agreement in directivity and magnitude with steady-state data.

Overall, the ASME nozzle acoustic results demonstrated that the transient noise data replicate the Boeing steady-state data to within ±2 or 3 dB on SPL versus full-scale frequency from 250 to 6300 Hz, as well as OASPL and PNL versus directivity angle. Table 53 summarizes the results of the entire battery of tests performed on the ASME nozzles, as well as the desired and achieved NPR and TTR jet conditions. The last column of the table describes the type of assessment discussed above for Figures 275 and 277, for each of the cases. The magnitude of EPNL values were shown to agree to within 1 to 3 dB, depending on test condition and nozzle scale. Repeatability of the results was found to be ±0.5 dB on a test-to-test basis and ±1 dB on a day-to-day basis.

Specific conclusions from the ASME nozzles include:

- Each of the transient nozzles tested exhibited the same overall trends in magnitude and directivity as the steady-state noise data. All transient tests showed agreement with the steady-state noise trends in OASPL and PNL versus angle.
- The 1/20-scale nozzle exhibited better than ±2 dB agreement on each test condition except for the 120° and 130° angles on the mid- and high-NPR cases, which deviated by around 3 dB. The 1/15-scale nozzle agreed to within ±2 dB at the mid- and high-NPR cases and to within ±3 dB on the 110° angle on the high-NPR case. Finally, the 1/10-scale nozzle agreed to within ±2 dB on the mid- and high-NPR cases and had the worst agreement of any nozzle at the low-NPR condition, deviating by 3 to 5 dB at 110°, 120°, and 130°.
- Transient nozzle-to-nozzle tests agreed within approximately 1 dB EPNL for the mid- and high-NPR cases. Each of the nozzles exhibited a higher value of EPNL, by about 1 or 2 dB, than the steady-state data at the mid-NPR condition. The 1/20-scale nozzle displayed the best agreement, with EPNL matched to within 0.5 dB for the low- and high-NPR conditions and within 1 dB for the mid-NPR condition.
- The use of multiple shock tube shots at the same operating condition was shown to reduce the uncertainty associated with transient acoustic measurements. Increasing the test time, through combined shock tube shots, demonstrated an improved convergence to the steady-state noise data. Systematic and run-to-run repeatability error prevent convergence to the theoretically achievable levels predicted, with around 30 to 35 milliseconds, or 2 to 3 shock tube shots, required for the best convergence.
- Run-to-run repeatability on jet conditions was found to be better than 1% on NPR and TTR and within 0.5 dB on SPL versus frequency.

Comparison of the performance of the LSMS mixer/ejector model is summarized in Table 54 for the cast aluminum chute rack and in Table 55 for the SLA chute rack. Table 56 is a comparison of the transient acoustic signatures obtained from the cast aluminum and SLA chute racks. The LSMS model is not symmetric, so variations in azimuthal angle, as well as variations with mixer area ratio were examined using the 1/12-scale model. A sample of the types of comparisons made, analogous to the ASME nozzles, is presented in Figures 279 and 280. Figure 279 shows that the agreement with the steady-state data is within 1 to 3 dB for the highest NPR condition tested. Figure 280 shows the variation with MAR at the low NPR condition on OASPL versus directivity angle.

Table 54. Summary of 1/12-Scale Cast Aluminum Chute Rack LSMS Model Performance

Desired		Achieved		LSMS Geometry		Comparison with Steady-State Assessment 250 to 4000 Hz Full-Scale Frequency Range
NPR	TTR	NPR	TTR	MAR	Azimuthal	
1.51	1.86	1.51	1.85	0.90	90Υ	± 2–4 dB on 100Υ, 110Υ, 120Υ, 130Υ, ± 3–5 dB on 70Υ
	1.86	1.50	1.88	0.98	90Υ	± 2–5 dB on 100Υ, 110Υ, 120Υ, 130Υ, ± 3–5 dB on 70Υ
2.48	2.48	2.48	2.48	0.90	90Υ	± 2–4 dB on 120Υ, 130Υ, ± 3–5 dB on 70Υ, 100Υ, 110Υ
	2.49	2.48	2.48	0.93	90Υ	± 4–5 dB on 120Υ, 130Υ, ± 4–6 dB on 70Υ, 100Υ, 110Υ
	2.48	2.49	1.49	0.98	90Υ	± 2–3 dB on 120Υ, 130Υ, ± 3–5 dB on 70Υ, 100Υ, 110Υ
3.43	2.97	3.49	2.89	0.90	90Υ	± 1–2 dB on 70Υ, 100Υ, 110Υ, 120Υ, ± 2–3 dB on 130Υ
	2.96	3.41	3.01	0.98	90Υ	± 1–2 dB on all directivity angles
1.51	1.86	1.53	1.87	0.90	24Υ	± 2–5 dB on 100Υ, 110Υ, 120Υ, ± 3–5 dB on 70Υ, 130Υ
	1.86	1.51	1.85	0.98	24Υ	± 2–4 dB on 100Υ, 110Υ, 130Υ, ± 3–4 dB on 70Υ, 120Υ
2.48	2.48	2.45	2.46	0.90	24Υ	± 3–4 dB on 120Υ, 130Υ, ± 3–5 dB on 70Υ, 100Υ, 110Υ
	2.49	2.47	2.48	0.93	24Υ	± 3–5 dB on 120Υ, 130Υ, ± 4–6 dB on 70Υ, 100Υ, 110Υ
	2.48	2.49	2.52	0.98	24Υ	± 2–3 dB on 120Υ, 130Υ, ± 3–5 dB on 70Υ, 100Υ, 110Υ
3.43	2.99	3.43	2.98	0.93	24Υ	± 1–2 dB on 70Υ, 100Υ, 110Υ, ± 2–3 dB on 120Υ, 130Υ
	2.96	3.45	2.97	0.98	24Υ	± 1–2 dB on 70Υ, 100Υ, 110Υ, 120Υ, ± 2–3 dB on 130Υ

Table 55. Summary of 1/12-Scale SLA Chute Rack LSMS Model Performance

NPR	TTR	NPR	TTR	MAR	Azimuthal	250–4000 Hz Full-Scale Frequency Range
1.51	1.86	1.52	1.86	0.90	24Υ	± 3–5 dB on 100Υ, 110Υ, 120Υ, ± 3–5 dB on 70Υ, 130Υ
	1.86	1.52	1.87	0.98	24Υ	± 3–4 dB on 100Υ, 110Υ, 130Υ, ± 3–4 dB on 70Υ, 120Υ
2.48	2.48	2.50	2.48	0.90	24Υ	± 3–4 dB on 120Υ, 130Υ, ± 3–5 dB on 70Υ, 100Υ, 110Υ
	2.48	2.51	2.52	0.98	24Υ	± 3–4 dB on 120Υ, 130Υ, ± 3–5 dB on 70Υ, 100Υ, 110Υ

Table 56. Summary of 1/12-Scale Cast Aluminum versus SLA Chute Rack Performance

NPR	TTR	NPR	TTR	MAR	Azimuthal	250–4000 Hz Full-Scale Frequency Range
1.51	1.86	1.52	1.86	0.90	24Υ	± 1–2 dB on all directivity angles
	1.86	1.52	1.87	0.98	24Υ	± 1–2 dB on 100Υ, 110Υ, 120Υ, 130Υ, ± 2–3 dB on 70Υ
2.48	2.48	2.50	2.48	0.90	24Υ	± 1–2 dB on all directivity angles
	2.48	2.51	2.52	0.98	24Υ	± 1–2 dB on all directivity angles

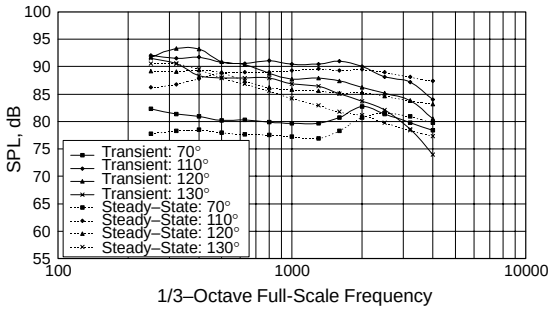

Figure 279. Comparison of 1/12-Scale LSMS: NPR = 3.43, TTR = 2.96, MAR = 0.98

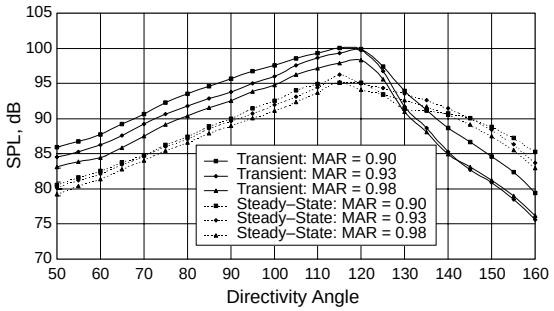

Figure 280. Comparison of 1/12-Scale LSMS: NPR = 1.51, TTR = 1.86

Specific conclusions from the LSMS investigation include:

- The SLA chute rack was robust enough to withstand even the highest nozzle pressures (3.43) and demonstrated agreement with the cast aluminum chute rack to within 1 or 2 dB.
- The transient and steady-state noise data agree to within 2 to 5 dB on SPL versus full-scale frequency, for all NPR and TTR, MAR and azimuthal angles studied thus far.
- The transient data tend to drop-off faster than the steady-state data at aft directivity angles, but on the whole are high by about 2 to 3 dB over the steady-state noise data.
- Variation with MAR was typically found to be on the order of 2 dB, whereas the steady-state data show variation of around 1 dB among the cases studied. It is hoped the enigmatic acoustic behavior associated with the 0.90 MAR condition will be clarified during future LSMS steady-state tests.
- Transient and steady-state data peaked at nearly the same directivity angle for all cases tested.
- Variation in azimuthal angle for the transient data was in agreement with the steady-state trends.
- EPNL values were typically 2 to 4 EPNdB higher for the transient data as compared to the steady-state noise data. The trends in EPNL values between the 1.51, 2.48, and 3.43 NPR condition showed agreement to about 1 to 2 EPNdB between the transient and steady-state data. Transient EPNL values were also in agreement with trends in MAR and azimuthal angle seen in the steady-state noise data.
- Use of multiple runs was found to reduce the uncertainty associated with making transient acoustic measurements with convergence being achieved after 2 or 3 shock tube shots.
- Run-to-run repeatability was on the order of 1 dB on a test-to-test basis.

Deviations between the transient and steady-state noise may be the result of a number of effects. Mixer/ejectors, such as the LSMS nozzle, are complicated fluid mechanical devices that are very sensitive to small changes in geometry and operating condition. Differences in throat area, Reynolds number, lobe trailing-edge thickness, and separation effects may play roles in the differences seen between the transient and steady-state noise data.

5.8.4.5 Concluding remarks

The shock tunnel was shown to be an efficient facility for generating and acquiring noise data that are in agreement with steady-state data taken on comparatively sized nozzles. The transient noise

data exhibited agreement with steady-state data over a full-scale frequency range, relevant to the HSCT program, to within ±2 to 4 dB for a majority of the nozzle and test combinations investigated. The facility can serve as a valuable tool for conducting jet noise research, with the cost of performing high-temperature jet noise experiments being retrenched by more than an order of magnitude. The short duration of the test time enables the nozzles to be made from inexpensive, rapid prototyping. Parametric testing can therefore be performed more economically and faster than in steady-state facilities, making transient shock tunnel testing a valuable tool to serve as a complimentary mode of investigation for jet noise research.

5.8.5 Fundamental Experiments on Mixing Enhancement

These experiments were conducted in the open-jet facilities and a wind tunnel housed in the test cells CW13 and CW17 (ERB) at NASA–Glenn. The primary objective was to investigate techniques for mixing enhancement and advance the understanding of flow mechanisms, in support of the HSR program. Following is a description of key research elements carried out under this program.

5.8.5.1 External Chevrons and Internal Mixer Tabs

The objective of the test was to investigate methods to increase mixing both outside and within the ejector by using tabs and chevrons. Early experiments focussed on the effect of tabs and chevrons placed at the exit of the ejector. All experiments with this nozzle involved cold flow without a secondary outer stream. Detailed data on vorticity inside and outside of the ejector were obtained at low speeds, and Pitot surveys were conducted at transonic conditions. Results were summarized in Reference 31; see also Reference 32. Later experiments with this nozzle focussed on use of tabs on the primary chutes and the resultant mixing enhancement within the ejector. For this purpose, GEAE provided a new set of chutes representing the design current at the time (1997). Various tab configurations were tried, and Pitot surveys within the ejector were conducted to assess the effects. Flow blockage and pumping were estimated. These experiments were conducted in close consultation with GEAE personnel and the HSR nozzle ITD team. The results led to certain tab configurations (“modified A Tabs”) that were later tried at GEAE for noise benefit. Promising noise benefits were noted in the latter experiments.

The nozzle configuration had an eight-lobe mixer of approximately 4.65 in^2 mounted in an 9.7-in-long ejector downstream of the mixer with dimensions 5 by 2.6 inches and a mixing area ratio of 1.0. Three external mixing devices were investigated: large chevrons, small chevrons, and tabs. The chevrons were isosceles triangles, aligned with the mean flow at the exit of the ejector. The small chevrons had base dimension 0.41 in, the large 0.83 in. The tabs were also isosceles triangles but bent 35° into the flow with blockage of approximately 0.3% per tab. The model, with the large external chevrons, is shown in Figure 281.

From detailed hot-wire data acquired at low speed inside the ejector, the main observations were that the streamwise vorticity generated by the lobed mixer persisted the length of the ejector, that this vorticity caused a complete interchange of high- and low-velocity regions in the cross sections of the flow, and that the longitudinal vorticity became organized to scale on the dimensions of the ejector box before the ejector exit.

Pitot surveys of the external plume were taken with each external mixing device in place. Figure 282 shows the results for a primary nozzle pressure ratio of 2.5 (cold). From this figure it can be seen

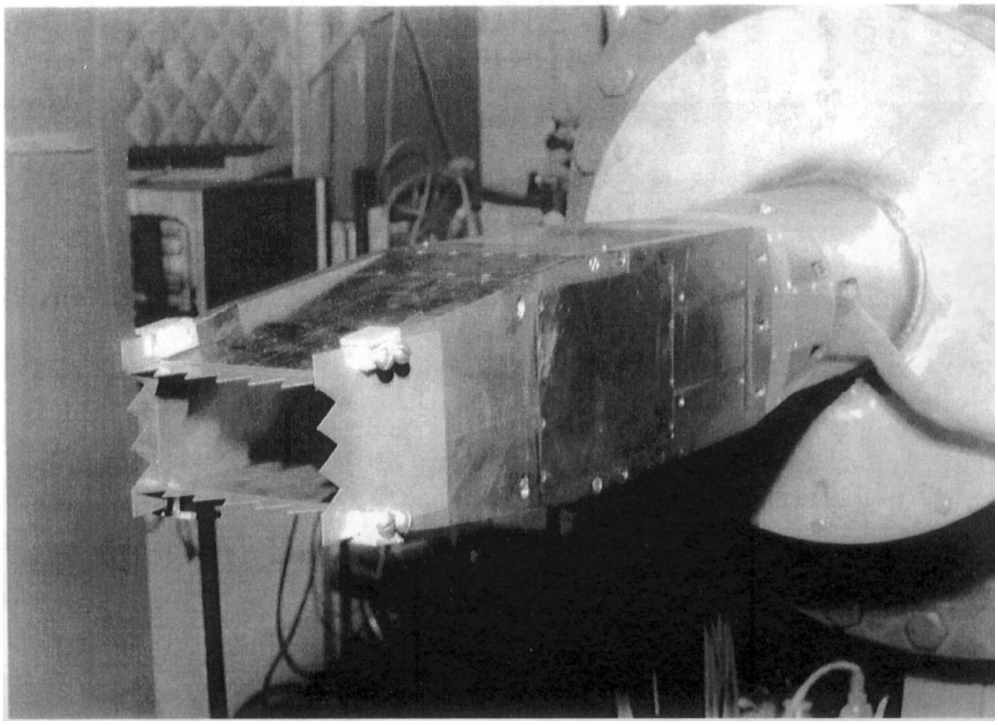

Figure 281. GEAE/ARL HSCT Mixer/Ejector Model Mounted in NASA–Glenn CW17 with Large External Chevrons

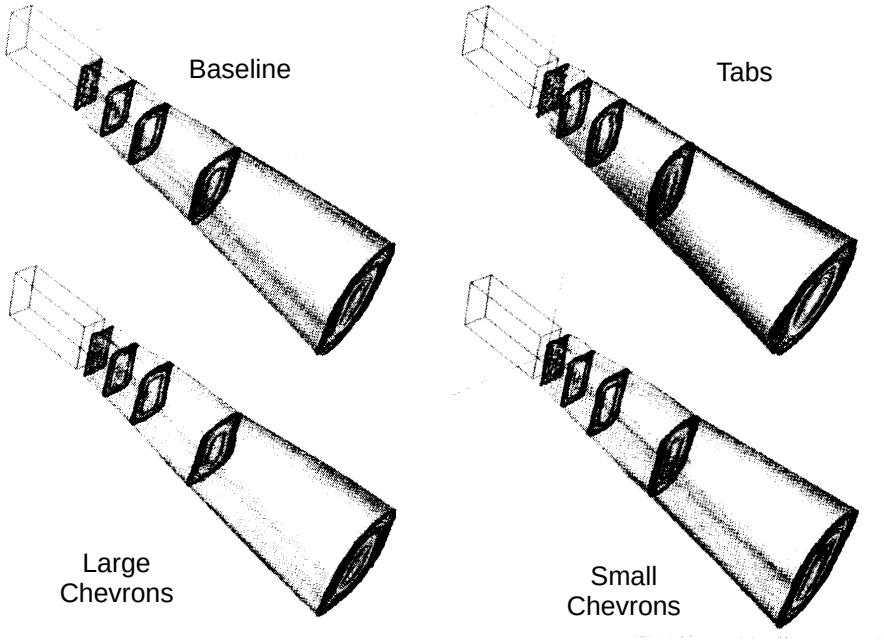

Figure 282. Plume Cross Sections for Different External Mixing Enhancement Devices, NPR=2.5, Cold

that the tabs had the most effect, both at the ejector exit and at the farthest downstream position where the plume is most circular of all the plumes. Figure 283 quantifies this in terms of peak Mach number at the different downstream locations. Also included in this plot is a simple rectangular nozzle. Comparing the rectangular nozzle with the baseline mixer/ejector, the effectiveness of the internal turbulent motion at enhancing the mixing immediately downstream is obvious. However, the decay rates for the baseline and the chevron cases are not much greater than with the rectangular nozzle. Only the tabs caused a sustained increase in decay rate.

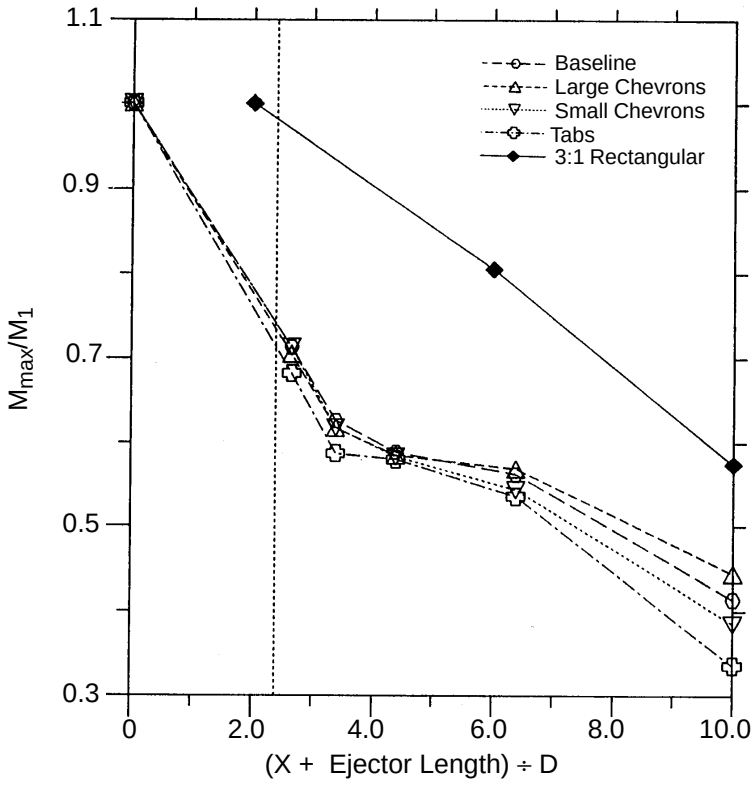

Figure 283. Peak Mach Number Decay in External Plume with Different External Mixing Enhancement Devices, NPR=2.5

5.8.5.2 Early Tabbed Mixer Studies: ACE and Lobed Mixer

Earlier experimental investigations were conducted with a single-lobed nozzle (eight lobes) and a small-scale model of the Boeing axisymmetric coannular-ejector (ACE) nozzle. Mixing characteristics with the lobed nozzle were studied with and without tabs. The ACE nozzle experiments were conducted in collaboration with Dr. J.M. Seiner of NASA–Langley. In the latter experiment, effects of tabs as well as porosity and aspiration through the central plug were studied. These results were summarized in Reference 33.

The most important observation of this study regarding applying tabs to the axisymmetric ACE nozzle was that applying greater numbers of tabs did not create more spread or mixing. Various sizes of 6, 12, and 24 tabs were tried; the greatest impact on mixing and on noise was obtained with the

6-tab configuration. The thrust loss for a given area blockage increased with the number of tabs, keeping the area constant.

The most important observation of this study regarding applying tabs to lobed mixers is summarized in Figure 284. This figure shows the jet cross section as visualized with various configurations of tabs. It is evident in the figure that the effect of the tabs is remarkable and very difficult to predict — it is not a simple linear relationship. Depending upon where extra flow expansion is needed, tabs can be applied to provide it.

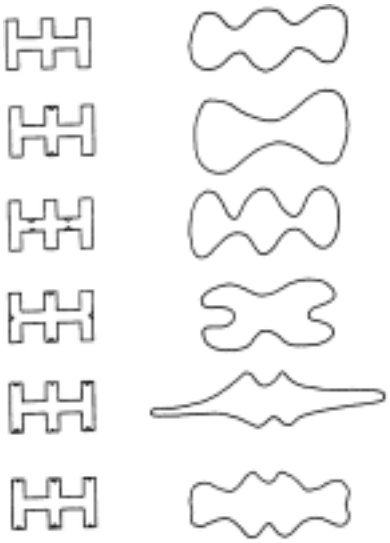

Figure 284. Effects of Various Tab Configurations on Flow Cross Section of Lobed Mixer

5.8.5.3 Fundamentals of Mixing Enhancement Via Tabs

A fundamental experiment studying the vorticity and small-scale structures as affected by multiple delta tabs in a two-stream, plane, mixing layer was conducted in the wind tunnel. This work is reported in Reference 34. A computational study for tabbed jets, using the NPARC code, was partially supported under this program (References 35 and 36). Several other fundamental studies on mixing and noise from jets were also partially supported under this program (References 37, 38, and 39).

Overall, it was found that tabs and other trailing-edge mixing enhancements accelerated mixing by introducing strong, large-scale axial vorticity. The degree of enhancement was determined first by the penetration and spacing of the tabs and second by the local static-pressure fields and boundary layers. Because of the complex interactions of axial vortices downstream of the tabs, simulations assuming periodic symmetry were often incorrect. Acoustically, tabs were found to reduce low-frequency jet noise — presumably by reducing effective jet velocity — but produced high-frequency noise from the increased turbulence and unsteady separation off the tabs.

5.9 Aero/Acoustic Collaborative Effort

5.9.1 Acoustic Data Interpretation

One of the aims of the *Aero Acoustic Collaborative Effort* (AACE) was to develop better understanding of the relationships between the aerodynamic and acoustic characteristics of the mixer/ejector nozzle. Nozzle designs that meet both acoustic and aerodynamic performance requirements could then be developed with less use of “cut and try” techniques. This has been a challenging objective.

This subsection is intended to provide a composite understanding of the acoustic features of the mixer/ejector nozzle that has evolved from analysis of acoustic and flowfield data acquired in different facilities, at different scales, and with the nozzle tested in isolation or installed on a wing. Semiempirical methods developed from the available data have also been employed to gain insight into the nozzle aeroacoustic features.

HSCT noise levels at the sideline and cutback certification points are dominated by jet noise. The metric used for evaluation of these levels is *effective perceived noise level*, an integration of the noise signal over a range of directivity angles and a broad range of frequencies. The semiempirical acoustic model of Subsection 5.6.2.1 represents our current level of understanding of the acoustic features of the mixer/ejector nozzle system. Here the acoustic field of the mixer/ejector nozzle is described in terms of three noise-generation regions (internal, premerged, and merged), each of which gives rise to a characteristic spectral and angular distribution. Each noise-generation region thus contributes to the overall EPNL, but the contributions vary. It is found that reduction of a particular noise component may increase the importance of another component or have a significant aerodynamic performance or weight penalty that would render the aircraft system economically nonviable.

Judicious selection of geometric and cycle parameters is needed to minimize the EPNL metric at sideline and cutback. The current discussion is grouped under:

- Geometric parameters such as SAR, ejector length, chute penetration, chute number, MAR, etc.
- Acoustic liner designs
- Mixing-enhancement devices
- Engine cycle conditions and free-stream Mach number
- Installation effects
- Effects of scale and the influence of the engine environment.

5.9.1.1 Geometric parameters

Out of several geometric parameters investigated, the significant parameters that influenced acoustics and had a significant impact on the overall nozzle system design are discussed here.

- Suppressor Area Ratio
- Ejector Length
- Chute Penetration
- Chute Number
- Mixing Area Ratio

Suppressor Area Ratio

For a given ejector inlet and chute aerodynamic design, increasing SAR increases ambient entrainment ratio (pumping) and results in reduced ejector exit velocity (because of the larger exit area) and a more uniform ejector exit velocity distribution (better mixed). This type of flowfield has been

shown to have lower levels of the merged noise component (reduced low frequency), which typically dominates in the shallow angles to the jet axis (aft) and contributes significantly to the EPNL in terms of duration correction. However, the increased entrainment gives rise to more intense mixing of the secondary and primary air, which results in more noise generation at the smaller length scales associated with chute width or hydraulic diameter. If such increased levels of the internal noise component are not effectively attenuated either by more acoustic treatment area or by more effective acoustic treatment, the benefit of the reduced merged noise component will not result in reduced EPNL. This was evident when the effect of SAR (2.5 versus 2.9) was investigated with the ejector walls fully lined and 5/9th lined. For the case with fully lined ejector walls, the SAR 2.9 nozzle had a lower EPNL than the SAR 2.5 for all jet velocities V_j. However, for the 5/9 lined nozzle, the SAR 2.9 EPNL is higher than that for the SAR 2.5 nozzle for $V_j < 2000$ ft/s and is lower for $V_j > 2000$ ft/s. As specific thrust increases, ($V_j \approx 2340$ ft/s), the eddy convection speed increases. This results in the increased dominance of the merged noise component as well as reduced treatment suppression. Increasing SAR from 2.5 to 2.9 with the fully lined ejector yielded about 2 EPNdB benefit at $V_j \approx 2340$ ft/s.

Ejector Length

For the full-width cold chute at the sidewall designs studied under the Gen 2 series of tests, increasing ejector length for a given cycle, ejector inlet, chute geometry, and SAR improves the noise reduction significantly by virtue of the following (see Section 5.7.1.4):

1. Increase in acoustic treatment area for suppression of the internal noise
2. Physical shrouding of internal noise sources
3. More uniformly mixed profile at the ejector exit resulting in lower premerged noise component at forward and peak noise angles

Increasing ejector length has been shown to reduce the entrainment ratio slightly, probably due to increased boundary layer thickness and reduced aerodynamic area. For a SAR 2.9 nozzle with fully treated walls, increasing the ejector length from 120 to 160 inches resulted in about 2 EPNdB benefit over the entire velocity range, for Mixer 8c. Spectral data clearly indicated the reductions were in the internal and premerged noise components. Small spectral reductions were noted at low frequencies at forward and peak angles for the longer ejector, as a consequence of more uniform exit velocity profile. However, a slight increase in low-frequency noise was noted at very shallow angles to jet axis, probably a consequence of reduced pumping. Increasing the ejector length for a true hard-wall case from 120 to 160 inches resulted in EPNL reductions of about 0.5 to 1.0 EPNdB over the jet velocity range. In the case of hard wall, the noise reductions are due to physical shrouding of noise sources and more uniform mixed profile at the ejector exit.

Care needs to be taken with regard to drawing general conclusions from these results in the light of data from Mixer 8H (with the half-width hot chute at the sidewall). Here there was significant acoustic benefit at 120 inches, attributed to more rapid mixing within the ejector, with little additional improvement with the increase in length.

Chute Penetration

Aerodynamic (flowfield) data on chute penetration variation (85%, 92.5%, and 100%) indicated that chute penetration has a significant effect on the mixing of primary and secondary streams and

external plume development (see Subsection 5.7.1.4). At 85% penetration, the secondary flow was principally near the ejector walls and the primary flow was near the nozzle axis, resulting in a highly (vertically) stratified flow field at the ejector exit. At 100% penetration, the hot primary flow and secondary flow mixed along the full height of the chutes, but the hot flow tended to stay near the ejector walls. This resulted in a well-mixed although slightly "inverted" velocity profile at the ejector exit. By far, 92.5% penetration achieved the most uniform mixing at the ejector exit. Lack of mixing in the case of 85% penetration (both within and outside the ejector), and subsequent lack of absorption of the internal noise by liners, resulted in higher noise levels at all jet velocities (about 2 EPNdB). PNL directivity and spectral comparisons indicate that the 85% penetration mixer resulted in higher levels at all directivity angles and almost at all frequencies. The 100% and 92.5% penetration mixers exhibit similar EPNL levels at most jet velocities of interest, although the 100% penetration mixer shows slightly lower EPNL at $V_j \approx 2600$ ft/s. This is principally due to the lower low-frequency noise of the 100% penetration mixer, resulting from the slightly reduced exit velocity (higher thrust loss) and "inverted" velocity profile.

Chute Number

Two principal noise-generation parameters influenced by chute number are shear perimeter (dividing the primary and secondary flows) and characteristic eddy length scale (influences peak frequency). The chute number was varied from 16 to 24 at a SAR of 2.5 (see Subsection 5.7.1.4). The chute aspect ratio (chute height/width) over this range of chute number is high enough that the mixing is controlled by shear perimeter rather than by streamwise vorticity. The Gen 1 nozzle designed by P&W had eight chutes with the chute aspect ratio less than 2 (see Subsection 5.7.5.3). In such designs there is room for the streamwise vortex to grow in the axial direction and contribute significantly to the mixing. Such is not the situation investigated in Subsection 5.7.1.4. It is noted that when the chute number was increased from 16 to 20, a reduction of about 2 EPNdB was obtained, whereas no significant acoustic differences were noted between 20 and 24 chutes. In general, the 16-chute mixer had higher levels of premerged and internal noise components than the 20- or 24-chute mixers. All had very similar merged noise content. This resulted in PNL differences at forward and peak angles and similar levels at very shallow angles to the jet axis. The 16-chute mixer showed more unmixed velocity profiles at the ejector exit both in the spanwise (chute to chute) and the vertical directions than the 20-chute mixer, thereby causing higher levels of internal and premerged noise components. The variation in chute number was not large enough to make a significant change in the Strouhal number associated with chute hydraulic diameter. Hence no systematic trend with peak frequency was evident (on a 1/3-octave band) with chute number variation.

Mixer Area Ratio

MAR has a significant effect on ejector internal aerodynamics (in terms of pumping, internal shock structures, and mixing), particularly at pressure ratios close to the mode transition. Reducing MAR was shown to shift the mode transition to higher nozzle pressure ratios. This in turn has a significant bearing on internal and premerged noise components. It is difficult to present a unified trend of noise characteristics with MAR due to the complex variation of internal flowfield and internal noise sources with MAR. Gen 2 tests (see Subsection 5.7.1.4) showed that the SAR 2.9 aerodynamic-shaped mixer (Mixer 8c) with 5/9 treatment exhibited EPNL reductions when MAR was reduced from 0.95 to 0.9. The reduction in ejector exit area as MAR is reduced from 0.95 to 0.9 tends to

reduce the entrainment slightly, with a concurrent slight increase in the mixed exit velocity. However, the reduction in entrainment tends to reduce the internal noise component. Thus, if the noise signature is dominated by internal noise (as is the case for Mixer 8), the slight reduction in entrainment and associated increase in external noise still resulted in a reduced EPNL. The increase in internal noise at MAR 0.95 can be offset by lining the whole ejector. Once the detailed aerodynamic and acoustic performances of the selected nozzle are determined, one can effectively use variable MAR capability to optimize the nozzle during takeoff for noise and aerodynamic performance.

5.9.1.2 Liner Designs

Acoustic liners have provided about 7.5 and 4+ EPNdB reductions at typical cutback and sideline, respectively, relative to a "true hard wall" for a mixer/ejector nozzle with 160-in long ejector and with a SAR 2.9 aerodynamic-shaped mixer (see Subsection 5.7.1.4). The liners are one of the most important elements for achieving noise goals. Several liner concepts and liner designs have been investigated in scale-model and laboratory tests. A liner design methodology has been developed that may be used to design bulk absorber liners that maximize noise suppression for different scale nozzle models (see Subsection 5.8.1.1). Early generation scale-model investigations indicated that bulk absorbers provided more noise suppression than single-degree-of-freedom liners. SDOF liners are tuned absorbers and are very effective over a narrow range of frequencies; whereas bulk absorbers provide suppression over a broad range of frequencies. This is a requirement for the mixer/ejector nozzle, which exhibits high internal noise levels over a broad range of frequencies.

Several bulk absorbers were investigated jointly between the CPC and EPM programs for acoustic suppression, material density, cost, and life considerations. T-Foam and silicon carbide foams were two materials that were investigated heavily in scale-model tests, and T-Foam was tested in the LSM nozzle. Gen 2 investigations (Subsection 5.7.1.4) showed that a "perforated hard wall" reduced entrainment compared to the "true hard wall," by virtue of the flow pulsating through the perforations, and had lower internal noise resulting in about 1 to 1.5 EPNdB reduction compared to the "true hard wall." At locations where treatment cannot be applied, it is worthwhile considering a "perforated hard wall" to achieve some noise reduction. SiC foam (200 and 100 ppi) and T-Foam bulks with the same face sheet gave very similar suppressions. Of the three bulks, 200-ppi SiC foam gave the largest noise reduction.

Several tests were conducted to investigate the contribution to noise reduction of liners at different axial locations within the ejector, as well as of liners on the flaps versus sidewalls (see Subsections 5.7.1.4 and 5.7.1.6). In general, liners in the aft portion of the ejector are more effective in reducing noise than those in the most forward segment. At cutback conditions, where the internal noise plays a more dominant role, one is able to discern the contribution to noise reduction by treatment at all axial locations. At sideline conditions, as the dominant sources move downstream, noise reduction (EPNL) due to treatment located in the forward segments becomes less significant. One also notices, at the peak PNL angle, the spectral reductions due to the forward segment of the liner in the 1 to 4 kHz region are also reduced, indicating treatment is becoming less effective as the grazing-flow Mach number on the liner increases. Acoustic treatment on the flaps alone (with hard-walled sidewalls) provided about 5 EPNdB suppression relative to the all-hard-wall configuration at the cutback condition and 90° orientation. Treatment on the sidewalls alone (with hard-walled flaps) provided about 1.5 EPNdB suppression under the same conditions, indicating that flap treatment was more effective than sidewall in this case. (Please note that the flaps have about 60% more

treatment area than the sidewalls). However, when both flaps and sidewalls were treated, approximately 7.5 EPNdB suppression was realized, indicating complex interactions of the incident sound field with the liners in the duct and radiation to the far field. The flap alone or sidewall alone treated configuration yielded approximately similar noise reductions at the 25° azimuthal location. At a $V_j \approx 1880$ ft/s, treated flaps alone provided about 4.2 EPNdB suppression; whereas treated sidewalls alone gave about 3.5 EPNdB suppression. However, when both flaps and sidewalls were treated approximately 6.2 EPNdB suppression was realized, further bolstering the argument for complex interactions of the sound field with the liners in the duct and radiation to the far field.

The liner design methodology used the extracted acoustic suppression (in terms of PWL) of the internal noise by treatment using the Stone method (see Subsection 5.8.1.1) and related it to the calculated acoustic suppression of a lined rectangular duct (modal analysis), through an empirical factor. The acoustic suppression is calculated as a function of liner impedance after accounting for temperature and grazing-flow effects. The liner impedance was related to the face-sheet properties and bulk absorber through a set of empirical relationships. Such a liner design methodology was used to recommend liners for the LSM and full-scale designs. The principal observation has been that the predicted EPNL reductions for different scales can be reasonably collapsed to a single curve if the liner depth is normalized by the linear scale factor (see Subsection 5.8.1.1) and that the optimum liner depth for a full scale nozzle is 2 inches. Deeper liners do not necessarily improve the noise suppression. The liner design methodology also prescribes optimum face sheet properties and bulk absorber resistivities for different nozzle scales.

5.9.1.3 Mixing-Enhancement Devices

Mixing-enhancement devices at the exit of the mixer as well as at the exit of the ejector have been investigated as a means of providing additional noise suppression at minimal thrust loss to meet the challenging noise goals.

Of several mixing-enhancement devices tested in the Gen 2/2.5/2.5A test series in GEAE's Cell–41, the so-called "reduced A tabs" and notches on Mixer 8h provided the most significant noise reductions. These configurations achieved the noise goals of the nozzle P5 and P6 metrics for sideline and cutback noise levels, respectively (see Subsection 5.7.1.4). Reduced A tabs on Mixer 8h provided about 1 and 2 to 3 EPNdB reduction at sideline and cutback conditions, respectively. Notches on Mixer 8h provided about 2 to 2.5 EPNdB benefit at both sideline and cutback. Flowfield features induced by these mixing devices within the ejector were measured using laser velocimetry through a glass sidewall. The basic mechanism is the introduction of additional streamwise vorticity to enhance mixing. Tabs behave as delta wings and generate strong vortices that enhance the mixing of primary and secondary flows. In the case of notches, the static pressure differential between the primary and secondary sides induces the primary flow to rush into the secondary side and thereby creates the streamwise vorticity and resultant mixing. The so-induced transverse velocity component implies a thrust loss.

One of the significant technical findings was that if, rather than applying a full set of A tabs to all the chutes, fewer tabs were applied to certain select chutes, there was a further noise reduction of approximately 1 EPNdB, with a lower inferred thrust loss. This became the so-called "reduced A tabs" configuration. The recommendation for this configuration was based on mixing enhancement experiments conducted in CW 13/17 (see Subsection 5.8.5). The principal lesson learned is that there probably is an optimum amount and location of injecting streamwise vorticity to enhance mixing

to get lower noise and it is not putting tabs on each chute. Another lesson learned in this investigation is that 1/7-scale model investigations of such devices (such as tabs) at the chute exit were hampered by the application technique (tack welding) in relatively narrow chute secondary passages, and this affected data repeatability. Improved fabrication techniques should be pursued to ensure that the application of such devices causes minimal surface disruption in primary and secondary passages.

Based on the above findings and lessons learned, "reduced A tabs" and "reduced notches" (notches at the location of "reduced A tabs") were tested in LSAF on the Gen 3.0 mixer to obtain noise and thrust performance data (see Subsection 5.7.1.6). Flowfield surveys were conducted at the nozzle exit to assess the mixing effectiveness of such devices compared to the baseline mixer case. The attachment schemes here were improved significantly compared to the Gen 2/2.5/2.5A test series. "Reduced notches" provided about 0.8 EPNdB reduction at both sideline and community locations with negligible effect on the thrust performance. For the fully treated ejector, the "reduced A tabs" provided about 2.0 EPNdB reduction over a broad range of NPR at both sideline and community locations with an associated thrust performance loss of approximately 0.5%. Acoustic data on the Gen 3.0 baseline mixer showed strong tones, in the 1 to 2 kHz frequency range, that were eliminated by the "reduced A tabs," and this contributed to the 2 EPNdB reduction. The Gen 3.0 mixer with the "reduced A tabs" provided 20 EPNdB and 16 EPNdB noise reduction relative to a reference conic nozzle at sideline and cutback conditions, respectively. The measured thrust coefficients adjusted for full-scale effects are 0.92 and 0.89 at sideline and cutback, respectively. This is a remarkable achievement of the program.

The Gen 3.5 "improved performance" mixer was designed with reduced primary flow angularity relative to the Gen 3.0 mixer and was also tested in LSAF (see Subsection 5.7.1.6). Another key feature of this mixer was the presence of a ½-width cold chute at the sidewall. The Gen 3.0 mixer had a ½-width hot chute. The purpose was to have colder, slower moving fluid next to the liner to increase noise suppression and reduce performance losses while at the same time avoiding the "cold hole" of unmixed secondary air at the nozzle exit associated with the full-width cold chute. The test data show that the Gen 3.5 mixer achieved about 1% improvement in thrust performance over the Gen 3.0 mixer. The Gen 3.5 mixer was also noted to be slightly quieter than the Gen 3.0 mixer at lower NPR's and about the same at higher NPR's. Mixing enhancement devices such as "reduced A tabs" were not investigated on the Gen 3.5 mixer. It should be noted that, until we understand the physical mechanisms of how the tabs work, it may be presumptuous to assume that similar levels of noise reductions are achievable with the "reduced A tabs" on the Gen 3.5 mixer.

Mixing-enhancement devices installed at the ejector exit (chevrons and vortex generating ramps) provided about 1 to 1.5 EPNdB reductions separately but annulled the benefit if used together (see Subsection 5.7.1.4). Most of the benefit of the chevron was attributed to the lengthening of the ejector rather than mixing enhancement. A chevron design that did not lengthen the ejector as much was tested on the Gen 3/3.5 mixers in LSAF (see Subsection 5.7.1.6), and lower noise benefit was measured. The chevron designs were constrained so as not to dip into the nozzle flow or external flow to prevent thrust loss at all conditions. Vortex-generation ramps also could induce significant thrust loss at supersonic cruise conditions.

5.9.1.4 Cycle Conditions and Free-Stream Mach Number

Simulation of an engine cycle in terms of jet total temperature and nozzle pressure ratio is very critical in jet noise experiments because the noise signature of supersonic jets consists of mixing

noise and possibly shock-associated broadband noise. Jet-mixing noise is a strong function of jet velocity, and shock noise is a strong function of NPR; thus, proper simulation of the cycle is crucial for the noise source simulation to be representative of the engine. Scaling for size is based on the Strouhal parameter.

As the jet velocity is increased along the throttle line, the noise components tend to increase but some at a faster rate than others. As V_j is increased, the eddy-convection Mach number increases, mixing of the primary and secondary streams becomes less efficient, the significantly stronger jet noise sources move downstream, and the techniques aimed at reducing the internal and pre–merged noise components (such as treatment designs, tabs/notches on chutes, CER etc.) become less effective in reducing the total EPNL. However, techniques aimed at reducing the merged noise component (such as SAR, chute penetration, chute number increase from 16 to 20 etc.) do yield total EPNL reductions (see Subsection 5.7.1.4). Review of data from several test programs indicates that noise-suppression techniques explored in this program become less effective for $V_j > 2400$ ft/s (where the noise suppression requirement increases). Hence, a practical limit of $V_j \simeq 2400$ ft/s for sideline is recommended from a cycle-selection consideration.

Within the constraints of $V_j < 2400$ ft/s, an engine cycle that achieves V_j by a higher T_7 (about 120°R) and lower NPR (such as F414 versus 3570.80 cycle) has been shown to reduce total EPNL by about 2 EPNdB after accounting for the required A_8 increase. The EPNL reduction is achieved due to the following physical mechanisms:

1. Reducing NPR at a given V_j results in increased pumping (ws/wp) and reduced ejector exit velocity and hence reduced merged noise.
2. Reducing NPR and increasing T_7 improves mixing of the primary and secondary streams.
3. Jet noise source strength reduces with jet density (that is, higher T_7).
4. Reduced NPR delays the subsonic to supersonic mode transition thereby reducing or eliminating external shock structures and associated shock broadband noise.

All these mechanisms have been shown to reduce all noise components. The noise-reduction benefit is to be assessed against the increased A_8 (weight and nozzle envelope implications) and material life cost (higher T_7).

Aircraft flight Mach number (M_0) is simulated in scale model jet noise facilities such as Cell 41/LSAF/NATR by immersing the jet in a free-jet moving at M_0 to capture the dynamic effect of flight on the jet noise sources. The received signal is corrected for the refraction and scattering effects of the free-jet shear layer and Doppler shifted to account for relative motion between the source and receiver. The effects of M_0 on the noise components of the mixer/ejector nozzle are different due to their locations and how the free-stream M_0 influences source strengths as well as propagation to the far field. The merged and premerged noise components located downstream of the nozzle exit plane experience the classical relative-velocity effect proportional to $[(V_{exit} - V_0) / V_{exit}]^{\sim 6}$ which reduces jet noise source strength. One notices significant reduction due to flight in low and middle frequencies (typically under 1 kHz). The source modification effect of flight on the internal noise component, unlike the case of the merged noise component, is basically through the slight increase in entrainment ratio compared to the static case (about 5%). However, the internal source must propagate through the ejector exit and or ejector inlet and suffer refraction

and scattering effects. There is very little noticeable effect of M_0 on the internal noise component when looking at scaled and extrapolated nozzle data..

5.9.1.5 Installation Effects

As the top inlet of the mixer/ejector needs to be closely integrated with the wing surfaces, there were concerns about any adverse impact of installation on the acoustic suppression of the mixer/ejector nozzle system. Early in the HSR program, the Gen 1, 1/7-scale, HAM mixer/ejector nozzle was installed on the in-board location of a semispan aircraft model (*Reference H* planform) and tested in the NASA–Ames 40×80 wind tunnel up to M_0 = 0.32 in 1995. NASA–Ames conducted a workshop in March 1996 to share the findings and data analyses performed by NASA and Industry members (HEAT Workshop). The noise measurements were principally acquired under the flight path with very limited data in line with the wing. An uninstalled test preceded the installed test at the same facility to quantify the effect of installation.

Within the scope of the measurements, installation effects on noise suppression were assessed to be small (less than 1 EPNdB increase) under the flight path. Ejector inlet rake measurements and flap static pressure measurements also indicated small effect of installation. There were concerns about the signal-to-noise ratio affecting the following measurements:

1. Forward quadrant microphone measurements at high tunnel Mach number (about 0.32).
2. All microphone measurements at cutback conditions.

Other concerns included acoustic reflectivity of the ground plane and potential near-field effects at low frequencies. Even with these limitations, the test gave valuable information about relatively minor impact of installation on middle to high frequencies (which would be the ones most affected by installation, if any), ejector nozzle aerodynamics in terms of pumping, and flap static pressure distributions.

5.9.1.6 Scaling and Influence of Engine Environment

There is technical risk in scaling acoustic data from 1/7-scale model nozzle tests to full–scale engine levels. Typically the 1/7-scale model nozzles are powered by a single stream (representing fully mixed fan and core streams) from test facilities with low in-flow turbulence and zero swirl. In the full-scale engine situation, due to the relatively short space between the turbine exit and the chute mixer, the fan and core streams are not well mixed; there could be remnant turbine exit swirl and higher levels of turbulence. Along with these differences, there is a lack of experience in scaling acoustic liners (in terms of face-sheet design parameters and bulk absorber properties) from 1/7 scale to full scale.

Comparison of acoustic data from the LSM (56% scale simulation) nozzle powered by the P&W F100–229 with data from the Gen 3 (LSM Similitude) 1/7-scale model showed the following:

- Applying flight effects from the Gen 3 model and taking cycle differences into account, when the two models were compared on an equal thrust basis the LSM levels were higher by about 1.5 EPNdB at both sideline and cutback conditions. Most of this difference was seen in the premerged portion of the spectrum, implying greater unmixedness at the ejector exit for the LSM.

- For the treated configuration, the LSM/LSMS difference was greater than for hard wall. The hard-wall difference represents the influence of the engine environment. The additional difference between the treated configurations represents the liner nonscalability. It must be remembered that manufacturing considerations at each scale limit the degree to which the liner can approach the optimal design. Factors such as face-sheet thickness and hole size do not scale directly. The bulk material properties were the same for both tests — although better suited for the 1/7-scale model.
- This exercise demonstrates that there is a risk associated with taking acoustic data from 1/7-scale models to full scale. More analysis is needed to quantify the details, but use of 1/7-scale nozzle data to demonstrate technology goals should make allowance for this.

5.9.2 Supporting Technology Development and Assessment

5.9.2.1 Tabs and Notches as Mixing-Enhancement Devices

One of the promising technologies explored during HSR was mixing enhancement by modification of the trailing edge of nozzles. Classically referred to as "tabs" for protuberances extending downstream and often into the flow at a nozzle lip or "notches" for serrations of the lip, these modifications enhance the mixing of shear layers and have a surprising impact on noise generated by the shear flow. In the HSR mixer/ejector nozzle there are two locations where such devices may be employed: the primary mixer and the ejector exit. During the HSR program, tabs were explored in some variety on the primary mixer along with a few notch configurations. At the ejector exit "chevrons," which can be viewed either as deep notches or as zero-penetration triangular tabs, were tried.

This subsection summarizes the history of tabs and notches as mixing-enhancement devices and briefly assesses application to HSR technology.

Triangle Tabs on Round Nozzles

The origins of tabs and notches are contentious to trace, possibly because much of the development came from military programs where they were used to reduce infrared signatures of engine plumes. Some of the earliest work in understanding the effects on jet flow focused on triangular tabs protruding into the flow at an angle. Results were dramatic in terms of modifying the plume cross section of a round jet, but the thrust loss was often cited as a major drawback, and introduction of tabs into the flow often brought about more high-frequency noise than was suppressed at low frequencies. However, given the philosophy of the mixer/ejector to mix the flow as quickly as possible inside the ejector and to use the ejector liner to absorb the resultant extra noise, this type of device was recognized early as a potential improvement to the basic mixer/ejector design. It remained to figure out how to apply it to lobed mixers for maximum benefit and minimal thrust loss.

Tabs on Mixer Lobes

HSR Tests at NASA–Lewis, 1995 – In 1995, a series of tests were run at the NASA Lewis NATR facility using the original P&W mixer/ejector model. The test screened potential propulsion-integration problems and various tab configurations on the eight-lobe, square-shouldered, "vortical" mixer.

At that time, tabs were attached to the tips of the lobes in the belief that this would enhance the mixing of the high-speed "hot spots" that appeared at the ejector exit downstream of the mixer lobes. During the test, after it was observed that the tabs were not having any effect on these hot spots or on the sound, researchers noted that CFD simulations traced the hot spots back to the midlobe region of the mixer, not the lobe tips. A hastily constructed tab configuration was added to the test that placed a single tab on the midpoint of each lobe. This configuration did improve mixing at the ejector exit plane and effected an acoustic benefit of roughly 1 EPNdB (see Figure 285).

Tabs on Simple Lobed Mixers at NASA–Lewis, 1993–1997 – The fluid mechanics of tabs on lobed mixers were studied in simple, small, cold models at NASA–Lewis in support of the hot-model test work being done in the anechoic rigs. The results of this effort are detailed in Subsection 5.8.5.

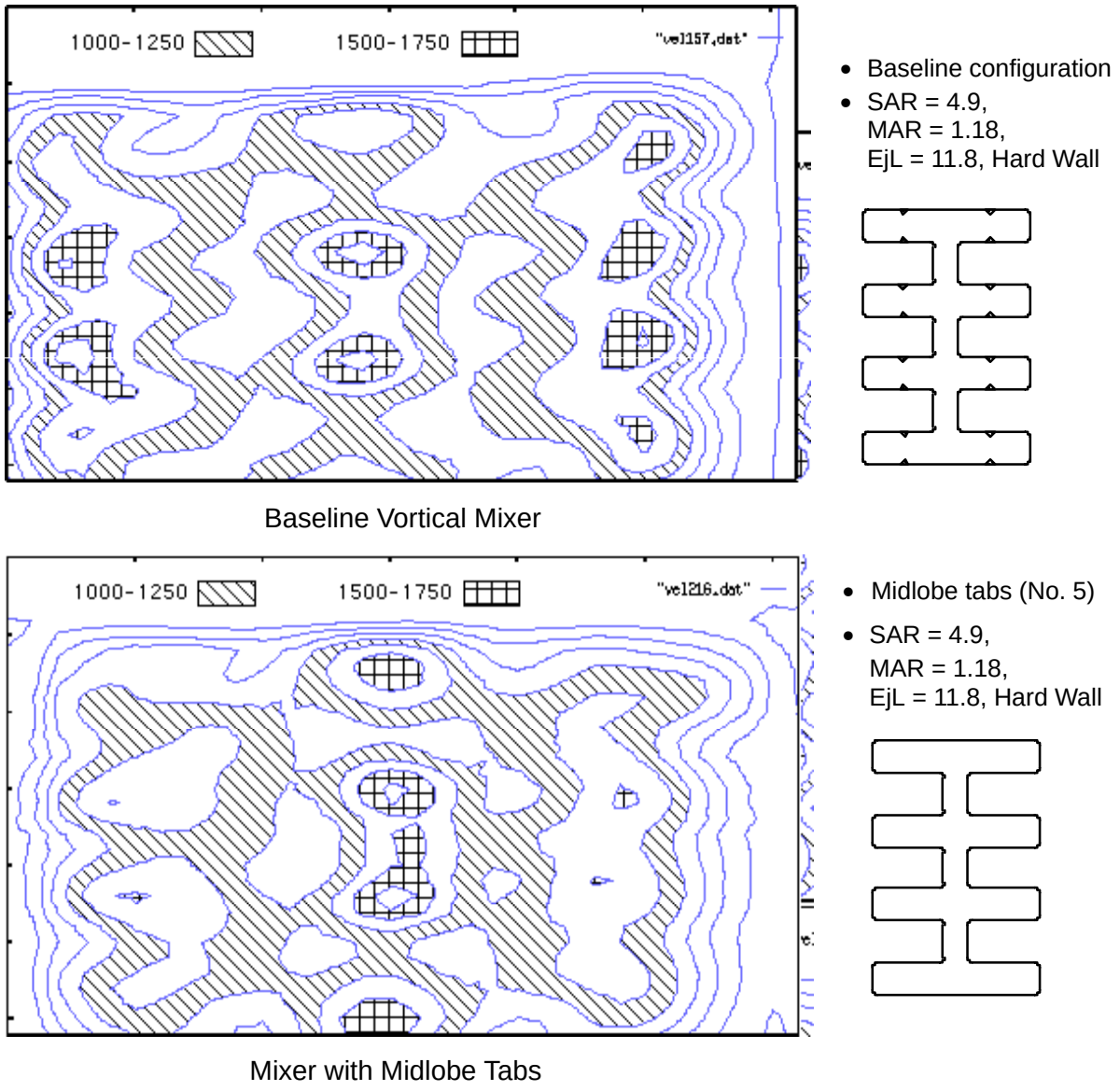

Figure 285. Velocity Contours for Baseline "Vortical" Mixer and Mixer with Midlobe Tabs

Tabs on HSR Gen 2.5 Mixers at GEAE – At the end of the HSR Gen 2.5 test entry in Cell 41, several tab configurations were tested for far-field acoustics and for internal flowfield using LV. The history of this effort became somewhat convoluted as two very different tab configurations were tried, the method of attachment modified the secondary side of the mixer, and this modification itself had a significant effect on the acoustics. The tests showed first showed that tabs could have a beneficial effect with more suppression than aerodynamic-performance loss. Not all configurations tried were successful, and certainly not all reasonable configurations were tried. (See Subsection 5.7.1.4 for further details.)

Notches on Mixer Lobes

Notches on HSR Gen 2.5 Mixer at GEAE – Notches were tested during the Gen 2.5 tests at GEAE Cell 41 as a target of opportunity. Having cut out dovetails in Mixer 8c to attach the "A" tabs, it was reasonable to make triangular notches into the dovetail material once the tabs had been ground off and before the dovetails were recut to reattach the tabs. These also showed a change in acoustic performance; based upon this information, it was recommended that a similar test should be done on a clean mixer during the Gen 3.5 test at Boeing's LSAF facility in 1999 (Figure 286).

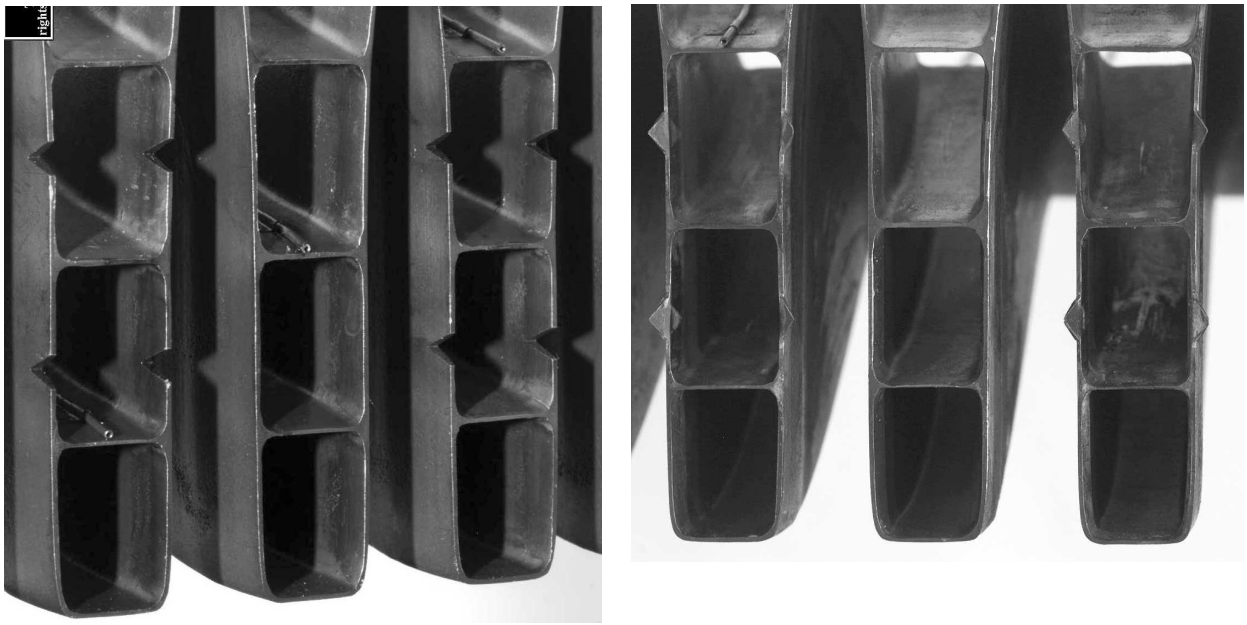

Gen 3.0 with "Reduced" Notches Gen 3.0 with "Reduced" A-Tabs

Figure 286. Mixing-Enhancement Devices Tested at 1/7 Scale

Chevrons on Ejector Exit

Gen 2.5 Experience – Chevrons can be viewed either as notches that touch at the trailing edge, so as to leave a sharp point, or as tabs that have zero penetration into the flow. These devices were tried on the ejector exit to increase the mixing of the external plume and thus reduce the externally generated, low-frequency noise. When first crudely applied to an ejector in the Gen 2.5 model at GEAE Cell 41, they had a significant, favorable effect of roughly 1.0 to 1.5 EPNdB. Further, it was

shown that this effect was more than would have been expected from an equivalent lengthening of the ejector. It should be noted in retrospect that the trailing edge of the Gen 2.5 model was very blunt and that such modification may have had benefits from sharpening the trailing edge that would not be found on a more aerodynamic model, as during the Gen 3.5 experiments.

Gen 3.5 Experience – In the Gen 3.5 tests it was decided to reevaluate ejector chevrons since the benefit was not understood and the range of applicability was in question. As can be gleaned from other sections of this report, the Gen 3.x model had significantly better external lines, finer trailing edges, and ejector trailing edges that were not coplanar. For whatever reason, the result from the Gen 3.5 test showed that the external chevrons did not make a significant difference in the acoustics (approximately 0.1 EPNdB). Our understanding of these devices remains imperfect, but the benefit was no longer bookkept as a technology that would be counted on in system studies for the airplane.

Final Assessment

Gen 3.5 Tests at LSAF – In the final test series, the "reduced A-tab" configuration that was tested on the Gen 3.0 half-hot sidewall mixer showed 2 to 3 EPNdB improvement in sound over the unmodified Gen 3.0 mixer at all angles and all power conditions. The aerodynamic penalty for these devices was measured to be less than 0.4% at takeoff condition. The notches were found to have less than 0.2% thrust loss while delivering roughly 1 EPNdB benefit for noise. The tabs were not tested on the Gen 3.5 mixer that already had a benefit both in noise and more significantly in thrust; however, it is felt that the benefits of tabs found on the Gen 3.0 mixer would also be found on the Gen 3.5 mixer if they were so applied. Given that current understanding of the effect of tabs on noise generation is very meager and only a few of the possible tab configurations had been tried, it also seems likely that other, more beneficial, configurations would be possible.

Current Understanding – The original concept for reducing mixer/ejector noise using tabs involved increasing the rate of mixing in the ejector. It was speculated that by increasing the rate of mixing in the ejector, the transverse gradients in the stream near and downstream of the ejector exit would be reduced, leading to reduced noise generation from these regions and increasing the noise generated upstream in the ejector. Here, so the thinking went, the liner would absorb the extra sound. This understanding has been challenged by the fact that the benefits are seen in the hard-wall configuration as well. In fact, the effect of liner position is the same as without the tabs, leading to the conclusion that the tabs actually reduce the noise generation. As the benefits are primarily observed at the high end of the frequency spectrum, it seems likely that the tabs are modifying the flow near the mixer to reduce noise generation. Another observation of note was that the often-significant "tone" observed around the NPR = 2.5 (cutback) power condition was entirely eliminated by the tabs. This is reminiscent of tones that occur when instabilities from compressible laminar shear layers set up a feedback and generate a strong tone from the impinging pressure wave on the nozzle lip. Just as in those situations the feedback is broken up by inserting tabs or other spatial perturbations to the nozzle lip, so too it seems that tabs remove this sound mechanism in the mixer/ejector nozzle. Clearly more work is required to study the details of this flow region internal to the ejector to understand the fluid mechanics of the tabs before the sound-generation effects can be optimized.

5.9.2.2 HSCT Mixer/Ejector Water Injection

Exhaust system noise levels are largely driven by velocity differences inside and exiting the nozzle system. By injecting water into the mixer/ejector, the water is vaporized, energy is removed from

the air streams, and the velocities are reduced. These reductions in velocity should then materialize as reductions in the radiated noise.

The impacts of water injection into a mixer/ejector were examined for the noise generated by the exhaust system as well as the aerodynamic performance. A one-dimensional analysis was completed to predict the effects of water injection either upstream of the mixer in the primary stream or into the mixing duct downstream of the mixer. These results were compared to relevant experimental data, and an independent analysis was also completed by Adroit Systems, Inc.

One-Dimensional Analysis

A one-dimensional mixer/ejector control volume analysis incorporated the effects of water injection/vaporization. The code assumed that the water was fully vaporized by the primary/secondary and that the flowfield exiting the exhaust system was uniform and fully mixed. Second-order effects due to heat transfer to the walls, wall friction, and changes in gas constants were ignored, and MAR = 1 was assumed for simplicity. A SAR of 2.86 was used for all the calculations, with a water injection area equal to 1% of the mixing duct (for injection in the mixing duct).

Using conservation of mass, momentum, and energy, the code iteratively solved for a given set of inlet primary and secondary total conditions, exit static pressure, and water injection mass flow rate. Upon convergence, the net thrust coefficient was calculated and compared to the zero-water-injection baseline configuration (both static and flight conditions were obtained). Jet noise reduction was estimated using the 7^{th} power law. (Basing potential noise reduction on V_{mix} alone can be very misleading; density effect is ignored, as are premerged and internal mixing sources.)

Results of the one-dimensional analysis showed potential for jet noise reductions of approximately 1 dB per 3.4% water injection rate (% of primary mass flow) for both sideline and cutback power settings. The maximum amount of vaporization potential is about 20% water injection. Net thrust coefficient increases were also observed with water injection, resulting in approximately 0.4% per dB noise reduction at sideline and 0.2% at cutback.

While detailed mechanical designs were not completed to examine the system required for water injection, estimates were made on the weight of plumbing, pumps, and a tank. These figures, in addition to the weight of the water at takeoff, were incorporated into an aircraft TOGW sensitivity analysis using 13,000-lbm TOGW / ΔEPNdB (sideline), 13,000-lbm TOGW / ΔEPNdB (cutback), 7,500-lbm TOGW / $\%\Delta C_{fn}$ at sideline, and 4,000-lbm TOGW / $\%\Delta C_{fn}$ at cutback. The TOGW weight analysis showed potential savings (using water injection) of greater than 15,000 lbm per dB of noise reduction. More detailed mechanical implementation analyses are needed, and the analysis did not account for the water weight only being carried during the takeoff phase.

Test Data

Several studies using water injection in simple nozzles have been performed over the last 40 years. These tests have typically shown limited noise reduction, along with thrust penalties. While these historical results are indicative of the performance of the primary stream with water injection upstream of the mixer in the hot-gas path, they are not relevant for predicting the results of mixer/ejector systems. The benefits achieved with an ejector system are largely due to the increased pumping of the secondary.

Test data most representative of water injection into the primary upstream of current mixer designs were obtained when off-cycle points were taken with varying primary total temperatures. These tests

showed that the premerged and merged noise were affected by the "water injection," but little change to the high-frequency internal noise resulted. The EPNdB change was approximately 1/3 to 1/2 that predicted by the ideal analysis. However, with internal-noise-reduction techniques such as rapid mixing devices, lobe-on-lobe, etc., water injection would generate a larger effect on the EPNL.

The only known test to date with water injection in an ejector system is documented in FAA–SS–72–42 "Supersonic Transport Noise Reduction Technology Summary." Water was injected both axially and radially into the mixing duct downstream of the primary nozzle. Several power conditions were tested, none of which match current HSCT cycles, but noise reductions were observed. Acoustic measurements were only taken at 90°, where internal noise is typically dominant. At that position, they observed PNLdB reductions up to 3dB with 20% water injection. These results are about ½ that predicted with the ideal one-dimensional analysis. In addition, configuration drawings indicate that vaporization would not be complete in this system, so less than ideal performance would be expected.

Adroit Systems Literature Search/Analysis

Adroit Systems, Inc. performed a literature search and analysis on exhaust system water injection. They found little relevant research documented in the open literature. A one-dimensional analysis was completed similar to that described above, and analysis was also performed on water-droplet vaporization rates and atomization requirements for the use of water injection in a typical HSCT exhaust system.

Conclusions and Recommendations

Analysis and experimental test results indicate that significant acoustic (more than 3 EPNdB), aerodynmic performance, and TOGW benefits are possible with water injection in mixer/ejector exhaust configurations. However, additional research is necessary to better understand the effects of water injection and obtain the full benefits of the vaporization process.

Recommendations for testing water injection in typical HSCT scale rig tests were documented. They included: (1) injection of the water into the primary stream upstream of the mixer, (2) an additional charging station to accurately determine the gas conditions before and after the water injection/vaporization, (3) additional analysis on water droplet trajectories, etc. to better understand the vaporization process and obtain complete vaporization prior to reaching the mixer, and (4) thrust and mass flow rate (air and water) measurement capability.

5.9.2.3 Lobe-on-Lobe Mixer

Large-Scale Mixer

Mixer/ejector exhaust system noise has been modeled assuming five sources, including: internal high-frequency mixing noise, premerged (jet nonuniformity) noise, and jet noise. While the noise is generated in a continuous spectra, the high-frequency mixing noise is often the major contributor of exhaust-system noise due to the sensitivity weightings applied to the sound pressure levels when calculating an EPNL. These noise sources peak downstream of the mixer, within the mixing duct, where high-energy, small-scale turbulent mixing occurs between the primary and secondary gas streams.

The objective of lobe-on-lobe mixer investigation was to decrease the scale of the high-energy, small-scale, turbulent mixing such that the peak frequency range radiated by the exhaust system is outside the peak annoyance range of the human ear. The aeroacoustic design methodology of the lobe-on-lobe mixer ejector will first be discussed, followed by acoustic predictions and aerodynamic test results. Mechanical design and analysis will then be summarized and conclusions presented.

Aeroacoustic Design Methodology – In the absence of acoustic treatment within the ejector, the spectral peak of noise radiated from previous HSCT mixer/ejector exhaust systems occured within the peak annoyance range of the human ear (approximately 2 to 4 kHz). Analysis indicated that a factor of seven in frequency "shift" would transition the HSCT radiated noise such that the dominant internal noise sources would lie outside the calculation range for EPNL. The noise generated by mixing flows is directly related to the length scale of the flow nonuniformities. Thus, to decrease the mixing length scale, minilobes were placed on the main lobe trailing edge to generate an array of $0.56 \times 1/7$-scale mixers within a 0.56-scale ejector mixing duct, as shown in Figures 287 and 288. Each section of the lobe-on-lobe rack should behave similar to the 1/7-scale model tests, with some interaction between sections (lack of walls). The mixing length should be very short relative to the mixing duct length (on the order of 1/7 the length), so acoustics liners would become more effective on internal noise sources and additional mixing length would reduce premerged noise due to exit flow nonuniformities. The main acoustic unknown is the interaction at the main lobe scale. However, with the rapid mixing of the minilobe racks, the main lobe length scale flow nonuniformities and generated noise should be much smaller amplitude than those for the baseline Gen 3 mixers.

Acoustic Predictions – State-of-the-art noise prediction methodology relies heavily on empirical data to generate a knowledge base within which noise predictions can be completed fairly successfully. Unfortunately, designs that are not within the experience base of the models (such as lobe-on-lobe) stretch the abilities of the acoustic prediction methods since assumptions are based on existing data and some physical understanding. Because of the empirical reliance of the existing acoustic codes, noise predictions for the lobe-on-lobe varied widely based on the assumptions used. Using assumptions broadly agreed to by the AACE community, noise reductions ranged from 3 to 8 EPNdB, with cutback having larger noise reductions than sideline by a couple dB.

As stated previously, the key unknown with lobe-on-lobe designs is the residual premerged and main lobe length-scale mixing noise sources. While noise is still generated at these frequencies, the amplitude depends on the degree of mixing of the minilobe racks and the interaction between different sectors of minilobes. If the mixing behaves essentially the same as an array of independent mixer racks, then the flow should be very well mixed by the end of the mixing duct, since the ejector box is equivalently seven times as long as previously tested configurations. This result would imply that premerged noise sources would be significantly reduced, and any mixing at the main lobe length scale would occur well within the mixing duct where acoustic treatment is highly effective. In addition, there is no reason to believe that the main lobe length scale nonuniformities should be nearly as large with an array of minilobe racks than a baseline configuration (such as Gen 3.0). However, the occurrence of an unknown noise source limiting the noise reduction potential of the lobe-on-lobe is a concern. For this reason, large (factor 7) shifts in the internal noise peak (mixer lobe width) are required to clearly show the internal spectra low frequency roll-off and expose unknown sources. A schematic of the acoustic effect that might be expected from the lobe-on-lobe is illustrated in Figure 289.

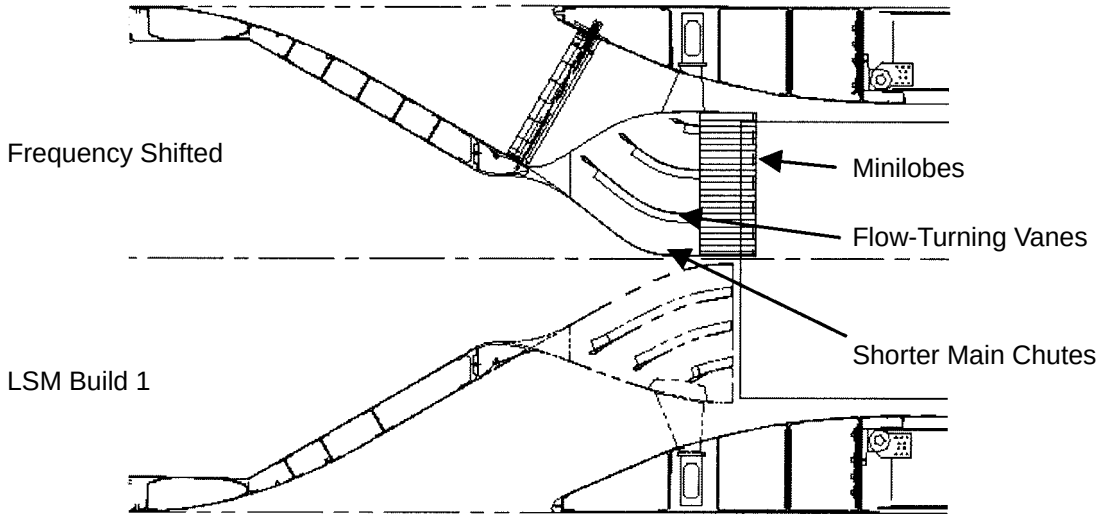

Figure 287. Lobe-on-Lobe Versus Baseline LSM1 Mixers (Side View)

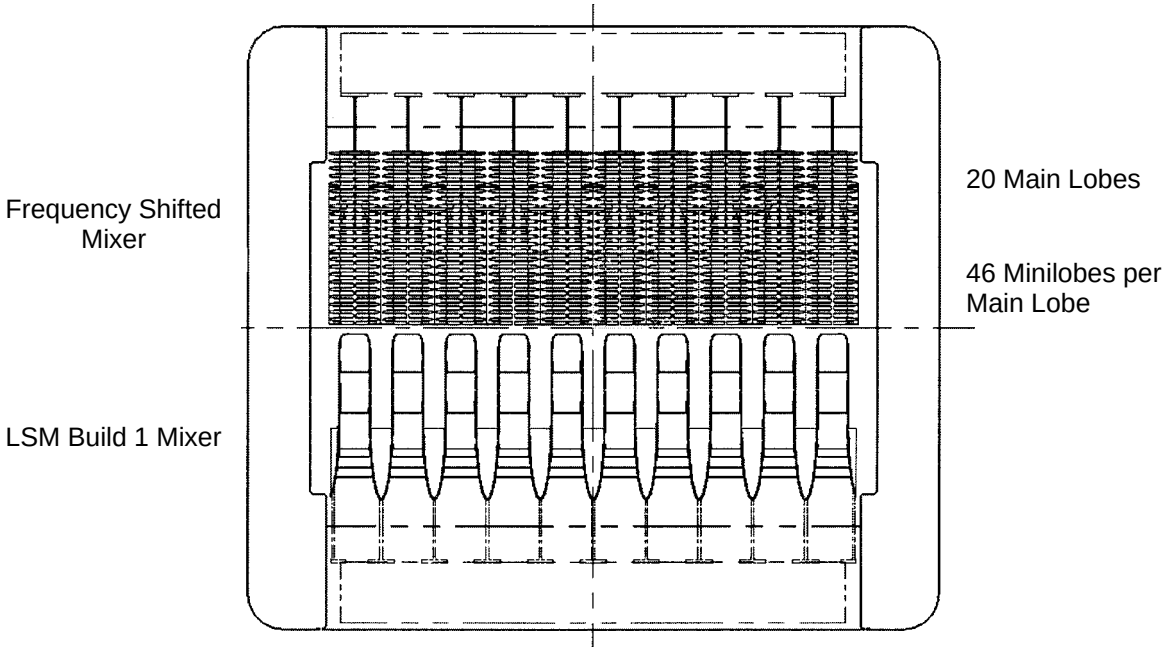

Figure 288. Lobe-on-Lobe Versus Baseline LSM1 Mixers (End View)

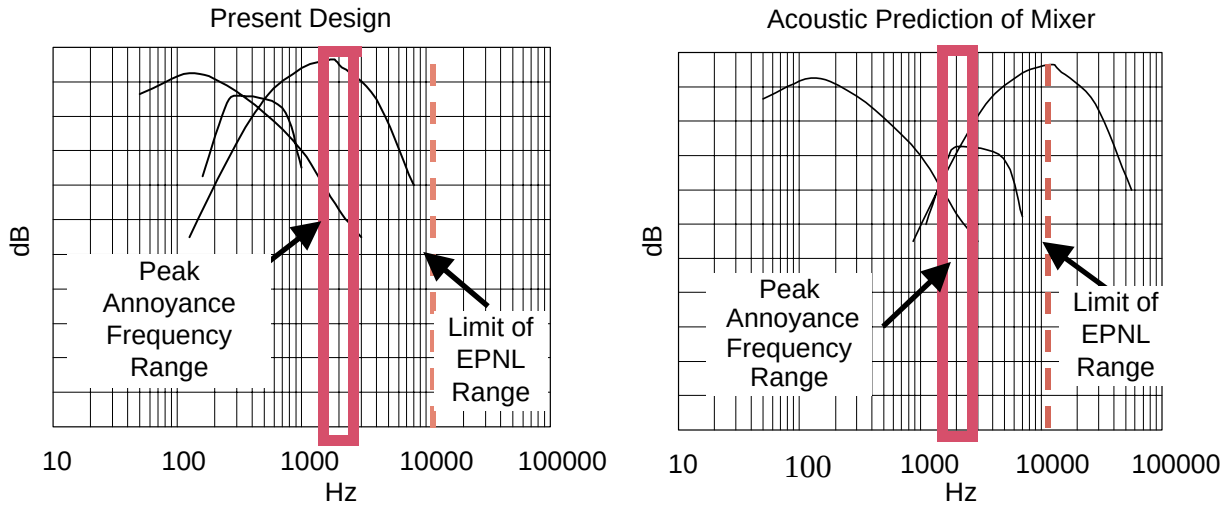

Figure 289. Schematic of Acoustic Spectral Changes Due to Lobe-on-Lobe Design

Aerodynamic Test Results – Concern over the aerodynamic performance of the LSM lobe-on-lobe design was mitigated through analytical analysis (1D and CFD) and empirical testing (C_{Vp} and CASL). Analytical studies typically consisted of aerodynamic loss effects, due to increased surface area at takeoff and cruise conditions, as well as base drag effects. CFD work on the primary flow showed fully attached boundary layers and high Cvp. A ¼-scale sector model was made for C_{Vp} testing, where both thrust and base pressures were measured. Although subsonic losses would be greater due to increased surface area within the main lobes, the supersonic wetted area is approximately the same as the baseline LSM1 mixer (Gen 3.0). Base drag and flow turning effects would also be higher for lobe-on-lobe, but the flow velocity is more axial exiting the primary than for the baseline mixer (which is a direct increase in axial thrust for the same total conditions). The combined effects result in a slightly higher net C_{Vp} for the lobe-on-lobe design than the baseline Gen 3 mixer.

CASL testing was also completed to address several concerns with the minilobe design. Calculations indicated that a scaled-down HPM lobe would separate with the minilobe inlet conditions, so several stretch factors (1.25, 1.70, and 2.17) were used on the lobes and then tested to measure the pressure recovery in the CASL facility. Testing showed that a stretch factor of 1.70 had the best pressure recovery within the Mach number range of interest while maintaining a margin of safety from separation. Vanes within the minilobes were also tested with three different vane geometries: floor aligned, straight angled, and area centered. All the vane geometries had significantly higher losses than without the vanes, but the floor-aligned vane was the best if vanes were required for structural integrity.

Because the minilobe regions near the secondary inlet ramp will be subjected to an angle of attack, CASL tests were completed to examine the effects of flow angularity onto the minilobes. 5°, 10°, and 12° were tested on the 1.70 stretch factor minilobe design, and additional pressure recovery losses were observed. The total pressure loss was about 1% at a shoulder Mach number of 0.45, but the losses rapidly increased for higher Mach numbers, particularly as incidence angles increased. For the LSM2 lobe-on-lobe geometry, flow angularity onto the minilobes was determined to not be a significant concern.

Mechanical Design and Analysis – Detailed mechanical design and structural analysis activities were completed on the lobe-on-lobe configuration, as the design was ready to manufacture when LSM2 testing was canceled (see lobe-on-lobe design review document). A great deal of interaction between mechanical design and aerodynamic engineers was performed to generate the optimal design that met the desired requirements. Thermal and pressure loading effects were examined with both linear and nonlinear analyses, and the results were used to generate the cold geometry such that the hot throat area was held constant relative to the baseline configuration. Low-cycle and high-cycle fatigue analyses were also completed. An expanded view of all the parts making up one main lobe of the lobe-on-lobe mixer rack assembly is shown in Figure 290.

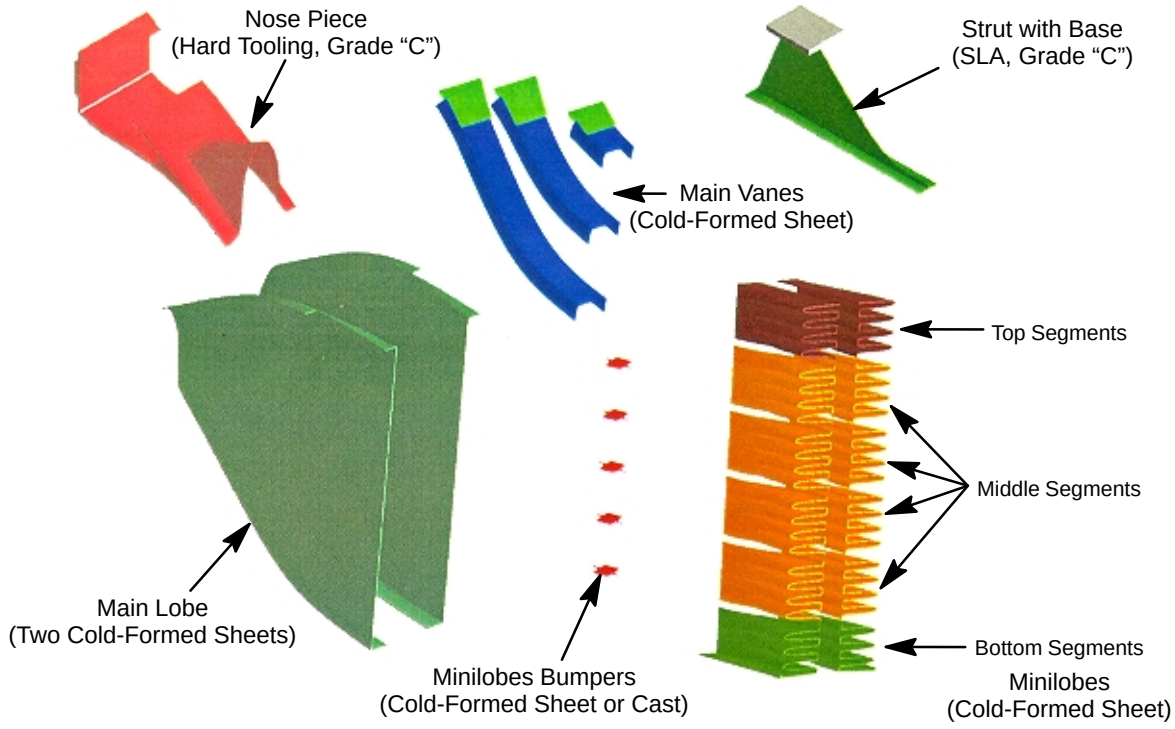

Figure 290. Expanded View of Lobe-on-Lobe Mixer Rack Assembly

With the 1.70 stretch factor minilobes it was found that the minilobe material thickness could be adjusted (within reasonable limits) such that vanes were not required in the minilobes to keep stresses within allowable limits. Bumpers (extremely short vanes) were placed between every other minilobe primary crown. The aerodynamic losses associated with the bumpers were estimated to be much less than would be induced by a full-length vane through the minilobe.

Lessons learned from the LSM1 mixer were incorporated into the lobe-on-lobe design. Cracks had initiated on the aft end of the LSM1 vanes due to LCF/HCF interactions caused by a misplaced weld, resulting in a punch load. To prevent this, the assembly layout drawings were clearly marked to preclude a weld in this region. The sidewall seals were redesigned to prevent crushing during mixer pressurization as happened in LSM1. To further add fidelity to the design analysis, a half-rack model was used to determine global deflections.

Summary and Conclusions – Detailed aerodynamic, acoustic, and mechanical activities were completed on the LSM lobe-on-lobe design. Aerodynamic analysis and experimental component

testing showed good aerodynamic performance, and acoustic predictions showed large potential noise reductions. These two performance criteria would lead to a very large reduction (26,000 to 90,000 lbm based on current sensitivities) in TOGW for the HSCT aircraft.

Mechanical design and structural analysis also showed the ability of the design to withstand engine scale testing, without the use of minilobe vanes and other high-loss devices. Manufacturing-technique lessons learned from LSM1 were incorporated into the design and manufacturing/fabrication plan of the LSM2 lobe-on-lobe mixer, as well as additional fabrication methods.

Scale-Model (1/7) Proof-of-Concept Design

The lobe-on-lobe mixer concept offers the potential for a large noise reduction as described in the previous discussion. However, the cost and risk of assessing the concept on the LSM prompted an effort to determine if the merit of the concept could first be assessed on a smaller scale, lower cost test. Thus, the proof-of-concept approach was conceived, the objective of which is to determine whether or not the net noise reduction estimated for the concept could be achieved without significant aerodynamic performance penalties.

Acoustic Definition – To create a lobe-on-lobe (LoL) model that could be operated at 1/7 scale, the designer had to first come to understand the relevant features of the LSM LoL design using the noise-source paradigms and models available. Obviously, the 56% model could not be simply scaled down, as the lobe dimensions would become so small compared with the minimum nozzle wall thickness that the nozzle would have a significant area taken up with blockage.

It was recognized that the concept was a new rendition of an idea that had been discovered during previous high-speed civil transport programs: break up the jet into many smaller jets, each with a much higher dominant frequency, to simultaneously reduce the total power generated and the noise received by the observer (because of more atmospheric attenuation of high-frequency sound). The problem with this approach had been in making such a nozzle aerodynamically viable. Since the original LoL concept proposed was being built upon a mixer design strategy that had been shown to be a good performer, it was decided to capture this aerodynamic performance knowledge but modify the lobe count to keep the dimensions acceptable at 1/7 scale and still provide the spectral separation required to demonstrate the acoustic impact of the concept. Conceptual design criteria included: the mixer area should be the same as the current 1/7-scale mixers, the lobe aspect ratios should be as high as possible, the gaps between racks should be minimal, and the width of the lobe flow area should be at least six times the lip thickness. This last criterion directly opposed the goal that was to maximize the number of minilobes or to maximize the lobe perimeter.

Several conceptual designs were rendered, and the Stone prediction code (uses mixer geometries and predicted secondary entrainment for noise modeling) was exercised on them. It was found that the effect of adding lobes became more pronounced as the number of minilobes increased but that the main influence was the effect at full scale of atmospheric attenuation on the higher frequency noise sources — something not appreciated previously. There were still some concerns about the passages being too small, both from manufacturability and Reynolds invariance standpoints, later addressed in the detail design review. A conceptual design was chosen that showed significant impact by adding 16 minilobes to 12 main lobes, both relative to the baseline main lobe mixer and to the current Gen 3.x 20-lobe mixer. Figure 291 shows the predicted acoustic performance of the 12/16 mixer. This was deemed a reasonable proof-of-concept test and recommended to the ITD team in December 1998. The design was passed on for further aerodynamic development.

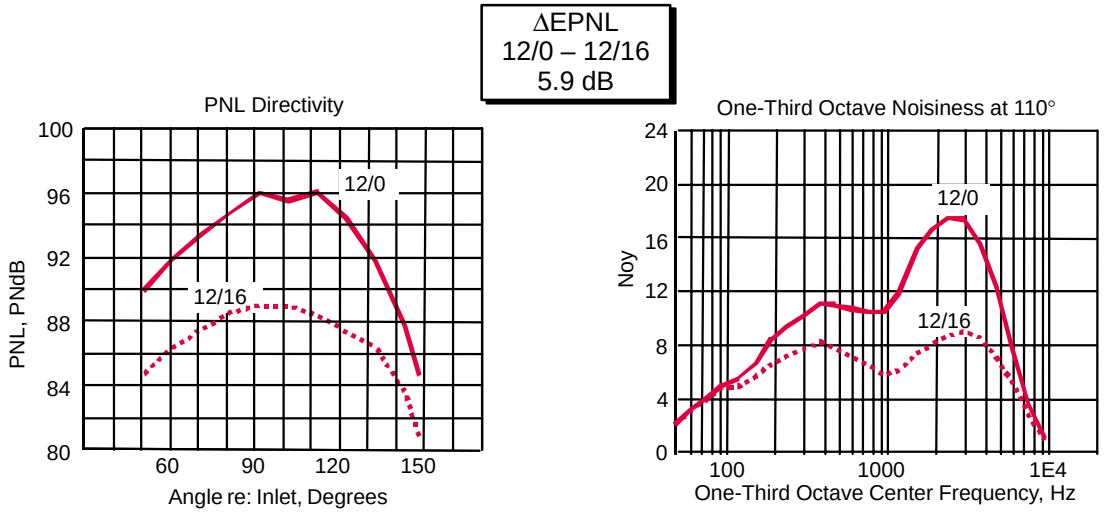

Figure 291. Predicted PNL and Typical Noy Spectra For Baseline and LoL Versions of 1/7-Scale Mixer

Aerodynamic Design and Analysis

The aerodynamic flowpath design of the 12×16-lobe, proof-of-concept mixer was conducted with two broad objectives as guidelines. The first was to provide a design with comparable performance relative to the 20×46 LSM design discussed above. The second objective was to deliver the flow to the ejector with no separation, in a manner similar to the 20×46 design, with no risk to the acoustic objective. To achieve these objectives, the overall aerodynamic-design approach for the proof-of-concept model was to leverage all of the aerodynamic development that had gone into the LSM 20×46 design (analytical studies, CFD studies, CASL tests, and C_{Vp} tests). This was accomplished by scaling the 20×46 design to maintain the same basic lobe shapes, turning rates, and area distributions. To facilitate this approach, the design and analysis was conducted at LSM scale to allow direct comparisons on a relative basis with the 20×46 design. This included scaling the required 1/7-scale model wall thicknesses up to LSM scale. Once the design was completed, the flowpath was scaled down to 1/7 scale for detailed mechanical design.

The main lobe was designed by maintaining the same side-view contour as the 20×46 design and proportionally widening the 20×46 design primary-side flowpath at any point to maintain the same flow area at any axial station. Wall-thickness differences for the 1/7-scale model were added to the secondary flowpath side.

The minilobes were designed in two steps. The first was to proportionally scale the length, width, and height of the 20×46 minilobe design to match the width of the main lobes and maintain the minilobe fineness ratio and wall curvatures. The second step was to proportionally widen the 20×46 minilobes design (in the same manner as the main lobes) to obtain the specified 16 minilobes per main lobe and to maintain the primary-side flow area distribution. The main and minilobe design approach is shown in Figure 292, and an isometric view of the resulting design is shown in Figure 293 compared with the 20×46 design. Approximately 20 cross-sectional area cuts for both mixers were compared to verify that the flow area distributions were retained.

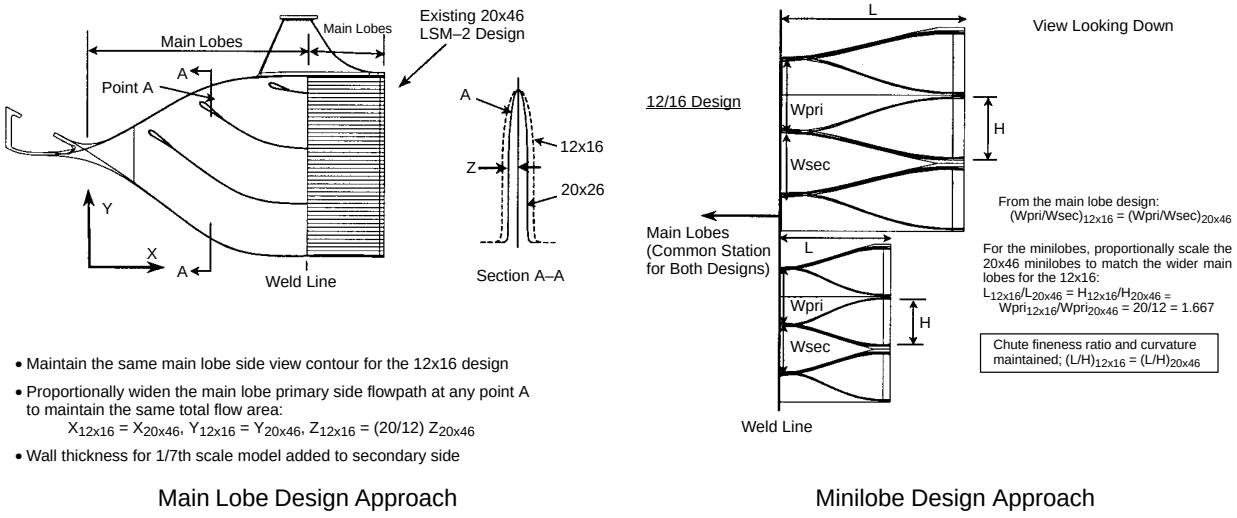

Figure 292. Main Lobe and Minilobe Design Approach

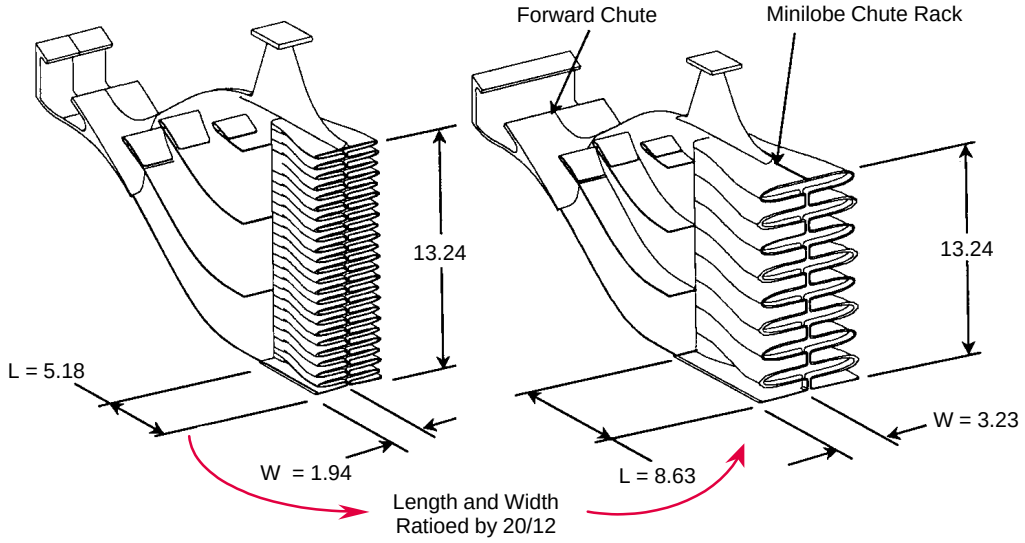

Figure 293. Comparison of 20x46 and 12x16 Lobe-on-Lobe Designs

Several concerns raised with this approach were addressed. It was thought that widening the main lobes might cause excessively high Mach numbers near the lobe leading edges due to the increased bluntness. A CFD analysis of the widened lobes indicated a small higher Mach number "bubble" (about 0.05 Δ Mach) at the lobe leading-edge corner, but it was not judged to be a concern. Because of the lengthening of the minilobes relative to the 20×46 design, the minilobe exit was moved 3.5 in farther aft into the ejector into a smaller duct area, thus higher Mach number regime. A CFD analysis with the chute exit moved to this location indicated a Mach number increase of about 0.08, and this was not considered to be a concern other than increasing secondary-side friction losses.

By definition, since the primary-side area distributions were retained, no change in friction loss should occur; in fact, friction losses should be lower than in the 20×46 design because of the reduced surface area due to the fewer number of lobes. Calculation of the secondary-side friction losses in both the main and minilobes indicated that the friction losses should be less than the 20×46 design primarily because the reduced surface area caused by fewer lobes off-set both the reduction in flow area in the main lobes due to increased wall thickness and the higher Mach numbers in the minilobes due to the farther aft location. Likewise, because of the reduced perimeter due to the fewer number of lobes, the base drag was determined to be lower than the 20×46 design in spite of the higher exit Mach number and increased trailing-edge thickness.

A diffusion of approximately 10% in the secondary-side area distribution was incurred because of the need in the 12×16 1/7-scale model design to transition from a 0.050-in wall thickness in the main lobes to 0.025 in at the start of the minilobes. Additionally, CASL tests of the 20×46 design with an initial vane design indicated flow separation off the vanes. The area diffusion coupled with initial 20×46 CASL result prompted a careful redesign of the turning vanes and a change in the location of the wall thickness transition. Subsequent CASL tests of the final vane design indicated total pressure wakes from the vanes comparable to those measured for the conventional mixers such as the Gen 3.0 and 3.4 mixers. It was concluded that the diffusion would not result in any appreciable vane separation.

Mechanical Design and Analysis

The 1/7-scale mechanical design features such as material, wall thickness, and mounting locations are based on previous 1/7-scale mixer configurations that have been tested with no structural problems. The key differences the LoL reresents from previous mixers are the number of chutes and the minilobes. The mechanical design analysis concentrated primarily on the minilobe features and not the main chutes.

The LoL mixer is designed to be manufactured from two Inco 718 forgings, one for the main lobes and one for the minilobes, and welded together. This manufacturing process was selected based on two factors. First, both Gen 3.5 and Gen 3.6 mixers were very difficult to cast (PCC) due to the thin-wall castings using gravity-fed sand casting process (the minilobe wall thickness is 0.025 in and the main lobe thickness is 0.050 i.). Second, it is estimated to cost more to cast the Gen 3.5 and Gen 3.6 mixers than to machine the parts. Discussions with Rich Tool and Die (an EDM machining company) resulted in positive feedback that the LoL mixer can be machined and welded to meet the drawing requirements.

The LoL mixer was designed for the maximum steady-state pressure and temperature condition expected in the model tests. The maximum condition is at an NPR of 4.0 at 1200°F. At this condition, changes in A_8 must be minimized and the lobes must not have any structural stresses greater than 120,000 psi for forging or 90,000 psi for casting.

A *Nastran* finite-element model analysis of the LoL configuration was built using the Unigraphics model definition. The area approximately 2 inches forward of the minilobes was constructed in the model to attenuate the boundary condition of the forward mixer attachment. Symmetric boundary conditions were used on the top and bottom to simulate adjacent lobe racks. The strut was fixed in the *y*-direction, which aids in supporting the lobes. The FEM had primary and secondary pressures distributions added. The primary pressure distribution was determined by using the cross-sectional

areas perpendicular to the centerline. From the cross-sectional areas, A/A*, P/P_T, and Mach number were determined and entered into the FEM. An ambient pressure of 14.7 psia was assumed, resulting in $P_7 = 14.7 \times 4 = 58.8$ psia. The secondary pressure distribution was obtained from Gen 3.0 test data. Eight pressure taps located on the bottom surface on the chutes were used to define the secondary pressure distribution.

The FEM stress results for a NPR 4 at a constant temperature of 1200°F are shown in Figure 294. The maximum stress is in the bumper pads, approximately 64,800 psi. This stress results in a 3σ margin of safety of 0.85 for forged material properties and 0.38 for cast material properties. A margin of safety greater than zero is considered acceptable.

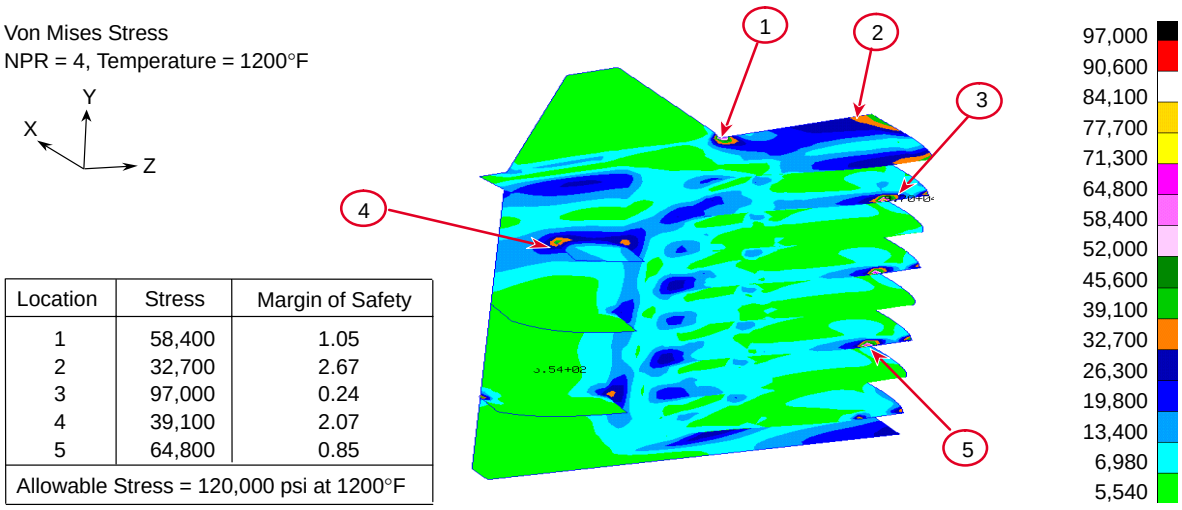

Location	Stress	Margin of Safety
1	58,400	1.05
2	32,700	2.67
3	97,000	0.24
4	39,100	2.07
5	64,800	0.85
Allowable Stress = 120,000 psi at 1200°F		

Figure 294. Calculated Minilobe Stress Distributions *Design has acceptable stress.*

A_8 deflection was calculated by using UniGraphics and the deflection results from the FEM. This area was then compared with the nominal A_8. The result was an area change of 1.58% due to pressure and temperature. The manufacturing tolerance is ±0.002, which equates to an A_8 change of ±1.55%.

In conclusion, the 1/7-scale LoL mixer has acceptable stresses and deflections for the maximum test condition.

5.9.2.4 Fan/Core Mixer Design

A fan/core (F/C) mixer is installed at the turbine frame exit to mix the cold fan and hot core engine gas streams efficiently. The primary objective of mixing the streams is to obtain a performance/SFC benefit for the low-bypass turbofan at cruise conditions. A challenging yet presumed-achievable goal of 80% mixing effectiveness to achieve this benefit was set for the program. In addition to the cruise performance benefit, effective mixing would minimize hot streaks in the nozzle gas stream which would also be favorable for reducing jet noise at takeoff and minimizing hot-metal streaking on the acoustic mixer.

Design Approach

The initial concept for the F/C mixer was a variable-geometry device called a variable-area bypass injector (VABI). This concept included mixer chutes that could be actuated into variable positions

to satisfy engine cycle requirements for a variable fan-to-core area split at the mixer exit. This was intended to optimize cycle efficiency across the flight regime. Several years prior to the termination of the CPC program, the added weight, cost, and complexity of a variable-geometry system led to cycle studies to reassess the need for a variable fan/core area match. The cycle studies indicated that the weight and cost savings for a fixed-geometry mixer with the area set to maximize performance gains at supersonic cruise would offset fuel burn increases at other flight conditions, and the fixed F/C mixer concept was incorporated into the design.

An initial deep-lobe mixer design was developed using simplified analytical methods and mixer design criteria developed by GEAE and P&W. Side and ends views of the design are shown in Figure 295. Full-quadrant CFD studies of this design were conducted in for the cruise and takeoff modes of operation. Results of these studies, to be briefly described in the following discussions, indicated that the cruise goal mixing effectiveness was not achieved (about 10% short). The CFD results indicated that a mixer with less penetration would improve the mixing, and a redesign was subsequently conducted. A CFD analysis of the redesign at both operating conditions was completed, but the results were unexpected. There was no improvement in the mixing, and flow separation on some areas was evident. It was apparent that the aerodynamic phenomena that influenced the mixing process was not understood for this component within the design space, and due to the CPC program termination no further work could be performed to improve the design and achieve the mixing goals. However, it was agreed within the aero community that a successful design could be accomplished with further technology development.

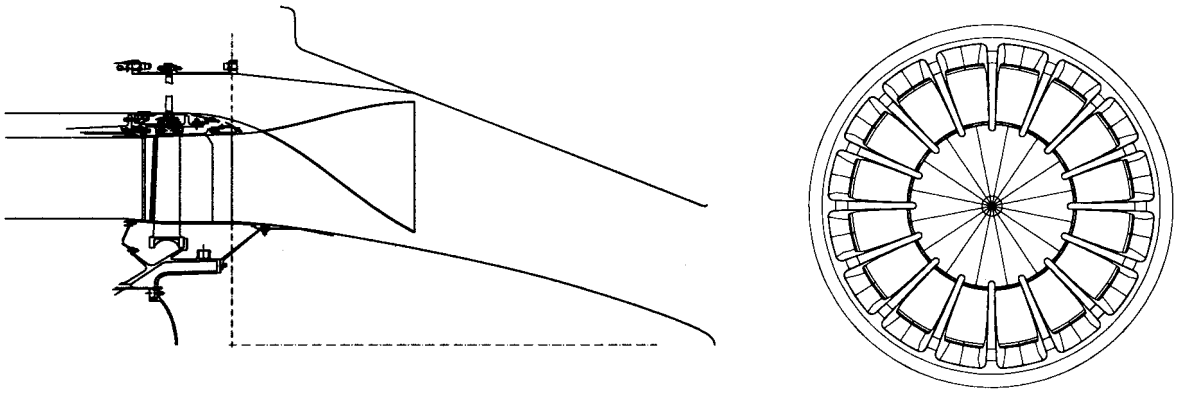

Figure 295. Initial Deep Lobe Fan/Core Mixer Design (May 98)

Cruise Mode CFD Results

A full-quadrant CFD analysis of the initial deep-lobe design F/C mixer was conducted in the cruise mode (T duct open and ejector inlet doors closed) at the Mach 2.4 cruise, power code 50, 3770.60 cycle conditions. The CFD solution started from just upstream of the turbine frame (frame not modeled in the solution), extended through the T duct and acoustic mixer, and ended a short distance downstream of the nozzle throat. A confluent F/C mixer (no lobes) was also analyzed to compare against the more complex and heavier lobed mixer to determine the net benefit of the lobed mixer approach. Both designs had a fan-to-core area ratio at the mixer exit of 0.28 (A_{16}/A_{56}) as defined by the cycle. The 2.1 million cell grid system was defined by ASE Technologies using the grid generator GRIDGEN, and GEAE conducted the CFD analysis using the FNS code STAR CD. Inputs to the solution included the cycle values of total pressure and temperature in the fan and core streams

coming into the mixer. Total temperature, Mach number, and velocity vector contours in axial, radial, and vertical planes were analyzed. Postprocessed results included the bypass ratio and mixing effectiveness.

Total temperature contours near the end of the centerbody and at the nozzle throat shown in Figure 296 indicate a flow inversion (colder fan air near the centerline and hot core flow in the outer regions of the duct) that did not fully mix out at the nozzle throat and resulted in a mixing effectiveness about 10% below the goal. Assessment of these and other results implied that a reduced-penetration mixer would lessen the flow inversion and increase mixing effectiveness at cruise. The confluent-mixer effectiveness was more than 40% below the goal, had a large hot slug of air at the centerline as expected, and verified that a lobed mixer was required to achieve the objectives stated previously.

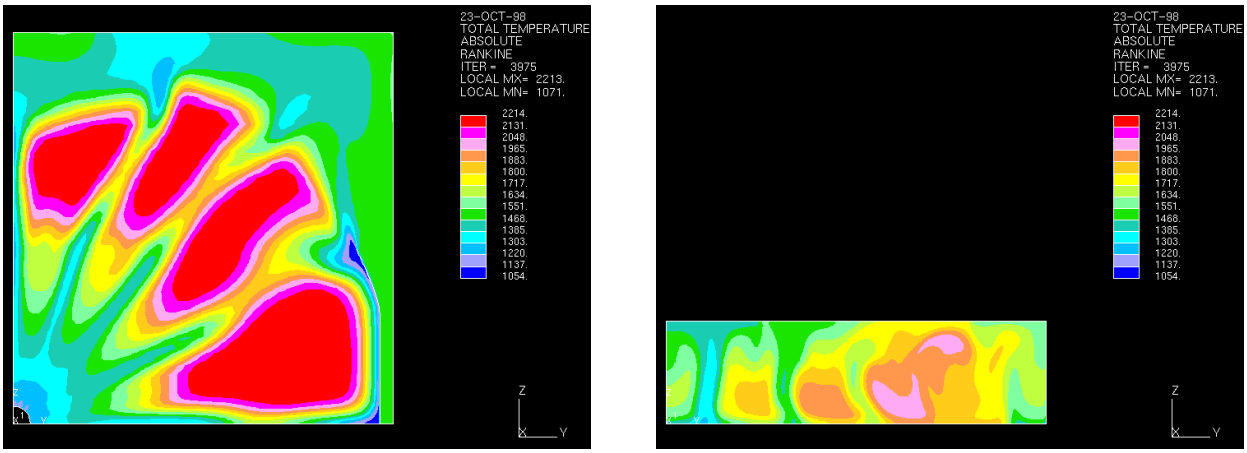

Near Centerbody Trailing Edge

At Nozzle Throat

Figure 296. Total-Temperature Contours for Initial Design F/C Mixer at Mach 2.4 Cruise

Based on these results (and the takeoff-mode CFD results in the following discussion), the mixer was redesigned with less penetration of the fan lobes into the core stream in an attempt to reduce the flow inversion. The fan lobe widths were increased accordingly to maintain the same 0.28 fan-to-core area ratio. The same total temperature contours near the end of the centerbody and at the nozzle throat, shown in Figure 297, were disappointing in that the flow inversion was not reduced but only spread out slightly. The mixing effectiveness was unchanged, and there was evidence of flow separation along the centerbody aft of the F/C mixer exit.

Takeoff Mode CFD Results

A full-quadrant analysis of the initial deep-lobe design was also conducted in the takeoff mode at the Mach 0.32, 689-ft, PC 50, 3770.60 cycle conditions. This CFD solution also started from just upstream of the turbine frame but terminated at the exit of the acoustic mixer. Only conditions at the exit of the acoustic mixer were of interest at the time. Combustion Research and Flow Technology, Inc. (CRAFT) defined the 6 million cell grid system using GRIDGEN and also conducted the CFD analysis using the FNS code CRAFT. Solution inputs included the appropriate cycle values of temperature and pressure; similar plots of total temperature, Mach number, and pressure at various stations and planes were analyzed.

Total temperatures near the end of the centerbody and at the exit of the acoustic mixer are shown in Figure 298. Similar to the cruise CFD results, a slug of cold fan air has collected near the

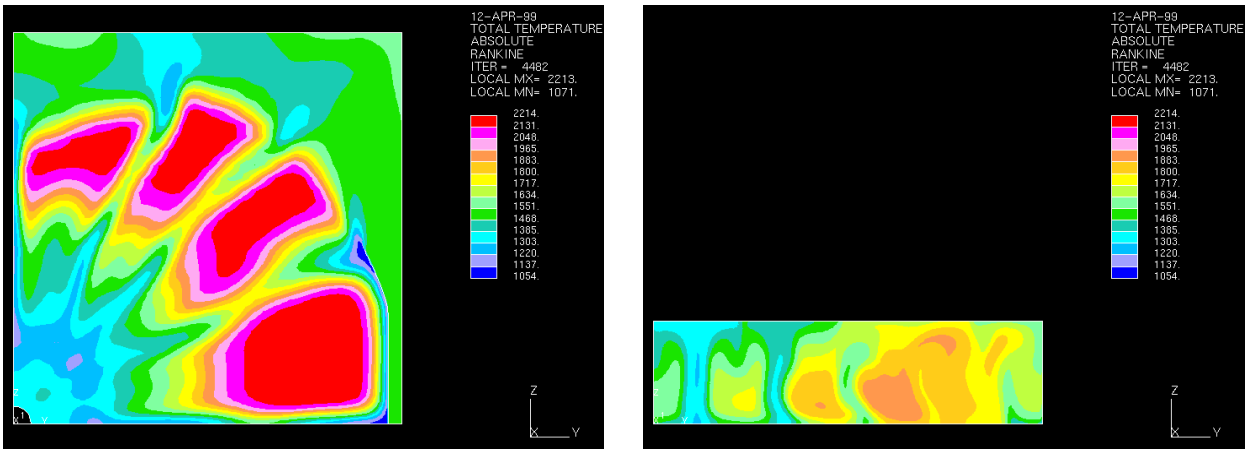

Near Centerbody Trailing Edge

At Nozzle Throat

Figure 297. Total-Temperature Contours for Revised Design F/C Mixer at Mach 2.4 Cruise

centerbody and persists to the exit of the mixer. In this case, the presence of the full T duct with the ejector inlet doors open and the transitioning of the flowfield from circular to rectangular has caused the flow near the centerbody to migrate to the side, resulting in the cold slug of air on either side of the centerbody. Once the flow pattern gets into the acoustic mixer, there is no mechanism that will allow the two streams to mix further.

The redesigned F/C mixer with reduced penetration was again run in the takeoff mode, this time at two cycle points, PC 50 and 47, to cover both mechanical and aeroacoustic conditions of interest, and an updated version of the 3770.60 cycle called 3770.54 was used. The same total temperature plots for the revised design are shown on Figure 299, and very little difference in the profiles is observed for these results.

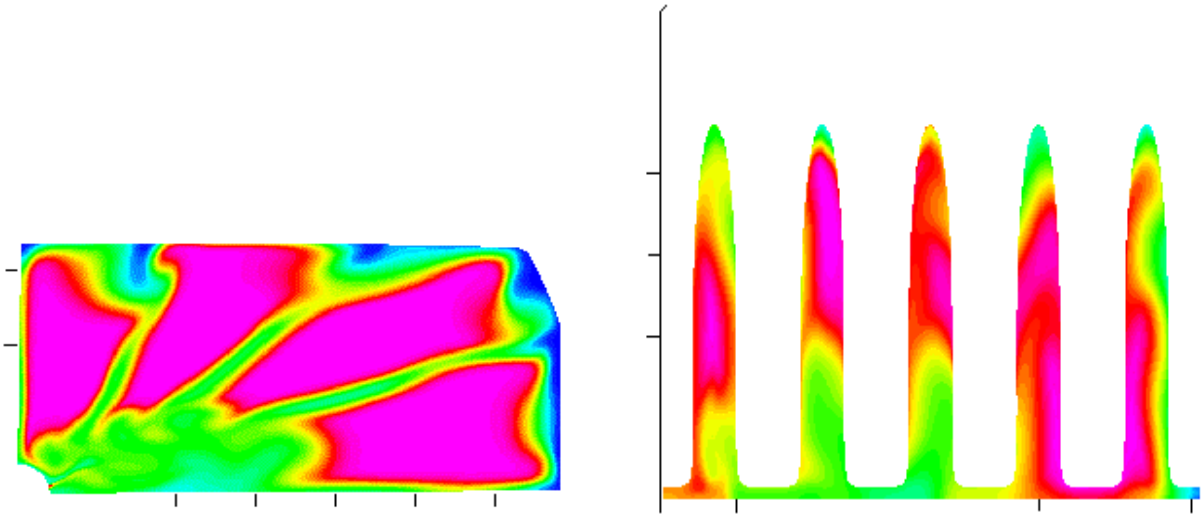

Near Centerbody Trailing Edge

At Mixer Chute Exit

Figure 298. Total-Temperature Contours for Initial Design F/C Mixer at Mach 0.32 Takeoff

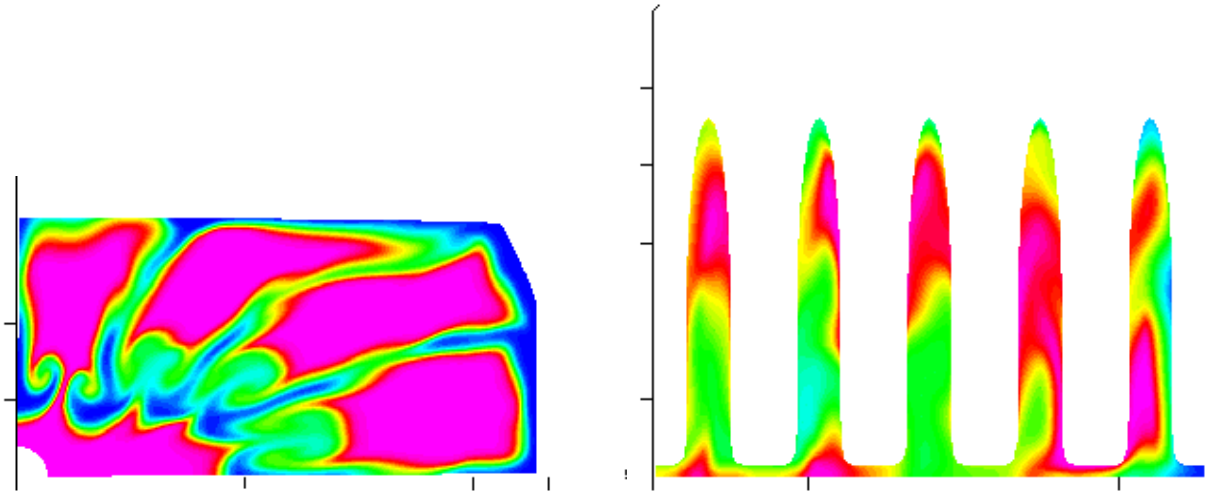

Figure 299. Total-Temperature Contours for Revised Design F/C Mixer at Mach 0.32 Takeoff

Scale-Model Test

All the 1/7-scale aeroacoustic testing conducted at Boeing and at GEAE has been with uniform entrance conditions (total pressure and temperature) to the mixer. There is concern in the acoustic community that nonuniformities in the flowfield coming out of the acoustic mixer, such as shown in Figures 298 and 299, may have a detrimental effect on the noise signature in the takeoff mode. Attempts to quantify the possible increase in noise have not led to a definitive answer, and it has been recommended that an acoustic test with the F/C mixer simulated be conducted following the CPC program to determine the effect on noise. As previously stated, it is recognized that the two F/C designs assessed thus far do not meet the cruise mixing-effectiveness goal for the program, but the goal is deemed achievable with further development. Thus, for purposes of obtaining a first assessment of the effect of nonuniform conditions on noise, the initial design F/C mixer was the better of the two analyzed and is recommended for testing on the 1/7-scale model.

5.9.2.5 Chevron Study

It was noted that certain advanced subsonic transport nozzles used chevrons that were somewhat similar to HSCT chevrons previously tested. Since mixed results had been obtained with the HSCT chevrons, it was decided to review the AST data in an attempt to establish whether chevrons would be expected to be beneficial for the HSCT nozzle and to gain some physical insights into the effects of chevrons. To some degree, the nozzles were similar; both had a hot central stream that was highly mixed (for certain AST cases) surrounded by a cooler stream, but there were enough differences to cast some doubt on direct application of results to the HSCT nozzle.

There were obvious differences in geometry such as the large boattail angle of the AST configuration, the presence of a centerbody, and the offset of the two exit streams, but these were probably not the most significant differences. The major difference was the presence of two distinct streams that both could be modified in the AST nozzle, which might drastically change the noise-generation dynamics of the AST nozzle relative to the HSCT nozzle. In addition, most of the flow modifications

(mixer nozzle or tabs) would occur upstream of any chevrons on the exit of the nozzle for the HSCT nozzle as opposed to downstream of the chevrons for the AST nozzle. It was also hypothesized that there was a very strong aeroacoustic coupling between the two streams in the AST tests that may make the actual performance of the mixing devices behave very differently than they would on an HSCT nozzle.

Application to HSCT

The most applicable cases to the HSCT nozzle in the AST tests were those where the core stream was modified and tested with and without chevrons on the fan stream. For these cases, the chevrons provided some incremental noise and thrust benefits, but the benefit was a function of the degree of modification to the core stream. When the core stream was highly disturbed the chevrons provided the most benefit, but when the disturbances were reduced the benefits of the chevrons decreased until there was even a slight penalty for the baseline core nozzle. These results may explain the differences in effectiveness of the chevrons for the various HSCT mixer nozzles, as they appear to indicate that no benefit should be expected from using chevrons on an HSCT nozzle when the flow is nearly uniform at the exit of the ejector.

Performance Versus Noise Reduction

The thrust data indicated that the addition of chevrons on the fan stream typically served to increase the thrust relative to those cases where only the core stream was modified. The mechanisms for this were unclear, but it appeared that the noise reduction due to the chevrons were not due to flow losses that decreased the thrust. It appeared that the addition of chevrons seemed to inhibit the growth of the core shear layer. This effect may have also been in part responsible for the decrease in thrust loss associated with the addition of the chevrons.

One other possible reason for the increase in the thrust could be a pressure increase on the centerbody of the fan stream. There were no pressure data taken to support this hypothesis, but it would be an important effect to test in the future. If there were a pressure recovery involved in the cases tested, it would imply that the chevrons would probably not provide a thrust benefit for the HSCT where there would be no centerbody. This would probably limit chevrons to cases where there was a centerbody or where there was a much higher emphasis on noise.

Physical Understanding of Noise-Reduction Mechanisms

Some insights into the physical mechanisms associated with the noise reduction of the chevrons were also gained. It was found that the reduction in noise was not simply due to a shorter potential core but more closely related to the volume of the shear layer and the turbulent intensities in the shear layer. The addition of the chevrons appeared to reduce the initial growth of the shear layer, as seen in Figure 300. Figure 300 shows that the normalized area of the shear layer was reduced immediately downstream of the exit when the chevrons were present, but the shear layer became thicker at locations further downstream. A complex interaction between the fan and core shear layers was observed with strong aeroacoustic coupling between the two. This coupling made it very difficult to isolate the particular effects of a mixing device as it affected both shear layers. It appeared that the mixing devices changed the character of the noise-generation mechanisms such that the peak noise-production region was modified by these devices. Finally, some recommendations for future studies were made that would help to further the understanding of how chevrons work.

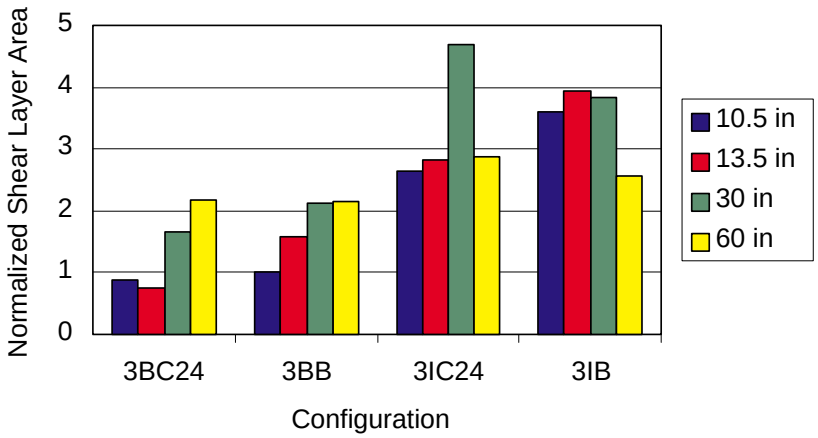

Figure 300. Effect of External Chevrons on the Shear Layer

5.10 Basis for Nozzle Data Supplied in Support of Airplane System Studies

5.10.1 Aerodynamic

The exhaust system performance characterization for the engine cycle decks has two models, one for the cruise mode and one for the noise suppression mode. These two models have a different basis for the predictions and are completely different in structure. For both modes, the location/station at which the aerodynamic loss accounting begins is at the exit of the F/C mixer, and it is known as the charging station. There is also a pressure loss model for the F/C mixer that is the same for both modes. It consists of a simple pressure drop within the mixer on both the fan and core. These pressure drops are based on *simple* analytical studies, and CFD results of the F/C suggest that the losses may be slightly high.

5.10.1.1 Cruise Mode

In the cruise mode, the exhaust system model is divided into two sections. The pressure loss model for the forward section was based on CASL scale-model test results of a modified sector of the flowpath conducted with both the subsonic and Mach 2.4 cruise throat areas (A_8). The change in CASL model flow coefficient in these tests was used to determine the pressure loss directly. It was assumed that the CD nozzle flow coefficient should not be affected by the presence of the mixer, and any reduction of flow measured in the CASL test with the addition of the mixer was attributed to a loss in pressure. The pressure loss increases with larger A_8, due to the higher Mach numbers within the duct, and it includes all the friction, turning, and expansion losses of the flow as it splits into the bypass area and passes through both sides of the acoustic mixer to the CD nozzle entrance, Station 7. The resulting total pressure provides the reference or charging station pressure for the nozzle thrust and flow coefficients. A 1/10-scale model of the exhaust nozzle in the cruise mode was designed and fabricated for testing in the NASA–Glenn CE22 static test stand. The model was designed to determine/validate the duct pressure loss using a more accurate, 3D version of this section of the flowpath. Program termination precluded such testing under CPC.

From Station 7 aft, the nozzle performance is characterized by a gross-thrust coefficient (C_{fg}). This thrust coefficient includes all the friction, angularity, expansion, and shock losses within the CD

nozzle. The predictions for these losses are based on FNS CFD analyses and Euler plus boundary layer calculations of 2DCD nozzles that has been validated by comparison of the CFD prediction with scale-model test data conducted in CE22 (see Subsection 5.7.3). Based on this validation, a subcode developed from the CFD output has been put together in the cycle deck to predict thrust coefficient for the CD nozzle given specific geometric inputs such as secondary flap length and angle and the cycle airflow conditions. The actual output of the code has been adjusted by +0.10% at Mach 2.4 cruise conditions (area ratios) down to 0 (no adjustment) at Mach 1.1 condition area ratios to reflect the validation comparison with the CE22 test data.

The CFD analyses had no accounting for any wall surface condition other than the usual smooth wall, and the CE22 scale-model tests likewise were conducted with conventional smooth-wall performance models. Thus, the C_{fg} as modeled in the data packs has no accounting for any extra friction drag or other momentum loss source due to the presence of the acoustic treatment panels. The 1/10-scale model previously mentioned for future testing in the CE22 test stand will have simulated acoustic panels with bulk absorber behind the face sheets in addition to conventional smooth-wall nozzles to obtain a first-time measurement of the acoustic panel thrust loss over a wide range of nozzle area ratios from subsonic to supersonic cruise.

An example plot of the thrust coefficient vs nozzle pressure ratio for the 3770.60 cycle is shown in Figure 301, and the corresponding area ratio schedule is shown in Figure 302. The area ratios are based on full expansion along the entire curve down to a floor value of 1.23. The full expansion selection is based on the assumption that maximum internal performance will be achieved at this condition. The 1.23 limit value has been set in all the cycle decks to provide margin for area ratio control such that the area ratio can not be equal to 1.0. This limit is based on initial mechanical design studies that evaluated control-system uncertainty and nozzle deflections due to aerothermal loads. It is set to avoid an aeromechanical instability that will occur for variable-geometry CD nozzles if an area ratio of 1.0 is reached. This floor compromises the low-ratio performance due to overexpansion losses as shown by the drop in C_{fg} at low pressure ratios. It is expected that the floor value could change in the future pending more detailed studies and system design definition.

Thrust losses due to leakage flow in the entire exhaust system are determined from a separate calculation as a change in C_{fg} and subtracted from the CFD based value. For the HSR program, the calculation was performed at the supercruise condition and assumed to be constant for all other flight conditions. The leakage loss was based on the effective leakage areas and estimates of the gas-stream static pressure and temperature at the leakage locations.

The flow coefficient in the cruise mode is also CFD based and accounts for both the change in primary nozzle half angle as A_8 varies and the 4.0-inch flowpath radius at the throat.

5.10.1.2 Noise-Suppression Mode

For the net-thrust coefficient (C_{fn}), the reference total pressure at the charging station is the mixed total pressure calculated in the cycle deck at the exit of the F/C mixer. It thus includes all the losses from that station aft including any friction, turning, shock, mixing losses of the primary and ejector air, and acoustic panel losses. Note that C_{fn} is also a net thrust coefficient in that it includes the ram drag of the ejector air. Any external friction or pressure drag of the nozzle is determined from drag tares performed in the 1/7-scale model tests and is bookkept in the airplane drag polars.

The cycle deck model for the takeoff coefficient is based on a 1D code having three key inputs of primary nozzle efficiency (C_s), inlet recovery (η), and ejector duct friction factor (f). The 1/7-scale

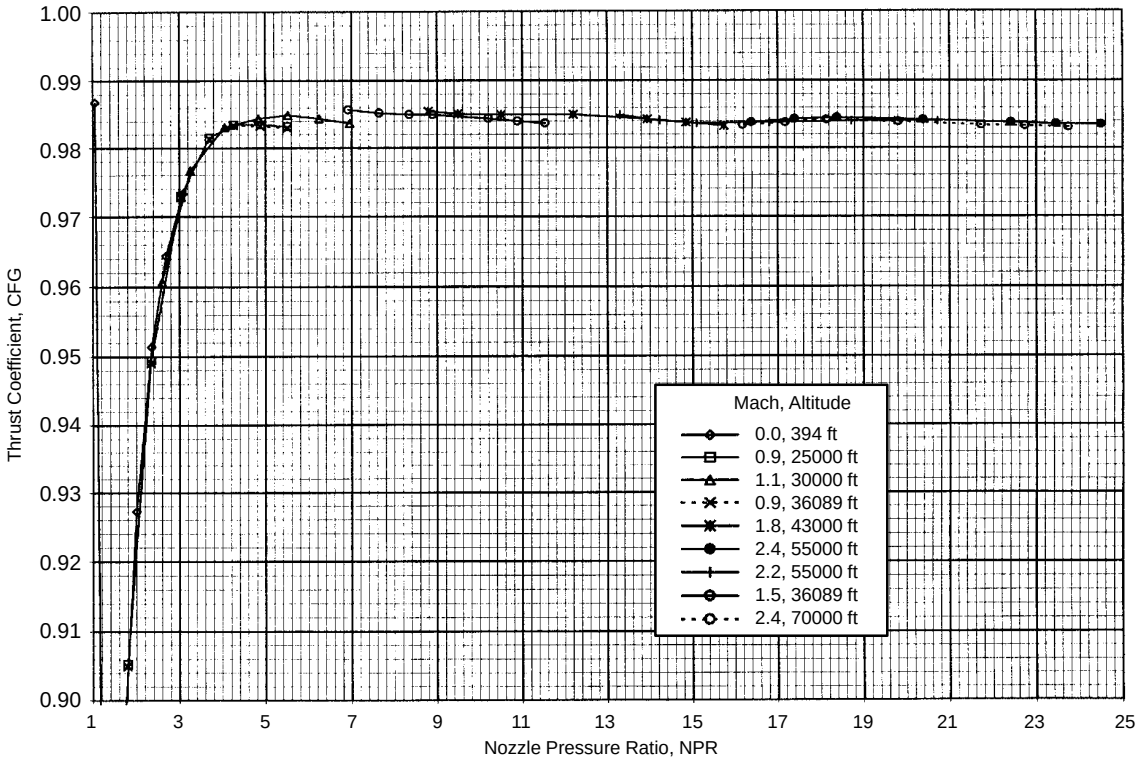

Figure 301. Nozzle Thrust Coefficient for MFTF 3770.60

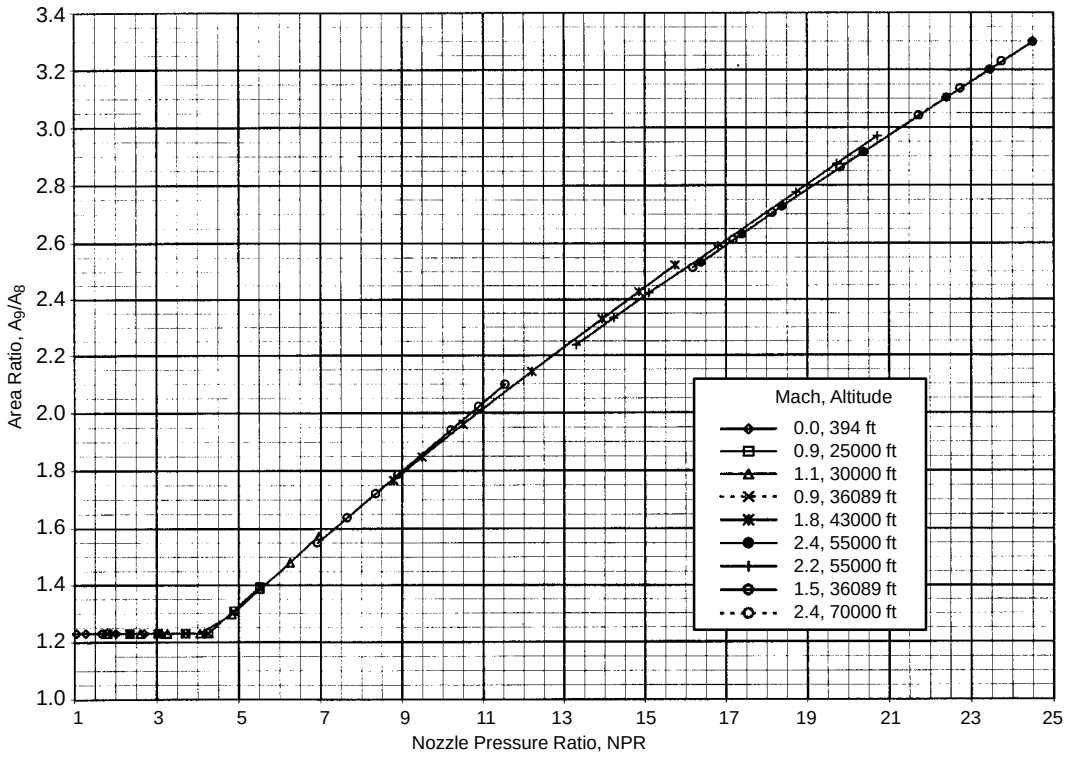

Figure 302. Nozzle Thrust Coefficient for MFTF 3770.60

model test data are scaled up to product size accounting for Reynolds number effects and other nonscaleable features such as mixer trailing-edge base thickness/drag and acoustic panel simulation. The 1D ejector code is then "calibrated" to the scaled model data at two Mach 0.32, 689-ft noise rating point conditions (sideline and cutback) such that the calculated C_{fn} from the 1D code match the scaled model data. This is done by adjusting the three prime inputs to reasonable values as determined by the nozzle aerodynamics team until the model data are matched. The code is then used to predict the nozzle performance at all other Mach numbers, altitudes, and power settings. For the actual data packs, however, the 1D code C_{fn} value with the status baseline nozzle was calibrated to the goal value of nozzle performance at the noise sideline operating condition rather than the scaled model data value. When trade studies were performed that involved nozzle geometric variations such as SAR, the 1D code had the capability for making adjustments to the baseline goal performance based on the nozzle geometric differences.

In the takeoff mode, the nozzle throat area is formed within the fixed-geometry acoustic mixer, resulting in a fixed A_8. The flow coefficient in this mode was a constant and was based on a combination of scale-model test results and analytical CFD studies.

5.10.2 Acoustic

Noise prediction is based on modeling the latest and "best" 1/7-scale test data. Deltas are applied to this modeled data to account for scaling and continued technology improvement (projections). The scaling to product size accounts for engine flow coming into the nozzle, for ejector lining differences, and for jet velocity differences. The technology projection Δ's account for anticipated improvements to the nozzle.

The latest prediction program used for airplane system studies was JN8C4. This program was a modeling of 1/7-scale data from the LSMS or Gen 3.0 nozzle. The key features of this nozzle were 2.9 SAR, 92.5% penetration, half hot sidewall, and a MAR of 95%. Modeling matched the spectral data as shown in Figure 303 and was within 0.2 EPNdB at sideline (3.43) and cutback (2.48) nozzle pressure ratios.

Scaling effects were evaluated in the HSR program by testing a large-scale mixer and a 1/7-scale equivalent called the *large scale mixer similitude* (LSMS). These tests resulted in a +3 EPNdB difference between the LSM and LSMS when both are extrapolated to product scale. Analysis of these data indicated that there were three primary causes of this difference.

First, the actual engine flow coming into the mixer was unmixed fan and engine core flow. (It had been decided not to include a fan/core mixer on the LSM test to determine how important it is.) Posttest data analysis indicated that l EPNdB of the difference was the unmixed fan/core streams.

Second, ejector lining for 1/7-scale testing attenuates a peak frequency for internal noise of over 20 kHz. At that frequency, virtually any lining configuration will work. The lining development program had concluded that if the right lining parameters could be found full-scale lining would attenuate more noise than model-scale lining. Lining materials that came close to the desired properties were not found until after the LSM testing. Approximately 1 EPNdB of the difference was that the lining suppression was less than model scale, when it potentially could provide more suppression.

The last difference is split between geometry details (LSM/LSMS) and product-scale thrust being better by about 2%. The higher thrust means that the ejector exit velocities, and to some extent

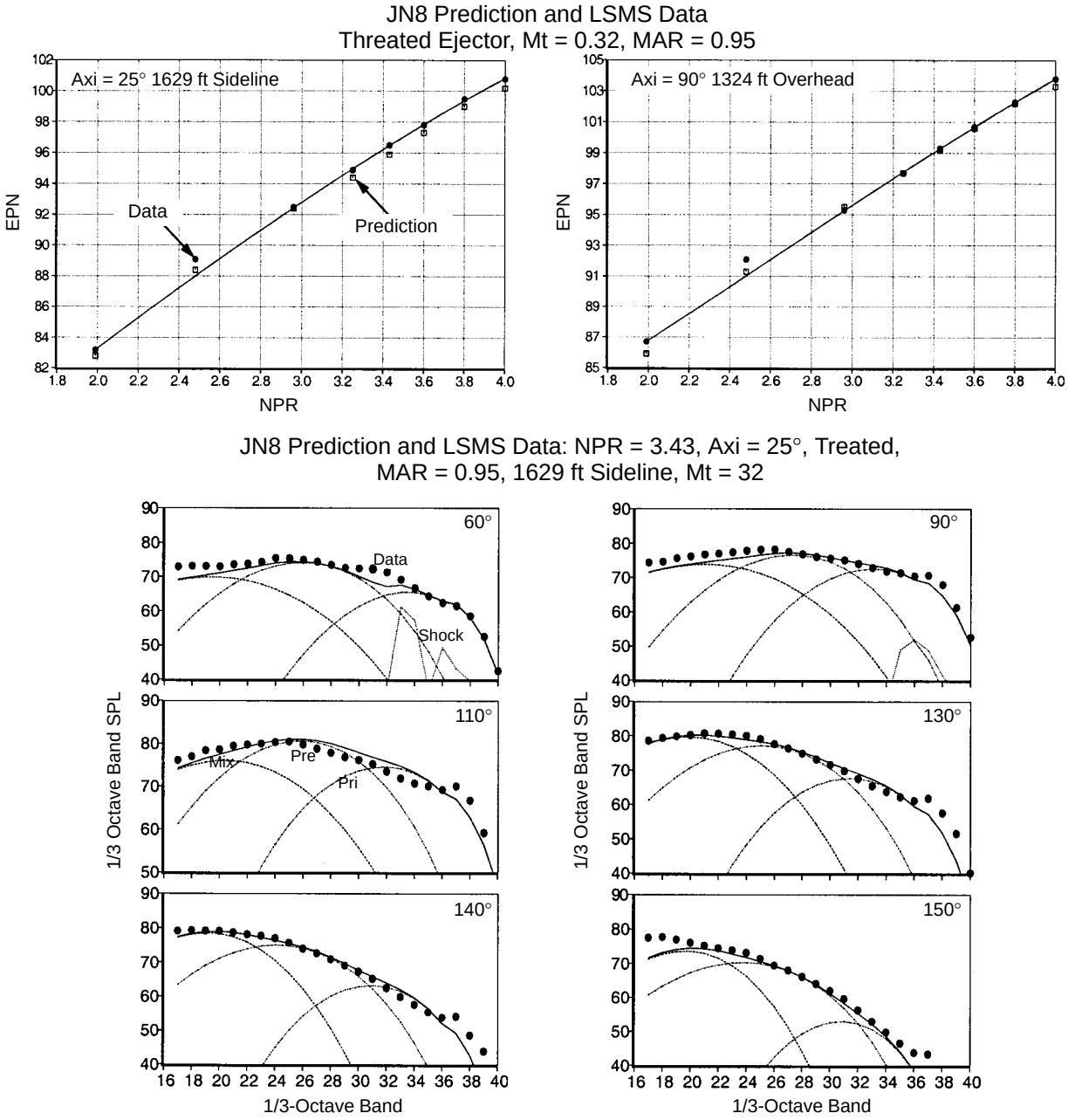

Figure 303. JN8C4 Versus LSMS Data

internal velocities, are higher. The higher velocities are inherent and will mean that scaled noise will be at least 0.5 EPNdB higher noise for LSM scale and product-scale nozzles.

Technology projections were also included to account for continued development of the mixer/ejector nozzle. This development was in four areas.

First, the mixer chutes were continually being modified, using CFD modeling, primarily to improve thrust performance. This also would affect noise performance but the relationship was not well understood. More gross modifications were the chute placement relative to the sidewall. The NRA

nozzle had a half-width hot chute adjacent to the sidewall. This was believed to cause high-velocity flow next to the sidewall, increasing the thrust loss due to friction and decreasing the lining attenuation. Gen 2 nozzles were a full cold chute next to the sidewall. This resulted in cold pockets in the exit profile, which were believed to reduce the nozzle noise suppression. The Gen 3 nozzle design was a half hot sidewall to eliminate the cold pockets. It did that, but lower thrust and lower lining attenuation were observed again. The Gen 3.5 nozzle was designed with half cold chutes next to the sidewall, and this proved to be both a noise and thrust performance benefit.

Second, mixing-enhancing devices were studied in elemental tests at NASA Langley and Glenn and by CFD modeling. Model-scale nozzle tests were conducted in Cell 41 at GEAE. Although no mixing design tool exists, progress was made. “Reduced A” tabs was the best configuration found. This provided more rapid mixing, improved the ejector lining suppression, and improved mixedness — reducing larger scale mixing noise. The net result was a 2-EPNdB improvement in noise at the cost of 0.5% loss in thrust coefficient. This is a favorable trade on the airplane.

Third, chevrons were tested with varying degrees of success. These are devices at the trailing edge of the ejector, and again they are not well understood. The best results achieved in the Gen 3.5 testing were not benefited by chevrons. They have been shown, however, with previous nozzles to provide as much as 1.0 EPNdB noise benefit with no impact on thrust.

Finally, the ejector lining can potentially be improved large scale over the model-scale results. This development would require large-scale testing to validate but was estimated from elemental testing and prediction codes. The benefits from these possible improvements were estimated for a 2007 certification date, which corresponds to a 2002 technology readiness date. This projection was reassessed for a 2015 certification date, or 2010 technology readiness date. For the technology to be considered ready, it should be demonstrated in a large-scale test. Model-scale demonstration would be approximately two years earlier. The detailed 2007 and 2015 projections are shown in Table 57. Mixing enhancers move ejector lining effectiveness closer to the mixer exit (five lobe widths) and this reduces the ejector length for the same treatment area. The EPN reductions were made on the noise sources; the totals shown are the results on the TC airplanes and are 1.2 EPNdB for the 2007 projection for sideline and 1.3 EPNdB for cutback noise. The 2015 projections are 4.0 EPNdB for sideline and 5.3 EPNdB for cutback.

Table 57. Projections for 2007 and 2015

Improvement	Noise Source	Sideline		Cutback		Approach	
		2007	2015	2007	2015	2007	2015
Internal Mixing: Tabs, Notches, etc.	Premerge	–1.8	–3.2	–1.8	–3.7	–1.8	–3.7
	Internal	0	–4.5	0	–4.0	0	–4.0
	Lining Area	5 Lobe Width		5 Lobe Width		5 Lobe Width	
Acoustic Lining	Internal	–0.6	–1.0	–0.7	–1.0	–0.7	–1.0
External Chevrons	All	–0.5	–1.2	–0.5	–2.1	–0.5	–2.1
Total Projection (ΔEPNdB)		–1.7	–4.3	–1.8	–5.6	–1.9	–7.0
Scaling Penalties	Premerge	+0.06	+0.3	+0.7	+0.4	+0.7	+0.4
	Merged	+0.5	+0.3	+0.6	+0.6	+0.6	+0.3
Net Benefit (ΔEPNdB)		–1.2	–4.0	–1.2	–5.3	–1.3	–6.7

The status of the nozzle development is the results of Gen 3.5 model-scale nozzle testing. These results indicate general demonstration of 2007 projections with an assumed 2% thrust benefit and a 0.5 EPNdB noise penalty for scaling to product size. The “reduced A” tabs were tested with the Gen 3.0 mixer, and the benefit was applied to the Gen 3.5 mixer.

5.10.3 Mechanical

The engine cycle datapacks were produced to support the aircraft system studies. These engine cycle datapacks, and ultimately the aircraft system studies, required geometry, weight, and center of gravity information for the exhaust nozzle. The following specific nozzle information was supplied in support of the engine cycle datapacks and system studies:

- divergent flap length
- nozzle internal width
- boattail flap length
- convergent/divergent flap hinge radius
- nozzle fore flange half height
- A_{max} (maximum nozzle nacelle projected area)
- A_{mix} (flowpath area at the ejector mixing plane)
- total nozzle weight
- nozzle center of gravity
- outer mold line defintion at supercruise
    - nozzle length
    - location of forward hinge point of the external flap
    - upper and lower boattail angles
    - sidewall boattail angle

The above listed nozzle data were supplied for all of the various engine cycles and SAR values requested as part of the many system studies. These nozzle data were generated using an *exhaust nozzle geometry and weight prediction tool* based on the product-scale version of the fixed-chute nozzle configuration as presented in the December 1995 Preliminary Design Review. Subsection 5.6.3.1 presents more details on the exhaust nozzle geometry and weight prediction tool and the basis of the data it generates.

5.11 Summary and Remaining Challenges

The objective of the HSCT nozzle CPC program was to develop a low-noise exhaust nozzle with high aerodynamic performance, low weight, and long life. When evaluated against that objective, the program was clearly a success. The final nozzle design demonstrated noise levels nearly 2 EPNdB below the program goal at cutback and only 0.2 EPNdB above the goal at sideline. In addition, technologies were demonstrated that would result in noises levels 1.8 EPNdB below the goal at sideline and 3.7 EPNdB below the goal at cutback. The nozzle takeoff performance exceeded

the original thrust coefficient goal of 0.945 and is projected to be within 0.007 of the more challenging goal of 0.960. The weight of the final nozzle design is estimated to be within 200 lbm of the goal of 7830 lbm, and potential weight savings concepts were identified that could lower the nozzle weight to more than 500 lbm below that goal. All of this was achieved with a design for a fully functional nozzle that can operate either in a suppression or a nonsuppression mode and translate between these modes. The many accomplishments are summarized in Subsection 5.11.1.

While the accomplishments were many, challenges remain. These challenges relate both to demonstration of the projections made relative to the program goals and to further enhancement of identified critical technologies that could lead to an even more successful nozzle design. These challenges are summarized in Subsection 5.11.2.

5.11.1 Summary

Although this summary is divided into three sections (acoustics, aerodynamics, and mechanical design), by no means should these disciplines be considered independent. In fact, one of the most important accomplishments of this program may have been the teaming of these three disciplines and the realization of designers for each discipline of how their requirements impacted the other disciplines.

5.11.1.1 Acoustics

Figure 304 is a summary of many of the aerodynamic and acoustic results from this program. Sideline noise reduction is plotted versus the percentage loss in takeoff thrust. Results from one of the early tests, of the Gen 1 NRA nozzle, gave the first indication that the noise goals could be reached with a feasible nozzle design. The nozzle demonstrated about 18 EPNdB noise reduction but with significant thrust loss. The interrelationship of noise and performance was quickly learned in the Gen 2 tests, where the thrust performance was greatly improved but the noise reduction decreased by about 4 EPNdB. The lessons learned from these tests and other supporting activities resulted in the nozzle design for the Gen 3 test, which had noise reduction similar to that of the Gen 1 model and thrust performance similar to that of the Gen 2 design. Tests of a large-scale model of the GEN 3 nozzle in an engine environment resulted in noise levels 1.5 EPNdB higher than those from the 1/7-scale model in the more ideal laboratory environment. The Gen 3.5 nozzle was the final nozzle tested in HSR, and it achieved the best results: maintaining noise performance at sideline and improving cutback noise by 1 EPNdB while improving thrust performance by 1%. This test series also evaluated the “reduced A” tab mixing-enhancer configuration that suppressed noise another 2 EPNdB with only a 0.5% thrust loss. This was tested with the Gen 3 mixer. More detailed summaries of the various acoustic tests are provided in the following subsections.

The Gen l 1/7-scale tests investigated several nozzle concepts. A 2D mixer/ejector, designated the NRA nozzle, was the first realistic nozzle to provide suppression on the order of what was needed. This nozzle was tested by GEAE in the Cell 41 facility. All of the following generation nozzles have been 2D mixer/ejectors that trace their origin to the NRA nozzle. One of the critical findings was a benefit for a 2D nozzle that reduced noise at the sideline azimuthal angle.

With the initial model-scale testing, concern was expressed as to the effect of installation on an airplane on ejector nozzle performance. To evaluate this, a test was conducted by NASA–Ames in the 40×80-ft wind tunnel. The question was: Is this a big effect, such that isolated testing is not valid,

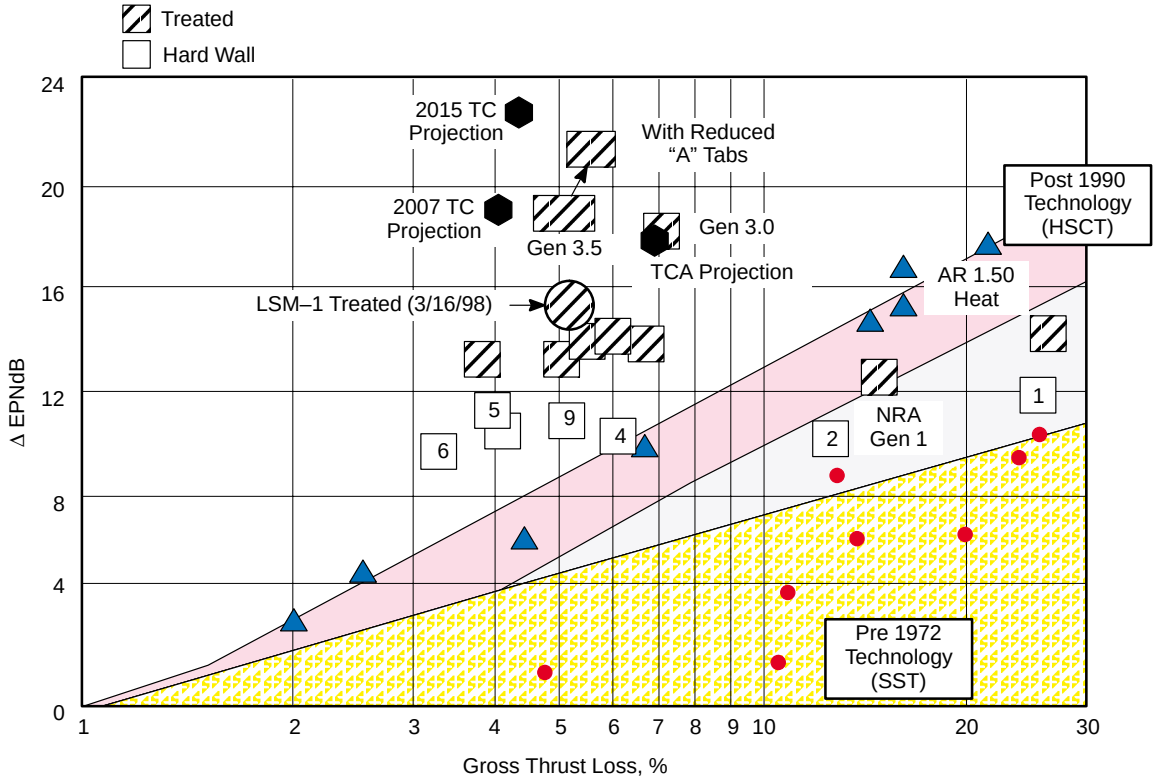

Figure 304. CPC HSR II Nozzle Test Data

or is it a small effect? This testing demonstrated that it is a small effect, and — even though a quantitative evaluation was not the objective — the data were good enough to apply a 0.8 EPNdB installation penalty to cutback noise, with no penalty to sideline or approach noise.

The Gen 2 nozzle incorporated changes to improve thrust performance and to represent a selected nozzle design, the *downstream mixer* nozzle. The DSM nozzle had a full cold chute next to the sidewalls, improved aerodynamic design of the chutes, peaked top versus square top, and an aspect ratio (mixer width/height) of 1.2 versus 1.5. This nozzle did improve thrust performance but lost a significant amount of the noise suppression of the NRA nozzle. These results are shown in Figure 304. Most of the parametric tests were done with this nozzle. The change to cold sidewalls was to improve thrust performance and the ejector acoustic lining performance of the sidewalls. To provide cold sidewalls, the number of primary (hot) chutes was reduced from 20 to 18. The loss in noise benefit was due to several factors. The number of chutes and chute shape reduced the mixing rate in the ejector. The lower aspect ratio reduced the azimuthal benefit found on the NRA nozzle by more than half. Parametric testing showed that noise reduced with SAR (Figure 305) and with chute penetration (Figure 306). Increasing SAR means a bigger nozzle, which means higher weight and drag. Increasing penetration reduced thrust performance. The parametric data made it possible to trade these effects and define the optimum nozzle for the airplane.

Gen 3 nozzles, also called *Large Scale Mixer Similitude*, went back to a 1.5 aspect ratio and 20 primary chutes. The chutes were arranged such that there was a half hot chute along each sidewall. SAR was selected at 2.9, and the penetration was fixed at 92.5%. The nozzle proved quite successful,

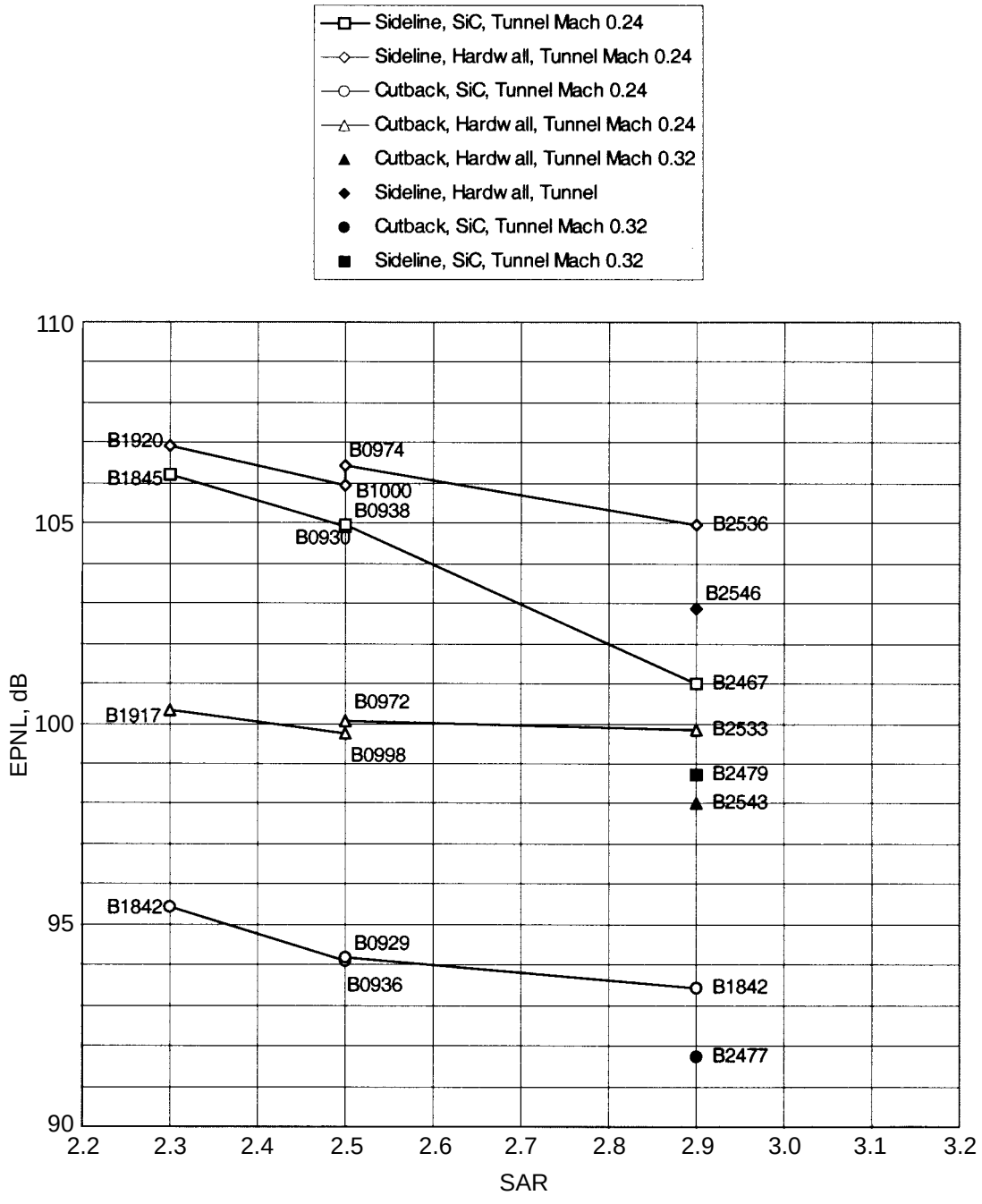

Figure 305. SAR Comparison, DSM Boeing Data Only

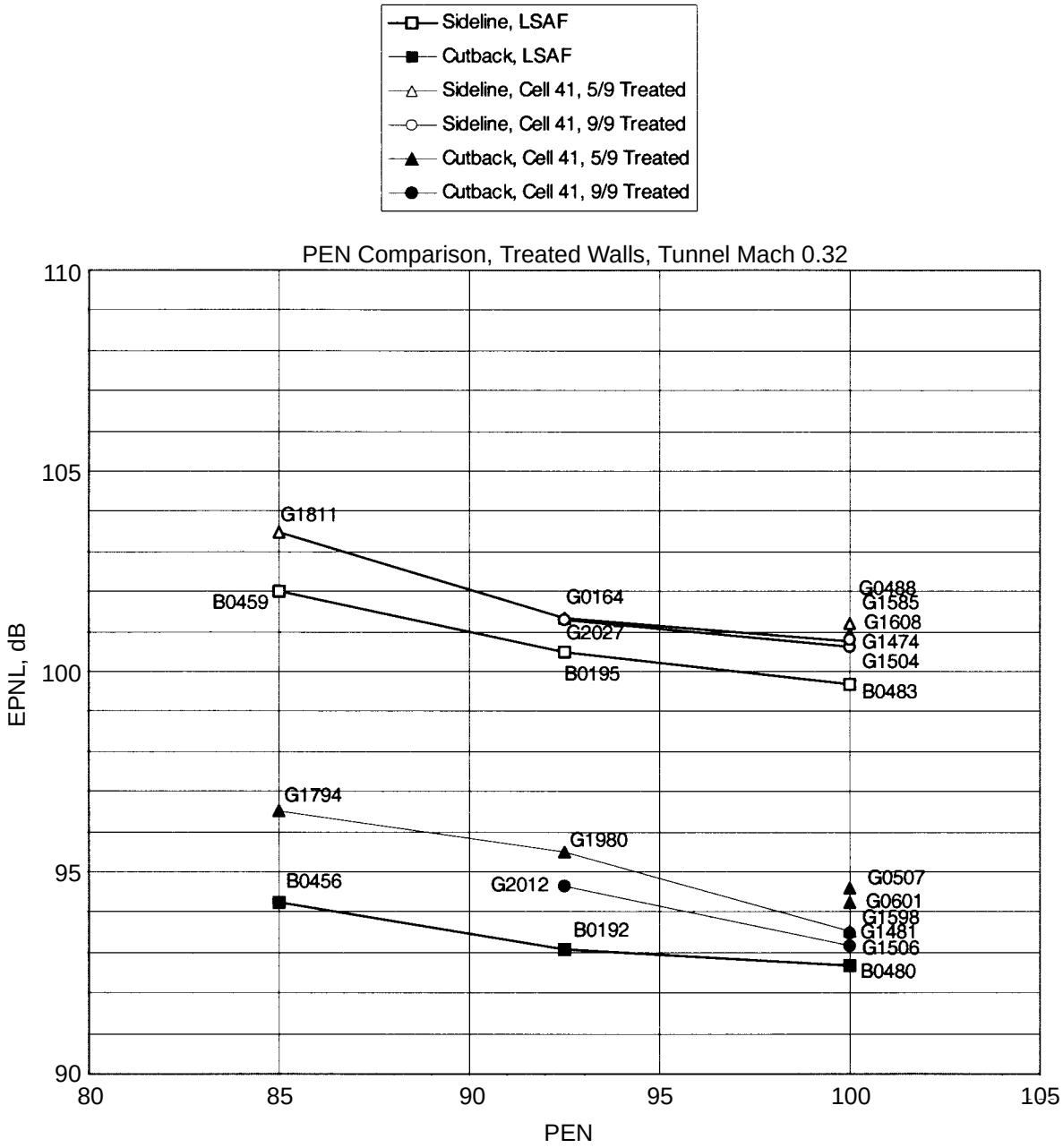

Figure 306. Suppressor Area Ratio (SAR) Noise Trends, DSM, with Treated Side Walls

with noise suppression back to NRA levels while retaining good thrust performance. Exit surveys and other measurements indicated that further improvements were possible.

The final nozzle tested under HSR was the Gen 3.5 nozzle. This nozzle went to a half cold chute along the sidewall and made another small modification to the chute shape to improve thrust performance. Again noise and thrust performance were improved, as shown in Figure 305. Enhancers were also being studied to improve mixing and thus the noise suppression of the nozzle. Many configurations of tabs and other devices were tested at the trailing edge of the mixer. Chevrons were tested at the trailing edge of the ejector. Most of this testing was in Cell 41 at GEAE. The best configurations found were then tested on a Gen 3 mixer in Boeing's LSAF, as part of the Gen 3.5 test series. The "reduced A" tabs provided a significant noise improvement at a small thrust penalty, Figure 304. Ejector acoustic lining is another important factor in optimizing noise suppression from a mixer ejector. Lining effectiveness is shown in Figure 307 plotted in terms of treatment area divided by cross-sectional flow area. This effectiveness depends on treatment location both downstream and circumferential. Noise sources inside the ejector are distributed downstream, and there propagation is influenced by the ejector flow. For a mixer without mixing enhancers, the treatment is virtually ineffective for the first 10 primary lobe widths downstream of the mixer exit. The lining becomes more effective the further downstream it is. Mixing enhancers (tabs) move these sources further upstream, and the lining becomes effective starting at five lobe widths and is more effective along the entire length. Lining was found to be more effective on the flaps than on the sidewalls, particularly under the flight path, as in cutback and approach noise.

Tests of a large-scale model of Gen 3 nozzle with an F100–PW–229 engine provided data that could be used to compare with the small-scale data obtained with more ideal inlet flow conditions. This comparison showed that large-scale nozzle was 1.5 EPNdB noisier than the small-scale nozzle. Analysis indicated that, with a good fan/core mixer, improving flow coming into the mixer and improved ejector acoustic lining could reduce this penalty to 0.5 EPNdB or less.

While overall progress in noise reduction was measured in terms of EPNL reductions, many supporting activities lead to this progress. Laboratory tests of acoustic liners provided valuable data to relate the acoustic impedance of various materials to the physical properties accounting for temperature and grazing-flow effects. Insertion-loss tests enabled development of models to predict liner noise suppression. Empirical models describing the total noise from mixer/ejector nozzles, in terms of the contributing noise sources, not only provided a means to extrapolate measured results but also provided much insight into the relative importance of the various mechanisms contributing to the total noise.

5.11.1.2 Aerodynamics

The overall accomplishments in aerodynamics were alluded to in the previous subsection. Takeoff thrust performance, in terms of thrust coefficient, improved dramatically during the program. Like the progress in acoustics, progress in aerodynamic performance resulted from many supporting activities. Fluid dynamic codes were adopted to make quantitative assessments of proposed changes. Results from CFD analyses were used to select mixer lobe designs for improved mixing, to minimize the possibility of separation in the ejector inlet, and to provide axial flow at the mixer exit plane. Since mixing inside the ejector and mixing just downstream of the ejector were the most important noise sources for the mixer/ejectors tested, much effort was directed toward understanding these processes through the use of flow-visualization measurements and CFD modeling. Examples are

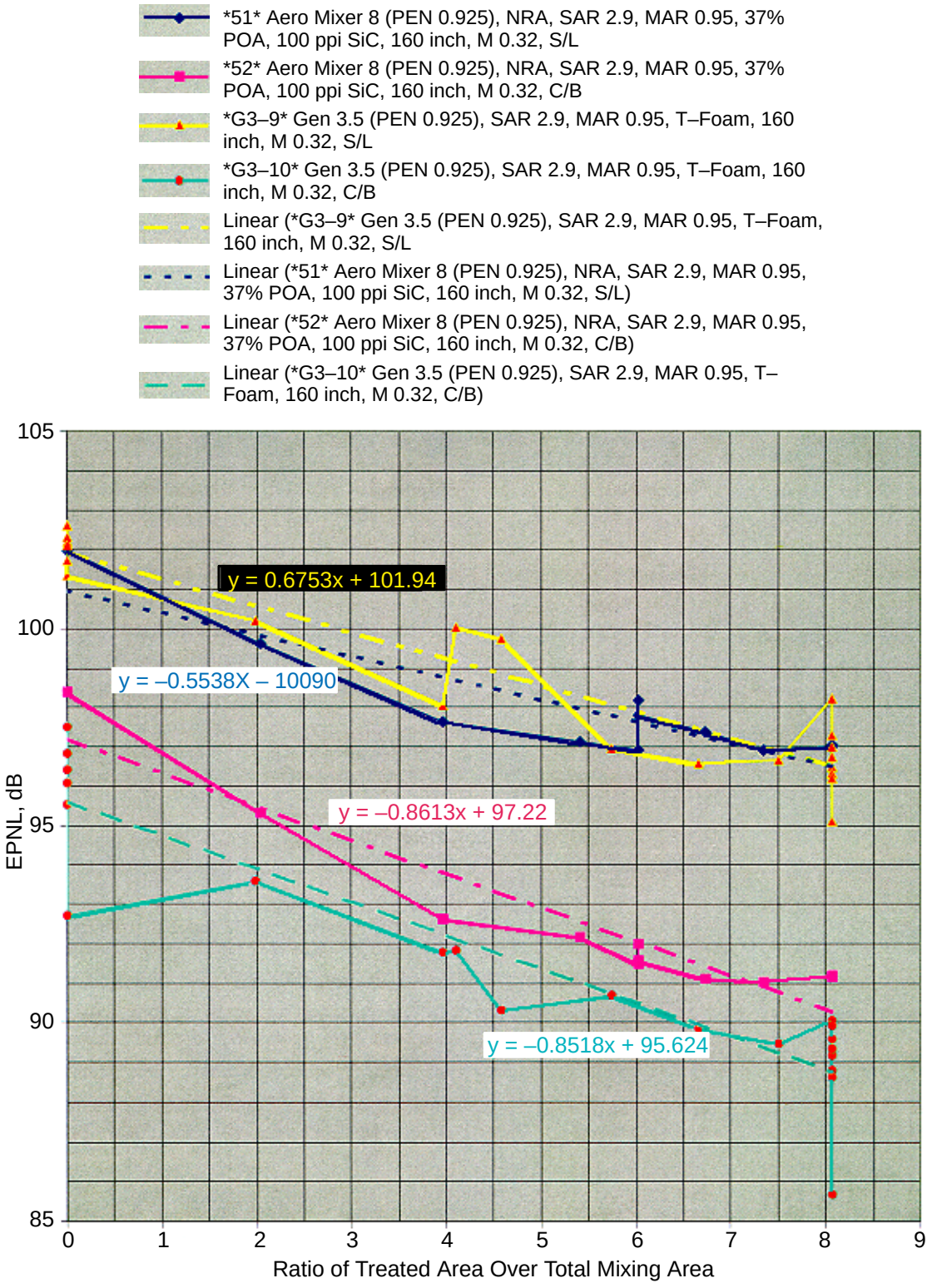

Figure 307. Noise Trends with Treatment Area

shown in Figure 308. CFD modeling was done in many locations; an example is shown in Figure 309. Although this area is far from adequately understood, much of our understanding comes from these efforts. Subelement testing was also used to develop an understanding of the mixing processes. These tests were conducted in the CASL rig at P&W in Florida, single-lobe testing at Boeing Seattle, and mixing enhancers at NASA–Glenn and NASA–Langley. Subelement tests have also been conducted at Universities. Results from these tests led to the highly successful use of tabs to enhance the mixing process within the ejector.

5.11.1.3 Mechanical Design

While the aerodynamic and acoustic disciplines concentrated on the takeoff configuration of the nozzle, the mechanical design had to consider all flight phases. There were many nozzle requirements to satisfy at subsonic cruise, transonic climb, and supersonic cruise that affected nozzle design. The mechanical design had to transition between suppressed and unsuppressed mode and meet boattail and performance objectives in all phases of flight. Strength and durability requirements also had to be met, all at the lowest weight. The final HSR design (see Subsection 5.5.2 and Figures 67 through 76) is estimated to meet all of these requirements and provide the configuration

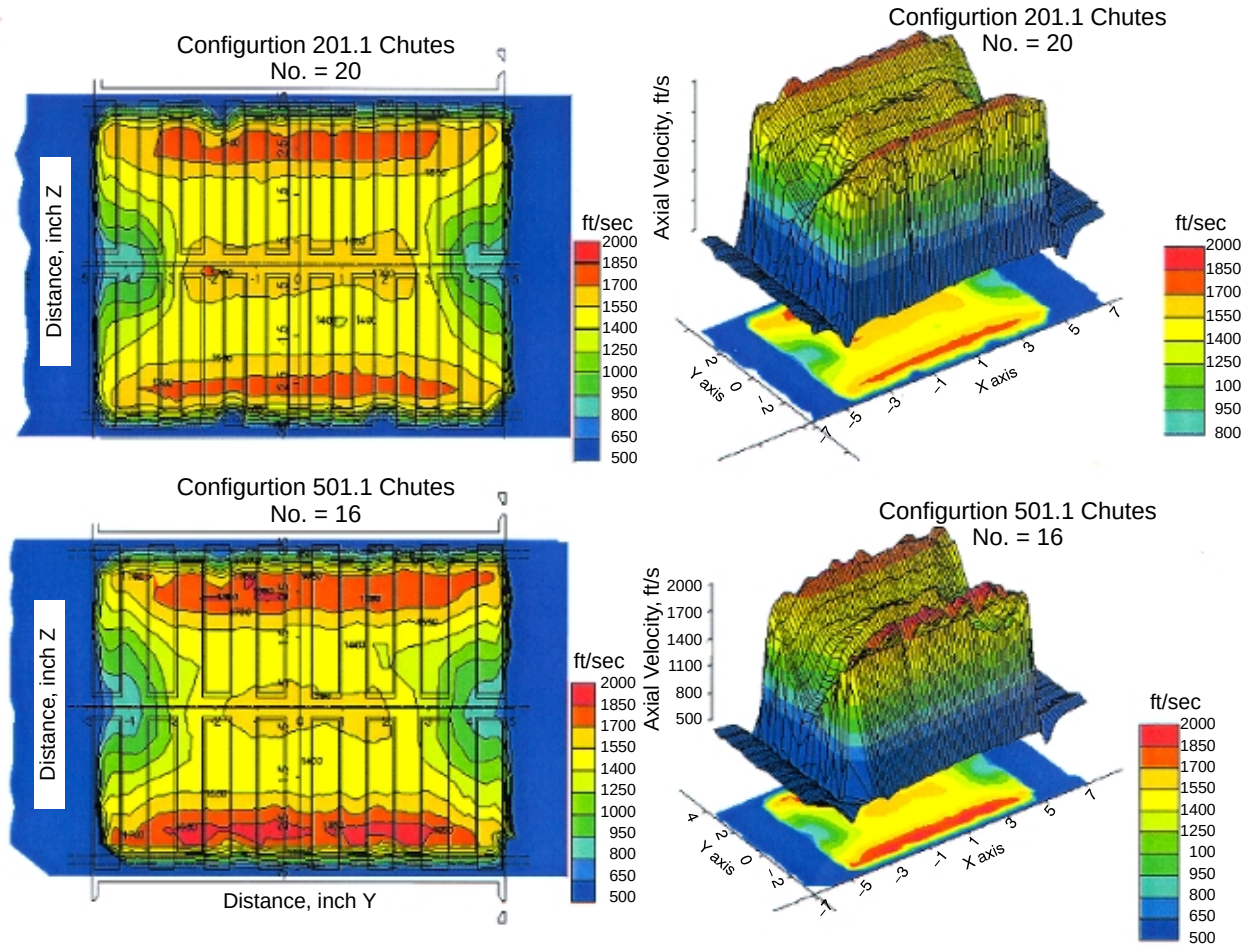

Figure 308. Exit Plane Velocity Contours – Chute Number Comparison MAR 0.95, 120-in Ejector, Sideline Condition

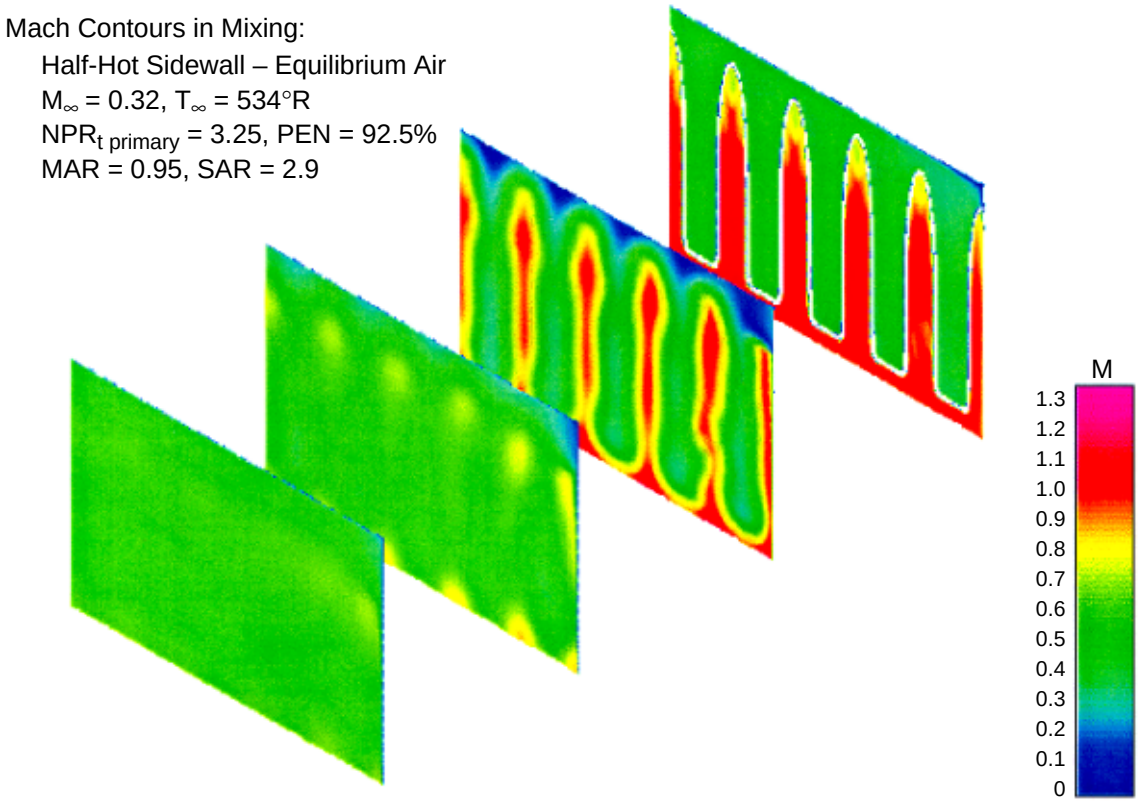

Figure 309. Nozzle Full-Quadrant Analysis, HAM Flowpath Results

and flowpath as tested in the Gen 3.5 model-scale nozzle. Weight estimates for this nozzle, as used in the system studies, included anticipated improvements in materials.

5.11.2 Remaining Challenges

5.11.2.1 Aerodynamic

At the closure of the HSR CPC program, several aerodynamic challenges remain. Following is a brief list of these challenges.

- Understanding the effect of acoustic treatment on thrust loss at small and large scales.
- Improving the robustness of the aerodynamic scaling effects procedure.
- Minimizing liner thrust loss while satisfying acoustic requirements.
- Understanding acoustic treatment effects on cruise performance. This includes two areas: basic acoustic treatment aerodynamic thrust loss and leakage around the divergent flap seals.
- Develop an understanding of the mechanisms of mixing-enhancement devices to allow design optimization.
- Improving mixer CFD analysis techniques with the inclusion of mixer vane simulation.
- Optimizing fan/core mixer design.

5.11.2.2 Acoustic

The following are the major challenges in acoustics foe mixer ejector nozzles:

- Validate the acoustic treatment design procedure that was developed in this program.
- Develop an understanding of the mechanisms of mixing-enhancement devices so the designs can be optimized.
- Develop the methodology to relate noise to the details of the flow field.
- Continue to develop methodologies for flight simulation and for extrapolating static data to flight.
- Validate the acoustic projections at large scale in an engine environment with flight simulation.

5.11.2.3 Mechanical

The following list comprises tasks the mechanical team identified goals to address:

- Complete CMC ejector/mixer design feasibility study.
- Perform nozzle weight-sensitivity studies based on varying nozzle kinematics parameters
- Develop flap train hot-gas-path seal
- Complete thermal profile sensitivity study for the ejector/mixer based on variations in fan/core mixer geometry
- Verify candidate SAVE event weight reduction ideas

5.11.3 Concluding Comment

Tremendous progress was achieved in developing a noise-suppression nozzle that will allow future supersonic transports to have a noise signature compatible with that of the future subsonic fleet without significant performance or weight penalties.

5.12 References

1. Federal Aviation Regulation Part 36, *Noise Standards: Aircraft Type and Airworthiness Certification.*
2. Allyn, D.M. and Lidstone, G.L., “Acoustic and Aerothermal Performance Test of the Axisymmetric Coannular Ejector Nozzle, Volume I – Aerothermal Performance,” NASA Contractor Report, April 1995.
3. Herkes, W., “Acoustic and Aerothermal Performance Test of the Axisymmetric Coannular Ejector Nozzle, Volume II – Acoustic Performance,” NASA Contractor Report, October 1995.
4. Kuhne, C.M., Uenishi, K., Leon, R.M., and Abdol–Hamid, K.S., “CFD Based 3D Aero Analysis System for High–Speed Mixer–Ejector Exhaust Nozzles,” AIAA Paper 94–2941, July 1994.

5. Frink, N.T., “Recent Progress Toward a Three–Dimensional Unstructured NavierStokes Flow Solver,” AIAA Paper 94–0061, January 1994.
6. Power, G.D., Cooper, G.K., and Sirbaugh, J.R., “NPARC 2.2 – Features and Capabilities,” AIAA Paper 95–2609, July 1995.
7. Bush, R.H., “A Three Dimensional Zonal Navier–Stokes Code for Subsonic Through Hypersonic Propulsion Flowfields,” AIAA Paper 88–2830, July 1988.
8. Bush, R.H., Power, G., and Towne, C., “WIND: The Production Flow Solver of the NPARC Alliance,” AIAA Paper 98–0935, January 1998.
9. Midea, A.C., Austin, T., Pao, S.P., DeBonis, J.R., and Mani, M., “High Speed Civil Transport (HSCT) Isolated Nacelle Transonic Boattail Drag Study and Results Using Computational Fluid Dynamics (CFD),” NASA TM HSR025, February 1996.
10. Barber, T..J., Chiappetta, L.M., DeBonis, J.R., Georgiadis, N.J., and Yoder, D.A., “Assessment of Parameters Influencing Prediction of Shear Layer Mixing,” Journal of Propulsion and Power, Vol. 15, No. 1, January 1999, pp 45–53.
11. Tew, D.E., “Streamwise Vorticity Enhanced Compressible Mixing Downstream of Lobed Mixers.” PhD Thesis, Massachusetts Institute of Technology, February 1997.
12. Teeple, B.S., “Optimization of Mixer–Ejector System for Supersonic Civilian Transport Aircraft,” PhD Thesis, Massachusetts Institute of Technology, May 1998.
13. Tew, D.E., Teeple, B.S., and Waitz, I., “A Mixer–Ejector Noise–Suppressor Model” AIAA 97–1692, 1997.
14. Morfey, C.L., and Szewczyk, V.M., “Jet Noise Modelling by Geometric Acoustics, Part 1. Theory and Prediction Outside the Cone of Silence,” *ISVR Technical Report No. 91*, Sept. 1977.
15. Morfey, C.L., and Szewczyk, V.M., “Jet Noise Modelling by Geometric Acoustics, Part 2. Theory and Prediction Inside the Cone of Silence,” *ISVR Technical Report No. 92*, October 1977.
16. Lighthill, M.J., “On Sound Generated Aerodynamically I. General Theory,” Proc. Roy. Soc. Series A Vol. 211 pp 564–587, 1952.
17. Mani, R. et al., “High Velocity Jet Noise Source Location and Reduction – Task 4 – Development/Evaluation of Techniques for ‘Inflight’ Investigation,” GE Contractor Report for DoT – FAA–RD–76–79, IV, February, 1977.
18. Amiet, R.K., “Correlation of Open Jet Wind Tunnel Measurements for Shear Layer Refraction,” AIAA Paper 75–532, 1975.
19. Shields, F.D. and Bass, H.E., “Atmospheric Absorption of High Frequency Noise and Applications to Fractional-Octave Bands,” NASA CR2760, 1977.
20. *Standard Values of Atmospheric Absorption as a Function of Temperature and Humidity,* Aerospace Recommended Practice ARP866A, Society of Automotive Engineers, Revised 3/15/75.
21. Salikuddin, M., Wisler, S., and Majjigi, R.K., “Acoustic, Flow Related and Performance Related Experimental Results for Generation 1.5 High Speed Civil Transport (HSCT) 2-Dimensional Exhaust Nozzles,” HSR046, December 1996.

22. Various Authors, “High-Lift Engine Aeroacoustics Technology (HEAT) NASA/Industry Workshop, Vol. I, Aerodynamic Presentations,” NASA CDCP–21010, March 1996.

23. Various Authors, “High-Lift Engine Aeroacoustics Technology (HEAT) NASA/Industry Workshop, Vol. II, Aeroacoustic Presentations,” NASA CDCP–21010, March 1996.

24. Salikuddin, M., Mengle, V.G., Shin, H–W, and Majjigi, R.K., “Acoustic and Aero–Mixing Experimental Results for Fluid Shield Scale Model Nozzles,” HSR024, January 1996.

25. Whitfield, C.E., “Axisymmetric Mixer Ejector Nozzle (AMEN) Tests in Cell 41,” HSR033, May 1996.

26. Schweiger, P. et al., “Results of Aero/Acoustic Tests and Analytical Studies of a Two–Dimensional Eight–lobe Mixer–Ejector Exhaust Nozzle at Takeoff Conditions,” HSR042, September 1966.

27. Majjigi, R.K. et al., “Low Noise Exhaust Nozzle Development,” HSR044, November 1996.

28. Schweiger, P., Salikuddin, M., et al., “Acoustic Tests of a Pratt & Whitney Two Dimensional, Eight Lobe Mixer–Ejector Nozzle at Takeoff Conditions in General Electric’s C–41 Acoustic Test Facility,” NASA Contract Report.

29. Allyn, D.D. and Lidstone, G.L, “Acoustic and Aerothermal Performance Test of the Near–fully Mixed Nozzle, Volume I – Aerothermal Performance,” NASA Contractor Report, April 1995.

30. Herkes, W., “Acoustic and Aerothermal Performance Test of the Near-Fully Mixed Nozzle, Volume II – Acoustic Performance,” NASA Contractor Report, October 1995.

31. Zaman, K.B.M.Q., “An Experiment on the Near Flow Field of the GE/ARL Mixer Ejector Nozzle,” NASA TM, Report HSR040 (LER), 1996.

32. “Internal Mixing Studied for GE/ARL Ejector Nozzle,” NASA TM 107350, 1996.

33. Zaman, K.B.M.Q., “Effect of Delta Tabs on Free Jets from Complex Nozzles,” NASA TM, Report HSR001 (LER), 1995.

34. Foss, J.K. and Zaman, K.B.M.Q., “Large and Small Scale Vortical Motions in a Shear Layer Perturbed by Tabs,” J. Fluid Mech., 382, 1999, pp 307–329.

35. Steffen, C.J., Reddy, D.R., and Zaman, K.B.M.Q., “Analysis of Flowfield from a Rectangular Nozzle with Delta Tabs,” 26th AIAA Fluid Dynamics Conf., San Diego, CA, Jun 19–22, 1995, AIAA 95–2146.

36. Reddy, D.R, Steffen, C.J., and Zaman, K.B.M.Q., “Computation of 3–D Compressible Flow from a Rectangular Nozzle with Delta Tabs,” ASME Gas turbine and Aeroengine Conf., Orlando, FL, June 2–5, 1997, 97–GT–257.

37. Zaman, K.B.M.Q., “Spreading Characteristics of Compressible Jets from Nozzles of Various Geometries,” J. Fluid Mech., 383, 1999, pp 197–228.

38. Zaman, K.B.M.Q. and Dahl M.D., “Aeracoustic Resonance with Convergent–ivergent Nozzles,” 37th Aerospace Sciences Meet., January 11–14, 1999, Reno, NV, AIAA 99–0164.

39. Zaman, K.B.M.Q. and Tam, C.K.W., “Subsonic Jet Noise from Non-Axisymmetric and Tabbed Nozzles,” 37th Aerospace Sciences Meet., January 11–14, 1999, Reno, NV, AIAA 99–0077.

REPORT DOCUMENTATION PAGE

Form Approved
OMB No. 0704-0188

1. AGENCY USE ONLY (*Leave blank*)	2. REPORT DATE	3. REPORT TYPE AND DATES COVERED
	May 2005	Final Contractor Report

4. TITLE AND SUBTITLE

Critical Propulsion Components
Volume 3: Exhaust Nozzle

5. FUNDING NUMBERS

WBS–22–714–09–447
NAS3–27235

6. AUTHOR(S)

Pratt & Whitney and General Electric Aircraft Engines

7. PERFORMING ORGANIZATION NAME(S) AND ADDRESS(ES)

Pratt & Whitney
Advanced Engineering Operations
P.O. Box 109600
West Palm Beach, Florida 33410

8. PERFORMING ORGANIZATION REPORT NUMBER

E–15051–3

9. SPONSORING/MONITORING AGENCY NAME(S) AND ADDRESS(ES)

National Aeronautics and Space Administration
Washington, DC 20546–0001

10. SPONSORING/MONITORING AGENCY REPORT NUMBER

NASA CR—2005-213584-VOL3

11. SUPPLEMENTARY NOTES

This research was originally published internally in September 2000. Pratt & Whitney, Advanced Engineering Operations, P.O. Box 109600, West Palm Beach, Florida 33410; and General Electric Aircraft Engines, Advanced Engineering Programs Department, One Neumann Way, Cincinnati, Ohio 45215–6301. Responsible person, Diane Chapman, Ultra-Efficient Engine Technology Program Office, NASA Glenn Research Center, organization code PA, 216–433–2309.

12a. DISTRIBUTION/AVAILABILITY STATEMENT

Unclassified - Unlimited
Subject Categories: 01, 05, and 07

Available electronically at http://gltrs.grc.nasa.gov

This publication is available from the NASA Center for AeroSpace Information, 301–621–0390.

12b. DISTRIBUTION CODE

13. ABSTRACT ***(Maximum 200 words)***

Several studies have concluded that a supersonic aircraft, if environmentally acceptable and economically viable, could successfully compete in the 21st century marketplace. However, before industry can commit to what is estimated as a 15 to 20 billion dollar investment, several barrier issues must be resolved. In an effort to address these barrier issues, NASA and Industry teamed to form the High-Speed Research (HSR) program. As part of this program, the Critical Propulsion Components (CPC) element was created and assigned the task of developing those propulsion component technologies necessary to: (1) reduce cruise emissions by a factor of 10 and (2) meet the ever-increasing airport noise restrictions with an economically viable propulsion system. The CPC-identified critical components were ultra-low emission combustors, low-noise/high-performance exhaust nozzles, low-noise fans, and stable/high-performance inlets. Propulsion cycle studies (coordinated with NASA Langley Research Center sponsored airplane studies) were conducted throughout this CPC program to help evaluate candidate components and select the best concepts for the more complex and larger scale research efforts. The propulsion cycle and components ultimately selected were a mixed-flow turbofan (MFTF) engine employing a lean, premixed, prevaporized (LPP) combustor coupled to a two-dimensional mixed compression inlet and a two-dimensional mixer/ejector nozzle. Due to the large amount of material presented in this report, it was prepared in four volumes; Volume 1: Summary, Introduction, and Propulsion System Studies, Volume 2: Combustor, Volume 3: Exhaust Nozzle, and Volume 4: Inlet and Fan/Inlet Acoustic Team.

14. SUBJECT TERMS

High speed civil transport; High speed research; Mixed-flow turbofan; Nozzles; Fixed-chute nozzle; Mixer/ejector

15. NUMBER OF PAGES

391

16. PRICE CODE

17. SECURITY CLASSIFICATION OF REPORT	18. SECURITY CLASSIFICATION OF THIS PAGE	19. SECURITY CLASSIFICATION OF ABSTRACT	20. LIMITATION OF ABSTRACT
Unclassified	Unclassified	Unclassified	